**Institut für Digitales und Autonomes Bauen**
Prof. Dr.-Ing. Kay Smarsly

TUHH

*Tagungsband*

# 35. Forum Bauinformatik

18. – 20. September 2024

**Herausgegeben von:**
Jan Stührenberg
Thamer Al-Zuriqat
Carlos Chillon Geck

FORUMBAUINFORMATIK

**Tagungsband des 35. Forum Bauinformatik 2024**
**Proceedings of the 35th Forum Bauinformatik 2024**
Technische Universität Hamburg

**Herausgegeben von**
Jan Stührenberg
Thamer Al-Zuriqat
Carlos Chillon Geck

**Layout & Satz**
Jan Stührenberg

Digitale Veröffentlichung über die Universitätsbibliothek der Technischen Universität Hamburg

**DOI:** 10.15480/882.13486

*Diese Veröffentlichung, ausgenommen Zitate und anderweitig gekennzeichnete Teile, ist unter der CC-Lizenz CC BY lizenziert.*
**Lizenzvertrag:** *Creative Commons Namensnennung 4.0 | http://creativecommons.org/licenses/by/4.0/*
*Das gedankliche Eigentum und die inhaltliche Verantwortung für die Beiträge liegt bei den jeweiligen AutorInnen.*

**Logo:** Forum Bauinformatik | www.forum-bauinformatik.de
**Umschlaggestaltung:** Jan Stührenberg | Technische Universität Hamburg

# Vorwort

Das Forum Bauinformatik dient seit 1989 regelmäßig dem Austausch im wissenschaftlichen Fachgebiet der Bauinformatik. Die mittlerweile 35. Ausgabe findet 2024 zum ersten Mal in Hamburg statt, am Institut für Digitales und Autonomes Bauen an der Technischen Universität Hamburg (TUHH). Die Bauinformatik erfreut sich in den letzten drei Jahrzehnten einer stetig zunehmenden Aufmerksamkeit. In verschiedensten Teilbereichen treffen vielfältige methodische und technologische Entwicklungen auf zunehmend komplexere Herausforderungen.

Das Forum Bauinformatik bietet Wissenschaftlerinnen und Wissenschaftlern aller akademischen Grade aus dem DACH-Raum die Gelegenheit, Themen und Forschungsergebnisse zu diskutieren und abgeschlossene Projekte zu präsentieren. Da sich die Arbeit der Teilnehmerinnen und Teilnehmer des Forum Bauinformatik nicht auf den deutschsprachigen Raum beschränkt, sondern vielfältig auch mit Partnern sowie Kolleginnen und Kollegen aus der internationalen Forschungsgemeinschaft erfolgt, freuen wir uns besonders, sowohl deutsch- als auch englischsprachigen Beiträgen eine Plattform bieten zu können.

In diesem Konferenzband sammeln wir die insgesamt 64 Beiträge aus 12 Sessions zu den Themenbereichen Künstliche Intelligenz und Maschinelles Lernen, Sensorik und Robotik, Building Information Modeling, Computer Vision, Organisation, Management und Linked Building Data, Nachhaltigkeit, Digitale Zwillinge sowie Simulation und Optimierung. Unser Dank gilt allen Autorinnen und Autoren sowie Betreuerinnen und Betreuern, die durch ihre Beiträge und Reviews zum Erfolg dieser Konferenz beigetragen haben. Wir wünschen allen Teilnehmenden eine spannende Konferenz mit inspirierenden Diskussionen und neuen Impulsen für ihre zukünftige Arbeit.

**Jan Stührenberg, Thamer Al-Zuriqat, Carlos Chillon Geck**

Hamburg, September 2024

# Preface

Since 1989, the Forum Bauinformatik has regularly provided a platform for exchanging scientific research and ideas in the field of computing in civil engineering. The 35th edition, hosted in 2024 at the Institute of Digital and Autonomous Construction at Hamburg University of Technology (TUHH), marks the first time the event is held in Hamburg. Over the years, computing in civil engineering has gained increasing attention, with diverse methodological and technological developments addressing challenges of growing relevance and complexity.

Within the Forum Bauinformatik, scientists of all academic levels from the DACH region are given the opportunity to discuss topics and findings to present their work, engage in discussions, and showcase projects. As the work of the participants of the Forum Bauinformatik is not limited to the German-speaking region, but is also carried out with partners and colleagues from the international research community, we are particularly pleased to offer a platform for both German- and English-language contributions.

This conference volume compiles 64 contributions from 12 sessions, covering artificial intelligence and machine learning, sensors and robotics, building information modeling, computer vision, organization, management und linked building data, sustainability, digital twins, as well as simulation and optimization.

We extend our sincere thanks to all authors and supervisors for their contributions through papers and reviews. We wish all participants a productive conference filled with engaging discussions and insights for future work.

**Jan Stührenberg, Thamer Al-Zuriqat, Carlos Chillon Geck**

Hamburg, September 2024

# Chronik des Forum Bauinformatik

| | |
|---|---|
| 1989 | Hochschule für Architektur und Bauwesen Weimar |
| | **Lehrstuhl für Informatik im Bauwesen** |
| 1990 | Brandenburgische Technische Universität Cottbus |
| 1991 | Technische Universität Berlin |
| 1992 | Ruhr-Universität Bochum |
| | **Lehrstuhl für Ingenieurinformatik im Bauwesen** |
| 1993 | Technische Universität München |
| | **Fachgebiet Bauinformatik** |
| 1994 | Technische Hochschule Darmstadt |
| | **Institut für Numerische Methoden und Informatik im Bauwesen** |
| 1995 | Universität Hannover |
| | **Institut für Bauinformatik** |
| 1996 | Brandenburgische Technische Universität Cottbus |
| | **Lehrstuhl für Bauinformatik** |
| 1997 | Technische Universität Dresden |
| | **Lehrstuhl für Computeranwendungen im Bauwesen** |
| 1998 | Bauhaus-Universität Weimar |
| | **Lehrstuhl für Informatik im Bauwesen** |
| 1999 | Technische Hochschule Darmstadt |
| | **Institut für Numerische Methoden und Informatik im Bauwesen** |
| 2000 | Technische Universität Berlin |
| | **Theoretische Methoden der Bau- und Verkehrstechnik, Institut für Bauingenieurwesen** |
| 2001 | Technische Universität München |
| | **Lehrstuhl für Bauinformatik** |
| 2002 | Ruhr-Universität Bochum |
| | **Lehrstuhl für Ingenieurinformatik im Bauwesen** |
| 2003 | Universität Hannover |
| | **Institut für Bauinformatik** |
| 2004 | Technische Universität Braunschweig |
| | **Institut für Computeranwendungen im Bauingenieurwesen** |
| 2005 | Brandenburgische Technische Universität Cottbus |
| | **Lehrstuhl für Bauinformatik** |
| 2006 | Bauhaus-Universität Weimar |
| | **Professur Informatik im Bauwesen** |
| 2007 | Technische Universität Graz |

| | |
|---|---|
| | **Institut für Bauinformatik** |
| 2008 | Technische Universität Graz |
| | **Institut für Informatik** |
| 2009 | Universität Karlsruhe |
| | **Institut für Industrielle Bauproduktion und Entwerfen** |
| 2010 | Technische Universität Berlin |
| | **Fachgebiet Bauinformatik, Institut für Bauingenieurwesen** |
| 2011 | University College Cork |
| | **Informatics Research Unit for Sustainable Engineering** |
| 2012 | Ruhr-Universität Bochum |
| | **Lehrstuhl für Informatik im Bauwesen** |
| 2013 | Technische Universität München |
| | **Lehrstuhl für Computergestützte Modellierung und Simulation** |
| | **Lehrstuhl für Architekturinformatik** |
| 2014 | Technische Universität Darmstadt |
| | **Institut für Numerische Methoden und Informatik im Bauwesen** |
| 2015 | Rheinisch-Westfälische Technische Hochschule Aachen |
| | **Geodätisches Institut, Lehrstuhl für Bauinformatik & Geoinformationssysteme** |
| 2016 | Leibniz Universität Hannover |
| | **Institut für Risiko und Zuverlässigkeit** |
| 2017 | Technische Universität Dresden |
| | **Institut für Bauinformatik** |
| 2018 | Bauhaus-Universität Weimar |
| | **Professur Informatik im Bauwesen** |
| 2019 | Technische Universität Berlin |
| | **Fachgebiet Bauinformatik und Fachgebiet Systemtechnik baulicher Anlagen** |
| 2021 | Technische Hochschule Darmstadt |
| | **Institut für Numerische Methoden und Informatik im Bauwesen** |
| 2022 | Technische Universität München |
| | **Lehrstuhl für Computergestützte Modellierung und Simulation** |
| | **Lehrstuhl für Architekturinformatik** |
| 2023 | Ruhr-Universität Bochum |
| | **Lehrstuhl für Ingenieurinformatik im Bauwesen** |
| 2024 | Technische Universität Hamburg |
| | **Institut für Digitales und Autonomes Bauen** |

# Inhaltsverzeichnis

**I Artificial Intelligence & Machine Learning** 1

**Sensitivity Analysis of Full-waveform LiDAR Data for Material Classification** . . . . . 2
Omar Aldohami and Hristo Vassilev

**Joint Triple Extraction for Construction Regulatory Documents using Graph Neural Networks** . . . . . 10
Sherief Ali

**Maschinelles Lernen zur Schadenserkennung bei Leichtbaubrücken mit beweglichen Massen** . . . . . 18
Georgios Dadoulis, Thamer Al-Zuriqat and Kosmas Dragos

**Using 2D scene graphs as an enabler for DT topology** . . . . . 26
Nayun Kim, Atacan Kural Avgoren, Mohammad Adnan Mohammad Alrabab'h, Fiona Collins and Changyu Du

**Generalising AI model performance for Non Destructive Testing in railway systems** . . 34
Georg Olm

**Enhancing Machining Feature Recognition in CAD Models through Transfer Learning on BRepNet** . . . . . 42
Konstantinos Gkrispanis

**Konzept zur KI-gestützten parametrischen Brückenmodellierung für ressourcen- und kostenoptimierte Bauwerksentwürfe** . . . . . 50
Jonas Wiederer, Simon Höng and Friedrich Eder

**SPARK: A Universal Approach to 3D Point Cloud Segmentation Using 2D Image Segmentation Models – Demonstration on Traffic Objects** . . . . . 58
Michael Disser, Vivien Volland and Gent Demiri

**AI in Critical Infrastructure -– Explainability and Models** . . . . . 66
Jens Wala

**Building facade evaluation using instance segmentation on thermal images** . . . . . 74
Gerda Cones, Fiona C. Collins and Florian Noichl

**Integrating Dynamic Environment Modelling with Reinforcement Learning for Fire Safety Design** . . . . . 82
Isabelle Fitkau

**II Sensors & Robotics** 90

**A scalable smart irrigation system based on Internet of Things technologies** . . . . . 91
Carlos Chillón Geck and Rami Nasr

**Robotikgestützte Werkzeuglogistik mit Quadrupeds für die Bauindustrie** . . . . . 99
Christian Kiebel, Dominik Lehmann, Sven Zentgraf and Patrick Herbers

**Underwater Spatial Field Monitoring with Small Scale Robots: An Experimental Study** 107
Nathalie Bauschmann

**Monitoring und Simulation von Roboterkinematik basierend auf digitalen Zwillingen für den Lehmdruck** . . . . . 115
Jasper Vollmert, Patricia Peralta and Aditya Tandon

**Continuous monitoring of construction sites using mobile machinery - a case study** . 123
Artem Bliznyuk, David Böken, Lennart Schinke and Jorge Luis Jiménez Aparicio

**Detection and elimination of strain reading anomalies in distributed strain sensing readings** . . . . . 131
Lisa Ulbrich

**Robotergestütztes Bauwerksmonitoring basierend auf eingebetteter Sensorik** . . . . . 139
Sergej Johann, Jan Stührenberg and Aditya Tandon

**Experimental evaluation of iPad Pro LiDAR, for building modeling and possibilities to connect with AI technologies** . . . . . 147
Nils Sören Krause and Miguel Guzmán-Merino

**Robot-based installation of nanostructured metal multilayers on civil infrastructure** . . 155
Niclas Spalek, Jan Stührenberg, Aditya Tandon, Maximilian Tourneau, Ayush Patel and Bastian Große

**Autonomous 3D Scanning of Construction Sites Using Terrestrial Laser Scanner and UGV** 163
Pranav Shevkar and Jan Luca Fahrendholz-Heiermann

**Autonome Navigation vierbeiniger Roboter für Bauwerksinspektionen** . . . . . 171
Aditya Tandon and Jan Stührenberg

**III Building Information Modeling** **179**

**Enhancing Compliance and Efficiency in Infrastructure Projects through Smart Standards** **180**
Sven Zentgraf, Susanne Wienholz, Sherief Ali, Andreas Bach, Iris Hindersmann and Jennifer Bednorz

**Deriving Fabrication Information from BIM for Automated Robotic Task Planning** . . . . **188**
Maikel Jean Silvo Brinkhoff and Mohammad Reza Kolani

**A framework for using heterogeneous data from digital building permits in urban mining** **196**
Marcel Heiß and Timo Bittner

**Nachhaltiges Bauen durch Building Information Modeling: Eine explorative Analyse und ein methodischer Ansatz zur Verbesserung der Ökobilanzierung** . . . . . **204**
Thujietha Thuraisingam, Nijanthan Mohan, Rolf Groß and Thomas Kleinow

**Nachhaltigkeitsbewertungen durch IoT-gestützte Auswertung von Nutzerverhalten im Rahmen des as-used BIM** . . . . . **212**
Maximilian Gehring and Yunquing Luo

**Developing rule-based model checking for verifying energy properties of windows: Promoting sustainable construction practices** . . . . . **220**
Janees Riyaz and Emara Merna

**Urban Tree Placement Analysis: A GIS-Based Approach for Identifying Suitable Planting Locations in Munich** . . . . . **228**
Roland Reitberger, Nayanesh Pattnaik and Ying Lu

**Integration of GIS data into 3D Space Partitioning to enhance architectural modeling** . **236**
Sebastian Oswald and Gresa Calliku

**Ein BIM-Reifegradmodell zur Messung der digi-talen Transformation von Infrastrukturbehörden** . . . . . **244**
Markus Boden

**Adding an extensive feedback loop for the creation and validation of functional requirements of BIM models** . . . . . **252**
Florian M. Becker and Daniel Napps

**Semi-automated assessment in fundamental BIM pedagogy for large cohorts** . . . . . **260**
Jiabin Wu, Sebastian Esser, Kasimir Forth, Ainur Kairlapova and Julian Gerstner

**Simplification of Polygons from Point Cloud Data for Automated Floorplan Generation** **268**
Antonio Carlone and Felix Gabler

**Incremental model updates in BIM: a critical analysis of the collaboration platform Speckle** **276**

Kai Dietmair, Sebastian Esser and Benedict Harder

**Automated IFC-based mesh refinement and quality control for indoor airflow simulations using OpenFOAM** . . . . . **284**
Anna Hochberger and Veronika Elisabeth Richter

**iDesignArch: Chatbot-supported architectural requirements management for inspiring building designs** . . . . . **292**
Jan H. Heinbach and Daniel Napps

**Ensuring Compliance in Construction: A Deep Dive into BIM Model Checking and Automated Code Verification** . . . . . **300**
Mohamed Helmy Ammar and Merna Emara

**IV Computer Vision** **308**

**Kombination von Thermographie und Laserscanning zur Erfassung und Visualisierung von Störstellen mittels BIM** . . . . . **309**
Melanie Müßle

**Automatic Detection of Shaft Locations in Site Plans** . . . . . **317**
Timo Santehanser and Phillip Schönfelder

**Automated Inspection of Obstructed Fire Extinguishers Using Amodal Instance Segmentation** . . . . . **325**
Jan H. Heinbach and Angelina Aziz

**Exploring Explainable AI for Symbol Detection in Construction Drawings** . . . . . **333**
Jan Michalak and Benedikt Faltin

**Comparison of Tracking Methods for Augmented Reality-Supported Damage Mapping of Grid Shell Structures** . . . . . **341**
Christian Rosenkranz and Pascal Mosler

**Enabling Component-Based Progress Monitoring on Construction Sites Through Image-Based Computer Vision** . . . . . **349**
Felix Friedl and Fabian Pfitzner

**V Organization, Management, & Linked Builing Data** **357**

**Berücksichtigung von Nutzeranforderungen bei der Planung von ÖPNV-Trassen: Eine Methode zur objektiven Bewertung und Empfehlungen im Kontext von Haltestellenstandorten** . . . . . **358**

Helena Hamann, Felix Petre and Martin Wogan

**Integration of Multi-Criteria Decision-Making in Heritage Building Information Management** **366**
Laura Fernandez Resta

**Automatisierte projektabhängige Filterung von technischen Regeln mit IDS** . . . . . **374**
Lennard Buttgereit and Merna Emara

**Geometric rule check with Answer Set Programming for barrier-free navigation** . . . . . **382**
Marian Kurzawa

**Informationsintegration in der Betriebsphase von Bauwerken: Eine diagnostikspezifische Ontologie im ICDD** . . . . . **390**
Paul-Christian Schuler, Yannic Stark and Mahsa Mirboland

**Enabling Circular Construction: Evaluating ICDD for Effective Deconstruction Processes** **398**
Victoria Jung

**VI Sustainability** **406**

**How can development plans promote the sustainability of construction projects?** . . . **407**
Jan Luther and Jonas Maibaum

**Distance-based Loss Function for Machine Learning in Image Segmentation of Concrete Cracks** . . . . . **415**
Baris Özcan and Fabian Alexander Schmiedecke

**Robotic Disassembly and Window Upgrading** . . . . . **423**
Begum Aktas and Mehrzad Esmaeili Charkhab

**VII Digital Twins** **431**

**DiggiTwin: End-to-end use of digital twins to realize a climate-neutral building stock** . **432**
Sriram Badri, Nijanthan Mohan, Marc Oyen and Lukas Schnittcher

**Presentation of an optimized process for generating analysis models in structural engineering using Graph Neural Networks** . . . . . **440**
Toni Nabrotzky

**Automatic conversion of real-world data from a German road infrastructure management system into a labelled property graph** . . . . . **448**
Ina Heise

**Model-Based-Systems-Engineering for bridges: Representing modular precast bridges with SysML** . . . . . 456
Benedict Harder and Sebastian Esser

**Implementing information container to link multi-models for Semantic Digital Twins** . . 464
Yingying Zhang

**VIII Simulation & Optimization** 472

**Building Resilience to Heatwaves: Parametric Simulation Approach Aiding Passive Design Strategies for Thermal Comfort in Future Climate** . . . . . 473
Agata Dalach

**A Comparative Study of Deep Learning and Evac4BIM in Building Evacuation Design** . 481
Patrick Berggold, Ann-Kristin Dugstad and Mohab Hassaan

**Anwendung des Simulationsmodells *Transreac* bei zweidimensionalem, korrosivem Angriff auf zementgebundene Baustoffe** . . . . . 489
Heike Heizmann

**Entwicklung eines Optimierungsverfahrens zur Strukturidentifikation von Brückenbauwerken** . . . . . 497
Lukas Guntermann and Bjarne Sprenger

**Neuartige selektive Massenskalierungsmethoden für transiente Analysen dünnwandiger Strukturen mit Volumenelementen und expliziter Zeitintegration** . . . . . 505
Moritz Hoffmann

**LLM Assistant for heterogeneous multi-robot system dynamic task planning** . . . . . 513
Miguel Guzmán-Merino and Nils Sören Krause

# Teil I

# Artificial Intelligence & Machine Learning

# Sensitivity Analysis of Full-waveform LiDAR Data for Material Classification

Omar Aldohami and Hristo Vassilev
Chair of Building Informatics and Geoinformation Systems and Geodetic Institute, RWTH Aachen University, Mies-van-der-Rohe-Str. 1, 52074 Aachen, Germany
E-mail(s): omar.aldohami@rwth-aachen.de, hristo.vassilev@gia.rwth-aachen.de

**Abstract:** Full-waveform (FWF) LiDAR can provide additional features which can be helpful to distinguish between different construction materials. However, due to its high volume FWF information is often discarded and not used for downstream analysis, such as material classification. This contribution investigates waveform processing, such as Gaussian decomposition, and modelling to extract important radiometric features from terrestrial laser scanning. In addition, geometric information is extracted by analysing point cloud neighbourhoods. The resulting combination of features is evaluated by means of sensitivity analysis to obtain their corresponding relevance to material classification. Specifically, the assessment is performed leveraging machine learning algorithms, such as support vector machines, and monitoring the influence of the model's performance depending on the combinatoric inclusion of the proposed individual features. To support the analysis, furthermore a rich dataset is presented, consisting of point clouds, waveform and image data of various urban and infrastructure scenes. Thereby the aim of the classification problem is to semantically segment the point clouds according to common materials such as concrete surfaces, vegetation or brick. This effort serves the goal of improving the automatic digitization of construction assets through the use of advanced remote sensing techniques.

*Keywords:* Digital Twin, Full-waveform, Laser scanning, Machine learning, Scan-to-BIM

Erschienen in Tagungsband 35. Forum Bauinformatik 2024, Hamburg, Deutschland, DOI: 10.15480/882.13519
© 2024 Das Copyright für diesen Beitrag liegt bei den Autoren. Verwendung erlaubt unter Creative Commons Lizenz Namensnennung 4.0 International.

## 1 Introduction

Over the last years, the demand for adopting modern data acquisition techniques, such as 3D laser scanning, for accurate Building Information Models (BIM) of existing buildings has increased in popularity. Such data include high resolution and high accuracy point cloud models which serve the purpose of downstream applications for models made using scan-to-BIM, which can range from as-built documentation, project renovations and additions, or facility management. Models made with scan-to-BIM are also very useful for comparing against as-planned models. A case study discussed the practical integration of 3D laser scanning with BIM in construction projects and demonstrated the significant impact of these technologies on improving project outcomes by enhancing as-built documentation and project information management [1].

With the introduction of full-waveform, FWF, LiDAR systems as an active remote sensing technique, emerged new possibilities for retrieving additional morphological features which can be used to enhance the automatic classification of urban areas. Typically, commercial LiDAR systems measure the first and last signal pulse, and some are capable of recording up to six echoes for each emitted pulse [2]. Due to the 3D structure of natural and artificial objects, the shape of the received signal can be extremely complex and these traditional discrete return systems can only provide the coordinates of the scattering objects. Conversely, full-waveform data capture the sequential 1D profiles of the landscape, where the laser beam, penetrating a cone-shaped volume due to diffraction, registers each object within this volume as distinct echoes in the waveform [3]. Full waveform return systems can therefore enhance user control over the interpretation of physical measurements and offer additional details about the reflectance of back-scattered objects. By combining full waveform feature extraction with machine learning, The aim is to assess the relevance of the additional waveform features in the specific use case of using TLS for "As-Is" / "As-Built" scan-to-BIM.

# 2 Research Background

## 2.1 Physical Operating Principle of FWF Systems

LiDAR is an active remote sensing technology that emits its own energy, unlike passive systems that rely on ambient light. LiDAR systems emit light signals toward the Earth's surface, which interact with objects like buildings and trees. The reflected light returns to the sensor, where it is detected and recorded. The time interval between the emission and return of the light signal, known as the two-way travel time, is used to calculate the distance traveled by the light signal, converting it into Cartesian coordinates. FWF LiDAR systems capture multiple reflections, or "returns," from a single laser signal, which are all recorded by the sensor. The returning light energy generates a waveform, representing the energy distribution detected by the sensor. Peaks in the waveform correspond to different objects encountered by the laser signal, such as branches or buildings. Analyzing these waveforms allows for extracting detailed morphological features, enhancing the classification and mapping of various objects within the scanned environment.

## 2.2 Development of FWF LiDAR

The development and application of full-waveform (FWF) LiDAR systems have significantly ad-vanced remote sensing. The first operational FWF LiDAR, the Laser Vegetation Imaging Sensor (LVIS), was developed by NASA in 1999. LVIS showcased the utility of recording entire waveforms for detailed vegetation analysis, capturing complex structural information of vegetation canopies [4]. The first commercial FWF LiDAR system was introduced in 2004, and today, companies like Riegl, Optech, Leica, and propose such an extension to their multiple pulse devices [5]. FWF LiDAR technology shows promise across various fields, for instance in forestry and environmental monitoring where it can facilitate precise tree species classification by capturing detailed waveform characteristics, improving accuracy in complex forest environments [6]. In coastal and underwater surveying, such as in the German Wadden Sea National Park, FWF LiDAR enhanced seabed map-ping and habitat structure analysis, highlighting its utility in environmental planning and conservation efforts in aquatic environments [7].

While FWF data have been used mainly for a large variety of land-cover mapping in forestry and vegetated areas using airborne laser scanning devices, theoretical assessment of the potential of such data has been barely tackled [8]. This is due to several factors: the complexity of waveform processing, the much larger data volume compared to multi-echo data, and the lack of standard formats and software solutions. Furthermore, FWF terrestrial laser scanning systems often exhibit more non-linearity in the scale characteristics of the system's response than observed in the FWF data acquired by airborne LiDAR systems. This is often due to the high dynamic range of the TLS targets (due to large range envelope) [9].

## 2.3 FWF Processing

Waveform processing in FWF LiDAR involves signal processing methods to decompose complex waveforms into identifiable echoes and model them using suitable mathematical functions. This process effectively characterizes different targets encountered by the laser pulse, extracting meaningful waveform-derived features.

### 2.3.1 Waveform Decomposition and Modelling

Initially, the goal is to maximize the detection rate of relevant peaks within the waveforms. This is done by waveform decomposition through which these complex waveforms are analyzed to identify the echo positions. An echo is generated when the laser signal reflects off an object and returns to the LiDAR sensor. The position of each echo within the waveform is critical as it relates directly to the physical location and characteristics of the object in the environment. Peak detection algorithms can help achieve this by identifying points in the data where the signal reaches a local maximum that is significant against the background noise. After detecting peaks, initial estimation of component numbers and values, is followed by parameter optimization to refine these estimates. Effective wave-form processing relies heavily on precise initial parameter estimation to prevent errors in echo characterization. Established techniques for optimization in the literature include the Expectation-Maximization algorithm, suitable for Maximum Likelihood estimates, and the Levenberg-Marquardt algorithm for non-linear least squares approaches [10]. Parametric modelling of echoes reveals detailed information about the surface or object from which the laser light was reflected. The shape of an echo depends on attributes like material reflectivity, object geometry, and laser beam angle. Gaussian functions, Lognormal, or a sum of generalized Gaussian (GG) curves often represent these echoes. Wagner et al. (2006) showed that more than 98% of observed waveforms with the Riegl system could be fitted with a sum of Gaussian functions. Asymmetric echoes, frequently observed in certain waveforms, necessitate adaptable parametric functions, capturing nuances such as skewness and scale [10].

### 2.3.2 Potential of FWF Features

FWF features capture detailed physical characteristics of targets, distinguishing different surfaces in urban environments. For instance, echo width and amplitude help identify vegetative or soft surfaces versus hard surfaces like roads. Reflectance variations can discern materials, which helps distinguish a building's concrete façade from glass windows, for example as shown in Figures 1 and 2 below.

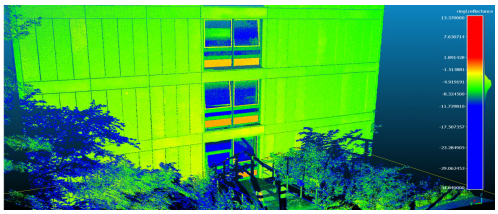

Figure 1: Reflectance variations

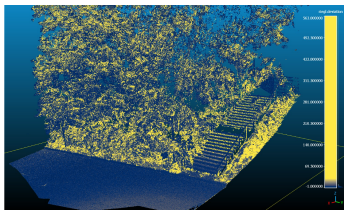

Figure 2: Deviation (echo width) variations

# 3 Methods

## 3.1 Study Area and Dataset

The following section describes the processing chain used in this study. Initially, the process begins with scanning the urban environment in the city of Aachen, Germany, focusing on areas which include both natural and man-made structures. Target selection was based on locations with various building facades made from different construction materials. RWTH Institute for Physical Chemistry and RWTH Chemistry Institute buildings were selected as the study areas. The selected classes of targets were to be located at different distances (ranges) from the scanner. Data acquisition targeted five classes of interest: Concrete, Bricks, Artificial ground, Natural ground, and Vegetation. The data was collected using the Riegl VZ-400 FWF Terrestrial Laser Scanner [11], for which dataset illustrations are shown in Figure 3.

Figure 3: Illustrations of dataset

## 3.2 FWF Processing

The following section describes the processing chain, depicted in Figure 4. Initially, the raw data is captured and exported in two formats: TLS LiDAR Waveforms (.wfm) and 3D point clouds (.rdbx). By combining the data found in those two formats, the point cloud generated by manufacturer's proprietary algorithms is merged with the raw full-waveform signal used in the process. The linking between the extracted point cloud and the corresponding location in the waveform data is facilitated through a timestamp. The waveform data consists of regions of interest (ROI), which are extracted from the entirety of the received signal during the on-board processing of the TLS. Although the ROI may initially vary in length, it was constrained to 32 values per point for consistency. Waveform processing involves the detection and modeling of peaks within the digitized echo signals, representing potential tar-gets or features. The findpeaks function from the SciPy library identifies local maxima based on

amplitude and other properties such as prominence and width. Prominence measures how much a peak stands out from the surrounding baseline, calculated as the vertical distance between the peak and the lowest con-tour around it that does not contain any higher peak. Peak width at a relative height is also calculated to ensure the peaks represent true signal characteristics. Once peaks are identified, a single Gaussian modelling is used in artificial classes which often exhibit single peak.

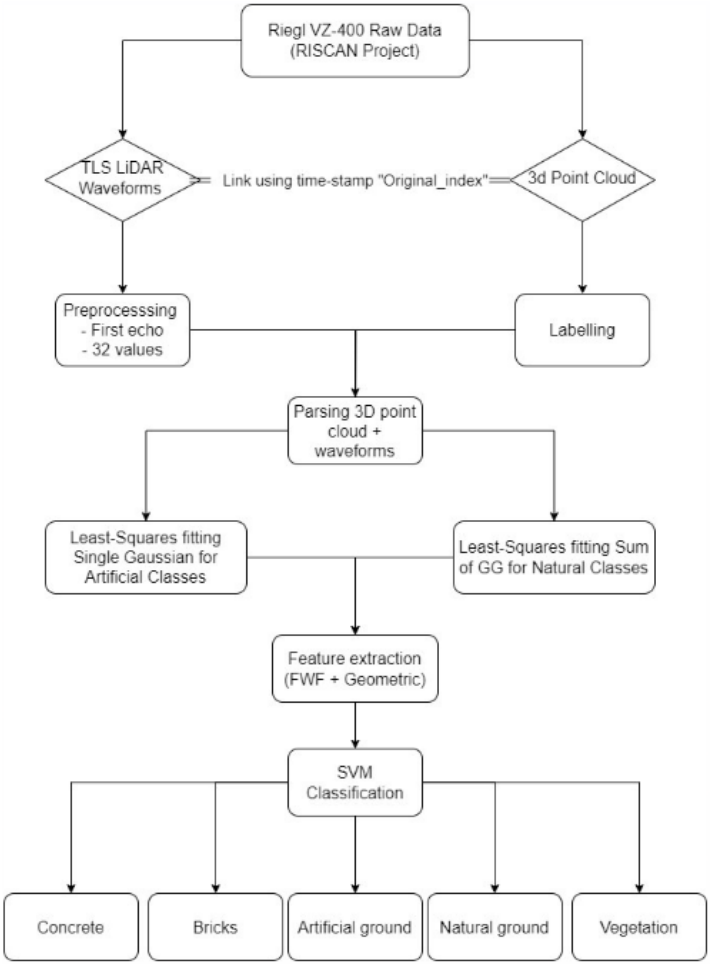


Figure 4: Flowchart for the processing chain.

The *curvefit* function in Scipy fits the data points of each detected peak by optimizing the parame-ters to minimize the difference between the fitted curve and the actual data points. The Gaussian fitting optimization utilizes the Levenberg-Marquardt algorithm which adeptly balances gradient descent and Gauss-Newton methods, optimizing parameter estimation for non-linear least squares problems. The algorithm starts with initial parameter guesses based on detected peak properties and enforces parameter bounds to ensure realistic solutions by handling up to 10,000 function evaluations (iterations). To assess the accuracy of the fit, Residuals, calculated as the difference be-tween observed data points and model-predicted values are measured with metrics such as R-squared and Root Mean Square Error (RMSE) to validate the model's effectiveness. An R-squared value of 0.9676 achieved indicates that approximately 96.76% of the variance in the dependent variable is explained by the model, suggesting a strong correlation and effective model performance. In complex environments

like natural ground and vegetation, waveforms often exhibit multiple peaks due to overlapping features or mixed material responses. A sum of generalized Gaussians model is then used to effectively fit the multiple peaks variations. This model captures diverse peak shapes which are noticed in natural classes. Fitting of waveforms is illustrated in Figure 5 below.

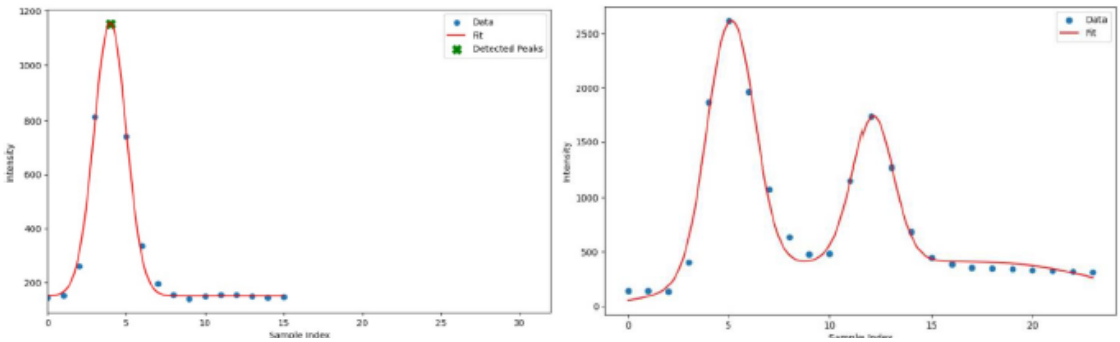


Figure 5: Left graph shows single Gaussian fitting for a 'Bricks' class waveform; right graph depicts a sum of generalized Gaussian fits for a 'Vegetation' sample.

### 3.3 Features of Interest

Several critical FWF features are extracted to characterize the waveform's profile, such as amplitude and mean, which indicate the peak intensity and central location of each peak, respectively, providing essential information on the strength and position of reflections. Sigma ($\sigma$), or the standard deviation of the Gaussian fit, illustrates the spread of the waveform around the mean, indicative of surface irregularities or scattering effects. Echo Width at Half Maximum (EWHM) quantifies the width at half-maximum intensity. The Peak Area under the Gaussian curve represents the total power of the reflected signal, correlating with the physical attributes of the reflecting surface. Flatness and Echo Asymmetry describe the peakedness and symmetry of the waveform, respectively, offering insights into the directional properties and uniformity of the reflecting surfaces. Statistical measures like Skewness and Kurtosis provide further description of the waveform's shape, assessing the asymmetry and tailedness which help distinguish material types based on reflective properties. Additionally, Peak Count and Average Inter-Peak Distance gauge the complexity of the waveform, which can be helpful to distinguish natural classes with multiple peaks from artificial ones. In addition, geometric local features were computed in Cloud Compare software. Roughness measures surface texture variation. Mean and Gaussian curvatures help distinguish surface shapes, such as flat, con-vex, and concave structures, useful for identifying man-made versus natural formations. Eigenvalues from principal component analysis yield shape descriptors like omnivariance, eigenentropy, and anisotropy, which indicate linear, planar, or volumetric features. Surface and volume density metrics quantify point distribution. Verticality assesses point alignment relative to the vertical axis, differentiating vertical structures like buildings from the ground plane. Figure 5 shows some derived features distinguishing between different classes. Feature selection strategy in this paper is based on ANOVA F-Score and SVM Coefficients for identifying the most informative features. ANOVA F-Score evaluates the impact of features based on statistical significance across groups, while SVM Coefficients reflect feature importance based on their role in the model's decision boundary.

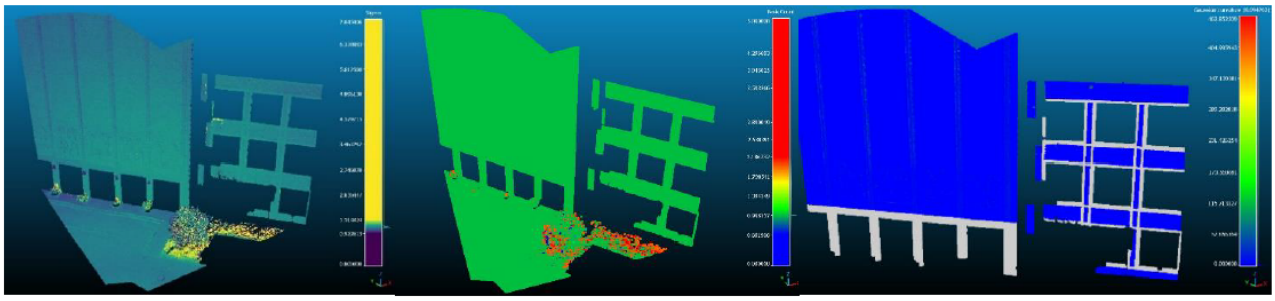

Figure 6: Derived features such as $\sigma$, peak count, and Gaussian curvature.

## 4 Results and Discussion

The model was trained on a dataset consisting of building facades with various materials and tested on a third building facade. Figure 6 illustrates the global feature ranking by averaging their importance across ANOVA F-Score and SVM Coefficient-based Feature Importance methods, with FWF features highlighted in bold. Additionally, a one-vs-one SVM approach with an RBF kernel was implemented to differentiate between natural and artificial classes. Using the FWF features, the recall and F1-score for natural classes increased from 0.75 and 0.86 to 0.86 and 0.92, respectively.

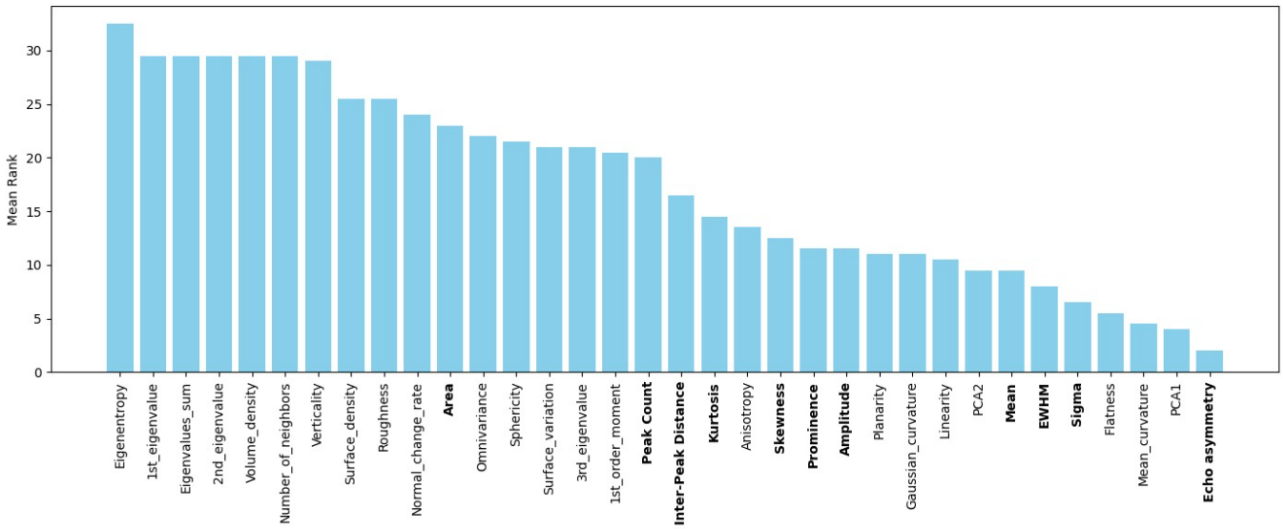


Figure 7: Global ranking using the two techniques. The mean rank is plotted for each feature.

## 5 Conclusion

This paper examined the classification of 3D point clouds in urban areas using terrestrial scanner full-waveform (FWF) data. The goal was to create an objective workflow to evaluate the impact of FWF features on classification. A supervised SVM classifier was used with a 34-component feature vector, including 11 FWF features. It was found that features like area, peak count, and average inter-peak distance are highly discriminative, while echo asymmetry and mean are less so. Future work could involve adding Riegl's proprietary features (reflectance, amplitude, deviation) and features from

radiometric calibration (cross-section, back-scatter coefficient) to improve classification. Additionally, data mining techniques could reduce feature redundancy before selection.

## References

[1] F. Sadeghineko, K. Lawani, and M. Tong, "Practicalities of incorporating 3d laser scanning with bim in live construction projects: A case study", *Buildings*, vol. 14, no. 6, p. 1651, 2024.

[2] A. Chauve, S. Durrieu, F. Bretar, M. Pierrot-Deseilligny, and W. Puech, "Processing full-waveform lidar data to extract forest parameters and digital terrain model: Validation in an alpine coniferous forest", *International Journal of Remote Sensing*, vol. 30, no. 19, pp. 5211–5237, 2009.

[3] C. Mallet, F. Bretar, M. Roux, U. Soergel, and C. Heipke, "Relevance assessment of full-waveform lidar data for urban area classification", *ISPRS Journal of Photogrammetry and Remote Sensing*, vol. 66, no. 6, Supplement, S71–S84, 2011.

[4] J. B. Blair, D. L. Rabine, and M. A. Hofton, "The laser vegetation imaging sensor: A medium-altitude, digitisation-only, airborne laser altimeter for mapping vegetation and topography", *ISPRS Journal of Photogrammetry and Remote Sensing*, vol. 54, pp. 115–122, 1999.

[5] F. Bretar, A. Chauve, C. Mallet, and B. Jutzi, "Managing full waveform lidar data: A challenging task for the forthcoming years", in *ISPRS Congress Proceedings*, ser. Part B1, ISPRS, vol. XXXVII, 2008, pp. 69–74.

[6] G. Zhao, A. Sanchez-Azofeifa, K. Laakso, C. Sun, and L. Fei, "Hyperspectral and full-waveform lidar improve mapping of tropical dry forest's successional stages", *Remote Sensing*, vol. 13, no. 19, p. 3830, 2021.

[7] D. Mader, K. Richter, P. Westfeld, J.-G. Nistad, and H.-G. Maas, "Analysis of the potential of full-waveform stacking techniques applied to coastal airborne lidar bathymetry data of the german wadden sea national park", *International Hydrographic Review*, vol. 29, no. 2, pp. 46–64, 2023.

[8] N. Chehata, L. Guo, and C. Mallet, "Airborne lidar feature selection for urban classification using random forests", in *International Archives of Photogrammetry, Remote Sensing and Spatial Information Sciences*, ser. Part 3/W8, vol. 38, 2009, pp. 207–212.

[9] M. Pashaei, M. J. Starek, C. L. Glennie, and J. Berryhill, "Classification of terrestrial lidar data directly from digitized echo waveforms", *IEEE Transactions on Geoscience and Remote Sensing*, vol. 61, 2023.

[10] M. Wagner, H. Ullrich, S. Ducic, M. Melzer, and N. Studnicka, "Gaussian decomposition and calibration of a novel small-footprint full-waveform digitising airborne laser scanner", *ISPRS Journal of Photogrammetry and Remote Sensing*, 2006.

[11] RIEGL Laser Measurement Systems GmbH, *Data sheet: Vz-400 terrestrial laser scanner*, 2017. [Online]. Available: http://www.riegl.com/uploads/tx_pxriegldownloads/10_DataSheet_VZ-400_2017-06-14.pdf.

# Joint Triple Extraction for Construction Regulatory Documents using Graph Neural Networks

Sherief Ali
Chair of Computing in Engineering, Ruhr-Universität Bochum, Universitätsstrasse 150
Gebäude IC 6-63, 44801 Bochum, Germany
E-Mail: sherief.ali@ruhr-uni-bochum.de

**Abstract:** The construction industry depends on regulatory documents, to guarantee the consistency and applicability of their operations, which is crucial for maintaining standards and protocols. Information extraction is a time-consuming and labor-intensive process, which aims to extract the relevant data from documents for definite operation. Extracting information and assigning it to a particular rule requires understanding the semantics of the sentences, essential for ensuring code compliance. One approach to address this concern is to parse the unstructured text into triples by extracting entities and their relation. This process enables the identification of subjects, objects, and relationships that provide a comprehensive understanding of the sentence. This paper proposes a joint entity and relation extraction model based on a graph neural network. The model is trained on construction regulatory documents sourced from Eurocode for design. The dataset undergoes preprocessing and labeling in the form of triples to assess the model's performance. The results demonstrate that the model can effectively predict the sentence triples. The model's prediction of sentence triples indicates the ability to capture complex semantic relationships within textual data, which can be transformed into a comprehensive knowledge representation.

*Keywords:* Information extraction, Relation extraction, Graph neural networks, Joint entity recognition, Code Compliance

Erschienen in Tagungsband 35. Forum Bauinformatik 2024, Hamburg, Deutschland, DOI: 10.15480/882.13507
© 2024 Das Copyright für diesen Beitrag liegt bei den Autoren. Verwendung erlaubt unter Creative Commons Lizenz Namensnennung 4.0 International.

## 1 Introduction

The Architecture, Engineering, and Construction (AEC) industry is characterized by continually pursuing innovation across various fronts. Among the evolving topics nowadays is code compliance. Regulatory documents play a role, providing the framework within which construction projects operate, from start to end. Traditionally, rules and regulations have been written and interpreted solely by humans. However, this human-centric approach has occasionally led to instances of

incompleteness, where specific conditions were left unaddressed, or contradictions emerged within regulatory frameworks [1]. The process of code compliance needs multiple iterations until all obligations are inspected, which requires a significant amount of money, time, and labor [2]. Significant efforts are being made to interpret the text through various approaches, including Joint Entity and Relation Extraction (JERE), deep learning techniques, and rule-based systems [3]. JERE involves identifying and extracting subject-predicate-object triples from textual data, providing a structured representation of information [4]. This structured representation has served as a foundation for semantic knowledge data representation, enabling a more comprehensive understanding and analysis of the data. Researchers frequently face challenges in accessing adequate construction regulatory documents and comprehensive datasets, encountering difficulties due to the limited availability of documents for thorough analysis and experimentation. Consequently, in some cases, researchers have utilized synthetic data to support their applications, as demonstrated by Bloch et al., by generating a dataset to facilitate the implementation of their methodology [5].

This study presents an approach for transforming unstructured text within construction regulatory documents into subject-relation-object triples. This transformation is achieved through the training of a Graph Neural Network (GNN), leveraging pre-trained BERT (Bidirectional Encode Representations from Transformers) embeddings for node representation. Our study aims to develop a solution for automating code compliance by deeply understanding the semantics of regulatory text. To the best of our knowledge, this study represents the first application of GNNs for the joint entity and relation extraction task on manually labeled construction regulatory documents.

## 2 Related studies

The interpretation of regulatory documents for automatic code compliance can be approached using three main methodologies: rule-based methods, deep learning approach, and JERE [3, 6]. Rule-based methods rely on predefined rules and logic to interpret and enforce compliance, which can be efficient but often lack flexibility and are costly to maintain. However, machine learning approaches utilize algorithms to learn from data, enabling more adaptive and scalable compliance checks. These methodologies help streamline the compliance process and reduce manual intervention [7].

Various initiatives are being undertaken to leverage artificial intelligence in enhancing the interpretation of regulations. For instance, Schönfleder and König [8] have presented a study to extract relevant terms from German regulatory documents utilizing a supervised deep learning transformer model BERT. BERT is a deep learning model designed to understand the context of words in a text by analyzing them in both directions [9]. In their study, the authors [8] have utilized a pre-trained BERT model for transfer learning, thereby eliminating the need for a large dataset. Another approach proposed by Zhong et al. [10], is for automatically extracting construction procedural constraints using a hybrid deep neural network. Their method has integrated bidirectional long short-term memory (Bi-LSTM) and conditional random field (CRF), achieving efficient

recognition of named entities and their relationships. The LSTM, a type of recurrent neural network (RNN), is well-known for its ability to effectively capture long-range dependencies in sequential data, and it has shown effective performance in text-mining tasks [11]. CRF is a statistical modeling method used in machine learning for structured prediction tasks and is popular, particularly in sequence labeling tasks, such as named entity recognition and part-of-speech tagging [12].

Several studies have employed a hybrid approach, combining multiple techniques, to maximize performance in information extraction tasks. Thus, these studies have combined JERE with deep learning, to privilege the performance of both techniques for a comprehensive understanding of natural language. Fu et al. [13] have proposed an end-to-end relation extraction model for joint entity and relation extraction. The GraphRel model leverages graph convolutional networks (GCNs) to jointly extract named entities and their relationships from unstructured text, providing a comprehensive understanding of the text. GCNs are a type of neural network designed to operate on graph-structured data, capable of encoding both graph structure and node features. In GCNs, each node in the graph represents an entity, and the edge between nodes represents relationships [14]. In a parallel endeavor, Zhao et al. [15] have proposed an approach called Representation Iterative Fusion based on Heterogeneous GNNs for Relation Extraction (RIFRE), to extract entities and relations as relational triples. The GNNs are designed to operate directly on graph-structured data, to model and process relationships between entities represented as nodes in a graph [16, 17]. In their study, the authors [15] have leveraged a graph-based representation, considering relations and words as nodes and iteratively fusing semantic information.

# 3 Methodology

In this section, the detailed methodology outlines the steps and processes involved in structuring our model. Additionally, a comprehensive explanation of how the joint entity and relation extraction model is designed. To test this methodology, an experiment is applied in Section **4** to evaluate the results and assess the performance of the approach.

## 3.1 Data preprocessing

Regulatory documents comprise various structures of information, and identifying the informative sentences is crucial for our joint entity and relation extraction model. Data preprocessing begins with identifying the document level of digital standards [18]. The documents need a comprehensive reading to capture the full context and content. The next step involves extracting sentences from the documents, which is crucial for maintaining the coherence and structure necessary for accurate entity and relation detection. Each sentence is then saved in a plain text (.txt) format. The extracted sentences are then cleaned by removing hyphens, as well as checking for proper punctuation, such as full stops, to ensure the text is clear and relevant for analysis.

## 3.2 Triplets tagging

The objective is to label the sentences for utilization in our joint model, aiming to extract triplets based on the subject-relation-object structure. To achieve this, the sentences undergo tagging using Label Studio [19], a tool tailored for efficient data labeling. Multiple relations could be in different sentences, therefore a thorough examination of the data extracted is needed to create a guideline for the relations. Given that multiple relations may exist across different sentences, a thorough examination of the extracted data is essential to establish a guideline for identifying these relations. Furthermore, both the subject and object within a sentence may consist of multiple words, which will be tested to assess the efficiency of our model in accurately determining these complex subject-object relationships.

## 3.3 Vector representation

To utilize the tagged sentences in the model, the data need to be transformed into numerical representations. This involves creating vector representations for each entity and relation involved. In our study, we adopt a two-node representation approach as conducted before [15], the first node represents words, utilizing embeddings from the pre-trained BERT model [20], particularly the token embeddings in the last hidden layer of BERT are utilized as word nodes. The second node represents relations, with pre-defined nodes assigned for each relation.

## 3.4 Joint entity and relation extraction

### 3.4.1 Graph Neural Network (GNN)

GNNs are instrumental in effectively capturing and modeling the complex dependencies between words and their relationships [16, 17]. The GNN operates on a heterogeneous graph where nodes represent both words and relationships, and edges denote the connections between them based on syntactic and semantic dependencies. The process begins with the initialization of node representations, where each word and relation node is assigned an initial embedding based on its features. Similar to the procedure applied in [15], the GNN then updates these node representations through the message-passing mechanism. In this mechanism, each node aggregates information from its neighbors to update its representation. The process enhances the model's ability to extract information and dependencies, enabling it to accurately extract triplets.

### 3.4.2 Joint triple extraction

To extract the information in the form of triplets, the procedure to apply is similar to studies [15, 21], which have the subject tagger and object tagger. The subject tagger detects all possible subjects in the word nodes. Specifically, two binary classifiers are employed to identify the beginning and end positions of the subject within the word nodes. The object tagger is utilized to complete the extraction of triples. This combined extraction method uses enhanced node representations to capture essential contextual and relational information, which is vital for accurate entity and relation extraction.

# 4 Experiment

## 4.1 Data preparation

To conduct our experiment on the proposed methodology, the focus is to experiment on construction regulatory documents because this area needs further studies. Therefore, the selected dataset is the Eurocode for the design [22]. The EN Eurocodes are a series of 10 European Standards, EN 1990 - EN 1999, but for our experiment, the choice is to initially test our methodology on the documents detailed in **Table 1**, to assess their effectiveness and suitability. The Eurocode documents exhibit a diverse text structure, including unstructured text written in normal paragraphs, as well as structured text presented in tables and figures. Our extraction process focuses on both the unstructured and structured text, aiming to effectively capture the relevant information from these different formats.

Table 1: Experimental Dataset

| Standard | Eurocode name |
|---|---|
| **EN 1990** | Basis of structural design |
| **EN 1991** | Actions on structures |
| **EN 1991** | Densities, self-weight, imposed loads for buildings |

To extract the text from the dataset, a comprehensive reading and understanding are conducted to have a clear insight. Consequently, the purpose is to identify and extract informative sentences from the code and gather them into a structured text file. The labeling process, as detailed in Section **3.2** proceeds by identifying the subject, relation, and object. Within our dataset, three distinct relations were extracted. The total number of tagged sentences is 300, encompassing 600 entities. As shown in **Figure 1**, sentences may have subjects or objects comprising multiple words. This aspect is integral to our model testing phase, to evaluate the model's proficiency in accurately extracting triplets.

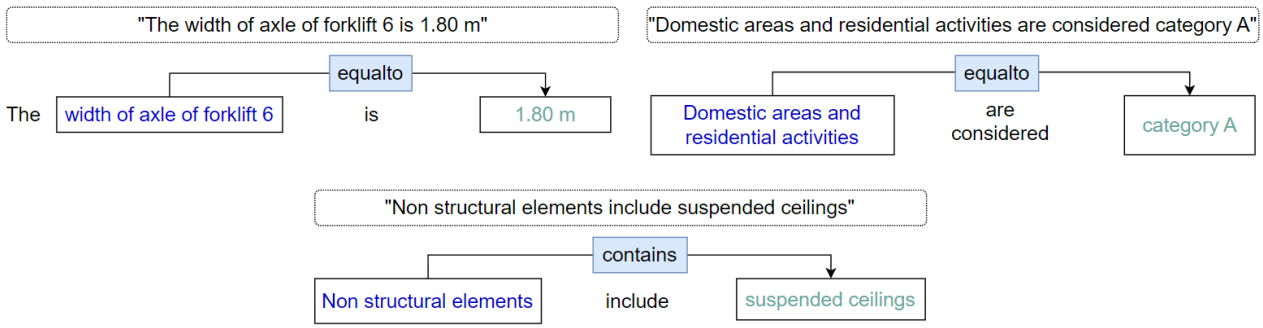


Figure 1: Dataset labeling

## 4.2 Model implementation

The model is trained by implementing the pre-trained BERT model (base-cased) as a foundation and adding the additional layers and components from vector representation, graph layer, and joint extraction on top of the pre-trained transformer. The dataset has been divided into three distinct subsets to optimize model performance: 70% of the data is allocated for training, 20% is reserved for validation, and the remaining 10% is for testing. Various hyperparameters are fine-tuned to optimize the model's performance. A regularizer with a value of 0.01 is added to address instability during training, improving the model's stability. Early stopping is implemented to prevent overfitting and a learning rate scheduler with patience of 10 epochs is used to adjust the learning rate, ultimately stabilizing at 0.1. The SGD optimizer is chosen for training the model, and the batch size is optimized to 16. Given the presence of long sentences with crucial information in our dataset, the maximum number of words in a sentence was set to 120. The model is trained for 60 epochs to ensure thorough learning.

## 4.3 Results and Discussion

Our model's performance is evaluated using precision, recall, and F1-score metrics, which are crucial for assessing the accuracy and robustness of relational triple extraction. The model demonstrates outstanding results as outlined in Table 2, achieving a precision of 86.4%, a recall of 88.2%, and an F1-score of 87.2%. The model results show that it accurately predicts the subject, relation, and object within sentences, correctly identifying the start and end points of both the subject and object and the relation between them. The F1 score varies during training, with the best score achieved at 91.3%. The results of this study cannot be directly benchmarked against several research due to the use of a newly developed dataset. This is a promising outcome, suggesting that our model is well-suited for information extraction tasks in the form of triples. This capability is particularly beneficial for the construction industry, which requires automated extraction of information from regulations to support digitization efforts.

Table 2: Evaluation of the model

| Evaluation metrics | Performance |
|---|---|
| **Precision** | 86.4 |
| **Recall** | 88.2 |
| **F1-Score** | 87.2 |

# 5 Conclusion and future work

The study has presented a model for joint entity and relation extraction utilizing GNN. The proposed model is trained on our own labeled dataset of Eurocode for design, demonstrating its capability to identify and predict sentence triples. Our findings has shown that the model not only predicts sentence triples accurately but also captures complex semantic relationships within the textual data. However, there are limitations to our study, particularly the size of the dataset. Increasing the amount of labeled data for training is essential for enhancing the model's accuracy and robustness. Regarding future work, we plan to label more data to expand the dataset, which we expect will improve the model's performance. Additionally, we aim to represent the extracted triplets in a comprehensive knowledge representation framework. This will further facilitate the transformation of textual information into structured, meaningful knowledge, advancing the utility of our approach in the construction regulatory domain and beyond.

## Acknowledgments

The author expresses his sincere appreciation to the Chair of Computing in Engineering for generously funding this research paper. Their support has played a pivotal role in facilitating the study and contributing to advancements in the field.

## References

[1] C. Eastman, J. Lee, Y. Jeong, and J. Lee, “Automatic rule-based checking of building designs,” Automation in Construction, vol. 18, no. 8, pp. 1011–1033, 2009, doi: 10.1016/j.autcon.2009.07.002.

[2] Borrmann and preidel, “BIM-based Code Compliance Checking,” 2018.

[3] Daniel Jurafsky, James H. Martin, “Speech and Language Processing,” 2023.

[4] Anthony Fader, Stephen Soderland, and Oren Etzioni, “Identifying Relations for Open Information Extraction,” 2011.

[5] Tanya Bloch, Andre Borrmann, Pieter Pauwels, “An alternative approach to Automated Code Checking - Application of Graph Neural Networks trained on synthetic data for an accessibility check case study,” 2023.

[6] S. Fuchs and R. Amor, “Natural Language Processing for Building Code Interpretation: A Systematic Literature Review,” *Proceedings of the 38th International Conference of CIB W78*, 2021.

[7] Nawari, “A Generalized Adaptive Framework (GAF) for Automating Code Compliance Checking,” *Buildings*, vol. 9, no. 4, p. 86, 2019, doi: 10.3390/buildings9040086.

[8] P. Schönfelder and M. König, “Deep Learning-Based Entity Recognition in Construction Regulatory Documents,” *Proceedings 38th International Symposium on Automation and Robotics in Construction (ISARC 2021)*, 2021, doi: 10.22260/ISARC2021/0054.

[9] J. Devlin, M.-W. Chang, K. Lee, and K. Toutanova, “BERT: Pre-training of Deep Bidirectional Transformers for Language Understanding,” 2019, doi: 10.48550/arXiv.1810.04805.

[10] B. Zhong *et al.,* “Deep learning-based extraction of construction procedural constraints from construction regulations,” *Advanced Engineering Informatics*, vol. 43, p. 101003, 2020, doi: 10.1016/j.aei.2019.101003.

[11] J. S. Sepp Hochreiter, “Long Short-Term Memory,” 1997, doi: 10.1162/neco.1997.9.8.1735.

[12] C. Sutton and A. McCallum, “An Introduction to Conditional Random Fields,”

[13] Tsu-Jui Fu, Peng-Hsuan Li, and Wei-Yun Ma, “GraphRel: Modeling Text as Relational Graphs for Joint Entity and Relation Extraction,” 2019, doi: 10.18653/v1/P19-1136.

[14] T. N. Kipf and M. Welling, “Semi-Supervised Classification with Graph Convolutional Networks,” 2017.

[15] K. Zhao, H. Xu, Y. Cheng, X. Li, and K. Gao, “Representation iterative fusion based on heterogeneous graph neural network for joint entity and relation extraction,” *Knowledge-Based Systems*, vol. 219, p. 106888, 2021, doi: 10.1016/j.knosys.2021.106888.

[16] P. Veličković, G. Cucurull, A. Casanova, A. Romero, P. Liò, and Y. Bengio, “Graph Attention Networks,”

[17] V. Garcia and J. Bruna, “Few-Shot Learning with Graph Neural Networks,”

[18] Damian A. Czarny, Gilles Bülow, Michael Noll, Dietmar Lochner, Damian A. Czarny, Jens Gayko, Jui Nahid Pervin, Christian Diedrich, Johannes Diemer, “Scenarios for Digitizing Standardization and Standards,” 2021.

[19] Tkachenko, Maxim, Malyuk, Mikhail, Holmanyuk, Andrey, & Liubimov, Nikolai, “Label Studio: Data labeling software,” 2020. [Online]. Available: https://github.com/heartexlabs/label-studio

[20] J. Devlin, M.-W. Chang, K. Lee, and K. Toutanova, “BERT: Pre-training of Deep Bidirectional Transformers for Language Understanding,”

[21] F. Li, Y. Song, and Y. Shan, “Joint Extraction of Multiple Relations and Entities from Building Code Clauses,” *Applied Sciences*, vol. 10, no. 20, p. 7103, 2020, doi: 10.3390/app10207103.

[22] British Standards Institution, “Eurocode: EN 1990 - EN 1999,”

# Maschinelles Lernen zur Schadenserkennung bei Leichtbaubrücken mit beweglichen Massen

Georgios Dadoulis[1], Thamer Al-Zuriqat[2] und Kosmas Dragos[2]

[1]Laboratory of Experimental Strength of Materials and Structures, Aristotle University of Thessaloniki, Aristotle University Campus, 54124 Thessaloniki, Greece

[2]Institut für Digitales und Autonomes Bauen, Technische Universität Hamburg, Blohmstraße 15, 21079 Hamburg, Deutschland

E-Mail: dadoulis@civil.auth.gr

**Abstract:** Leichtbaubrücken sind Fahrzeugverkehr ausgesetzt, bei dem die Gewichte der Fahrzeuge – insbesondere bei Schwerverkehr – häufig mit dem Eigengewicht der Brücke vergleichbar sind. Diese beweglichen Massen führen zu einem komplexen dynamischen Verhalten, das über herkömmliche Strategien zur Schadenserkennung nur unzureichend analysiert werden kann. Dieser Beitrag beschreibt ein Konzept zur Schadenserkennung bei Leichtbaubrücken unter Verwendung von maschinellem Lernen (ML). Es wird ein ML-Modell zur Klassifizierung von Bauwerksschäden entwickelt, unter Verwendung von Simulationen traniniert und mittels realen Messdaten in einem Laborversuch validiert. Die Validierung zeigt, dass das ML-Modell geeignet ist, Bauwerksschäden an Leichtbaubrücken zu identifizieren, auch unter variierenden dynamischen Bedingungen, die durch die beweglichen Massen verursacht werden.

*Keywords:* Künstliche Intelligenz, Machinelles Lernen, Schadenserkennung, Fahrzeuglasten, Leichtbaubrücken, bewegliche Massen.

Erschienen in Tagungsband 35. Forum Bauinformatik 2024, Hamburg, Deutschland, DOI: 10.15480/882.13527
© 2024 Das Copyright für diesen Beitrag liegt bei den Autoren. Verwendung erlaubt unter Creative Commons Lizenz Namensnennung 4.0 International.

## 1 Einleitung

Die Materialreduzierung beim Brückenbau erfordert besondere Sorgfalt, um unerwartete Schwingungen zu vermeiden, wie sie beispielsweise bei der Eröffnung der Millennium Bridge (London, Großbritannien) im Jahr 2000 auftraten [1]. Brücken müssen den Schwingungen, die durch Betriebslasten wie dem Fahrzeugverkehr verursacht werden, standhalten [2]. Bei Leichtbaubrücken können Gewichte der Fahrzeuge mit dem Eigengewicht vergleichbar sein und werden als „bewegliche Massen“ betrachtet, was zu einem komplexen, nicht-stationären Problem führt, das vom klassischen Problem der „bewegliche Massen“ in der Strukturdynamik abweicht [3]. Herkömmliche Strategien zur Schadenserkennung gehen kaum auf das Problem der beweglichen Massen ein, da experimentelle Techniken sowie Strategien zum Bauwerksmonitoring (engl. Structural Health Monitoring, SHM) in der Regel auf Datenanalysemethoden basieren, die auf stationäre Probleme abgestimmt sind [4]. Auch Studien zu beweglichen Lasten auf Balken erfassen das Problem der Schadenserkennung bei beweglichen Massen nicht.

Die Schadenserkennung an Trägern mit beweglichen Massen wurde bisher nur sporadisch behandelt. In [5] wurden von einem intakten Brückenmodell vor und nach einer Schadensinduktion die Verschiebungen über die Zeit verglichen, in [6] wurden die Reaktionsgrenzen von Euler-Bernoulli-Trägern mit strukturellen Schäden aus theoretischer Sicht abgeschätzt, und in [7] wurden die Wavelet-Transformationskoeffizienten des experimentell abgeleiteten modalen Parameters zur indirekten Schadenserkennung verwendet. Bei den vorgenannten Ansätzen beruht die Schadenserkennung auf Verschiebungen oder auf der Genauigkeit der experimentell abgeleiteten modalen Parametern, was bei instationären Problemen kaum gewährleistet ist. Aus diesem Grund könnte die Schadenserkennung bei Trägern mit beweglichen Massen von einem Ansatz profitieren, der Beschleunigungsdaten verwendet, wie sie beim SHM gesammelt und von modernen Berechnungswerkzeugen verarbeitet werden [8].

Diese Arbeit stellt einen Ansatz zur Schadenserkennung vor, der auf früheren Arbeiten zur Fehlerdiagnose mithilfe maschinellen Lernens (ML) aufbaut [9]. Insbesondere wird ein ML-Modell zur Klassifizierung von Mustern in Beschleunigungsdaten für strukturelle Schadensszenarien entwickelt. Das in dieser Arbeit verwendete ML-Modell ist ein faltendes neuronales Netzwerk (engl. Convolutional Neuronal Network, CNN), das mit simulierten, „markierten“ Beschleunigungsdaten trainiert wird, die vordefinierten strukturellen Zustandsszenarien entsprechen. Nach Abschluss des Trainings wird die Klassifizierung mit realen Beschleunigungsdaten durchgeführt. Der hier vorgeschlagene Ansatz wird in einem Laborversuch validiert, die Fähigkeit des CNNs zur Erkennung von Bauwerksschäden, die durch den teilweisen Verlust der Festigkeit an einer Stütze eines Stahlträgers dargestellt werden, nachweisen. Die nächsten Abschnitte dieses Beitrags erörtern den Ansatze, gefolgt von den Validierungstests. Der Beitrag endet mit einer Zusammenfassung und Schlussfolgerungen sowie einem Ausblick auf zukünftige Forschungsarbeiten.

## 2 Schadenserkennung bei Leichtbaubrücken mit beweglichen Massen

In diesem Abschnitt werden zunächst die Simulationen zur Erstellung von markierten Beschleunigungsdaten erläutert. Anschließend werden das CNN-Modell und der Trainingsprozess vorgestellt, einschließlich der Vorbereitung der Beschleunigungsdaten.

### 2.1 Simulation des Problems der bewegten Masse

Die Bewegungsgleichung einer Leichtbaubrücke mit einer beweglichen Masse, modelliert als kontinuierlicher Euler-Bernoulli-Balken (Abbildung 1), wurde in einer früheren Arbeit der Autoren nachgewiesen [10]:

$$\rho A\ddot{w} + c\dot{w} + EIw'''' = m\left[g - \ddot{w} - 2v\dot{w}' - v^2 r''\right]\delta\left(x - vt\right), \tag{1}$$

wobei $\rho$ die Materialdichte, $A$ die Querschnittsfläche des Balkens, $E$ der Elastizitätsmodul, $I$ das Trägheitsmoment des Balkens in vertikaler Richtung, $c$ der Dämpfungskoeffizient, $w$ die vertikale Verschiebung der neutralen Achse des Balkens, $\delta$ das Dirac-Delta, $x$ die räumliche Koordinate in Längsrichtung des Balkens und $t$ die Zeit ist. Die Geschwindigkeit der bewegten Masse wird mit $v$ und die Oberflächenrauheit mit $r$ bezeichnet. Schließlich gilt $\dot{w} = \partial w/\partial t$, $\ddot{w} = \partial^2 w/\partial t^2$, $w'''' = \partial^4 w/\partial x^4$, $r'' = \partial^2 r/\partial x^2$.

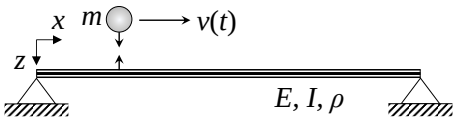


Abbildung 1: Bernoulli-Euler-Balken mit beweglicher Masse

Gleichung (1) wird durch die Modalanalyse $w(x,t) = \varphi_n(x)q_n(t)$ $(n = 1\ldots p)$ gelöst, wobei $\varphi_n(x)$ die $n$-te sinusförmige „Eigenfunktion“ (Wellenfunktion) und $q_n(t)$ die $n$-te „generalisierte“ Koordinatenfunktion ist. Durch Einsetzen von $p$ Modal-Analyse-Komponenten in Gleichung (1) und Ausnutzung der Orthogonalität der Eigenfunktionen und Vormultiplikation von Gleichung (1) mit $\boldsymbol{\varphi}(x)^T$ $(\boldsymbol{\varphi}(x) = [\varphi_1(x),\varphi_2(x),\ldots,\varphi_p(x)])$ wird ein $p\times p$-System von Differentialgleichungen erhalten (ausgedrückt in Matrixform):

$$\begin{aligned}
&\mathbf{M}(t)\ddot{\mathbf{q}}(t)+\mathbf{C}(t)\dot{\mathbf{q}}(t)+\mathbf{K}(t)\mathbf{q}(t)=\mathbf{F}(t)\\
&\mathbf{M}(t)=\mathbf{I}+m\boldsymbol{\varphi}\boldsymbol{\varphi}^T,\ \mathbf{C}(t)=diag(2\xi_n\omega_n)+2mv\boldsymbol{\varphi}\boldsymbol{\varphi}'^T,\ \mathbf{K}(t)=diag(\omega_n^2)+mv^2\boldsymbol{\varphi}\boldsymbol{\varphi}''^T,\\
&\mathbf{F}(t)=mg\boldsymbol{\varphi}-mv^2r''\big(x(t)\big)\boldsymbol{\varphi},\ \xi_n=c/\big(2\rho AL\omega_n\big),\ \ \omega_n=n^2\pi^2/L^2\sqrt{EI/(\rho A)}.
\end{aligned} \tag{2}$$

Gleichung (2), die eine Reihe gewöhnlicher Differentialgleichungen zweiter Ordnung repräsentiert, wird mithilfe der Zustandsraumformulierung in eine Reihe gewöhnlicher Differentialgleichungen erster Ordnung umgewandelt,

$$\dot{\mathbf{y}}(t)=\left[-\mathbf{A}^{-1}(t)\mathbf{B}(t)\right]\mathbf{y}(t)+\mathbf{A}^{-1}(t)\mathbf{h}(t) \tag{3}$$

$$\mathbf{A}(t)=\begin{bmatrix}\mathbf{0} & \mathbf{M}(t)\\ \mathbf{M}(t) & \mathbf{C}(t)\end{bmatrix},\ \mathbf{B}(t)=\begin{bmatrix}-\mathbf{M}(t) & \mathbf{0}\\ \mathbf{0} & \mathbf{K}(t)\end{bmatrix},\ \dot{\mathbf{y}}(t)=\begin{bmatrix}\dot{\mathbf{q}}(t)\\ \mathbf{q}(t)\end{bmatrix},\ \ \mathbf{h}(t)=\begin{bmatrix}\mathbf{0}\\ \mathbf{F}(t)\end{bmatrix}, \tag{4}$$

die für jeden Zeitpunkt $k$ durch eine Eigenwertanalyse der nicht symmetrischen Matrix $(-\mathbf{A}_k)^{-1}\mathbf{B}_k$ gelöst wird, was zu komplexen Eigenwerten $\boldsymbol{\Lambda}_k$ und einer Eigenvektormatrix $\boldsymbol{\Psi}$ führt:

$$\boldsymbol{\Lambda}_k=diag(\boldsymbol{\lambda}_{n,k}),\boldsymbol{\lambda}_{n,k}=\begin{bmatrix}e^{\lambda_{n,k}} & 0\\ 0 & e^{\bar{\lambda}_{n,k}}\end{bmatrix},\ \lambda_{n,k}=\xi_{n,k}\omega_{n,k}\pm i\omega_{n,k}\sqrt{1-\xi_{n,k}^2},\quad \xi_{n,k}\neq\xi_n. \tag{5}$$

$$\mathbf{y}_k=\boldsymbol{\Theta}_k\left(\boldsymbol{\Theta}_{k-1}\right)^{-1}\mathbf{y}_{k-1}+\boldsymbol{\Theta}_k\int_{k-1}^{k}\left(\boldsymbol{\Theta}_s\right)^{-1}\mathbf{A}_k^{-1}\mathbf{h}_k ds,\qquad \boldsymbol{\Theta}_k=\boldsymbol{\Psi}_k\boldsymbol{\Lambda}_k. \tag{6}$$

Die $q(t)$-Funktionen werden zusammen mit den Eigenfunktionen verwendet, um die vertikalen Verschiebungsfunktionen $w(x,t)$ zu rekonstruieren. Die vertikalen Verschiebungsfunktionen werden wiederum verwendet, um die Beschleunigungsdaten („Simulationsdaten“) zu erzeugen, die für das Training des CNN-Modells verarbeitet werden.

## 2.2 Training eines neuronalen Netzwerks zur Erkennung von Schäden

Aufgrund der Nichtstationarität des Problems der beweglichen Massen ist eine Vorbereitung der Daten erforderlich, sodass der gekoppelte Zeit-Frequenz-Inhalt der Simulationsdaten widergegeben wird [11]. Deshalb erfolgt die Vorbereitung der Daten über die Gabor-Transformation [12],

$$G_w(\kappa) = S\left[\sum_{j=1}^{N} \ddot{w}(x,t_j) z_j e^{-i2\pi\kappa j/N}\right]^2, \ \kappa = N \cdot f / f_s \ , \tag{10}$$

wobei $G_w$ der Gabor-Koeffizient ist und $\kappa$ der Index des diskreten Frequenzbereichs der Frequenz $f$, für den eine diskrete Menge von Simulationsdaten der Länge $N$ betrachtet wird, die mit der Frequenz $f_s$ ($f_s = 1/\Delta t$) abgetastet werden. Die Fensterfunktion wird als $z_j$ (z. B. Gauß-Funktion oder Hann-Fenster) bezeichnet, und $S$ ist ein Skalierungsfaktor. Gabor-Koeffizienten werden in der Regel als Farbkarte dargestellt, im Folgenden als Gabor-Transformationsbild bezeichnet.

Nach der Erstellung der Gabor-Transformationsbilder wird das CNN-Modell zur Klassifizierung der Bilder in Schadensszenarien entwickelt. Ein typisches CNN-Layout, das in Abbildung 2 dargestellt ist, besteht aus einer Eingabeschicht (engl. „Input Layer“, IL), einer Abfolge von faltenden Schichten (engl. „Convolution Layers“, CL) und Pooling-Schichten (engl. „Pooling layers“, PL), (mindestens) einer vollständig verbundenen Schicht (engl. „Fully Connected Layer“, FC), einer Ausfallschicht (engl. „Dropout Layer“, DrL) und einer Klassifizierungs- oder Ausgabeschicht (engl. „Output Layer“). Die CL führen „gleitende“ Faltungsoperationen über Bildbereiche mit quadratischen Kernels aus. Das Ergebnis jeder CL ist eine Merkmalskarte, die einer Aktivierungsfunktion zugeführt wird, um die CNN mit einer Nichtlinearität zu versehen, die für die Lösung nicht-trivialer Probleme erforderlich ist. Die Aktivierungen werden an die PL weitergeleitet, die die Aktivierungen über gleitende Fensterberechnungen entweder den Durchschnitts- oder den Maximalwerte verdichtet. Auf die letzte PL folgen mindestens eine FC und eine DrL, die die verdichteten Aktivierungen kombinieren und zufällige Ausschlüsse von Aktivierungen vornehmen, um eine Überanpassung zu verhindern. Die DrList mit der Ausgabeschicht verbunden, die die Klassen enthält.

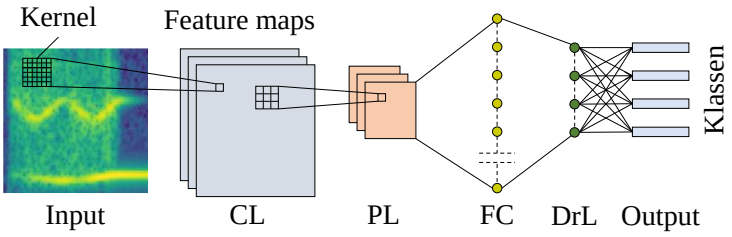


Abbildung 2: Layout einer typischen CNN-Seite

Das Training (d.h. die Feinabstimmung der Kernels) erfolgt mithilfe eines „markierten“ Datensatzes von Gabor-Transformationsbildern, einschließlich Bildern von der intakten Struktur und von Simulationen von Schadensszenarien. Der markierte Datensatz wird zu 70 % in Trainingsdaten, 20 % in Validierungsdaten und 10 % in Testdaten aufgeteilt aufgeteilt. Der Trainingssatz wird in Iterationen durch das CNN geleitet, um den Fehlergradienten an der Ausgabeschicht vorherzusagen, und zurückgeleitet, um die Kerne gemäß einem Optimierungsalgorithmus und einer Lernrate zu aktualisieren. Der Validierungssatz wird nach einer Reihe von Iterationen regelmäßig durch das CNN geleitet, um eine Überanpassung des CNN an den Trainingssatz zu vermeiden. Der Testsatz wird am Ende des Trainings durch das CNN geleitet, um die Leistung des CNN zu überprüfen. Die Validierungstests, einschließlich Simulationen eines Balkens mit einer beweglichen Masse, Datenvorverarbeitung und Training eines CNN-Modells zur Schadensklassifizierung, werden im nächsten Abschnitt vorgestellt.

# 3 Laborversuch zur Validierung

Die Validierung des vorgestellten Ansatzes umfasst einen Laborversuch, die in diesem Abschnitt vorgestellt werden. Zunächst wird der Versuchsaufbau erörtert, gefolgt von den Simulationen zur Erstellung des markierten Datensatzes, dem Training des CNN-Modells, dem Laborversuch und den Ergebnissen.

## 3.1 Versuchsaufbau und Simulationen

Der Laborversuch wird an einem einfach gestützten HEB100-Stahlträger durchgeführt, der ein verkleinertes Modell einer Leichtbaubrücke darstellt, die von einer beweglichen Masse überquert wird (Abbildung 3). Der Querschnitt des Trägers hat die Abmessungen 100×100×10×6 (mm) (Breite × Höhe × Flanschdicke × Stegdicke). Die Gesamtlänge der neutralen Achse des Trägers beträgt 5830 mm. Der Träger ist Teil eines Versuchsaufbaus, der verstellbare Streben umfasst, die sicherstellen, dass der Träger waagerecht ausgerichtet ist. Der Träger wird nur an seinen Enden gestützt, d. h. die mittleren Streben stützen den Träger nicht. Die Versuchsanordnung umfasst Rollen, die es ermöglichen, dass sich Massen entlang der Längsachse des Trägers bewegen können, sowie einen Motor, der die Geschwindigkeit der Massen steuert.

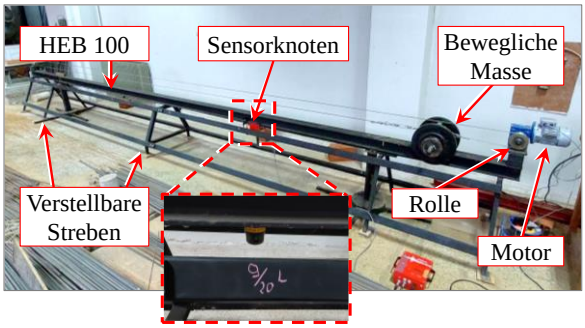


Abbildung 3: Versuchsaufbau

Es wird ein analytisches Modell des Balkens entwickelt und zur Simulation der Bewegung einer sich bewegenden Masse über den Balken verwendet, wobei $E$ und $\rho$ jeweils 198.5 GPa und 7650·kg/m$^3$ betragen, wie aus Vorversuchen geschätzt wurde. Die Masse und die Geschwindigkeit werden im Zufallsverfahren gewählt, um mehrere Simulationsszenarien zu entwickeln, wobei $m$ Werte von 10 kg bis 40 kg und $v$ Werte zwischen 0.2 m/s und 0.5 m/s annehmen. Es werden zwei strukturelle Zustände betrachtet, ein Zustand für den intakten Träger und ein Zustand, bei dem von einem Verlust der Festigkeit an einer Stütze ausgegangen wird, d. h. durch Ersetzen der vertikalen Stütze durch eine Translationsfeder, was einer Erosion des Untergrunds des Fundaments ähnelt, z. B. als Folge von Abnutzung. Für jeden Zustand werden 500 Simulationen durchgeführt, wobei die Beschleunigungsdaten bei $9L/20$ vom Träger mit $f_s$ = 128 Hz berechnet werden. Der Grund, aus dem die Mitte des Balkens vermieden wird, ist, dass die zweite Eigenfunktion, die zur Reaktion beiträgt, durch eine antisymmetrische Sinusform mit einem Nulldurchgangspunkt in der Mitte charakterisiert ist. Für jede Klasse werden 500 Gabor-Transformationsbilder erstellt, die den markierten Satz bilden, der für das Training des CNN-Modells verwendet wird. In Abbildung 4 sind beispielhafte Abbildungen von Gabor-Transformationsbildern für beide Zustände dargestellt, die die Variation der ersten beiden Eigenfrequenzen für beide strukturellen Zustände veranschaulichen. Wie in den Abbildungen zu

sehen ist, verringert der Verlust der Fixierung an der Stütze die Eigenfrequenzen, der Variationstrend ist jedoch in beiden Zuständen ähnlich.

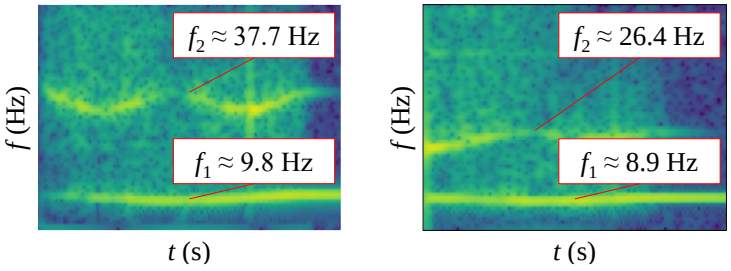


Abbildung 4: Gabor-Transformation für den intakten Balken (links) und für den beschädigten Balken (rechts)

## 3.2 Training des CNN-Modells

Zur prototypischen Implementierung des Ansatzes wird das MATLAB-Tool für maschinelles Lernen eingesetzt und ein einfaches Layout für das CNN-Modell entwickelt, das in Abbildung 5 dargestellt ist. Es ist an die Eingabe von Gabor-Transformationsbildern und die Anzahl der berücksichtigten Klassen angepasst.

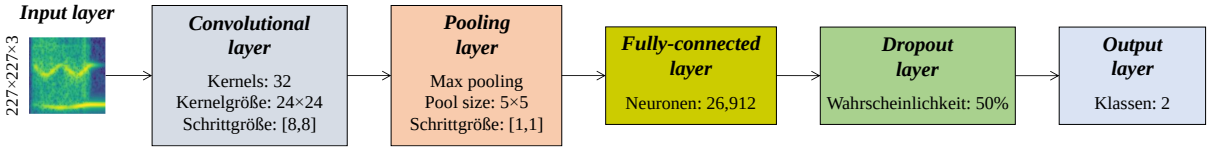


Abbildung 5: Das in dieser Studie definierte CNN-Layout

Während des Trainings wird der „Adam“-Optimierer – ein stochastischer Gradientenabstieg-Optimierungsalgorithmus – für die Feinabstimmung der Kernel in jeder Iteration eingesetzt [13]. Die anfängliche Lernrate wird auf 0,001 festgelegt, die Batch-Größe (Anzahl der Bilder für jede Iteration) beträgt 30 Bilder und die Validierungsfrequenz wird auf alle 30 Iterationen festgelegt. Die Lernrate wird alle 117 Iterationen um den Faktor 0,5 reduziert. Nach 122 Iterationen wird eine hohe Trainingsgenauigkeit von 98 % erreicht. Vor der Anwendung des CNN-Modells mit Beschleunigungsdaten aus dem Versuchsaufbau wird die Klassifizierungsfähigkeit des CNN-Modells anhand des Testdatensatzes überprüft. Der Klassifizierungstest ergab, dass jedes Bild des Testdatensatzes korrekt klassifiziert wurde, was einer Genauigkeit von 100 % entspricht.

## 3.3 Laborversuch

Es werden Beschleunigungsdaten mithilfe eines drahtlosen Lord Microstrain G-Link-200-Sensorknotens erfasst, der Beschleunigungen von bis zu ±8 g in drei Achsen und einer Abtastrate von bis zu 4096 Hz messen kann [14]. Der Laborversuch besteht aus zwei Experimenten, die den in den Simulationen verwendeten Zuständen entsprechen und 30 Kombinationen von Massen- und Geschwindigkeitswerten für jeden Zustand verwenden. Die Massen nehmen Werte von 13 kg, 18 kg, 23 kg, 27 kg und 38 kg an, und die Geschwindigkeitswerte reichen von 0,25 m/s bis 0,5 m/s mit einer Schrittweite von 0,05 m/s. Der Verlust der Festigkeit wird durch das Anbringen einer Feder zwischen dem Trägerende und seiner Stütze realisiert. Die Beschleunigungsdaten werden für jedes Experiment in der Nähe der Mitte des Balkens an einem Punkt erfasst, der sich $9L/20$ vom

Balkenende entfernt befindet, wie in Abbildung 4 dargestellt. Wie in den Simulationen wird eine Abtastfrequenz von 128 Hz wird verwendet. Die Beschleunigungsdaten aus jedem Experiment werden zur Erstellung eines Gabor-Transformationsbildes verwendet, sodass ein Satz von 60 Gabor-Transformationsbildern entsteht, die in das CNN-Modell eingespeist werden. Die Gabor-Transformationsbilder werden dem CNN-Modell zugeführt und in die beiden Klassen eingeteilt, die den betrachteten Zuständen entsprechen. Die Ergebnisse werden in der folgenden Matrix zusammengefasst:

Tabelle 1: Matrix für die Experimente

| | Intakt | Beschädigt |
|---|---|---|
| Intakt | 30 | 0 |
| Beschädigt | 1 | 29 |

Die Ergebnisse zeigen deutlich, dass das CNN-Modell in der Lage ist, reale Beschleunigungsdaten korrekt zu klassifizieren. Von den Gabor-Transformationsbildern des intakten Balkens wird nur ein Experiment als „beschädigt“ falsch klassifiziert, während die entsprechenden Bilder des beschädigten Balkens alle korrekt klassifiziert werden. Darüber hinaus dienen die Ergebnisse als Beweis für die Aussagekraft des vorgeschlagenen Konzepts und für die Übertragbarkeit des CNN-Trainings von Simulationen auf die reale Welt.

## 4 Zusammenfassung und Schlussfolgerungen

In dieser Arbeit wurde ein Ansatz zur Erkennung von Schäden an Leichtbaubrücken vorgestellt, die durch Euler-Bernoulli-Balken repräsentiert werden. Dieser Ansatz basiert auf simulierten Beschleunigungsdaten, mit denen ein CNN trainiert wird, um die Daten in vordefinierte Schadensszenarien einzuordnen. Anschließend wird das CNN mit realen Beschleunigungsdaten angewendet. Der vorgeschlagene Ansatz wurde in einem Laborversuch an einem Stahlträger mit einer beweglichen Masse validiert. Die Ergebnisse haben gezeigt, dass das CNN (1.) mit hoher Genauigkeit anhand von simulierten Beschleunigungsantwortdaten trainiert werden kann und (2.) auf reale Anwendungen übertragen werden kann, sofern das analytische Modell hierfür kalibriert wird. In zukünftigen Arbeiten könnten mehrere Schadensszenarien, die während der Lebensdauer von Leichtbaubrücken auftreten können, untersucht werden und der vorgeschlagene Ansatz zu einem Konzept für SHM weiterentwickelt werden.

## Danksagungen

Die Autoren danken der Deutschen Forschungsgemeinschaft (DFG) für die Unterstützung im Rahmen der Sacheihilfe mit dem Geschäftszeichen SM 281/20-1, für die Unterstützung der Hellenic Foundation for Research and Innovation (HFRI) unter Förderkennzeichen 6255 sowie dem Bundesministerium für Digitales und Verkehr (BMDV) für die Unterstützung im Rahmen der Projekte „IDA-KI“ (Förderkennzeichen 19FS2013B) und „KaSyTwin“ (Förderkennzeichen 19FS2059C) im Rahmen des mFUND-Programms. Die in dieser Arbeit vorgestellten Ergebnisse wurden mithilfe der Hochleistungsrecheninfrastruktur der Aristotle University Thessaloniki im Rahmen der Deutsch-Griechichen Kooperation mit der Technischen Universität Hamburg erzielt. Alle in diesem Beitrag

geäußerten Meinungen, Erkenntnisse, Schlussfolgerungen oder Empfehlungen sind die der Autoren und spiegeln nicht unbedingt die Ansichten der DFG, der HFRI oder des BMDV wider.

## Referenzen

[1] P. Dallard, T. Fitzpatrick, A. Flint, A. Low, R. Ridsdill Smith, M. Willford, and M. Roche, "London Millennium Bridge: Pedestrian-induced lateral vibration", *ASCE Journal of Bridge Engineering*, 6(6), pp. 412-417, 2001.

[2] K. Smarsly and Y. Petryna, "A Decentralized Approach towards Autonomous Fault Detection in Wireless Structural Health Monitoring Systems," in *Proceedings of the 7th European Workshop on Structural Health Monitoring* (*EWSHM*) *2014*, Nantes, France, July 8, 2014.

[3] A. Firus, *A Contribution to Moving Force Identification in Bridge Dynamics*. Wiesbaden, Germany: Springer Vieweg, 2023.

[4] K. Dragos, F. Magalhães, G. D. Manolis, and K. Smarsly, "Frequency-domain synchronization of structural health monitoring data", *Journal of Sound and Vibration*, 571(118017), 2024.

[5] C. Bilello and L. A. Bergman, "Vibration of damaged beams under a moving mass: theory and experimental validation", *Journal of Sound and Vibration*, 274(3-5), pp. 567-582, 2004.

[6] A. Cicirello, "On the response bounds of damaged Euler–Bernoulli beams with switching cracks under moving masses", *International Journal of Solids and Structures*, vol. 172-173, pp. 70-83, 2019.

[7] Y. Zhan, F. T. K. Au, and J. Zhang, "Bridge identification and damage detection using contact point response difference of moving vehicle", *Structural Control Health Monitoring*, 28(12), e2837, 2021.

[8] K. Smarsly, D. Hartmann, and K. H. Law, "Structural Health Monitoring of Wind Turbines Observed by Autonomous Software Components – 2nd Level Monitoring," in *Proceedings of the 14th International Conference on Computing in Civil and Building Engineering*, Moscow, Russia, June 27, 2012.

[9] T. Al-Zuriqat, C. Chillón Geck, K. Dragos, and K. Smarsly, "Adaptive fault diagnosis for simultaneous sensor faults in structural health monitoring systems", *Infrastructures*, 8(3), p. 39, 2023.

[10] G. Dadoulis and G. D. Manolis, "Dynamic response of a damaged bridge model traversed by a heavy point mass", *Journal of Sound and Vibration*, 551(117613), 2023.

[11] H. Fritz, J. Peralta, D. Legatiuk, M. Steiner, K. Dragos, and K. Smarsly, "Fault diagnosis in structural health monitoring systems using signal processing and machine learning techniques", in *Structural Health Monitoring Based on Data Science Techniques*, A. Cury, D. Ribeiro, F. Ubertini, and M. D. Todd, Eds. Cham, Switzerland: Springer, pp. 143-164, 2022.

[12] S. Qian and D. Chen, "Discrete Gabor transform", *IEEE Transactions on Signal Processing*, 41(7), pp. 2429-2438, 1993.

[13] D. P. Kingma and J. Ba, "Adam: A method for stochastic optimization", presented at the *3rd International Conference on Learning Representations*, San Diego, CA, USA, May 7, 2015.

[14] Microstrain Sensing, *Microstrain Sensing Product Datasheet: G-Link-200*. Williston, VT, USA: Parker Hannifin Corp., 2020.

# Using 2D scene graphs as an enabler for DT topology

Nayun Kim*, Atacan Kural Avgoren*, Mohammad Adnan Mohammad Alrabab'h*, Fiona Collins and Changyu Du
*equally contributed to this work
The Chair of Computational Modeling and Simulation, Technical University of Munich, Arcisstraße 21, 80333 Munich, Germany
E-mail(s): ny.kim@tum.de, atacan.avgoren@tum.de, m.alrababh@tum.de, fiona.collins@tum.de, changyu.du@tum.de

**Abstract:** Scan-to-BIM research has gained significant attention, yet many reconstruction methodologies overlook the crucial topological relationships in Building Information Modeling (BIM). To address this challenge, we propose using Scene Graphs to capture contextual relationships in images, focusing on hallways and offices at the Technical University of Munich (TUM). Our approach involves fine-tuning an existing Scene Graph Generation (SGG) model and proposing an in-house model both aiming to predict scene graphs, by integrating object detection and predicate detection methods. The fine-tuned SGG model with the benchmark archived the recall@50 of 95.57 in predicate classification mode. Comparatively, our in-house model attained a recall of 65.12 for the overall scene graph generation. Despite these promising results, some limitations remain, such as low object detection accuracy and the exclusion of non-relationships, as well as the evaluation being limited to qualitative comparisons and was done independently for each method. These limitations highlight areas for future work. Nevertheless, this study offers a proof of concept for integrating scene graph predictions into Scan-to-BIM workflows while identifying areas for further improvement.
*Keywords:* Closed-Vocabulary 2D Scene-Graph, Computer Vision, Rule-Based ML, Transfer Learning, Digital Twin

Erschienen in Tagungsband 35. Forum Bauinformatik 2024, Hamburg, Deutschland, DOI: 10.15480/882.13529
© 2024 Das Copyright für diesen Beitrag liegt bei den Autoren. Verwendung erlaubt unter Creative Commons Lizenz Namensnennung 4.0 International.

## 1 Introduction

In this work, we explore the use of scene graph generation to enhance the Digital Twinning method and Scan-to-BIM process. Current Scan-to-BIM methodologies often overlook crucial topological relationships, leading to incomplete representations of buildings and spaces. This limitation is particularly evident in complex environments like spaces with open areas or void spaces, where spatial definitions rely on more than just physical proximity. Scene graphs can capture intricate semantics by explicitly modeling objects (e.g., doors, windows, walls) and their relationships (e.g., "hang-on",

"above"). By integrating 3D scene graphs into the Scan-to-BIM process, we aim to improve the accuracy of classification and clustering, especially in these sophisticated spatial arrangements. Our main goal is to investigate methods for automatically enriching Scan-to-BIM images with object and relationship semantics. This approach has the potential to significantly enhance the handling of complex spaces and improve the overall accuracy of digital twin creation in the built environment.

## 2 Literature Review

Several studies have explored methods for generating scene graphs from images. Zellers et al. [1] introduced the Stacked Motif Network (MOTIFNET) for scene graph parsing, which captures higher-order dependencies in scene graphs. Tang et al. [2] presented VCTREE, a model that dynamically constructs tree structures to capture visual context in images. Both models were evaluated on general datasets like Visual Genome and showed improvements in scene graph generation. Some research shows the application of relationship-based structures similar to scene graphs in construction and building information modelling. Bueno and Bosché [3] emphasize the importance of understanding relationships between elements in construction projects. They demonstrate how these relationships provide vital semantic and topological context, enabling precise validation and quality control in specific domains like railways. While these studies have advanced scene graph generation, they lack specific focus on building components. Common datasets like COCO and Visual Genome omit crucial building elements such as walls, roofs, and floors, vital objects in building context, leaving a gap in relationship definitions for these objects. Our research addresses this limitation by investigating how existing scene graph models perform in a building context. We aim to evaluate their applicability and performance when dealing with building-specific components and relationships, an area not thoroughly explored in previous studies. This work seeks to contribute to scene graph generation techniques tailored for the built environment, potentially enhancing Scan-to-BIM processes and digital twinning in the building domain.

## 3 Methodology

We employ two approaches for building-related scene graph generation. The first approach involves fine-tuning the Scene Graph Generation with the Visual Genome Benchmark (SGGVG) Model developed by Kaihua Tang et al., which is a PyTorch implementation of their paper [4]. This model was initially trained on a widely adopted Visual Genome (VG) split [5], which contains 108k images with the most frequent 150 object categories and 50 predicate categories. This model builds on a pre-trained, but relatively old versioned, Faster R-CNN model for object detection [6]. The second approach utilizes an in-house model based on a Multi-Layer Perceptron (MLP) and leverages the recent pre-trained weights of the Faster R-CNN model.

### 3.1 Data Preparation

The dataset used in this study is derived from the research by Pan et al. [7], consisting of images from buildings at the Technical University of Munich (TUM). It includes 377 images with 23 object classes, ranging from predominant elements like walls, roofs, and ceiling lights to smaller objects such as light switches and manual call points, all annotated with segmented masks. To provide a

consistent dataset for both methodologies, we converted the segmented masks into bounding boxes (Bbox). We then used a rule-based Python script to automate the annotation of obvious predicates and performed semi-automated manual annotation for the scene graph, including 13 predicate classes. No annotations were made for non-relationships. For the first approach, it was necessary to convert the common dataset into the Visual Genome format. We used the Iterative Message Passing (IMP) [8] toolkit to compress the data into the H5 format, making it compatible with the pre-trained models.

### 3.2 SGG with Fine-tuned Benchmark Model

As illustrated in Figure 1, The SGGVG model builds upon the Mask R-CNN framework [9] by adding a relation head for scene graph generation. By toggling specific components, the model supports three modes of inference: Predicate Classification (PredCls), using only the Relation Head for predicate prediction, Scene Graph Classification (SGCls), using the Box Head and Relation Head for predicates and bounding box prediction, and Scene Graph Detection (SGDet), using all components for all prediction including scene graph.

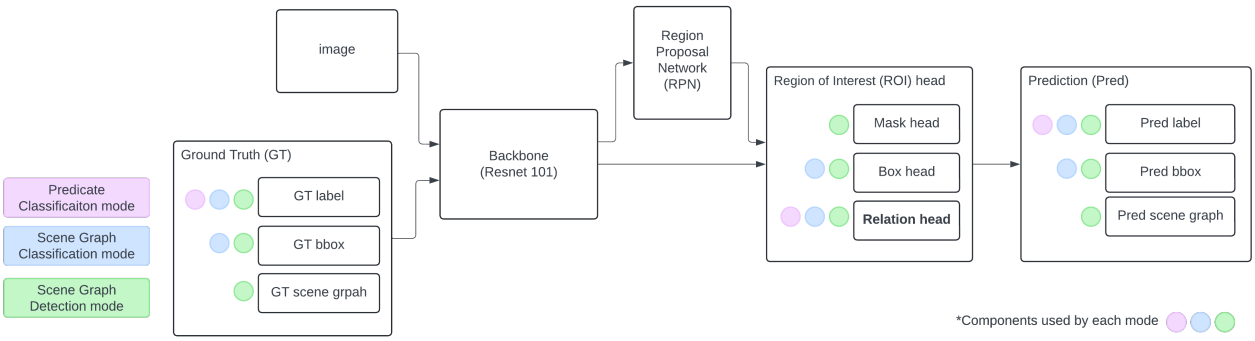


Figure 1: Flow diagram of SGGVG Model

SGGVG model can perform various object detection and predicate detection inferences. For object detection, it can utilize pre-trained weights from Faster R-CNN [6] and Mask R-CNN [9]. For predicate detection, it supports various methods for prediction during inference, including MOTIFS [1], Iterative Message Passing (IMP) [8], VCTree [1], and the Unbiased-Causal-TDE [4] model. The repository [10] offers pre-trained weight of the SGGVG model, trained and evaluated on the Visual Genome benchmark [5], which contains 108k images with the most frequent 150 object categories and 50 predicate categories [4]. The pre-trained object detector utilizes a Faster R-CNN with a ResNeXt-101-FPN backbone, achieving mAP scores of 26.35 and 28.14 on the VG validation and test sets, respectively [10]. The pre-trained SGGVG model is trained in SGDet mode, utilizing all components for scene graph generation. In Predicate Classification (PredCls) mode, which only evaluates the relation head, the model achieves Recall@20, Recall@50, and Recall@100 scores of 59.64, 66.11, and 67.96, on VG dataset respectively. Before fine-tuning, qualitative testing with sample images revealed that the pre-trained model failed to accurately detect primary objects in the building context, leading to irrelevant scene graphs in SGDet mode [7]. Consequently, we decided to fine-tune both the relation head and the Faster R-CNN model using our custom VG dataset.

### 3.3 SGG with In-house Model

In the In-house Model, we followed two main steps: Object Detection and Predicate Detection. In the first step, our model predicts objects in the images along with their labels and bounding box coordinates. In the second step, the predicate detection model predicts the predicates between these detected objects. Performance metrics for each step of this model are discussed in section 4.2.

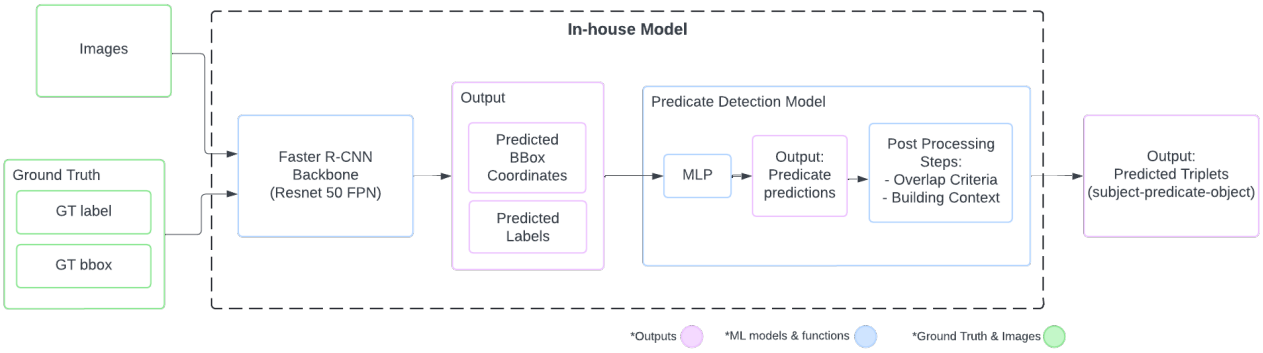


Figure 2: Flow diagram of In-house Model

As first step, we implemented a object detection method to detect objects in images using the Faster R-CNN model with a ResNet-50 backbone. This model effectively captures detailed features and precise object borders on a image. The model was fine-tuned to detect 23 specific classes relevant to our dataset, such as door, window, wall, ceiling and stair. Our Predicate Detection Model identifies predicates between objects in images using their locations and labels. It begins with a Multi-Layer Perceptron (MLP) to predict potential predicates, which are then refined by post-processing filters that eliminate irrelevant predicates and ensure logical spatial topology. The MLP model processes bounding box coordinates and object labels, which are predicted by the Object Detection Model, to detect various predicate types. It uses ReLU activation and dropout to prevent over-fitting, transforming input features into a robust 64-dimensional space, and finally predicts predicates with a softmax function. During training, the MLP model addresses class imbalance by assigning more weight to less frequent classes in the dataset. For instance, our dataset contains numerous instances of lighting but very few of hand-rails. This balancing approach enhances prediction accuracy and prevents overfitting. The process involves feeding data batches, calculating loss, and adjusting model parameters over multiple epochs.

Post-processing consists of two steps: Overlap Criteria and Building Context. The Overlap Criteria filtration calculates the intersection area between bounding boxes of two objects, classifying predicates into high, low, or nearly-none overlap categories. This validation ensures that predicted predicates make logical spatial sense, e.g., "mounted-on" requiring high overlap and "adjacent-to" needing minimal overlap, aligning with typical building and construction arrangements. Building Context filtration ensures the model's predictions are relevant by limiting them to a predefined set of valid subject-predicate-object triplets specific to the building domain. These predefined triplets, representing possible subject-predicate-object combinations, were created from our manual annotations on the

images. These triplets prevent irrelevant predicates and ensure contextual accuracy within the building domain.

# 4 Results

## 4.1 SGG with Fine-tuned Benchmark Model

As illustrated in Figure 1, The SGGVG model builds upon the Mask R-CNN framework [9] by adding a relation head for scene graph generation. By toggling specific components, the model supports three modes of inference: Predicate Classification (PredCls), using only the Relation Head for predicate prediction, Scene Graph Classification (SGCls), using the Box Head and Relation Head for predicates and bounding box prediction, and Scene Graph Detection (SGDet), using all components for all prediction including scene graph.

Table 1: Comparison of Original (left) and Fine-tuned (right) Model performance (Recall@k)

| Mode | R@20 | R@50 | R@100 |
|---|---|---|---|
| PredCls | 59.5 | 66.0 | 67.9 |
| SGCls | 35.8 | 39.1 | 39.9 |
| SGDet | 25.1 | 23.1 | 36.9 |

| Mode | R@20 | R@50 | R@100 |
|---|---|---|---|
| PredCls | 94.24 | 95.57 | 95.57 |
| SGCls | 48.17 | 50.90 | 51.89 |
| SGDet | 8.44 | 8.99 | 9.21 |

In the PredCls mode, we observed a significant improvement of about 35%, achieving an accuracy of over 90%. The SGCls mode also showed an enhancement, with accuracy increasing by approximately 10%. However, in the SGDet mode, the fine-tuned model unexpectedly achieved lower scores than the original model. This underperformance in SGDet mode can be attributed to several factors. The bbox head used for predictions in this mode struggled to detect objects in our dataset. This difficulty originates from the pre-trained Faster R-CNN model's initially low accuracy (around 35%) for object detection. Additionally, there was a mismatch between our building-centric dataset and the Visual Genome dataset used for pre-training, which lacks building-related objects. Furthermore, resizing our images from 2592x1728 to 1028x684 which was configured for training the model before resulted in the loss of small objects such as switches and lighting fixtures.

## 4.2 SGG with In-house Model

The Jaccard index, also known as the Intersection over Union (IoU), was calculated for the object detection component of the project, resulting in a score of 92.12%. This high score indicates a strong overlap between the detected objects and the ground truth, as detailed in the accompanying Table 2.

Table 2: Performance metrics of the Object Detection Model in the In-house Model

| Model | Input | Output | IoU (Jaccard Index) |
|---|---|---|---|
| fine-tuned Faster RCNN | Images | Object bbox coordinates and labels | 92.12 |

For the Predicate Detection Model, two sets of inputs were tested: the first using ground truth bounding boxes and labels, and the second using predicted boxes and labels from the previous Object Detection Model. The use of ground truth bounding boxes and labels resulted in higher accuracy metrics. This may be due to some missing or mislabeled objects in the Object Detection Model.

Table 3: Performance metrics of the Predicate Detection Model in the In-house Model

| Input | Output | Recall | Precision | F1-Score |
|---|---|---|---|---|
| GT BBox and Labels | Triplets (s,v,o) | 71.17 | 38.03 | 49.59 |
| Predicted BBox and Labels | Triplets (s,v,o) | 65.12 | 36 | 46.36 |

## 5 Discussion

Our research compares two scene graph generation methodologies: a fine-tuned benchmark model (SGGVG) and an in-house model. The SGGVG model, pre-trained on a dataset with 75% background pairs as non-relationships [4], predicts and ranks predicates and handles the case of non-relationship. It presents top K final predictions with confidence scores, including possible non-relationships, and is therefore evaluated using Recall@K. Unlike the SGGVG model, our in-house model does not handle non-relationship cases. Instead, it assumes that a relationship exists for all input pairs. It predicts predicates between each object in the images and then applies a confidence level filtration to eliminate those below 50%. Subsequently, it applies two post-processing filters: Building Context and Overlap Criteria. Training the in-house model with non-relationship pairs may enhance its effectiveness and make it more applicable to other datasets. We offer a qualitative comparison to highlight each model's strengths.

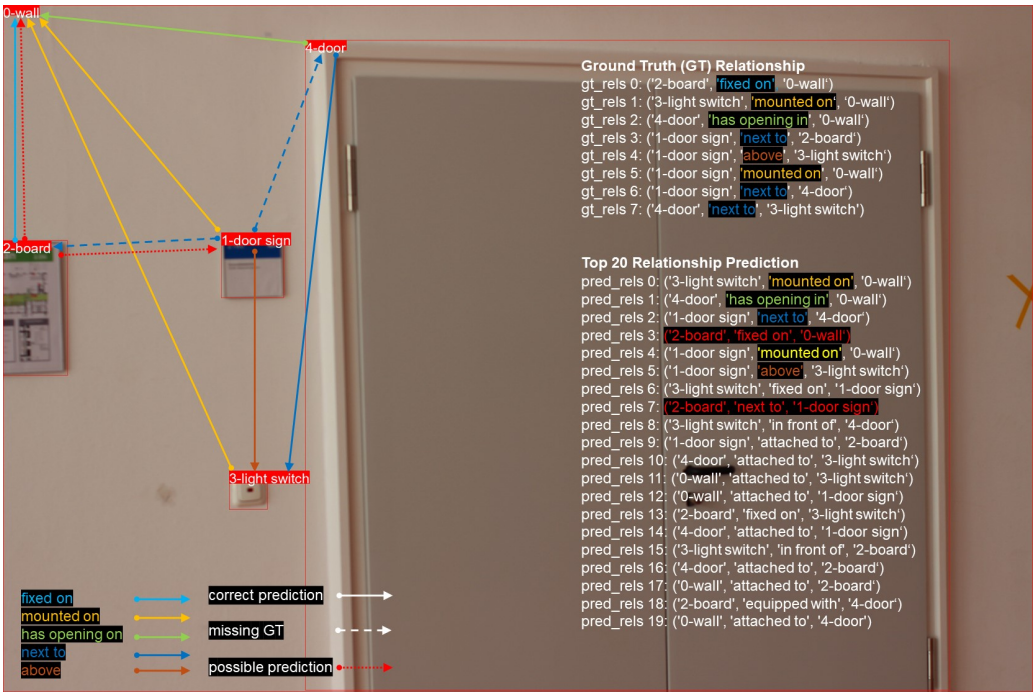


Figure 3: Visualization in predicate prediction from SGG with Fine-tuned Benchmark Model

For qualitative comparison, we visualized the predictions of both models on a sample image. Figure 3 shows the inference results of the fine-tuned SGGVG model in PredCls mode. Out of 8 total predictions, the top 6 match the ground truth, while the model failed to detect 2 'next to' predicates. This is likely due to the 'next-to' class having an accuracy of 85.22%, significantly lower than other classes which exceed 95% accuracy. Moreover, the model's 8th ranked prediction was 'board' 'next-to'

'door sign', which, although not present in the ground truth annotation, is semantically correct. This demonstrates the model's ability to not only predict predicates missing from the ground truth but also to evaluate non-relationships by ranking predictions. Such capability allows for a more comprehensive assessment of the model's performance beyond the limitations of ground truth annotations. Figure 4 shows the inference results of the In-House model. It's predictions cover all ground truth predicates. In addition to these predictions, it has detected four extra predicates which are reasonable.

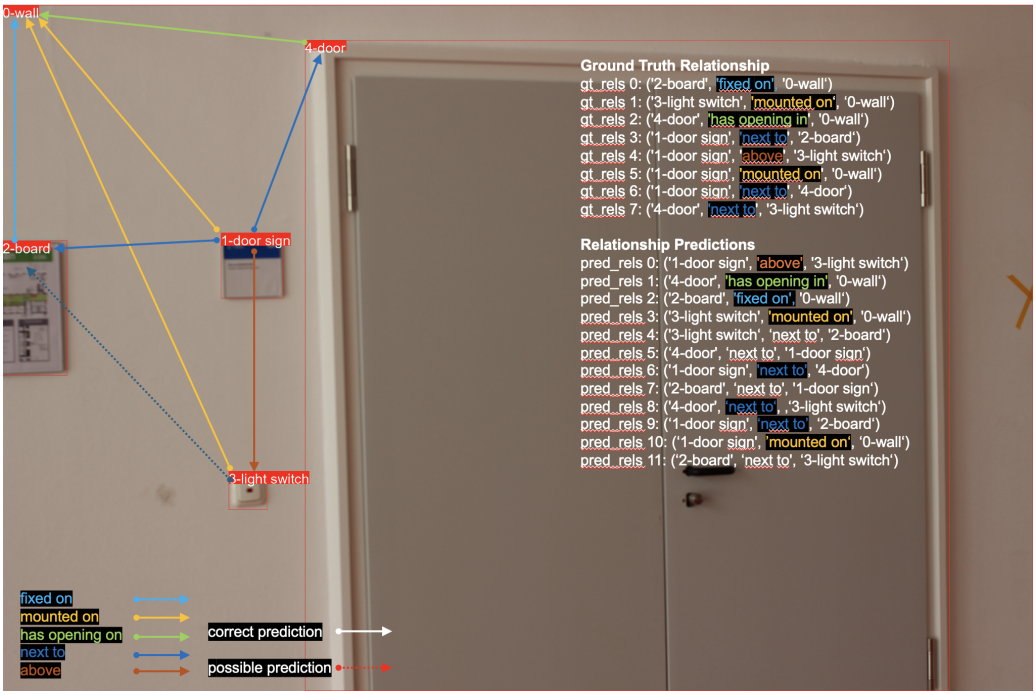


Figure 4: Visualization in predicate prediction from SGG with In-house Model

Future improvements for SGGVG could include updating its object detection model, while our in-house model could be enhanced by adding non-relationship prediction and addressing training bias.

## 6 Conclusion

This study investigated the application of scene graph generation techniques in the built environment domain, revealing both potential and limitations. Our findings highlight that while open-source computer vision models are effective for general object and relationship recognition, they face constraints in specialized domains like the built environment, emphasizing the need for domain-specific training data. We demonstrated methods for applying scene graph generation to built environment applications through fine-tuning a benchmark model and developing a domain-specific model, analyzing the merits of each approach. Our research indicates the potential of scene graph generation to enrich the Scan-to-BIM process with topological information, while also highlighting the need for further investigation into which specific relationships (e.g., "mounted-on", "next-to", "attached-to") are most critical for BIM topology. Future work should focus on developing built environment-specific datasets, improving results with modern object detection models, and integrating these technologies into Scan-to-BIM workflows. In conclusion, this study lays the groundwork for enriching the Scan-to-BIM process with

topology, which is crucial for creating parametric models and enhancing spatial reasoning capabilities. By capturing relationships between building elements, we contribute to the digital transformation of the built environment sector, enabling more sophisticated and context-aware digital building models.

## Author Contributions

Nayun Kim, Atacan Kural Avgoren, and Mohammad Adnan Mohammad Alrabab'h contributed equally. Kim led the "SGG with Fine-tuned Benchmark Model" section, Avgoren the "SGG with in-house model" section, and Alrabab'h the "Data preparation" and "Literature Review" sections. Fiona Collins and Changyu Du supervised the research.

## References

[1] R. Zellers, M. Yatskar, S. Thomson, and Y. Choi, "Neural motifs: Scene graph parsing with global context", *Proceedings of the IEEE Conference on Computer Vision and Pattern Recognition (CVPR)*, 2018. DOI: 10.48550/arXiv.1711.06640. arXiv: 1711.06640 [cs.CV]. [Online]. Available: https://doi.org/10.48550/arXiv.1711.06640.

[2] K. Tang, Y. Niu, J. Huang, J. Shi, and H. Zhang, "Learning to compose dynamic tree structures for visual contexts", *IEEE Transactions on Pattern Analysis and Machine Intelligence*, vol. 42, no. 7, pp. 1801–1814, 2019.

[3] M. Bueno and F. Bosché, "Pre-processing and analysis of building information models for automated geometric quality control", in *Automation in Construction*, vol. 165, 2024. DOI: https://doi.org/10.1016/j.autcon.2024.105557. [Online]. Available: https://www.sciencedirect.com/science/article/pii/S0926580524002930.

[4] K. Tang, Y. Niu, J. Huang, J. Shi, and H. Zhang, "Unbiased scene graph generation from biased training", *IEEE Transactions on Pattern Analysis and Machine Intelligence*, vol. 43, no. 7, pp. 1872–1888, 2020.

[5] R. Krishna, *Visual genome: Connecting language and vision using crowdsourced dense image annotations*, https://paperswithcode.com/dataset/visual-genome, 2017.

[6] S. Ren, K. He, R. Girshick, and J. Sun, "Faster r-cnn: Towards real-time object detection with region proposal networks", 2015.

[7] Y. Pan, A. Braun, I. Brilakis, and A. Borrmann, "Enriching geometric digital twins of buildings with small objects by fusing laser scanning and ai-based image recognition", *Automation in Construction*, vol. 129, p. 103 808, 2022.

[8] D. Xu, Y. Zhu, C. B. Choy, and L. Fei-Fei, "Github - scene-graph-tf-release", 2017.

[9] F. et al., *Github - maskrcnn-benchmark: Fast, modular reference implementation of instance segmentation and object detection algorithms in pytorch*, https://github.com/facebookresearch/maskrcnn-benchmark, 2019.

[10] K. Tang, Y. Niu, J. Huang, J. Shi, and H. Zhang, *Github repository - scene graph benchmark*, https://github.com/KaihuaTang/Scene-Graph-Benchmark.pytorch, 2020.

# Generalising AI model performance for Non Destructive Testing in railway systems

Georg Olm[1]
[1]Department of Civil System Engineering, Technische Universität Berlin
E-mail(s): georg.olm@tu-berlin.de

**Abstract:**

Maintaining railway systems is an essential task during operation of such public infrastructure, but the methods have remained unchanged in Germany for decades. Advancements in ML modeling, Simulation Techniques, and Data Management enable possibilities to accelerate the shift to more efficiently digitized evaluation processes. This research aims to analyze the capabilities of generalization of a previously identified Deep Learning model, trained on real-field ultrasonic data from regular inspection runs, and augmented by simulated defects. As this cannot be done by the usually applied summary statistics, it is necessary to analyze the model performance following the questions of how well the model learns data pattern explicitly, can interpolate between the trained parameters, and whether it did not overfit on specific simulation pattern. This is done by applying selective sampling strategies and an analysis of interesting results. The findings indicate a good fit for explicit patterns with an AUC of 0.964, while interpolation between parameters is successful only in specific use cases. Finally, we conclude that the model likely learns background patterns from simulations and may not necessarily apply simulated defects to real-world scenarios.
*Keywords:* Machine Learning, Railway Maintenance, Sensor Data, NDE

Erschienen in Tagungsband 35. Forum Bauinformatik 2024, Hamburg, Deutschland, DOI: 10.15480/882.13521
© 2024 Das Copyright für diesen Beitrag liegt bei den Autoren. Verwendung erlaubt unter Creative Commons Lizenz Namensnennung 4.0 International.

## 1 Introduction

Deep Learning-enabled AI models provide the potential to perform many tasks efficiently and can enhance the implementation of digitized processes. Rail inspection, essential for maintaining structural integrity and ensuring reliable infrastructure, has seen little change in methodology in recent decades. Evaluators still need to manually examine a lot of data collected on the maintenance train. Ultrasonic testing remains the primary data source for detecting internal rail defects. Evaluators must go through a long training period in order to learn the complex interactions between different signals and to sufficiently distinguish between normal expected indications and actual defects, which require actions. Once trained for the task, assessors can very quickly evaluate a single ultrasonic image for defects. Complex interactions in a large amount of data, which can be examined easily with experience, describe a prime use case for deep learning.

### 1.1 State of research

The field of ultrasonic-based railway maintenance, with its large volume of data requiring manual evaluation, presents significant opportunities for deep learning model applications. The research by Tang, De Donato, Besinović, *et al.* [1] and Chenariyan Nakhaee, Hiemstra, Stoelinga, *et al.* [2] provides an overview of how AI is used in the field of railway maintenance. Both emphasize the possibilities for AI methods in railway maintenance and see a growing number of published research in that field. They also see a lack of sufficient and meaningful data to train models suitable for the real world in the field spanning across most publications. Real defects, in particular, are scarce in general datasets. A common approach to overcome this problem is to generate synthetic data. Uhlig, Alkhasli, Schubert, *et al.* [3] conducted a review study on how synthetic and augmented ultrasonic data are used in multiple domains of NDE. They point out the huge potential of this approach as it enables meaningful training data sizes in the first place, but need to acknowledge that despite increasing interest in the last years its application remains low, compared to overall publications about AI in NDE. Using synthetic data for railway maintenance has not been explicitly researched by them, although it is generally considered part of the NDE field. Nevertheless, respective research has been conducted in the railway domain, but not in a way that reflects the applicability in the real world [4], [5].

This research focuses on utilizing large amounts of real field testing data from actual inspections, which contain all noise and ambiguous signals and allow real-world conclusions to be drawn. In addition, the lack of defect data in the field data will be overcome by introducing simulated defects into the training process. Both solve common gaps in this field of research.

Data collection followed the methods described by Armbruster, Heckel, and Fenger [6] and simulated according to Zhang and Heckel [7]. Neural networks are typically evaluated by looking at aggregate statistics that describe the model performance, e.g. precision, recall, area under the curve (AUC), or true positive and false positive rates (TPR, FPR). Before this research, a suitable model architecture has already been identified by assessing these indicators. The results can be seen in Table 1. It consists of six blocks of bidirectional LSTM layer, with 115 hidden units each including a residual step, which is followed by a multi-head attention layer following typical architecture from the literature [8], [9].

Table 1: Model performance overview of already identified model architecture. This model is used to during the research of this paper.

| AUC | TPR-Defect | FPR-Defect | TPR-Artefact | FPR-Artefact |
|---|---|---|---|---|
| 0.964 | 0.894 | 0.001 | 0.962 | 0.04 |

## 2 Research Method

Although these values look promising, considering proper hyperparameter tuning still offers capabilities for improvement, they need to be evaluated cautiously. Based on these summary metrics, it cannot be fully understood how well the trained patterns, especially through mutually exclusive division of defects and artifacts between simulated and field data, can be applied in the real world. Therefore, it is necessary to explore finer-grained parameters, to examine the model's capability to generalize

between the real world and the simulated pattern. This examination follows questions that are deriving from exploratory principles found in the basic literature [10], [11].

1. How well is the model classifying the learned pattern? – **Learning Explicit**
2. Can the model interpolate on data it has not explicitly been trained on? – **Learning Implicit**
3. Did the model prevent to learn undesired patterns? - **Not Learning**

The first question resembles the traditional deep learning questionnaire the most and can be answered through the summary statistics already assessed in Table 1 and a further confusion matrix in Figure 3.

Simulated defects are described by physical parameters (e.g., length, height, and angle) in greater detail than can be assessed through the evaluation of actual test data. Computational and time constraints prevent simulating all possible parameters. The model can only be trained on a finite set of defects and therefore needs to be able to interpolate between these values. Assessing this performance requires a very specific sampling strategy before training, which enables a statistical comparison of predictions within the sampled parameters and outside of them.

Finally, it is critical to differentiate classes between simulations and field data. It should be assumed that specific patterns are distinct in the simulated data, caused by the simulation process. Based on the currently available data, almost all artifact classes are from the field data and all defect classes are simulated. This differentiation is completely hidden in the summary statistics. Based on these assumptions, it is necessary to check whether the model is actually capable of classifying the defect data in reality or just detecting specific simulations. This must be taken into account in the preparation of the data and the artifact types sampled accordingly.

## 2.1 Data Preparation

Source data consists of 1,144 m of simulated data and 14,656 m of selected field data around indications, both of which will be converted into windowed sequences of size 115 mm with a stride of 10 mm. Depending on the actual question and task, it is necessary to define metrics that can be observed to assess the model's performance for not trained on testing data sets. **Explicit learning** on artifact detection and classification will be measured with ROC-AUC, combined with True Positive Rate (TPR) and False Positive Rate (FPR) for artifacts and defects. These fundamental results can already be seen in Table 1.

Testing for **implicit learning** results demands a more refined sampling strategy. Because the goal is to see out-of-training sample prediction on physical parameters, such as length, height, angle, it makes sense to only sample specific values for training and validation and keep a holdout set for testing. The amount of simulated data is currently still limited and the most variability is in the simulations length parameter. The sampling strategy is depicted in Figure 1. Variations of defects with drillings of lengths 3, 12, and 24 millimeters will be in the training and validation data, whereas lengths 6, 9, 15, 18, and 21 millimeters only occur in the testing dataset.

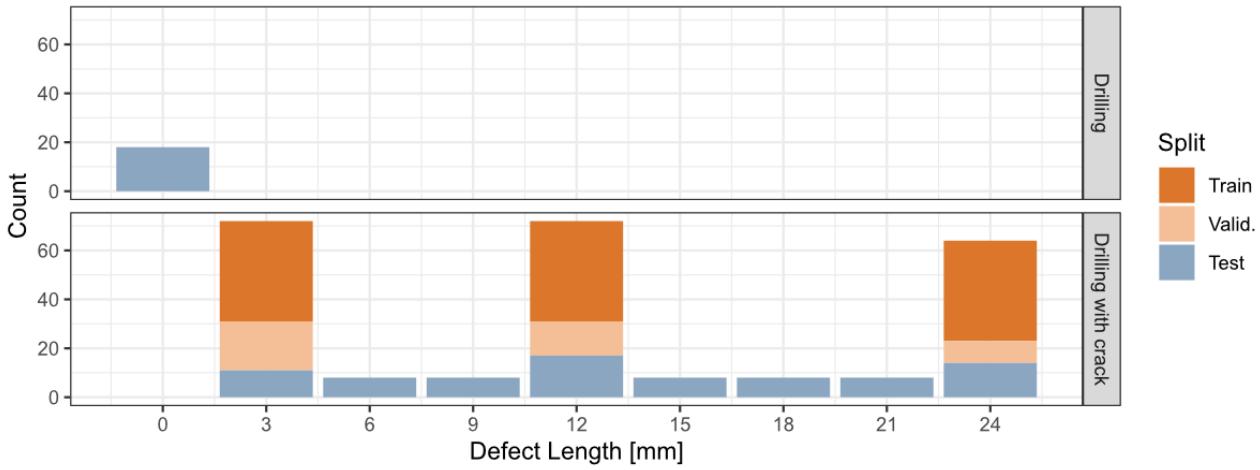


Figure 1: **Simulation Split** between training and testing the model. Data points with parameters used during training are further considered as *In Sampling* data and parameters, which are exclusively in the testing data will be considered as *Out of Sampling* data. This follows the question of the models implicit learning capabilities.

To assess whether the model learned an undesirable pattern, a special holdout simulation of a drilling without a crack has been created, and its sampling can also be seen in Figure 1. This artifact frequently occurs in the field data and its pattern should be well learned by the model. Consequently, misclassifications of simulations should closely align with those observed in field data.

# 3 Data and Results

## 3.1 Model Performance

The performance metrics of the model, based on Table 1 suggest a promising ability to learn the ultrasonic pattern, in general. An AUC of 0.964 confirms this, although a proper trade-off between TPR and FPR needs to be determined by domain experts before a final conclusion is possible. FPR and TPR are of the same categories. The values indicate a practical usability, but a deeper evaluation of why individual classifications happen or fail should be done before an assessment can be concluded. Looking at the FPR for artifacts of 0.04 demands special attention. Due to the very large number of normal rails in the inspection process, 4% false positive can lead to a large number of unnecessary signals for human evaluation. This value needs to be evaluated on a larger sample of measurements to fully assess the impact of defect and artifact detection on the overall performance of the model in detecting and classifying indications.

## 3.2 Parameter prediction

Figure 2 compares the difference in predicting in-sample and out-of-sample length parameters of rail indications, specifically drillings with crack under four different angles 0, 45, 90 and 135 degrees starting from a vertical crack on top of the drilling. Separation by angle is based on the underlying question, whether performance is dependent on the angle of crack expansion. The relative error is the highest for 0º angle, which is justifiable, as a vertical angle is hard to fully capture with the ultrasonic

angle beam probe. It also has a very apparent difference between the in- and out-of-sample values, which is much closer for the remaining categories. The relative error for all estimations seems very high, with typical relative errors leading up to 100% of their actual length.

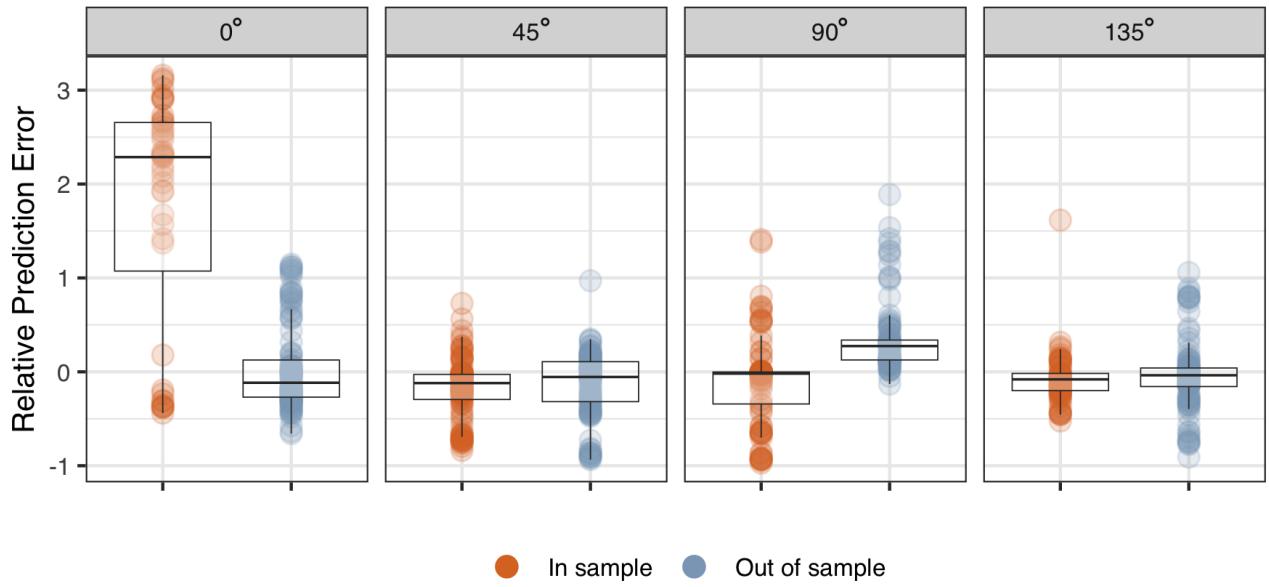


Figure 2: Comparative scatterplot of relative **Prediction Error Comparison**. Data grouping by angle of crack expansion. Color indicates whether the data defect parameter where also in training set or exclusively in test set. Data points augmented by boxplots to increase interpretability.

Table 2 describes the effect of sampling per angle based on Welch's t-test. For the 0º angle group we see the largest effect for out of sample estimation of around -1.701 and very low effects for 45º and 135º. The effects of sampling are very significant for 0º and 90º and not significant 45º and 135º.

Table 2: Influence of sampling strategy on error by angle

| angle | effect term | estimate | conf.low | conf.high | std.error | p.value |
|---|---|---|---|---|---|---|
| 0º | out of sample | -1.701 | -1.974 | -1.428 | 0.138 | 1.34e-24 |
| 45º | out of sample | 0.036 | -0.054 | 0.125 | 0.046 | 0.432 |
| 90º | out of sample | 0.432 | 0.314 | 0.551 | 0.060 | 1.43e-11 |
| 135º | out of sample | 0.041 | -0.060 | 0.141 | 0.051 | 0.426 |

### 3.3 Effect of simulation pattern

Figure 3 provides more details for individual classifications. As can be expected from Table 1, most artifacts are classified correctly. Each failing classification should be closely examined to assess the actual model behavior, but the current research question is about the classification difference between simulations and field data. With regard to drillings with cracks, there is only one misclassification as a drilling. Considering cracks with a length of 3 mm are hardly visible in a data resolution of 3x3 mm, much more of these classifications would have been expected. Regarding the exclusively held out

simulated drillings, all are misclassified as drilling with crack. For simulated head defects, the results are similar. No misclassification of head defects as drillings or welds can be seen. There are only missed head defects. This can be expected because some head defects are simulated in a very close proximity to the UT entry shadow and are prone to be missed.

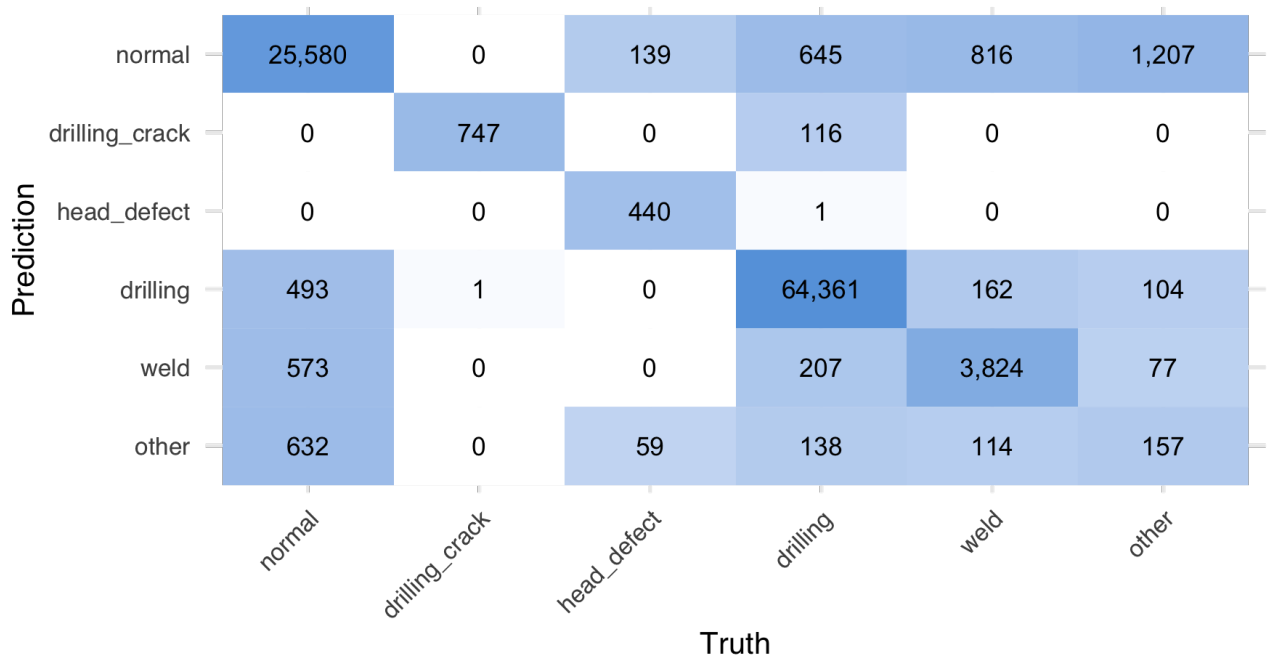


Figure 3: **Confusion Matrix** of all classified sequences in the validation set. Color scale is pseudo log transformed.

## 4 Discussion

The principal performance metrics appear to be good, but require more attention in the details. Besides a general drive to improve the results, it is necessary to perform closer examinations of failed classifications. It might not necessarily be the model that causes the problem, but the data which have certain properties that remained undefined. These can be indications that could not be properly labeled in the preparation phase or even new indications that were not considered even to be a problem. For example, certain noise levels can cause problems for the model and make the data unusable for defect detection. This realization might flow back into the inspection process, which could be adjusted to create cleaner data that are easier to classify.

The interpolation of the defect size for values that were specifically excluded in the training process shows mixed results. There are no significant differences in the predictions for 45 and 135 degree angles. The difference is significant for 90 degree and very large, as well as significant for 0 degree angle defects. In general, the error range is large, with error between -100% and 100% relative to the original size. The values have been normalized to generate a meaningful statistic with regard to difference between sampled and non-sampled values. Conclusions about the general quality of predictions cannot be drawn on the basis of these results. Different measures are necessary to do that, for example, the mean absolute error, which needs to be discussed in future research. From

these results, it is only possible to conclude that interpolation between learned defect sizes works for specific angles. A more thorough examination for predictions of 0º angle is necessary to understand how the models behave for this edge case.

Based on the confusion matrix in Figure 3, it must be assumed that the model learns to differentiate between the simulated and the real field data very well. Thereby a prioritization of data type over actual class is visible through the classification of simulated drillings as drillings with cracks and the lack of expected misclassifications for very small defects. In order to omit the theory that the model can generalize from simulation onto field defects, an explicit test for that case is needed but could not be completed due to a lack of data. Therefore, it is not possible to draw a final conclusion about this. There are examples in the literature where simulations can be generalized onto real data, such as Pyle, Bevan, Hughes, *et al.* [12], but the current data cannot reject doubts and even provides further evidence to assume that the model does not learn to classify real field data based on simulations.

However, interpretation of the results should be cautious and subject to certain limitations. In order to assess the models FPR a larger scale of normal rail data is needed and should be done with a special additional testing dataset to account for the overwhelming size of normal rail in reality. The data size for simulated defects is still relatively small. The work on further simulation continues and will be evaluated in further studies. In addition to creating more balance between field and simulation, equalizing different size parameter of defects will be key to this work. This research points out the possibility of failing generalization between simulations and real field data but cannot provide solutions to solve it. This needs to be done in future research, as possible approaches are still available for exploration. One solution can be a further assessment of the differences between simulations and field data. Knowledge about this can lead to an improved way to simulate defects and prevent deviating data pattern at the source. Another way of solving the problem might be an adjusted training method. Currently, training occurs naively with a combined set of simulations and field data. Training the model with a dedicated data set at different levels can yield more general results. Therefore, an approach of transfer learning should be implemented which first trains the model weights for field data and fine-tunes specific layers with simulated data afterwards.

## 5 Conclusion

This research provides valuable insights into the questions of how a deep learning model can generalize from trained data to new data. First, the model is capable of learning the pattern of defects and artifacts from ultrasonic testing data from the field and from simulations. Although further optimization and parameter tuning will be necessary to provide optimal value for the real world. Second, interpolating on different out-of-sample defect lengths works for specific angles of expansion and fails for difficult edge cases. For future research, it must be assessed whether the error in predicting the actual defect length is in an acceptable range to be applied in a productive system. Third, by observing the different classification of simulation and field data, it seems very likely that the model learned characteristic patterns, which are distinct from simulation and differentiate them from the actual field data. It is not clear whether this prevents a classification of real field defects, as this could not have been tested for now. However, a consequent assumption needs to be that the model did not learn to classify the

simulated pattern in the real field. Further work needs to specifically address this problem and how it might be solved by adjusting the training process or the simulations themselves.

## 6 Acknowledgements

This research is part of the project AIFRI, which is funded by the German Federal Ministry of Digital and Transport as part of the mFUND innovation initiative with a total of € 2.416 million.

## References

[1] R. Tang, L. De Donato, N. Besinović, *et al.*, “A literature review of artificial intelligence applications in railway systems”, *Transportation Research Part C: Emerging Technologies*, vol. 140, p. 103 679, 2022.

[2] M. Chenariyan Nakhaee, D. Hiemstra, M. Stoelinga, and M. van Noort, “The recent applications of machine learning in rail track maintenance: A survey”, in *Reliability, Safety, and Security of Railway Systems. Modelling, Analysis, Verification, and Certification: Third International Conference, RSSRail 2019, Lille, France*, Springer, 2019, pp. 91–105.

[3] S. Uhlig, I. Alkhasli, F. Schubert, C. Tschöpe, and M. Wolff, “A review of synthetic and augmented training data for machine learning in ultrasonic non-destructive evaluation”, *Ultrasonics*, vol. 134, p. 107 041, 2023.

[4] J. M. Ha, H. M. Seung, and W. Choi, “Autoencoder-based detection of near-surface defects in ultrasonic testing”, *Ultrasonics*, vol. 119, p. 106 637, 2022.

[5] H. Mahajan and S. Banerjee, “A machine learning framework for guided wave-based damage detection of rail head using surface-bonded piezo-electric wafer transducers”, *Machine Learning with Applications*, vol. 7, p. 100 216, 2022.

[6] R. Armbruster, T. Heckel, and S. Fenger, “Die gläserne schiene-fortgeschrittene ultraschallschienenprüfung”, *ZfP-Zeitung*, vol. 121, pp. 65–68, 2010.

[7] T. Zhang and T. Heckel, “Virtuelle referenzschienen nach din en 16729-1 für die ultraschallprüfung von verlegten eisenbahnschienen”, 2023.

[8] F. Karim, S. Majumdar, H. Darabi, and S. Harford, “Multivariate lstm-fcns for time series classification”, *Neural Networks*, vol. 116, pp. 237–245, 2019.

[9] B. Sirisha, S. Naveena, G. Palanki, and P. Snehaa, “Multivariate time series sensor feature forecasting using deep bidirectional lstm”, *Procedia Computer Science*, 2023.

[10] F. Chollet, *Deep learning with Python*. Simon and Schuster, 2021.

[11] I. J. Goodfellow, Y. Bengio, and A. Courville, *Deep Learning*. MIT Press, 2016.

[12] R. J. Pyle, R. L. Bevan, R. R. Hughes, R. K. Rachev, A. Ait Si Ali, and P. D. Wilcox, “Deep learning for ultrasonic crack characterization in nde”, *IEEE Transactions on Ultrasonics, Ferroelectrics, and Frequency Control*, 2020.

# Enhancing Machining Feature Recognition in CAD Models through Transfer Learning on BRepNet

Konstantinos Gkrispanis[1]
[1]Chair of Computational Modeling and Simulation, Technical University of Munich, Arcisstraße 21, 80333 Munich, Germany
E-mail(s): konstantinos.gkrispanis@tum.de

**Abstract:** Industrial products are initially designed using Computer-Aided Design (CAD) systems, which employ Boundary Representation (B-Rep) models for precision and efficiency. During the manufacturing process it is important to identify machining features in CAD models, as this enhances the ability to analyze, process and manufacture them. This study proposes a deep learning approach that employs transfer learning to enhance the identification and segmentation of these features. BRepNet [1], a novel neural network designed to operate directly on B-Reps, is adapted by integrating pre-trained weights and adding a modified segmentation head to refine feature identification. By freezing the backbone network and training only the segmentation head, the approach minimizes computational demands and accelerates training times. This makes deep learning more feasible for real-world applications requiring rapid deployment and high accuracy. Tested on the MFCAD dataset, the proposed architecture achieves near state-of-the-art accuracy, with 0.998 accuracy in feature identification for the version with the freezed backbone and 0.999 for the fully fine-tuned version. The study highlights the effectiveness of transfer learning in achieving high accuracy with fewer resources, demonstrating the potential for more efficient and robust CAD model analysis.
*Keywords:* Geometric Deep Learning, CAD learning, B-Rep, CAD segmentation, Machining features

Erschienen in Tagungsband 35. Forum Bauinformatik 2024, Hamburg, Deutschland, DOI: 10.15480/882.13539
© 2024 Das Copyright für diesen Beitrag liegt bei den Autoren. Verwendung erlaubt unter Creative Commons Lizenz Namensnennung 4.0 International.

## 1 Introduction

Computer-Aided Design (CAD) is an important tool in a wide variety of industries, especially in construction. Its ability to allow precise control and modification of highly intricate designs has transformed the creative processes. Almost any physical object that exists in the world was initially designed by means of CAD. Recent advancements in AI are set to revolutionize this field by automating many aspects of the design process. AI algorithms can analyze, interpret and even generate CAD models. However, there advancements bring challenges; traditional deep learning approaches for machining feature recognition are computationally expensive, often requiring extensive training time and significant computational resources.

This study leverages transfer learning to adapt existing deep learning models more efficiently. By modifying and freezing parts of the network, this approach significantly accelerates training times.

Various data formats are used to represent CAD models. The most common are: Boundary Representation (B-Rep), Point Clouds and Meshes. In this work, B-Rep will be utilized as it provides a precise and mathematically accurate representation of 3D objects.

Boundary Representation (B-Rep) is a method for representing a 3D shape by defining the limits of its volume. This approach describes a three dimensional volume through its limiting surfaces and as a result, it provides precise control over the object's geometry. It is a fundamental data format for CAD models, encoding a high level of parametric details. This data format allows for a detailed understanding of the complexities in CAD models. A solid is represented as a collection of connected surface elements, which define the boundary between interior and exterior points. Usually, a Vertex-edge-face graph is part of the B-Rep data structures. This graph offers a clear and organized way to represent the relationships between vertices, edges and faces.

A commonly used data structure in B-Rep to efficiently manage and navigate these relationships is the Winged-Edge. This data structure enhances the representation by storing the edges that connect vertices and edges that bound faces. It also provides direct access to neighboring elements, which is particularly useful for operations such as edge flipping, mesh refinement and geometry editing. The Winged-Edge structure is a powerful tool for handling complex geometric data as it supports complex topological queries and modifications. In Figure 1, Winged-Edge walk is illustrated.

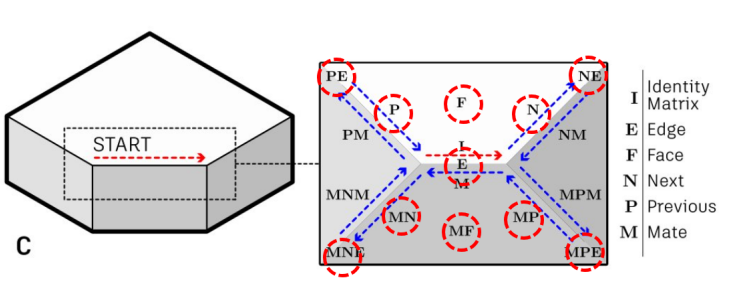


Figure 1: Winged Edge

The main contributions of this work are:

- First application of BRepNet on the MFCAD dataset, which is specifically designed for machining feature recognition.
- Significant reduction in the number of trainable parameters of the deep learning model. This reduction not only enables faster training times but also maintains high accuracy, demonstrating the effectiveness of this approach.

## 2 Background

Numerous models have been evaluated on the MFCAD dataset, each demonstrating notable performance. UV-NET [2], is a novel neural network architecture designed to operate directly on B-Rep

data. UV-Net represents 3D CAD models by exploiting the U and V parameter domains of curves and surfaces. PointNet++ [3], is a hierarchical neural network built upon the original PointNet [4] that captures local structures in point clouds by leveraging metric space distances. Another neural network designed to learn on point clouds is DGCNN [5]. The primary goal is to leverage local geometric structure while maintaining permutation invariance, which is crucial for point cloud processing tasks such as segmentation.

Table 1: Segmentation accuracy per face and number of parameters for MFCAD dataset.

| **Network** | **Accuracy per face (%)** | **Number of parameters** |
|---|---|---|
| UV-Net [2] | **99.95** | 1.23M |
| PointNet++ [3] | 91.35 | 1.42M |
| DGCNN [5] | 90.99 | 0.53M |
| MeshCNN [6] | 99.89 | 2.29M |
| Cao et al [7] | **99.95** | 0.53M |
| Hierarchical CADNet (Adj) [7] | 98.24 | 4.49M |
| Hierarchical CADNet (Edge) [7] | 99.90 | 6.60M |

MeshCNN [6], is a convolutional neural network designed for analyzing triangular meshes. It applies convolution operations on mesh edges, treating them as the basic building blocks, similar to pixels in an image. In [7], efficient representations of 3D CAD models were developed and used with graph neural networks for the recognition of machining features. Hierarchical CADNet [7] encodes information about the surface geometry and face topology of CAD models. A hierarchical graph is used to represent both the B-Rep face adjacency and the facets of a triangular mesh, capturing both the topology and geometry of the CAD model.

However, as illustrated in Table 1, the majority of these models possess a significantly high number of parameters, which can lead to increased computational complexity, resource consumption and longer training times. Moreover, many of these models require the conversion of the original STEP files into alternative data formats such as meshes or point clouds. This process is time consuming and also adds an additional layer of complexity to the workflow. Such transformation requirements can hinder the efficiency of the model deployment and utilization in practical applications.

# 3 Methodology

To tackle the challenges outlined in Section 2, a modified BRepNet architecture that significantly reduces the number of trainable parameters is introduced. This optimization is accomplished by utilizing transfer learning, where pre-trained weights from the 360Fusion dataset are loaded into BRepNet. By freezing the backbone network's weights, the training process is concentrated on an improved segmentation head, streamlining the learning process and boosting efficiency.

## 3.1 Dataset

MFCAD is a segmentation dataset consisting of 15,488 CAD models with labeled machining features. It was developed to enhance the automation of generating and segmenting 3D CAD models, making it a valuable tool for advancing machine learning applications in manufacturing and design [8]. In

a comparative study, both graph-based and voxel-based deep learning algorithms were tested for their ability to segment CAD models. The experiments highlighted that graph-based approaches were particularly effective in identifying and recognizing complex machining features, outperforming voxel-based methods in both accuracy and efficiency. The labeled models within the MFCAD dataset provide a rich basis for further research and development in feature recognition and segmentation, with examples of these annotated models presented in Figure 2. This dataset serves as a benchmark for evaluating advanced geometric deep learning techniques applied to CAD model analysis.

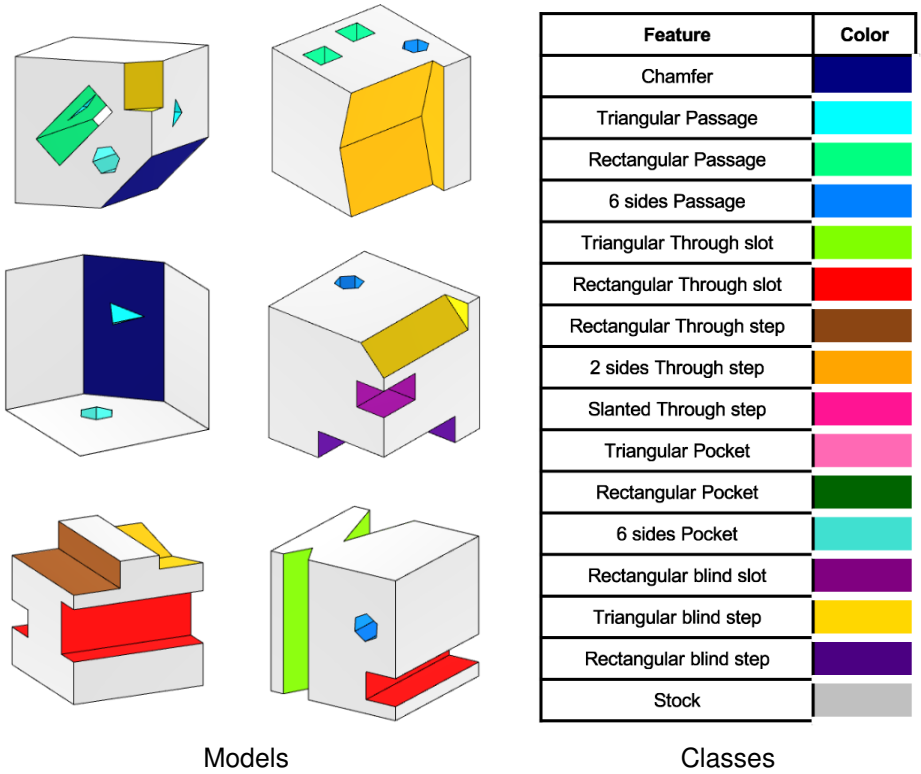


Figure 2: Models from MFCAD dataset and the color annotation for the classes.

### 3.2 BRepNet

As already discussed, the model used in this paper is the BRepNet [1]. BRepNet is another novel neural network with major contribution on this field. It is specifically designed to operate directly on B-Rep data structures. The main goal of this model is to enhance the segmentation of B-Rep models in CAD applications. BRepNet defines convolutional kernels with respect to oriented edges in the B-Rep data structures. It identifies a small collection of faces, edges and coedges in the neighborhood of each coedge, using specific learnable parameters to detect patterns in these feature vectors. The model introduces topological walks to navigate through the data structure, utilizing matrices representing next, previous and mating adjacency relationships. Kernels can have different configurations. These configurations, determine how the network captures and processes the geometric and topological information from the B-rep structure. Each kernel configuration defines a unique set of topological walks that traverse the model, aggregating information from neighboring faces, edges and coedges. From

experiments in [1], it was shown that the best balance of segmentation accuracy and computational efficiency was provided by *winged edge* kernel. In [1], a dataset of CAD models with 8 machining features, named 360FusionDataset, was also presented. BRepNet's architecture is shown in Figure 3.

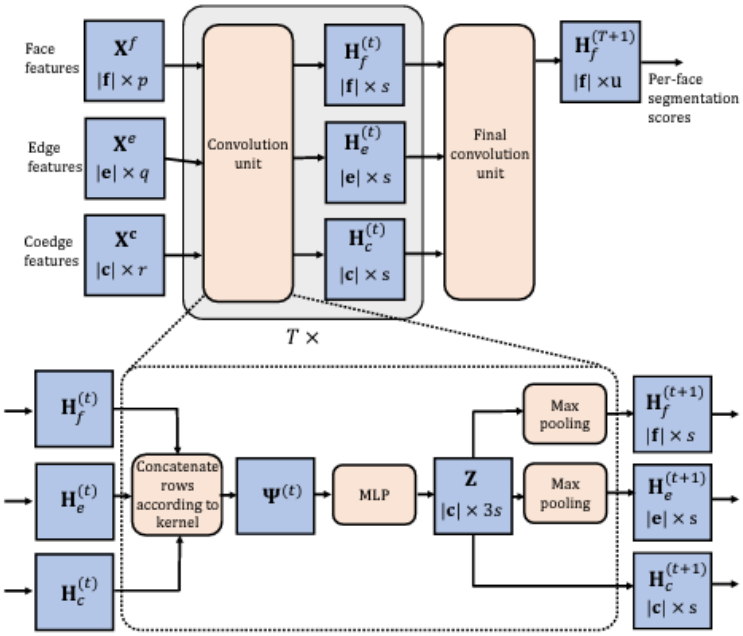


Figure 3: Original BRepNet architecture [1].

Geometric features are extracted from faces, edges and coedges, including surface types, edge geometry, edge convexity and additional flags indicating properties like edge closure and coedge direction. BRepNet achieves higher accuracy and IoU for segmentation tasks compared to methods using meshes and point clouds.

### 3.3 Modified Architecture & Experimental Setup

The core of the methodology lies in the modified BRepNet architecture. The original BRepNet was used as a backbone network for feature extraction, while the final convolutional unit (see Figure 3) was replaced with a custom segmentation head. This new segmentation head utilizes 1D convolutional layers, which are capable at capturing information from neighboring entities. In Figure 4, the modified architecture is plotted. To further enhance the model's performance and prevent overfitting, dropout layers were included in the segmentation head.

In order to leverage the principles of transfer learning, pre-trained weights from the 360Fusion dataset were loaded into the backbone network. These weights were frozen, ensuring that their values remained unchanged during the training phase. Only the segmentation head was subjected to training. While the original BRepNet has approximately 1.8 million parameters, the segmentation head has only approximately $142k$ parameters. By allowing only the segmentation head to be trainable, the model significantly reduces its computational requirements, enabling it to be trained on devices with limited computational resources. This technique minimizes the risk of overfitting and also speeds up the training process due to the reduced number of trainable parameters.

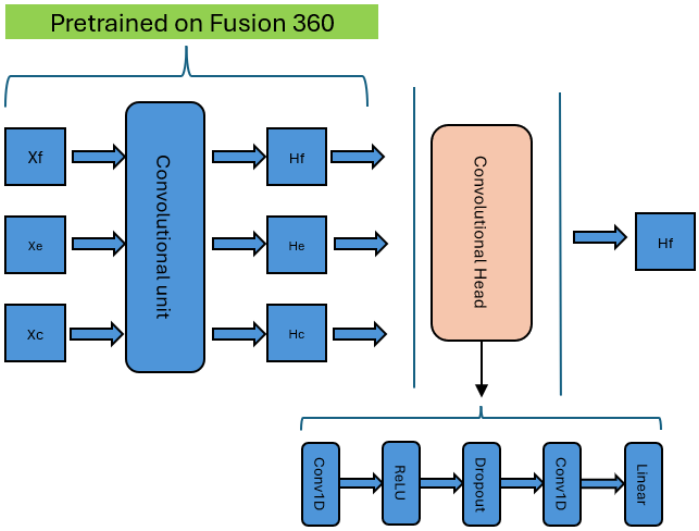


Figure 4: Modified architecture

The experiments conducted are listed below:

- Training the original BRepNet from scratch to recognize MFCAD classes.
- Fine-tuning the pre-trained BRepNet from the 360Fusion dataset on MFCAD classes.
- Using a modified architecture with pre-trained weights from BRepNet, fine-tuning only the segmentation head.

For all experiments, the learning rate was set to 0.001 and the batch size to 64. The data was split following the original paper's methodology: 60% for training, 20% for validation, and 20% for testing.

## 4 Results

This section presents the performance of the modified BRepNet architecture in comparison with other state-of-the-art models, as shown in Table 2.

The advantages of the proposed pipeline are clearly demonstrated. The results indicate that with significantly fewer trainable parameters, the BRepNet can achieve performance levels close to the top performing state-of-the-art models. This highlights the critical trade-off between model performance and computational efficiency.

Additionally, the benefits of transfer learning are underscored by these results. By leveraging pre-trained weights from 360Fusion dataset, the BRepNet results in faster training times and reduced computational load. The robustness and the efficiency of the proposed modification is showcased here, as this approach accelerates the training process and enables the model to generalize well.

The results in Table 3, present the performance of the three models implemented in this paper, in terms of Intersection over Union across all machining features of MFCAD dataset. It is evident that both the fine-tuned and modified versions of BRepNet achieve consistently high IoU values, often approaching or equal to 1.0. This demonstrates their robustness in accurately identifying MFCAD's classes. The

Table 2: Trainable parameters and accuracy of different models

| Model | Trainable parameters | Accuracy |
|---|---|---|
| **Finetuned BRepNet** | 1.8M | **0.999** |
| **Modified BRepNet** | **142k** | 0.988 |
| BRepNet from scratch | 1.8M | 0.975 |
| UV-Net [2] | 1.23M | 0.999 |
| PointNet++ [3] | 1.42M | 0.913 |
| DGCNN [5] | 0.53M | 0.909 |
| MeshCNN | 2.29M | 0.998 |
| Cao et al [7] | 0.53M | **0.999** |
| Hierarchical CADNet (Adj) [7] | 4.49M | 0.982 |
| Hierarchical CADNet (Edge) [7] | 6.60M | **0.999** |

modified BRepNet even with fewer trainable parameters, performs comparably well to the fine-tuned version, especially in critical feature classes. The slight decreases in performance for certain classes, such as the Chamfer and Triangular through slot, will be the focus of future optimizations.

Table 3: Comparison of BRepNet models with fine-tuned and modified versions

| Class | Intersection over Union | | |
|---|---|---|---|
| | **BRepNet** | **BRepNet fine-tuned** | **Modified BRepNet** |
| Chamfer | 0.995 | 0.995 | 0.986 |
| Triangular Passage | 0.998 | 0.999 | 0.998 |
| Rectangular Passage | 0.998 | 0.999 | 0.999 |
| 6 sides Passage | 0.999 | 1.0 | 0.950 |
| Triangular through slot | 0.999 | 0.998 | 0.979 |
| Rectangular through slot | 0.998 | 0.999 | 0.999 |
| Rectangular through step | 0.503 | 0.997 | 0.985 |
| 2 sides through step | 1.0 | 1.0 | 0.998 |
| Slanted through step | 0.521 | 0.997 | 0.988 |
| Triangular pocket | 1.0 | 1.0 | 0.998 |
| Rectangular pocket | 1.0 | 1.0 | 0.998 |
| 6 sides pocket | 1.0 | 1.0 | 0.988 |
| Rectangular blind slot | 1.0 | 1.0 | 0.999 |
| Triangular blind step | 1.0 | 1.0 | 0.978 |
| Rectangular blind step | 1.0 | 1.0 | 0.999 |
| Stock | 0.999 | 0.999 | 0.999 |

## 5 Conclusion

In conclusion, this study has demonstrated that the modified BRepNet, enhanced through transfer learning, provides a robust and efficient solution for CAD model segmentation. At first, the model benefits from the feature extraction capabilities of the original BRepNet. Consequently, by freezing the backbone network and concentrating on training only a custom lightweight segmentation head, the proposed approach achieves high accuracy with reduced computational demands.

The application of transfer learning has been particularly effective, allowing for faster times and improved generalization across different CAD model datasets. It is worth mentioning, that there is no need to transform the data to other formats as the BRepNet is designed to operate directly on B-Reps.

Further works could explore optimizing the segmentation head to enhance performance in classes where IoU scores were lower than expected. Additionally, expanding the application of this model to other types of geometric data or integrating other machine learning techniques could be promising.

## References

[1] J. G. Lambourne, K. D. Willis, P. K. Jayaraman, A. Sanghi, P. Meltzer, and H. Shayani, “Brepnet: A topological message passing system for solid models”, in *Proceedings of the IEEE/CVF conference on computer vision and pattern recognition*, 2021, pp. 12 773–12 782.

[2] P. Jayaraman, A. Sanghi, J. Lambourne, *et al.*, “Uv-net: Learning from boundary representations”, Jun. 2021, pp. 11 698–11 707. DOI: 10.1109/CVPR46437.2021.01153.

[3] C. R. Qi, L. Yi, H. Su, and L. J. Guibas, “Pointnet++: Deep hierarchical feature learning on point sets in a metric space”, *Advances in neural information processing systems*, vol. 30, 2017.

[4] R. Q. Charles, H. Su, M. Kaichun, and L. J. Guibas, “Pointnet: Deep learning on point sets for 3d classification and segmentation”, in *2017 IEEE Conference on Computer Vision and Pattern Recognition (CVPR)*, 2017, pp. 77–85. DOI: 10.1109/CVPR.2017.16.

[5] Y. Wang, Y. Sun, Z. Liu, S. E. Sarma, M. M. Bronstein, and J. M. Solomon, “Dynamic graph cnn for learning on point clouds”, *ACM Transactions on Graphics (tog)*, vol. 38, no. 5, pp. 1–12, 2019.

[6] R. Hanocka, A. Hertz, N. Fish, R. Giryes, S. Fleishman, and D. Cohen-Or, “Meshcnn: A network with an edge”, *ACM Transactions on Graphics (ToG)*, vol. 38, no. 4, pp. 1–12, 2019.

[7] A. R. Colligan, T. T. Robinson, D. C. Nolan, Y. Hua, and W. Cao, “Hierarchical cadnet: Learning from b-reps for machining feature recognition”, *Computer-Aided Design*, vol. 147, p. 103 226, 2022.

[8] *Graph Representation of 3D CAD Models for Machining Feature Recognition With Deep Learning*, vol. Volume 11A: 46th Design Automation Conference (DAC), International Design Engineering Technical Conferences and Computers and Information in Engineering Conference, Aug. 2020, V11AT11A003. DOI: 10.1115/DETC2020-22355.

# Konzept zur KI-gestützten parametrischen Brückenmodellierung für ressourcen- und kostenoptimierte Bauwerksentwürfe

Jonas Wiederer[1], Simon Höng[1] and Friedrich Eder[1]
[1]Ostbayerische Technische Hochschule Regensburg, Seybothstraße 2, 93053 Regensburg, Germany
E-mail(s): jonas.wiederer@oth-regensburg.de, simon.hoeng@oth-regensburg.de, friedrich.eder@oth-regensburg.de

**Abstract:** Brückenbauwerke stellen eine wesentliche Komponente einer soliden Infrastruktur dar. Wegen vernachlässigter Instandsetzungsmaßnahmen und sich verändernder Anforderungen sind für eine Vielzahl dieser Bauwerke in Deutschland Ersatzneubauten notwendig. Diese Arbeit adressiert die Herausforderungen der Ressourcenverschwendung durch wiederholten Arbeitsaufwand bei individuellen Brückenentwürfen für die angesprochenen Bauwerke. Es wird ein parametrisches Entwurfsmodells in *Siemens NX* entwickelt, um den Entwurfsprozess zu beschleunigen und eine einfache Anpassung an die entsprechenden Rahmenbedingungen zu ermöglichen. Zudem wird eine effektive Methode zur Anbindung an die Kostenermittlungssoftware *RIB iTWO* vorgestellt, die eine nachgelagerte Kostenkalkulation nach DIN 276 ermöglicht. Aufbauend darauf wird ein Optimierungsworkflow vorgestellt, welcher verschiedene Faktoren einbindet, um einen hochwertigen Bauwerksentwurf zu erzielen. Hierbei wird die Einbindung von Techniken aus dem Bereich der Künstlichen Intelligenz angestrebt. Die vorgestellte Methodik soll die Wirtschaftlichkeitsbewertung und Entscheidungsfindung für die Realisierung der Brückenentwürfe erleichtern und somit zu einer effizienteren Nutzung von Ressourcen im Brückenbau beitragen.
*Keywords:* Building Information Modeling (BIM), Parametric Modeling, Artificial Intelligence (AI), Industry Foundation Classes (IFC), Design Automation

Erschienen in Tagungsband 35. Forum Bauinformatik 2024, Hamburg, Deutschland, DOI: 10.15480/882.13506
© 2024 Das Copyright für diesen Beitrag liegt bei den Autoren. Verwendung erlaubt unter Creative Commons Lizenz Namensnennung 4.0 International.

## 1 Motivation

Über zehn Prozent des deutschen Bruttoinlandsprodukts werden für Bauinvestitionen verwendet[1]. Bei einem gesamten nominalen Bauvolumen von 565,3 Mrd. € fallen etwa 20 Prozent auf den Tiefbau im privaten und öffentlichen Sektor [2]. Hierzu zählen auch Brückenbauwerke, welche für die Infrastruktur von besonderer Bedeutung sind. Diese ermöglichen die Durch- und Überquerung von Bauwerken, Straßen oder auch geographischer Merkmale wie Täler und Flüsse. Aufgabe der Baubranche ist,

[1]https://www.bauindustrie.de/fileadmin/user_upload/Bauwirtschaft-im-Zahlenbild-2023-A5_final.pdf
[2]https://www.bbsr.bund.de/BBSR/DE/veroeffentlichungen/analysen-kompakt/2024/ak-01-2024-dl.pdf

diese neuralgischen Infrastrukturbauwerke in Betrieb zu halten. Durch regelmäßige Kontrollen können Schwachstellen und Mängel identifiziert und entsprechende Sanierungs- und Instandhaltungskonzepte entwickelt und schließlich umgesetzt werden. Da die Hälfte der Brücken bereits in den 1960er und 1970er Jahren gebaut wurden[3] kommt es nicht selten vor, dass sich eine Sanierung des betroffenen Bauwerks aus wirtschaftlichen Gründen nicht lohnt. Somit ist der Rückbau der Bestandsbrücke und der anschließende Neubau ein übliches Vorgehen. In Deutschland gibt es (Stand 2024) rund 39.500 Brückenbauwerke unterschiedlicher Ausprägung (Bauweise, Material, Gesamtlänge) auf Bundesfernstraßen; rund zwei Drittel davon weisen eine geringere Gesamtweite als 30 Meter auf.[4] Die Gesamtlänge einer Brücke ist ein guter Indikator zur Abschätzung des entsprechenden Planungs- und Fertigungsaufwands. Der Grund hierfür sind spezielle Bauverfahren wie beispielsweise Vorschubrüstungen oder Taktschiebeverfahren, die bei kurzen Brücken nicht üblich sind. Diese komplexeren Bauverfahren betreffen daher lediglich ein Drittel aller Brückenbauwerke. Die kürzeren Brücken sind grundsätzlich weniger komplex und damit ist auch der Planungsaufwand geringer. Hierbei kommen häufig sog. Richtzeichnungen zum Einsatz. Das bedeutet, dass viele dieser Brücken einen ähnlichen Aufbau haben, jedoch für jedes Projekt neu geplant werden müssen. Der Einsatz digitaler Werkzeuge wie Building Information Modeling (BIM), parametrische Brückenmodelle und Künstlicher Intelligenz (KI) können hier einen Beitrag zur Steigerung der Effizienz bei der Planung dieser Bauwerke leisten.

## 2 Stand der Technik

Die Erstellung von parametrischen Brückenmodellen bietet zahlreiche Vorteile wie einen effizienteren Designprozess und eine einfachere Anpassung an verschiedene Rahmenbedingungen. Die Relevanz dieser Methodik wird durch mehrere Studien in der Literatur belegt. Eine umfassende Untersuchung zu einem parametrischen BIM-Ansatz zur Brückenkonstruktion und -analyse wird in [1] präsentiert. Darin wurde ein parametrisiertes und steuerbares Brückenmodell über die visuelle Programmierstelle Rhino Grasshopper erstellt und mittels des Grasshopper-Tekla Live Link Plugins nach Tekla Structures transferiert. Der Schwerpunkt dieses Ansatzes liegt auf der Entwicklung eines flexiblen und anpassbaren Workflows zur effizienten Variantenuntersuchung. Ein umfassender Einblick in die grundlegenden Methoden und das Vorgehen bei der Erstellung eines parametrisierten und assoziativ gekoppelten Brückenmodells wird in [2] gegeben. Eine Erweiterung des IFC-Formats zur Unterstützung der Parametrik in Brückenmodellen wird in [3] vorgestellt. Dort wurde das IFC-Bridge Format durch eine semantische Beschreibung ergänzt, sodass die Parametrik der Brückenmodelle beim Datenaustausch erhalten bleibt. Dadurch wird ein mächtiger, offener und neutraler Standard zum Austausch von Brückenmodellen gefördert. Die Vorteile, die Modellierungstools aus dem Bereich des Maschinenbaus, wie *Siemens NX*, im Kontext der parametrischen Modellierung gegenüber den in der Baubranche typischerweise verwendeten Tools bieten, wurden in [4] aufgezeigt. Etablierte BIM-Autoren-Software wie Revit oder ArchiCAD fokussieren sich eher auf den Bereich des Hochbaus und eignen sich damit nur bedingt für die Erstellung parametrisch vollbestimmter Brückenbaumodelle. Um die Potenziale der parametrischen Modelle voll auszuschöpfen, ist es sinnvoll zu untersuchen, inwiefern sich diese Modelle zur Optimierung eines Bauwerks nutzen lassen. [5] präsentiert ein

[3] https://www.bast.de/DE/Statistik/Bruecken/Brueckenstatistik.pdf
[4] https://www.bast.de/DE/Publikationen/Regelwerke/Ingenieurbau/Entwurf/RiZ-ING-Gesamt.pdf

computergestütztes Werkzeug zur Optimierung von Brückenkonstruktionen, speziell für durchlaufende, vorgespannte Betonkastenträger-Straßenbrücken mittels des Harmony-Search-Algorithmus. Durch den Einsatz verschiedener Module werden optimale Konstruktionsparameter berechnet, die den festgelegten Anforderungen entsprechen. Der automatisierte Datenaustausch mit Fachsoftware ermöglicht eine tiefere Evaluation der Parameter. Moderne KI-Technologien erweisen sich als besonders geeignet zur Optimierung von Parametern und Modellen. Eine Arbeit zur Optimierung parametrischer Modelle mithilfe von KI wird in [6] präsentiert. Dort wurde sich mit der Anwendung von KI-Technologien zur automatisierten Verbesserung parametrischer Modelle befasst. Anhand eines parametrischen Modells für eine Stahlrahmenhalle wurden verschiedene Regressionstechnologien genutzt. Dazu wurde eine Schnittstelle zum Finite-Elemente-Programm SOFiSTiK implementiert, welches die Prädiktionen der KI bezüglich der Parameter der Stahlrahmenhallen an ein Eingabefile übergibt und die Berechnung und Bemessung anstößt. Die Arbeit zeigt, dass ein prototypischer KI-basierter Assistent zur Vorbemessung von Stahlrahmenhallen erfolgreich umgesetzt werden konnte.

In dieser Arbeit wird ein Konzept für die effizientere Planung und Bewertung von Brückenbauwerken beschrieben. Dafür werden Erkenntnisse aus den aufgeführten Arbeiten genutzt und für einen spezifischen Workflow weiterentwickelt. Die Grundlage für diesen Workflow liefert ein parametrisch-assoziatives Brückenmodell in *Siemens NX*. Im Zuge dessen wurden Ansätze entwickelt, fachfremde (Maschinenbau-)Software mit domänenspezifischer Bausoftware zu verbinden. Damit können durch nachgelagerte Prozesse das Bauwerk bewertet und Parameter angepasst werden. Inwiefern dies auch durch KI-Techniken (z.B. Reinforcement Learning) erfolgen kann, wird abschließend diskutiert. Ein solcher ganzheitlicher Workflow, der speziell für parametrische Brückenmodelle in *Siemens NX* entwickelt wurde, scheint ein bisher unveröffentlichter Ansatz zu sein.

# 3 Methodik

Die beschriebene Methodik verfolgt das Ziel, einen möglichst automatisierten Workflow von der Brückenkonstruktion bis hin zu entscheidungsrelevanten Prozessen wie Kostenermittlungen oder Tragwerksanalysen zu ermöglichen. Informationen, die in diesen nachgelagerten Prozessen gewonnen werden, lassen sich zur Optimierung des Bauwerksentwurfs verwenden, was beispielsweise durch die Berücksichtigung wirtschaftlicher oder strukturmechanischer Kenngrößen erfolgen kann. Um eine durchgängige Umsetzung einer automatisierten Optimierung zu ermöglichen, muss das Bauwerk einen möglichst hohen Parametrisierungsgrad aufweisen. Aus den im Stand der Technik aufgeführten Gründen wurden in dieser Arbeit die Modelle mit *Siemens NX* konstruiert und weiterverarbeitet. Die so entstandenen parametrischen Modelle, lassen sich in nachgelagerten Workflows von Mensch und Maschine (z.B. in Form von KI Agenten) gleichermaßen editieren. Die Integration von Algorithmen aus dem Bereich des maschinellen Lernens hat hier das Potential, sich als ein leistungsfähiges Werkzeug für den Bauwerksentwurf zu erweisen.

## 3.1 Konzept

Ausgehend von einem konstruierten, voll-parametrischen Brückenmodell sollen nachgelagerte Prozesse (Kostenermittlung, Tragwerksanalyse etc.) möglichst automatisch angesteuert werden und damit den Entwurfsprozess verbessern. Parameterwerte (Breite, Höhe etc.) und Trassierungsinfor-

mationen (Absteckpunkte, Lageplan, Gradiente etc.) sind entsprechende Steuervariablen über die ein Brückenmodell beschrieben werden kann. Die Eingabe erfolgt über eine Produktvorlage (*Product Template*), bei der Werte und Bauteiltypen angepasst werden. Um das Modell für bauspezifische Software nutzen zu können, werden die generierten Daten im IFC-Schema abgespeichert und anschließend in unterschiedlichen Analysesoftwaren (AVA-Software, Tragwerksanalyse etc.) evaluiert. Das oben beschriebene Konzept wird durch die Bewertung der Wirtschaftlichkeit mit der 5D Software *RIB iTWO*, exemplarisch untersucht. So werden Positionen eines einmalig erstellten, generischen Leistungsverzeichnisses (LV) über sogenannte Matchkeys (bauteilbezogene Primärschlüssel) einzelnen Bauteilen zugeordnet. Die Kopplung zwischen LV-Positionen und BIM-Objekten ermöglicht somit eine objektbezogene Attributsabfrage (Geometrie, Material, Typ etc.), die dazu verwendet wird, Mengen in das verbundene LV zu übertragen. Aus den Mengen und zugehörigen Einheitspreisen (EP) kann je Bauteil(gruppe) eine Kostenschätzung erfolgen, womit sich die Kenngröße Kosten für jeden Entwurf automatisiert ermitteln lässt. Durch die jeweilige zyklische Rückgabe dieses Ergebnisses können die Parameter angepasst und eine neue Modellvariante entwickelt werden. Der neue Input kann durch die planende Person oder auch durch eine künstliche Intelligenz retrospektiv angepasst werden. Dadurch entsteht eine Optimierungsschleife, die so lange durchlaufen werden kann, bis eine oder mehrere definierte Zielfunktionen, wie beispielsweise minimale Kosten und optimale Auslastung des Tragwerkes, erreicht sind.

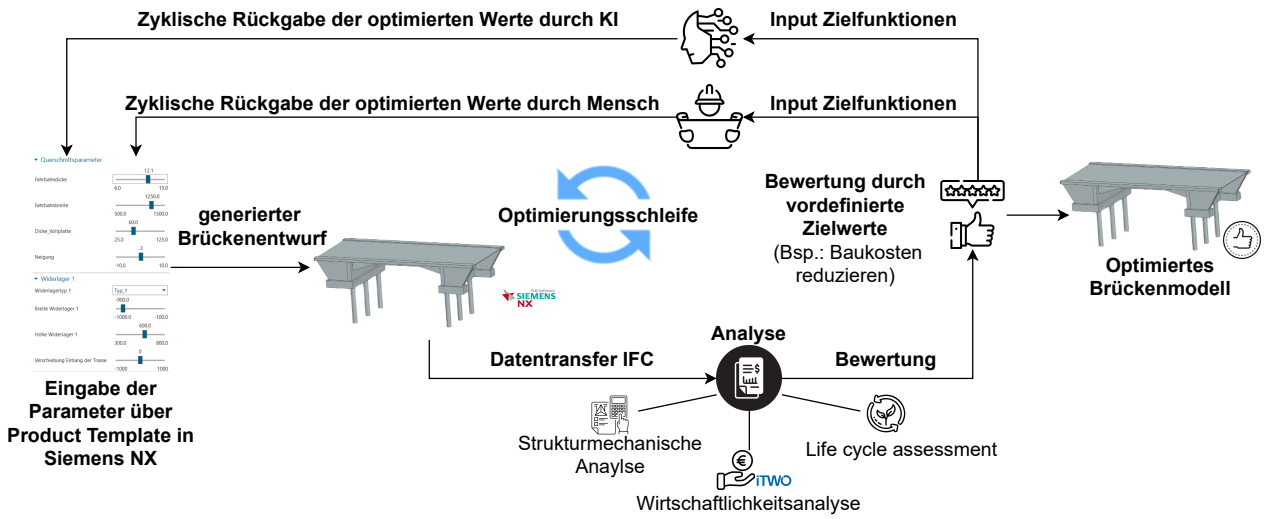


Abbildung 1: Zirkulärer Optimierungsworkflow für Brückenbauwerke

## 3.2 Aufbau des parametrischen Modells

Die Grundlage für den kompletten Workflow bildet das parametrisch aufgebaute Brückenmodell in *Siemens NX*. Für den Konstruktionsprozess wurde gemäß der Top-Down-Methode gearbeitet, da sie komplexe und fehlerfreie Änderungen präzise ermöglicht. Die Methode hat den Vorteil, dass bei der Änderung einzelner Bauteile alle abhängigen Bauteile assoziativ angepasst werden. Das Konzept baut auf vorab definierten Referenzen auf, die in übergeordneten Baugruppen abgespeichert werden und für alle weiteren Bauteile als hierarchischer Container dienen. Für das Brückenmodell werden Trasse, Widerlagertypen und Parameter (Querneigung, Steghöhe etc.) als Steuergrößen

genutzt. Die jeweiligen Koordinaten für die Führungslinie wurden als CSV-Datei über die visuelle Programmierschnittstelle (*Algorithmic Modeling*) importiert und weiterverarbeitet. Mit dieser Methode wird gewährleistet, dass unterschiedliche Koordinaten eingelesen und damit Brücken direkt und ohne manuelle Änderungen realisiert werden können. Die einzelnen Komponenten der Brücke (Widerlager, Unterbau, Oberbau, Kappen etc.) werden als rein geometrische Körper aufgebaut, anhand der Führungslinie positioniert und ausgerichtet.

### 3.3 Erzeugung der Modellinstanz über die Parameter

Um ein Modell zu erzeugen, müssen zuerst Koordinaten in Form einer CSV-Datei eingelesen werden. Nach dem Import werden alle Bauteile generiert und können anschließend für jedes Projekt modifiziert werden. Schnelle Änderungen sind durch Produktvorlagen im Product Template Studio (PTS) möglich, im Template können Anpassungen durch verschiedene Änderungsfunktionen in Echtzeit durchgeführt werden. Mit der Auswahlfunktion können unterschiedliche Bauteiltypen ohne Verzögerung aktiviert und getestet werden. Zusätzlich werden zu jedem Bauteil Informationen hinzugefügt, die ähnliche Bauteile gruppieren und jedes Bauteil zusätzlich in Form von Matchkeys eindeutig identifizieren.

### 3.4 Datenaustausch

Der IFC-basierte Datenaustausch macht es möglich, Schnittstellen zu unterschiedlichen, fachspezifischen Autorensoftwares zu nutzen. So wurde die Bewertung der Wirtschaftlichkeit in Form einer Kostenschätzung nach DIN 276 mit *RIB iTWO* durchgeführt. Zur Erstellung bauspezifischer Fachmodelle in *Siemens NX* mussten beim Konstruieren zusätzliche Schritte unternommen werden, da alle Bauteile nur als geometrische Körper ohne spezifische Metadaten gespeichert werden. Diese fehlenden semantischen Informationen werden jedoch in *RIB iTWO* benötigt, um den in Abschnitt 3.1 beschriebenen Prozess umzusetzen. Zur Umsetzung des Workflows wurden jedem Bauteil ein alphanumerischer *Matchkey* zugeordnet, der sowohl Gruppen- als auch individuelle Zuordnungen ermöglicht.

### 3.5 Verarbeitung der Daten in der Zielsoftware

Das Modell wird als IFC-Datei über den BIM Qualifier nach *RIB iTWO* importiert und die Modellqualität (bezogen auf die Verarbeitbarkeit des Datensatzes) überprüft. Für die weiteren Prozesse in der Software wird die Datei in das sog. CPIXML-Format überführt und freigegeben. Für eine automatisierte Kostenschätzung werden Mustervorlagen in *RIB iTWO* für das sog. Ausstattungsdokument, das sog. Bemusterungsdokument und das LV erstellt. Im Ausstattungsdokument werden mit sog. Quantity-Takeoff-Abfragen (QTO) die geforderten Mengen ermittelt. Die Mengen können direkt in *RIB iTWO* berechnet oder über Attributabfragen aus den vorhandenen Informationen gezogen werden. Die Verknüpfung der Bauteile zu den Abfragen funktioniert über Objektauswahlgruppen. Diese werden im Bemusterungsdokument zugeordnet. Für eine Objektauswahlgruppe werden die in *Siemens NX* erstellten Matchkeys als Connector gespeichert, die die Bauteile mit der Ausstattung verbinden. Bei Änderung des Brückenentwurfs in der Ursprungssoftware muss das Modell neu in *RIB iTWO* importiert werden. Die Verknüpfungen werden dann automatisch aktualisiert. Das Ausstattungsdokument besitzt eine ähnliche Struktur wie das LV, deswegen können Positionen und enthaltene Informationen

übernommen werden. Kosteninformationen können manuell hinzugefügt oder durch Plug-Ins direkt in *RIB iTWO* geladen werden.

### 3.6 Rückgabe der Bewertung

Die Rückgabe und Verarbeitung der Ergebnisse ermöglichen es, in weiteren Schritten den Entwurf zu modifizieren. Durch die Vorgabe von Zielfunktionen können Änderungen durchgeführt und die Parameter abgeändert werden. Im durchgeführten Validierungsbeispiel werden kostenrelevante Daten in Form einzelner Positionen eines LVs zurückgegeben, die von der planenden Person weiterverarbeitet werden können. Im Anwendungsbeispiel werden ausschließlich kostenrelevante Informationen zyklisch verarbeitet. Weitere Prozesse, beispielsweise in Form einer strukturmechanischen Analyse, können ebenfalls durchgeführt werden. Damit ist auch die Einbeziehung mehrdimensionaler Zielwerte (z.B. Ergebnisse aus Kosten und Tragwerksanalyse) in die Optimierungsschleife denkbar. Hier kann eine Bewertungsmatrix genutzt werden, die ein optimales Ergebnis für die verwendeten Analysen nutzt. Für umfangreichere Gesamtanalysen kann der Einsatz von KI gewinnbringend genutzt werden. Sobald alle Parameter ihr Optimum erreicht haben, ist das Brückenmodell fertig und kann für die nächsten Planungsschritte verwendet werden.

## 4 Anwendungsbeispiel: Automatisierter Modellaustausch für Kostenermittlung

Durch die vorliegenden Dateien ist es möglich, individuelle Brückenentwürfe durch die Eingabe von Parameterwerten zu generieren. Der Import der Koordinaten als CSV-Datei gibt die Linienführung vor, die Quantität der Punkte kann die Modellqualität erhöhen und komplexere Linienführungen nachbilden. Mit der Parametereingabe im *Product Template* werden die Dimensionen der Brücke angepasst, vor allem Querschnittswerte des Ober- und Unterbaus, und Parameter wie Kreuzungswinkel, Spannweite und Schlankheit können ebenfalls durch die Auswahlmöglichkeiten aktiviert werden. Aus der Bibliothek können unterschiedliche Widerlagertypen für den Entwurf genutzt werden. Die Brücke wird als IFC-Datei nach *RIB iTWO* exportiert und analysiert. Beim Erstellen eines Projekts in der Software müssen die gespeicherten Mustervorlagen einmalig importiert werden, sodass ein automatischer Workflow durchgeführt werden kann. Im Ausstattungsdokument sind alle Bauteile mit den jeweiligen QTO-Mengenabfragen gelistet und durch die Verknüpfung der Informationen mit den Bauteilen über Matchkeys in der Bemusterung werden die Mengen direkt berechnet. Die Verbindung zwischen dem Ausstattungsdokument mit LV-ähnlicher Struktur und dem späteren LV ermöglicht eine Kostenschätzung. Die Kosten werden durch die planende Person eingegeben oder können durch Plug-ins eingefügt werden. Das generierte LV gibt Aufschluss über die Kosten der jeweiligen Bauteile. So können zyklisch Änderungen der jeweiligen Parameter vorgenommen und schnelle Adaptionen durchgeführt werden. Das modifizierte Modell wird daraufhin erneut in *RIB iTWO* importiert und die Kosten dafür aktualisiert.

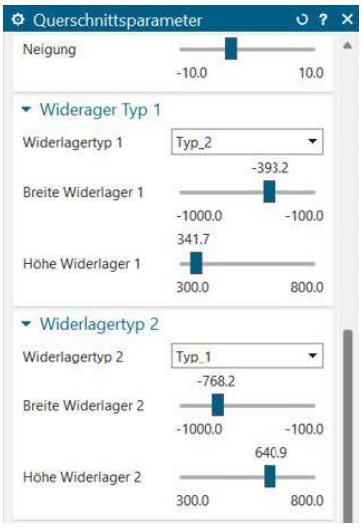


Abbildung 2: Definition der Parameterwerte

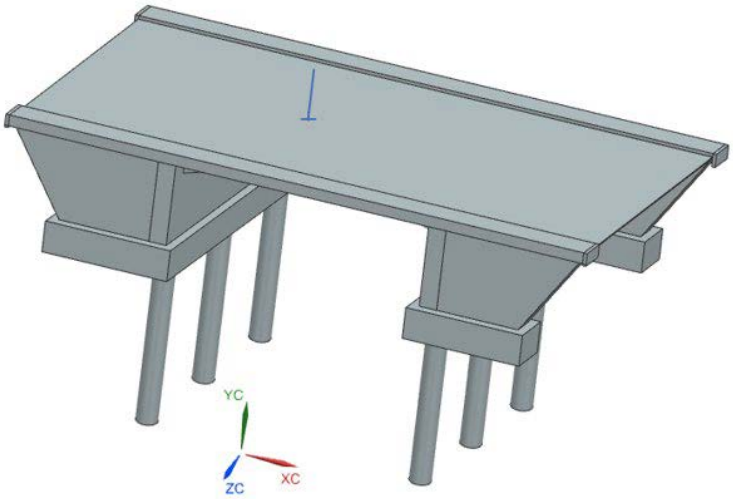


Abbildung 3: Generierter Brückenentwurf in Siemens NX

| Struktur | OZ | Kurz-Info | Kurztext | Menge | ME | Einheitspreis | Gesamtbetrag | WE |
|---|---|---|---|---|---|---|---|---|
| | 1 | | **Gesamtmodell** | | | | **8.962,29** | **EUR** |
| | 1. | | Brückenmodel | | | | 8.962,29 | EUR |
| | 1. 1. | | Oberbau | | | | 0,00 | EUR |
| | 1. 2. | | Unterbau | | | | 8.962,29 | EUR |
| § | 1. 2. 10. | | Ortbeton Sauberkeitsschicht | 1,716 | m2 | 0,00 | 0,00 | EUR |
| § | 1. 2. 20. | | Ortbeton Fundament Widerlager auf Pfeiler | 99,581 | m3 | 90,00 | 8.962,29 | EUR |
| § | 1. 2. 30. | | Ortbeton Flügel | 37,089 | m3 | 0,00 | 0,00 | EUR |
| § | 1. 2. 40. | | Ortbeton Kammerwand mit Aufagerbank | 76,274 | m3 | 0,00 | 0,00 | EUR |
| | 1. 3. | | Gründung | | | | | |

Abbildung 4: Beispielhaftes LV mit Kostenschätzung in RIB iTWO

## 5 Diskussion und Fazit

Mit der Integration eines parametrisch-assoziativen Brückenmodells in die Prozesse der modellbasierten Kostenermittlung wurde die Grundlage für das in der Methodik beschriebene Konzept geschaffen. In einem nachgelagerten Prozess wurden die Kosten als evaluierendes Beispiel berechnet. Für die Modellierung in *Siemens NX* konnte aufgezeigt werden, dass die Integration domänenspezifischer, semantischer Informationen (Bauteiltypen, Kostengruppen etc.) in ein generisches parametrisches Modell für den korrekten Datentransfer notwendig ist. Der erzeugte Modellentwurf ist aufgrund seiner Parametrik flexibel einsetzbar und kann durch den Import neuer Koordinaten für unterschiedliche Projekte verwendet werden. Mithilfe von angelegten Vorlagen und Bibliotheken werden Bauteile automatisch zugeordnet und Analysen in unterschiedlichen Bereichen ermöglicht. Dies hängt vor allem davon ab, welche Konnektoren (strukturmechanische Analyse, Kosten, Life Cycle Assessment etc.) für die Optimierungsschleife(n) integriert werden sollen und welchen Einfluss diese auf den Entwurf haben. Für die Bewertung des Modellentwurfs kann die Optimierungsschleife mit KI-Techniken wie dem Machine Learning effizienter durchgeführt werden. Eine Möglichkeit bietet hierfür der im Brückenbau von [5] erfolgreich angewandte Harmony-Search-Algorithmus. Der Algorithmus erzeugt

dabei neue Parameterwerte und vergleicht die generierten Modelle nach bestimmten Zielwerten miteinander. Die planende Person kann für die Entwürfe individuelle Zielwerte, wie maximale Gesamtkosten, vorgeben und bis zum Trennungskriterium die Optimierungsschleife durchführen. Da das Modell komplett parametrisch aufgebaut ist, sind Varianten durch einen Algorithmus leicht zu generieren. Insgesamt stellt die beschriebene Methode einen vielversprechenden Ansatz zur Verringerung des Planungsaufwandes von Brückenbauwerken dar. Insbesondere durch die detaillierte Ausarbeitung der beschriebenen automatisierten und KI-basierten Feedback-Schleife soll das Potential dieses Ansatzes in künftiger Forschung genauer evaluiert werden.

## Acknowledgements

Diese Veröffentlichung wurde im Rahmen des KIFa Projekts vom BMWK auf Basis einer Entscheidung des Deutschen Bundestages gefördert.

Zudem danken wir Prof. Dr. Michael Kraus für die Kooperation im Rahmen dieses Forschungsthemas.

## Literatur

[1] V. Boretti, L. Bohórquez, P. Palumbo, R. Asso und D. Masera, »A Parametric BIM Approach for Bridge Design and Analysis«, in *Shell and Spatial Structures*, S. Gabriele, A. Manuello Bertetto, F. Marmo und A. Micheletti, Hrsg., Cham: Springer Nature Switzerland, 2024, S. 609–618. DOI: 10.1007/978-3-031-44328-2_63.

[2] M. Obergrießer, *Digitale Werkzeuge zur integrierten Infrastrukturbauwerksplanung*. Wiesbaden: Springer Fachmedien, 2017. DOI: 10.1007/978-3-658-16782-0.

[3] Y. Ji, A. Borrmann, J. Beetz und M. Obergrießer, »Exchange of Parametric Bridge Models Using a Neutral Data Format«, *Journal of Computing in Civil Engineering*, Jg. 27, Nr. 6, S. 593–606, Nov. 2013. DOI: 10.1061/(ASCE)CP.1943-5487.0000286.

[4] K. Lukas, Y. Ji, M. Obergriesser und A. Borrmann, »Parametrische Modellierung von Brückenbauwerken«, in *Tagungsband Des 20. Forum Bauinformatik*, 2008.

[5] T. García-Segura, V. Yepes und J. Alcalá, »Computer-support tool to optimize bridges automatically«, *International Journal of Computational Methods and Experimental Measurements*, Jg. 5, Nr. 2, S. 171–178, März 2017. DOI: 10.2495/CMEM-V5-N2-171-178.

[6] R. Fisch, E. Stecker und M. A. Kraus, »Maschinelles Lernen beim Entwurf und der Bemessung von Stahlrahmenhallen«, *Stahlbau*, Jg. 92, Nr. 6, S. 332–344, 2023. DOI: 10.1002/stab.202200054.

# SPARK: A Universal Approach to 3D Point Cloud Segmentation Using 2D Image Segmentation Models – Demonstration on Traffic Objects

Michael Disser[1], Vivien Volland[2] and Gent Demiri[1]
[1]Institut für Numerische Methoden und Informatik im Bauwesen, Technische Universität Darmstadt, Franziska-Braun-Straße 7, 64287 Darmstadt, Deutschland
[2]FG Geodätische Messsysteme und Sensorik, Technische Universität Darmstadt, Franziska-Braun-Straße 7, 64287 Darmstadt, Deutschland
E-mail(s): disser@iib.tu-darmstadt.de, vivien.volland@tu-darmstadt.de

**Abstract:** The generation of point clouds using LIDAR or photogrammetry is used in various fields of (civil) engineering and allows to capture the geometry of scenes or objects. The categorisation of objects and their segmentation has to be done either manually or using isolated solutions with limited functionality. This paper presents the general purpose application SPARK, which uses 2D object recognition to perform automated 3D object segmentation in point clouds. The point cloud mesh is imported into the Unity game engine and an orthographic camera is flown over the mesh to capture images. 2D object segmentation CNNs are then used to classify and mask the detected objects. This information is projected onto the mesh using raycasts to create a three-dimensional localisation of the classified points in the scene. These points are clustered into bounding boxes and used to localise elements in the original point cloud and to create classified sub-point clouds. The workflow is demonstrated in the SPARK application using the example of capturing road objects with the object segmentation models pre-trained on the ADE20K and Cityscapes datasets. A case study with three point clouds of urban street scenes is performed and the results and applicability are discussed.
*Keywords:* Point Cloud, Segmentation, Computer Vision, 2D-3D Transformation, Gaming Engine

Erschienen in Tagungsband 35. Forum Bauinformatik 2024, Hamburg, Deutschland, DOI: 10.15480/882.13515
© 2024 Das Copyright für diesen Beitrag liegt bei den Autoren. Verwendung erlaubt unter Creative Commons Lizenz Namensnennung 4.0 International.

## 1 Introduction

Point clouds are a reliable, accurate tool for capturing geometric objects and are used in civil engineering for as-built documentation of environments and buildings. In geodesy, LIDAR (Light Detection and Ranging) using TLS (Terrestrial Laser Scanning) or MLS (Mobile Laser Scanning) and photogrammetry are common methods for generating point clouds. Point clouds provide a geometric representation of objects and environments. However, when used as a project-related data source, the semantic context of the represented objects must be identified and individual relevant objects must be (manually)

labelled or separated. This separation of point cloud objects is necessary to enable integration into model-based planning processes such as BIM (Building Information Modelling) or for simulations such as digital twins using as-built geometry. While automated methods exist for the recognition of various simple geometric bodies and some objects (see Chapter 2), the latter in particular are isolated solutions and in practice the majority of objects are identified and segmented manually. Training CNNs (Convolutional Neural Networks) for object recognition directly on point clouds is time-consuming and hardware-intensive, and generating data sources and labelling is labour-intensive [1].
The aim of this work is to present a generally applicable workflow that is capable of automatically recognising, localising and geometrically describing a large number of different objects for different use cases. Since a large number of labelled datasets already exist for training 2D image segmentation models (see Chapter 2), these will be used to support 3D object segmentation. Alternatively, users can train their own 2D image segmentation models by labelling images and training CNN models and include them in the workflow. In order to use the image segmentation models for 3D segmentation of point clouds, a game engine application has been developed that automatically generates photos in a game engine, segments them using the CNN models, projects the results back onto the point cloud (mesh) and thus creates a spatial reference. This spatial reference can then be used to identify the classified objects in the original point cloud and, if desired, create sub-point clouds of the isolated objects. The presented application allows the creation of segmented, labelled three-dimensional point clouds of specific objects and a hierarchical understanding of the scene can be generated. The segmented point clouds can also be used as labelled data for training 3D object recognition algorithms. The workflow is generally valid and is implemented on the example of traffic related objects and validated on three different point clouds.

## 2 Related Work

Point clouds acquired by methods such as terrestrial laser scanning (TLS), mobile laser scanning (MLS) or unmanned aircraft systems (UAS) often consist of millions of 3D points. The segmentation and classification of objects within point clouds is the subject of research for various application purposes. To segment and classify objects, 2D and/or 3D parts of point clouds are subdivided. A common method is the use of deep learning, especially CNNs, and feature identification algorithms.
K-means clustering (a method for vector quantization; also used for cluster analysis) of 3D point clouds is one approach to classify 3D points [2], [3]. In addition to classifying each point, [3], [4] use algorithms such as RANSAC (Random sample consensus) to detect planes within point clouds. [5] also uses RANSAC in combination with region growing algorithms to detect planes and thus semi-automatically detect objects in interior point clouds. [1] present a deep learning framework, including k-means clustering, that predicts a semantic label for each point in a 3D point cloud. They use point neighbourhoods and loss functions to refine feature spaces. Similar methods are used by [6], [7]. [2] extracts 3D and 2D geometric features by considering the local neighbourhood of each 3D point and projecting them onto a horizontal plane to extract the 2D features. Many segmentation and classification methods focus on indoor scenes. A common dataset for analysing outdoor scenes is the KITTI dataset, which is often used for autonomous driving scenarios [1]. [8] used this dataset for a real-time 3D object detector called PIXOR (ORiented 3D object detection from PIXel-wise neural

network predictions) to operate on point clouds. [8] outputs accurately oriented bounding boxes in real dimensions in a bird's eye view. Another common method is to use 3D voxel grids or 2D projections on surfaces in combination with CNNs [9], [10]. [9] discretises the projection into a 2D image and applies 2D convolutions. Another work focusing on outdoor scenarios with traffic-related objects is by [11]. The deep learning algorithm KPConv is used in combination with the NPM3D dataset. This dataset contains an outdoor scenario including poles, benches, bins and signs. Semantic segmentation combined with partial local neighbourhood segmentation is performed on the MLS data. Another technique for point cloud segmentation is the use of meshes. [12] used aerial and autonomous LIDAR point clouds and RGBD cameras for indoor floor and wall detection. The input data are 2D point sets, 3D point clouds and meshes. After mesh smoothing, dominant plane normal estimation, planar segmentation and polygon extraction, their system, called Polylodar3D, outputs planes and corresponding polygon representations. For outdoor scenarios, they also use the KITTI dataset, which is analysed from a bird's eye view. Raycasting is another method of detecting the location of points within a point cloud for more accurate segmentation. [13] use a raycasting approach to detect changes in point clouds of large urban areas. [14] also use a raycasting method in combination with a deep neural network, but for geolocating people and determining distances for search and rescue scenarios using UAS imagery.

In addition to the KITTI dataset, other datasets, their trained classes and their features were analysed for their suitability in the road infrastructure use case. ADE20K [15] and COCO [16] contain a wide range of common objects and are suitable for general use case independent analysis. Citycapes [17], KITTI [18] (both German) and BDD100K [19] (American) labelled road specific and urban objects like roads, signs, traffic lights, poles for use cases like autonomous driving. GTSRB [20] has over 40 different types of German road signs and can be used to specify which road sign is recognised.

The approach of the paper combines several of the above methods: pre-trained CNN-DL algorithms with 2D views of meshed point clouds, raycasting, and the final mapping of the segmented and classified traffic-related objects back onto the point cloud. To the authors' knowledge, such an approach does not yet exist.

## 3 The SPARK Application

The main requirement of the application is to be able to transfer the results of 2D object segmentation algorithms to the 3D point cloud. To ensure transferability to other use cases, it should be possible to combine matching object segmentation algorithms in a modular way. In order to generate images from different positions and angles, an automation of the image generation is required that allows (partial) automation based on user input for parameters and camera path. The application should be able to handle large point cloud meshes and their colliders, but there is no requirement for the application to run in real time, as no user input should be made at runtime. The results of the segmentation in 3D space should be clustered and the instances should be geometrically described, classified and exported in an applicable data scheme. To cover a wide range of use cases, the application should be scalable, have modular functionality and run on conventional hardware and applications.

To meet these requirements, a workflow concept is developed and an application called SPARK (Segmentation Processing and Analysis for Recognizing Keyobjects) is implemented. The described

workflow consists of modifications of point clouds with external consumer software as well as the application, which consists of different scripts and designed GameObjects in the game engine Unity, and the management of the different object segmentation algorithms through Python scripts. The modules of the workflow are shown in the Figure 1 and described in the following sections.

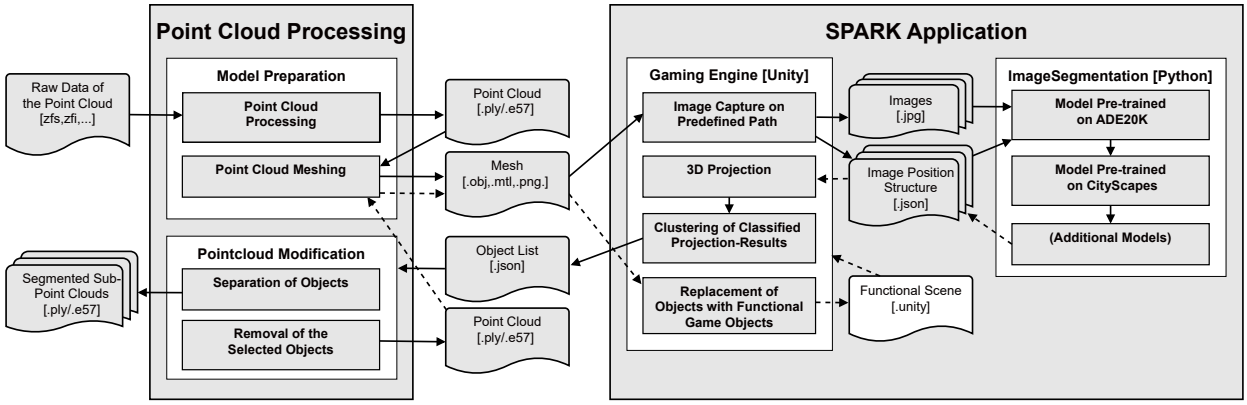


Figure 1: Overview of the SPARK application.

## 3.1 Pointcloud Preparation

Once the raw data of a scene has been captured, it needs to be processed so that it can be stored as a point cloud. The point cloud is meshed so that it can physically interact with the mesh collider in Unity. The results are then exported as an .obj with material and texture files.

## 3.2 Image Retrieval

To generate images from the point clouds for object recognition, an orthographic camera is moved along a path that takes images at fixed user-defined intervals. The path is a GameObject containing a line renderer with a polyline (see Figure 2). The goal is to capture all objects to be detected from at least three sides in order to draw a bounding box around the object (see Section 3.5). By rotating the camera at each capture point, images are taken from different directions, depending on the user's parameter settings for the GameObjects script. As a result, objects along the path are captured from different angles and directions as the camera moves past them. An orthographic camera was chosen to make it easier for the recognition algorithms in Section 3.5 to recognise objects compared to perspective cameras. It is also easier to recalculate the 3D points using the orthographic camera setting. The images are stored in a folder and the recording details of each image recording are stored using a class schema and saved as .json.

## 3.3 Image Segmentation

After the camera completes its path, an external Python script is triggered to analyse the captured images to identify and segment objects. The script uses a machine learning model to detect objects and and mark them with bounding boxes and masks. For the mask, not every pixel is used, but every n-th value, to produce a relatively detailed list of results, but not too many raycasts in the next step. For SPARK, different models are used that have been pre-trained with the Tensorflow Deeplab_v3 models

using the ADE20K [15] dataset and the Cityscapes [17] dataset (available at [1]). These datasets were chosen to get a mix of common objects and German urban street objects, as the point clouds are also generated on German scenes. The backbones used are MobileNetV2, MobileNetV3 and Xception. An example of the results of the Cityscapes dataset pre-trained on Deeplab_v3 can be seen in Figure 3.

Figure 2: Example of a manually created camera path; Current camera-POV in the bottom right corner.

Figure 3: Masking of the image object segmentation using Cityscapes.

### 3.4 3D Projection to the Mesh

The results of the image segmentation Python script are returned as output to the Unity application and embedded into the existing class structure. The instance of the captured image is updated with information about the objects detected within it, including the object's classes, locations, bounding boxes and masks. The user can filter the classes of objects to be included in the projection process to exclude irrelevant objects such as sky or void. The next step is to project the collected 2D information of the masked objects on each image into the three-dimensional mesh of the urban scene. To do this, the camera moves and orients itself to the exact orientation and position where the image was taken. Each label mask is iterated, and the two-dimensional pixel values of each object are also iterated. Each two-dimensional pixel coordinate is converted to the base plane (rectangle) of the orthographic camera. From this point, a raycast is created, oriented in the same direction as the camera view (perpendicular to the camera's base plane). This raycast represents the view direction of the renderer for that exact pixel. Therefore, the first part of the urban scene mesh hit by the raycast represents the object captured by the camera. This hitpoint is a three-dimensional representation of the two-dimensional object segmentation, as shown in Figure 4. By doing this for all pixels in the mask, and for multiple images with multiple positions and orientations, each detected object is now tagged with a multitude of classified coordinates.

### 3.5 Segmentation and Replacement

For each detected class, all 3D points are clustered using the DBSCAN algorithm. Each cluster result is then identified as an instance of the object and a bounding box is created to distinguish the points as part of the instance. The instance number, class label, bounding box geometry and identified

[1]Tensorflow Model-Zoo: https://github.com/tensorflow/models/blob/master/research/deeplab/g3doc/cityscapes.md

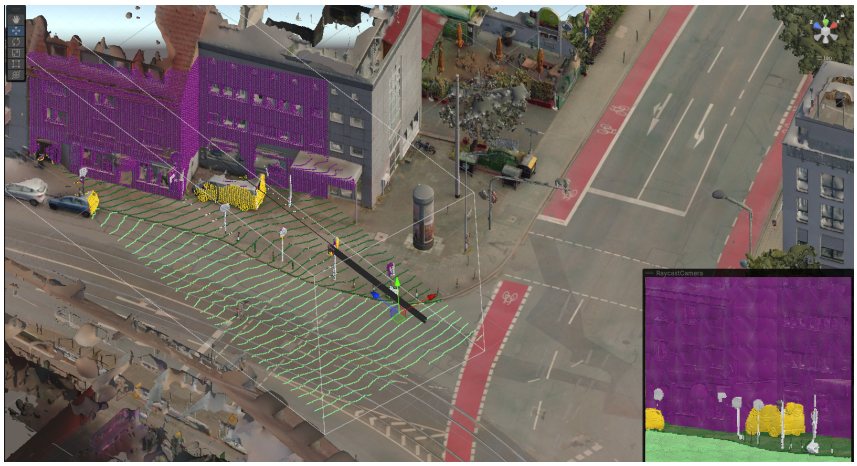

Figure 4: Visualisation of the segmentation results with lines and spheres as 3D representation of the raycast hits.

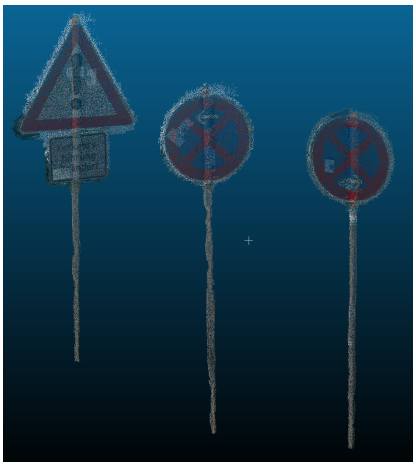

Figure 5: Point clouds of separated street signs and poles.

points are then exported as .json. This information is then used by another Python script which has two options: First, it can separate the detected objects as sub-point clouds, generating smaller point clouds with all points between the respective bounding boxes. This can be used to create classified point clouds consisting only of these objects. These can be used to create instances of realistic GameObjects or as training data for object detection in 3D point clouds. On the other hand, some classes can be selected by the user to be cut out of the whole point cloud. This can be used to replace these objects in the mesh for functional or interactive GameObjects. For example, the traffic lights in the original mesh could be replaced with functional traffic lights in the game engine by placing a functional GameObject at the position of the bounding box.

## 4 Results and Outlook

To validate the concept and application, three point clouds were generated in different types of urban scenes. While two of the point clouds contain large road crossings (one in the city centre and one in a vegetation-rich area), the third was in a relatively object-free environment. Two of the point clouds were generated using the NavVis VLX (v1) mobile laser scanner and one was generated using the Z+F 5016 imager. The raw data was processed using Z+F Lasercontrol and Scantra as well as the NaVis Ivion cloud application. Meshing was done using RealityCapture, Meshlab and CloudCompare. The results for the point cloud of an urban crossing with the detection can be seen in Figure 4 and the separation of traffic signs the associated poles in Figure 5.

The SPARK application and the case study proved that the workflow of the concept is a suitable method to detect and segment objects in point clouds. The modularity of the application allows it to be used for different use cases and can be adapted by the users through the parameters they can set for the GameObjects. Compared to relying only on images taken from the point cloud produced by scanners or photogrammetry, the paper approach has the advantage of generating images from different perspectives than the original images, resulting in better detection of objects due to better visibility and user-defined angles. The approach works even if the images have not been provided to the user or if only a mesh is available. The objects detected by the 2D object segmentation

algorithms can be seamlessly projected into the 3D world. Some pixel coordinates at the edge of the objects missed their target, which can be solved by omitting the edge pixels. As the results are highly dependent on the quality of the mesh and the object segmentation models, the functionality of the method is limited by the quality of these algorithms. This was particularly the case for small or thin objects such as road signs and traffic light poles. Depending on the quality of the mesh, these objects became bulky and sometimes unidentifiable. At this stage of the application, multiple objects of the same class next to each other are grouped as one object by the clustering algorithm. A solution to this would be to use instance segmentation algorithms such as those used in the BDD100K dataset [19]. The next step for the application is to introduce new segmentation algorithms to detect different types of objects. Lane detection, as introduced in BDD100K [19], can be used to identify the different lanes. The detected objects can be compared with publicly available information for traffic related objects such as those from OpenStreetMap or Mapillary. Scalability needs to be tested with larger datasets and also with point clouds produced by photogrammetry to enable larger scale capture of road infrastructure. Other use cases can be tested to ensure universal applicability. For larger or very detailed meshes, the use of the original mesh as a mesh collider was identified as a performance limiting bottleneck. To overcome this, an invisible lower poly mesh could be used for the collider. In addition, image quality could be improved by using Gaussian splats or a visualisation of the point cloud itself combined with a low-poly mesh collider to interact with the raycasts.

## References

[1] F. Engelmann, T. Kontogianni, J. Schult, and B. Leibe, “Know What Your Neighbors Do: 3D Semantic Segmentation of Point Clouds”, en, in vol. 11131, Dec. 2018, pp. 395–409. DOI: 10.1007/978-3-030-11015-4_29.

[2] M. Weinmann, B. Jutzi, and C. Mallet, “Feature relevance assessment for the semantic interpretation of 3D point cloud data”, en, *ISPRS*, vol. II-5/W2, pp. 313–318, Nov. 2013. DOI: 10.5194/isprsannals-II-5-W2-313-2013.

[3] D. Iwaszczuk, T. Koch, and U. Stilla, “Innenraumrekonstruktion aus semantisch angereicherten 3D Punkten und Linien”, de, *DGPF, Band 26*, 2017. DOI: https://doi.org/10.1007/s41064-017-0029-9.

[4] J. Schmidt, V. Volland, D. Iwaszczuk, and A. Eichhorn, “Detection of Hidden Edges and Corners in SLAM-Based Indoor Point Clouds”, en, *ISPRS*, vol. XLVIII-1/W1-2023, pp. 443–449, May 2023. DOI: 10.5194/isprs-archives-XLVIII-1-W1-2023-443-2023.

[5] J. López Iglesias, J. A. Diaz Severiano, P. E. L. Amorocho, *et al.*, “Revision of Automation Methods for Scan to BIM”, in *XXIX INGEGRAF*, Logroño, Spain: Springer Nature Switzerland AG, 2019, pp. 482–490.

[6] S. A. Bello, S. Yu, C. Wang, J. M. Adam, and J. Li, “Review: Deep Learning on 3D Point Clouds”, en, *Remote Sensing*, vol. 12, no. 11, p. 1729, May 2020. DOI: 10.3390/rs12111729.

[7] C. R. Qi, L. Yi, H. Su, and L. J. Guibas, *PointNet++: Deep Hierarchical Feature Learning on Point Sets in a Metric Space*, en, Jun. 2017. [Online]. Available: http://arxiv.org/abs/1706.02413.

[8] B. Yang, W. Luo, and R. Urtasun, *PIXOR: Real-time 3D Object Detection from Point Clouds*, en, Mar. 2019. [Online]. Available: http://arxiv.org/abs/1902.06326.

[9] X. Chen, H. Ma, J. Wan, B. Li, and T. Xia, *Multi-View 3D Object Detection Network for Autonomous Driving*, en, Jun. 2017. [Online]. Available: http://arxiv.org/abs/1611.07759.

[10] M. Engelcke, D. Rao, D. Z. Wang, C. H. Tong, and I. Posner, *Vote3Deep: Fast Object Detection in 3D Point Clouds Using Efficient Convolutional Neural Networks*, en, Mar. 2017. [Online]. Available: http://arxiv.org/abs/1609.06666.

[11] S. Yousefimashhoor, "Deep learning on MLS Point Clouds: Feasibility of Improving Semantic Segmentation Result Using Part Segmentation", en, Tech. Rep., Jul. 2022. [Online]. Available: https://essay.utwente.nl/91777/1/Yousefimashhoor_MA_ITC.pdf.

[12] J. Castagno and E. Atkins, *Polylidar3D - Fast Polygon Extraction from 3D Data*, en, Jul. 2020. [Online]. Available: http://arxiv.org/abs/2007.12065.

[13] J. Gehrung, M. Hebel, M. Arens, and U. Stilla, "A Voxel-Based Metadata Structure for Change Detection in Point Clouds of Large-Scale Urban Areas", en, *ISPRS Ann. Photogramm. Remote Sens. Spatial Inf. Sci.*, vol. IV-2, pp. 97–104, May 2018. DOI: 10.5194/isprs-annals-IV-2-97-2018.

[14] G. Paulin, S. Sambolek, and M. Ivasic-Kos, "Application of raycast method for person geolocalization and distance determination using UAV images in Real-World land search and rescue scenarios", en, *Expert Systems with Applications*, vol. 237, p. 121 495, Mar. 2024. DOI: 10.1016/j.eswa.2023.121495.

[15] B. Zhou, H. Zhao, X. Puig, *et al.*, *Semantic Understanding of Scenes through the ADE20K Dataset*, 2016. DOI: 10.48550/ARXIV.1608.05442. [Online]. Available: https://arxiv.org/abs/1608.05442.

[16] T.-Y. Lin, M. Maire, S. Belongie, *et al.*, *Microsoft COCO: Common Objects in Context*, Feb. 2015. [Online]. Available: http://arxiv.org/abs/1405.0312 (visited on 01/23/2024).

[17] M. Cordts, M. Omran, S. Ramos, *et al.*, *The Cityscapes Dataset for Semantic Urban Scene Understanding*, Apr. 2016. DOI: 10.48550/arXiv.1604.01685. [Online]. Available: http://arxiv.org/abs/1604.01685.

[18] A. Geiger, P. Lenz, C. Stiller, and R. Urtasun, "Vision meets robotics: The KITTI dataset", en, *The International Journal of Robotics Research*, vol. 32, no. 11, pp. 1231–1237, Sep. 2013. DOI: 10.1177/0278364913491297.

[19] F. Yu, H. Chen, X. Wang, *et al.*, *BDD100K: A Diverse Driving Dataset for Heterogeneous Multitask Learning*, 2018. DOI: 10.48550/ARXIV.1805.04687.

[20] J. Stallkamp, M. Schlipsing, J. Salmen, and C. Igel, "The German Traffic Sign Recognition Benchmark: A multi-class classification competition", in *IJCNN*, San Jose, CA, USA: IEEE, Jul. 2011, pp. 1453–1460. DOI: 10.1109/IJCNN.2011.6033395.

# AI in Critical Infrastructure – Explainability and Models

Jens Wala
Research Training Group KRITIS, Technical University of Darmstadt, Dolivostraße 15,
64293 Darmstadt, Germany
E-Mails: wala@kritis.tu-darmstadt.de

**Abstract:** Critical infrastructures such as power grids, transportation networks, and water systems are essential to national economies and societal well-being. Integrating Artificial Intelligence (AI) into these systems could enhance productivity and operational resilience. However, the adoption of AI in critical infrastructures necessitates a focus on explainability to ensure transparency, trust, and regulatory compliance. This paper explores inherently explainable models (IEMs) and post hoc explainable models (PHEMs) within the domain of critical infrastructures. By examining regulatory requirements, analyzing different AI models designed for explainability, and comparing these models, this paper provides a comprehensive overview of strategies for selecting AI systems that enhance transparency and compliance. The findings underscore the importance of choosing appropriate AI models to ensure safe, reliable, and legally accountable AI implementation in critical infrastructure, ultimately supporting societal functions and public safety.
*Keywords:* Explainable Artificial Intelligence, Critical Infrastructure, Interpretability, Resilience, Transparency

Erschienen in Tagungsband 35. Forum Bauinformatik 2024, Hamburg, Deutschland, DOI: 10.15480/882.13498
© 2024 Das Copyright für diesen Beitrag liegt bei den Autoren. Verwendung erlaubt unter Creative Commons Lizenz Namensnennung 4.0 International.

## 1 Introduction

Critical infrastructures such as power grids, transportation networks, and water systems form the backbone of national economies and societal well-being. These infrastructures are complex socio-technical systems that require robust monitoring and control mechanisms to ensure efficient and uninterrupted service [1]. Traditionally, automation in critical infrastructure control has relied on control theory and rule-based systems [2]. Control theory is a branch of mathematics dealing with the behavior of dynamic systems with inputs. It uses feedback loops to maintain a system's desired output despite disturbances. In a rule-based system, the logic is explicitly programmed, making the decision-making process easily understandable and verifiable.

Integrating Artificial Intelligence (AI) into these systems could revolutionize their operational capabilities, leading to significant enhancements in productivity and potential reductions in human

resource needs. This evolution is particularly pertinent in the ongoing global skilled worker shortage, which has placed additional pressure on maintaining operational resilience [3].

However, adopting AI technologies in critical infrastructures is not without challenges. Key among these is the need for explainability [3]. Explainability pertains to the ability of stakeholders to understand and trust the decisions made by AI systems [3]. This transparency is crucial for operational trust and compliance with legal standards [4]. Recent legislative developments, such as the European Union's Artificial Intelligence Act (AIA) and Canada's Artificial Intelligence and Data Act (AIDA), have set forth stringent requirements for AI explainability [4], [5], [6]. These regulations aim to ensure that AI systems are effective but also accountable and fair, mitigating risks associated with opaque decision-making processes.

This paper delves into the dual paradigms of inherently explainable models (IEMs) and post hoc explainable models (PHEMs) within the critical infrastructure domain. The paper outlines strategies for selecting AI systems that enhance transparency and compliance by exploring these models, thereby supporting robust and legally sound AI implementation in critical infrastructures. The ensuing sections will review regulatory requirements, analyze different AI models designed for explainability, and compare these models in terms of their practical applications, challenges, and benefits in real-world settings.

## 2 Related Works

The paper by Panigutti et al. [4] explores how the EU's AIA addresses the challenges of AI system opacity. It discusses the Act's transparency and human oversight requirements, particularly for high-risk AI systems. The authors argue that while the Act does not mandate the use of explainable AI (XAI) techniques or transparent-by-design models, it demands comprehensive documentation and effective oversight measures. The paper highlights the limitations of current XAI methodologies. It emphasizes that AI systems can achieve trustworthiness through appropriate transparency and oversight rather than relying solely on technical explainability.

Zschech et al. [7] compare five generalized additive models (GAM) to four black-box learning approaches, classic decision trees, and linear regression, given their performance and degree of interpretability. Both regression and classification tasks have been tested. On twelve datasets, they could show that GAMs outperform the other tested approaches on five of them and find that the discrepancy between the model's performances is minuscule. Tests have been conducted with the recommended parameters provided by the developers of the respective models. Nonetheless, they show that GAM-based models offer a promising direction for achieving both interpretability and competitive predictive performance. The study highlights the potential of intrinsically interpretable models as ethical and technically viable alternatives to black-box models, particularly in critical decision-making areas.

# 3 Regulatory Requirements for AI Explainability

The EU proposed a framework called the Artificial Intelligence Act (AIA) to regulate artificial intelligence in 2021 [5]. The European Parliament unanimously approved the Act on 13 March 2024 [5]. The Act classifies the use of AI into different risk stages depending on the application [3]. Minimal risk applications are those where the AI's impact is deemed negligible, such as spam filters or AI-enabled games. Limited risk applications involve systems that may pose some risk but are not likely to result in significant harm. These include chatbots and virtual assistants. High-risk applications involve AI systems that significantly impact the rights and safety of individuals [8]. These include AI used in healthcare, transportation, and power grids. Unacceptable risk applications are outright prohibited due to their potential for significant harm, such as social scoring by governments or systems that manipulate human behavior.

Critical infrastructure is categorized as high-risk due to the potentially severe consequences that failures or mismanagement in these systems can cause. High-risk systems must meet stringent requirements for transparency and interpretability [8]. This ensures that the decisions made by AI systems can be understood and trusted by human operators [4]. Interpretability is crucial for compliance with legal standards and maintaining operational trust, especially in sectors where AI decisions directly affect human lives and societal functions.

This leads to the following research questions:

- **RQ1:** How can AI models be designed to ensure interpretability and compliance with the regulatory standards set by the EU AIA in high-risk critical infrastructure applications?
- **RQ2:** What are the best practices for implementing and maintaining explainable AI systems in critical infrastructure to enhance transparency, trust, and operational efficiency?

# 4 AI Models for Explainability

Deploying AI models in critical infrastructure necessitates a balance between performance and interpretability. Given the high risk associated with critical infrastructure operations, stakeholders must be able to understand and trust the decisions made by AI systems. This chapter delves into two paradigms of AI explainability: Inherently Explainable Models (IEMs) and Post Hoc Explainable Models (PHEMs), exploring their applications, benefits, and challenges in the context of critical infrastructure.

## 4.1 Inherently Explainable Models (IEMs)

Inherently explainable or interpretable models (IEMs) are designed with transparency as a fundamental feature. These models are constructed so humans can easily understand their operations and decision-making processes. IEMs' characteristics include simplicity, transparency, and ease of interpretation. This allows stakeholders to trust and verify the outputs of these models, making them particularly suitable for high-risk environments like critical infrastructure.

Rule-based automation involves systems that follow predefined rules to perform tasks. These rules are typically "if-then" statements derived from expert knowledge. Rule-based models are easy to understand and implement because they rely on logical conditions that dictate the system's actions. For instance, in a water supply system, a rule might state that if the water level in a reservoir drops below a certain point, a pump should be activated.

Decision trees and linear regression are fundamental types of inherently explainable models. Decision trees are structured as a series of binary decisions, represented as branches, which lead to different outcomes, represented as leaves [9]. The tree's structure makes it straightforward to follow the decision-making process from the root to any leaf, providing clear insight into how a particular decision was reached [9]. Linear regression, on the other hand, models the relationship between a dependent variable and one or more independent variables by fitting a linear equation to observed data. Its simplicity and the direct nature of the relationships it models make linear regression highly interpretable.

Generalized Additive Models (GAMs) extend linear models by including non-linear relationships between the dependent and independent variables while maintaining interpretability [7]. GAMs achieve this by representing the model as a sum of smooth functions of the predictor variables [7]. The advantage of GAMs lies in their ability to provide transparent predictions that can capture complex patterns in the data without sacrificing interpretability [7]. In the context of critical infrastructure, GAMs can be particularly useful. For example, in water supply monitoring and control, a GAM could predict water demand based on temperature, time of day, and historical usage patterns. By understanding these relationships, an autonomous system can make resource allocation and system management decisions and provide operators with the relevant decision information.

These inherently explainable models are crucial for maintaining transparency and trust in critical infrastructure systems. They ensure that the decision-making processes are effective but also understandable and verifiable by human operators, aligning with the stringent requirements for transparency and accountability set forth by regulations like the EU AIA.

### 4.2 Post-Hoc explainable models

In contrast to inherently explainable models, black box models are complex, and their decision-making processes are not easily interpretable [10]. These models, such as deep neural networks and complex ensemble methods, often yield highly accurate predictions but at the cost of transparency [10]. To address this issue, various methods have been developed to make the decisions of these models more understandable.

Post-hoc explainability refers to techniques applied after a model has made its predictions to interpret and explain the results.

One prominent post-hoc explainability technique is Local Interpretable Model-agnostic Explanations (LIME) [10], [11]. LIME works by locally approximating the black box model around a specific prediction with a simpler, interpretable model. By perturbing the input data slightly and observing the

changes in the model's output, LIME constructs a local surrogate model that explains the behavior of the black box model for that particular instance [11]. This approach is valuable for providing instance-level explanations, making understanding why a model made a specific prediction easier.

Another widely used method is SHapley Additive exPlanations (SHAP) [10], [11]. SHAP values are derived from cooperative game theory and represent the contribution of each feature to the model's prediction [11]. By considering all possible combinations of feature values, SHAP provides a consistent and fair attribution of feature importance [11]. This method ensures that the explanations are accurate and theoretically grounded, making it a powerful tool for understanding complex models.

Integrated Gradients is another technique that attributes a neural network's prediction to its input features [12]. It works by computing the gradients of the model's output to its inputs, integrated along a path from a baseline (such as a zero vector) to the actual input [12]. This method highlights the features that contribute most to the prediction, offering insights into the inner workings of the neural network and helping to explain the model's decisions more intuitively.

Post-hoc explainability techniques are essential for making the decisions of black box models more transparent. They enable stakeholders to gain insights into the functioning of complex AI systems, ensuring that these systems can be trusted and their decisions can be validated.

## 5 Comparative Analysis

Following the exploration of Post-Hoc Explainable Models (PHEMs) and Inherently Explainable Models (IEMs), the following table provides a detailed comparison. This comparison uses the following aspects to highlight differences between the explainability approaches:

**Design Philosophy:** This aspect describes the fundamental AI model creation approach. It contrasts the built-in transparency of IEMs with the performance-first approach of PHEMs.

**Transparency** refers to how easily humans can understand the model's decision-making process. It compares the clear, interpretable process of IEMs with the initially opaque nature of PHEMs.

**Compliance:** This aspect addresses how well the models meet regulatory requirements for transparency and accountability, particularly in regulations like the EU AIA.

**Complexity Handling:** This aspect compares how well each model type can handle complex patterns and large datasets, highlighting the trade-offs between simplicity and performance.

**Performance:** This refers to the overall effectiveness of the models in completing their assigned tasks, especially for highly complex problems.

**Trust and Verification:** This aspect addresses how easily stakeholders can trust and verify the decisions made by the AI models, which is crucial in critical infrastructure applications.

| Aspect | Inherently Explainable Models (IEMs) | Post-Hoc Explainable Models (PHEMs) |
|---|---|---|
| **Design Philosophy** | Built with transparency and simplicity from the ground up. | Focused on performance; explanations are derived after the model is built. |
| **Transparency** | High transparency; the decision-making process is clear and interpretable. | Limited initial transparency; relies on additional techniques for explanations. |
| **Compliance** | Meets regulatory requirements for transparency and accountability. | Requires supplementary methods to meet transparency standards. |
| **Complexity Handling** | May struggle with very complex patterns; simplicity can limit performance. | Excels in handling complex patterns and large datasets. |
| **Performance** | Generally lower than black-box models for highly complex tasks. | Higher performance due to complexity but at the cost of initial opacity. |
| **Trust and Verification** | High, as decisions can be easily traced and understood. | Trust needs to be established through post-hoc explanations. |

The EU AIA emphasizes the need for transparency and accountability in AI systems, particularly those classified as high-risk, such as those used in critical infrastructure. In this context, inherently explainable models (IEMs) are uniquely positioned to meet these requirements due to their built-in transparency. By design, IEMs offer a clear and interpretable decision-making process that aligns with the stringent transparency standards mandated by the AIA. This intrinsic interpretability is crucial for critical infrastructure systems where decisions impact public safety, security, and overall societal well-being. Human operators and regulatory bodies can verify and understand the actions of IEMs, which fosters trust and ensures compliance with legal standards.

In contrast, post-hoc explainable models (PHEMs) provide explanations after the model has made its predictions. While PHEMs can offer high performance and handle complex tasks effectively, they require additional techniques to render their decisions interpretable. This adds a layer of complexity and potential uncertainty, making them less straightforward to deploy in highly regulated environments like critical infrastructure.

Therefore, within the framework of the EU AIA, IEMs are the preferred choice for operating critical infrastructure control and monitoring systems. Their inherent transparency provides a robust

foundation for compliance, making them reliable tools for maintaining operational trust and legal accountability.

## 6 Discussion

The integration of AI in critical infrastructure presents both opportunities and challenges. The analysis reveals a preference for Inherently Explainable Models (IEMs) in this context, primarily due to their alignment with regulatory requirements like the EU AIA. Generalized Additive Models (GAMs) offer a promising balance between performance and interpretability.

The skilled worker shortage in critical infrastructure sectors adds urgency to AI adoption. IEMs potentially allow for faster integration and training of existing staff. However, this must be balanced against possible performance trade-offs compared to more complex models.

The tension between performance and explainability remains a key challenge. While Post-Hoc Explainable Models (PHEMs) often offer superior performance in complex tasks, their lack of inherent transparency poses challenges for regulatory compliance and stakeholder trust. Future research should focus on narrowing this gap, potentially through hybrid approaches.

Looking ahead, evolving regulations will continue to shape AI development in critical infrastructure, potentially driving global standards towards greater emphasis on explainability. However, this focus should not compromise system performance or security.

In conclusion, while IEMs offer the most promising path for AI in critical infrastructure, the field remains dynamic. Successful implementation will require collaboration between AI developers, infrastructure managers, policymakers, and ethicists to ensure AI enhances critical infrastructure's resilience, efficiency, and trustworthiness.

## 7 Conclusion

This paper has explored the role of explainable AI models in critical infrastructure, highlighting the preference for Inherently Explainable Models (IEMs) due to their alignment with regulatory requirements and operational needs. While IEMs, particularly Generalized Additive Models, balance performance and interpretability, the tension between model complexity and explainability remains challenging.

The skilled worker shortage in critical infrastructure sectors underscores the urgency of AI adoption, with IEMs potentially offering easier integration and staff training. However, evolving regulations will continue to shape AI development in this field, emphasizing the need for transparency without compromising performance or security.

Moving forward, successful AI implementation in critical infrastructure will require collaboration among AI developers, infrastructure managers, policymakers, and ethicists. Future research should focus on enhancing IEM capabilities, standardizing explainability evaluation frameworks, and

studying the long-term impacts of explainable AI in critical systems. This approach is key to leveraging AI to enhance critical infrastructure's resilience, efficiency, and trustworthiness while meeting regulatory demands.

## References

[1] A. Fekete, Kritische Infrastruktur und Versorgung der Bevölkerung: Klimawandel, Epidemien, digitale Transformation und das Risikomanagement. in essentials. Berlin, Heidelberg: Springer Berlin Heidelberg, 2022. doi: 10.1007/978-3-662-65047-9.

[2] Simrock, “Control Theory,” CERN. Accessed: Jun. 25, 2024. [Online]. Available: https://cds.cern.ch/record/1100534/files/p73.pdf

[3] P. Laplante and B. Amaba, “Artificial Intelligence in Critical Infrastructure Systems,” Computer, vol. 54, no. 10, pp. 14–24, Oct. 2021, doi: 10.1109/MC.2021.3055892.

[4] Cecilia Panigutti, Ronan Hamon, and Isabelle Hupont, “The role of explainable AI in the context of the AI Act,” presented at the Conference on Fairness, Accountability and Transparency, Jun. 2023. doi: 10.1145/3593013.3594069.

[5] “EU AI Act: first regulation on artificial intelligence | News | European Parliament.” Accessed: Jun. 16, 2023. [Online]. Available: https://www.europarl.europa.eu/news/en/headlines/society/20230601STO93804/eu-ai-act-first-regulation-on-artificial-intelligence

[6] Innovation, Science and Economic Development Canada, “The Artificial Intelligence and Data Act (AIDA) – Companion document.” Accessed: Dec. 08, 2023. [Online]. Available: https://ised-isde.canada.ca/site/innovation-better-canada/en/artificial-intelligence-and-data-act-aida-companion-document

[7] P. Zschech, S. Weinzierl, N. Hambauer, S. Zilker, and M. Kraus, “GAM(e) changer or not? An evaluation of interpretable machine learning models based on additive model constraints.” arXiv, Apr. 19, 2022. doi: 10.48550/arXiv.2204.09123.

[8] “ANNEX III AI-Regulation (Proposal) - HIGH-RISK AI SYSTEMS REFERRED TO IN ARTICLE 6(2).” Accessed: Aug. 10, 2023. [Online]. Available: https://lexparency.org/eu/52021PC0206/ANX_III/

[9] J. R. Quinlan, “Simplifying decision trees,” Int. J. Man-Mach. Stud., vol. 27, no. 3, pp. 221–234, Sep. 1987, doi: 10.1016/S0020-7373(87)80053-6.

[10] A. B. Arrieta et al., “Explainable Artificial Intelligence (XAI): Concepts, Taxonomies, Opportunities and Challenges toward Responsible AI.” arXiv, Dec. 26, 2019. Accessed: Dec. 11, 2023. [Online]. Available: http://arxiv.org/abs/1910.10045

[11] S. Lundberg and S.-I. Lee, “A Unified Approach to Interpreting Model Predictions.” arXiv, Nov. 24, 2017. doi: 10.48550/arXiv.1705.07874.

[12] M. Sundararajan, A. Taly, and Q. Yan, “Axiomatic Attribution for Deep Networks.” arXiv, Jun. 12, 2017. doi: 10.48550/arXiv.1703.01365.

# Building facade evaluation using instance segmentation on thermal images

Gerda Cones, Fiona C. Collins and Florian Noichl
Chair of Computational Modeling and Simulation, Technical University of Munich, Arcisstraße 21, 80333 Munich, Germany
E-mail(s): gerda.cones@tum.de, fiona.collins@tum.de, florian.noichl@tum.de

**Abstract:** To advance building energy efficiency assessments, Deep Learning (DL) technologies such as image segmentation can be leveraged to expedite evaluations. Previous research has applied instance segmentation to compute U-values of doors, walls, windows and facades, or has applied semantic segmentation to identify thermal anomalies. This work focused on training a DL instance segmentation model on a rudimentary dataset to discern and categorize different facade elements, including windows, doors, walls, floors, and thermal anomalies. The fine-tuned Mask RCNN ResNet-50+FPN model yielded the following segmentation Average Precision (AP) values: 45.6 (mean AP), 65.2 (window glazing), 53.5 (window), 34.9 (wall) and 17.2 (thermal bridge). The bounding box AP for thermal bridges, 28.6, highlights the model's ability to detect thermal bridges. The results presented in this paper indicate the potential for applying DL instance segmentation to thermal images to identify thermal bridges and estimate U-values using the Infrared Thermovision Technique (ITT). The dataset can be found in https://github.com/gerdac/thermal-images-instance.

*Keywords:* Thermal performance assessment, deep learning, instance segmentation, dataset

Erschienen in Tagungsband 35. Forum Bauinformatik 2024, Hamburg, Deutschland, DOI: 10.15480/882.13553
© 2024 Das Copyright für diesen Beitrag liegt bei den Autoren. Verwendung erlaubt unter Creative Commons Lizenz Namensnennung 4.0 International.

## 1 Introduction

The demand for accurate, rapid and accessible thermal performance assessments of buildings is becoming increasingly larger due to the urgency for efficient buildings. Thermography is being employed to evaluate buildings' envelopes and identify building defects' role on energy performance [1]. A critical factor in understanding heat loss is thermal transmittance, expressed as U-value, which can be determined using theoretical and in-situ methods [2]. However, it is not possible to develop accurate numerical models without knowing the internal structure [3]. Therefore, in-situ building inspections necessitate non-destructive investigations [4] to determine thermal bridging performance [3]. It is crucial to account for thermal bridges' higher heat losses while assessing the building's envelope thermal performance [3]. This work is based on a proof of concept for the integration of Infrared Thermovision Technique (ITT), a non-destructive quantitative infrared thermography (QIRT) technique developed by Albatici, Tonelli, and Chiogna [5] to calculate U-values, and Deep Learning (DL) image segmentation for analyzing thermal images as an approach for enhancing building thermal

performance assessments. This integration brings together the qualitative and quantitative aspects of infrared thermography. The work presented in this paper comprises the development of a rudimentary dataset, transfer learning and preliminary results for DL instance segmentation of windows, walls, doors and thermal bridges within thermal images.

## 2 Related Works

Infrared thermography is useful and time-efficient for in-situ assessment of the overall structure, especially for visible and invisible material defects, moisture and thermal failures [4]. When performing energy assessments, the determination of U-values is imperative [2]. The most widely used methods for U-value determination are the theoretical method, the heat flow meter (HFM) method, the simple hot box-heat flow meter method (SHB-HFM), the thermometric method (THM) and QIRT [2]. QIRT methods use infrared thermography to measure surface temperature, emissivity and reflected temperature [2]. ITT is a QIRT technique for determining U-values and employing the quantitative aspect of infrared thermographhy.

The automation of the qualitative aspect of infrared thermography through image segmentation rises as a possibility thanks to deep learning. However, the ground truth for thermal anomaly segmentation are subject to the potential subjective interpretation of thermographers and the difficulty of establishing definitive boundaries for different anomaly types [6]. One anomaly can be annotated by one expert as a single anomaly, while another expert may separate it into multiple anomalies [6]. This is likely a contributing factor to why image segmentation has not been extensively implemented on thermal images of buildings.

Instance segmentation was employed in the work of Sadhukhan, Peri, Sugunaraj, *et al.* [7] to develop a data-driven three-layered framework to calculate the heat-loss or U-values. Transfer learning was employed on approximately 500 thermal images from campus buildings at the University of North Dakota to train a Mask R-CNN model. The Average Precision (AP) at confidence level 0.50 was 0.67 for windows and 0.46 for facades. The mean Average Precision (mAP) was 0.56. The detection of windows outperformed that of facades, but the mask accuracy as evaluated by IoU was significantly more accurate for facades than windows; the IoUs were 0.50 and 0.05, respectively. To calculate the U-values, the manually annotated thermal images were used instead of the masks obtained from the Mask R-CNN model. Cumulative U-value calculations were used. [7]

## 3 Methodology

Accurate U-value calculations and comprehensive thermal analysis of building facades hinge upon the ability to precisely segment and classify individual components within thermal images. The methodology focuses on creating a specialized dataset for training the model to detect and categorize critical facade elements, such as walls, windows, and thermal anomalies, to accurately estimate U-values.

A dedicated dataset of thermal images collected under controlled weather conditions was manually labeled to train the model. The instance segmentation approach utilizes state-of-the-art tools such as Detectron2 and employs transfer learning strategies to expedite the training process.

Figure 1 depicts the envisioned DL-based approach. The approach is the following: thermal images are used as input for a DL image segmentation model, which results in instance masks for windows, walls, and thermal anomalies. The masks are then visualized for confirmation. These instance masks are then processed using weather and emissivity data to calculate U-values employing the ITT. This work comprises the mentioned steps up to the instance visualization.

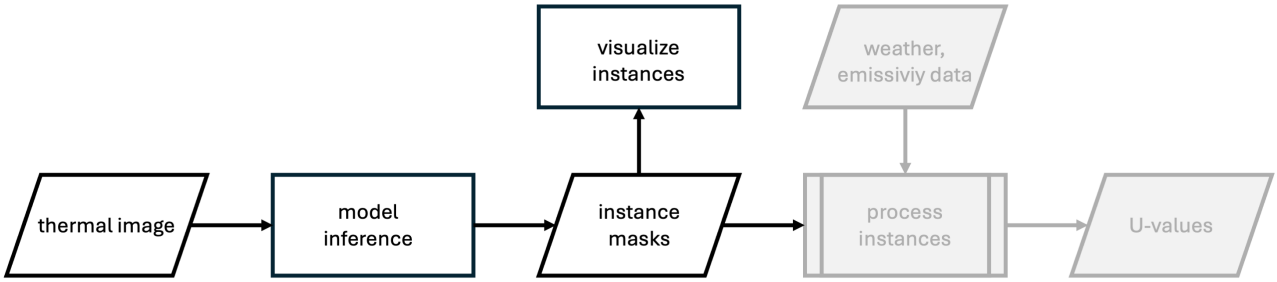


Figure 1: Proposed DL-based Approach for U-value calculation using thermal images. Greyed-out steps are not developed in this work.

### 3.1 Collection of Thermal Images for Dataset Development

To develop the dataset, weather.com was used to check whether the predicted weather conditions adhered to the 24 hours and 12 hours requirements and recommendations outlined in table 1, which tabulates the weather condition requirements and recommendations outlined in [5], [8]–[11]. Adherence to the recommendations and requirements is imperative, as stated in [8] moisture on the wall, radiant heat exchange, and solar radiation can render the values obtained using the thermograph unreliable. Especially with very porous materials, as the thermal conductance of materials is strongly influenced by temperatures and moisture conditions [12]. During collection, a FLIR A50 camera was used to collect thermal radiometric images over the course of two days. The sensors and data loggers listed in table 2 were utilized to confirm the weather condition during collection was as per table 1.

Table 1: Thermal Images Collection Requirements and Recommendations

| Collection conditions | 24 hours before | 12 hours before | During collection |
|---|---|---|---|
| Overcast skies | ▤ [8] | ■ [5] | ■ |
| No solar radiation | - | ▤ [9], [10] | ■ [5] |
| Dry facade | - | - | ■ [5], [8], [11] |
| $\Delta T = T_{int} - T_{out} > \frac{3}{U}$ | ■ [9] | ■ | ■ |
| $\Delta T \geq 5$ ℃ | ■ [9] | ■ | ■ |
| $\Delta T \geq 10$ ℃ | ▤ [10] | ▤ | ▤ |
| $\Delta T \leq \pm 30\%$ | ▤ [10] | ▤ | ▤ |
| $\Delta T_{int} \leq \pm 2$ ℃ | - | - | ■ [9]–[11] |
| $\Delta T_{out} \leq \pm 5$ ℃ | - | - | ■ [9], [11] |
| $\Delta T_{out} \leq \pm 10$ ℃ | ■ [11] | ■ [11] | - |
| Hourly $\overline{v} \leq 5$m/s | ■ [5] | ■ | - |
| $v \leq 0.5$m/s | - | - | ■ [5] |

Recommendations ▤ and Requirements ■.

Table 2: Equipment list

| Equipment | Data collected |
|---|---|
| FLIR A50 camera (serial number 89800406) | thermal, RGB and MSX images |
| anemometer (turbulence testo probe) | wind speed, absolute pressure (m/s, hPa) |
| hygrometer (humidity/temperature testo probe) | humidity, temperature (%RH, ℃) |
| thermometer (globe testo probe Ø 5.9") | temperature (℃) |
| testo data logger and software | logs data from testo probes |
| pyranometer (LICOR LI-200R) | solar radiation (W/m$^2$) |
| LICOR light sensor logger with GPS | GPS coordinates and logs pyranometer data |

### 3.2 Dataset Development

After collecting the thermal images, the images were labelled using V7Labs' online data training platform, V7 Darwin, from v7labs.com. V7Lab's Darwin is an AI data engine that facilitates the labelling process using auto-annotate models. The process is the following: input data, create a workflow, establish the classes, check the data quality and export the labelled data. The classes were: wall, thermal bridge, window (glazing, frame), door (panel, frame), floor, other, foliage, and sky. The classes foliage and sky were discarded and not included in model training.

### 3.3 Model Training and Transfer Learning

The model training and transfer learning was performed in Google's Colaboratory notebooks. The methodology encompassed the following steps. First, Detectron2 [13] was installed and the Detectron2 utilities required were imported. The labelled dataset was pulled directly from V7 Darwin. Then the training, validation and testing splits were established and registered. The training data was then visualized to ensure the labels and metadata were correct. The Detectron2's default trainer's configurations were updated. The Mask RCNN R50-FPN 3x, trained on COCO Instance Segmentation, was chosen as the pre-trained model weights from Detectron2's Model Zoo [13]. A data augmentation program employing transformations to increase variability during the training process was implemented using a custom trainer by modifying the DatasetMapper. The specific transformations applied were: RandomCrop, RandomBrightness, RandomContrast, RandomSaturation, RandomLighting, and RandomFlip. Detectron2's COCOEvaluator [13] was then used to evaluate the models' metrics during training on the training and validation splits. Ultimately, the model was evaluated on the testing split.

## 4 Results

This section delineates the dataset development and inference performance results. Specifics regarding the dataset are outlined and the parameters and benchmarking results of the model are investigated.

### 4.1 Dataset Development

During a 2-day dataset collection period, 577 thermal, 118 RGB, and 114 MSX images were taken of various buildings within the borough of Maxvorstadt, Munich, Germany. The locations are mapped in fig. 2. From these 577 thermal images, several were of the same facade, or from buildings with very

similar construction structures. Therefore, a reduced amount of images were labelled, as the quantity and variety provided by the total dataset could be emulated using data augmentation. Therefore, the following criteria were implemented when filtering the images for labelling. Firstly, images of each building inspected were chosen for labelling, to provide the largest variety of window, door, and wall configurations. The second criterion was using images with several instances to provide highly variable training images when cropping transformations were applied. Thirdly, to improve the class balance, several images containing only walls and thermal bridges were also labelled. The thermal images were labelled using V7 Darwin. The final classes distribution can be seen in table 3, and the labelled and unlabelled images can be found in https://github.com/gerdac/thermal-images-instance.

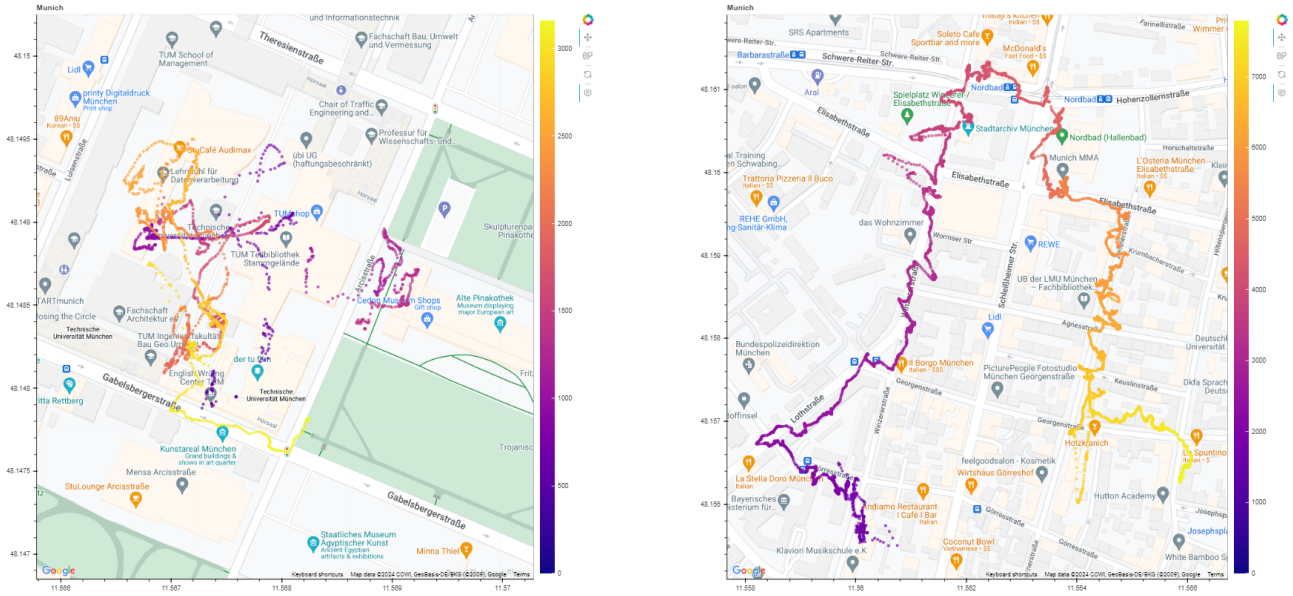


(a) GPS locations day 1.

(b) GPS locations day 2.

Figure 2: GPS locations during dataset collection

## 4.2 Inference Performance

The training hyperparameters used are outlined in table 4, and the AP and AP50 metrics for bounding boxes and segmentation masks are tabulated in table 5. The model demonstrated adequate detection precision to facilitate image segmentation, enabling U-value calculations directly from the segmentation masks, provided no foreign objects for which the model was not extensively trained on were in the foreground. However, the model was unable to identify all thermal bridges in the images. For the thermal bridge above and below the central window in fig. 3 (a), it was likely due to the dispersed appearance of the thermal bridge. The model should have been able to identify the parking sign and the thermal bridges under the top left window due to their stark contrast against the wall. However, due to the undersized training dataset, the model is only able to confidently identify sections of the facade and specific thermal bridges. Lowering the confidence threshold yielded different masks for the thermal bridges and the parking sign, as illustrated in fig. 3. Although lowered thresholds compromise the reliability of precise U-value calculations, the potential for employing differentiated thresholds for thermal bridges warrants consideration, given their irregular shapes and the importance of their

accurate detection in comprehensive building facade analysis. Furthermore, the segm/AP50 values were compared against [7], a related instance segmentation works focused on detecting the following building elements: doors, roofs, facades, beams and windows. Sadhukhan, Peri, Sugunaraj, *et al.* [7] presented AP25, AP50, and AP75 values for windows, facades, and their average in Table 12 of their study. Their model achieved AP50 values of 0.67 and 0.46 for windows and facades, respectively [7]. Comparatively, the model exhibited superior performance in these classes. However, AP values for the remaining classes were not disclosed, likely stemming from class imbalance challenges given the inherent ratio of windows and doors in buildings. This imbalance complicates the model's training process by biasing the more frequently represented classes, which affects the precision and recall of less common classes. [7] encountered similar challenges in detection accuracy, resorting to using their manually annotated images for the U-value calculations of the windows, walls and roofs.

Table 3: Class Distribution

| | Label Classes | Instances |
|---|---|---|
| 1 | wall | 169 |
| 2 | thermal bridge | 344 |
| 3 | window | 389 |
| | a glazing | 796 |
| | b frame | 275 |
| 4 | door | 16 |
| | a panel | 12 |
| | b frame | 13 |
| 5 | floor | 23 |
| 6 | other | 165 |

Table 4: Training Hyperparameters

| Hyperparameter | Value |
|---|---|
| Training split | 75% |
| Validation split | 15% |
| Testing split | 10% |
| Batch | 4 |
| Learning rate | 0.0005 |
| Iterations | 4000 |
| Regions of interest | 128 |

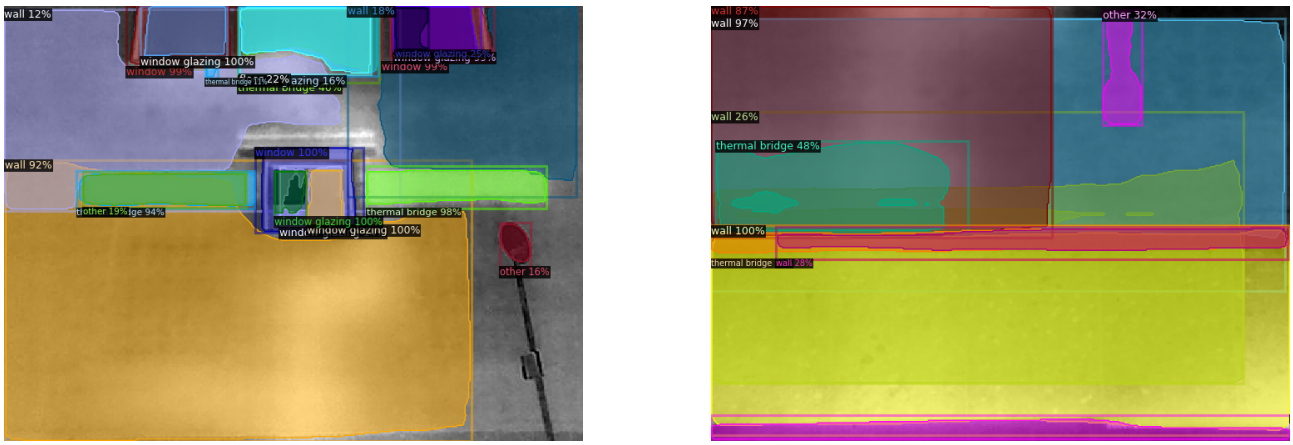


(a) Inference with 10% threshold

(b) Inference with 20% threshold

Figure 3: Segmented images at 10 m using different threshold levels.

## 5 Outlook

The future of thermal performance assessments could be based on non-intrusive U-value calculations or the identification of thermal bridges using deep learning instance segmentation. To enhance the

Table 5: AP values for bounding box and segmentation per class

| Class | bbox/AP | bbox/AP50 | segm/AP | segm/AP50 |
|---|---|---|---|---|
| wall | 39.7 | 67.1 | 34.9 | 50.4 |
| thermal bridge | 28.6 | 43.7 | 17.2 | 40.1 |
| window | 58.5 | 86.1 | 53.5 | 79.5 |
| window glazing | 61.3 | 92.8 | 65.2 | 92.8 |
| window frame | 0.0 | 0.0 | 0.0 | 0.0 |
| door | 70.0 | 100.0 | 80.0 | 100.0 |
| door panel | 80.0 | 100.0 | 80.0 | 100.0 |
| door frame | 0.0 | 0.0 | 0.0 | 0.0 |
| floor | 90.0 | 100.0 | 90.0 | 100.0 |
| other | 47.9 | 85.1 | 45.1 | 66.5 |

accuracy of the approach, improvements to the class balance and the implementation of panoptic segmentation could be pursued.

Improving the balance of the classes is a key factor for improving the model. For a fully functioning robust model all aspects of a facade should be included. Additionally, the instances labelled "other" were in fact different types of objects that are typically present in front of a facade. For future models, it could be beneficial to separate these items even further, or to leverage existing models that can identify these common items such as bikes, cars, people, and light fixtures.

For thermal bridges with dispersed heat loss and amorphous shapes, integrating instance and semantic segmentation, as in panoptic segmentation, offers a promising approach to delineating various facade elements while simultaneously flagging the presence of thermal bridges. Panoptic segmentation's dual capability to classify both discrete objects and amorphous regions, could be particularly effective for implementing the thermal bridge-specific Anomaly Identification Metric as developed by Kakillioglu, Masri, Pan, *et al.* [6], which severs the one-to-one instance dependency associated with instance segmentation. Leveraging the semantic component of the panoptic model to label pixels as thermal anomalies, irrespective of their sizes and shapes, while achieving accurate segmentation of building facade elements, has the potential to result in a robust model for thermal inspections.

## 6 Conclusion

This work contributes significantly to the advancement of building energy efficiency through the development of a rudimentary database to fine-tune an existing DL instance segmentation Mask RCNN ResNet-50+FPN backbone model for the analysis of thermal images. The model yielded the following AP values: 45.6 (mAP), 65.2 (window glazing), 53.5 (window), 34.9 (wall) and 17.2 (thermal bridge). The bounding box AP for thermal bridges, 28.6, suggests the model is able to detect thermal bridges but struggles with their amorphous shapes. This work sets the foundation for implementing DL instance segmentation on thermal images to identify thermal bridges and compute U-values using ITT.

## References

[1] T. Rakha, Y. E. Masri, K. Chen, E. Panagoulia, and P. D. Wilde, “Building envelope anomaly characterization and simulation using drone time-lapse thermography”, *Energy and Buildings*, vol. 259, Mar. 2022. DOI: 10.1016/j.enbuild.2021.111754.

[2] D. Bienvenido-Huertas, J. Moyano, D. Marín, and R. Fresco-Contreras, *Review of in situ methods for assessing the thermal transmittance of walls*, Mar. 2019. DOI: 10.1016/j.rser.2018.12.016.

[3] M. O’Grady, A. A. Lechowska, and A. M. Harte, “Application of infrared thermography technique to the thermal assessment of multiple thermal bridges and windows”, *Energy and Buildings*, vol. 168, pp. 347–362, Jun. 2018. DOI: 10.1016/J.ENBUILD.2018.03.034.

[4] A. Tavukçuoğlu, “Non-destructive testing for building diagnostics and monitoring: Experience achieved with case studies”, *MATEC Web of Conferences*, vol. 149, p. 01 015, 2018. DOI: 10.1051/matecconf/201814901015.

[5] R. Albatici, A. M. Tonelli, and M. Chiogna, “A comprehensive experimental approach for the validation of quantitative infrared thermography in the evaluation of building thermal transmittance”, *Applied Energy*, vol. 141, pp. 218–228, Mar. 2015. DOI: 10.1016/j.apenergy.2014.12.035.

[6] B. Kakillioglu, Y. E. Masri, C. Pan, *et al.*, “A performance metric for the evaluation of thermal anomaly identification with ill-defined ground truth”, in *EG-ICE 2021 Workshop on Intelligent Computing in Engineering, Proceedings*, 2021, pp. 401–410.

[7] D. Sadhukhan, S. Peri, N. Sugunaraj, *et al.*, “Estimating surface temperature from thermal imagery of buildings for accurate thermal transmittance (u-value): A machine learning perspective”, *Journal of Building Engineering*, vol. 32, 2020. DOI: 10.1016/j.jobe.2020.101637.

[8] G. Dall’O’, L. Sarto, and A. Panza, “Infrared screening of residential buildings for energy audit purposes: Results of a field test”, *Energies*, vol. 6, pp. 3859–3878, 8 2013. DOI: 10.3390/en6083859.

[9] *Thermal Performance of Buildings-Qualitative Detection of Thermal Irregularities in Building Envelopes-Infrared Method*, BS EN 13187:1999. London, UK, May 1999.

[10] *Thermal insulation — Qualitative detection of thermal irregularities in building envelopes — Infrared method*, ISO 6781:1983(E). Switzerland, 1983.

[11] D. Bienvenido-Huertas, R. Rodríguez-Álvaro, J. J. Moyano, F. Rico, and D. Marín, “Determining the u-value of facades using the thermometric method: Potentials and limitations”, *Energies*, vol. 11, 2 Feb. 2018. DOI: 10.3390/en11020360.

[12] G. Ficco, F. Iannetta, E. Ianniello, F. R. D. Alfano, and M. Dell’Isola, “U-value in situ measurement for energy diagnosis of existing buildings”, *Energy and Buildings*, vol. 104, pp. 108–121, Jul. 2015. DOI: 10.1016/j.enbuild.2015.06.071.

[13] Y. Wu, A. Kirillov, F. Massa, W.-Y. Lo, and R. Girshick, *Detectron2*, https://github.com/facebookresearch/detectron2, 2019.

# Integrating Dynamic Environment Modelling with Reinforcement Learning for Fire Safety Design

Isabelle Fitkau[1]

[1]Department of Civil Systems Engineering, Institute of Civil Engineering, Technische Universität Berlin, Gustav-Meyer-Allee 25, 13355 Berlin, Germany

E-Mails: i.fitkau@tu-berlin.de

**Abstract:** Escape path planning belongs to the domain of fire safety design in buildings, ensuring the safety of individuals during emergencies. Applied Reinforcement Learning (RL) research has focused on optimizing training for simple evacuation scenarios. Research findings indicate that agents can learn to escape environments using path-planning methods. However, it has yet to be considered in depth how immediate changes to the environment affect the learning process. By using dynamic environment modeling, the agent can learn to modify floor plans based on the results of escape paths. This approach leads towards a performance-based validation tool, where the results of evacuation path planning can be used to, e.g., support regulatory compliance checks. Our work focuses on creating a reinforcement learning environment that simulates a floor plan to train the agent to identify escape paths and strategically optimize the layout by placing the exits for evacuation. The environment creation is based on a grid-based environment using a discrete action space. This allows for fast prototyping since learning in environments with fewer choices leads to less variability of outcomes and facilitates comparison with existing research, which the study addresses regarding reproducibility and comparability of the environments and the robustness of the algorithm's outcomes.

*Keywords:* reinforcement learning, fire safety design, dynamic environment modeling, performance-based validation

Erschienen in Tagungsband 35. Forum Bauinformatik 2024, Hamburg, Deutschland, DOI: 10.15480/882.13532
© 2024 Das Copyright für diesen Beitrag liegt bei den Autoren. Verwendung erlaubt unter Creative Commons Lizenz Namensnennung 4.0 International.

## 1 Introduction

Fire safety is a multifaceted domain within construction, impacting various other areas. For example, including openings can influence structural design, while fire safety systems like sprinklers can affect MEP design. Additionally, the layout of escape routes can significantly impact the overall floor plan. The collaboration between floor plan designers and those responsible for compliance checking is

not just beneficial but crucial for the safety of the building's occupants. Ensuring compliance with prescribed and safety goal-oriented fire safety requirements involves a lengthy process, as automated methods also demand extensive knowledge [1]. The building design must be continually updated to reflect changes made by designers from other fields to meet fire safety standards. Escape paths, crucial for ensuring the safety of occupants, represent a fire safety aspect of floor plan design that must comply with cross-domain fire safety requirements. These are closely linked to room layouts, door placements, component parameters, and systems such as fire extinguishers. The principle of reinforcement learning (RL), which utilizes machine learning to optimize a simulation environment through continuous adaptation and learning, has been explored in existing research [2] - [4]. This research primarily focuses on optimizing training specifications to determine escape paths in static environments that do not change dynamically.

However, the application of RL in modifying floor plans based on escape path knowledge has yet to be thoroughly explored. A key question is whether an RL agent can be trained to develop fire-safe floor plans or improve existing ones by simulating escape path scenarios and making corresponding adjustments to the layout. The goal of setting up an environment for training an RL agent to recognize escape paths and strategically position fire safety elements, such as doors, based on pathfinding outcomes by incorporating dynamic environment modeling into the agent's learning process has been addressed only in a preliminary form [5]. This work presents the initial approaches that facilitate the development of a performance-based validation tool. It employs a more complex yet still straightforward methodology, which, through its implementation, focuses on identifying efficient and feasible environmental variables. These variables can then be utilized to describe the optimal environment for the specified use cases. Utilizing a grid-based environment with a discrete action space fulfills the requirement for more efficient prototyping.

The paper opens by reviewing the latest research and categorizing its contributions. It then describes the background and methodology for developing the prototype with dynamic environment modeling and shares initial results. The paper ends with a discussion of future research directions.

## 2 Background

Understanding that learning occurs through interaction with the environment is essential to grasp the nature of learning. Reinforcement learning (RL) is a computational method centered on goal-directed learning through interaction and maximizing reward signals. This approach involves discovering which actions yield the highest rewards through trial and error, without direct instructions, and observing the long-term consequences of actions [6].

RL has been used to model human behavior and interactions during emergencies in escape scenarios. While RL environments do not necessarily depend on visual representation, appropriate visualization can enhance realism and facilitate the agent's tasks by tracking its actions. For instance, one study simulates realistic fire scenarios and tests pre-trained agents on a large, complex building model represented solely as a graph, demonstrating scalability without visuals. The results indicate that combining off-policy, model-free algorithms improves performance in real-world fire evacuation

emergencies [2]. Several studies advocate for explicit visualization methods. One research paper employs a grid-based approach to pathfinding, discussing how an agent decides on escape routes [7]. Another study examines evacuation routes in a single room with multiple exits and obstacles [4]. Additionally, a framework using deep reinforcement learning in a 3D environment simulates crowd evacuation, analyzing how height, mass, and exit width affect evacuation dynamics [3]. Another piece of research applies RL to enhance emergency evacuation drills, using a controlled 3D environment where an agent trained as an evacuation leader streamlines the evacuation process for more efficient management [8]. Others employ tools such as Unity to adapt to the real-world needs of case studies that require it, such as active shooter incidents. The subsequent analysis then considers the understanding, implementation, and investigation of the impact of building design parameters on evacuations [9].

Despite the advancements, existing research critiques these models' static nature and lack of real-world features [2] - [4]. Dynamic environment modeling for escape scenarios using continuous ranging state and action spaces shows promise but necessitates extensive test runs and prolonged training [5]. Further research is needed on dynamic (non-stationary) modeling approaches within environments that yield faster results, such as using discrete action spaces to influence the decision-making process. Our proposed research framework aims to fill these gaps by integrating dynamic modeling into RL environments for escape scenarios, addressing the limitations of current models.

## 3 Methodology

Planning escape routes for emergency evacuation scenarios focuses on pathfinding individuals affected by the situation. Human movement patterns, which form these escape routes, can be modeled using various approaches. Our prototype movement is modeled using discrete action spaces within a grid-based environment. This approach translates navigation through the floor plan into numerical values, such as 0 for moving left, 1 for moving right, and 2 for moving straight. The agent then moves through the floor plan by executing these actions, progressing from point A (the starting point) to point B (the emergency exit or terminated state), thereby learning the escape path within the environment.

Concurrently, the agent must learn to apply the insights gained from escape path learning to modify the floor plan. This process involves adapting to changes in the environment during the agent's learning or training episodes. Therefore, the environment model must support a suitable action space and dynamic changes to facilitate effective learning and adaptation. Dynamic environment modeling refers to the capacity to alter the state of the environment within an ongoing episode in response to actions taken by an agent or external factors. Depending on the task, most RL environments within modeling frameworks remain stationary throughout an episode (initialized at the start and reset at the end). In evacuation scenario planning, pathfinding maps human movement through escape routes. These movement patterns can be modeled using simulations that support dynamic environment modeling, essential for adapting the floor plan during training. As the agent learns and

interacts with the environment, this approach enhances the applicability of the learned escape paths under varying conditions.

In our work, we employed the technique of prototyping to generate initial results for our approach. This entailed a continuous loop of developing, testing, demonstrating/visualizing, and refining the RL environment. Prototyping is beneficial as it allows us to improve the model iteratively, ensuring it accurately reflects real-world conditions and effectively adapts escape paths. This method aligns with our approach by enabling hypothesis testing, repeated experimentation, and ongoing refinement based on visualized results. A summary of RL modeling frameworks was conducted to develop an effective workflow for the simultaneous learning of escape paths and design decisions. This entailed the utilization of Farama's *Miniworld* [10] for the modeling of the environment, implementing reliable and widely-used RL algorithms via *Stable Baselines 3* [11], and *wandb.ai* [12] for the logging and tracking of experiments. The model was trained using the Proximal Policy Optimization Algorithm (PPO) [13].

# 4 Results

## 4.1 The environment

The agent's objective is to navigate from a starting point, designated as A, to a goal location, defined as B. The agent is randomly positioned at various starting locations, as described in section 4.2. The agent learns to navigate to B, the terminated state, solely through the input provided by the environment setup, the action and observation space, and the reward function.

The prototype we are discussing is a simple setup of three rooms and a hallway on an 8x20m floor. Four walls surround the arena, which are fixed in size and cannot be escaped. Another five walls separate the floor, each separating two rooms. The hallway has a door leading to a staircase, representing the terminated state (the target) where the agent reaches safety (see Figure 1). The partition walls have a sensor that detects the agent's touch when he decides to move through it, automatically creating a door. This door, represented by a passage, is placed where the agent touched the partition wall, enabling the agent to pass from one room into the other (see Figure 2). During reset, all placed doors are removed.

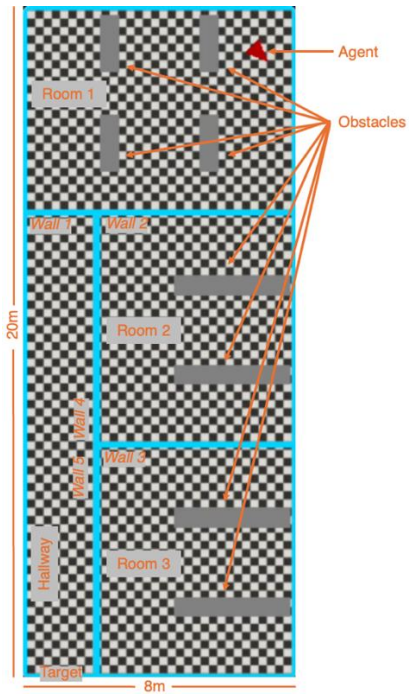


Figure 1: The environment set-up.

The duration of an episode is set to 3000 steps before resetting for a new episode. This timeframe was identified as pertinent for the agent to explore and locate the target in initial test runs. Tables 1 and 2 present the action and observation spaces. The rewards have been refined during several

prototyping steps and are meant to foster fast escape times. We tend to model a realistic environment that includes design aspects such as regulatory requirements (e.g., hallways have higher fire resistance requirements) without introducing too many biases simultaneously.

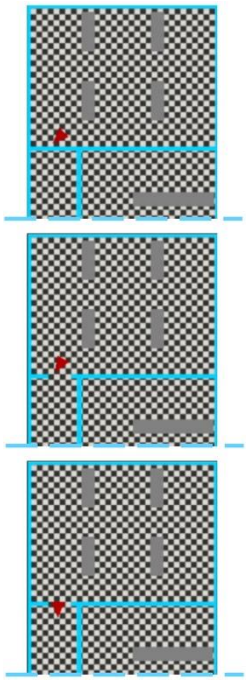

Figure 2: Dynamic environment modeling during an episode (example Room 1; applies to all walls once per episode).

The rewards are given as follows:

1. *reward += 1 / (distance_to_terminal + 1)* for reducing the distance to the target, else:
   *reward -= 0.5 / (distance_to_terminal + 1)*
2. *reward += 100* for creating a door
3. *reward += 0.5* for being in the hallway
4. *reward += 3000* for step-count < 1000,
   *reward += 2000* for 1000 < step-count < 2000,
   *reward += 1000* for 2000 < step-count < 3000
   for termination
5. *reward -= 500* for truncation

The prototype resulted in some assumptions (partly adjusted from [5]) and parameters being set as 1) fixed set up of floor plan walls, 2) no orientation/sight included for the agent – the agent neither has knowledge of the escape path nor a lidar sight or else implemented, 3) the door he positions through walking towards the exit has a fixed size and cannot be moved again during an episode and 4) the obstacles represent simplified furniture (e.g., office tables) and do not move or change sizes during training.

Table 1: Action Space.

| turn_left | turn_right | move_forward | action_space |
|---|---|---|---|
| 0 | 1 | 2 | discrete(3) |

Table 2: Observation Space.

| agent position | direction of agent | target B position | distance to target B | encoded room name | observation_ space |
|---|---|---|---|---|---|
| x, y, z | angle | x, y, z | length | [1, 0, 0, 0] | Box(11) |

## 4.2 The findings

Preliminary results indicate that when using the environment described in section 4.1, the agent can learn to navigate the environment for the trained number of steps and position doors within the floor plan based on its learned optimal escape path. The mean reward throughout the training can differ slightly for the mean length of an episode as the agent is randomly placed in a room by episodes reset, frequently changing the distance and location to the target.

Transfer learning during prototyping, resulting in the training results below (see Figure 3). *Run 0* has been conducted by placing the agent in four starting positions in Room 1 randomly. The resulting paths are shown in Figure 3a. After discovering and solving an environmental bug of too large of the

obstacles bounding boxes, we reran the training but overfitted to the former solution of *run 0*. Then, we conducted *run 1* using the 6mio-global step result model from *run 0*, representing half of the experiences and final learnings of *run 0*-agent (see Figure 4), which led to more exploratory and expected results (see *run 1*-paths of Figure 3b). Then, we transferred the final learning of *run 1* and added three starting positions A in Room 2, resulting in seven starting positions A for *run 2*. For the last *run 3*, we added three starting positions A in Room 3 to the existing ones, leaving us with ten starting positions A and the final learning of run 2, which resulted in the learning of paths shown in Figure 3b. Figure 4 presents the transferred learning from one run to another. Except for the described reusing of run 0 for run 1, all the other transfers used the learning results at the end of each training run, e.g., final learning at 9mio global steps of *run 1* for the start of *run 2*.

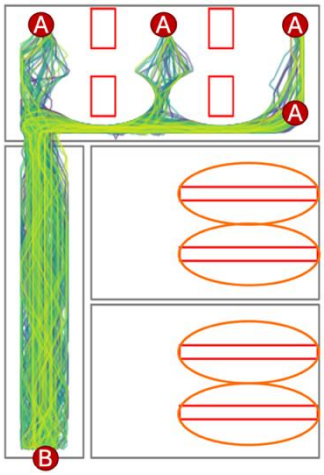


Figure 3a: Prelimary paths shown for *run 0*. Bounding boxes of obstacles represented with orange circles.

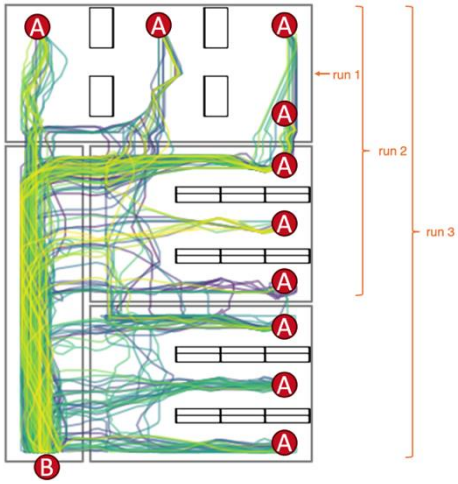


Figure 3b: Visualization of paths and sequence of runs after resolving the environmental bug of bounding boxes.

Figure 3: A typical sequence of prototyping. The paths shown in 3a (*run 0*) resulted from the fact that the obstacles bounding boxes prevented the agent from moving in certain areas (orange circles). After resolving the environmental bug, 3b shows the transfer learning results (*run 1*, then *run 2*, then *run 3*).

## 5 Discussion and Conclusion

This paper presents a novel approach to integrating dynamic environment modeling within a reinforcement learning (RL) framework. The objective is to optimize escape paths in evacuation scenarios. The agent modifies its environment dynamically by placing doors and learning optimal escape routes through interaction and adaptation. The discrete state and action space, operating within the defined range of motion, yielded usable, rapid results and facilitated additional refinement steps within the prototype method.

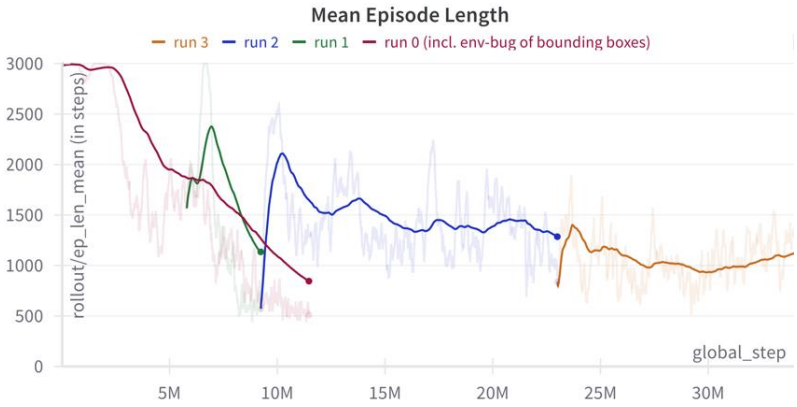


Figure 4: The agents mean episode length. *run 0* equals the training results shown in Figure 3a. To avoid overfitting: training *run 1* starts using the 6mio-global step result model from *run 0*.

Nevertheless, several limitations require further attention in future research. The static nature of the floor plan and the fixed size of components like doors restrict the adaptability of our model. Implementing scalable solutions for floor plan creation and additional building elements will assist in creating more realistic scenarios. Implementing scalable solutions for floor plan creation and additional building elements will assist in creating more realistic scenarios. The preliminary results indicate that incorporating orientation awareness and lidar sight could enhance the agent's human-like characteristics, thereby improving the efficacy of the training process. Furthermore, investigating the integration of semantic knowledge (e.g., hot-encoded room names) of learning outcomes would enhance the model's realism. Fine-tuning the algorithm's hyperparameters is paramount to achieving stable learning. Implementing advanced strategies to avoid local optima could enhance the current prototype’s complexity and deceptive rewards [14]. The PPO algorithm [13] proved beneficial; however, the dynamic environment setup requires an in-depth sensitivity analysis of variables and parameters.

This novel approach to escape path planning in a dynamic RL environment demonstrates promising results, indicating both feasibility and potential benefits for performance-based validation, such as developing authority compliance checks. Future work will focus on enhancing the environment's scalability and flexibility and fine-tuning algorithms to reflect realistic conditions better. This research contributes to advancing adaptive RL systems, which can inform the design of safer floor plans for fire safety.

## References

[1] I. Fitkau and T. Hartmann, “An ontology-based approach of automatic compliance checking for structural fire safety requirements,” *Adv. Eng. Inform.*, vol. 59, p. 102314, Jan. 2024, doi: 10.1016/j.aei.2023.102314.

[2] J. Sharma, P.-A. Andersen, O.-C. Granmo, and M. Goodwin, “Deep Q-Learning With Q-Matrix Transfer Learning for Novel Fire Evacuation Environment,” *IEEE Trans. Syst. Man Cybern. Syst.*, vol. 51, no. 12, pp. 7363–7381, Dec. 2021, doi: 10.1109/TSMC.2020.2967936.

[3] D. Zhang *et al.*, “Deep reinforcement learning and 3D physical environments applied to crowd evacuation in congested scenarios,” *Int. J. Digit. Earth*, vol. 16, no. 1, pp. 691–714, Oct. 2023, doi: 10.1080/17538947.2023.2182376.

[4] Y. Zhang, Z. Chai, and G. Lykotrafitis, “Deep reinforcement learning with a particle dynamics environment applied to emergency evacuation of a room with obstacles,” *Phys. Stat. Mech. Its Appl.*, vol. 571, p. 125845, Jun. 2021, doi: 10.1016/j.physa.2021.125845.

[5] I. Fitkau and T. Hartmann, “Applying Reinforcement Learning for Design Decisions on Fire Safety Requirements in a Fire Evacuation Environment,” in *Proceedings of the 31st EG-ICE International Workshop*, Vigo, Spain, Jul. 2024. Accessed: Aug. 25, 2024. [Online]. Available: https://3dgeoinfoeg-ice.webs.uvigo.es/proceedings

[6] R. S. Sutton and A. G. Barto, *Reinforcement learning: an introduction*, Second edition. in Adaptive computation and machine learning series. Cambridge, Massachusetts: The MIT Press, 2018.

[7] P. Wongsai and W. Pawgasame, “A Reinforcement Learning for Criminal’s Escape Path Prediction,” in *2018 5th Asian Conference on Defense Technology (ACDT)*, Hanoi: IEEE, Oct. 2018, pp. 26–30. doi: 10.1109/ACDT.2018.8593191.

[8] N. Sinpan, P. Sasithong, S. Chaudhary, S. Poomrittigul, N. Leelawat, and L. Wuttisittikulkij, “Simulative Investigations of Crowd Evacuation by Incorporating Reinforcement Learning Scheme,” in *Proceedings of the 6th International Conference on Algorithms, Computing and Systems*, Larissa Greece: ACM, Sep. 2022, pp. 1–5. doi: 10.1145/3564982.3564983.

[9] R. Liu, W. Wu, B. Becerik-Gerber, and G. M. Lucas, “Enhancing Building Safety Design for Active Shooter Incidents: Exploration of Building Exit Parameters using Reinforcement Learning-Based Simulations,” in *Proceedings of the 31st EG-ICE International Workshop*, Vigo, Spain, Jul. 2024. Accessed: Aug. 25, 2024. [Online]. Available: https://3dgeoinfoeg-ice.webs.uvigo.es/proceedings

[10] M. Chevalier-Boisvert *et al.*, “Minigrid & Miniworld: Modular & Customizable Reinforcement Learning Environments for Goal-Oriented Tasks,” Jun. 23, 2023, *arXiv*: arXiv:2306.13831. Accessed: Jul. 07, 2024. [Online]. Available: http://arxiv.org/abs/2306.13831

[11] A. Raffin, A. Hill, A. Gleave, A. Kanervisto, M. Ernestus, and N. Dormann, “Stable-Baselines3: Reliable Reinforcement Learning Implementations,” *J. Mach. Learn. Res.*, vol. 22, no. 268, pp. 1–8, 2021.

[12] L. Biewald, “Experiment Tracking with Weights and Biases.” 2020. [Online]. Available: https://www.wandb.com/

[13] J. Schulman, F. Wolski, P. Dhariwal, A. Radford, and O. Klimov, “Proximal Policy Optimization Algorithms,” 2017, *arXiv*. doi: 10.48550/ARXIV.1707.06347.

[14] Q. Wu, S. Zhao, F. Zhou, H. Zhang, Y. Huang, and K.-K. Ma, “Cognitive Escape Reinforcement Learning for Complex Decision Making,” Mar. 23, 2023. doi: 10.21203/rs.3.rs-2661516/v1.

# Teil II

# Sensors & Robotics

# A scalable smart irrigation system based on Internet of Things technologies

Carlos Chillón Geck and Rami Nasr
Institute of Digital and Autonomous Construction, Hamburg University of Technology, Blohmstraße 15, 21079 Hamburg, Germany
E-mail: carlos.chillon.geck@tuhh.de

**Abstract:** Internet of Things (IoT) technologies have reduced the need for manual labor in agriculture by facilitating the automation of irrigation processes. To automate irrigation, IoT-based irrigation systems consisting of low-cost hardware components have been proposed, aiming at optimizing irrigation and reducing overall costs. However, the design of IoT-based irrigation systems is based on ad-hoc solutions that lack scalability and integration capabilities. This paper presents a scalable smart irrigation system based on IoT technologies, developed using the OPC Unified Architecture (OPC UA). The system includes low-cost hardware components with embedded computing and IoT communication capabilities as well as an open-source IoT platform, which is validated in a laboratory test. The results of the validation test highlight the effectiveness of the scalable smart irrigation system in enhancing water resource management and operational efficiency.

*Keywords:* Smart irrigation, Internet of Things, OPC UA, scalable systems.

Erschienen in Tagungsband 35. Forum Bauinformatik 2024, Hamburg, Deutschland, DOI: 10.15480/882.13494
© 2024 Das Copyright für diesen Beitrag liegt bei den Autoren. Verwendung erlaubt unter Creative Commons Lizenz Namensnennung 4.0 International.

## 1 Introduction

As the global population continues to grow, projected to surpass 8.5 billion by 2030, the challenges of food security and water scarcity become more pronounced [1]. Thus, innovative irrigation solutions in agriculture are essential to meet the increasing food demands and to ensure sustainable agricultural practices. In particular, wireless sensor networks and Internet of Things (IoT) technologies have reduced the need for manual labor, making automation in agriculture more feasible [2]. Numerous studies on precision agriculture and smart irrigation systems have explored different approaches to enhance water efficiency [3]. Several studies proposed low-cost IoT-based prototypes that optimize water usage through automatic control of irrigation based on soil moisture and environmental conditions for intelligent scheduling [4]. Yet, research often overlooks scalability and integration aspects into irrigation systems. Ensuring compatibility among different hardware components is crucial to achieve flexibility that supports diverse infrastructures, ranging from agricultural farms to urban

gardening. Scalable systems may be adapted to various agricultural operations, from small farms to large plantations, and it may be easily upgraded when operations expand. Integration with diverse technologies, such as drones and satellite imaging, also requires scalability and integration among different technologies for effective decision-making.

Few studies focus on scalability and integration in smart irrigation. For example, IoT with aerial mapping technologies using mesh networks for sensor communication and cloud computing for data processing and storage have been proposed [5], also including data from wireless sensor networks for precision agriculture [6]. Other research focuses on automating irrigation with multi-agent systems [7], which inherently enable scalability by managing an increasing number of sensors and agents [8]. However, scalability and integration are not explicitly addressed. To address this gap, in this paper, the OPC Unified Architecture (OPC UA) is adopted to implement a scalable smart irrigation system using IoT technologies. OPC UA provides a framework for integrating devices and systems across manufacturers and communication protocols [9]. By leveraging an OPC UA server, scalability is explicitly addressed, structuring data and communication. OPC UA enhances scalability and facilitates asset integration, allowing smart irrigation systems to adapt and expand to meet evolving demands and technological advancements.

# 2 Design of a scalable smart irrigation system

## 2.1 System requirements

In Table 1, the functional requirements that define the operational capabilities of a scalable smart irrigation system are summarized. Requirements not directly related to scalability are (1) actuators enabled by automated control algorithms, (2) user-friendly interfaces with features including visualization of information for decision-making, data querying and analysis features, alerts for system fault detection, and (3) efficient data storage. Moreover, non-functional requirements are considered for developing of the system include cost efficiency and security.

Table 1: Functional requirements of a scalable smart irrigation system.

| Requirements | Description |
|---|---|
| Semantic richness | Semantically enrich data with metadata and context to enable comprehensive understanding of irrigation data and instantiatino of system elements based on a formal asbtract model. |
| Data integration | Collect data from various devices, including a robust data ingestion connector, designed to interface with specified external communication protocols for collecting real-time data from various sources. |
| Scalability and modularity | Provide scalability, capable of expanding to accommodate additional sensors or devices without significant modifications to the core system architecture. |

## 2.2 System architecture

The system architecture is defined based on the requirements listed above. The proposed system integrates an OPC UA framework into an IoT layered architecture using standard information modeling. In Figure 1, the interconnected system layers are illustrated, encompassing agents, each of which devised to solve specific tasks:

- *Assets layer*: The physical components, such as sensor nodes and actuators, are interfaced with the digital system.
- *Integration layer*: In this layer, embedded software standardizes the raw data collected by sensors into a consistent format for further processing.
- *Communication layer*: Receives information on which data must be collected and uses standard protocols for data communication.
- *Information and aggregation layer*: The OPC UA server is the centerpiece of this layer. OPC UA employs an information model, serving as a schema to standardize the sensor data. The information model enables integrating sensor data regardless of the source and format and facilitates model instantiation.
- *Functional layer:* In this layer, the data is stored and irrigation schedules are created, which are then executed to control the irrigation process efficiently.
- *Business layer:* Translates the operational efficiencies into business value, producing visual analytics for strategic planning and decision-making. Real-time ("live") monitoring and the ability to override automated decisions are provided through a dashboard.

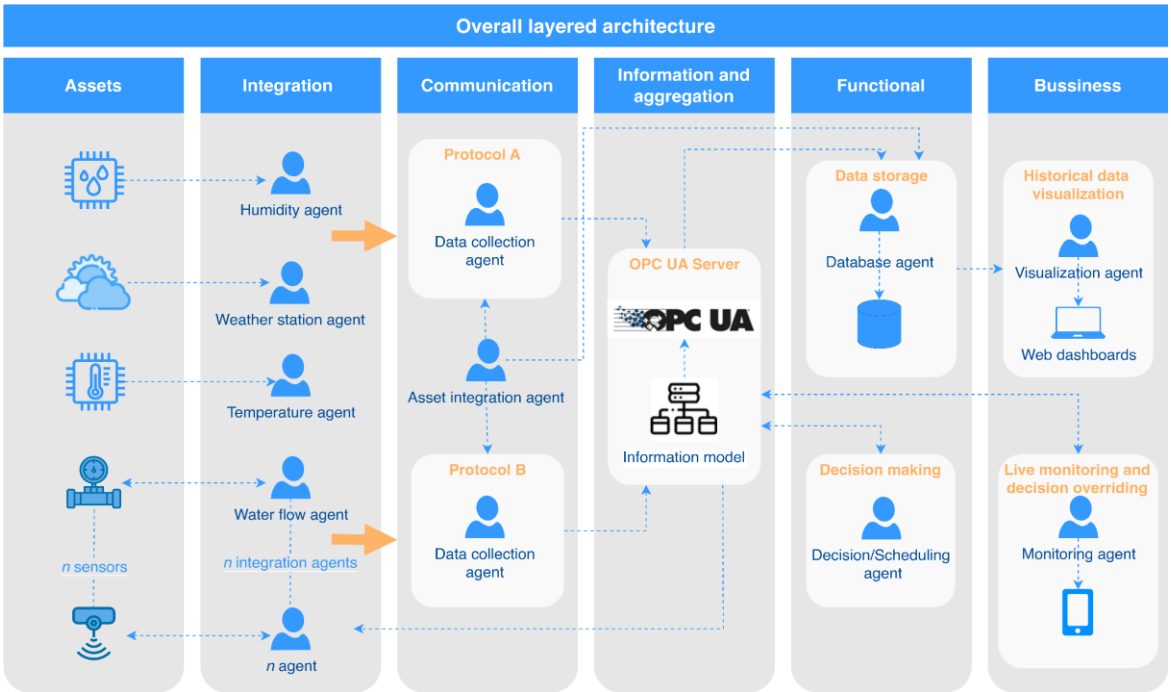


Figure 1: Layered architecture of the smart irrigation system.

# 3 Implemention of the smart irrigation system

This section describes the prototype implementation of the smart irrigation system, with emphasis of the agents situated in the different layers intoroduced above.

## 3.1 Assets and integration layer

The assets layer encompasses the hardware used to create the smart irrigation system. For implementation, the hardware components listed in Table 2 are used with a pump and relays. The ESP-32 S3 microcontrollers handle real-time data collection from the sensors and control the actuators based on the input signals received from the Raspberry Pi. The integration layer is where diverse sensors represented by dedicated agents, in which a Raspberry Pi serves as the central hub, aggregating data from the microcontrollers, running decision-making algorithms, and providing a user interface for monitoring and control. The integration layer employs common industrial communication protocols, such as message queuing telemetry transport (MQTT) for lightweight and efficient messaging, to forward standardized and semantically enriched data to the communication layer. The hardware components are chosen with respect to reliability, cost-effectiveness, and compatibility with IoT-based smart irrigation systems.

Table 2: Hardware components, as part of the asset layer.

| Component | Quantity | Purpose |
|---|---|---|
| AZ Delivery v1.2 capacitive soil moisture sensor | 2 | Measure and monitor the soil humidity levels. |
| Analog devices DS18B20 temperature sensor | 2 | Measure and monitor the soil temperature levels. |
| Sparkfun HC-SR04 ultrasonic sensor | 1 | Measure and monitor the water level in the tank. |
| DNT weather station pro | 1 | Collect environmental data. |
| WHADDA 12 V solenoid valve | 3 | Control the flow of water. |
| Espressif ESP32 S3 microcontroller | 2 | Primary acquisition and control units for sensors and actuators. |
| Raspberry Pi 4 Model B 4 Gb | 1 | Central processing unit for system management, data processing and visualization. |

### 3.2 Communication layer

Communication agents enable data transfer from the integration layer to the information and aggregation layer. Data is ingested and mapped to the OPC UA server. The communication flow is initiated by a JSON file, that serves as a guiding schema for the data collection agents, detailing key elements for the system operation. The data description file (i) specifies the communication protocol to trigger the relevant data collection agent, (ii) enumerates data points, (iii) lists node IDs to map data onto the relevant variable nodes in the OPC UA server, and (iv) describes the structure for data storage within the database. The JSON file guides the data flow from the integration layer to subsequent layers, ensuring cohesive system operation.

### 3.3 Information and aggregation layer

The OPC UA server that hosts the information model lies in the information and aggregation layer, serving as the foundation of the smart irrigation system architecture. The foundation of the scalability of the system lies in the design of an OPC UA *types model*. The types model enables instantiation of OPC UA *instance models*, facilitating the system to accommodate an expanding array of assets and subsystems for defining a wide range of generic object types, variable types, data types, interface types, and standardized hierarchal relations and information models. Thus, to model a new scalable smart irrigation system, four key categories, i.e. *Actuators*, *Sensors*, *WeatherData*, and *IrrigationControl* are required. A UML schema of the scalable smart irrigation system implemented in this work is shown in Figure 2.

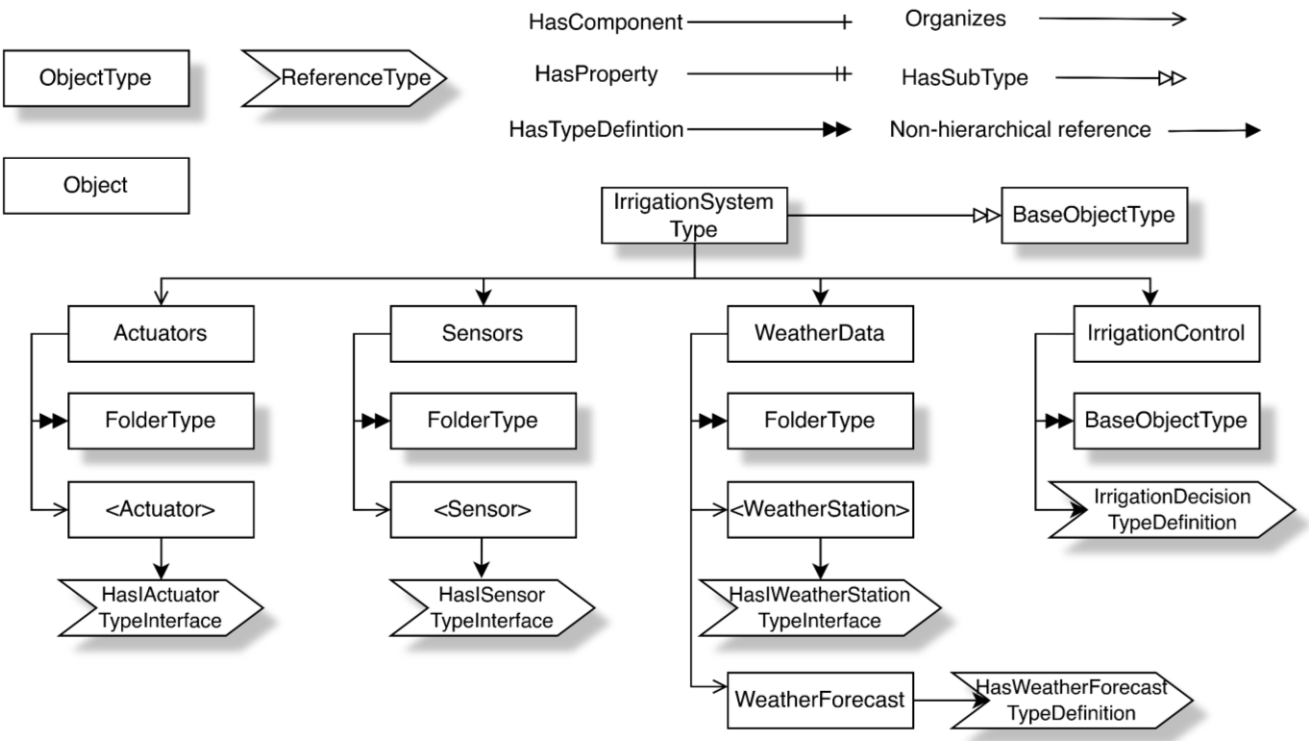


Figure 2: Schema of the scalable smart irrigation system.

### 3.4 Functional layer

In this layer, the database agent, hosted on Node-RED, is responsible for the systematic storage of data to InfluxDB that is hosted as a local instance on the Raspberry Pi. The decision agent processes data from the OPC UA server to determine the most efficient irrigation schedules and triggers the irrigation process. The event-based control algorithm, implemented in Python and running on the Raspberry Pi, considers minimum soil moisture levels and weather forecasts.

### 3.5 Business layer

To facilitate the visualization of historical data, Grafana, an open-source web service for data analytics, is hosted on the Raspberry Pi. The Grafana dashboard displays various metrics related to soil moisture, temperature, water levels, and irrigation schedules. Historical data can be accessed and visualized, enabling analysis of past irrigation events and environmental conditions. Historical data visualization allows for trend analysis, performance monitoring, and compliance reporting, enabling users to make informed decisions based on past patterns and system performance. In addition, a manual override option allowing user control to intervene when the irrigation system does not function as expected.

## 4 Validation of the smart irrigation system

Validation tests are conducted using two prototype implementations of the smart irrigation system, (i) system 1 ($S_1$), an indoor setup without consideration of weather forecasting, and (ii) system 2 ($S_2$), an indoor setup that considers outdoor conditions with weather forecasting. Both systems, implemented in compliance with the above specifications, are planted with garden cress and are supposed to have optimal soil humidity levels of 70%, which is the optimal soil moisture for garden cress growth. The soil moisture sensor provides consistent moisture readings within an accuracy range of ±4% and a response time of under 1.5 s for detecting moisture changes.

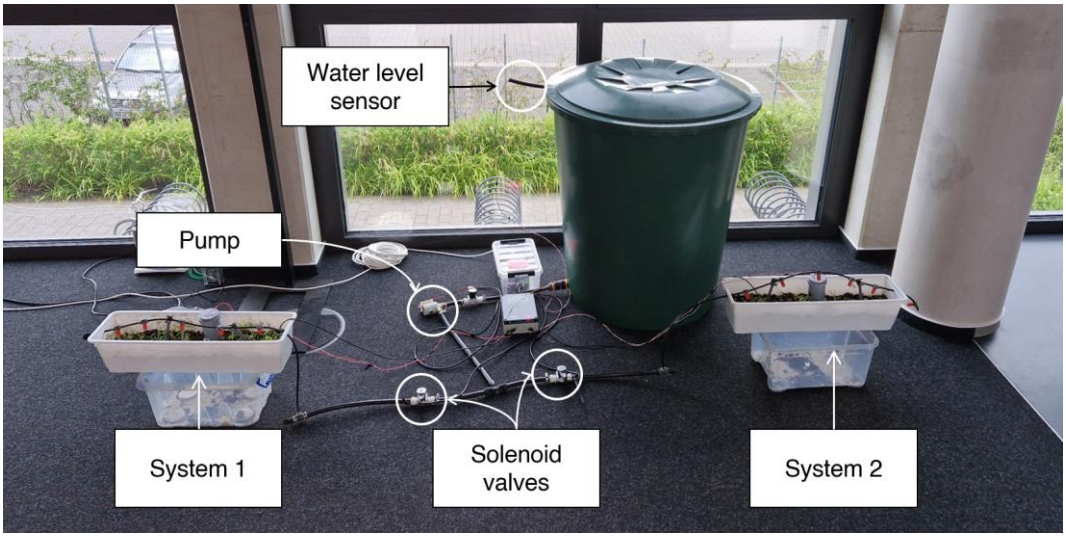


Figure 3: Validation test setup.

System $S_1$ is designed to maintain the soil humidity at the desired level through automated irrigation. The validation process involves monitoring soil humidity, water consumption, and the growth of garden cress over a 10-day period. The soil humidity sensors continuously measure the moisture content in the soil, and data is collected and analyzed to ensure the system maintained the daily soil humidity at the optimal level of 70%. The total water used by the system is 2.21 l. The growth of garden cress is monitored as an indicator of the system effectiveness, and the garden cress reached a height of 12 cm. Figure 4 illustrates the soil humidity of System $S_1$ over the 10-day period.

System $S_2$ incorporates weather forecasting to adjust irrigation schedules based on predicted rainfall, aiming to optimize water usage. Although the setup is implemented indoors for validation purposes, it considers outdoor conditions to validate the effect of integrating weather data. Soil humidity is maintained at 70%, such as with system $S_1$, but system $S_2$ adjusts irrigation based on real-time sensor data and weather forecasts. The total water used by system $S_2$ is 1.92 l, showing a reduced water consumption in comparison to $S_1$. The growth of garden cress is monitored as an indicator of the system effectiveness, reaching a height of 9 cm, 3 cm smaller than the cress used in $S_1$, arguably due to the smaller amount of water. Figure 5 illustrates the soil humidity of $S_2$ over the 10-day period.

Figure 4: Soil humidity and total water consumption of $S_1$.

Figure 5: Soil humidity and total water consumption of $S_2$

## 5 Summary and conclusions

This paper has presented a scalable smart irrigation system to enhance water resource management and operational efficiency. The system integrates IoT-based hardware components, including sensor nodes, actuators, a weather station, and IoT platforms. The novelty of the system lies in integrating an OPC UA framework into an IoT layered architecture using formal information models. Thus, the smart irrigation system can be scaled to adapt to agricultural fields or urban gardening applications. Two prototype implementations of the system have been validated, using outdoor conditions using weather forecasts and indoor conditions. In the validation tests, optimal soil moisture levels have been kept, demonstrating the effectiveness of the system to irrigate without human intervention. The OPC UA framework ensures semantic richness, standardized data, and efficient instantiation of new elements of the system. Future research may integrate machine learning to improve control algorithms for different setups and deployment in real agricultural or urban environments, including different sensors and actuators to validate the scalability and integration capabilities of the system, which in this paper is shown in an indoor environment.

## References

[1] M. van Dijk, T. Morley, M. L. Rau, & Y. Saghai, “A meta-analysis of projected global food demand and population at risk of hunger for the period 2010–2050,” Nat Food, 2(7), pp. 494-501, 2021

[2] V. V, R. A. C, V. S. R. R, A. K. P, S. M. R, and S. B. M, “Implementation of IoT in Agriculture: A Scientific Approach for Smart Irrigation,” in 2022 IEEE 2nd Mysore Sub Section International Conference (MysuruCon), pp. 1-6, 2022

[3] H. Osman, M. Mahmud, A. Hassan, & A. Ali, “A bibliometric analysis of the evolution of IoT applications in smart agriculture,” Ingénierie des systèmes d information, 28, pp. 1495-1504, 2023

[4] O. Friha, M. A. Ferrag, L. Shu, L. Maglaras, & X. Wang, “Internet of Things for the Future of Smart Agriculture: A Comprehensive Survey of Emerging Technologies,” IEEE/CAA Journal of Automatica Sinica, 8(4), pp. 718–752, 2021

[5] C. Cambra, S. Sendra, J. Lloret, & L. Garcia, “An IoT service-oriented system for agriculture monitoring,” in 2017 IEEE International Conference on Communications (ICC), pp. 1–6, 2017

[6] P. Sanjeevi, S. Prasanna, B. Siva Kumar, G. Gunasekaran, I. Alagiri, & R. Vijay Anand, “Precision agriculture and farming using Internet of Things based on wireless sensor network,” Transactions on Emerging Telecommunications Technologies, 31(12), p. e3978, 2020

[7] Smarsly, K. & Law, K. H, “Coupling Wireless Sensor Networks and Autonomous Software for Integrated Soil Moisture Monitoring” in 10th International Conference on Hydroinformatics. Hamburg, Germany, 2012.

[8] G. Villarrubia, J. De Paz, D. Hernández de la Iglesia, & J. Bajo, “Combining Multi-Agent Systems and Wireless Sensor Networks for Monitoring Crop Irrigation,” Sensors, 17, p. 1775, 2017

[9] A. Veichtlbauer, M. Ortmayer & T. Heistracher, “OPC UA integration for field devices” IEEE 15th International Conference on Industrial Informatics (INDIN), Emden, Germany, pp. 419-424, 2017

# Robotikgestützte Werkzeuglogistik mit Quadrupeds für die Bauindustrie

Christian Kiebel[1], Dominik Lehmann[1], Sven Zentgraf[1] and Patrick Herbers[1]
[1]Lehrstuhl für Informatik im Bauwesen, Ruhr-Universität Bochum, Universitätsstraße 150, 44801 Bochum, Deutschland
E-mail(s): christian.kiebel@rub.de, dominik.lehmann@rub.de, sven.zentgraf@rub.de, patrick.herbers@rub.de

**Abstract:** Dieser Beitrag stellt die Umsetzung eines praktischen Beispiels vor, um die potenziellen Anwendungen der Robotik in der Baulogistik aufzuzeigen. Mit der zunehmenden Integration von Industrie 4.0-Technologien in den Produktionssektor hat die Robotik eine zentrale Rolle übernommen, da sie Effizienzsteigerung und Automatisierung bietet. Um diese Vorteile auf den Bausektor zu übertragen, wird ein theoretisches Konzept anhand eines praktischen Beispiels umgesetzt. Die Grundlage dafür ist *Spot*, ein von Boston Dynamics entwickelter Roboterhund. Unter Verwendung der API und des Software Development Kits wurde eine automatisierte Routine programmiert, die einen bestimmten Arbeitsablauf auf einer Baustelle simuliert. Um die praktische Anwendbarkeit zu veranschaulichen, wurde *Spot* mit einem neuen Zusatzmodul ausgestattet, in dem Proben oder Werkzeuge gelagert werden können. Zusätzlich wurde *Spot* mit einem Greifarm ausgestattet, der es ihm ermöglicht, Objekte aus dem Zusatzmodul zu entnehmen. Im Mittelpunkt dieser Untersuchung stand die Frage, ob *Spot* in der Lage ist, den programmierten Autowalk einschließlich der Anbringung des Zusatzmoduls und der darin enthaltenen Gegenstände auch dann durchzuführen, wenn unvorhergesehene Hindernisse auftreten oder die vorgegebene Route blockiert ist. Die Ergebnisse zeigen, dass *Spot* diese Aufgabe erfolgreich bewältigt hat, was die Machbarkeit und das Potenzial der Integration von Robotertechnologie im Bausektor verdeutlicht.
*Keywords:* Robotik, Automatisierung, Additive Fertigung

Erschienen in Tagungsband 35. Forum Bauinformatik 2024, Hamburg, Deutschland, DOI: 10.15480/882.13526
© 2024 Das Copyright für diesen Beitrag liegt bei den Autoren. Verwendung erlaubt unter Creative Commons Lizenz Namensnennung 4.0 International.

## 1 Einleitung

Im Kontext der industriellen Entwicklung markiert der Unterschied des technologischen Fortschritts und der Automatisierung zwischen der Fertigungsindustrie und dem Bauwesen eine Diskrepanz. Während die Fertigungsindustrie durch weitreichende Automatisierungsprozesse und den Einsatz fortschrittlicher Technologien charakterisiert wird, steht das Bauwesen diesen Entwicklungen noch vergleichsweise zurückhaltend gegenüber [1]. Ein deutlicher Indikator für diesen Unterschied lässt sich anhand der Produktivitätsentwicklung in diesen Sektoren ablesen. Während die allgemeine

Wirtschaftsleistung zwischen 1991 und 2021 um 45 Prozent anstieg und das verarbeitende Gewerbe sogar einen Produktivitätssprung von 90 Prozent verzeichnen konnte, erlebte das Baugewerbe einen Rückgang der Arbeitsproduktivität um 4,2 Prozent [2]. Im Vergleich zu anderen Wirtschaftsbereichen ist es den Unternehmen im Baugewerbe somit nicht gelungen, ihre Produktivität signifikant zu verbessern.

Die zunehmende Integration von Robotik in das Bauwesen erfolgt aufgrund der Erkenntnisse und Erfolge in der industriellen Anwendung. Roboter, welche durch ihre Fähigkeit, physische Belastungen für die Arbeiter minimieren und monotone sowie arbeitsintensive Tätigkeiten übernehmen, stellen einen beträchtlichen Mehrwert dar [3]. Diese Arbeit konzentriert sich darauf, das Potenzial der Robotik zur Unterstützung und Optimierung von Prozessen im Bauwesen zu evaluieren, speziell im Bereich der Baustellenlogistik. Trotz der noch hohen Anschaffungskosten der Robotikhardware wird durch steigende Lohnkosten der Einsatz von Robotik auf der Baustelle unabdingbar sein. Die Verteilung von Material und Werkzeug auf einer Baustelle ist mit dem gesamten Bauprozess eng verbunden. Eine Unterstützung der Baustellenlogistik durch Robotik könnte so den Weg zu einer komplett autonomen Baustelle bereiten.

Ziel dieser Arbeit ist, ein Szenario der Baustellenlogistik, den Werkzeugtransport, durch den Einsatz mobiler, autonomer Robotik zu unterstützen. Wir verwenden *Spot*, einen vierbeinigen Roboter von Boston Dynamics, der über fortschrittliche autonome Gleichgewichts- und Navigationsfähigkeiten verfügt. *Spot* soll dabei in der Lage sein, Gegenstände aufzuheben, zu verstauen, und an einen anderen Ort zu liefern. Dabei müssen verschiedene Aspekte berücksichtigt werden, wie das Gewicht der Payloads, der Massenschwerpunkt, und die Transportsicherheit.

## 2 Verwandte Arbeiten

Ein anschauliches Beispiel für den praktischen Einsatz von *Spot* zeigt sich im verstärkten Gebrauch dieser Technologie bei der Deutschen Bahn. Im Artikel “Roboterhund unterstützt digitale Instandhaltung der DB” [4] wird die Anwendung von *Spot* detailliert beschrieben und verdeutlicht den Beitrag zur digitalen Wartung und Instandhaltung: *“Der Laufroboter reduziert Laufwege, objektiviert Prüfungsergebnisse und ermöglicht den Wegfall von aufwendigen Grubenarbeiten unter dem Zug. Die Mitarbeitenden werden bei körperlich anstrengenden Arbeiten entlastet und gewinnen Zeit für wertschöpfende Tätigkeiten. So können die Instandhaltungskosten gesenkt und der Fachkräftemangel abgefedert werden.”*

Follini, Terzer, Marcher u. a. [5] stellen ein Projekt vor, in dessen Zentrum die Entwicklung einer Roboterplattform steht, die in der Lage ist, einem Arbeiter auf der Baustelle zu folgen und dabei dynamische Hindernisse automatisiert zu umgehen. Die Reduktion von Muskel-Skelett-Erkrankungen der Arbeitnehmer auf Baustellen stellt ein wesentliches Ziel des Projekts dar. Die Übernahme schwerer körperlicher Arbeit durch die Maschine ermöglicht es, die Belastung der Arbeitnehmer zu reduzieren. Der Arbeiter fungiert dabei lediglich als Leitfigur, um sich schneller auf der Baustelle zurechtzufinden.

Emig, Siegele und Terzer [6] präsentieren mögliche Steigerungen des Automatisierungsgrades von Bauvorhaben sowie aktuelle Herausforderungen, wie beispielsweise dynamische und unsichere Randbedingungen bei der Umsetzung auf der Baustelle. Im Artikel werden diverse Maschinen vor-

gestellt, die zur Umsetzung der Digitalisierung auf der Baustelle beitragen könnten. Dazu gehören beispielsweise auch verfahrbare Plattformen zum Transport von Baumaterialien.

Bei der Implementierung von Robotertechnologien auf Baustellen sind wichtige Faktoren zu berücksichtigen, die den Einsatz derzeit teilweise unmöglich machen, diese Probleme und mögliche Lösungen werden von Dindorf und Wos [7] behandelt. Zwar geht es den Autoren nicht direkt um den Materialtransport auf der Baustelle, sondern um ein mobiles robotergestütztes Maurersystem (RBS), aber die Probleme, die bei der Umsetzung auf der Baustelle auftreten, sind die gleichen wie bei der robotergestützten Werkzeuglogistik auf der Baustelle. Dazu zählen anfängliche Kostenbarrieren, die hohen Vorlaufkosten für die Herstellung und den Betrieb der Bauroboter. Will [8] thematisiert neue Möglichkeiten zur Automatisierung von Baumaschinen und Bauprozessen. Der Autor kommt zu dem Schluss, dass im Hochbau die Implementierung von Assistenzsystemen zur Unterstützung und Entlastung der Arbeitskräfte eine entscheidende Rolle spielt.

## 3 Methodik

Das Ziel dieser Forschungsarbeit ist die Entwicklung und Bewertung einer simulierten Laufroute unter Einsatz von *Spot*, einem vierbeinigen autonomen Roboter von Boston Dynamics. *Spot* kann sowohl über ein Tablet für direkte Befehle als auch programmatisch über speziell entwickelte Software-Schnittstellen gesteuert werden. Ein zentraler Bestandteil der autonomen Steuerung ist die AutoWalk-Schnittstelle. AutoWalks sind vom Benutzer aufgenommene Laufrouten, die vom Roboter vollautonom abgelaufen werden können. Darüber hinaus ist *Spot* mit Fischaugenkameras und Stereokameras ausgestattet, die ihm eine kontinuierliche Umgebungswahrnehmung und damit die Vermeidung von Kollisionen ermöglichen. *Spot* kann neben den bereits fest eingebauten Kameras noch bis zu 14kg Payload tragen.

Unter Verwendung der Boston Dynamics API (*Application Programming Interface*) wird eine Laufroute erstellt, die *Spot* autonom durchlaufen soll. Dabei wird eine speziell angefertigter Payload integriert, der bis zu einem definierten Maximalgewicht beladen werden kann. Die Laufroute wird in zwei Szenarien getestet: erstens auf einer hindernisfreien Strecke und zweitens auf einem Weg, der durch ein Hindernis blockiert wird. Ziel dieser Evaluation ist es, zu überprüfen, ob *Spot* in der Lage ist, sich die Laufroute zu merken und das Hindernis eigenständig zu umgehen oder anzuhalten. Diese Simulation zielt darauf ab, die praktische Anwendbarkeit von *Spot* auf Baustellen und in ähnlichen Arbeitsumgebungen zu demonstrieren, wobei die Fähigkeit zur autonomen Navigation und Hindernisvermeidung im Mittelpunkt steht.

Ein praktisches Anwendungsbeispiel bildet eine alltägliche Situation auf einer Baustelle, bei der ein Arbeiter einen Winkelschleifer aus einem Magazincontainer benötigt, jedoch der weitläufige Weg dorthin ineffizient ist. In diesem Szenario wird der Winkelschleifer in einen speziell für *Spot* entwickelten und auf ihm befestigten Payload gelegt. Anschließend wird *Spot* so programmiert, dass er den Winkelschleifer direkt zum Arbeiter transportiert. Ziel ist es, zu demonstrieren, dass *Spot* den programmierten Weg bei wiederholter Durchführung zuverlässig absolviert, auch wenn kleine Hindernisse auftreten oder geringfügige Änderungen im Gelände vorliegen. Dies minimiert den

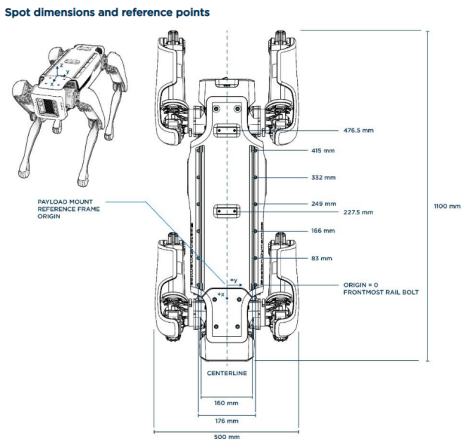


Abbildung 1: *Spot* Abmessungen und Bezugspunkte von oben

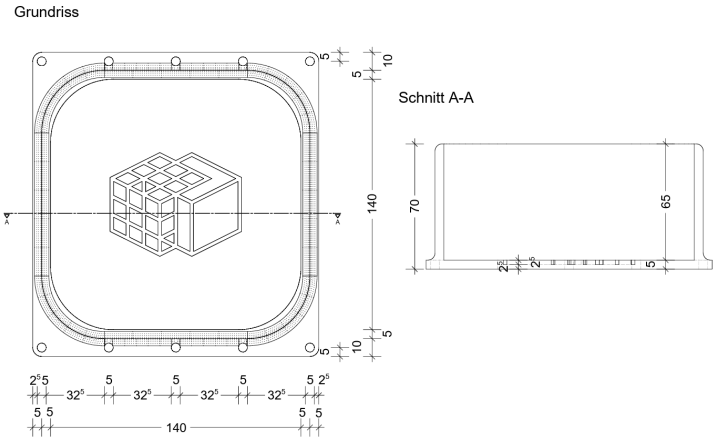


Abbildung 2: Konstruktionszeichnungen mit Bemaßung

Bedarf, die Laufroute für jede Lieferung neu anzupassen. Die Entwicklung eines maßgeschneiderten Rahmens und eines tragbaren Behälters ist dabei essenziell. Der Rahmen wird dauerhaft an *Spot* befestigt, während der Behälter für flexible Einsätze konzipiert wird. Durch genaue Vermessung und Berücksichtigung des maximal zulässigen Gewichts gemäß den Herstellerempfehlungen wird sichergestellt, dass der Payload die Funktionsfähigkeit von *Spot* nicht beeinträchtigt. Dieses Projekt soll nicht nur die Machbarkeit des automatisierten Transports von Werkzeugen und Materialien auf Baustellen verdeutlichen, sondern auch Perspektiven für zukünftige Erweiterungen eröffnen, wie die Einbindung fortgeschrittener Navigationsalgorithmen und die Optimierung des Payload-Designs für vielfältigere Einsatzmöglichkeiten.

## 3.1 Vorgehen Additive Fertigung

In diesem Abschnitt wird der Prozess der Entwicklung und Herstellung der Payloads für *Spot* beschrieben. Um sicherzustellen, dass *Spot* in Zukunft auch mit empfindlichen Werkzeugen auf der Baustelle beim Transport zurechtkommt, wurde in der Projektarbeit beispielhaft ein Alltagsgegenstand gewählt. Um zu zeigen, wie gut *Spot* auch mit zerbrechlichen Dingen umgehen kann, wurden Getränkeflaschen aus Glas als Testobjekt ausgewählt. Die Intention bestand darin, die Flaschen so auf *Spot* zu befestigen, dass sie sicher stehen, jedoch auch einfach wieder abgenommen werden können. Für die Bewältigung dieser Herausforderung wurde eine Transportbox entworfen.

Abb. 1 zeigt die Bemaßung des Roboters, Abb. 2 die Konstruktuionszeichnung der entworfenen Transportbox. Die Transportbox wurde für vier Glasflaschen (ca. 70mm Radius) entworfen. Die inneren Maße der Box betragen 145mm $\times$ 145mm und eine Höhe von 70mm. Wände und Boden der Transportbox wurde mit einer Dicke von fünf Millimetern entworfen, um eine ausreichende Stabilität für das Tragen von Flaschen zu gewährleisten. Um die strukturelle Integrität zu verstärken, wurde um die Box herum eine Randversteifung eingefügt, in der Schraubenlöcher für die Befestigung angebracht wurden. Dabei wurde ein Abstand von zehn Millimetern an den Seiten vorgesehen, an denen Schrauben angebracht werden, während an den anderen Seiten ein Abstand von fünf Millimetern eingehalten wurde. Damit auch andere Flaschen in dieser Box transportiert werden

Abbildung 3: Transportbox mit Abstandshalter für kleinere Flaschen

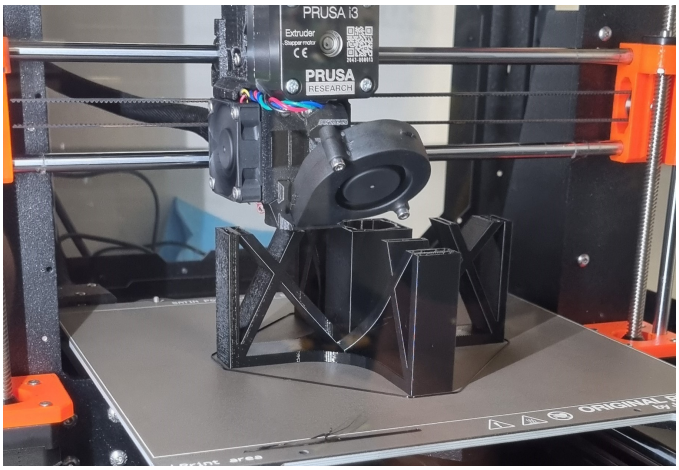


Abbildung 4: Druck des Abstandshalters mit Querstreben

können, wurde für die Box ein Abstandshalter entworfen und gedruckt, der für 0,25-Liter-Flaschen geeignet ist. Dieser ist in Abb. 3 zu sehen.

Die im Druckverfahren verwendeten Kunststoffe machen das endgültige Modell leicht und gleichzeitig robust genug, um den vorgesehenen Zweck zu erfüllen. Abb. 4 zeigt den Druck des Abstandhalters, Abb. 5 die montierte Transportbox mit Ladung.

### 3.2 Vorgehen Autowalk

Für die autonome Navigation des Roboters wurde die Autowalk API von Boston Dynamics verwendet. Die Steuerung von *Spot* erfolgte über einen Tablet-Controller, der mittels einer Wi-Fi-Verbindung die drahtlose Kommunikation mit dem Roboter ermöglichte. Durch die Nutzung des Tablets konnten Wegpunkte aufgenommen werden, die die Route des Autowalks bilden. Die Wegpunkte beinhalten die Pose des Roboters und visuelle Orientierungspunkte (z.B. Fiducials), welche während der Aufnahme sichtbar waren. Die Wegpunkte werden in etwa 1m Abständen aufgezeichnet und auf das Tablet übertragen. Ist der Roboter Hindernissen gegenübergestellt, muss eine alternative Route gesucht werden. Dafür muss die aufgenommene Route in einen Graphen übertragen werden, in dem alle Posen untereinander verlinkt werden. Dadurch wird es auch möglich, jeden einzelnen Punkt des Graphen gezielt anzusteuern. Neben den automatisch aufgenommenen Wegpunkten besteht auch die Möglichkeit, manuell Wegpunkte zu setzen. Diese Funktionalität ermöglicht eine präzise Steuerung und Anpassung der Laufroute, um eine optimale Navigation und Wiederholbarkeit der Route zu gewährleisten.

### 3.3 Vorgehen Beladung

Für eine autonome Baustellenlogistik ist die Beladung und Entladung ein zentraler Bestandteil. Damit der Roboter ohne externe Hilfe Ladung aufnehmen und ablegen kann, wurde ein Roboterarm der Marke *Kinova Gen 3* auf dem Rücken von *Spot* montiert (siehe Abb. 6). Die Stromversorgung des Arms erfolgte über eine externe Stromquelle, ein integrierter Anschluss an die Batterie von Spot ist aber denkbar. Der Roboterarm hat eine Reichweite von 90cm und eine Bewegungsfreiheit von 6 Degrees

Abbildung 5: *Spot* mit beladener Transportbox

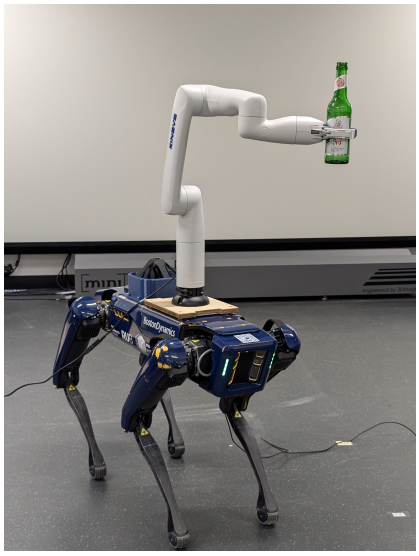

Abbildung 6: Montierter *Kinova Gen 3* Roboterarm mit Ladung

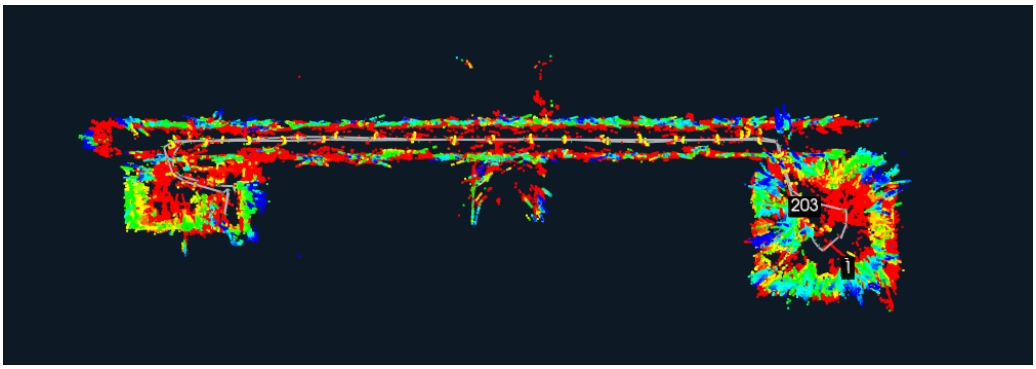


Abbildung 7: Aufgenommene Route des Autowalks und Punktwolke

of Freedom (6-DoF). Der Arm kann Objekte mit einem Gewicht von 2kg heben, 4kg wenn nahe am Schwerpunkt. Das Eigengewicht des Arms von 7kg erlaubt die Nutzung als Payload für *Spot*, jedoch beschränkt diese *Spot*'s gesamte Traglast von 14kg. Der Arm verschiebt den Masseschwerpunkt des Roboters erheblich. Deswegen ist zu empfeheln, den Arm nur zu bedienen, wenn *Spot* in einer stabilen Position auf dem Boden sitzt. In Tests konnte der bearmte Roboter in Sitzposition 0,5l Flaschen problemlos heben und in dem gedruckten Aufbau verstauen. Auch ein Entladen konnte erfolgreich getestet werden.

## 4 Ergebnisse

Um das Gleichgewicht und die Navigation des Roboters zu prüfen, wurde ein Testlauf gestartet. Zunächst wurden die in Kapitel 3.1 beschriebenen Payloads für *Spot* entsprechend registriert. Der Schwerpunkt der Transportbox inkl. Flaschen wurde vermessen und in *Spot*'s Konfiguration angegeben. Diese Justierungen sind wichtig, um die Stabilität und Bewegungsdynamik zu optimieren, insbesondere hinsichtlich seines Aufsteh- und Bewegungsverhaltens sowie der Lastverteilung auf seinem Rücken.

Eine Laufroute von 40m entlang eines Flurs und zwei Räumen inklusive Rückweg wurde entsprechend des Vorgehens in Kapitel 3.2 aufgezeichnet (siehe Abb. 7). Die Laufroute enthält enge Passagen durch Türen sowie Hindernisse in From von Kisten in den Räumen. Die Überprüfung der aufgenommenen Laufroute bestätigte die erfolgreiche und fehlerfreie Funktionsweise. *Spot* ist in der Lage, zu einem spezifizierten Wegpunkt zu navigieren und im Anschluss an den Ausgangspunkt zurückzukehren. Selbst bei der Anpassung der Laufroute mit einem Hindernis findet *Spot* eigenständig einen alternativen Weg, um die geplanten Wegpunkte sequenziell abzuarbeiten. Diese Fähigkeit zeigt sich besonders vorteilhaft in dynamischen Umgebungen wie Baustellen.

Nach der Montage der mittels 3D-Druck hergestellten Transportbox als Payload auf *Spot*s Rücken wurde ein AutoWalk-Test durchgeführt, um die Funktionalität und Belastbarkeit der Konstruktion zu überprüfen. Im Rahmen des Tests demonstrierte *Spot* seine Stabilität und Mobilität mit Lasten, indem er sowohl aufstehen als auch sich hinlegen konnte, ohne dass die transportierten Bierflaschen – jeweils 0,5 Liter – umfielen oder Schaden nahmen. Dies bestätigt die Eignung der Transportbox in Verbindung mit *Spot* für den sicheren Transport von Gegenständen. Während des Tests navigierte *Spot* von einem Labor über einen Flur bis zur Kaffeeküche des Lehrstuhls und legte sich dort auf den Boden. Für die Rückkehr zum Ausgangspunkt stand *Spot* wieder auf, drehte sich um und bewegte sich zurück zur Startposition. Dabei musste lediglich eine konstante WiFi-Verbindung aufrecht erhalten werden, um die Steuerung und Notstopp-Funktion via Laptop zu erhalten. Dies unterstreicht die Bedeutung der Berücksichtigung von Reichweitengrenzen bei der Planung von autonomen Operationen auf Baustellen oder in ähnlichen Umgebungen, insbesondere wenn ferngesteuerte Überwachung und Steuerung vorgesehen sind.

## 5 Schlussfolgerung und Ausblick

Die Ergebnisse dieser Arbeit verdeutlichen, dass *Spot* effektiv für den Transport von Materialien und Werkzeugen auf Baustellen eingesetzt werden kann. Die Kombination mit der additiven Fertigung im 3D-Drucker macht es möglich, Halterungen für jeden Zweck herzustellen und diese dann auf *Spot* anzubringen. Durch die Aufnahme eines Autowalks war es möglich, *Spot* autonom navigieren zu lassen. Dies würde einen Einsatz von automatisierter Logistik über die Baustelle ermöglichen, zum Beispiel als Werkzeuganforderung oder Materialverfolgung und Verteilung. Auch ist ein Fernzugriff möglich, sodass externe Fachkräfte Proben nehmen oder andere Arbeiten durchführen können, ohne auf die Baustelle zu kommen. In Zeiten des Fachkräftemangels würde das einen effizienteren Einsatz von Arbeitskraft ermöglichen.

Die Fähigkeit von *Spot*, Hindernisse zu erkennen und zu umgehen, unterstreicht die fortgeschrittene Technologie und Flexibilität, die Robotiksysteme in das Bauwesen einführen können. Dieser Aspekt ist besonders relevant, da er zeigt, dass der Einsatz von Robotern nicht auf vorhersehbare oder streng kontrollierte Umgebungen beschränkt ist, sondern auch in den dynamischen und oft unvorhersehbaren Bedingungen einer Baustelle effektiv sein kann. Die erfolgreiche Integration der zusätzlichen Payloads und die Anpassung der Bewegungsfähigkeiten von *Spot* basierend auf dem Gewicht und Schwerpunkt der transportierten Gegenstände zeigen das Potential für eine Vielzahl von spezialisierten Anwendungen. Diese Anpassungsfähigkeit eröffnet neue Möglichkeiten für die

Nutzung von *Spot* in verschiedenen Phasen des Bauprozesses, von der initialen Erkundung und Datenakquisition bis hin zum Transport von Baumaterialien und Werkzeugen.

In weiterführender Forschung sollten die autonomen Fähigkeiten des Roboters untersucht und erweitert werden. Für den Werkzeug- und Materialtransport ist eine visuelle Erkennung und Klassifizierung notwendig um das automatische Beladen zu ermöglichen. Für einen sicheren Einsatz von mobilen Robotern auf der Baustelle ist ein Umgebungsverständnis nötig, welche Gefahren erkennen und vermeiden kann. Weiterhin sollten andere Konfigurationen von Robotern getestet werden, wie radbasierte Roboter für erhöhte Transportkapazität, oder humanoide Roboter für mehr Flexibilität. Auch weitere Forschung in Interaktionsmöglichkeiten zwischen menschlichen Arbeitern und mobilen Robotersystemen wie *Spot* können dazu beitragen die Akzeptanz und effektive Zusammenarbeit auf der Baustelle zu fördern.

## Literatur

[1] T. Bock, »The future of construction automation: Technological disruption and the upcoming ubiquity of robotics«, *Automation in Construction*, Jg. 59, S. 113–121, 2015. DOI: 10.1016/j.autcon.2015.07.022.

[2] Hauptverband der Deutschen Bauindustrie e.V., *Produktivität im Bau(haupt-)gewerbe – ein statistischer Befund*, 2022. Adresse: https://www.bauindustrie.de/zahlen-fakten/publikationen/brancheninfo-bau/produktivitaet-im-bauhauptgewerbe (besucht am 26. 03. 2024).

[3] T. Afflerbach, *Serviceroboter: Digitalisierung von Dienstleistungen aus Kunden-, Mitarbeiter- und Managementperspektive* (essentials). Wiesbaden, Germany und Heidelberg: Springer Gabler, 2021. DOI: 10.1007/978-3-658-35624-8.

[4] Deutsche Bahn AG, »Roboterhund unterstützt digitale Instandhaltung der DB«, 2023. Adresse: https://www.deutschebahn.com/resource/blob/11859294/810ba4ea054e62aae448612d9bcdf42e/Laufroboter_Faktenblatt-data.pdf (besucht am 26. 03. 2024).

[5] C. Follini, M. Terzer, C. Marcher, A. Giusti und D. T. Matt, »Combining the Robot Operating System with Building Information Modeling for Robotic Applications in Construction Logistics«, *Advances in Service and Industrial Robotics*, S. 245–253, 2020. DOI: 10.1007/978-3-030-48989-2_27.

[6] J. Emig, D. Siegele und M. Terzer, »Digitalisierung und KI in der Baurobotik: Eine Analyse der aktuellen Entwicklungen und zukünftigen Potenziale«, *Künstliche Intelligenz im Bauwesen*, S. 413–429, 2024. DOI: 10.1007/978-3-658-42796-2_24.

[7] R. Dindorf und P. Wos, »Challenges of Robotic Technology in Sustainable Construction Practice«, *Sustainability*, Jg. 16, Nr. 13, 2024. DOI: 10.3390/su16135500.

[8] F. Will, »Automatisierte Baumaschinen und Bau-Robotik«, in *Auf dem Weg zu einer nachhaltigen, effizienten und profitablen Wertschöpfung von Gebäuden: Grundlagen – neue Technologien, Innovationen und Digitalisierung – Best Practices*. Springer Fachmedien Wiesbaden, 2022, S. 335–360. DOI: 10.1007/978-3-658-34962-2_20.

# Underwater Spatial Field Monitoring with Small Scale Robots: An Experimental Study

Nathalie Bauschmann[1]
[1]Institute of Mechanics and Ocean Engineering, Hamburg University of Technology,
Eißendorfer Straße 42, 21073 Hamburg, Germany
E-mail(s): nathalie.bauschmann@tuhh.de

**Abstract:** Autonomous underwater vehicles (AUVs) can serve as efficient and cost-effective mobile sensor nodes for monitoring of underwater environments and construction sites such as marinas or nuclear storage ponds. In field exploration, the information collected by the AUV is used to construct a probabilistic field belief model of the environmental field. This can then be used to integrate an information metric into the path planning step. In this paper, a Gaussian Process-based field belief for a scalar, 2D underwater environmental field is investigated. The main contribution is the extensive experimental validation using real measurements. For testing purposes, a radiation field is mimicked using electro-magnetic carrier signals emitted by spatially distributed active beacons. Leveraging the attenuation of these signals underwater, the AUV measures the received signal strength. In literature so far, field exploration frameworks in the underwater domain are typically validated in experiments by simulating the field itself and the resulting measurements. While sensor noise can be integrated relatively easily, this still constitutes an over-simplification due to model imperfections. Moreover, this approach neglects other effects resulting from e. g. dynamic motion as the AUV interacts with the environment or field anomalies due to obstacles. Hence, an experimental investigation under realistic conditions is expected to deliver insights.

*Keywords:* Probabilistic field modeling, underwater robotics, Gaussian Process regression

Erschienen in Tagungsband 35. Forum Bauinformatik 2024, Hamburg, Deutschland, DOI: 10.15480/882.13531
© 2024 Das Copyright für diesen Beitrag liegt bei den Autoren. Verwendung erlaubt unter Creative Commons Lizenz Namensnennung 4.0 International.

## 1 Introduction

Autonomous underwater field exploration constitutes a promising task for mobile robots acting as mobile sensor nodes. With the continuous advances in miniaturization of computation technology, small-scale autonomous underwater vehicles (AUVs) are expected to play a prominent role in monitoring and exploration of environmental systems; an example of a small-scale underwater robot is depicted in Figure 1. Environmental 2D spatial fields of interest include radiation, oil concentration, temperature or total dissolved oxygen.

In field exploration, the information, i. e. measurements, collected by the AUV is used to construct a probabilistic field belief model of the environmental field. This information-theoretic metric can then be

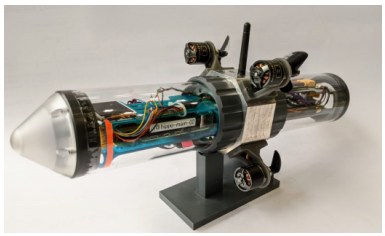

Figure 1: Example of a small-scale AUV used for spatial field mapping, the HippoCampus $\mu$AUV [7].

used in the AUV's path planning to save time during the mission. Consider the scenario of developing exploration algorithms for mobile underwater robots targeting environmental field monitoring, such as radiation fields. While investigating stationary spatial fields constitutes an obvious first step, their representation in submerged scenarios is challenging. This work studies the suitability of electromagnetic fields to mimic these fields. A focus lies on investigating potential disturbances, as antenna misalignments.

There has been extensive research on field exploration frameworks in the underwater domain. However, if these frameworks are validated experimentally, the field itself and the resulting measurements typically are simulated. A core reason being that time-constant fields are difficult to obtain. While sensor noise can be integrated relatively easily, this still constitutes an over-simplification, due to model imperfections. More importantly, this approach neglects other effects resulting from e. g. dynamic motion of the AUV.

One of the first works to deploy a field exploration algorithm in the real world is Cui et al. [1]. The authors map a 2D temperature field using a selective basis function Kalman filter. However, during the field experiments using four robots, they use simulated temperature measurement. Kemna et al. [2] use a log-Gaussian Process to map biological data, e. g. algae bloom. For the sake of simplicity, in field experiments in the subsequent publication [3], the authors use bathymetry data instead as a simple scalar field. This comes with the advantage of being fairly static in time and the possibility, to compose a ground truth model. A more in-depth field trial analysis is provided in [4]. Stankiewicz et al. use a Gaussian Process (GP) to model scalar environmental phenomena, namely dissolved oxygen measurements for water quality monitoring. Another example of using bathymetry data for field modeling is presented in [5].

In conclusion, the use of real-life measurement data in underwater field exploration frameworks is limited to physical, biological or chemical properties of large-scale outdoor environments. There are no examples of field belief modeling for confined environments such as nuclear storage ponds. This work explores the feasibility of using electro-magnetic (EM) carrier signals for underwater field exploration. Notably, received signal strength (RSS) data have been used in field modeling in other domains, e. g. using GP regression in an indoor environment in [6].

## 2 Modeling Electro-Magnetic Spatial Underwater Fields

In this work, we investigate the usage of 433 MHz EM carrier signal emitted by an active beacon to mimick a radiation field. Leveraging the attenuation of these signals underwater, a receiver antenna can measure the RSS. This section describes, first, the physical model of the radiation pattern and

attenuation of the antennas and, second, the hardware design of the measurement system consisting of the receiver and transmitter side. Finally, a GP-based field belief model is presented.

### 2.1 Electro-magnetic carrier signals underwater

Inspired by their usage in recent efforts in underwater localization [8], [9], omnidirectional dipole antennas emitting EM carrier signals of constant magnitude are used in this work. Omnidirectional dipole antennas display a doughnut-shaped radiation pattern. Therefore, the highest gain is achieved for receivers in the horizontal plane. The signal power varies with both the angle between a transmitter and receiver antenna, as well as the vertical distance between them. The 3D spatial attenuation characteristics of EM waves underwater, using omnidirectional antennas, are examined in detail by Kwak et al. [10].

The difference in EM wave power $S_R$ on receiver side and EM wave power $S_T$ on transmitter side is the RSS. This can be expressed as a function of the range $R$ between receiver and transmitter antenna according to [8] as

$$\text{RSS} = S_\text{R} - S_\text{T} = -20 \log_{10} R - 20\ R\,\alpha \log_{10} e + \Gamma. \tag{1}$$

Here, $\Gamma$ is an offset factor that represents antenna and environmental influences for the transmitter and $\alpha$ is the attenuation constant of the planar wave. The parameters $\Gamma$ and $\alpha$ can be calculated explicitly if variables such as polarization loss factor, transmitting and receiving antenna gains and the attenuation factor are known. Alternatively, they can be determined through calibration, as described in [11].

### 2.2 Hardware Design

In the following, the hardware design is described. The transmitter unit consists of the Radiometrix™ USX2 module to generate the EM carrier signal in the 433 MHz band. As for the antenna, off-the-shelf dipole 2 dBi wifi antennas are used on the transmitter and receiver side. This is possible since the wavelength is shortened underwater. Therefore, the 433 MHz band sufficiently matches the characteristic wavelength of wifi systems in air, which operate at 2.4 GHz.

The receiver side consists of three main components: a commercial 2 dBi dipole wifi antenna, a modified Digital Video Broadcasting-Terrestial (DVB-T) USB dongle, and a single board computer (SBC), as depicted in Figure 2a. The NooElec™ NESDR Mini DVB-T USB dongle can process analog EM signals within a range of 24-1700 MHz, using software defined radio (SDR). After demodulation and analog digital conversion, the signals are transmitted as data sample to the SBC, a Raspberry Pi 4b, via USB interface. The SBC runs a fast Fourier transform on the samples to compute the RSS at the expected frequency in the power spectrum. A more in-depth description can be found in [11].

### 2.3 Field Belief Modeling

A common method for spatial modeling, also known in geostatistics as Kriging, is GP regression [12]. GP regression relies on two primary assumptions: spatial regularity, where measurements taken in close proximity are physically correlated, and Gaussian (zero-mean) measurement noise. The GP is completely defined by a mean function and its covariance matrix. While it is a non-parametric model, its performance is affected by hyperparameters, which are the kernel's parameters.

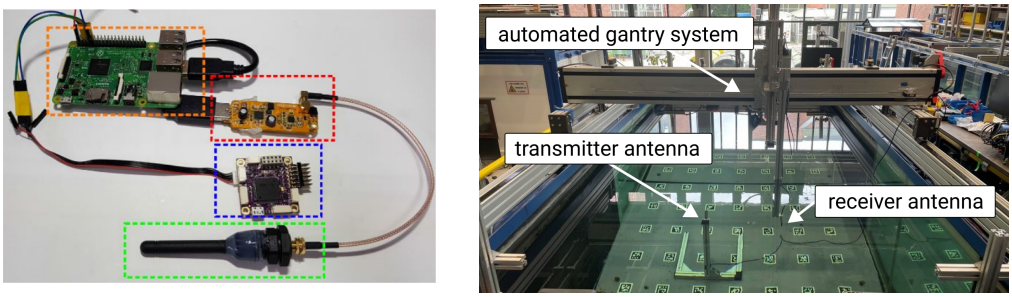


(a) (b)

Figure 2: (a) Components of EM receiver measurement setup: antenna (green), DVB-T dongle (red) and Raspberry Pi 4 single board computer (orange), (b) Experimental setup consisting of stationary transmitter beacon inside fresh water tank, receiver beacon on automated gantry system.

For the GP's kernel, a combination of the squared exponential function kernel [12] and a white noise covariance function is used, resulting in

$$k(\mathbf{x}, \mathbf{x}') = \sigma_f^2 \exp\left(-\frac{1}{2}\sum_{k=1}^{2}\frac{\left(x_{i,k} - x_{j,k}\right)^2}{l_k^2}\right) + \sigma_n^2 \delta_{\mathbf{x}_i,\mathbf{x}_j}, \tag{2}$$

with position $\mathbf{x} \in \mathcal{R}^2$ and the hyperparameter vector $\theta = \left[l_1, l_2, \sigma_f^2, \sigma_n^2\right]^\top$. Here, $\sigma_f^2$ is the signal variance, which determines the vertical scale of the function, and $\sigma_n^2$ is the variance of the noise. The parameters $l_k$ are length scales in each dimension, which determine the level of correlation between measurements. Moreover, $\delta_{\mathbf{x}_i,\mathbf{x}_j}$ is the Kronecker delta function. The hyperparameters are optimized using the log-marginal likelihood as cost function [12] and the L-BFGS-B algorithm.

# 3 Analysis

The goal of the investigation is to, first, collect a 2D baseline field of the RSS values used as the ground truth in the following. Second, the sensitivity to possible error sources as they will occur with dynamic vehicle motions is investigated. Third, a *proof-of-concept* is shown to analyze how well a GP can capture the EM field's spatial characteristics. Finally, the results are discussed.
The experiments are conducted within a 2×4×1.5 m fresh water tank. A single stationary transmitter beacon is placed inside the tank. The receiver antenna is mounted on an automated gantry system, see Figure 2b.

## 3.1 Baseline

The RSS data is recorded in an evenly-spaced grid, with a distance of 5 cm between waypoints. At each waypoint, 80 measurements are recorded in a period of 3 s and the mean is taken. The results are depicted in Figure 3. It can be seen that the measured RSS value decreases with distance to the emitting beacon. However, interference effects roughly matching the ~0.5 m wavelength can be observed.

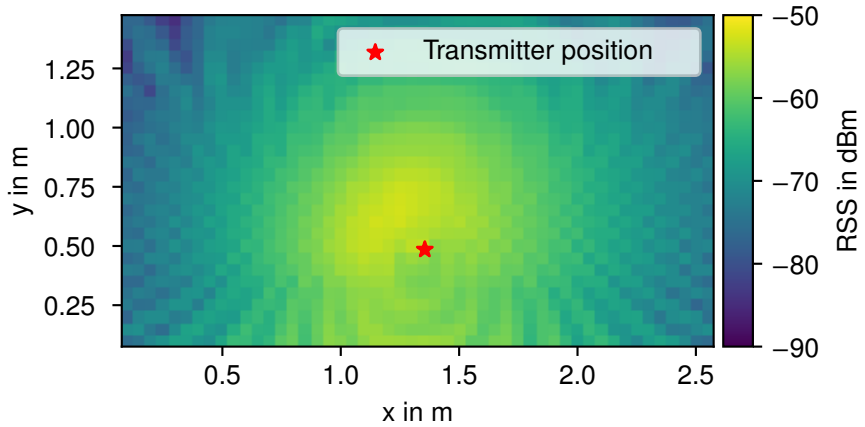


Figure 3: Baseline RSS measurement in fresh water tank, exhibiting interference effects.

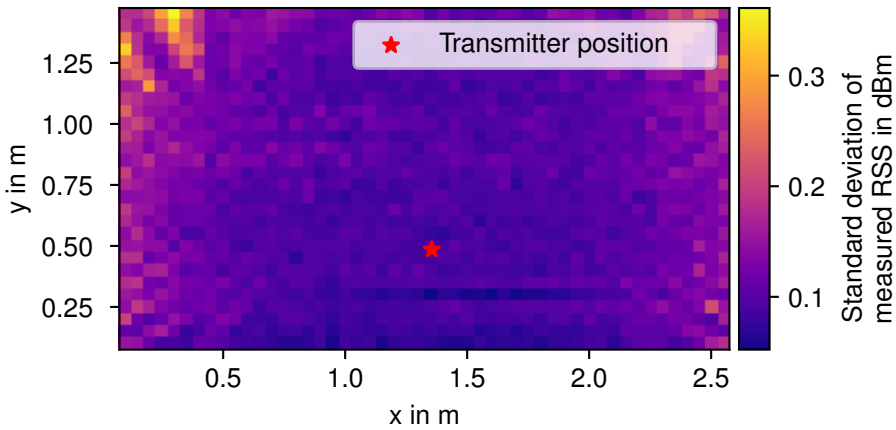


Figure 4: Standard deviation of baseline measurement.

### 3.2 Sensitivity to Alignment Errors

When the receiver antenna is deployed on an actual AUV, the dynamic motion is expected to affect the measurement. Even with extensive controller tuning, increasing forward thrust typically results in a pitch movement as well. Moreover, while the motion of the AUV is constrained to a 2D plane, depth control cannot be assumed to be perfect. Therefore, the effects of antenna misalignments, caused by relative tilts and vertical shifts between the receiver and transmitter antenna, are investigated in the following.

The RSS data is recorded on the same waypoint grid as in Section 3.1. Figure 5 depicts the error in RSS values compared to the baseline for antenna tilts of -20, -10, 10, and 20 degrees, as well as 10 cm and 20 cm vertical shift between the receiver and transmitter. It can be seen that the errors resulting from angle misalignment are comparatively small. However, for antenna tilts, an interesting effect can be observed. On one side of the transmitter antenna (right-hand side of Figure 5(a)-(d)), the measured RSS values *increase*, while on the other side, they decrease compared to the baseline. The maximum antenna gain and therefore the highest measured RSS value is expected for exact horizontal and angular alignment of antennas. Therefore, the increase in RSS in this setup can be

explained by an existing tilt or vertical offset in the baseline setup.
Moreover, the vertical displacement of the receiver antenna has a strong effect on the measured RSS value close to the transmitter antenna, as expected due to the doughnut-shaped radiation characteristics where the gain decreases above the antenna.

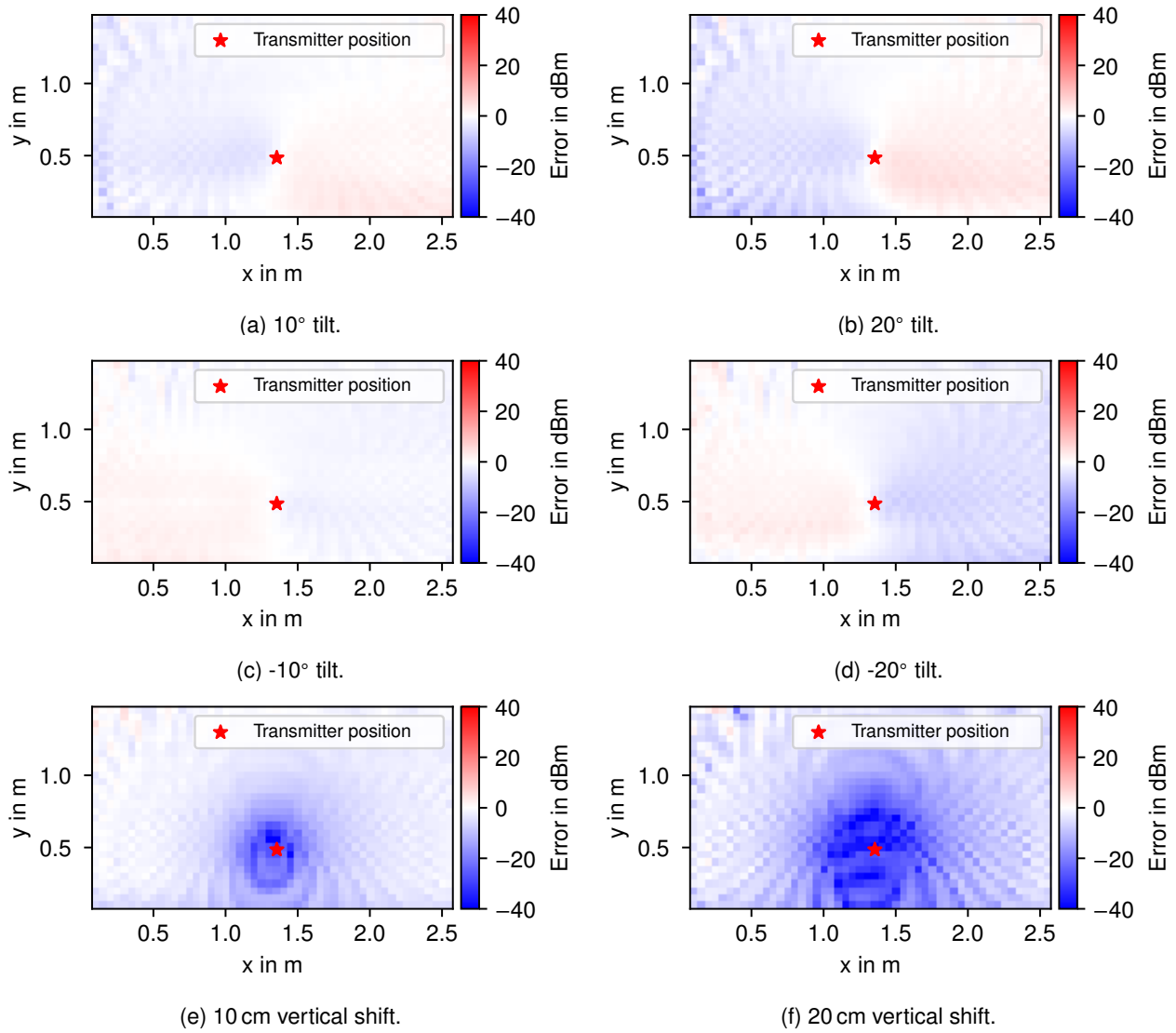


(a) 10° tilt.

(b) 20° tilt.

(c) -10° tilt.

(d) -20° tilt.

(e) 10 cm vertical shift.

(f) 20 cm vertical shift.

Figure 5: RSS error compared to baseline for different antenna misalignments. For angle shift, antenna is tilted around the x-axis.

### 3.3 Gaussian Process Regression Proof-of-Concept

As a first step towards leveraging EM measurements for underwater field exploration, general feasibility of modeling a 2D spatial RSS field using GP regression is demonstrated in the following. For this, 15 measurements are drawn at random positions. Figure 6 shows the predicted mean compared to the baseline measurement, with contour lines displayed at identical values. The results show a good fit for the absolute predicted RSS value, while the interference effects are not present in the model.

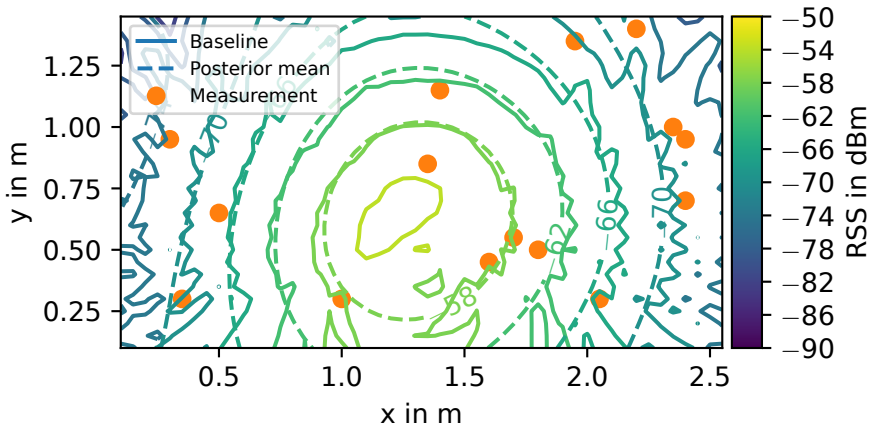


Figure 6: Predicted (dashed line) vs baseline (solid line) RSS values. 15 Measurements used for fitting the GP.

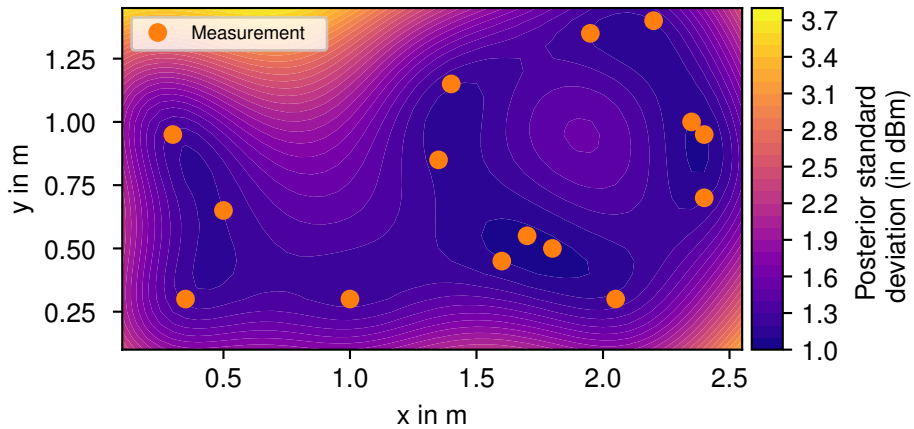


Figure 7: Uncertainty: posterior standard deviation of predicted RSS values after 15 measurements.

Moreover, Figure 7 depicts the uncertainty of the model, i. e. posterior standard deviation of each predicted RSS value. Around the measurements, the uncertainty is low, whereas in unexplored areas, the uncertainty is higher.

## 4 Conclusion

This work examines using EM carrier signals, precisely their attenuation, for underwater spatial field exploration. A stationary transmitter antenna emits a constant signal, while a mobile receiver antenna measures the RSS. The error analysis shows that the RSS measurements are very sensitive to vertical offsets between antennas in close proximity to the transmitter antenna. This is due to the radiation characteristics of the omnidirectional dipole antennas used. Comparatively, angle errors have less effect on the RSS. Modeling the RSS using a GP-based field belief was shown to be feasible.
As a next step, the measurement device will be deployed on a real robot, using this data to actively explore a spatial field. To overcome the shown sensitivity to angle and height misalignments, different antenna designs can be explored. Hemispherical antennas are promising due to their hemispherical radiation pattern. Alternatively, predicting errors using the robot's pose can be investigated.

## References

[1] R. Cui, Y. Li, and W. Yan, “Mutual information-based multi-auv path planning for scalar field sampling using multidimensional rrt”, *IEEE Transactions on Systems, Man, and Cybernetics: Systems*, vol. 46, no. 7, pp. 993–1004, 2015.

[2] S. Kemna, J. G. Rogers, C. Nieto-Granda, S. Young, and G. S. Sukhatme, “Multi-robot coordination through dynamic voronoi partitioning for informative adaptive sampling in communication-constrained environments”, in *2017 IEEE International Conference on Robotics and Automation (ICRA)*, IEEE, 2017, pp. 2124–2130.

[3] S. Kemna, H. Heiarsson, and G. S. Sukhatme, “On-board adaptive informative sampling for auvs: A feasibility study”, in *OCEANS 2018 MTS/IEEE Charleston*, IEEE, 2018, pp. 1–10.

[4] P. Stankiewicz, Y. T. Tan, and M. Kobilarov, “Adaptive sampling with an autonomous underwater vehicle in static marine environments”, *Journal of Field Robotics*, vol. 38, no. 4, pp. 572–597, 2021.

[5] G. Flaspohler, V. Preston, A. P. Michel, Y. Girdhar, and N. Roy, “Information-guided robotic maximum seek-and-sample in partially observable continuous environments”, *IEEE Robotics and Automation Letters*, vol. 4, no. 4, pp. 3782–3789, 2019.

[6] N. Fung, J. Rogers, C. Nieto, H. I. Christensen, S. Kemna, and G. Sukhatme, “Coordinating multi-robot systems through environment partitioning for adaptive informative sampling”, in *2019 International Conference on Robotics and Automation (ICRA)*, IEEE, 2019, pp. 3231–3237.

[7] D. A. Duecker, N. Bauschmann, T. Hansen, E. Kreuzer, and R. Seifried, “Hippocampusx–a hydrobatic open-source micro auv for confined environments”, in *2020 IEEE/OES Autonomous Underwater Vehicles Symposium (AUV)*, IEEE, 2020, pp. 1–6.

[8] D. Park, K. Kwak, J. Kim, and W. K. Chung, “3d underwater localization scheme using em wave attenuation with a depth sensor”, in *2016 IEEE international conference on robotics and automation (ICRA)*, IEEE, 2016, pp. 2631–2636.

[9] D. A. Duecker, T. Johannink, E. Kreuzer, V. Rausch, and E. Solowjow, “An integrated approach to navigation and control in micro underwater robotics using radio-frequency localization”, in *2019 International Conference on Robotics and Automation (ICRA)*, IEEE, 2019, pp. 6846–6852.

[10] K. Kwak, D. Park, W. K. Chung, and J. Kim, “Underwater 3-d spatial attenuation characteristics of electromagnetic waves with omnidirectional antenna”, *IEEE/ASME Transactions on Mechatronics*, vol. 21, no. 3, pp. 1409–1419, 2016.

[11] D.-A. Duecker, A. R. Geist, M. Hengeler, *et al.*, “Embedded spherical localization for micro underwater vehicles based on attenuation of electro-magnetic carrier signals”, *Sensors*, vol. 17, no. 5, p. 959, 2017.

[12] C. E. Rasmussen and C. K. Williams, *Gaussian Processes for Machine Learning*. MIT Press, 2006.

# Monitoring und Simulation von Roboterkinematik basierend auf digitalen Zwillingen für den Lehmdruck

Jasper Vollmert, Patricia Peralta, Aditya Tandon
Institut für Digitales und Autonomes Bauen, Technische Universität Hamburg,
Blohmstraße 15, 21079 Hamburg, Germany
E-Mail: jasper.vollmert@tuhh.de

**Abstract:** Die additive Fertigung auf Lehmbasis, auch bekannt als Lehmdruck, hat das Potenzial, den Lehmbau effizienter zu gestalten, als es mit bisherigen Verfahren möglich ist. Allerdings sind die Probleme, die sich aus nicht berücksichtigten kinematischen Effekten (z. B. Ruckbewegungen) von Lehmdruckrobotern, auch bekannt als Lehmdrucker, ergeben, nach wie vor ungelöst und beeinträchtigen die Qualität der gedruckten Bauteile. Um den Lehmdruck zu verbessern, muss die Roboterkinematik im Druckprozess untersucht werden. In diesem Beitrag wird ein auf digitalen Zwillingen basierendes Framework zum Monitoring und zur Simulation von Druckprozessen vorgestellt, um den Einfluss der Roboterkinematik auf Druckprozesse zu untersuchen. Das Framework basiert auf einer substanzwissenschaflich abgesicherten Referenzarchitektur für digitale Zwillinge und wird prototypisch für einen Lehmdrucker implementiert, der aus einem horizontalen Gelenkarmroboter und einem linearen Ram-Extruder besteht. Das Framework wird über das Monitoring und die Simulation von Druckprozessen einer mit Lehm gedruckten Wand validiert. Die Ergebnisse zeigen, dass die ungewollten kinematischen Effekte, die während des Druckprozesses auftreten, durch das Framework abgeschwächt werden können und das Framework als Grundlage für das autonome Drucken von Lehm dienen kann.

*Keywords:* Additive Fertigung (AM), digitale Zwillinge (DT), Lehmdruck, Roboterkinematik

Erschienen in Tagungsband 35. Forum Bauinformatik 2024, Hamburg, Deutschland, DOI: 10.15480/882.13540
© 2024 Das Copyright für diesen Beitrag liegt bei den Autoren. Verwendung erlaubt unter Creative Commons Lizenz Namensnennung 4.0 International.

## 1 Einführung

Lehm als Baumaterial ermöglicht kostengünstiges und nachhaltiges Bauen. Technische Schwierigkeiten im Lehmbau begrenzen jedoch den Übergang vom traditionellen Lehmbau zum digitalen Bauen [1]. Um die Digitalisierung des Lehmbaus voranzutreiben, kann der Lehmbau mit additiver Fertigung („Additive Manufacturing“, AM) und intelligenten Sensortechnologien gekoppelt

und hierbei das in anderen Bereichen, wie dem Betondruck, gewonnene AM-Fachwissen genutzt werden [2].

Das Potenzial von lehmbasiertem AM in der Bauindustrie wurde durch Projekte und Prototypen aufgezeigt, wie in [3] beschrieben. Detailliertere Studien zur Bewertung von erdbasiertem AM wurden durchgeführt, wobei der Schwerpunkt auf Hardwarelösungen für Extruder [4], Materialentwicklung für optimiertes rheologisches Verhalten [1], strukturelle Leistung von Komponenten [5] und Prozessverbesserung durch parametrische Werkzeugwegplanung und Extrusionsregelung [6] lag. Darüber hinaus wird die Materialextrusion üblicherweise für die erdgebundene AM angepasst. Dabei werden AM-Systeme verwendet, die hauptsächlich auf Robotersystemen basieren, ähnlich wie die AM-Systeme, die für den Betondruck verwendet werden [7]. AM-Systeme, die gemeinhin als „Drucker“ bezeichnet werden, zielen auf einen präzisen Materialauftrag ab, wobei geringfügige Abweichungen in Position oder Ausrichtung zu Druckproblemen führen können [8].

Obwohl die additive Fertigung – und insbesondere der Lehmdruck – ein Forschungsgebiet von zunehmender Relevanz ist, wurde dem Einfluss kinematischer Effekte auf die Genauigkeit von AM-Systemen im Lehmdruck bisher nur wenig Aufmerksamkeit geschenkt. Unberücksichtigte kinematische Effekte, wie ruckartige Bewegungen und Vibrationen, können zu Abweichungen in der Position und Ausrichtung der Extruder sowie in der Kontinuität des Materialauftrags führen und die Qualität der gedruckten Komponenten beeinträchtigen [9]. Deshalb sind weitere Anstrengungen erforderlich, um die Auswirkungen der Roboterkinematik im Druckprozess zu untersuchen. Von der Interaktion zwischen Prozess und Material bis hin zur Prozessregelung ist die Roboterkinematik der Schlüssel zur Definition des Roboterverhaltens, der Randbedingungen, der Prozessparameter und der Regelungsstrategien. Bestehende Ansätze im Lehmdruck erfordern aufwändige Trial-and-Error, um eine effiziente Prozesssteuerung zu gewährleisten, bevor qualitativ hochwertige gedruckte Komponenten erzielt werden können. Die Erstellung eines digitalen Zwillings kann das Verständnis der Roboterkinematik verbessern und dazu beitragen, Probleme, die bei Druckprozessen auftreten können, zu mindern.

In diesem Beitrag wird ein auf digitalen Zwillingen basierendes Framework vorgestellt und implementiert, um den Einfluss der Roboterkinematik auf den Druckprozess für den Lehmdruck zu untersuchen. Digitale Zwillinge sind virtuelle Gegenstücke physischer Einheiten, die „physischen Zwillinge“, die synchronisiert werden, um den Zustand der physischen Einheit zu reflektieren [10]. Hier werden digitale Zwillinge für das Monitoring und die Simulation des Lehmdrucks eingesetzt, um Druckprobleme aufgrund von kinematischen Effekten zu identifizieren und zu mindern. Der auf digitalen Zwillingen basierende Ansatz wird für einen Lehmdrucker implementiert und validiert, wobei ein digitaler Zwilling (DT) mit einem physikalisch orientierten Ansatz entwickelt wird, um Geometriemodelle, Mehrkörpermodelle und kinematische Modelle zu integrieren.

# 2 Ein auf digitalen Zwillingen basierendes Framework für den Lehmdruck

Das DT-basierte Framework ermöglicht das Monitoring und die Simulation von Druckprozessen, die digitale Darstellung von Bewegungen von Lehmdruckern und die Identifikation potenzieller Probleme in Druckprozessen, die durch kinematische Effekte verursacht werden können.

Das Monitoring und die Simulation von Roboterbewegungen hilft bei der Identifizierung von Abweichungen in der Position der Extruder von vordefinierten Trajektorien, die die Materialabscheidung behindern können. Durch die Bewertung der Abweichungen in der Extruderposition ist es möglich, Probleme aufgrund kinematischer Effekte in Druckprozessen während des Entwurfs und der Planung von Druckprojekten zu mindern. In diesem Beitrag geht es um die Identifizierung von Punkten mit erhöhter Vibration und ruckartigen Bewegungen in Druckprozessen, die Vorhersage damit verbundener Probleme und die Definition von Regelungsstrategien zur Minderung von Druckfehlern.

Digitale Zwillinge für Lehmdrucker werden auf der Grundlage einer von den Autoren zuvor entwickelten Referenzarchitektur für digitale Zwillinge konzipiert [11]. Der DT verwendet eine geschichtete, serviceorientierte Systemarchitektur, um die Funktionen und Verhaltensweisen von Lehmdruckern (d. h. physischen Einheiten) in einer digitalen Umgebung darzustellen (Abbildung 1).

## 2.1 Ein digitaler Zwilling für Lehmdrucker

Das DT-basierte Framework wurde für einen Lehmdrucker, einen SCARA-Roboter mit 3 Freiheitsgraden (DOF) implementiert. Der digitale Zwilling für den 3-DOF SCARA-Lehmdrucker, bestehend aus einem Scara Roboter mit Linearantrieb Extruder, wird mit MATLAB und Simulink [12] als Modellierungs- und Simulationswerkzeug implementiert. Ein geometrisches Modell des Lehmdruckers wird verwendet, um ein Mehrkörpermodell zu erstellen, dass die Komponenten und die physikalischen Wechselwirkungen zwischen den Komponenten des Robotersystems darstellt und zu einem Mehrkörpersystem mit starren Körpern führt, wie in Abbildung 2 dargestellt. Darüber hinaus wird ein kinematisches Modell , dass die Roboterglieder und -gelenke auf der Grundlage der DH-Parameter des Roboters berücksichtigt [13]. Mit dem Kinematikmodell werden die Positionen der einzelnen Gelenke der Roboter durch eine numerische Lösung des Problems der inversen Kinematik geschätzt, wobei ein numerischer Löser auf der Grundlage des Levenberg-Marquardt-Algorithmus verwendet wird. Durch die Integration und Replizierung des Robotermodells in das Modell der Simulationsumgebung werden Monitorings- und Simulationsdienste entwickelt. Die Dienste replizieren die Bewegung von Lehmdruckern für benutzerdefinierte Trajektorien und prozessbezogene Parameter (z. B. Druckgeschwindigkeit und Materialbeladung) unter Verwendung von PID-Reglern, um das Verhalten des Lehmdruckers basierend auf einer Rückkopplungsschleife für die Gelenkpositionen anzupassen. Im folgenden Unterabschnitt wird ein Überblick über den Simulationsdienst gegeben.

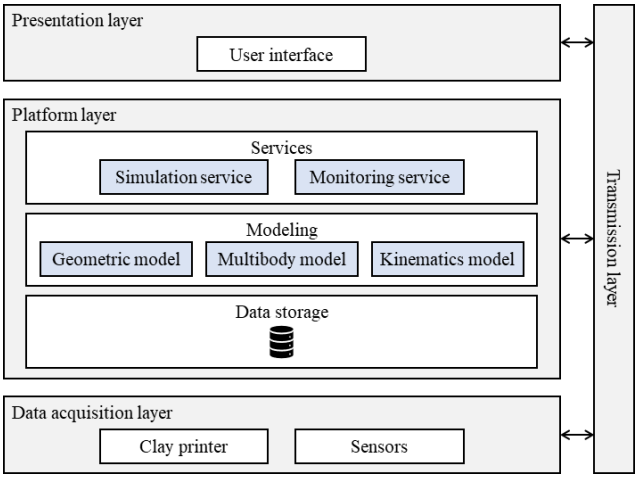


Abbildung 1. Systemarchitektur für den digitalen Zwilling für den Lehmdruck.

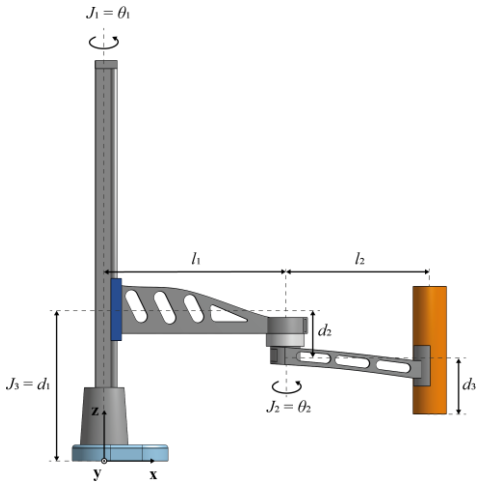


Abbildung 2. Mehrkörpermodell des SCARA-Lehmdruckers.

Der Simulationsdienst wird mit dem Simscape-Simulationswerkzeug in Simulink implementiert, wie in Abbildung 3 dargestellt. Um die Bewegung des Lehmdruckers zu simulieren, verwendet der Simulationsdienst Zieltrajektorien, Zielendzeiten und die Materialnutzlast als Eingaben. Die Zieltrajektorien sind definiert als ein Vektor von Zielpunkten $\boldsymbol{p}_i = (x_i , y_i , z_i )$, die die Koordinaten des Extruders darstellen. Aus den Zieldruckgeschwindigkeiten werden jedem Zielpunkt diskretisierte Zeitschritte zugewiesen und ein trapezförmiges Geschwindigkeitsprofil erzeugt. Der Block für inverse Kinematik löst die Zieltrajektorie numerisch in geschätzte Gelenkpositionen ($\theta_1 , \theta_2 , d_1$) auf. Die geschätzten Gelenkpositionen werden den PID-Reglern zugeführt, die die Gelenkpositionen in prozessbezogene Parameter für Drehmoment und Kraft umwandeln. Die Drehmoment- und Kraftparameter werden zur Vorhersage des Verhaltens des Lehmdruckers verwendet, ausgedrückt als Ausgangstrajektorie, Ausgangsgeschwindigkeit, Ausgangsbeschleunigung und Ausgangsdrehmoment. Zur Verfeinerung der Simulation wird eine Rückkopplungsschleife eingesetzt, um die tatsächlichen Fügepositionen, die aus der Ausgangsbahn abgeleitet werden, an die PID-Regler zurückzugeben. Mithilfe des Monitoringdiensts werden Punkte erhöhter Vibrationen und Ruckbewegungen als Spitzen im Ausgangsdrehmoment bzw. in der Ausgangsgeschwindigkeit identifiziert. Im folgenden Abschnitt wird die Validierung des DT-basierten Frameworks vorgestellt.

## 2.2 Fallstudie

Die Fallstudie beschreibt den Druckprozess einer Teststruktur, die aus einem rechteckigen Wandelement mit einer gezackten Innenstruktur besteht. Der Druckprozess für jede Schicht ist in drei Schritte unterteilt, nämlich Umfangsstruktur, Füllstruktur und Schichtübergang. Zunächst wird die Umfangsstruktur der Wand gedruckt, indem Material entlang des Umrisses der Wand aufgetragen wird, wie in Abbildung *4* dargestellt. Zweitens wird die Füllstruktur der Wand gedruckt, die für Stabilität sorgt. Drittens fährt der Extruder in eine Ausgangsposition zurück, während er zur nächsten Schicht übergeht und den Extruder auf die nächste Schichthöhe bewegt. Dieser Vorgang wird so lange wiederholt, bis das Wandelement fertig gedruckt ist.

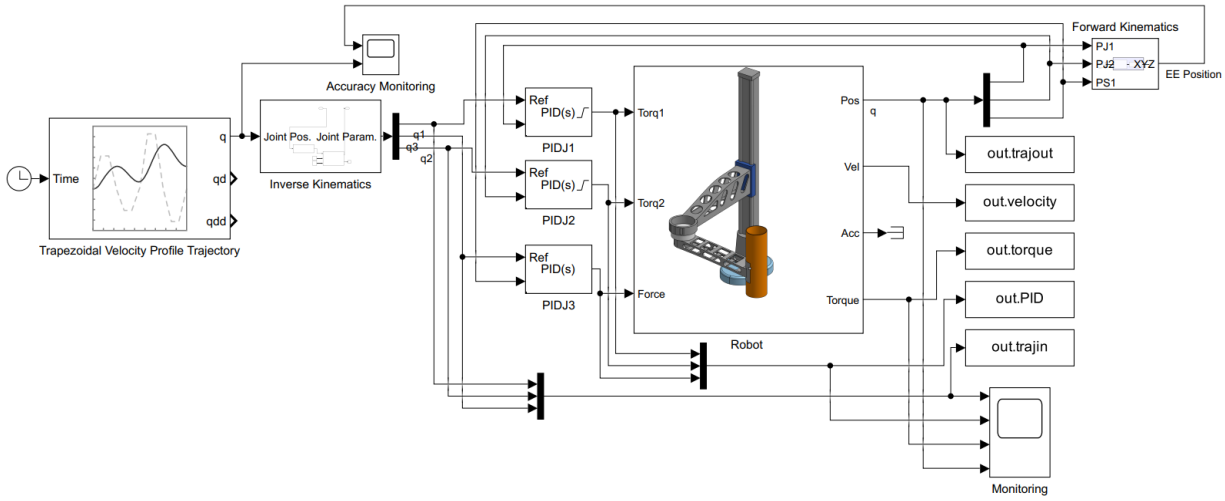


Abbildung 3. Simscape-Simulationsarchitektur.

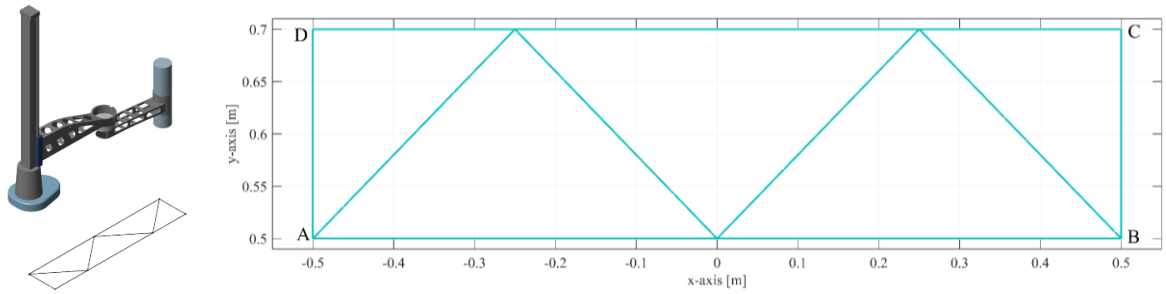


Abbildung 4. Teststruktur (Druckreihenfolge A, B, C, D, A, B)

## 2.3 Ergebnisse

Der Zieldruckpfad für das Wandelement wird als Zieltrajektorie für die Simulation mit einer Zieldruckgeschwindigkeit von 0,1 m/s definiert. Um mögliche Änderungen der Genauigkeit während des Druckprozesses zu untersuchen, wird die Materialbeladung des Extruders während des gesamten Simulationsprozesses variiert. Das Material wird Schicht für Schicht aufgetragen, so dass die Materialbeladung mit jeder weiteren Schicht konstant abnimmt. Aufgrund der geringen Druckgeschwindigkeit, bleibt die Materiallast über jede Schicht nahezu konstant. Die Beziehung zwischen prozessbezogenen Parametern, der Materialbeladung, und den kinematischen Effekten sind einige der wichtigsten Unsicherheitsfaktoren für den SCARA-Lehmdrucker. Um die Beziehungen zwischen den Parametern zu untersuchen, werden vier Druckszenarien mit unterschiedlichen Materialbeladungen eingeführt. Die Materialbeladung beginnt bei voller Extrusionskapazität und wird in jedem Szenario um ein Drittel der Kapazität verringert, bis der Extruder vollständig entleert ist. Die Gewichtsveränderung wird als Veränderung der Masse und Trägheit modelliert. Deshalb werden die vier Druckszenarien, die einer Materialauslastung von 100 %, 66 %, 33 % und 0 % entsprechen, in den nachfolgenden Simulationsergebnissen verglichen.

Der tatsächliche Druckpfad, d. h. die Ausgangstrajektorie, wird beobachtet und als Abweichungsdiagramm für jedes Gelenk dargestellt (Abbildung 5). Die Abweichung für jede Gelenkposition wird anschließend mit Simulationen mit unterschiedlichen Materialnutzlasten verglichen, die 100 %, 66 %, 33 % und 0 % der Materialnutzlast umfassen. Die Ergebnisse zeigen, dass das Modell des Lehmdruckers den angestrebten Druckpfad mit nur geringen Abweichungen verfolgt. Es ist zu beobachten, dass anfängliche Abweichungen durch die Einschwingzeit der PID-Regler entstehen. Außerdem werden die Fehler an den Ecken der gedruckten Struktur mit der Verringerung der Materialbeladung vergleichsweise reduziert. Darüber hinaus ist zu beobachten, dass die Ausgangsdrehmomente über die Simulationsexperimente hinweg abnehmen, insbesondere an ihren Spitzen (Abbildung 6), und die Ausgangsgeschwindigkeiten während der Simulationsexperimente gleich bleiben. Im Vergleich dazu nimmt die Kraft für das Gelenk $J_1$ aufgrund der abnehmenden Materialbeladung im Extruder ab, die Fehler über die gesamte Simulation sind jedoch vernachlässigbar.

Die Ergebnisse von Experimenten, die in der Simulationsumgebung durchgeführt wurden, zeigen, dass die geschätzten Gelenkpositionen für die Gelenke des Lehmdruckers die Zieltrajektorien mit minimaler Abweichung erfolgreich verfolgen. Die Simulationsumgebung zeichnet sich durch Echtzeitleistung und latenzfreie Schätzung der Gelenkpositionen aus und ist zudem robust gegenüber Robotersingularitäten. Die Ergebnisse validieren somit das implementierte Simulationssystem für weitere Experimente mit realen Daten, um Extrusionsratenfehler aus den Simulationsdaten zu bewerten und Regelungsstrategien zu definieren.

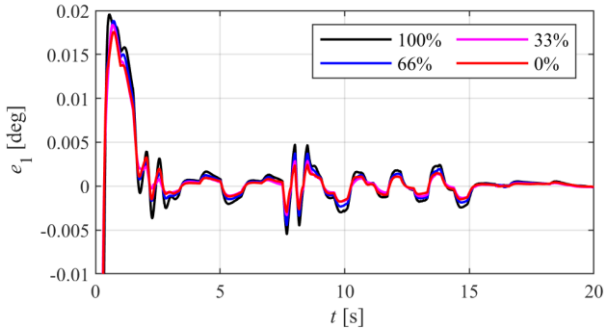


Abbildung 5. Fehlerverfolgung für die Position des Gelenks $J_1$.

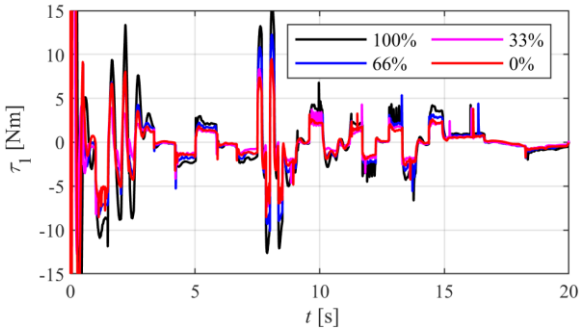


Abbildung 6. Drehmoment des Gelenks $J_1$.

## 3 Zusammenfassung und Schlussfolderungen

In dieser Arbeit wurde der Einfluss der Roboterkinematik auf den Druckprozess mit Hilfe eines auf einem digitalen Zwilling basierenden Ansatzes untersucht. Ein digitaler Zwilling wurde entwickelt, um die Bewegung von Lehmdruckern nachzubilden und dadurch Druckprobleme zu identifizieren, die durch kinematische Effekte verursacht werden, und um die Druckwegplanung zu validieren. Zur Validierung wurde der Druckprozess an einem 3-DOF SCARA Lehmdrucker simuliert.

Zur Umsetzung des Konzept des digitalen Zwillings wurde eine etablierte Referenzarchitektur für digitale Zwillinge verwendet [14] und auf die Erkenntnissen im Bereich intelligenter Sensortechnologien zurückgegriffen [15], die mit dem Lehmdruck gekoppelt wurden. Der digtiale Zwilling wurde konkret mit Hilfe von Modellierungs- und Berechnungswerkzeugen für die Modellierung der Geometrie, des Mehrkörpersystems und der Kinematik des SCARA-Lehmdruckers umgesetzt. Als Eingangsparameter verwendet der vom digitalen Zwilling bereitgestellte Simulationsdienst die inverse Kinematik, um die Bewegungen des Roboters anhand von Zieltrajektorien, Zieldruckgeschwindigkeiten und der Materialbeladung des Extruders zu replizieren. Die Validierung wurde an einem rechteckigen Wandelement mit einer gezackten Innenstruktur unter Berücksichtigung unterschiedlicher Materialbeladungen durchgeführt. Zur Darstellung der Simulationsergebnisse wurden Vergleichskurven verwendet. Es wurde festgestellt, dass sich die Genauigkeit des Lehmdruckers verbessert, wenn die Materialnutzlast während des Druckvorgangs aufgrund von Materialextrudierung abnimmt. Die Ergebnisse zeigen, dass der Ansatz, der für die Modellierung eines SCARA-Lehmdruckers verwendet wurde, praktikabel ist. Das Modell stellt eine robuste und schnelle Simulationsumgebung dar, die zur Optimierung kinematischer Abweichungen verwendet werden kann.

Zusammenfassend lässt sich festhalten, dass Probleme, die sich aus der Roboterkinematik ergeben, durch die Bewertung von Druckparametern über Simulationen der Druckerbewegungen durch die Entwicklung geeigneter Druckstrategien entschärft werden können. Die Validierung wurde an einer Teststruktur durchgeführt, bei der kinematische Effekte durch Vibrationen und Ruckbewegungen zu erwarten sind, z. B. erhöhte Fehlerraten an scharfen Ecken. Der vom digitalen Zwilling erbrachte Simulationsdienst stößt jedoch an seine Grenzen, da Sensordaten aus dem SCARA-Lehmdrucker als Eingaben benötigt werden, um den Kompromiss zwischen Druckgenauigkeit und Druckgeschwindigkeit weiter zu analysieren. In Zukunft könnte die Forschung auf die Entwicklung von DT-Diensten für das Echtzeitmonitoring und Geräteregelung beim Lehmdruck zur Archivierung des adaptiven Drucks ausgeweitet werden.

## Danksagungen

Die Autoren bedanken sich für die Unterstützung durch die Deutsche Forschungsgemeinschaft (DFG) im Rahmen der Sachbehilfen mit den Geschäftszeichen SM 281/17-1 und SM 281/22-1 sowie durch die Technische Universität Hamburg im Rahmen des Juniorprojekts „Digitalization of earth printing to advance climate-informed engineering“ im Programm I$^3$. Unser herzlicher Dank geht auch an die HC Hagemann GmbH & Co. KG, Hamburg, Deutschland, für die großzügige Bereitstellung der für diese Studie genutzten Infrastruktur. Die in diesem Beitrag geäußerten Meinungen, Erkenntnisse, Schlussfolgerungen und Empfehlungen sind die der Autoren und spiegeln nicht notwendigerweise die Meinung der vorgenannten Institutionen und Partner wider.

## References

[1] Perrot, A., Rangeard, D., & Courteille, E. (2018). 3D printing of earth-based materials: Processing aspects. *Construction and Building Materials*, 172(2018), S. 670-676.

[2] Smarsly, K., Peralta, P., Luckey, D., Heine, S., & Ludwig, H.-M. (2020). BIM-based concrete printing. In: *Proceedings of the International ICCCBE and CIB W78 Joint Conference on Computing in Civil and Building Engineering 2020*. Sao Paolo, Brasilien, 18.08.2020.

[3] Wolf, A., Rosendahl, P.L., & Knaack, U. (2022). Additive manufacturing of clay and ceramic building components. *Automation in Construction*, 133(2022), 103956.

[4] Gomaa, M., Jabi, W., Veliz Reyes, A., & Soebarto, V. (2021a). 3D printing system for earth-based construction: Case study of cob. *Automation in Construction*, 124(2021), 103577.

[5] Gomaa, M., Vaculik, J., Soebarto, V., Griffith, M., & Jabi, W. (2021b). Feasibility of 3DP cob walls under compression loads in low-rise construction. *Construction and Building Materials*, 301(2021), 124079.

[6] Peralta, P., Heine, S., Ludwig, H.-M., & Smarsly, K. (2020). A BIM-based approach towards additive manufacturing of concrete structures. In: Proceedings of the 27th International Workshop on Intelligent Computing in Engineering (EG-ICE). Berlin, 01.07.2020.

[7] Kontovourkis, O. & Tryfonos, G. (2020). Robotic 3D clay printing of prefabricated non-conventional wall components based on a parametric-integrated design. Automation in Construction, 110(2020), 103005.

[8] Dörfler, K., Dielemans, G., Lachmayer, L., Recker, T., Raatz, A., Lowke, D., & Gerke, M. (2022). Additive manufacturing using mobile robots: Opportunities and challenges for building construction. Cement and Concrete Research, 158(2022), 106772.

[9] Dai, C., Lefèbvre, S., Yu, K., Geraedts, J.M.P., & Wang, C.C.L. (2020). Planning jerk-optimized trajectory with discrete time constraints for redundant robots. IEEE Transactions on Automation Science and Engineering, 17(4), S. 1711-1724.

[10] Tao, F., Cheng, J., Qi, Q., Zhang, M., Zhang, H., & Sui, F. (2018). Digital twin-driven product design, manufacturing and service with big data. The International Journal of Advanced Manufacturing Technology, 94(2018), S. 3563-3576.

[11] Smarsly, K., Ahmad, M. E., Peralta, P., Al-Zuriqat, T., Al-Nasser, H., Dragos, K., & Chillón Geck, C. (2024). Digital twins, architectures, and elements in civil engineering – A multivocal literature review. In: Proceedings of the 20th International Conference on Computing in Civil and Building Engineering (ICCCBE). Montréal, Kanada, 25.08.2024.

[12] MathWorks (2024). Simulink: Simulation and model-based design, online: https://de.mathworks.com/products/simulink.html. Zugriff am 27.03.2024.

[13] Denavit, J. and Hartenberg, R.S. (1955). A kinematic notation for lower-pair mechanisms based on matrices. Journal of Applied Mechanics, 22(2), S.215-221.

[14] Smarsly, K., Peralta, P., Dragos, K., Ahmad, M. E., Al-Zuriqat, T., Chillón Geck, C., & Al-Nasser, H., (2024). A multivocal literature review of digital twins, architectures, and elements in civil engineering. In: Proceedings of the 11th European Workshop on Structural Health Monitoring (EWSHM). Potsdam, 10.06.2024.

[15] Smarsly, K. & Tauscher, E. (2016). Monitoring information modeling for semantic mapping of structural health monitoring systems. In: Proceedings of the 16th International Conference on Computing in Civil and Building Engineering (ICCCBE). Osaka, Japan, 06.07.2016.

# Continuous monitoring of construction sites using mobile machinery - a case study

Artem Bliznyuk[1], David Böken[1], Lennart Schinke[1] and Jorge Luis Jiménez Aparicio[1]
[1]Institute of Man-Machine Interaction, RWTH Aachen University, Ahornstraße 55, 52074 Aachen. Germany
E-mail(s): bliznyuk@mmi.rwth-aachen.de, boeken@mmi.rwth-aachen.de, schinke@mmi.rwth-aachen.de, jimenez@mmi.rwth-aachen.de

**Abstract:** Regularly monitoring construction sites is essential for progress tracking and safety evaluation during a construction project. Conventional methods rely on periodic surveys and manual data collection through site personnel. Additionally, current research investigates the use of unmanned ground/aerial vehicles. However, both approaches present limitations, such as time and labor inefficiency, or unreliable navigation and susceptibility to harsh outdoor conditions. In this paper, we present a novel approach for site monitoring by augmenting mobile construction machinery with sensors and leveraging their mobility onsite. To validate this approach, a wheel loader was equipped with a setup consisting of LiDAR, Camera, and GNSS sensors and deployed it over multiple months during a real road construction project. This paper analyzes the setup's performance during outdoor operation and the quality of the collected data for the implementation of automated and continuous mapping. Afterward, the encountered challenges and advantages of our approach are discussed. The results demonstrate the feasibility of using mobile machinery for this task and are a first step for an automated site monitoring system.

*Keywords:* outdoor monitoring, construction site, mobile machinery, LiDAR, automation

Erschienen in Tagungsband 35. Forum Bauinformatik 2024, Hamburg, Deutschland, DOI: 10.15480/882.13516
© 2024 Das Copyright für diesen Beitrag liegt bei den Autoren. Verwendung erlaubt unter Creative Commons Lizenz Namensnennung 4.0 International.

## 1 Introduction

Monitoring the state of a construction site is an integral process of every construction project. Time and resource management, quality control, and safety evaluation are directly dependent on the employed monitoring methods, as they require information about what is done onsite, when and by whom. Conventional monitoring is mostly achieved through periodic reports by the foreman and more extensive bi-weekly to monthly visits to the site. Important observations are noted on a site plan, supported by comments and photographs. This approach is time-inefficient, relies almost entirely on frequent manual labor, and is error-prone due to its subjective nature [1]. Moreover, such documentation tends to come from different sources and in different formats, making it more difficult to analyze and manage it [2].These issues are being tackled by the current trend of automated data collection via unmanned aerial or unmanned ground vehicles (UAV/UGV), which, however, has

barriers of its own [3], [4]. One important issue is robust navigation in the dynamic, rough and often unstructured environments of construction sites. Moreover, unmanned vehicles must avoid collisions or obstructions of workers and machines.
In comparison, mobile machinery (e.g. a wheel loader) already constantly traverses the construction site and operates near areas where construction is actively taking place. Equipping it with sensors normally used with UGVs results in a mobile mapping system (MMS) that operates "autonomously", as it does not require additional personnel to control the vehicle apart from the already employed machine operator. This paper explores this approach of automated site monitoring by first presenting the design and deployment of a demonstrator on a real construction site, and then analysing the gathered monitoring data and discussing the strengths and weaknesses of this approach.

## 2 Related works

MMSs are used in several domains for automatically obtaining updated and accurate geospatial data. Some of the domains where MMSs have been extensively utilized include road asset management and condition assessment, Building Information Modeling for archaeological reconstruction and transportation infrastructure analysis, emergency and disaster response, riverine vegetation mapping and detection, tree detection and measurement and digital heritage conservation [5].
On construction sites, UAVs are often the choice for a MMS and are mainly used for inspection and surveying [3]. An example for real-time reconstruction of a construction site was demonstrated by Shang and Shen [6] by using Visual Simultaneous Location and Mapping (SLAM). Since UAVs normally need an operator and are susceptible to bad weather, there is a trend to combine them with UGVs for better results. The general idea is to use the UAV's aerial view of the scene to provide the UGV with a clearer understanding of its surroundings and allow for robust navigation. This strategy was implemented, for example, by Kim et. al. [7] for an outdoor environment and by Asad et. al. [8] for an indoor environment, respectively. Other methods are extensively described by Rao et al.[9], however, almost all identified use cases for monitoring dynamic environments used stationary sensor setups. Only two examples mention mobile sensors setups—one on a car for earthwork monitoring and another on a crane for safety monitoring of crane operation.
Typical sensors used in MMSs are light detection and ranging (LiDAR) and high-resolution cameras for data acquisition of objects and areas of interest, as well as global navigation satellite system (GNSS) and inertial measurement unit (IMU) for positioning and georeferencing. However, there is no single, standardized MMS setup that is widely adopted because the selection of sensors depends on several use case specific factors such as budget, sensor availability, scene contents, processing strategies and accessible platforms for the MMS mounting [5].

## 3 System design

### 3.1 Physical setup

For this study, a wheel loader was equipped with a setup of different sensors, shown in Figure 1. It consists of a monocular webcam at the front, four LiDARs (*Ouster OS1-64*, two *Velodyne VLP-16* and *Blickfeld Cube 1*) pointing in different directions and a *GNSS receiver*. This selection was motivated

by the availability of the sensors to the authors. As shown on the top left in Figure 1, the sensors and a control cabinet, that houses the hardware infrastructure, were mounted on a rack consisting of aluminum profiles. This allows the entire setup to be pre-assembled, tested and initially calibrated. All sensors, the switch cabinet and its cable glands had an ingress protection rating of at least IP66. The whole setup was then installed on the roof of a wheel loader, as shown on the bottom left in Figure 1. Consequently, operations on the construction site only had to be interrupted for a short time. The mobility and versatility of a wheel loader on-site motivated its choice for this study. The chosen machine was a CAT 908M provided by the construction company working on the site. Apart from possibly different mounting techniques and positions of the sensors, this setup can be adapted to different models and even types of construction machines.

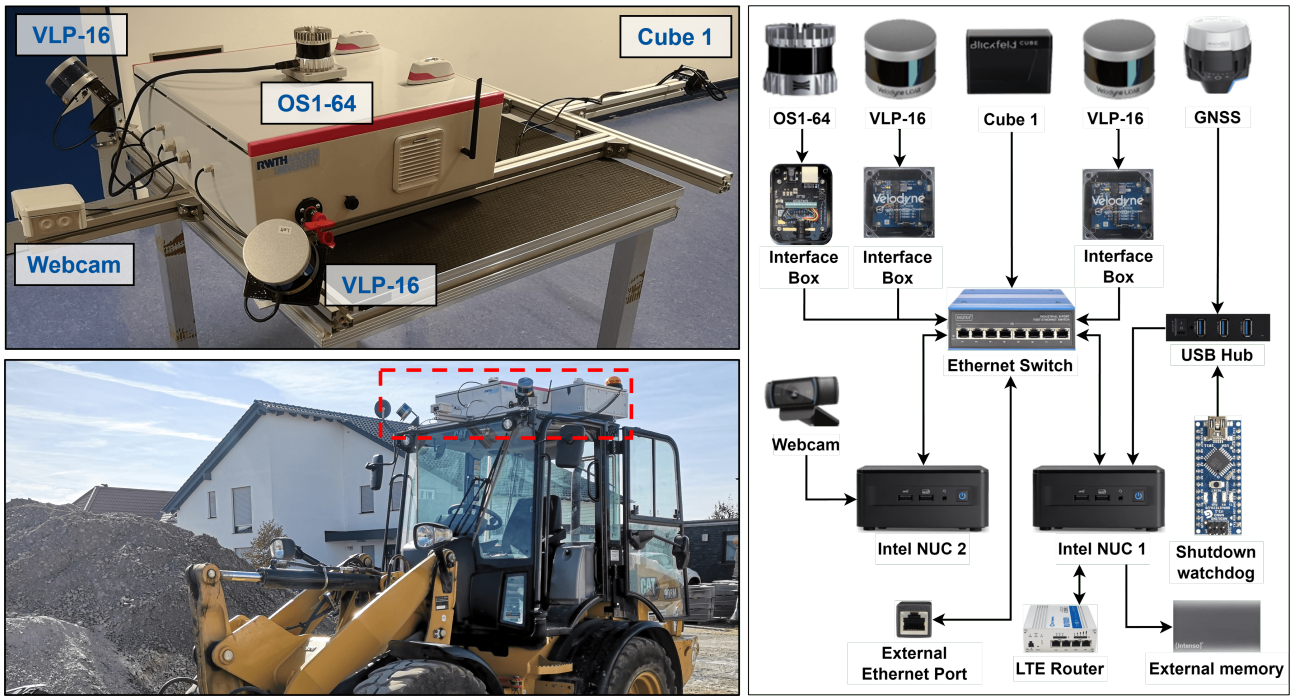


Figure 1: Top left: Sensor setup with positions of visible sensors. The GNSS receiver is inside the switch cabinet. Bottom left: Sensor setup mounted on the wheel loader[1]. Right: Schematic structure of sensor setup.

The right side of Figure 1 shows the internal architecture of the setup. It was connected to the 12 V battery of the wheel loader. One exception is the shutdown watchdog, which is connected to both ignition and continuous plus to detect when the wheel loader is turned off to safely power down the sensor system and prevent unwanted power drainage. Electrical components such as voltage converters or fuses are left out of the diagram for better readability.

### 3.2 Software setup

Minimizing interference with usual processes during active construction was an important design goal of the measurement system. To achieve this, easy on-site and remote access to the actual software

[1]An additional switch cabinet can be seen. Its only function was to store the rather expensive sensors during longer downtimes, such as winter break, as the particular site didn't offer any security measures against vandalism or theft.

stack was implemented. Additionally, the system was programmed robustly, so short issues during a recording did not corrupt the whole file.
The implemented software stack is based on *Ubuntu 22.04* with *ROS2 iron* running on two *Intel NUCs*, distributing the workload between them. The communication between the NUCs, as well as several sensors, was done via an Ethernet network (see Figure 1). An external RJ45 jack and a bridged Wi-Fi Hotspot from one of the NUCs granted access to this network. Everything was saved to two solid-state drives (SSDs) connected to the system via *USB3*. To automatically distribute the recordings across both drives, *MergerFS*[2] was used. It combined both SSDs into one large drive by distributing the files evenly between them. The new and flexible standard *MCAP* was chosen as the format for the recordings. In order to upload the recordings to a storage system for further processing, the drives were exchanged regularly, circa every two weeks.
The load of recording was shared between both NUCs. While the first mainly managed the LiDAR sensors, GNSS, and the actual recording, the second NUC was responsible for the camera input and image compression. Every ROS component was configured to be part of the system auto-start via *systemd*, as well as the trigger for recording using *ROS bags*. By distributing everything to its own process, managed by systemd, a failure in one part of the system was not cascaded to another part, and the rest of the data remained usable. Additionally, a service was implemented to monitor the LiDAR data to trigger a restart of the drivers and sensors in case they stopped sending data. To facilitate a clean shutdown, the ignition of the wheel loader is monitored by the shutdown watchdog. If the ignition is turned off for a certain duration, both NUCs individually trigger a shutdown, resulting in a clean recording stop. In case this did not work, there was a safety relay in front of the complete system, which cuts power to everything after 3 min, to avoid draining the battery and causing problems for the actual construction work.
As the system is intended to run without regular involvement, a remote monitoring functionality was added. This included a remote accessing tool as well as regular notifications that e.g. reported startup times or current drive usage to better plan the next drive change. A remote monitoring tool was used to provide *ssh* access to the running system to inspect and resolve possible problems. The internet connection was provided through a USB LTE Modem connected to one of the NUCs. The internet was bridged into the local network as well, allowing the GNSS to download Real-Time Kinematic correction data from a Satellite Positioning Service[3], so it could work independently of any locally setup reference point.

## 4 Experiments

The setup was mounted on a wheel loader for several months to validate the proposed approach and investigate the resulting coverage of the construction site. The selected site is a final road construction project with an area of approximately 16000 m² and a house stock of 80 %. The sensor setup stayed on the machine from September 2023 until May 2024, experiencing different challenging weather conditions. During this time, data was collected on 75 full workdays. The setup turned itself on only when the wheel loader started operating. This results on average in nine individual measurements per

[2]https://github.com/trapexit/mergerfs
[3]https://sapos.de

day with an average duration of 153 min (min. 3 min, max. 300 min). A standard deviation of 71 min reflects the fluctuations in operational times.

Figure 2 shows a synchronized example of the three main data types collected with the described setup. The top left pane displays the camera image, oriented towards the wheel loader's shovel, providing a direct view of the materials being handled by the machine. The bottom left map shows the GPS signal over time, with the specific point in time indicated by a darker dot in the map. Finally, the right pane shows a 3D view of the four LiDAR sensors used, with the machine's direction of view depicted as a red arrow. The gravel pile visible on the right side of the camera image can also be recognized in blue within the point clouds, slightly further in the direction of view. Some house fronts and multiple containers can be seen on the left of the machine. The OS1-64, positioned on top, covers the mid to long-range environment displayed here with dark blue points. Both VLP-16 sensors complement it with measurements directly around the wheel loader. The left sensor is displayed in orange and the right one in green. The Cube 1 at the rear is dedicated to measuring the space behind the machine, with its points concentrated in a small area behind the machine. The acquired LiDAR

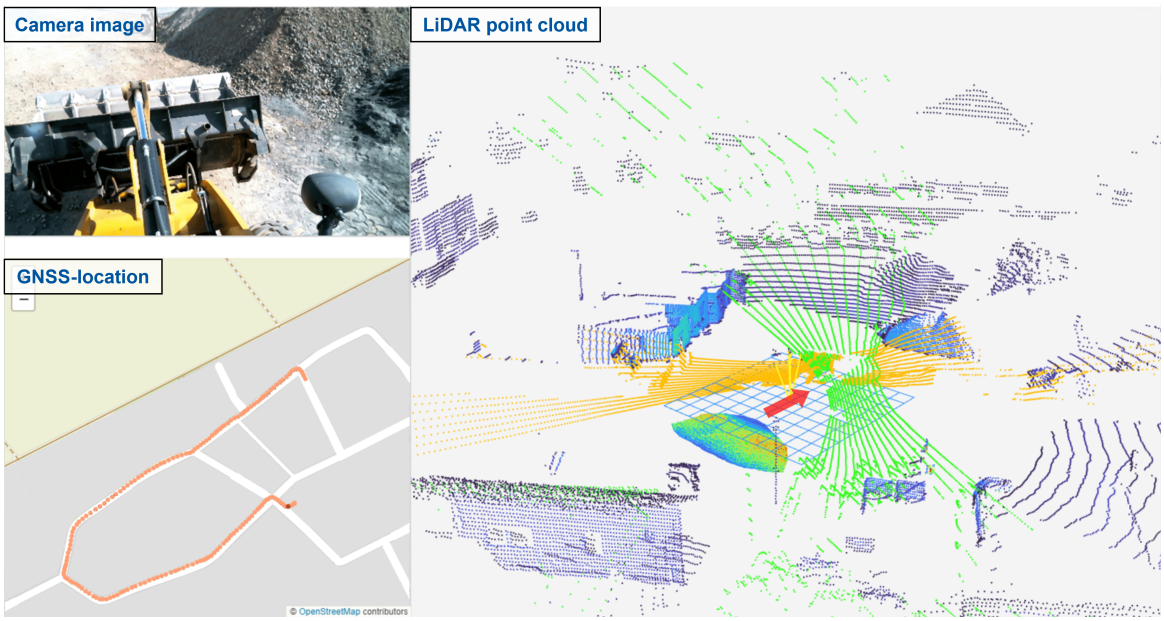


Figure 2: Visualization example of the collected data: Camera images (top left), GPS coordinates (bottom left), and LiDAR point clouds (right). These are shown at the same point in time. The red arrow symbolizes the direction the machine is facing.

scans were assembled into point clouds of the environment using a SLAM-based algorithm[4] as the first iteration of data processing. A visual examination of the recordings showed good quality of the dataset. Figure 3 illustrates the successful recreation of the construction site environment. The left and right sub-figures depict the same location several days apart, with clearly noticeable changes to the site. In the top right quadrants, a short wall and an earth heap were removed, the area evened, and an outline for future construction created. Additionally, multiple palettes with stones and some barriers were moved during pavement work, as seen on the left sides of the sub-figures. This exemplifies the

[4]https://github.com/rsasaki0109/lidarslam_ros2

usability of the data for automatic and continuous mapping. Further iterations of the processing will also include images from the camera.

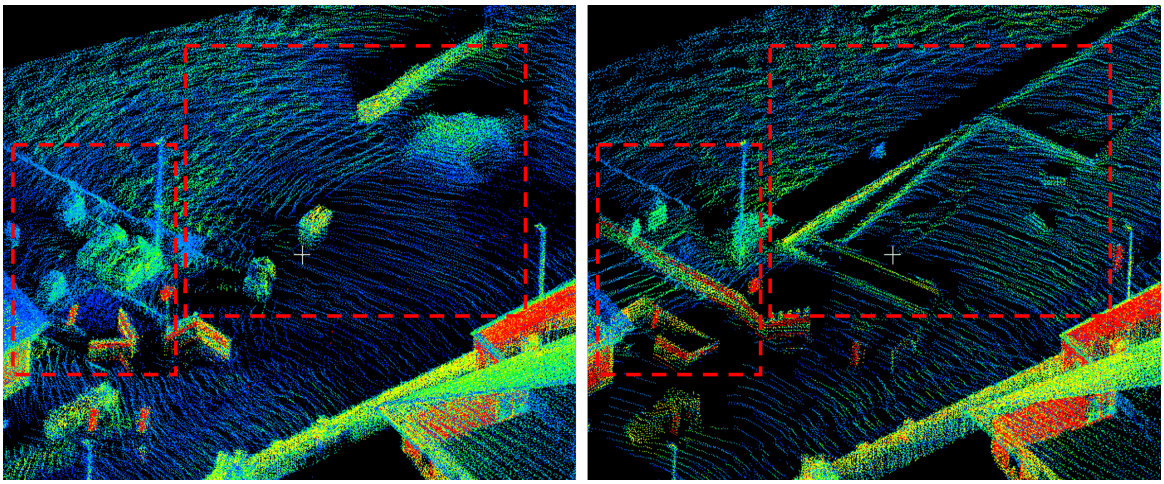

Figure 3: Generated point clouds of the same area from two different scans a few days apart. The progress on the site can be seen from left to right sub-figure, especially inside the corresponding highlighted area. The points are colored by the return intensity of the laser.

## 5 Discussion

The conducted experiments confirm some of the assumed advantages of using mobile construction machines as mapping systems. Two of the main concerns of UGVs on construction sites are robust navigation in the often unstructured and dynamic environment, and safety and acceptance by the other agents on-site [10]. Both topics have been successfully addressed through the non-invasive design of the equipment and the use of the already employed machine. Aside from a brief session, where the setup was mounted and connected to the power supply, the workers made no changes to their work schedule or task execution while enabling mobile mapping on the site. Furthermore, this approach diminishes possible fears of future competition with robots on the construction site, as it only extends the performance of the existing workforce.

As the technical setup was deployed on a real construction site during autumn, winter and spring, it was exposed to a rough working environment. Rain, dust, direct sunlight or low temperatures are normally formidable challenges for other mobile mapping systems. However, during the complete duration of the experiment, no technical failures or deterioration of measurement quality were observed. Only one issue was encountered when a power plug got loose through the vibration of the wheel loader. Luckily, this can be easily prevented in a future iteration by using a latching type of plug.

The positioning and selection of the LiDAR sensors enabled a comprehensive coverage of the surrounding area at relevant heights, providing sufficient resolution to effectively recognize objects and structures within the environment. Notably, the Cube 1 positioned in the rear offers highly detailed measurements of the ground, which could be used for soil condition studies. The front-facing camera collects image data crucial for texture-dependent object detection, particularly for identifying materials handled by the machine. This enhances the detailed monitoring of relevant objects and materials processed by the machine.

However, the field of view and angle of the camera limit the visible area, restricting material recognition based on texture to the frontal area only. This limitation can be addressed by incorporating additional cameras to cover a wider angle of the environment. Another challenge encountered with the current setup is the heterogeneity of the sensors, which require more computational power to execute fusion algorithms for data consolidation. This issue can be mitigated by employing a factory pre-calibrated sensor suite.

Analysis of the wheel loader pathing showed that although the machine traversed and mapped the majority of the site, some areas were rarely visited, yielding no updates. This can be explained in two ways: construction was simply happening somewhere else as those parts have been mostly finished, or alternatively, tasks were carried out by different machines at that time, as only one of two wheel loaders on this site was equipped with sensors. To achieve complete coverage, all involved machines should participate in the monitoring process. Another possibility is an automatic evaluation of the achieved coverage that warns if an area has not been visited in a while.

Lastly, continuous monitoring always raises the question about total surveillance of workers near the proposed MMS or the privacy of people living next to the construction site. As a result, further development of this system needs a built-in anonymization of people, license plates, predefined areas, etc. in the point clouds and images as well as a secure and transparent access policy to the data and the derived insights.

## 6 Conclusion

In this paper, a new approach to construction site monitoring was presented. By equipping mobile construction machines with typical sensors used for mobile mapping, the state of their surroundings can be surveyed. This solution can safely navigate the site and does not require additional personnel, as the already employed human operator simply carries out his usual tasks, giving it an edge over current unmanned aerial/ground vehicle based approaches. A demonstrator was built and mounted on a wheel loader. It consisted of four LiDARs, one camera and a GNSS receiver, giving a broad all-round view. The hardware infrastructure was mounted inside a switch cabinet on top of the machine and the power connected to its battery. The modified machine was used on a real construction site for several months during autumn, winter and spring. Remarkably, this setup worked robustly in the rough environment and gathered reliable data about the changes to the surroundings. This demonstrated the feasibility of the approach and builds the basis for an automated site monitoring system.

The next steps consist of further processing and automatic extraction of changes on the site between different points in time, such as position of materials and digital elevation models, and then validating the results with data from the site surveyor. Additionally, future iterations of the sensor setup will include more cameras to improve image coverage of the environment. A factory pre-calibrated sensor suite will be used to reduce the computational load and streamline data integration. This also offers the opportunity to implement the data processing directly on the edge computer and connect it to a digital twin of the site, which stores and visualizes the construction progress. Finally, multiple machines can be equipped and used at the same time to provide a more complete picture of the construction site.

## Acknowledgements

The presented research was conducted as a part of the project “Off-Highway Twins 2" funded by the program "mFUND" of the German Federal Ministry of Digital and Transport under grant ID: 19FS2036A.

## References

[1] J. Teizer, “Status quo and open challenges in vision-based sensing and tracking of temporary resources on infrastructure construction sites”, *Advanced Engineering Informatics*, vol. 29, no. 2, pp. 225–238, 2015. DOI: 10.1016/j.aei.2015.03.006.

[2] S. Karimi, R. G. Braga, I. Iordanova, and D. St-Onge, “Semantic Optimal Robot Navigation Using Building Information on Construction Sites”, *ISARC Proceedings*, pp. 57–64, 2021. DOI: 10.22260/ISARC2021/0010.

[3] A. A. Molina, Y. Huang, and Y. Jiang, “A Review of Unmanned Aerial Vehicle Applications in Construction Management: 2016–2021”, *Standards*, vol. 3, no. 2, pp. 95–109, 2023. DOI: 10.3390/standards3020009.

[4] H. I. Moud, A. Shojaei, and I. Flood, “Current and Future Applications of Unmanned Surface, Underwater, and Ground Vehicles in Construction”, *Construction Research Congress*, pp. 106–115, 2018. DOI: 10.1061/9780784481264.011.

[5] M. Elhashash, H. Albanwan, and R. Qin, “A Review of Mobile Mapping Systems: From Sensors to Applications”, *Sensors*, vol. 22, no. 11, p. 4262, 2022. DOI: 10.3390/s22114262.

[6] Z. Shang and Z. Shen, “Real-time 3D Reconstruction on Construction Site using Visual SLAM and UAV”, *Construction Research Congress*, pp. 305–315, 2018. DOI: 10.1061/9780784481264.030.

[7] P. Kim, J. Park, Y. K. Cho, and J. Kang, “UAV-assisted autonomous mobile robot navigation for as-is 3D data collection and registration in cluttered environments”, *Automation in Construction*, vol. 106, p. 102 918, 2019. DOI: 10.1016/j.autcon.2019.102918.

[8] K. Asadi, A. Kalkunte Suresh, A. Ender, *et al.*, “An integrated UGV-UAV system for construction site data collection”, *Automation in Construction*, vol. 112, p. 103 068, 2020. DOI: 10.1016/j.autcon.2019.103068.

[9] A. S. Rao, M. Radanovic, Y. Liu, *et al.*, “Real-time monitoring of construction sites: Sensors, methods, and applications”, *Automation in Construction*, vol. 136, p. 104 099, 2022. DOI: 10.1016/j.autcon.2021.104099.

[10] C. Follini, M. Terzer, C. Marcher, A. Giusti, and D. T. Matt, “Combining the Robot Operating System with Building Information Modeling for Robotic Applications in Construction Logistics”, in *Advances in Service and Industrial Robotics*, 2020, pp. 245–253. DOI: 10.1007/978-3-030-48989-2_27.

# Detection and elimination of strain reading anomalies in distributed strain sensing readings

Lisa Ulbrich[1]
[1]Hentschke Bau GmbH, Zeppelinstr. 15, 02625 Bautzen, Germany
E-Mails: ulbich.lisa@hentschke-bau.de

**Abstract:** Distributed strain sensing (DSS) is increasingly used in structural health monitoring (SHM). Unlike conventional measurement technology, DSS allows for quasi-continuous measurement of strains with high spatial resolution, enabling the recording of global strain changes in the structure. However, DSS readings are subject to process-related interference, such as dropouts and strain reading anomalies (SRA). SRA can hinder data analysis during postprocessing or even falsify the results. Because of high amount of data produced by DSS, it is crucial to detect and remove SRA from DSS readings during automated preprocessing. Outlier removing methods from literature were analysed for their potential application to DSS readings. Based on this analysis, a sliding median z-score had been proposed, implemented in the *fosanalysis* framework and applied to various DSS readings for validation and to determine suitable parameters.
*Keywords:* Strain Reading Anomalies, Distributed Fibre Optic Sensors, Distributed Strain Sensing

Erschienen in Tagungsband 35. Forum Bauinformatik 2024, Hamburg, Deutschland, DOI: 10.15480/882.13497
© 2024 Das Copyright für diesen Beitrag liegt bei den Autoren. Verwendung erlaubt unter Creative Commons Lizenz Namensnennung 4.0 International.

## 1 Introduction

### 1.1 Distributed strain sensing in structural health monitoring

*Distributed fibre optical sensors (DFOS)* become increasingly relevant in structural health monitoring (SHM). Unlike traditional measurement techniques (e.g. strain gauges), DFOS can capture global changes in strain within the structure, making them suitable for both event-related and event-independent SHM purposes. Of particular interest is distributed strain sensing (DSS), based on coherent optical frequency domain reflectometry (cOFDR) of Rayleigh backscatter [1]. This measurement technique provides strain readings with an accuracy of up to 1 µm/m, measurement rates of up to 250 Hz, and spatial resolution of up to 0.65 mm [2] and therefore allows the monitoring of crack patterns and crack development in concrete structures [3] and facilitates the detection of deformations [4] within a structure. Hence, DSS has enormous potential for predictive maintenance [5]. For more detailed understanding of the principal of DSS, please refer to [3].

## 1.2 Strain Reading Anomalies (SRA)

Due to the application of cOFDR, process-related disturbances in the DSS readings like dropouts and SRA occur [6, 7]. Dropouts are measurement points for which no strain reading is available, while SRA manifest as significant local peaks in strain readings [7]. A strain peak is considered a SRA if it exhibits a considerable deviation from the previous and following measurement, in space and/or time (i.e. space and/or time domain) [8].

In [7], SRA in DFOS strain readings on reinforcing bars were analysed using a ODiSI-A OBR. It was shown, that SRA often occur at neighbouring sensor positions and thus form so-called anomalistic areas [7]. These anomalistic areas occur preferably in highly strained sensor sections or sections with high strain gradients [7]. Furthermore, SRA have been classified into harmful and harmless SRA [7]. Harmful SRA (HF-SRA) occur at the same sensor position at all measurement times, while harmless SRA (HL-SRA) only occur at certain times. In contrast to HL-SRA, HF-SRA only exhibit an abrupt increase along the time axis and then remain constant, which means that no more actual strain values are registered at this sensor positions [7, 8].

The presence of SRA can impede accurate data analysis during postprocessing or even lead to false results. Thus, elimination of strain reading anomalies is vital to ensure accurate and reliable results in SHM using DSS [1, 7]. However, the ideal approach is to prevent or minimize SRA through technical measures e.g. selecting an appropriate sensor [8]. If technical measures fail to prevent SRA, detecting and removing SRA is necessary as part of the data preprocessing [8].

## 1.3 Outlier elemination methods

In the following, elimination methods from other fields of application are also considered, which is why the term "outliers" is used instead of SRA. Usually, there are two strategies to deal with outliers:

1) **Smoothing methods** can align outliers with the measurement but do not remove them. Common smoothing methods are sliding average [1, 9], sliding median [1, 10], locally weighted scatterplot smoothing (LOWESS), spline interpolation, and Savitzky-Golay filter [9]. However, smoothing methods are disadvantageous for typical postprocessing applications (e.g., crack width calculation), as they replace actual measurement values with calculated (other) values and thus could falsify postprocessing results [9].

2) **Detection methods** use thresholds to detect and subsequently remove outliers. Detection methods are, e.g., geometrical threshold method (GTM) [8], polynomial interpolation comparison method (PICM) [8], and z-value-based methods [11]. Defining a threshold can be challenging as it should neither erroneously exclude genuine values (false positive) nor disregard outliers (false negative).

Both strategies can be applied to space or time domains or simultaneously to both domains. For DSS readings the strain state can vary significantly over time, whereas a change in strain over

distance is usually limited due to the close proximity of the measuring points in the physical structure [8].

Z-score-based methods, including z-value, modified z-score and Whitaker-Hayes z-score [11], differ from other detection methods by increasing the exaggeration of an outlier, making it easier to determine a threshold. Additionally, these methods can be fully automated, unlike PICM, making them highly efficient for analyzing large datasets. Due to these favorable properties, z-score-based methods show great potential for detecting SRA and will be elaborated on further.

While z-score is based on the mean, modified z-score uses the median [11]. Since the median itself is more stable against outliers, the difference between modified z-score of actual measurement values $z_{AMV}$ and z-score of SRA-values $z_{SRA}$ is more significant. Thus, modified z-score has a greater potential for SRA detection in DSS than z-score [11]. The modified z-score $z_i$ is calculated as follows:

$$z_i = \left| 0.6745 \cdot \frac{y_i - \tilde{y}}{\mathrm{MAD}} \right| \tag{1}$$

Where $y_i$ is the measurement value $i$, $\tilde{y}$ is the median of all measured values $y$. The term $y_i - \tilde{y}$ is called absolute deviation (AD). $\mathrm{MAD}$ is the median of all AD's. The multiplier 0.6745 compensates for the asymptotic distortion when calculating $\mathrm{MAD}$ from standard distribution [12].

The Whitaker-Hayes z-score according to [13] uses the median of $\Delta_i = y_i - y_{i-1}$. Since in DSS readings $\Delta_i$ is significant between SRA and their predecessor as well as their successor, there might be significant $z_{AMV}$, that can be classified false positive. Another issue appears with anomalistic areas. Up to the values of neighbouring SRA, $\Delta_i$ might be small, resulting in small $z_{SRA}$. In this case, the result is false negative. Last but not least, dropouts next to SRA lead to missing AD values and thus to missing $z_{SRA}$, resulting in false negative classification.

All in all, modified z-score shows the greatest potential for SRA detection in DSS readings. However, DSS readings with wide measurement value range, i.e. due to cracks, lead to $z_{AMV}$ close to $z_{SRA}$ due the shift of the median resulting in higher AD. Therefore, the modified z-score is not reliable for SRA detection in DSS readings with a wide measurement value range.

## 2 Sliding modified z-score

In order to overcome the issues of modified z-score described before, a combination of sliding median and modified z-score called sliding modified z-score $sz_i$, is proposed as follows:

$$sz_i = \left| 0.6745 \cdot \frac{\varepsilon_i - \widetilde{\varepsilon_{(\iota \pm r)}}}{\mathrm{MAD}} \right| \tag{2}$$

where $\varepsilon_i$ is the strain measurement value $i$ and $\widetilde{\varepsilon_{(\iota \pm r)}}$ is the median of all strain measurement values in the radius $r$ (sliding median). Thereby, term $\varepsilon_i - \widetilde{\varepsilon_{(\iota \pm r)}}$ is called the AD from the sliding median. $\mathrm{MAD}$ is the median of all AD's from the sliding median.

In contrast to median $\tilde{y}$, the sliding median $\widetilde{\varepsilon_{(\iota\pm r)}}$ leads to a median close to $\varepsilon_i$ and thus to smaller AD. In order to reduce the AD for $\varepsilon_{AMV}$ but not for $\varepsilon_{SRA}$, $r$ has to be choosen small enough to get $\widetilde{\varepsilon_{(\iota\pm r)}}$ close to $\varepsilon_{AMV}$, but wide enough minimize influence by SRA.

Due to the sliding median, AD can possibly tend towards 0. Thus, MAD might be 0 and $sz_i$ cannot be calculated. In that case, MAD is replaced by the mean of all AD's from the sliding median (MeanAD). In order to compensate for asymptotic distortion when calculating MeanAD from a standard distribution, the multiplier has to be replaced by 0.7979 [12].

In order to classify and sort out SRA, a threshold $t$ has to be defined. If $sz_i$ exceeds $t$, $\varepsilon_i$ is identified as SRA and replaced by a dropout:

$$sz_i > t \rightarrow SRA \tag{3}$$

In order to validate the algorithm and find a suitable $r$, various DSS readings where processed in the space domain with different $r$. All readings were from an ODiSi 6100 from Luna Innovation Inc. using monolithic Epsilon Sensors from Nerve-Sensors. The performance of the sliding modified z-score was validated regarding the resulting distance $\Delta sz$ between maximum sliding modified z-score the actual measurement values $\max z_{AMV}$ and minimum sliding modified z-score of the SRA's $\min z_{SRA}$. A high $\Delta sz$ allows determination of a reliable $t$, which neither erroneously excludes genuine values (no false positive) nor disregards outliers (no false negative). In case of $\Delta sz \leq 0$ definition of $t$ is not possible.

## 3 Demonstration strain readings from single crack

A dataset of DSS readings from a single crack in a prestressed concrete girder in 4-point bending is used for demonstration. The dataset contains a single SRA at x = 0,039 m and a variety of dropouts in the neighborhood. The SRA was varied regarding the difference S between the latest available $\varepsilon_{AMV}$ and $\varepsilon_{SRA}$ in a range between +5000 µm/m and -5000 µm/m, see *figure 1*.

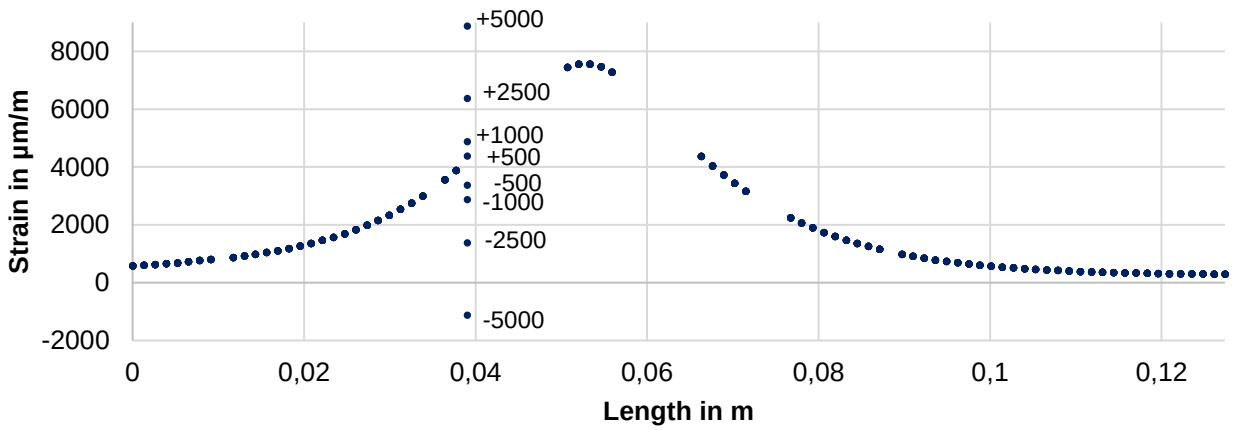


Figure 1: Predefined Dropouts and SRA's in the crack area.

Sliding modified z-score was applied to the DSS reading for each SRA variation with radius $r$ = 1…15. Examples for the resulting distances $\Delta sz$ are shown in *Figure 2*.

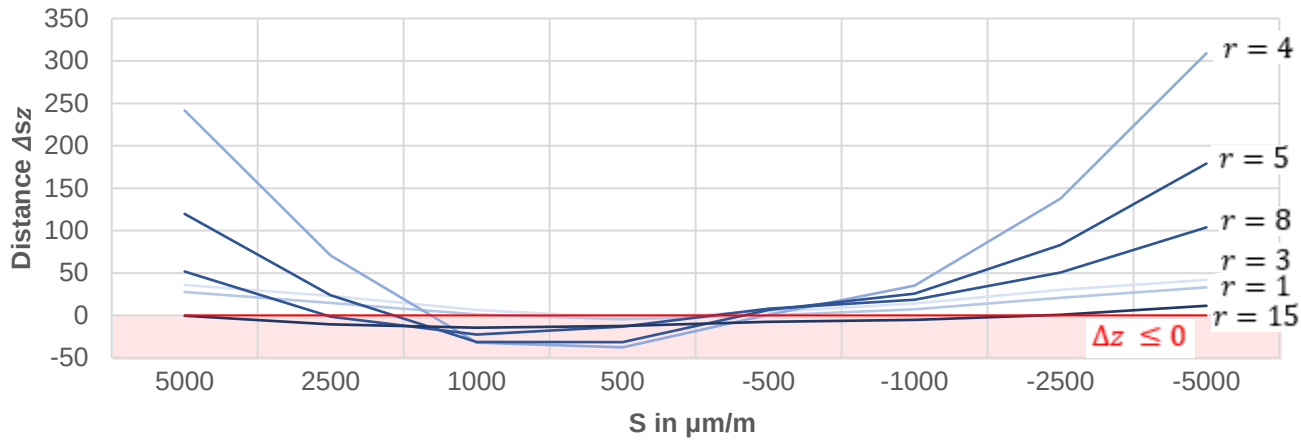


Figure 2: Distance $\Delta z$ between $\max z_{AMV}$ and $\min z_{SRA}$.

For $r$ = 1-3 all SRA can be detected, except for $S$ = 500 µm/m. However, $\Delta sz$ is quiet small for all SRA. The highest $\Delta sz$ can be reached with $r = 4$ or 5. For $r = 4$ or 5 only SRA with S = 500 µm/m and S = 1000 µm/m can not be detected. Thus, $r = 4$ and 5 are most promising for removing SRA. While with $r = 4$, SRA still have high impact on sliding median $\widetilde{\varepsilon_{(\iota \pm r)}}$, with $r = 5$ SRA have less impact. For higher $r$, $\Delta sz$ becomes smaller and fewer SRA can be detected.

## 4 Validation on strain readings with multiple cracks

In order to validate algorithm and parameters, the proposed modified z-score has been applied to DSS readings of prestressed concrete beams with multiple cracking, see *figure 3*. Due to pre-stressing and multiple cracking strain readings show a wide range between appr. -220 µm/m and +12 000 µm/m. While reading 1 has only one SRA (a1) at x = 2.7963 m, reading 2 has an accumulation of four SRA (a2 to d2) next to each other at x = 0.7475 m … 0.7527 m forming an anomalistic area, with one dropout between. Parameter $r$ was set to 4 and 5.

For reading 1, it delivers a high $\Delta sz$ with both $r$, see *Figure 4*. For reading 2, the resulting $\Delta sz$ are much smaller, see *Figure 5*. Furthermore, the resulting $\Delta sz$ differ up to $|S|$ of the SRA. Thereby, $|S|$ is the absolute difference between the latest available $\varepsilon_{AMV}$ and $\varepsilon_{SRA}$. SRA with $|S| > 6900$ µm/m (a2 and d2) result in positive $\Delta sz$ and are thus possible to recognise and eliminate by a suitable threshold *t*. SRA with $|S| < 1500$ µm/m (b2 and c2) result in negative $\Delta sz$ and can not be detected anymore. $r = 4$ results in higher $\Delta sz$ also in reading 2.

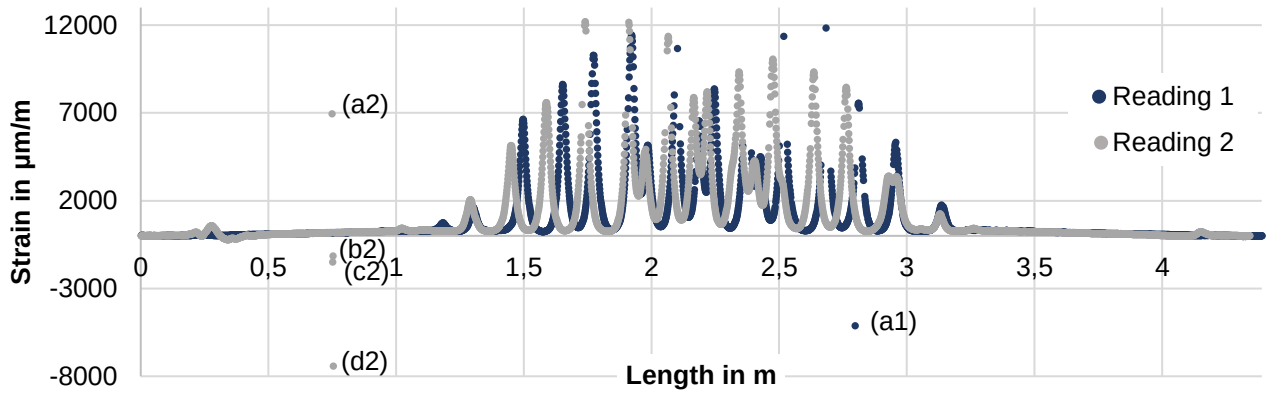


Figure 3: DSS reading 1 and 2.

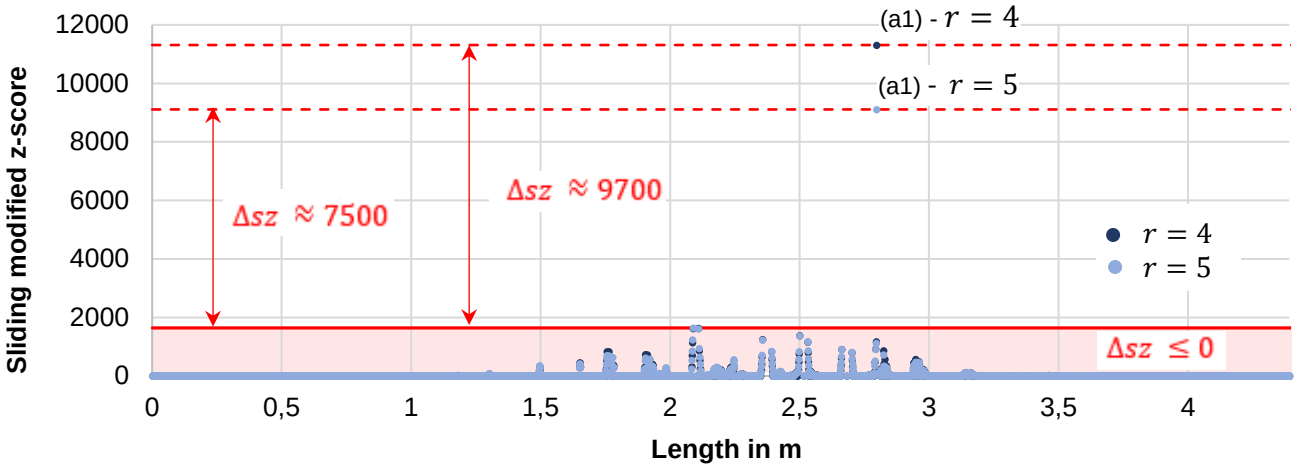


Figure 4: Sliding modified z-score for DSS reading 1 with $r = 4$ and $5$.

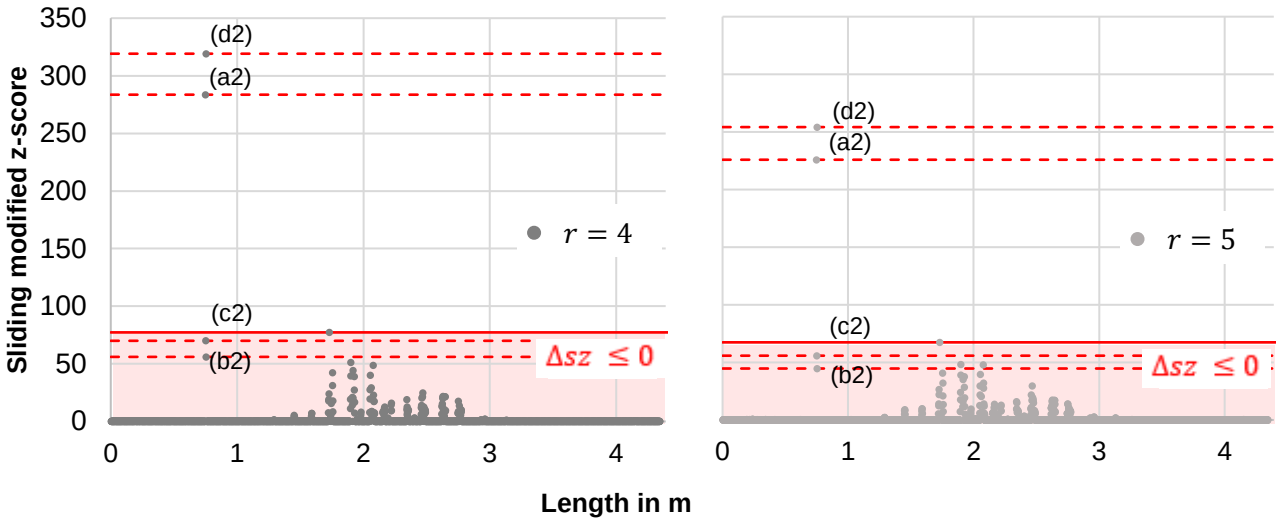


Figure 5: Sliding modified z-score for DSS reading 2 with $r = 4$ and $5$.

## 5 Discussion

The application of the sliding modified z-score on a single crack shows, that $r = 4$ and $5$ are most promising for SRA detection. $r > 5$ increases AD, resulting in a smaller $\Delta z$. For $r < 4$ sliding median is influenced by SRA, resulting in small AD and a smaller $\Delta sz$. Furthermore, the closer an SRA is to the actual measurment values, the smaller is $\Delta sz$. The smaller $\Delta sz$, the less likely is a threshold t for DSS readings with a wide range of measured values, which neither ignores outliers nor sorts out real measured values.

The validation shows, that sliding modified z-score works well with $r = 4$ and $5$ for DSS readings with a wide range of measured values and with high SRA. It allows defining a threshold, which neither erroneously exclude genuine values nor disregard outliers. In reading 2, the anomalistic area influences the median, resulting in a low AD for SRA. Additionally, MAD becomes 0 and has been replaced by MeanAD, which is, due to the impact of SRA, higher than MAD. Thus, for smaller SRA $\Delta sz$ got negative. In order to avoid this, $r$ has to be increased, when there are two or more SRA next to each other.

## 6 Conclusion

Sliding modified z-score has shown to allow reliably detecting and removing SRA in DSS readings. Currently, the definition of a proper threshold *t* seems to be specific to the dataset. An automatic definition of threshold *t* would enable an automated SRA removal in DSS readings. Since small SRA have only minor or neglible impact on postprocessing results, automatic SRA removal can be limited to large and medium SRA's in most practical applications. The impact of SRA on postprocessing applications, such as crack detection, crack width calculation and others, has to be investigated.

Sliding modified z-score will be published in fosanalysis v0.4 .The software fosanalysis is available as free/libre open source software at https://github.com/TUD-IMB/fosanalysis.

## Acknowledgements

This article presents results of the research project IDA-KI (Automated assessment of monitoring data for infrastructure constructions using AI and IoT), funded by the Federal Ministry for Digital and Transport, Germany, within the innovation program mFUND (funding reference: 19FS2013C).

## References

[1] B. Richter, M. Herbers, and S. Marx, "Crack monitoring on concrete structures with distributed fiber optic sensors – Toward automated data evaluation and assessment," *Structural Concrete*, vol. 25, no. 2, pp.1465-1480, Nov. 2023. doi: 10.1002/suco.202300100.

[2] Luna Innovations Inc., *Optical Distributed Sensor Interrogator Model ODiSI 6: User's Guide,* 2020. [Online] Available: https://lunainc.com/sites/default/files/assets/files/resource-library/ODiSI%206100%20User%20Guide.pdf. [Accessed: Jun. 8, 2024.]

[3] O. Fischer, S. Thoma and S. Crepaz, „Distributed fibre optic sensing for crack detection in concrete structures", *Civil Engineering Design,* vol. 1, Jul. 2019. doi: 10.1002/cend.201900008.

[4] C. Monsberger and W. Lienhart, "Distributed Fiber Optic Shape Sensing of Concrete Structures", *Sensors,* vol. 21, no. 18, Sept. 2021. doi: 10.3390/s21186098.

[5] M. Herbers, B. Richter, B. Schwarz, and S. Marx, „Messtechnische Überwachung von Spannbetonbauteilen mit faseroptischen Sensoren," In Proc. 12. Symposium Experimentelle Untersuchungen von Baukonstruktionen, 2023. doi: 10.25368/2023.143.

[6] S. Poe and M. Davis, Luna Innovations Inc., Personal emails (Jan. 2024).

[7] M. F. Bado, J. R. Casas, and A. Barrias, "Performance of Rayleigh-Based Distributed Optical Fiber Sensors Bonded to Reinforcing Bars in Bending," *Sensors,* vol. 18, no. 9, Sept. 2018. doi: 10.3390/s18093125.

[8] M. F. Bado, J. R. Casas, and J. G. i Esteve, "Post-processing algorithms for distributed optical fiber sensing in structural health monitoring applications," *Structural Health Monitoring,* vol. 20, no. 2, Jun. 2020. doi: 10.1177/1475921720921559.

[9] T. Janiak, H. Becks, B. Camps, M. Classen, and J. Hegger, "Evaluation of distributed fibre optic sensors in structural concrete," *Materials and Structures,* vol. 56, no. 159, Oct. 2023. doi: 10.1617/s11527-023-02222-9.

[10] T. O'Haver, *A pragmatic Introduction to Signal Processing with application in scientific measurements*, 2024. [Online]. Available: https://terpconnect.umd.edu/~toh/spectrum/. [Accessed: May 3, 2024.]

[11] N. Coca, "Removing Spikes from Raman Spectra with Anomaly Detection: Whitaker-Hayes algorithm in Python", *Towards Data Science,* Nov. 2019. [Online]. Available: https://towardsdatascience.com/removing-spikes-from-raman-spectra-8a9fdda0ac22. [Accessed: Feb. 12, 2024.]

[12] IBM, "Modified z score", 2024. [Online]. Available: https://www.ibm.com/docs/en/cognos-analytics/11.1.0?topic=terms-modified-z-score. [Accessed: Mar. 16, 2024.]

[13] D. A. Whitaker and K. Hayes, "A simple algorithm for despiking Raman spectra," *Chemometrics and Intelligent Laboratory Systems,* vol. 179, Jun. 2018. doi: 10.1016/j.chemolab.2018.06.009.

# Robotergestütztes Bauwerksmonitoring basierend auf eingebetteter Sensorik

Sergej Johann[1,2], Jan Stührenberg[1] und Aditya Tandon[1]

[1]Institut für Digitales und Autonomes Bauen, Technische Universität Hamburg, Blohmstraße 15, 21079 Hamburg, Deutschland

[2]Bundesanstalt für Materialforschung und -prüfung, Unter den Eichen 87, 12205 Berlin, Deutschland

E-Mails: sergej.johann@bam.de, jan.stuehrenberg@tuhh.de, aditya.tandon@tuhh.de

**Abstract:** In den letzten Jahrzehnten hat sich das Bauwerksmonitoring (engl. „Structural Health Monitoring“, SHM) zu einer nützlichen Ergänzung routinemäßiger Inspektionen entwickelt. SHM ermöglicht die frühzeitige Erkennung von Schäden an Bauwerken und dadurch die frühe, und somit kostengünstige, Durchführung von Reparatur- und Wartungsarbeiten. Mit dem Aufkommen drahtloser Technologien und Fortschritten in der Informations- und Kommunikationstechnologie werden Bauwerke zunehmend mit drahtlosen Sensorknoten ausgestattet, um für SHM relevante Bauwerksdaten zu erfassen, zu analysieren und zu übertragen. Eine vielversprechende Methode für SHM ist die direkte Einbettung von Sensoren in den Beton. In diesem Beitrag wird ein Sensorsystem zur Einbettung in Beton vorgestellt, das in der Lage ist, die im Beton aufgenommenen Bauwerksdaten auszuwerten. Die Sensoren werden bei Bedarf von vierbeinigen Robotern mittels Radio Frequency Identification (RFID) ausgelesen und mit Energie versorgt, was einen automatisierten und effizienten Prozess ermöglicht. Der prototypische Prozess zur automatischen Erfassung von Bauwerksdaten mit eingebetteter Sensorik und vierbeinigen Robotern wird durch Tests in einer Büroumgebung validiert. Die Ergebnisse der Tests bestätigen die automatische und effiziente Erfassung von Bauwerksdaten, die eine frühzeitige Erkennung von Bauwerksschäden, auch von nicht sichtbaren Schäden, ermöglicht, und eine folgerichtige Weiterentwicklung des modernen Bauwerksmonitorings repräsentiert.

*Keywords:* Radio Frequency Identification (RFID), Bauwerksmonitoring (SHM), eingebettete Sensorik, vierbeinige Roboter, autonome Navigation

Erschienen in Tagungsband 35. Forum Bauinformatik 2024, Hamburg, Deutschland, DOI: 10.15480/882.13502
© 2024 Das Copyright für diesen Beitrag liegt bei den Autoren. Verwendung erlaubt unter Creative Commons Lizenz Namensnennung 4.0 International.

## 1 Einleitung

Structural Health Monitoring (SHM) ist für eine kosteneffiziente Instandhaltung von Bauwerken durch rechtzeitige Schadenserkennung von großer Bedeutung. In den letzten Jahren wurden vermehrt

drahtlose Sensorknoten in SHM-Systeme integriert, um den Installationsaufwand zu verringern und die Flexibilität und Skalierbarkeit im Vergleich zu kabelgebundenen SHM-Systemen zu verbessern [1]. Die Einbettung von Sensoren in Beton ist vielversprechend für drahtloses SHM, da Degradationsprozesse – wie Korrosion im Stahlbeton [2] – an der Oberfläche von Bauelementen, wo drahtlose Sensorknoten normalerweise installiert werden, kaum sichtbar sind. Die Herausforderungen bei Ansätzen, die eingebettete drahtlose Sensoren verwenden, liegen in der Energieautonomie und in der Datenabfrage [3]. Eine kontinuierliche Stromversorgung ist bei eingebetteten Sensoren kaum möglich, und die Abfrage von Daten kann insbesondere bei großen Bauwerken mit vielen eingebetteten Sensoren umständlich sein. Drahtlose eingebettete Sensoren, die effizient mit Strom versorgt und abgerufen werden können, und damit eine Datenerfassung über die gesamte Dicke von Strukturelementen ermöglichen, könnten das SHM erheblich verbessern.

Eine vielversprechende Technologie für die drahtlose Energieversorgung ist die Radiofrequenz-Identifikation (RFID), die zunehmend im Bausektor zur drahtlosen Identifizierung und Überwachung von Objekten eingesetzt wird. Darüber hinaus wird die Durchführung groß angelegter Inspektionen von Bauwerken während der Bauphase durch mobile Roboter erleichtert, die zunehmend auf Baustellen eingesetzt werden. Die aktuelle SHM-Praxis kann von den beiden oben genannten Technologien, RFID und mobile Robotik, profitieren.

Eine Übersicht zur Integration von RFID-Technologie und SHM findet sich in [4]. Ansätze, die mobile Roboter für SHM einsetzen, werden in [5] behandelt. Dabei sind Laufroboter mit fortschrittlichen Fortbewegungstechniken, die eine verbesserte Manövrierfähigkeit und Anpassungsfähigkeit an unterschiedliche Umgebungen bieten, besonders interessant für SHM [6]. Der Integration von RFID in mobile Roboter zur Steigerung der Effizienz von SHM, z.B. zur Erleichterung des Einsatzes eingebetteter Sensoren, wurde bisher jedoch kaum Beachtung geschenkt.

In diesem Beitrag wird eine Methode zur Einbettung drahtloser Sensoren in Betonstrukturen vorgeschlagen. Die in den Beton eingebetteten Sensoren zeichnen SHM-Daten auf, um den Zustand der Struktur zu bewerten. Vierbeinige Roboter werden eingesetzt, um die in den Beton eingebetteten Sensoren bei Bedarf automatisch über RFID mit Strom zu versorgen und die SHM-Daten drahtlos zu erfassen. Die automatische Erfassung von SHM-Daten minimiert die menschliche Interaktion und erhöht die Effizienz.

Der Beitrag ist wie folgt gegliedert. In Abschnitt 2 werden die Methodik und die Implementierung für den Einsatz der robotergestützten und in den Beton eingebetteten Sensoren, einschließlich der automatischen Erfassung der SHM-Daten mit vierbeinigen Robotern, beschrieben. In Abschnitt 3 werden Validierungstests vorgestellt, die in einer Büroumgebung durchgeführt wurden, um die automatische Datenerfassung der eingebetteten Sensoren zu demonstrieren. Abschnitt 4 schließt den Beitrag mit einer Zusammenfassung und Schlussfolgerungen.

# 2 RFID für robotergestützte, in Beton eingebettete Sensoren

Die Beschreibung der in diesem Abschnitt vorgestellten Methodik beginnt mit einem Überblick über die RFID-Technologie, einschließlich der Komponenten, die zum Auslesen der SHM-Daten von den in den Beton eingebetteten Sensoren verwendet werden. Anschließend werden die Anbringung der RFID-Komponenten an vierbeinigen Robotern und der Prozess der automatischen Erfassung von SHM-Daten von den in den Beton eingebetteten Sensoren mithilfe von vierbeinigen Robotern beleuchtet.

## 2.1 RFID-Technologie

Die RFID-Technologie ermöglicht (i) die Stromversorgung und (ii) die Datenübertragung von den in den Beton eingebetteten Sensoren zu den Lesegeräten. Abbildung 1 veranschaulicht die RFID-Komponenten, die zur Durchführung von Messungen im Rahmen des SHM erforderlich sind. Zu den wesentlichen Komponenten gehören RFID-Tags, die die SHM-Daten aufnehmen, und RFID-Lesegeräte, die die Informationen und SHM-Daten von den RFID-Tags lesen und die Daten zur weiteren Verarbeitung übermitteln. RFID-Lesegeräte senden elektromagnetische Wellen aus, um die RFID-Tags zu aktivieren und die von den RFID-Tags empfangenen SHM-Daten auszulesen, zu speichern, zu verwalten und zu analysieren. RFID-Antennen sind die Kommunikationsschnittstelle zwischen den RFID-Tags und den RFID-Lesegeräten. Die Energieübertragung erfolgt über elektromagnetische Felder, so dass die Tags ohne Energiespeicher arbeiten können. In diesem Beitrag sind die RFID-Tags so konzipiert, dass sie Daten von Temperatur-, Feuchtigkeits- und Drucksensoren für das SHM erfassen.

## 2.2 Automatisierte Erfassung der Sensordaten mit Hilfe von Laufrobotern

Um eine automatisierte und effiziente Erfassung von SHM-Daten von in Beton eingebetteten Sensoren zu ermöglichen, werden die RFID-Komponenten auf einem vierbeinigen Roboter installiert, wie in Abbildung 2 dargestellt. Das RFID-Lesegerät ist über eine universelle asynchrone Empfänger/Sender-Schnittstelle (UART) mit dem Roboter verbunden. Die RFID-Antenne ist am Endeffektor eines Roboterarms angebracht, der auf dem vierbeinigen Roboter montiert ist. Der Roboterarm ermöglicht es, die Antenne nahe an die eingebetteten RFID-Tags heranzubewegen.

Für die automatisierte Erfassung von SHM-Daten von mehreren in Beton eingebetteten Sensoren, die in einem zu inspizierenden Gebäude verteilt sind, ist der vierbeinige Roboter mit einer zuverlässigen autonomen Bewegungsplanung ausgestattet. Die Bewegungsplanung beruht auf einer Echtzeit-Wahrnehmung der Umgebung, um detaillierte Karten zu erstellen, die genaue Lokalisierung innerhalb der Karten zu ermöglichen und Hindernisse zu erkennen. In dieser Studie verwendet der vierbeinige Roboter die weit verbreitete Kombination aus einem 3D-Light-Detection-and-Ranging (LiDAR)-Sensor und einer Inertialmesseinheit (IMU) für die Wahrnehmung, wie in Abbildung 2 dargestellt. Da die Bewegungsplanung in 3D und in Echtzeit auf eingebetteten Plattformen wie vierbeinigen Robotern erhebliche rechnerische Herausforderungen mit sich bringt [7], werden die 3D-LiDAR-Daten auf die horizontale 2D-Ebene projiziert, um eine überschaubare

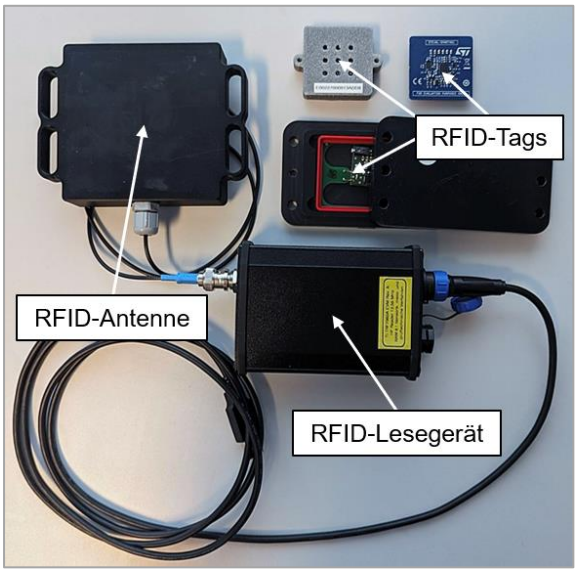


Abbildung 1: Prototypische RFID-Komponenten für die eingebetteten Sensoren.

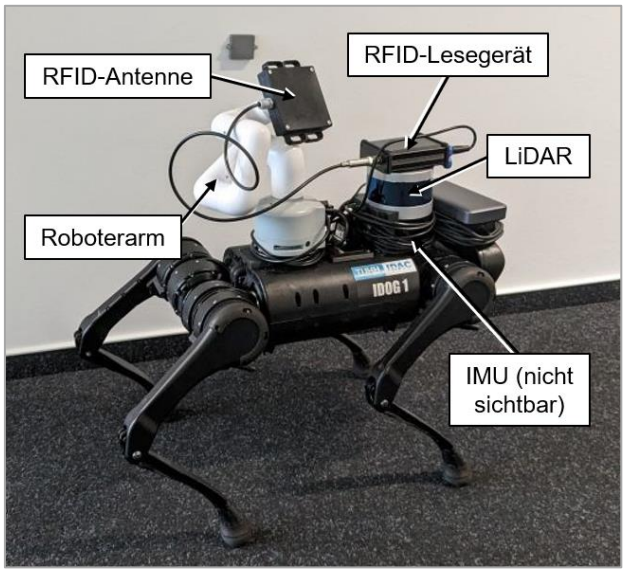


Abbildung 2: Am vierbeinigen Roboter angebrachte RFID-Komponenten.

Datenverarbeitung zu gewährleisten. Die Bewegungsplanung erfolgt durch die Darstellung des vierbeinigen Roboters als holonomer Roboter in der horizontalen 2D-Ebene mit einer rechteckigen Grundfläche, die dem physischen Raum entspricht, den der vierbeinige Roboter einnimmt. Die Bewegungsplanung basiert auf der Architektur des Robot Operating System (ROS).

Der Prozess der automatisierten Erfassung der SHM-Daten von in den Beton eingebetteten Sensoren besteht aus den folgenden Schritten:

- Erstellen einer Karte der Umgebung,
- Planung von Inspektionsaufgaben durch Bereitstellung von Zielposen in der Karte
- Planung und Verfolgung von Trajektorien zu den Zielposen und
- Erfüllung der Inspektionsaufgaben durch Bewegen der RFID-Antenne mit dem Roboterarm zu den RFID-Tags an den Zielposen, um SHM-Daten auszulesen.

Die Karte der Umgebung wird mit einem SLAM-System (Simultaneous Localization and Mapping) erstellt, genauer gesagt mit dem SLAM-System „Cartographer“ [8]. Cartographer verwendet die auf die horizontale 2D-Ebene projizierten LiDAR-Daten und die IMU-Messungen zur Erstellung einer statischen 2D-Umgebungskarte, die als Occupancy Grid Map kodiert ist und die Umgebung als gleichmäßig verteiltes Gitter darstellt, wobei jede Gitterzelle eine Wahrscheinlichkeit des Vorhandenseins von Hindernissen enthält.

Die Planung von Inspektionsmissionen erfolgt mithilfe eines Frameworks basierend auf hierarchischen endlichen Automaten. Inspektionsmissionen bestehen aus Zielposen und Inspektionsaufgaben, die beide als einzelne Zustände modelliert werden. Übergänge zwischen den Zuständen werden auf der Grundlage des Ausführungsstatus der einzelnen Zustände definiert. Der Automat wird mit Hilfe der SMACH-Bibliothek [9] in der ROS-Architektur implementiert. Zur intuitiven

Planung von Inspektionsaufgaben wurde ein Planungspanel im ROS-Visualisierungstool RViz entwickelt, das es ermöglicht, Zielposen auf den erstellten Karten zu markieren und Inspektionsaufgaben zu den Zielposen hinzuzufügen.

Zur automatischen Ausführung von Inspektionsaufträgen lokalisiert sich der vierbeinige Roboter in der Karte der Umgebung, plant Pfade zu den Zielpositionen der Inspektionsaufträge, folgt den Pfadplänen während Hindernisse umgangen werden, und führt die Inspektionsaufgaben an den jeweiligen Zielpositionen aus. Zur Lokalisierung in der Karte verwendet der vierbeinige Roboter den Lokalisierungsmodus des Cartographer-Systems. Im Lokalisierungsmodus werden projizierte LiDAR-Daten mit vorher erstellten Karten abgeglichen, so dass der vierbeinige Roboter seine anfänglich unbekannte Position in der Karte finden und anschließend verfolgen kann. Der A*-Suchalgorithmus wird verwendet, um Trajektorien, die hier als "globale Pläne" bezeichnet werden, von den aktuellen Positionen der Roboter zu Zielpositionen in statischen Karten der Umgebung zu planen. Um dynamische oder statische Hindernisse (die z.B. in veralteten Karten auftreten können) zu kompensieren und eine kollisionsfreie Navigation zu gewährleisten, wird ein lokaler Planer verwendet. Der lokale Planer erfasst mithilfe der LiDAR-Daten dynamische und statische Hindernisse um den Roboter herum in lokalen Kostenkarten, die Mindestabstände zwischen dem vierbeinigen Roboter und den Hindernissen sicherstellen. Der lokale Planer passt grobe globale Pläne für ein kurzes Zeitfenster in der Nähe des vierbeinigen Roboters mit hoher Frequenz an und gibt Bewegungssteuerungsbefehle an den Roboter. Für den lokalen Planer wird der Ansatz der Timed Elastic Bands (TEB) verwendet [10], der zeitoptimale Trajektorien generiert.

Sobald Roboter eine Zielpose neben einem RFID-Tag erreicht haben, bewegt er die am Endeffektor angebrachte RFID-Antenne in Richtung des RFID-Tags. Nach der Messung für eine vordefinierte Zeit wird der Roboterarm eingezogen und der Roboter bewegt sich zur nächsten Zielpose.

## 3 Validierung und Ergebnisse

Die Anwendbarkeit der vorgeschlagenen Methodik zur automatischen Erfassung von SHM-Daten mit einem vierbeinigen Roboter wird in Validierungstests gezeigt. Die Tests werden in einer Büroumgebung mit zwei RFID-Tags durchgeführt, die in 3D-gedruckten Gehäusen an einer Wand befestigt sind. Der bei den Tests eingesetzte vierbeinige Roboter „IDOG“ basiert auf dem Roboter Unitree A1 von Unitree Robotics und ist mit dem Velodyne Puck LITE LiDAR und einer LORD MicroStrain 3DM-GX5-25 IMU zur Lokalisierung, Kartierung und Navigation ausgestattet [11]. Weiterhin ist der Roboterarm myCobot 280 von Elephant Robotics auf dem IDOG montiert, der die RFID-Antenne hält. Der IDOG wird zunächst ferngesteuert, während mit dem Cartographer-System eine Karte erstellt wird. Die Inspektionsmission wird geplant, indem in der Karte neben den RFID-Tags Zielposen angegeben und mithilfe des Planungspanels Inspektionsaufgaben hinzugefügt werden. Nach dem Speichern der Mission wird die Mission fünfmal wiederholt. Während der Wiederholung der Mission läuft der IDOG automatisch zu den Zielposen, sammelt SHM-Daten von den eingebetteten Sensoren, und visualisiert Karte, Trajektorie und SHM-Daten in RViz.

Die generierte Karte der Büroumgebung einschließlich der beiden Zielposen ist in Abbildung 3 dargestellt. Abbildung 4 und Abbildung 5 zeigen Momentaufnahmen der automatischen Erfassung der SHM-Daten in den Missionswiederholungen. In Abbildung 4 sind der globale Plan, der lokale Plan und die tatsächliche Trajektorie des IDOGs dargestellt. Der lokale Plan weicht vom globalen Plan ab, um Hindernissen, in diesem Fall einem Passanten, auszuweichen. Abbildung 5 zeigt die Erfassung von SHM-Daten durch die in den Beton eingebetteten Sensoren. Nach Erreichen einer Zielposition (Abbildung 5a) bewegt der IDOG den mit der Antenne ausgestatteten Roboterarm in Richtung des RFID-Tags (Abbildung 5b) und sammelt SHM-Daten. Nach einer Messdauer von 10 Sekunden zieht der IDOG den Roboterarm zurück und bewegt sich zur nächsten Zielposition. Die vom IDOG gesammelten Daten sind in Tabelle 1 aufgeführt und umfassen Luftfeuchtigkeit, Druck und Temperatur für zwei Zielposen. Bei allen fünf Missionswiederholungen ist der IDOG in der Lage, die Inspektionsmission erfolgreich abzuschließen, indem es zu allen Zielposen navigiert.

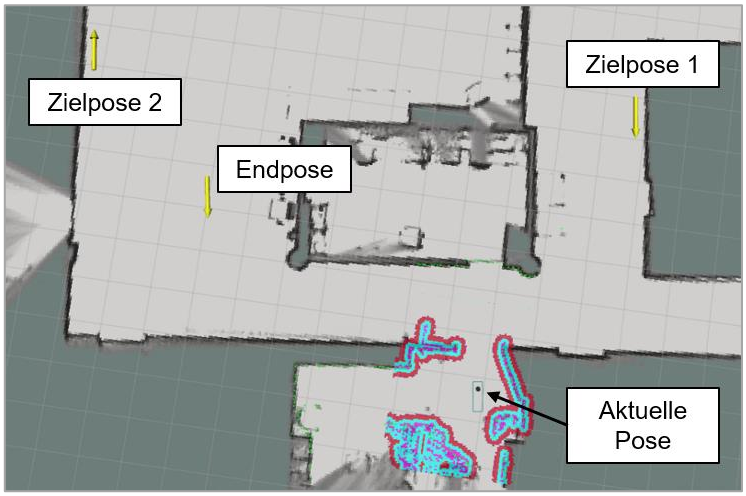


Abbildung 3: Generierte Karte der Umgebung mit Zielpositionen der Inspektionsmission.

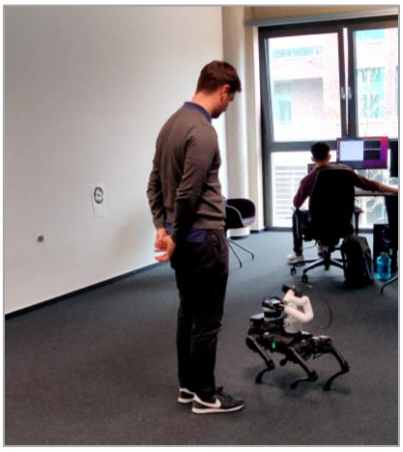

(a) Umlaufen eines Passanten

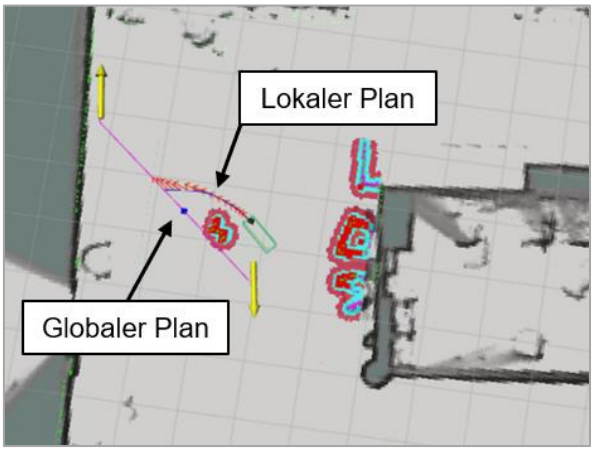


(b) Abweichung zwischen globalem und lokalem Plan

Abbildung 4: Hindernisvermeidung während der Durchführung der Inspektionsmission.

(a) IDOG bei Erreichen einer Zielposition

(b) Erfassung von SHM-Daten

Abbildung 5: Vom IDOG automatisch erfasste SHM-Daten in einer Zielposition.

Während der Validierungstests konnten die SHM-Daten bei der Zielpose 1 in zwei Wiederholungen aufgrund von Ungenauigkeiten bei der Lokalisierung der RFID-Tags und der Positionierung der RFID-Antenne nicht abgerufen werden. Um die Gesamtleistung zu verbessern und die Fehlertoleranz bei SHM-Inspektionseinsätzen zu erhöhen, muss die Genauigkeit der RFID-Tag-Lokalisierung und der Positionierung der Antenne erhöht werden, um Ausfälle bei der SHM-Datenerfassung zu vermeiden.

Tabelle 1: Vom IDOG erfasste SHM-Daten während der Valdierungstests.

| **Test Nr.** | | 1 | 2 | 3 | 4 | 5 |
|---|---|---|---|---|---|---|
| **RFID-Tag 1** | Temperatur [°C] | 24 | - | 24 | - | 24 |
| | Luftfeuchtigkeit [%] | 55 | - | 56 | - | 56 |
| | Druck [hPa] | 1210 | - | 1210 | - | 1210 |
| **RFID-Tag 2** | Temperatur [°C] | 25 | 25 | 25 | 24 | 24 |
| | Luftfeuchtigkeit [%] | 47 | 47 | 56 | 56 | 56 |
| | Druck [hPa] | 1001 | 1001 | 1004,5 | 1004,5 | 1004,5 |

## 4 Zusammenfassung und Schlussfolgerungen

SHM ist zu einer wertvollen Ergänzung regelmäßiger Inspektionen geworden. Robotergestützte, in Beton eingebettete Sensoren für SHM stellen ein vielversprechendes Werkzeug dar, um SHM weiterzuentweckeln, die Informationsverarbeitung weitergehend zu automatisieren und Sensordaten aus dem Inneren von Bauelementen zu erfassen. In diesem Beitrag wurde eine Methodik robotergestützter, in Beton eingebetteter Sensoren für SHM vorgestellt und auf einem vierbeinigen Roboter implementiert. Es wurden Validierungstests in einer Büroumgebung durchgeführt, um die Anwendbarkeit der vorgeschlagenen Methodik zur automatischen Erfassung von SHM-Daten zu demonstrieren. Der vierbeinige Roboter hat erfolgreich und automatisch die SHM-Daten von den in der Büroumgebung verteilten Sensoren erfasst und dabei Hindernisse vermieden. Zusammenfassend lässt sich feststellen, dass sich die Kombination aus RFID-

Technologie und robotergestützter Inspektionen als vielversprechender Ansatz erwiesen hat, um die derzeitigen SHM-Praktiken in Richtung automatisierter und digitalisierter Prozesse voranzutreiben. Obwohl die Validierungstests erfolgreich verlaufen sind, besteht Verbesserungspotenzial hinsichtlich der Genauigkeit der robotergestützten, automatischen Lokalisierung der RFID-Tags. Darüber hinaus kann die Integration mit Building Information Modeling (BIM) helfen, den Ansatz weiter zu automatisieren, indem den Robotern Karten der Bauwerke zur Verfügung gestekllt und die erfassten SHM-Daten mit den Objekten in den BIM-Modellen verknüpft werden.

## Referenzen

[1] Dragos, K. & Smarsly, K., 2015. A comparative review of wireless sensor nodes for structural health monitoring. In: Proceedings of the 7th International Conference on Structural Health Monitoring of Intelligent Infrastructure, Turin, Italy, 7/1/2015.

[2] Strangfeld, C., Johann, S., & Bartholmai, M., 2019. Smart RFID sensors embedded in building structures for early damage detection and long-term monitoring. Sensors, 19(24), 5514.

[3] Johann, S., Strangfeld, C., Müller, M., Mieller, B., & Bartholmai, M., 2017. RFID sensor systems embedded in concrete - requirements for long-term operation. Materials Today: Proceedings, 4(5), S. 5827-5832.

[4] Zhang, J., Tian, G. Y., Marindra, A. M., Sunny, A. I., & Zhao, A. B, 2017. A review of passive RFID tag antenna-based sensors and systems for structural health monitoring applications. Sensors, 17(2), 265.

[5] Tian, Y., Chen, C., Sagoe-Crentsil, K., Zhang, J., & Duan, W., 2022. Intelligent robotic systems for structural health monitoring: Applications and future trends. Automation in Construction, 139, 104273.

[6] Smarsly, K., Dragos, K., Stührenberg, J., & Worm, M., 2023. Mobile structural health monitoring based on legged robots. Infrastructures, 8(9), 136.

[7] Wellhausen, L. & Hutter, M., 2023. Artplanner: Robust legged robot navigation in the field. Field Robotics, 3(1), S. 413-434.

[8] Hess, W., Kohler, D., Rapp, H., & Andor, D., 2016. Real-time loop closure in 2D LIDAR SLAM. In: Proceedings of the International Conference on Robotics and Automation, Stockholm, Sweden, 5/16/2016.

[9] Bohren, J. & Cousins, S., 2010. The smach high-level executive. IEEE Robotics & Automation Magazine, 17(4), S. 18-20.

[10] Rösmann, C., Feiten, W., Wösch, T., Hoffmann, F., & Bertram, T., 2012. Trajectory modification considering dynamic constraints of autonomous robots. In: Proceedings of ROBOTIK 2012; 7th German Conference on Robotics. Munich, Germany, 3/21/2012.

[11] Smarsly, K., & Dragos, K., 2024. Advancing civil infrastructure assessment through robotic fleets. Internet of Things and Cyber-Physical Systems, 4(2024), S. 138-140.

# Experimental evaluation of iPad Pro LiDAR, for building modeling and possibilities to connect with AI technologies

Nils Sören Krause[1] and Miguel Guzmán-Merino[1]
[1]AI for Sustainable Construction, University of Rostock,
Justus-von-Liebig-Weg 2, 18059 Rostock, Germany
E-mail(s): nils.krause@uni-rostock.de, miguel.merino@uni-rostock.de

**Abstract:** Measuring buildings is a recurring task when recording construction progress and existing buildings in BIM-models. LiDAR (Light Detection and Ranging) surveying systems allow fast and precise recording of environments but are usually not attractive in terms of price of widespread use. Nowadays, modern mobile devices equipped with LiDAR sensors offer a cost-effective alternative for measuring environments or structures. This Paper experimentally investigates to which extent the iPad Pro, with its various software solutions and the LiDAR technology available today, can be used to create building models. Four experiments were conducted to reflect real-life situations: (i) scanning closed space, (ii) scanning loop of a larger area, (iii) the range of the LiDAR sensor, and (iv) its accuracy as well as the functionality of direct automatic modeling of BIM-models compared to professional systems. The experimental investigations show that the iPad Pro can already be used to capture point clouds with minor quality reduction. Furthermore, the post-processing of the scan data using artificial intelligence is being investigated to derive further research questions on how the scan data can be automatically evaluated and the quality of the derived 3D building models can be improved.

*Keywords:* BIM, LiDAR, Point-cloud, iPad Pro, AI

Erschienen in Tagungsband 35. Forum Bauinformatik 2024, Hamburg, Deutschland, DOI: 10.15480/882.13511
© 2024 Das Copyright für diesen Beitrag liegt bei den Autoren. Verwendung erlaubt unter Creative Commons Lizenz Namensnennung 4.0 International.

## 1 Introduction

Many engineers and architects might find that as-built surveys can be carried out more efficiently with 3D laser scanners. With a variety of LiDAR devices offering different accuracies, ranges, and features, the opportunities for innovation are enormous. The low-cost system of the iPad Pro was selected for the study compared to a professional system, the BLK2GO from Leica. The iPad Pro offers many new possibilities due to its low purchase price. For example, it increases distribution and availability, is easy to use, serves as an alternative to professional systems, has versatile applications in the construction industry, and promotes development and research in the field of LiDAR technology because it is affordable for everyone. However, the most important question is how accurate the

generated data is and what can be done with this data. To this, the experimental studies aim to use the iPad Pro to explore its applications, identify the most effective software solutions, and determine the accuracies of the system. Through four different experimental investigations, we will find out how this technology can improve today's construction industry and make it more digital. The experiments are divided into: (i) scanning a closed space, (ii) scanning a loop of a larger area, (iii) evaluating the range of the LiDAR sensor, and (iv) its accuracy as well as the functionality of direct automatic modeling of BIM-models. The collected data will be analyzed to determine which applications are best suited for further research into the evaluation of scan data using artificial intelligence, up to and including the BIM-model, thus paving the way for groundbreaking advances. The state-of-the-art section of this paper establishes a link to previous publications, highlights progress to date, and outlines important points for future developments. In addition, it shows how AI can further improve the processing of the recorded data and what possibilities already exist today. The methods section provides background information on the experiments carried out. The results section presents the analyzed data and the paper concludes with a discussion of the results.

# 2 State-of-the-Art

## 2.1 LiDAR

There are already evaluations of the performance of the LiDAR scanner in the iPad Pro, such as those by Teo and Yang [1]. The results are evaluated in terms of the potential for the subsequent creation of 3D BIM-models. The investigations in the study were divided into dynamic and static tests. As a result of the study, it was found that the LiDAR scanner installed in the iPad Pro was able to achieve accuracy of up to 1 mm concerning a reference plane in static tests, explicitly related to a straight wall and mounted on a tripod. Furthermore, it was found that the deviations in the dynamic test, which was carried out as a loop, were within 80 % of the recorded points generating a deviation of 1 cm with the iPad Pro. As a result, it was concluded that it is possible to create precise point clouds with the iPad Pro under certain conditions. However, the accuracy was not sufficient to achieve the accuracy required by the USGSA BIM guidelines for 3D point clouds. In the USGSA BIM guide, the accuracy is divided into four different levels and ranges from ± 3 mm to ± 51 mm [2]. The technology was used for large-scale structures in a publication by Luetzenburg, Kroon, and Bjørk [3], measuring a coastal cliff in Denmark. It was found that the LiDAR sensors installed in the iPhone 12 achieved an accuracy of ± 1 cm for small objects with a side length of > 10 cm. For larger objects with dimensions of 130×15×10 m, the system achieved an absolute accuracy of ± 10 cm. A study by Vacca [4] is based on the evaluation of the LiDAR sensor built into the iPad Pro in relation to the documentation of architectural and cultural heritage. The investigations were carried out using software applications from Polycam, Sitescape, 3DScannerApp, and Scaniverse. As a result of the study, it was found that the Apple LiDAR sensors can be used to document and create 3D models, but the shape and texture should not be complex.

## 2.2 AI technologies

The approaches to as-built surveys do not only refer to the data basis of point clouds, BIM-models or components are created from construction drawings using AI models. Al-Wesabi [5] describes an

approach for extracting information from German infrastructure projects. The study presents promising results for the automatic creation of digital building models but does not provide a definitive solution. Further areas are covered in a publication by Schoenfelder, Stebel, Andreou, *et al.* [6] which dealt with the extraction of text information from as-built plans. A data set for text recognition from floor plans was created, applied, and compared with various deep learning algorithms. In the end, the study shows which algorithm performed the best text recognition and explains of further development. The acquisition of data from the 2D-floor plans is carried out as described in a publication by Gard and Barreiro [7] by first converting the plan information into the Json-format. The data obtained in Json-format is then converted into a 3D model and saved in Ifc-format. Components such as walls, ceilings, floors, windows, and doors are recognized. The BIMKIT-project also describes Ifc-model generation, which, according to the forward schematic description, is converted from Json-format into an Ifc-model using AI. However, according to the current project status, no training data is yet available for the AI [8]. Furthermore, there are similarities to the BIM-SPEED project, in which there is an application that automatically models walls within a point cloud, in line with the topic [9]. However, the overall picture after recording a point cloud up to the parameterized building model is missing. Initial approaches can be found for infrastructure structures. As-built surveys are usually carried out using laser scanners, as described by H. Mischo [10]. The further modeling and processing of the data is still carried out manually. In a publication by Jaekel, Goelzhaeuser, Schmitt, *et al.* [11] the manual modeling is transformed into a partially automated generation of digital infrastructure projects. A first approach is shown in which an existing bridge for maintenance management was successfully digitized. Another promising approach to partial automation is provided by Bednor [12] or Qin, Zhou, Hu, *et al.* [13], where the process, from data acquisition through laser scanning to export, i.e. the provision of modeled data, is explained. It is also established that it is possible to derive BIM-models from 3D point clouds. In a further study on point cloud recording in indoor areas by Stojanovic, Trapp, Richter, *et al.* [14] two different DL-algorithms are described. These are the DL-algorithm PointNett++ [15] and the Inception V3 [16] algorithm. The study by Stojanovic et al. shows that both algorithms are suitable for the segmentation of point clouds from mobile scanning systems.

## 3 Methodical

The LiDAR scanners are evaluated through various experimental analyses. The experiments are designed to obtain information on the accuracy of the different applications and systems. The software applications in Table 1 were selected based on the export formats. The .ply format was used for the investigations of the point clouds. For automatic model generation, the focus was on the Ifc-format. Experiment (i) was carried out as part of a semi-dynamic investigation on a tripod with the device swiveling and rotating around its axis. Experiments (ii), (iii), and (iv) were conducted in a dynamic experiment to provide the slam algorithms with sufficient data to process the scans. Figure 1 shows the experiments, which reference is taken, and the used applications with the analysis process of the data. To analyze the point clouds, the apps 3DScannerApp [17], RTAB-Map [18], and Scaniverse [19] are used. For experiment (iv) the applications Magicplan [20] and Metaroom [21] were chosen.

Table 1: List of iPad Pro applications and export formats for LiDAR-Scanning, which were compared, based on the export formats.

| Application | Export format |
|---|---|
| Polycam | .dae, .dxf, .fbx, .gltf, .las, .obj, .ply, .pts, .raw, .stl, .usdz, .xyz |
| Magicplan | .ifc, .obj, .usdz |
| 3D-Scanner-App | .e57, .glb, .gltf, .las, .obj, .pcd, .ply, .pts, .stl, .usdz, .xyz |
| Canvas Lite | .dae, .dwg, .ifc, .kit, .plan, .rvt |
| OpalAi | .e57, .glb, .gltf, .las, .obj, .pcd, .ply, .pts, .stl, .xyz |
| Metaroom | abc, .dae, .dxf, .fbx, .glb, .gltf, .ifc, .obj, .rdf, .skp, .stl, .usd, .zip |
| SiteScape | .e57, .ply |
| 3D-Scanner | .dae, .glb, .obj |
| Metascan | fbx, .gltf, .laz, .obj, .ply, .stl, .usdz, .xyz |
| Scaniverse | .fbx, .glb, .las, .obj, .ply, .ply, .stl, .usdz |
| RTAB-Map | .ply |
| LiDAR-Scanner | .ohj, .ply, .stl, .usdz |

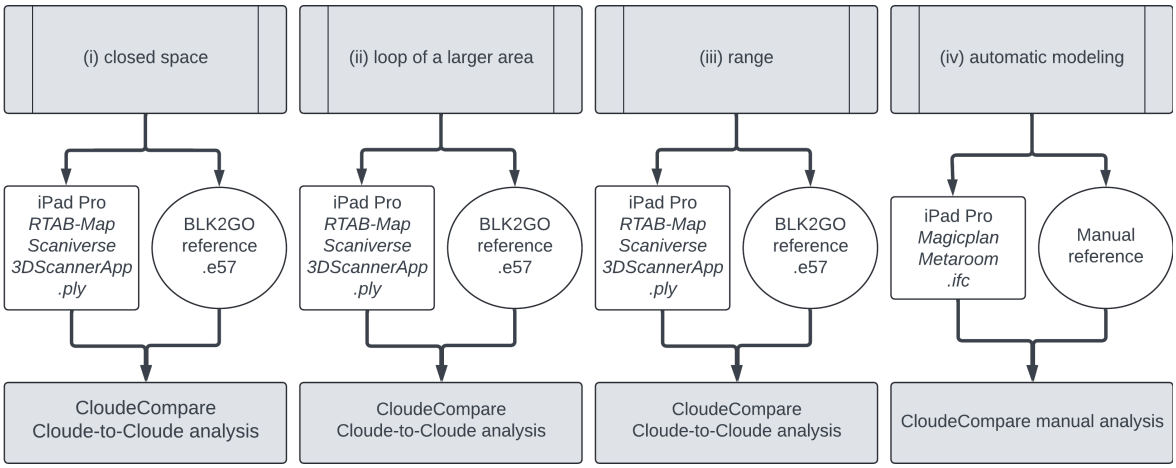


Figure 1: Sequence of the proposed experiments with implementation components, export formats and result analysis. The graphic applies to all experiments carried out in this work.

## 4 Results

Experiments (i) and (ii) were carried out in comparison with the professional BLK2GO system. In (i), an error was detected in the reference point cloud, shown in Figure 2, which influences the maximum distance of the point deviation. However, the error does not affect the average deviation of the point clouds, as it occurs consistently and only increases the error of the maximum distance. Apart from the error described above, the process was carried out quickly and efficiently using the iPad Pro. After aligning the scans from the experiment (ii), it became clear that the generated point clouds from the iPad Pro software applications are inherently distorted, as shown in Figure 3. The phenomenon of inclined positions would lead to major errors in the model in later modeling. For this reason, no modeling was carried out in this regard. Only by interpreting an assumed course of the spatial lines would the model become usable. In both cases (i) and (ii), the smallest deviations were found in the application of RTAB-Map.

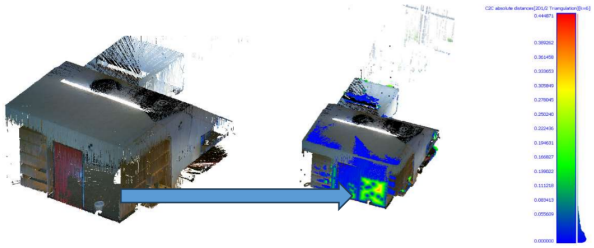

Figure 2: Error in experiment (i), showing a missing Wall in the scanned reference point cloud, scanned by the BLK2GO system, the error depends on the static scan process.

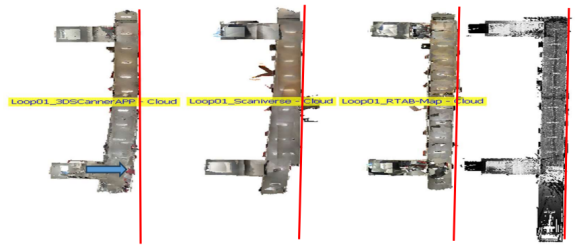


Figure 3: Scanned loops, out of experiment (ii). Shows the inclined positions, of the scanned point clouds. From left to right side: 3DScannerApp, Scaniverse, RTAB-Map, BLK2GO.

The experiment (iii) was evaluated by manually selecting points on the targets, shown in Figure 4. The left picture shows a point cloud, generated with the iPad Pro LiDAR, and the right side is a point cloud generated by the BLK2GO, to compare both clouds. The reference values for the distance between the targets were determined using a laser distance meter. During the experiment, it was also recognized that the LiDAR applications in the iPad Pro are no longer able to generate sufficient data from a distance of 3 m when used statically, shown in Figure 5. A dynamic approach was chosen for the further execution of the experiment (iii). The RTAB-Map application delivered again the lowest deviations.

Figure 4: Process of the manual measuring in the point clouds, between the used target markets in experiment (iii), to get the length between target markets in the Software CloudeCompare. From left to Right side: Scaniverse, BLK2GO.

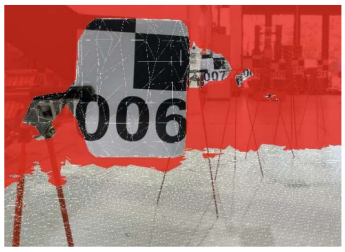


Figure 5: Example out of a static scan experiment, which didn´t work to get the length of 5 m, only 2 m. The density of the point cloud was too low, experiment (iii).

In experiment (iv), models were generated by a modeling process automated by the software using edge detection, shown in Figure 6. These models were compared with reference values using a laser distance meter. The iPad Pro was hand-held and dynamically moved through the room, to represent realistic use. A trivial geometry consisting of rectangular structures, a window, and doors was captured. No problems were encountered during the survey. In a second run, the detection of a structure with sloping roofs was evaluated. With the applications listed, it was not possible to capture the sloping structures and transfer them to an Ifc-model. The roof pitches are not shown in the model, see Figure 7, only the knee walls are shown. The interesting fact is that the edge detection and the storage of three-dimensional objects in the form of Ifc objects usually have higher accuracy than the point cloud for a closed recorded space.

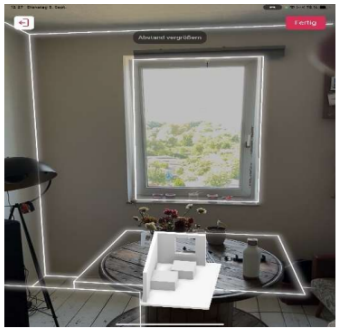

Figure 6: An example, of how the automatic modeling process is shown in the App Metaroom, on the left side. On the right side an example of the Ifc-Model from the measured room, the same application and room.

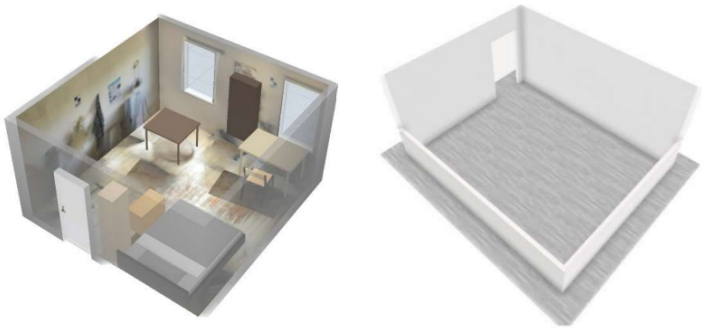

Figure 7: Exported Ifc-model, from experiment (iv), shows the knee wall and the missing sloped walls.

For the intended comparison between the professional system (BLK2GO) and the iPad Pro, meaningful values can be taken from investigations (i), (ii), and (iii). In general, the recorded deviations of the systems are far apart. The deviations of the iPad Pro range from 1.3 cm to 9.2 cm across all applications used, while for the deviations of the BLK2GO, the average deviations are within a narrow range of 0.1 to 1.03 cm. The applications for automated model creation are currently in an experimental state and are not suitable for commercial use. This is due to the limited possibilities for further processing and the lack of capabilities for recording more complex spatial geometries. However, according to the USGSA, the accuracy would be sufficient for an inventory in individual rooms for the Metaroom application. The results of the deviations are shown in the Table 2 presented.

Table 2: Evaluation results of all experiments, with a comparison of the results for existing work

| **Experiment** | **Dim.** [m] | **Dev. Ref.** [cm] | **Dev.** [cm] USGSA | [cm] Producer | [cm] Luetz. | **Total** [cm] |
|---|---|---|---|---|---|---|
| (i) closed space all | 5.4x4.6x2.6 | 1.90 | ± 0.6- ± 1.3 | - | - | 1.3-0.77 |
| (i) Scaniverse | 5.4x4.6x2.6 | 1.88 | ± 0.6- ± 1.3 | - | - | 1.28-0.75 |
| (i) RTAB-Map | 5.4x4.6x2.6 | 1.35 | ± 0.6- ± 1.3 | - | - | 0,75-0.05 |
| (i) 3DScannerApp | 5.4x4.6x2.6 | 2.48 | ± 0.6- ± 1.3 | - | - | 1.88-1,18 |
| (ii) loop all | 66x2,5x2,2 | 12-17 | - | - | ± 10 | 2-7 |
| (iii) range Apple | 1 | 1.8 | - | ± 0.8 for 50 | - | 1 |
| (iii) range Apple | 2 | 3.4 | - | ± 1.8 for 150 | - | 1.6 |
| (iii) range Apple | 3 | 3.4 | - | ± 5.3 for 300 | - | 1.9 |
| (iii) range Apple | 4 | 8.8 | - | ± 5.3 for 300 | - | 3.5 |
| (iii) range Apple | 5 | 9.2 | - | ± 5.3 for 300 | - | 3.9 |
| (iii) range BLK2GO | 1 | 1.03 | - | ± 1 | - | 0.03 |
| (iii) range BLK2GO | 2 | 0.1 | - | ± 1 | - | -0.9 |
| (iii) range BLK2GO | 3 | 0.1 | - | ± 1 | - | -0.9 |
| (iii) range BLK2GO | 4 | 0.9 | - | ± 1 | - | -0.1 |
| (iii) range BLK2GO | 5 | 0.4 | - | ± 1 | - | -0.6 |
| (iv) Metaroom | 4.3x4.4x2.7 | 0.3-1.3 | 0.6-1.3 | - | - | -0.3-0 |
| (iv) Magicplan | 4.3x4.4x2.7 | 2.8-22.5 | 0.6-1.3 | - | - | 2.2-21.2 |

## 5 Discussion and Conclusion

The various tests have shown how the deviations of the LiDAR scanner in the iPad Pro turn out in rooms of different sizes or complexity. The results clearly reflect that there are still differences between the low-cost system of the iPad Pro and the professional system, the BLK2GO. The recorded deviations can also be verified with values from other related publications. Thus, from the perspective of the study (i), a statement by Teo and Yang [1] can be confirmed. It can be concluded that the iPad Pro is suitable for recording point clouds in rectangular, single rooms. However, it should be noted that the accuracy of these point clouds are not sufficient according to the USGSA. When recording loop (ii), the tolerance is exceeded many times over, which is why this investigation is not discussed further in connection with such a statement. An average deviation of 14.9 cm was achieved in the examination of loop (ii) from the corridor. In terms of accuracy alone, this appears to be an acceptable deviation in the point clouds. It should also be noted that it is difficult for algorithms to ensure the correct alignment of point clouds in corridors, for example. In the evaluation of the experiment, it was also determined that the point clouds recorded using the iPad Pro are twisted within themselves. Based on this observation, it does not make sense to use (ii) for subsequent modeling. In the evaluation and segmentation of point clouds, there are many different approaches for increasing efficiency using AI. However, there is a lack of an overall standardized approach to the parameterized building model according to the BIM-concept. There are also AI applications for analyzing buildings from point cloud data and for processing as-built plans into BIM-models. In further research, the entire procedure for automated model creation from point cloud data could be viewed from a new perspective. Does the data have to be represented as currently known parameterized components or is a mesh/volume-based approach within the point cloud with the addition of the required semantic information sufficient? Furthermore, the automatic creation of models should be considered, with regard to the possibilities of data set generation for machine learning. By scanning with iPad Pro per LiDAR, a model and the corresponding point cloud of trivial structures can be generated directly. In coming research articles we take a look into getting clean point cloud Data from the commonly available AI models. We are going to train and test the commonly available AI models for as-built survey construction with these data.

## References

[1] T.-A. Teo and C.-C. Yang, “Evaluating the accuracy and quality of an ipad pro’s built-in lidar for 3d indoor mapping”, *Developments in the Built Environment*, vol. 14, 2023.

[2] U. G. S. Administration, *Gsa bim guide series 03*, 2009. [Online]. Available: http://en.fm-engineering.ru/int/GSA_BIM_Guide_Series_Laser_Scaning.pdf.

[3] G. Luetzenburg, A. Kroon, and A. A. Bjørk, “Evaluation of the apple iphone 12 pro lidar for an application in geosciences”, *Scientific Reports*, vol. 11, no. 1, 2021.

[4] G. Vacca, “3d survey with apple lidar sensor—test and assessment for architectural and cultural heritage”, vol. 6,

[5] Al-Wesabi, "Extracting information from old and scanned engineering drawings of existing buildings for the creation of digital building models", in *Skatulla, S., Beushausen, H. (eds) Advances in Information Technology in Civil and Building Engineering*, Springer, Cham, 2023.

[6] P. Schoenfelder, F. Stebel, N. Andreou, and M. Koenig, "Deep learning-based text detection and recognition on architectural floor plans", *Automation in Construction*, vol. 157, 2024.

[7] N. Gard and A. C. Barreiro, "Towards automated digital building model generation from floorplans and on-site images", in *34. Forum Bauinformatik*, 2023.

[8] *Bimkit*, 2024. [Online]. Available: https://bimkit.eu.

[9] *Bim-speed*. [Online]. Available: https://www.bim-speed.eu.

[10] J. S. H. Mischo, *Vom 3-d-laserscan zum bim-modell: Ein erfahrungsbericht aus dem stahlbrueck-enbau*. [Online]. Available: http://dx.doi.org/10.1002/bate.201900031.

[11] J.-I. Jaekel, P. Goelzhaeuser, A. Schmitt, *et al.*, *Teilautomatisierte generierung von digitalen infrastrukturmodellen mittels multi-datenfusion*, 2023.

[12] J. Bednor, *2. Fachkongress Digitale Transformation der Verkehrsinfrastruktur: Fachtagung Ueber Planung, Bau, Betrieb, Unterhalt, Rueckbau von Bruecken, Tunneln, Schienen, Strassen, Wasserwegen digital* (Einsatz kuenstlicher Intelligenz zur Generierung von BIM-Bestandsmodellen im Straßenbrueckenbau). expert verlag GmbH, 2023.

[13] G. Qin, Y. Zhou, K. Hu, D. Han, and C. Ying, "Automated reconstruction of parametric bim for bridge based on terrestrial laser scanning data", *Advances in Civil Engineering*, 2021.

[14] V. Stojanovic, M. Trapp, R. Richter, and J. Doellner, "Comparison of deep-learning classification approaches for indoor point clouds", 2020. [Online]. Available: https://www.dgpf.de/src/tagung/jt2020/proceedings/proceedings/band_29/dgpf2020_tagungsband_29_ebook.pdf.

[15] C. R. Qi, L. Yi, H. Su, and L. J. Guibas, "Pointnet++: Deep hierarchical feature learning on point sets in a metric space", *CoRR*, 2017. [Online]. Available: http://arxiv.org/abs/1706.02413.

[16] C. Szegedy, V. Vanhoucke, S. Ioffe, J. Shlens, and Z. Wojna, *Rethinking the inception architecture for computer vision*, 2016.

[17] L. Labs, *3d scanner app™*, version 1.1.5, 2023. [Online]. Available: https://apps.apple.com/de/app/3d-scanner-app/id1419913995.

[18] M. Labbe, *Rtab-map*, version 0.21.2, 2021. [Online]. Available: https://github.com/introlab/rtabmap.

[19] Niantic, *Scaniverse*, 2023. [Online]. Available: https://scaniverse.com/.

[20] Magicplan, *Magicplan*, 2023. [Online]. Available: https://www.magicplan.app/.

[21] Metaroom, *Metaroom*, 2023. [Online]. Available: https://amrax.ai/de/metaroom-app/.

# Robot-based installation of nanostructured metal multilayers on civil infrastructure

Niclas Spalek[1], Jan Stührenberg[2], Aditya Tandon[2], Maximilian Tourneau[1], Ayush Patel[2], and Bastian Große[2]

[1]Institute for Metal and Composite Structures, Hamburg University of Technology, Denickestraße 17, 21073 Hamburg, Germany

[2]Institute of Digital and Autonomous Construction, Hamburg University of Technology, Blohmstraße 15, 21079 Hamburg, Germany

E-Mails: niclas.spalek@tuhh.de, jan.stuehrenberg@tuhh.de

**Abstract:** Fatigue, particularly in welded joints, causes premature failure of civil infrastructure, an increase in maintenance costs, and safety risks. Nanostructured metal multilayers, applied via electrodeposition, represent a novel treatment to enhance the fatigue strength of welded joints by introducing residual compressive stress during the deposition process, reducing surface roughness and strengthening resistance against extrusions. Nanostructured metal multilayer (NMM) patches may be utilized to postpone crack initiation, restrict the propagation of structural damage, and prolong the life of civil infrastructure. With advancements in robotic technologies, automated robot-based processes may be employed to ensure accuracy and consistency when installing nanostructure patches. In this paper, a methodology for automated robot-based installation of NMM patches on welded joints of civil infrastructure is proposed. Mobile robots, equipped with robotic arms, autonomously navigate to welded joints and install NMM patches using electrodeposition. To validate the methodology, NMM patches are installed and tested under laboratory conditions in small-scale experiments. As a result, integrating NMM technology and robot-based automation, presented in this study, demonstrates a promising approach towards prolonging the lifetime of civil infrastructure.

*Keywords:* Mobile robots, nanostructured metal multilayers, weld detection, electrodeposition

Erschienen in Tagungsband 35. Forum Bauinformatik 2024, Hamburg, Deutschland, DOI: 10.15480/882.13549
© 2024 Das Copyright für diesen Beitrag liegt bei den Autoren. Verwendung erlaubt unter Creative Commons Lizenz Namensnennung 4.0 International.

## 1 Introduction

The infrastructure crisis is continuously unfolding. Globally, an increasing number of bridges have reached a critical state, with cracks impairing the structural integrity of steel-based infrastructure. The growing volume of heavy vehicle traffic is identified as a significant factor contributing to the premature aging of bridges. In Germany, the past three decades have seen an increase in freight

transport of over 70% [1]. At the same time, 40% of railway bridges are older than 80 years and 40% of motorway bridges are older than 50 years [2], rendering structural health monitoring (SHM) a valuable tool of increasing importance for infrastructure maintenance [3].

Due to increasing traffic, bridges, alongside all other steel-based infrastructure, experience aging, referred to as “fatigue”, with welded connections being the weakest points. To strengthen welded connections against fatigue, post-weld treatments may be applied [4]. As robots have become prevalent in infrastructure inspection and maintenance [5], robots may advantageously be used to apply post-weld treatments on civil infrastructure. In this paper, first results of a post-weld treatment based on nanostructured metal multilayer (NMM) patches on welded connections is presented. Furthermore, a methodology for the installation of the NMM patches in an automated robot-based process on civil infrastructure is described.

The remainder of this paper is organized as follows. In section 2, NMMs and a prototype for installing NMM patches are described. In section 3, a methodology for the robot-based installation of NMM patches is proposed. Section 4 shows validation tests and results concerning the fatigue behavior of NMMs, and the installation of NMM patches under laboratory conditions. Finally, section 5 contains a summary of the paper, conclusions, and potential future work.

## 2 Nanostructured metal multilayers

In steel-based construction, welded connections are prone to cyclic loading due to intrinsic microstructural and geometrical changes [6]. A coating of Cu/Ni NMM applied on welded seams has been observed to increase the fatigue behavior of welded samples, as published before in [6-8]. Therein, a thin film is electrodeposited on the fatigue susceptible areas of structures, i.e. the welded connections. The film consists of numerous individual Cu and Ni layers, each with a layer thickness of 15 nm and 35 nm, respectively. The NMM is 9 µm thick with a Ni-levelling layer in between the steel substrate and the NMM film. The combination of an increase in mechanical properties due to the Hall-Petch effect [10], which results in a metallically bonded hard coating, inhibiting the formation of persistent slip bands [11], and changing the residual stress states, thus reducing critical notch stresses due to the welding process [12] are thought to be responsible for the effect of the NMM post-weld treatment.

To facilitate the potential of the NMM post-weld treatment, the technology has to be applicable in the field. For civil infrastructure, in specific, the need for a mobile deposition unit for NMM patches is essential, as the demounting of large-scale parts is either not possible or cumbersome and expensive. As a solution, a mobile deposition unit to install NMM patches is developed, which is shown in Figure 1. The essential components of a mobile deposition unit are a container for the electrolyte, the tubing, and the unit capable of performing the deposition. To deploy NMM patches, the mobile deposition unit is pressed onto the welded connection, the chamber is filled with the Cu/Ni sulphate-based electrolyte and by applying the respective current densities in alteration, i.e. 0.45

mA/cm$^2$ for copper and 22 mA/cm$^2$ for nickel, a NMM is deposited onto the weld seam and its proximity.

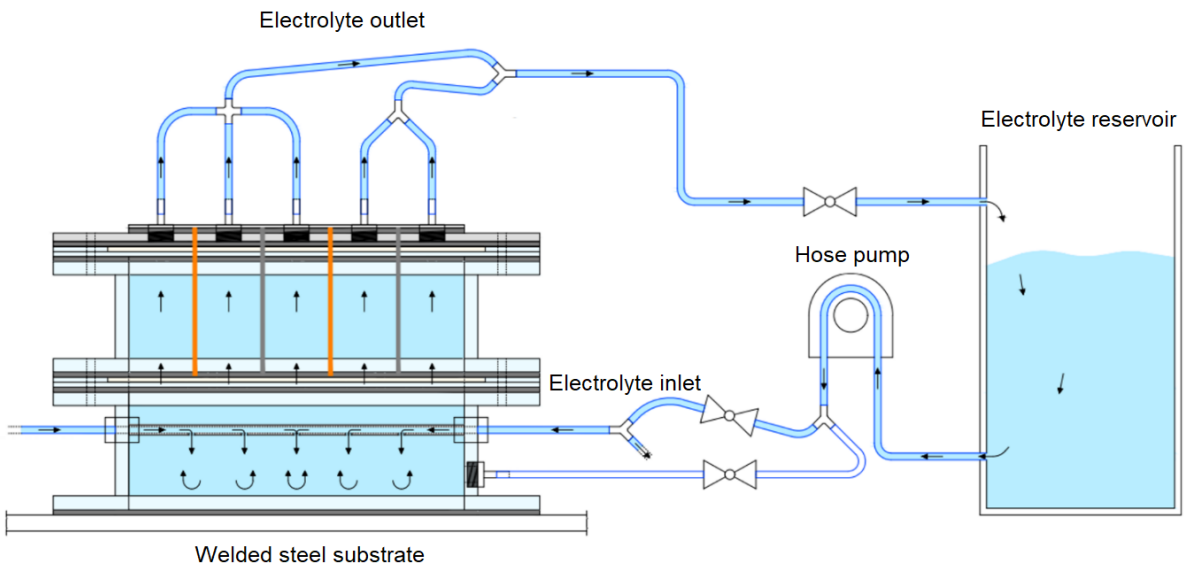


Figure 1: Mobile deposition unit for NMM patch installation.

## 3 A methodology for robot-based installation of NMM patches

This section describes a methodology to enable automated robot-based installation of NMM patches to welded joints of civil infrastructure using mobile robots. Mobile robots allow autonomous navigation to critical points of civil infrastructure. In this study, the IDOG robotic platform is used as a technological basis [5]. A robotic arm is mounted on the platform with a mobile deposition unit attached to the end effector of the robotic arm. The robotic arm allows fine positioning of the mobile deposition unit to align with the welded joints. To detect the welded joints, a camera is mounted on the robotic arm. An eye-in-hand calibration process [13] is utilized to simultaneously estimate the translation and rotation components of the rigid transformation from the camera frame to the end effector frame. Leveraging state-of-the-art object detection in images using convolutional neural networks [14], welded joints are detected and localized in the images by bounding boxes. Since cameras provide a mapping to a 2D plane (where depth information is lost), a time-of-flight sensor is attached to the robotic arm alongside the camera to measure distances and recover depth information. Upon detection of welded joints, the coordinates of bounding boxes, transformations from the camera frame to the end effector frame, and distance information from the time-of-flight sensor to welded joints allow the computation of full 6 degree-of-freedom (DoF) transformations from the end effector to welded joints. By multiplying the 6 DoF transformations with the current poses of the end effector, the poses of welded joints are computed in the robot-base frames. To enable the installation of NMM patches, the robotic arm is positioned at an installation pose, i.e. at a fixed position from the weld. The installation pose is fed into the inverse kinematics module to obtain goal

positions in the joint space of the robot. The robotic arm subsequently moves the mobile deposition unit to the welded joints for the installation of the NMM patches. The tests conducted to validate the methodology are presented in the subsequent section.

## 4 Validation tests and results

This section shows the validation tests that are conducted (i) to assess the fatigue behavior of NMM patches, (ii) to assess the performance of NMM patches under laboratory conditions, and (iii) to validate the methodology proposed for automated robot-based installation of NMM patches. To evaluate the fatigue behavior of post-weld treatments, different variants of post-weld treatments are tested, as shown in Figure 2. Dogbone samples are prepared in agreement with DIN 50100 [15] in the following configurations: (a) as-welded, (b) machined, (c) high-frequency-mechanical-impact (HFMI) treated, and (d) NMM post-weld treated. A cross-sectional scanning electron microscope (SEM) image and a laminar build-up of the NMM are depicted in (e) and (f), respectively, to highlight the nano-laminate structure of the NMM.

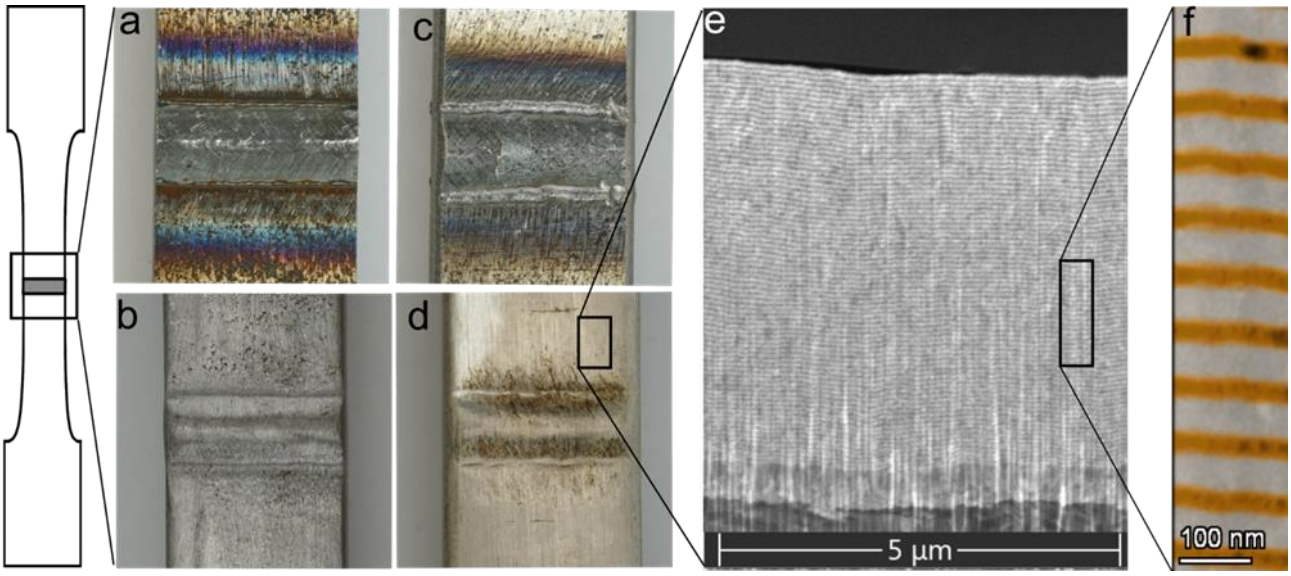


Figure 2: Dogbone sample with welds (a) in the as-welded condition, (b) after polishing the weld proximity, (c) after HFMI post-weld treatment, and (d) after application of the NMM post-weld treatment. (e) Cross-sectional SEM image showing the nanostructured build-up and (f) transmission electron microscopy (TEM) image showing the individual layers highlighted in orange (Cu) and grey (Ni).

Fatigue testing is conducted and evaluated in accordance with DIN 50100 [13]. The results are shown in Figure 3, in which the 5% quantile of the S-N curves are plotted to highlight the substantial change of fatigue strength of the NMM-treated weld in comparison with the as-welded and HFMI-post-weld treated weld; for more details on the results, the reader is referred to [9]. The NMM post-weld treatment shows a superior increase in fatigue strength of the weld compared to HFMI

treatment, while ensuring high reliability in fatigue strengthening, which manifests itself in the reduced scatter of results. According to Eurocode 3, the fatigue strength class design parameters for structures under cyclic loading can be read out at N = 2 x $10^6$ cycles.

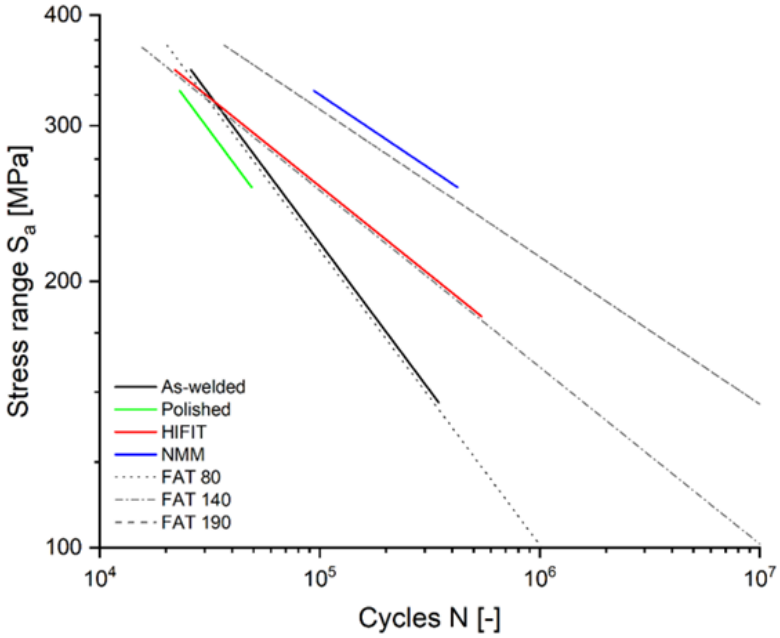


Figure 3: S-N curves of the 5% quantiles compared to the respective design-based FAT classes.

To assess the performance of NMM patches using the mobile deposition unit, an NMM patch is applied under laboratory conditions (Figure 4a). A thorough coating without any flaking, delamination, or other forms of defects can be seen, which is fundamental for the installation of NMM patches in the field. For further analysis, SEM images of the NMM cross section are acquired to gauge the nanoscale application quality (Figure 4b). In Figure 4a, the laminar build-up can be detected, while deviations from the planar coating can be seen. Particularly, in comparison to Figure 2e, the differences are noticeable. Although deviations from the planar coating are visible, no defects such as holes, voids, or delaminations can be found.

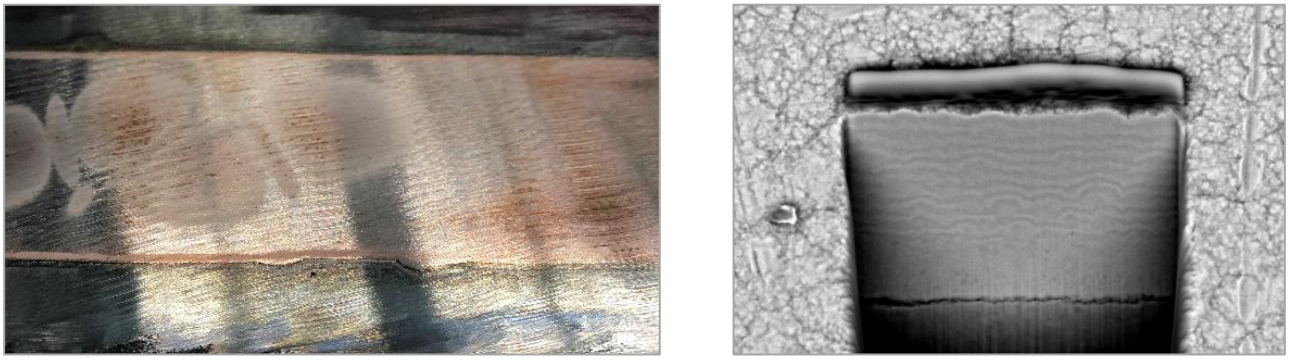

Figure 4: (a) Deposited nanolaminate thin film, (b) SEM image of the NMM cross-section.

Since the prototype of the mobile deposition unit is heavy for the robotic equipment available to the authors, the methodology for automated robot-based installation of NMM patches is tested exemplarily on a small scale. Figure 5a depicts the test equipment, including the IDOG robot with a robotic arm, introduced in [14], as a mobile robot platform, equipped with a robotic arm. A camera and a time-of-flight distance sensor are attached to the robotic arm. The mobile deposition unit, mounted at the end-effector of the robotic arm, is mimicked by a gripper in an open configuration. Details on autonomous navigation of the IDOG using light detection and ranging (LiDAR) sensors and the inertial measurement unit (IMU) are presented in [16].

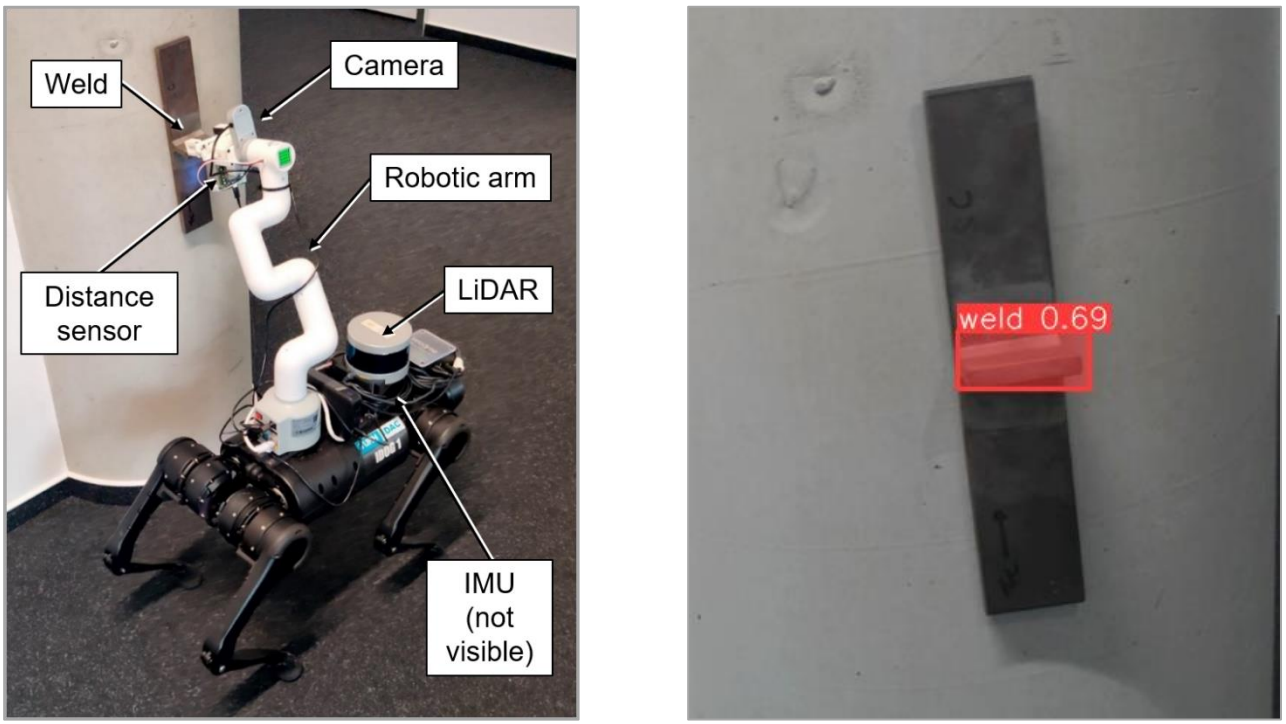


Figure 5: (a) Test equipment and (b) weld detected by the IDOG mobile robot.

To validate the methodology for automated robot-based installation of NMM patches, tests are conducted in an indoor environment with weld samples mounted on concrete pillars that emulate welds on existing civil infrastructure. A mapped environment, as described in [16], is utilized to enable autonomous navigation of the IDOG to goal locations in the vicinity of weld samples. Upon arriving at the goal locations, welds are successfully detected by the IDOG, as depicted in Figure 5b. However, false positives and low confidence scores during weld detection are also observed, indicating the need for a larger and more diverse weld dataset to be utilized for the training of the neural network. Upon detecting a weld, the robotic arm is successfully positioned towards the weld, as shown in Figure 5a.

## 5 Summary and conclusions

Fatigue, primarily in welded joints, is one of the primary factors that contribute to the failure of civil infrastructure. NMMs applied via electrodeposition may enhance the fatigue strength of welded joints. NMM patches may be installed by automated robot-based processes on civil infrastructure to ensure accuracy and consistency. In this paper, the fatigue behavior of NMM patches have been investigated and tested. A prototype of a mobile deposition unit has been developed to install NMM patches in the field. A methodology proposed to install NMM patches in automated robot-based processes has been investigated and validated. In conclusion, the improvement in the fatigue behavior of NMM patches allows adapting the design of civil infrastructure to either (i) increase the lifetime of structures, while leaving the structures unchanged, (ii) reduce the dimensions of load-bearing components, thereby decreasing material usage, (iii) or a combination of the above. While for bridges, reducing dimensions of load-bearing components is most likely prohibitive, since load-bearing components of reduced dimensions would exacerbate other load cases than fatigue, increasing the lifetime of bridges is of great interest. Furthermore, the results obtained in this study indicate that automated robot-based installation of NMM patches holds significant potential to prolong the lifetime of civil infrastructure. For future installation, a bridge in the harbor of Hamburg has been identified to further improve the approach toward robot-based installation of nanostructured metal multilayers on civil infrastructure.

## References

[1] Deutsches Zentrum für Luft- und Raumfahrt, 2022. Güterverkehr in Deutschland - Verkehrsmittel im Vergleich. Accessed on: 07/05/2024. [Online]. Available: https://www.dlr.de/de/aktuelles/nachrichten/daten-und-fakten/gueterverkehr-in-deutschland-verkehrsmittel-im-vergleich

[2] Geißler, K., 2014. Handbuch Brückenbau. Wiley-VCH Verlag GmbH, Berlin, Germany.

[3] Theiler, M., Dragos, K. & Smarsly, K., 2017. BIM-based design of structural health monitoring systems. In: Proceedings of the 11th International Workshop on Structural Health Monitoring (IWSHM). Stanford, CA, USA, 09/12/2017.

[4] Chmelko, V., Margetin, M., & Harakal, M., 2018. Notch effect of welded joint. MATEC Web of Conferences, 165, 21003.

[5] Smarsly, K., Dragos, K., Stührenberg, J., & Worm, M., 2023. Mobile structural health monitoring based on legged robots. Infrastructures, 8(9), 136.

[6] European Committee for Standardisation, 2005. EN 1993-1-9: Eurocode 3: Design of steel structures - Part 1-9: Fatigue.

[7] Brunow, J., Spalek, N., Mohammadi, F., & Rutner, M., 2023. A novel post-weld treatment using nanostructured metallic multilayer for superior fatigue strength. Scientific reports, 13(1), 22215.

[8] Brunow, J., & Rutner, M., 2021. Das Nanolaminatpflaster – Schweißnahtnachbehandlung für bisher unerreichte Lebensdauerverlängerung. Stahlbau, 90(9), pp. 691–700.

[9] Brunow, J., Gries, S., Krekeler, T., & Rutner, M., 2022. Material mechanisms of Cu/Ni nanolaminate coatings resulting in lifetime extensions of welded joints. Scripta Materialia, 212, 114501.

[10] Anderson, P. M., & Li, C., 1995. Hall-Petch relations for multilayered materials. Nanostructured Materials, 5(3), pp. 349–362.

[11] Dodaran, M. S., Wang, J., Shamsaei, N., & Shao, S., 2020. Investigating the interaction between persistent slip bands and surface hard coatings via crystal plasticity simulations. Crystals, 10(11), 1012.

[12] Wang, Y.-C.,Misra, A. & Hoagland, R. G., 2006. Fatigue properties of nanoscale Cu/Nb multilayers. Scripta Materialia, 54(9), pp. 1593–1598.

[13] Tsai, R. Y. & Lenz, R. K., 1989. A new technique for fully autonomous and efficient 3d robotics hand/eye calibration. IEEE Transactions on Robotics and Automation, 5(3), pp. 345–358.

[14] Redmon, J., Divvala, S., Girshick, R., & Farhadi, A., 2016. You Only Look Once: Unified, real-time object detection. In: Proceedings of the 2016 IEEE Conference on Computer Vision and Pattern Recognition (CVPR). Las Vegas, NV, USA, 6/27/2016.

[13] DIN 50125:2022-08, 2022. Prüfung metallischer Werkstoffe – Zugproben. Deutsches Institut für Normung, Berlin, Germany.

[14] DIN 50100:2016-12, 2016. Schwingfestigkeitsversuch - Durchführung und Auswertung von zyklischen Versuchen mit konstanter Lastamplitude für metallische Werkstoffproben und Bauteile. Deutsches Institut für Normung, Berlin, Germany.

[15] Johann, S., Stührenberg, J., Tandon, A., Dragos, K., Bartholmai, M., Strangfeld, C., & Smarsly, K., 2024. Implementation and validation of robot-enabled embedded sensors for structural health monitoring. In: Proceedings of the 11th European Workshop on Structural Health Monitoring (EWSHM). Potsdam, Germany, 06/10/2024.

[16] Tandon, A., Stührenberg, J., Dragos, K., & Smarsly, K., 2024. Autonomous navigation of quadruped robots for monitoring and inspection of civil infrastructure. In: Proceedings of the 20th International Conference on Computing in Civil and Building Engineering (ICCCBE). Montréal, Canada, 08/25/2024.

# Autonomous 3D Scanning of Construction Sites Using Terrestrial Laser Scanner and UGV

Pranav Shevkar[1] and Jan Luca Fahrendholz-Heiermann[1]
[1]Chair of Individualized Production in Architecture, RWTH Aachen University, Aachen, Germany
E-mail(s): shevkar@ip.rwth-aachen.de, fahrendholz@ip.rwth-aachen.de

**Abstract:** Accurate representation of construction sites for Artificial Intelligence (AI) processing and process monitoring demands complete 3D point clouds. Conventionally, a tripod-mounted terrestrial laser scanner (TLS) is employed for generating 3D point clouds at multiple locations, followed by post-processing, which is time-consuming. This paper proposes an autonomous scanning system integrating TLS with an Unmanned Ground Vehicle (UGV) to generate 3D point clouds. The approach employs frontier-based exploration to autonomously navigate the robot to optimal scan waypoints within predefined GPS-marked areas on an outdoor construction site. Subsequently, the high accuracy and long-range TLS scanner record a point cloud, which is registered, and a new optimal waypoint for the robot is computed. This iterative exploration and scanning process continues until the point cloud is complete and no new scanning frontier is identified within the scan area. The effectiveness of the newly developed autonomous scanning technique is evaluated through a comparative analysis of number of scan positions, point cloud completeness, and the time needed for manual scanning of outdoor construction sites. the proposed pipeline enables efficient collection of high-quality point clouds in outdoor environments, laying the groundwork for further artificial intelligence processing.
*Keywords:* 3D point cloud generation, ROS, autonomous exploration, terrestrial laser scanner, wave-front frontier detection

Erschienen in Tagungsband 35. Forum Bauinformatik 2024, Hamburg, Deutschland, DOI: 10.15480/882.13544
© 2024 Das Copyright für diesen Beitrag liegt bei den Autoren. Verwendung erlaubt unter Creative Commons Lizenz Namensnennung 4.0 International.

## 1 Introduction

Point cloud data technology has become a vital component of the construction industry, offering numerous applications that significantly enhance various aspects of construction projects. A primary application of point cloud data is in 3D model reconstruction, which includes both geometric and semantic model reconstruction. Additionally, point cloud data is crucial for quality inspection tasks, such as dimensional quality inspection, surface quality inspection, and displacement inspection [1]. Furthermore, 3D point clouds are instrumental in generating 3D data [2] and are utilized on construction sites for progress monitoring as well as raw material monitoring. This enables automated comparisons between the as-built and the as-planned state, allowing early detection of deviations during the construction process[3], [4].

This research is focused on the generation of point clouds on construction sites, specifically in outdoor environments. Flying laser scanners such as the 'Leica BLK2FLY', tower crane mounted laser scanners such as 'Blickfeld cube 1' as well as Terrestrial Laser Scanners (TLS) are particularly suited for outdoor scanning. This study focusses on TLS scanners due to their high dimensional accuracy and capability to generate dense point clouds. These scanners typically incorporate complex optics, motors, single-board computers, MEMS sensors, GPS antennas, and batteries for capturing and processing point clouds. However, manually scanning outdoor environments using a tripod is labor-intensive and time-consuming, highlighting the need for automated laser scanning solutions. Although tower crane-mounted laser scanners enable faster scanning, they are prone to increased blind spots caused by shadowing. On the other hand, flying laser scanners provide lower detail, are highly dependent on the weather conditions, and strict aviation regulations which can limit their usage in certain areas [5].

In this study, we utilize a Riegl VZ-400i terrestrial laser scanner mounted on an INNOK Heros 224 mobile robot. This setup allows for remote navigation to the desired scan positions. On larger construction sites, such as the one in this study, approximately 10 scans from various positions are required to construct a comprehensive and detailed point cloud, which remains a time-consuming process. To address these challenges, we propose an autonomous scanning system that integrates TLS and an UGV for optimal and fully autonomous 3D point cloud creation in outdoor environments. This system leverages a streamlined pipeline to enhance efficiency and reduce the time and labor associated with point cloud generation on construction sites.

The paper is organized as follows: Section 2 introduces related works; Section 3 describes the proposed system; Section 4 presents the experimental analysis; discussions about the current implementation are mentioned in Section 5; and finally, our conclusions are presented in Section 6.

## 2 Related Work

Autonomous 3D scanning of built environments was first developed by Surmann et al. [6] where they used a UGV equipped with a 3D laser scanner for navigation. The next best view (NBV) was selected based on the highest information gain value. In [7], Strand et al. proposed a 2D grid-based next best view strategy for 3D scanning of indoor environments. In this approach, navigation-specific information of the 3D world was projected onto a 2D grid. A weighting function was computed by simulating laser beams in 360° to select the next best viewpoint. Kim et al. introduced the Ground Robot Mapping Infrastructure (GRoMI) for dynamic SLAM-based navigation for 3D scanning using multiple 2D scanners [8]. Researchers in [9] developed a two-stage strategy for pose planning in outdoor environments. First, a 2D map was used as a reference to create a rough initial 3D model of the environment. This model was then used to plan the next best view in the second stage. Liang et al. used a TLS-based laser scanner on a UGV for autonomous scanning and implemented a UFOMap-based next best view algorithm for optimal scanner placement [10].

While there have been several studies on the development of autonomous 3D scanning using TLS and UGV, most research has focused on indoor scanning. This study specifically aims to automate the 3D scanning process in outdoor environments with minimal prior information.

# 3 Methodology

## 3.1 Hardware

For scanning the construction sites, a Riegl VZ-400i terrestrial laser scanner is used which provides predefined scanning patterns. Pattern 'Panorama40' is chosen for this application as it provides 34mm resolution at a distance of 50 m. This pattern records 22.5 Mio points at a frequency of 1200 kHz in 45 seconds.

To conduct the scanning autonomously, we employ the HEROS 224 robot from Innok Robotics as the UGV. This mobile robot has a compact footprint (920 x 730 x 440 mm), which enables it to navigate in tight spaces. With its sturdy construction and high ground clearance of 141 mm, it can easily traverse rough terrain. The UGV can carry a maximum payload of 200 kg. It is equipped with a SICK safety laser scanner for obstacle detection and an Xsens MTI-30 IMU, which provides absolute orientation through the fusion of accelerometer, gyroscope, and magnetometer data. Additionally, an Emlid Reach RS2+ multi-band RTK GNSS receiver is retrofitted on the rear side of the UGV to facilitate GPS-based navigation.

To securely mount the Riegl scanner to the Innok UGV, a custom fixture is installed on the front side of the robot. This fixture holds the Riegl scanner securely while allowing for easy mounting and unmounting. The UGV with the Riegl TLS is shown in Figure 1.

Figure 1: Innok UGV mounted with the Riegl TLS

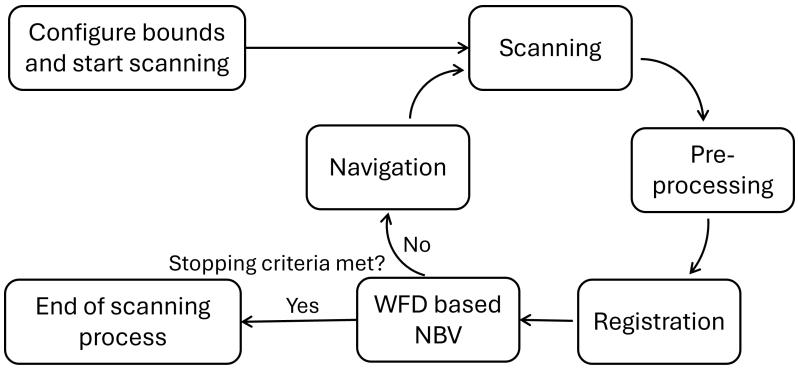


Figure 2: Flowchart of the implemented autonomous scanning pipeline

## 3.2 Software

Figure 2 provides an overview of the scanning pipeline of the developed system. The prior information for starting the algorithm includes a list of GPS coordinates that acts as a boundary for the scanning which is defined in a YAML file. The pipeline comprises five distinct modules that operate in a loop to capture the point cloud of the construction site which is similar to the work presented in [10]. These

modules are scan acquisition, pre-processing, frontier detection, navigation, and registration. Each module is further divided into sub-modules, which are discussed in detail in the following sections.

### 3.2.1 Scan acquisition module

The ROS2 package `ros-riegl-vz`, provided by RIEGL Laser Measurement Systems GmbH, was used for the development of scanner control and point-cloud data acquisition nodes. This package enables the writing of ROS2 nodes for configuring scan parameters, scanner control, and point cloud acquisition. The scanner, UGV computer, and processing computer are all connected to the same WLAN network, allowing the topics to be discoverable over the network.

Scanning is triggered automatically using a ROS2 service when the robot reaches the defined scanning location. Predefined parameters such as scan pattern, level of detail, fast scan registration mode, and GPS bounds are used. These parameters significantly affect the scan duration; hence, selecting the optimal pattern and level of detail that meets the requirements is crucial. Subsequently, the acquired scan is published over a topic as a `sensor_msgs/PointCloud2` message, which can take between 2 to 3 minutes with the selected configuration depending on the size of the point cloud.

### 3.2.2 Pre-processing

In the pre-processing module, every scan undergoes initial processing before further operations on the point cloud. During scanning, a large number of points outside the area of interest are captured, resulting in unnecessary accumulation of points in the registered point cloud. This not only increases the size of the point cloud but also extends processing times. To mitigate this issue, each scan is initially cropped using GPS bounds to remove extraneous points and reduce the size of the 3D scan. The first scan is established as the global reference scan, with its origin serving as the reference system origin.

Next, the cropped scan undergoes down-sampling to further reduce the number of points, utilizing a voxel size of 0.5 meters. Subsequently, Fast Point Feature Histograms (FPFH) are computed for both the source and target point clouds. These FPFH values play a crucial role in computing the initial global RANSAC transformation.

### 3.2.3 Registration

In the registration module, a transformation matrix is calculated and applied to the newly pre-processed point cloud to align it with the reference point cloud. Initially, a coarse principal axis alignment is performed using a transform obtained from the robot pose. Fine alignment is then done using point-to-plane ICP algorithm using the Open3D library which is available for Python [11]. Point-to-plane ICP requires normal estimation which is done using the hybrid KD-tree approach. In this research, the search radius was set to 0.1m and maximum number of nearest neighbors for this search to 30. This returns a registration result, which includes the refined transformation matrix that best aligns the new point cloud to the previous registered point cloud.

### 3.2.4 Next Best View Waypoint Computation

Each time a new scan is acquired, it undergoes transformation using the registration-derived transformation matrix. The point cloud is subsequently filtered along the z-axis based on parameters minZ and maxZ. The minZ parameter is configured to remove ground undulations, while maxZ ensures the robot navigates around structures such as shelters at the construction site, not considering them as obstacles. This filtered point cloud is then down-projected to generate an Occupancy Grid Map (OGM). The robot's current absolute pose is calculated by fusing GPS, IMU, and magnetometer sensor data. The Wavefront Frontier Detection (WFD) algorithm, implemented as a ROS2 node, identifies all frontiers in the OGM larger than twice the robot's size. The median pose of each frontier is computed and sorted based on Euclidean distance from the robot's current pose. Using the Nav2 package in ROS2, the robot navigates towards the closest frontier median. If the path planner fails to compute a path to the nearest frontier, the next closest frontier is selected iteratively [12]. Upon reaching the median pose, a new scan is acquired, and the process repeats. Offline mapping from the SLAM toolbox integrates the down-projected submap with the global map [13].

## 4 Experimental Analysis

To evaluate the effectiveness of the developed pipeline, we conducted an experiment on a reference construction site on the Melaten Campus of RWTH Aachen University covering an area of approximately $4000\,\mathrm{m}^2$. The chosen site featured a diverse array of elements, including tower cranes, excavators, containers, shelters, and various other construction materials.

First, the GPS coordinates of the scan area were recorded in the configuration file of the planning and processing node. The area is visualized on the map in Figure 3 below.

Figure 3: Visualization of the scan area on a map

Next, a scan was captured following the process outlined in Figure 2. The robot then moved to the next scan location determined by the WFD algorithm. After each scan, the OGM was updated with

the occupancy information computed by down-projecting the transformed 3D point cloud, and new frontiers were explored. During navigation, the robot avoided obstacles detected by the Sick laser scanner and re-planned the route to the goal location. During experimentation, we optimized the frontier area to avoid navigation to smaller frontiers and carefully adjusted the maximum height to allow the robot to pass through shelters without entering other open doors.

In this case study, the robot computed 12 frontiers to cover the complete construction site within the given GPS bounds. Every point cloud captured by the TLS scanner was successfully registered. However, some gaps were found in the registered point cloud at locations where the robot could not successfully plan a path. The scan locations are shown in the top view of the registered point cloud in Figure 4.

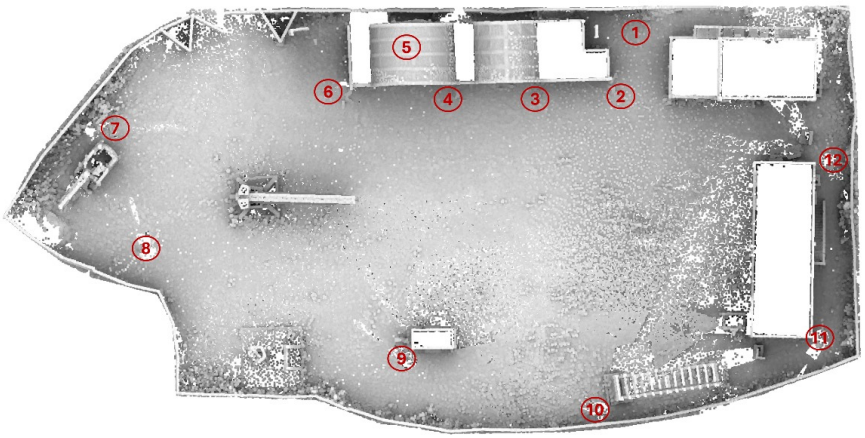


Figure 4: Sequence of scans acquired using the WFD algorithm for getting the scanner position

To compare the efficacy of the proposed pipeline, an experienced colleague performed a manual scanning process of the same construction site. Using the manual method, 16 scans were required to cover the entire site. An experimental comparison between the manual and autonomous scanning methods is presented in Table 1. The comparison shows that the automated method required fewer scans and less time to cover the construction site. The automated method results in fewer points compared to the manual scanning process due to reduced redundancy in scanning the same areas.

Table 1: Comparison of Automated and Manual Methods

| Method | #Scans | #Points | Time | Pre-processing time |
|---|---|---|---|---|
| Automated | 12 | 6,545,862 | 1 h | 0 |
| Manual | 16 | 9,542,703 | 2 h | 2 h |

The pre-processing time is zero in case of the proposed automated method as the pre-processing is conducted on-the-fly and the point-cloud is registered. In case of manual method, the point-clouds must be downloaded from the TLS and then processed in a software such as RiSCAN PRO to get the registered point-cloud.

## 5 Discussion

The proposed solution follows the "stop-scan-plan-go" scanning pattern, contrasting with the "scanning-while-navigating" pattern that requires continuous planning and exploration using the SLAM technique's lifelong mapping algorithm. Although "scanning-while-navigating" approaches, such as those in [8] and [14], are efficient, they often generate noisy point clouds, rendering them unsuitable for capturing architectural details. In comparison, automated Terrestrial Laser Scanning (TLS) methods, as discussed in [10], are more precise. Additionally, some researchers have suggested computing the NBV using unknown voxels [15]. However, our research found that this method is most effective in closed environments.

Implementing an automated TLS system mounted on an UGV can lead to a high initial cost but the reduction in labor costs alone can be significant, as UGVs eliminate the need for skilled operators and can work continuously without breaks or fatigue. Considering an initial UGV cost of €60,000, amortized over 30 projects and maintenance cost of €200 per project, the total operational cost would be €2200 per project. Labour cost with a skilled worker taking €20 per hour for a 20 day project would be €3200 per project. While there is an upfront cost associated with implementing an automated TLS system on a UGV platform, the long-term benefits often outweigh these initial expenses through substantial reductions in labor costs, increased operational efficiency, and enhanced safety measures.

## 6 Conclusion

This research presents an autonomous UGV-based scanning method tailored for outdoor environments, requiring minimal prior information and human intervention. The method achieves scanning accuracy comparable to that of an experienced human operator, with a reduced number of scans. This was validated through testing on a reference construction site.

Future work will focus on optimizing the algorithm to analyze gaps in the point clouds and compute a NBV pose to address them. Additionally, this research can be expanded to include the identification and analysis of specific construction elements, such as sand piles, for volumetric data extraction.

## Funding

This work is part of the KI for BauChain research project funded by Zukunftbau, Bundesinstitut für Bau-, Stadt- und Raumforschung (BBSR), and Bundesministerium für Wohnen, Stadtentwicklung und Bauwesen (BMWSB) (project number 10.08.18.7-22.15).

## References

[1] Q. Wang and M.-K. Kim, “Applications of 3d point cloud data in the construction industry: A fifteen-year review from 2004 to 2018”, *Advanced Engineering Informatics*, 2019. DOI: 10.1016/j.aei.2019.02.007.

[2] C. Thomson and J. Boehm, “Automatic Geometry Generation from Point Clouds for BIM”, *Remote Sensing*, vol. 7, no. 9, pp. 11 753–11 775, 2015. DOI: 10.3390/rs70911753.

[3] A. Braun, A. Borrmann, S. Tuttas, and U. Stilla, “BIM-Basead Progress Monitoring”, in *Building Information Modeling*, 2018, pp. 527–544.

[4] J. Fahrendholz, L. Kirner, and S. Brell-Cokcan, “Entwicklung und umsetzung einer automatisierten baufortschrittsüberwachung mittels deep learning basierend auf punktwolken und bauinformationsmodellen”, in *IoC - Internet of Construction*, S. Brell-Cokcan and R. Schmitt, editors, Wiesbaden: Springer Vieweg, 2024. DOI: 10.1007/978-3-658-42544-9_22.

[5] A. Rao, M. Radanović, Y. Liu, *et al.*, “Real-time monitoring of construction sites: Sensors, methods, and applications”, *Automation in Construction*, vol. 136, p. 104 099, Apr. 2022. DOI: 10.1016/j.autcon.2021.104099.

[6] “An autonomous mobile robot with a 3d laser range finder for 3d exploration and digitalization of indoor environments”, *Robotics and Autonomous Systems*, vol. 45, no. 3, pp. 181–198, 2003. DOI: https://doi.org/10.1016/j.robot.2003.09.004.

[7] M. Strand and R. Dillmann, “Using an attributed 2d-grid for next-best-view planning on 3d environment data for an autonomous robot”, Jul. 2008, pp. 314–319. DOI: 10.1109/ICINFA.2008.4608017.

[8] P. Kim, J. Chen, and Y. Cho, “Slam-driven robotic mapping and registration of 3d point clouds”, *Automation in Construction*, vol. 89, pp. 38–48, May 2018. DOI: 10.1016/j.autcon.2018.01.009.

[9] P. S. Blaer and P. K. Allen, “Data acquisition and view planning for 3-d modeling tasks”, in *2007 IEEE/RSJ International Conference on Intelligent Robots and Systems*, 2007, pp. 417–422. DOI: 10.1109/IROS.2007.4399581.

[10] N. Liang, Y. P. Ang, K. Yeo, X. Wu, Y. Xie, and Y. Cai, “Bimbot for autonomous laser scanning in built environments”, *Robotics*, vol. 13, p. 22, Jan. 2024. DOI: 10.3390/robotics13020022.

[11] Q.-Y. Zhou, J. Park, and V. Koltun, “Open3D: A modern library for 3D data processing”, *arXiv:1801.09847*, 2018.

[12] A. Topiwala, P. Inani, and A. Kathpal, “Frontier based exploration for autonomous robot”, *arXiv:1806.03581*, 2018.

[13] S. Macenski and I. Jambrecic, “Slam toolbox: Slam for the dynamic world”, *Journal of Open Source Software*, vol. 6, p. 2783, May 2021. DOI: 10.21105/joss.02783.

[14] J. Zhang and S. Singh, “Loam : Lidar odometry and mapping in real-time”, *Robotics: Science and Systems Conference (RSS)*, pp. 109–111, Jan. 2014.

[15] D. Duberg and P. Jensfelt, “Ufomap: An efficient probabilistic 3d mapping framework that embraces the unknown”, *IEEE Robotics and Automation Letters*, Aug. 2020. DOI: 10.1109/LRA.2020.3013861.

# Autonome Navigation vierbeiniger Roboter für Bauwerksinspektionen

Aditya Tandon und Jan Stührenberg
Institut für Digitales und Autonomes Bauen, Technische Universität Hamburg, Blohmstraße 15, 21079 Hamburg
E-Mails: aditya.tandon@tuhh.de, jan.stuehrenberg@tuhh.de

**Abstract:** Robotersysteme werden für automatisierte Inspektionen von Infrastrukturbauwerken eingesetzt, um die Inspektionsgenauigkeit zu erhöhen und die betriebliche Effizienz zu verbessern. Vierbeinige Roboter verfügen über ausgefeilte Fortbewegungstechniken, die eine große Stabilität, Manövrierfähigkeit und Anpassungsfähigkeit in komplexen bzw. schwierig zugänglichen Gebäuden ermöglichen. Für den zuverlässigen autonomen Betrieb von vierbeinigen Robotern sind robuste Navigations- und Regelungssysteme erforderlich, die jedoch mit zunehmender Komplexität der Bauwerke nicht optimal funktionieren oder die von vierbeinigen Robotern gebotene Flexibilität nicht ausnutzen. Um den autonomen Betrieb von vierbeinigen Robotern zu erleichtern, wird in diesem Beitrag ein Framework zur Bewegungsplanung vorgestellt, der aus einem sampling-basierten globalen Planungsansatz, den Batch Informed Trees*, und dem lokalen Planungs- und Regelungsansatz Timed Elastic Band besteht. Das vorgeschlagene Framework beinhaltet zusätzlich den Cartographer-Algorithmus zur Lokalisierung, der einen erfolgreichen autonomen Betrieb und die Navigation in Innenräumen ermöglicht. Das Framework wird auf vierbeinigen Robotern unter Verwendung einer verteilten Softwarearchitektur eingesetzt, die die Planung und Ausführung von Inspektionsaufgaben mit Hilfe einer Basisstation und autonomen Navigationsfunktionen in Echtzeit auf den mobilen Robotern ermöglicht. Zur Validierung des Frameworks werden Inspektionsmissionen in einer Büroumgebung mit Hindernissen geplant und ausgeführt. Die Ergebnisse zeigen, dass das Framework robuste Echtzeit-Hindernisvermeidungsfunktionen bereitstellt und eine zuverlässige Pfadplanung und Lokalisierung mit geringer Latenzzeit ermöglicht.
*Keywords:* Vierbeinige Roboter, autonome Navigation, Simultaneous Localization and Mapping (SLAM), Bewegungsplanung, Inspektionsplanung

Erschienen in Tagungsband 35. Forum Bauinformatik 2024, Hamburg, Deutschland, DOI: 10.15480/882.13500
© 2024 Das Copyright für diesen Beitrag liegt bei den Autoren. Verwendung erlaubt unter Creative Commons Lizenz Namensnennung 4.0 International.

## 1 Einleitung

Der Verfall von Infrastrukturbauwerken stellt ein erhebliches Risiko für die öffentliche Sicherheit dar. Infrastrukturbauwerke erfordern ein kontinuierliches Monitoring und regelmäßige Inspektionen, um

einen sicheren Betrieb zu gewährleisten [1]. Bestehende manuelle Monitoring- und Inspektionsverfahren können jedoch zeitaufwändig, arbeitsintensiv, gefährlich, und teuer sein. Die Einführung robotergestützter, automatisierter Monitoring- und Inspektionsverfahren hat das Potenzial, die Produktivität zu steigern, die Sicherheit zu erhöhen und die Kosten zu senken [2].

Mobile, mit Sensoren ausgestattete Roboter wurden bereits erfolgreich für Inspektionsaufgaben eingesetzt [3], wobei bisher spezialisiertes Personal wie Gebäudeinspektoren und Roboterbediener erforderlich waren. Jüngste Fortschritte in der Robotik haben den Einsatz mobiler Roboter zur automatischen Durchführung visueller Inspektionen vorangetrieben [4]. Insbesondere werden vermehrt vierbeinige Roboter eingesetzt, die Hindernisse überwinden, Treppen steigen und schwere Nutzlasten tragen können. Um robotergestützte automatische Inspektionen zu ermöglichen, müssen vierbeinige Roboter in der Lage sein, zuverlässig autonom zu arbeiten. Dafür werden in der Regel Bewegungsplanungssysteme eingesetzt, die die Umgebung in Echtzeit wahrnehmen, den Roboter lokalisieren, Pfade planen, Hindernisse vermeiden und die Roboter so auf kollisionsfreien Trajektorien zu Zielpositionen bewegen. Bestehende Bewegungsplanungssysteme für vierbeinige Roboter nutzen häufig Ganzkörperregelungen für die Planung des Fußkontakts und Erreichbarkeitsüberprüfungen [5], um eine umfassende Bewegungsplanung im Gelenkraum zu ermöglichen. Das Bewegungsproblem in Ganzkörperregelungen kann jedoch hochdimensional und nichtlinear sein, was die Lösung des Problems in Echtzeit komplex und rechenaufwändig macht. Die Komplexität rechenintensiver Ganzkörperregelungen ist in herkömmlichen Innenräumen kaum gerechtfertigt, da die Berechnung präziser Fußkontakte weniger wichtig ist. Stattdessen kann eine Gangstrategie, die das Gleichgewicht des Roboters aufrechterhält, ausreichend sein. In diesem Beitrag wird ein Framework zur Bewegungsplanung vierbeiniger Roboter für automatisierte Inspektionen präsentiert. Das Framework entkoppelt das Bewegungsplanungsproblem in (i) ein High-Level-Aufgabenraumproblem und (ii) ein Low-Level-Gelenkraumproblem, um einen effektiven Echtzeitbetrieb von vierbeinigen Robotern zu gewährleisten. Innerhalb der Frameworks wird ein Missionsplanungmodul verwendet, um die Planung und Ausführung von Inspektionsaufgaben zu ermöglichen.

Der Beitrags ist wie folgt gegliedert. Abschnitt 2 beschreibt den Entwurf und die Implementierung des Frameworks für automatische Inspektionen. In Abschnitt 3 werden die zur Validierung des Frameworks durchgeführten Tests sowie deren Ergebnisse vorgestellt. Abschnitt 4 schließt mit einer Diskussion der Ergebnisse, einer Zusammenfassung und einem Ausblick auf mögliche zukünftige Arbeiten.

## 2 Ein Framework zur Bewegungsplanung für automatische Bauwerksinspektionen

Das Framework zur Bewegungsplanung für automatische Bauwerksinspektionen ist in Abbildung 1 dargestellt. Da Roboter in einer dynamischen Welt operieren, muss eine zuverlässige Echtzeitleistung der Module des Bewegungsplanungsframeworks gewährleistet sein, um Kollisionen

zu vermeiden. Daher basiert das Framework auf einer verteilten Robot Operating System (ROS)-Architektur, die es ermöglicht, Module auf Roboter und Computer zu verteilen. Die Auslagerung von Modulen auf Computer reduziert die Rechenlast der Roboter und erleichtert den Echtzeitbetrieb. Das Missionsplanungsmodul, das für den Echtzeitbetrieb nicht entscheidend ist, wird daher auf einem Computer implementiert. Zusätzlich wird das Framework in ein High-Level-Aufgabenraumproblem und ein Low-Level-Gelenkraumproblem entkoppelt. Die Entkopplung der Probleme führt zu zwei Problemen mit reduzierter Komplexität, die unabhängig voneinander gelöst werden können. Das High-Level-Task-Space-Problem befasst sich mit der Planung kollisionsfreier Pfade für den Roboter und der Erzeugung von Zielgeschwindigkeiten im Task-Space. Die Low-Level-Bewegungsausführung verwendet eine Gangstrategie, um die Zielgeschwindigkeiten unter Beibehaltung des Gleichgewichts und der Stabilität des Roboters zu erreichen, wobei eine Hochfrequenzkommunikation verwendet wird. Da die High-Level-Bewegungsplanung unter Verwendung vollständiger 3D-Darstellungen in Echtzeit auf eingebetteten Plattformen nach wie vor sehr rechenaufwändig ist [5], wird eine hybride Strategie angewandt, die die 3D-Umgebung in 2D approximiert. Die Bewegungsplanung auf oberer Ebene im Aufgabenraum wird daher durch die Darstellung des vierbeinigen Roboters als holonomer Roboter im SE(2)-Zustandsraum mit einem rechteckigen Roboterfußabdruck entsprechend der Größe des Roboters erreicht. Durch die Entkopplung kann der Low-Level-Controller mit hohen Frequenzen arbeiten und so eine robuste und stabile Fortbewegung in unebenem Gelände und bei Vorhandensein von externen Störungen gewährleisten. Als Basis der Implementierung wird der ROS-Navigationsstack genutzt. In den folgenden Abschnitten werden die Kernmodule des Frameworks vorgestellt.

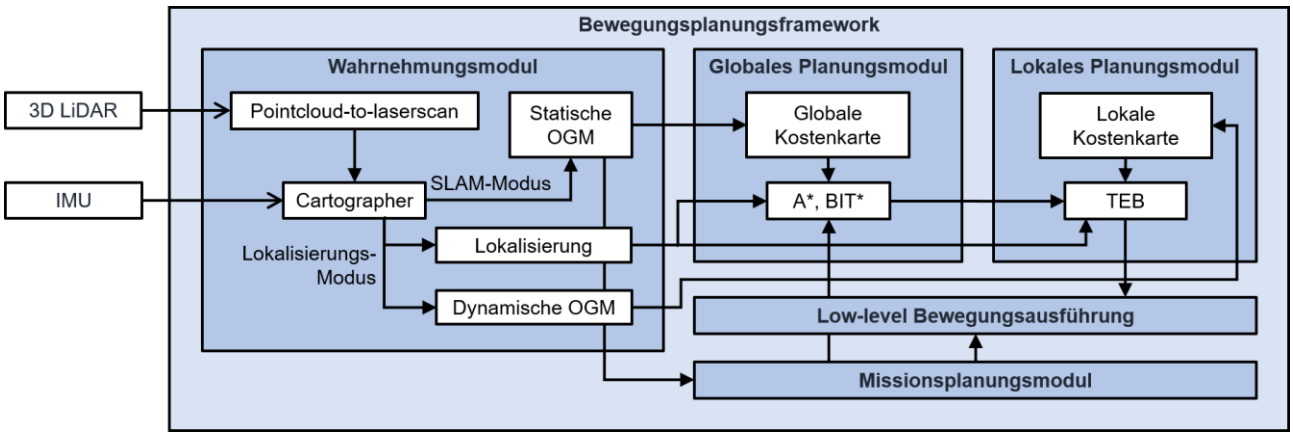


Abbildung 1: Framework zur Bewegungsplanung für automatische Bauwerksinspektionen.

## 2.1 Wahrnehmungsmodul

Die Bewegungsplanung erfordert die Wahrnehmung der Umgebung, um Karten der Umgebung zu erstellen, sich innerhalb der Karten zu lokalisieren und dynamische Hindernisse zu erkennen. In diesem Beitrag wird die Wahrnehmung durch einen LiDAR (Light Detection and Ranging)-Sensor ermöglicht, ergänzt durch eine Inertialmesseinheit (IMU). Da die Bewegungsplanung und Navigation im SE(2)-Zustandsraum durchgeführt wird, werden die 3D-Punktwolkendaten durch Abbildung auf

die horizontale Ebene in 2D-Laserscandaten umgewandelt. Das simultane Lokalisierungs- und Kartierungssystem (SLAM) „Cartographer“ [6] nutzt die 2D-Laserscan- und IMU-Daten, um eine Karte der Umgebung zu erstellen und sich innerhalb der Karte zu lokalisieren. Cartographer operiert dabei in zwei Modi: Im SLAM-Modus zur Erzeugung einer statischen Occupancy Grid Map (OGM) und im Lokalisierungsmodus zur Positionierung des Roboters auf der statischen OGM.

## 2.2 Globales Planungsmodul

Das globale Planungsmodul ermöglicht Robotern, durchführbare, sichere und optimale Pfade zu Zielposen zu planen, indem es mögliche Kollisionen mit Hindernissen in der statischen Karte überprüft und Entfernung, Zeit und/oder Energie minimiert. Für die Suche werden graphenbasierte oder sampling-basierte Bahnplanungsalgorithmen verwendet. Das globale Planungsmodul verwendet die NavfnROS-Implementierung des graphbasierten Planungsalgorithmus A*. A* arbeitet auf einer diskretisierten und statischen Belegungsrasterkarte und garantiert mit einer zulässigen Heuristik eine optimale Lösung. Sampling-basierte Pfadplanungsalgorithmen nehmen zufällige Stichproben im Konfigurationsraum und konstruieren einen Graphen, indem sie Punkte mit Kanten verbinden, wenn sie kollisionsfrei sind. ROS-kompatible C++-Implementierungen von sampling-basierten Planungsalgorithmen werden aus dem globalen Planungsmodul OmplPlanner [7] verwendet. Die Implementierungen der Planungsalgorithmen Rapid-Exploring Random Trees (RRT*) und Informed-RRT* werden unverändert verwendet, während der OmplPlanner um den Planungsalgorithmus Batch-Informed Trees (BIT*) erweitert wurde.

## 2.3 Lokales Planungsmodul

Das lokale Planungsmodul nutzt die vom globalen Planungsmodul geplanten Pfade. Um Hindernissen Rechnung zu tragen, die während der Kartierung möglicherweise nicht erfasst wurden, passt das lokale Planungsmodul Trajektorien für ein kurzes Zeitfenster in der unmittelbaren lokalen Umgebung des Roboters mit hoher Frequenz an, um eine kollisionsfreie Navigation zu ermöglichen. Das lokale Planungsmodul nutzt Sensordaten vom Wahrnehmungsmodul um eine lokale Karte inklusiver dynamischer und statischer Hindernisse zu erstellen, die sich um den Roboter herum befinden. Um minimale Abstände zwischen Robotern und Hindernissen zu gewährleisten, werden Kostenkarten eingesetzt. Kostenkarten ergänzen die OGMs, indem sie den benachbarten belegten Zellen Reisekosten zuweisen. Das lokale Planungsmodul verwendet den TEB (Timed Elastic Bands)-Ansatz für die lokale Planung [8]. Der TEB-Planungsansatz modifiziert bestehende globale Pläne, indem er die virtuellen Anziehungskräfte der globalen Pläne und die Abstoßungskräfte von Hindernissen ausgleicht. Der TEB-Planungsansatz generiert zeitoptimale Trajektorien, wobei kinodynamische Beschränkungen eingehalten und minimale Abstände um Hindernisse eingehalten werden. Da vierbeinige Roboter holonomische Roboter sind, wird die Strafe für Querbewegungen im TEB-Planungsansatz abgeschwächt. Dadurch wird die Generierung von Trajektorien mit Geschwindigkeiten und Beschleunigungen in allen Richtungen im SE(2)-Zustandsraum gefördert.

### 2.4 Missionsplanungsmodul

Um automatisierte Bauwerksinspektion zu ermöglichen, wird ein Missionsplanungsmodul eingesetzt. Das Missionsplanungsmodul umfasst eine Benutzerschnittstelle für die sequentielle Planung, Ausführung und Verwaltung von Inspektionsaufgaben und -missionen und verwaltet die roboterbezogene Sicherheit und Funktionalität. Inspektionsmissionen sind als hierarchische endliche Zustandsautomaten modelliert. Inspektionsmissionen bestehen aus Missionsaufgaben, die als einzelne Zustände modelliert sind, und Übergänge zwischen den Zuständen, die auf der Grundlage des Ausführungsstatus der jeweiligen Aufgaben definiert werden. Die Inspektionsmissionen werden mit Hilfe der SMACH-Bibliothek im ROS-Framework implementiert [9] und lassen sich intuitiv mit einer grafischen Benutzeroberfläche im ROS-Visualisierungstool RViz erstellen. Zielposen werden durch das Markieren von Pfeilen auf der statischen OGM zu einer Inspektionsmission hinzugefügt. Die grafische Benutzeroberfläche ermöglicht das Speichern, Laden und Ausführen von Inspektionsmissionen. Zusätzlich kann über die grafische Benutzeroberfläche der Betriebs- und Bewegungsstatus des Roboters eingesehen und kontrolliert werden, um beispielsweise die Ausführung eines Auftrags zu unterbrechen.

## 3 Validierungstests und Ergebnisse

Das in diesem Beitrag präsentierte Framework wird in einer Büroumgebung validiert, um die Funktionalität und Echtzeitleistung zu bewerten. Zunächst wird das Wahrnehmungsmodul des Frameworks validiert, indem eine statische OGM der Umgebung mit dem SLAM-Modus von Cartographer erstellt und die Lokalisierung in der statischen OGM mit dem Lokalisierungsmodus von Cartographer getestet wird. Anschließend werden mit dem Missionsplanungsmodul Inspektionsmissionen in der statischen OGM geplant, um das globale Planungsmodul und das lokale Planungsmodul des Frameworks zu validieren. Das Framework wird auf einem vierbeinigen Roboter vom Typ „Intelligent Documentation Gadget“ (IDOG) implementiert [10]. Die Büros sind mit beweglichen Möbeln ausgestattet, die die räumliche Anordnung der kartierten Umgebung verändern können und somit als statische Hindernisse fungieren. Personen, die sich in den Büros bewegen, stellen dynamische Hindernisse dar.

Zur Validierung des Wahrnehmungsmoduls wird Cartographer verwendet, um eine statische OGM der Umgebung zu erstellen und anschließend den Roboter auf der statischen OGM zu lokalisieren. Der LiDAR wird mit einer Frequenz von 10 Hz und die IMU mit 100 Hz betrieben. Der IDOG wird manuell gesteuert, während der SLAM-Modus von Cartographer die OGM mit einer Auflösung von 0,05 m/Pixel erstellt. Die Karte hat eine Länge von ca. 780 Pixeln und eine Breite von 400 Pixeln, was 39 m × 20 m entspricht. Nach dem Start des Lokalisierungsmodus von Cartographer wird die zunächst unbekannte Position des IDOG in der Karte innerhalb von Sekunden bestimmt.

Zur Validierung des globalen Planungsmoduls werden Inspektionsmissionen in der statischen OGM erstellt, die als Missionen mit mehreren Wegpunkten angelegt sind. Das globale Planungsmodul plant Pfade zwischen den Wegpunkten, die anhand von Pfadlänge und Planungszeit verglichen

werden. Wie in Abbildung 2 dargestellt, werden in der statischen OGM drei Wegpunkte ausgewählt, die verschiedene Herausforderungen simulieren. Die Validierung wird für die Algorithmen BIT*, Informed-RRT*, RRT* und A* durchgeführt.

Abbildung 2: Inspektionsmission zur Validierung des globalen Planungsmoduls.

Die Validierungstests zeigen, dass bis auf RRT* alle globalen Planungsalgorithmen ausschließlich kollisionsfreie Pfade zwischen den Wegpunkten in den Tests erzeugen. Daher werden weitere Pfadplanungstests mit RRT* aufgegeben. Die Ergebnisse sind in Tabelle 1 dargestellt. Die von A*, BIT* und Informed-RRT* geplanten Pfade haben vergleichbare Längen. Der A*-Algorithmus weist eine um eine Größenordnung geringere Planungszeit auf als die anderen stichprobenbasierten Planungsalgorithmen mit einem Planungsbudget von einer Sekunde. Die Ergebnisse in dieser Studie deuten darauf hin, dass die globale Bewegungsplanung in 2D und in der vergleichsweise kleinen Validierungsumgebung schneller vom graphenbasierten A*-Algorithmus gelöst wird. Für künftige Bahnplanungen in 3D und in großen Umgebungen wird BIT*, der den Stand der Technik darstellt, zusätzlich zum A*-Algorithmus in das Bewegungsplanungssystem integriert. Der A*-Algorithmus wird für die Planung in 2D und kleinen Umgebungen verwendet.

Tabelle 1: Weglänge und Planungszeit der globalen Planungsalgorithmen.

| Weg-punkt | A* | | BIT* | | Informed-RRT* | | RRT* | |
|---|---|---|---|---|---|---|---|---|
| | Länge (m) | Zeit (s) | Länge (m) | Zeit (s) | Länge (m) | Zeit (s) | Länge (m) | Zeit (s) |
| 1 | 18.878 | 0.082 | 18.795 | 1.037 | 19.732 | 1.035 | 26.747 | 1.034 |
| 2 | 11.544 | 0.288 | 11.621 | 1.051 | 11.535 | 1.085 | - | - |
| 3 | 08.815 | 0.085 | 08.816 | 1.032 | 08.811 | 1.039 | - | - |

Die Validierung der Funktionalität und Echtzeitleistung des lokalen Planungsmoduls wird durch mehrere Tests durchgeführt, die sowohl die An- und Abwesenheit von Hindernissen als auch die Durchquerung von offenen Räumen und schmalen Passagen beinhaltet. In Abwesenheit von Hindernissen zeigt sich, dass die tatsächliche Trajektorie des Roboters eng mit dem globalen Plan übereinstimmt. Lediglich in einigen Segmenten sind leichte Abweichungen vom globalen Plan zu beobachten. Statische Hindernisse, wie beispielswiese verschobene Möbel, werden durch vom Wahrnehmungsmodul empfangene Sensordaten der lokalen Kostenkarte des Roboters hinzugefügt, wie in Abbildung 3a dargestellt. Das lokale Planungsmodul plant um das Hindernis herum (blaue

Trajektorie), obwohl der globale Plan mit dem statischen Hindernis kollidiert (lila Trajektorie). Wie in Abbildung 3b zu sehen ist, ist der IDOG in der Lage, das Hindernis erfolgreich zu umgehen.

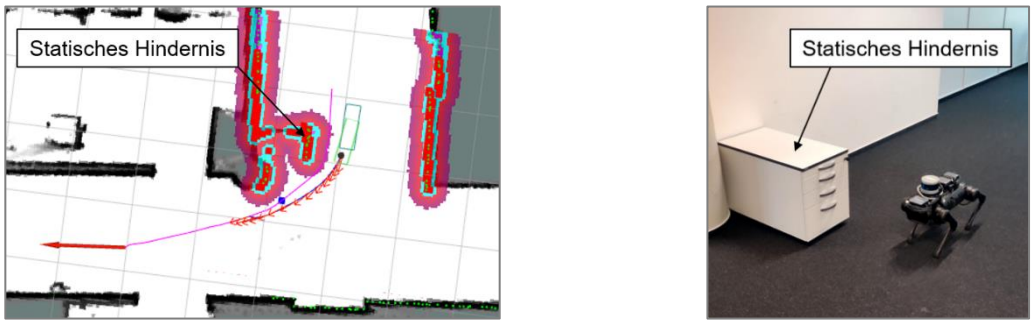


(a) Plan um statisches Hindernis herum (b) IDOG umgeht das Hindernis

Abbildung 3: Ausführung eines lokalen Plans auf engem Raum und um Ecken.

Um die Navigation durch schmale Passagen zu validieren, werden Wegpunkte in zwei Räume platziert, die die Durchquerung von Türen mit einer Breite von 1,05 m und 0,8 m erfordern. Die Tests zeigen, dass der IDOG in der Lage ist, erfolgreich einen globalen Pfad zu planen, den Pfad lokal abzustimmen und in Echtzeit zu navigieren, während ein ausreichender Abstand zu den Türpfosten eingehalten wird. Während die autonomen Navigationsfähigkeiten um Hindernisse herum und durch enge Passagen zufriedenstellend sind, wird in schmalen Passagen ein oszillierendes Verhalten zwischen dem vom IDOG verfolgten Pfad und dem globalen Plan beobachtet (Abbildung 4), dennoch kann der IDOG den globalen Plan vervollständigen.

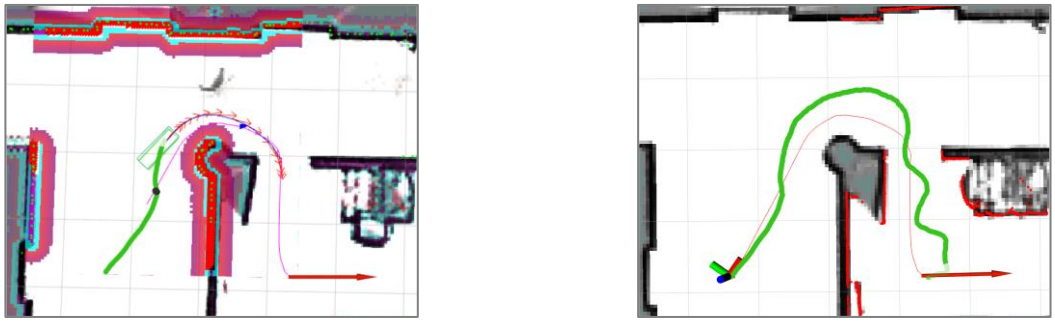

(a) Lokaler Plan um die Ecke. (b) Durchgeführte Trajektorie um die Ecke.

Abbildung 4: Ausführung eines lokalen Plans auf engem Raum und um Ecken.

## 4 Zusammenfassung und Schlussfolgerungen

Der Verfall baulicher Infrastruktur erfordert ein kontinuierliches Monitoring und regelmäßige Inspektionen, um einen sicheren Betrieb zu gewährleiste. Um ein robotergestütztes, automatisiertes Monitoring und Inspektionen mit vierbeinigen Robotern zu erreichen, ist die Verwendung von Bewegungsplanungssystemen unerlässlich. Das in dieser Studie vorgestellte Framework entkoppelt das Bewegungsplanungsproblem in ein High-Level-Aufgabenraumproblem und ein Low-Level-Gelenkraumproblem für den Echtzeitbetrieb von vierbeinigen Robotern. Der sampling-basierte globale Planungsalgorithmus BIT*, der A*-Algorithmus und der lokale Planungsansatz TEB werden für die Steuerung von Robotern und die Vermeidung von Hindernissen unter Einsatz einer verteilten

Software-Architektur auf dem vierbeinigen IDOG-Roboter und einem Computer implementiert. Inspektionsmissionen wurden in einer Büroumgebung mit statischen und dynamischen Hindernissen geplant und in Validierungstests vom IDOG erfoglreich ausgeführt. Die Ergebnisse zeigen, dass das Bewegungsplanungsframework in Echtzeit arbeiten kann, statische und dynamische Hindernisse erfolgreich umgehen kann und schmale Türen durchqueren kann, obwohl hier ein unerwünschtes oszillierendes Verhalten der Roboterbewegung zu beobachten ist. Zusammenfassend lässt sich festhalten, dass das Framework eine nützliche Grundlage für die automatisierte Inspektion von baulicher Infrastruktur mit vierbeinigen Robotern darstellt. Zukünftige Arbeiten werden das oszillierende Verhalten des Bewegungsplanungsframeworks beim Durchqueren schmaler Passagen untersuchen und abmildern. Darüber hinaus werden spezifische Inspektionsaufgaben implementiert werden.

## Referenzen

[1] Smarsly, K., Law, K. H., & König, M., 2011. Autonomous structural condition monitoring based on dynamic code migration and cooperative information processing in wireless sensor networks. In: Proceedings of the 8th International Workshop on Structural Health Monitoring 2011. Stanford, CA, USA, 09/13/2011.

[2] Smarsly, K. & Dragos, K., 2024. Advancing civil infrastructure assessment through robotic fleets. Internet of Things and Cyber-Physical Systems, 4(2024), S. 138-140.

[3] Smarsly, K., Dragos, K., Stührenberg, J., & Worm, M., 2023. Mobile structural health monitoring based on legged robots . Infrastructures, 8(9), 136.

[4] Halder, S. & Afsari, K., 2023. Robots in inspection and monitoring of buildings and infrastructure: A systematic review. Applied Sciences, 13(4), 2304.

[5] Wellhausen, L. & Hutter, M., 2022. Artplanner: Robust legged robot navigation in the field. Field Robotics, 3(1), S. 413-434, 2023.

[6] Hess, W., Kohler, D., Rapp, H., & Andor, D., 2016. Real-time loop closure in 2D lidar slam. In: Proceedings of the 2016 Int. Conf. on Robotics and Automation. Stockholm, Schweden, 5/16/2016.

[7] Sucan, I. A., Moll, M., & Kavraki, L. E., 2012. The open motion planning library. IEEE Robotics & Automation Magazine 19(4), S. 72-82.

[8] Rösmann, C., Feiten, W., Wösch, T., Hoffmann, F., & Bertram, T., 2012. Trajectory modification considering dynamic constraints of autonomous robots. In: Proceedings of ROBOTIK 2012; 7th German Conference on Robotics. München, Deutschland, 5/21/2012.

[9] Bohren, J. & Cousins, S., 2010. The smach high-level executive. IEEE Robotics & Automation Magazine, 17(4), S. 18-20.

[10] Johann, S., Stührenberg, J., Tandon, A., Dragos, K., Bartholmai, M., Strangfeld, C., & Smarsly, K., 2024. Implementation and validation of robot-enabled embedded sensors for structural health monitoring. In: Proceedings of the 11th European Workshop on Structural Health Monitoring. Potsdam, 06/10/2024.

# Teil III

# Building Information Modeling

# Enhancing Compliance and Efficiency in Infrastructure Projects through Smart Standards

Sven Zentgraf[1], Susanne Wienholz[2], Sherief Ali[1], Andreas Bach[2], Iris Hindersmann[3] and Jennifer Bednorz[3]

[1]Chair of Computing in Engineering, Ruhr-Universität Bochum, Universitätsstraße 150, 44801 Bochum, Germany

[2]Schüßler-Plan Digital GmbH, Grafenberger Allee 293, 40237 Düsseldorf, Deutschland

[3]Bundesanstalt für Straßenwesen (BASt) , Brüderstraße 53, 51427 Bergisch Gladbach, Deutschland

E-mail(s): sven.zentgraf@ruhr-uni-bochum.de, SWienholz@schuessler-plan.digital, sherief.ali@ruhr-uni-bochum.de, abach@schuessler-plan.digital, hindersmann@bast.de, bednorz@bast.de

**Abstract:** The BIM master plan aims to achieve comprehensive implementation of BIM technology in federal road construction by 2025. This technology is already being used extensively in the planning phase, supported by integrating digital models created and exchanged by existing standards and guidelines. Rule-based, semi-automated test procedures ensure model quality and compliance with regulations. However, one drawback is that the necessary information is usually only available in non-machine-readable continuous texts and illustrations. An essential part of the project is therefore the conversion of traditional regulations into Smart Standards, which are serialized as XML documents according to the NISO STS to optimize their management and the provision of the contained information. In preparation, the suitability of existing regulations was analyzed and ten regulations were transferred to the NISO STS, considering the current version of the federal road construction object catalog. Furthermore, a concept for the description of information requirements and checking rules in the regulations was developed. The converted Smart Standards are integrated into the checking systems and the checking rules entered are tested on a model. Finally, recommendations for the management and administration of the Smart Standards were formulated.

*Keywords:* Building information modeling (BIM), design automation, algorithms, energy simulation

Erschienen in Tagungsband 35. Forum Bauinformatik 2024, Hamburg, Deutschland, DOI: 10.15480/882.13537
© 2024 Das Copyright für diesen Beitrag liegt bei den Autoren. Verwendung erlaubt unter Creative Commons Lizenz Namensnennung 4.0 International.

## 1 Introduction

Building Information Modeling (BIM) is a collaborative working method in the construction industry that accompanies and supports the increasing digitization in planning, construction, and operation. BIM models can contain geometric information, alphanumeric information, and documentation. They can be used for planning control, construction process simulation, quantity and cost estimation, and many

other applications [1]. In a BIM-based project, each discipline, such as structural engineering, creates a discipline-specific model corresponding to their work. These models vary in content depending on the intended purpose and the project phase. The individual discipline models are integrated into a coordination model, at designated times This integration enables interdisciplinary collaboration, coordination, and review. This step ensures that the content of the models is as error-free as possible both, individually and in the shared context [2].

The successful implementation of BIM in the federal highway construction sector relies on the continuous development and maintenance of exchange formats and software programs. This enables organizations such as the Autobahn GmbH, the DEGES, and state road construction administrations to utilize BIM in multiple projects [3]. However, implementing such projects is not solely dependent on technical aspects. Adherence to existing standards, regulations, and guidelines is also a crucial factor. These requirements, which are typically available in printed or digital formats such as PDFs, serve as the foundation for the planning and execution of construction projects. Integrating these non-machine-readable requirements into the various BIM processes is a time-consuming and error-prone challenge [4].

This research aims to develop a procedure for the creation, management, and application of so-called Smart Standards for federal highway construction. The National Information Standards Organization (NISO) Standard Tag Suite (NISO STS) will be utilized for this purpose. NISO STS provides an XML-based data format for the comprehensive description of standards, norms, and regulations. [5] This will facilitate the accessibility of regulatory requirements in a machine-readable format, thereby enabling their integration into verification tools or modeling instruments. In the long term, this should result in increasing compliance with regulatory requirements during the creation and implementation of planning models, as well as facilitating the conformity check of models, for example, within building permit reviews. To prepare for the conversion, the existing regulations are analyzed to ascertain their suitability. Ten regulations are then transferred into NISO STS, taking into account the current version of the Federal Highway Construction Object Catalog. Furthermore, a conceptual schema for delineating information requirements and validation rules within the regulations is devised. The implemented Smart Standards were integrated into a verification system, and the entered verification rules were tested on a model. Finally, procedures for managing and administering Smart Standards, that address technical and organizational issues, were presented.

## 2 Background

This chapter provides an overview of the relevant research and concepts for this study. It specifically addresses verifying information requirements and validation rules concerning building models and the concept of Smart Standards.

The BIM methodology allows that digital models are consistently utilized throughout the entire lifecycle of the modeled structure. When creating such a 3D model, numerous guidelines from modeling standards and regulations are typically considered and integrated into the building model [1]. With the help of quality assurance measures, such as geometric collision checks and the verification of semantic conditions, the correctness of the model data can be guaranteed. This involves developing examinations that first perform a formal check of information requirements and then conduct a technical

rule check to ensure accurate representation and modeling of building elements [6]. Based on the work of Nuyts, Bonduel, and Verstraeten [7], these two types of checks can be further specified and divided. The formal validation first checks for the presence of all relevant attributes of an object, and then ensures that the specified values meet the specified requirements. (e.g., data type, unit, and value range). The following technical rule check is divided into checking relational dependencies, mathematical formulas, and conditional constraints [7].

The technical implementation of model checking can be realized using different checking and query languages separable in IFC-based, open data, and semantic web approaches [7]. IFC-based approaches focus on technologies like MVD [8] and IDS [9]. The open data approaches focus on more generalized technologies like the XML-Schema Definition (XSD) and the Extensible Stylesheet Language Transformation (XSLT) to validate the correctness of model data. Within semantic web approaches ontologies like the ISOProps Ontologies [10] are used together with SPARQL [11] and SHACL [12] to validate the contents of a building model. A more detailed overview of rule languages and their use, is given by Nuyts, Bonduel, and Verstraeten [7], Stepien, Vonthron, and König [6] and Tomczak, Berlo, Krijnen, *et al.* [1].

In the construction industry, regulations are an important tool for defining legally binding requirements for the design and execution of construction projects. The growing number of text-based standards makes compliance difficult, as the required specifications must be manually extracted and prepared for digital use. [1] In addition, current information exchange is often limited to specific data catalogs, which hinders cross-domain collaboration and increases workload. To address these limitations, the Initiative Digital Standards (IDiS) of DIN e.V. focuses on creating digital standards that are accessible and usable by both humans and machines. To achieve this, specific action plans have been developed that outline the necessary steps to ensure that standards are mature, readable, implementable, and interpretable. This process outlines five distinct levels of autonomy in the way standards are created and used, leading to the development of Smart Standards [4].

The levels of autonomy range from paper format (Level 0) and digital documents (Level 1) to machine-readable documents (Level 2) where the structure and granular contents can be extracted. This progresses to machine-readable contents with identifiable information units and their relationships (Level 3), machine-interpretable contents linked with execution and application data (Level 4), and finally, machine-controllable contents that can be autonomously adjusted and published by automated processes (Level 5). To effectively implement the rules for automated compliance checking of Building Information Models, Level 3 or higher digital standards are required. This means that the standards must be mature enough to be interpreted and applied by humans and machines. In this work, the standards considered are first converted into Level 2 documents and then extended to Level 4.

## 3 Initial Review of Road Construction Regulations

This chapter focuses on the preliminary investigations conducted on road construction regulations to identify which ten regulations are most suitable for conversion into smart standards at Autonomy Level 2 in terms of effort and benefit, and which two are chosen to be implemented as Level 4 standards in the scope of this paper. For this purpose, the first step was to define metrics for the cost-benefit assessment.

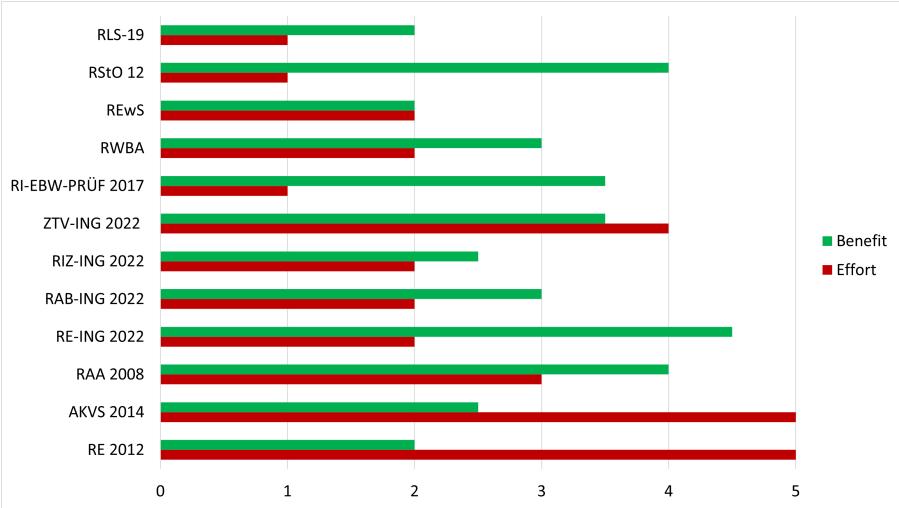


Figure 1: Result of the cost/benefit assessment

The criteria for estimating the effort required to convert road construction regulations into the NISO STS format include several key factors. First, the scope of the regulations is analyzed, considering the length and volume of texts, tables, illustrations, charts, and forms within the documents. The total number of pages serves as an initial indicator of the content to be converted, with larger volumes requiring more time and resources. Second, the complexity of the text structure plays a crucial role in the conversion process. Third, the presence and complexity of tables and figures within the regulations significantly impact the conversion effort. Complex tables and detailed illustrations require precise handling to ensure an accurate transfer and to avoid errors. Lastly, the informational content within figures and forms must be assessed. It is essential to differentiate whether these elements contain critical information or serve merely as supplementary aids for human understanding.
The following benefit assessment of the regulations involves evaluating two main criteria on a scale from one to five. The first criterion is the practical market relevance and frequency of use, where regulations frequently applied and highly relevant to everyday work processes receive higher ratings. The second criterion is the derivability of checking rules, which includes the potential for automating validation processes and simplifying workflows through transforming regulations. This criterion depends on the structure and clarity of the regulation, as only clearly formulated and verifiable contents can be automated.

After completing the effort and benefit assessment, the results were summarized by contrasting the effort required to digitize each regulation (Figure 1 red lines) with the benefit of having the regulation available in digital form (Figure 1 green lines). Based on the effort and benefit assessments, ten regulations were selected for conversion into NISO STS documents with autonomy Level 2. Additionally, the RE-ING and the RStO are chosen for the enrichment to autonomy Level 4 due to their good benefit-to-effort ratio.

# 4 Creation of Digital Standards

Creating a digital standard at Autonomy Level 2 involves converting text-based regulations, such as PDF and Word documents, into a format that is readable and processable by both humans and machines. The NISO STS standard, used for this purpose, offers extensive capabilities for structuring documents in XML. The conversion begins with selecting the appropriate XML version and integrating the necessary Document Type Definitions (DTD) and an optional stylesheet for later formatting. Subsequently, the title page is described separately from the document body. In the next step, the text body structures, like text, illustrations, tables, charts, forms, and formulas, are converted into XML following NISO STS guidelines. A detailed technical description of this conversion process is beyond the scope of this paper instead, the technical documentation of NISO STS is referenced. [4].

The created digital standard is enriched with information requirements and validation rules to create a Level 4 standard. For clarity, the terms *information requirements* and *validation rule* are collectively referred to as *information elements* below. The integration of information elements is done through *term sections*, which are defined at the end of each text-bearing section. A *section type* attribute distinguishes whether the section contains information requirements or validation rules. The information elements mentioned for the first time in the relevant section are listed in each of these sections.

The *term section* for information requirements contains *term entries*, which describe terms and concepts found in information elements. Each entry in a *term section* is assigned a globally unique ID (GUID) generated according to RFC 4122 standards. After specifying the ID, an *index term*, containing *term* element, indicates whether the defined information requirement is a property or a property group. Within a *language set* element, the language of the information element can be defined and additional details can be provided within a *definition* element. *TIG (Term Information Group)* elements allow for various descriptions, such as a preferred term, an accepted synonym (*admittedTerm*), acronyms, and a name for digital processing.

Similar to the approach for information requirements, the validation rule is organized within an XML structure to define and manage the rules and their associated information elements. Each validation rule is identified by a globally unique identifier (GUID). The main definition of the validation rule resides within the *term entry*, where it is specified as a validation rule using a *term* element. An additional *source* element may reference an external file, such as an IDS file, which contains the implemented validation rule. The rest of the definition follows the structure used for information requirements.

In addition, the concept of validation rules includes multiple lists, for example, one list defines the conditions for the validation rule, while another list defines the objects to be included in the validation. This concept can be extended by further lists if necessary. The standardization body should prescribe the allowed values for the *list-type* attribute ensuring uniform naming conventions across different working groups. The elements for *code* and *formulas* can provide detailed information on the implementation and necessary parameters. The *code* element allows pseudocode or fully developed code in a programming language, which is useful when validation rules are not delivered as ready-to-implement components with the standard document. The *formula* element is used to include mathematical formulas written in Mathematical Markup Language (MathML), illustrating essential calculations or

Figure 2: Developed Desite BIM Plugin and the tested BIM Model

logic of the validation rule. The definition of the validation rule is concluded with an optional *paragraph* element, which provides a comprehensive explanation for enhancing human understanding.

## 5 Evaluation

To verify the applicability and machine processability of the concept presented in section 4, a plugin for DESITE BIM was developed. DESITE BIM[1] is a BIM software solution from thinkproject that serves as a coordination platform used during planning, execution, and facility management. It enables project-related BIM applications by visualizing, analyzing, checking, and linking model data, supporting various functions such as model and collision checks, schedule creation through 4D simulations, and quantity take-offs. The result of the development and an example bridge model are shown in Figure 2.

The first step in checking the validation requirements of the selected regulation is to read the prepared, machine-interpretable validation rules. Therefore the loaded standard is scanned for term sections containing information elements.
The extracted term sections can then be searched for additional tags to retrieve overarching information, such as the name or definition of the validation rule. Once the basic data is captured, the lists, code, and source elements can be accessed for validation requirements.
In the example shown in Figure 2, a checking rule was loaded to validate the clearance height under the newly designed bridge. The formal check first verifies whether the model contains all objects and attributes required for the subsequent technical validation, and that the attributes are valid in terms of data type, characteristics, and value ranges. The succeeding technical validation uses the previously checked objects and attributes to check that the requirements specified in the check rules are also met. The illustrated example checks whether the modeled clearance profiles (yellow boxes in Figure 2) have a minimum height of 4.70 m and whether they interfere with the planned bridge at any point. There are no collisions present in the shown example, there the check is successful.
The evaluation shows that using digital standards facilitates the extraction and preparation of constraints and creates an improved basis for integrating and using such constraints in common software

[1] https://www.thinkproject.com/de/products/vdc-manager/

products. The use of digital standards contributes to increased efficiency and harmonization in the areas of standardization, testing, and rule management. However, the process of creating such digital standards is currently relatively labor-intensive. For continuous use, methods need to be developed to partially or fully automate the conversion to XML-based standards and the integration of information requirements and test rules.

## 6 Conclusion

The BIM masterplan aims for comprehensive implementation in federal highway construction. BIM applications in road construction and civil engineering are carried out under existing standards and guidelines, with digital models being used for data exchange and quality assurance. These models enable both the implementation of specific use cases and general project evaluations, whereby the model quality and conformity with guidelines can be checked, in some cases automatically. Standards and regulations will be digitized in the future to enable more efficient testing processes like digital standards.

The present study evaluates digital standards in terms of their benefits and effort and examines the creation and management of digital regulations. Ten regulations were converted to Level 2 and two were extended additionally to Level 4, based on the autonomy levels of the Smart Standards initiative. The conversion process included the current object catalog of the German Federal Highway Administration. Methods for describing and integrating information requirements and validation rules in digital standards were developed. The applicability of the developed concept was demonstrated using a self-implemented plugin for DESITE BIM.

The results of this study highlight the benefits of digital regulations combined with model checks and advocate for the digitization of analog regulations. However, several key points must be addressed to enable the widespread use of digital standards. Firstly, software solutions must be developed to create and manage standards that directly generate NISO STS-compliant documents. While existing solutions are available on the market, their practical suitability still needs to be assessed. In addition to technical adjustments, the approach to developing standards should be revised. This includes ensuring that requirements are explicitly formulated during the creation or versioning of regulations to facilitate the generation of information requirements and validation rules. Furthermore, images and illustrations in regulations should only be used as supplementary elements to aid human understanding, as automated processes struggle to extract explicit knowledge that is not textually depicted.

In conclusion, it is important to note that the digitization of regulations as digital standards provides significant opportunities to streamline the use of standards, thereby enhancing compliance in planning, construction, and implementation processes.

## Acknowledgments

This paper is based on parts of the research project carried out at the request of the Federal Ministry For Digital and Transport and its Network of Experts “Knowledge - Ability - Action”, represented by the Federal Highway Research Institute, under research project FE-No. 02.0463/2022/ARB. The authors are solely responsible for the content. We would like to thank the members of our project’s advisory board for their useful advice and feedback.

## References

[1] A. Tomczak, L. v. Berlo, T. Krijnen, A. Borrmann, and M. Bolpagni, “A review of methods to specify information requirements in digital construction projects”, *IOP Conference Series: Earth and Environmental Science*, vol. 1101, no. 9, p. 092 024, 2022. DOI: 10.1088/1755-1315/1101/9/092024.

[2] A. Borrmann, *Building Information Modeling: Technologische Grundlagen und Industrielle Praxis* (VDI-Buch Ser). Wiesbaden: Springer Fachmedien Wiesbaden GmbH, 2015.

[3] BMDV, *Masterplan für die Digitalisierung im Bundesfernstraßen-Bau*, 2.07.2024. [Online]. Available: https://bmdv.bund.de/DE/Themen/Digitales/Building-Information-Modeling/BIM-Fernstrassen/building-information-modeling.html.

[4] D. A. Czarny, J. Diemer, M. Schacht, *et al.*, *Scenarios for digitizing standardization and standards*. [Online]. Available: https://www.din.de/resource/blob/801106/0251eb1280a9a97e53285d42d3bf1fea/whitepaper-idis-en-data.pdf.

[5] NISO Standards Tag Suite Working Group, *ANSI/NISO Z39.102-2017, STS: Standards Tag Suite*, Baltimore, MD, 2017-06. DOI: 10.3789/ansi.niso.z39.102-2017.

[6] M. Stepien, A. Vonthron, and M. König, “OpenBIMRL – An open format for code compliance checking of complex functional requirements from a regulation to the BIM model”, in *Proceedings of 30th EG-ICE: International Conference on Intelligent Computing in Engineering*, European Group for Intelligent Computing in Engineering, editor, 2023.

[7] E. Nuyts, M. Bonduel, and R. Verstraeten, “Comparative analysis of approaches for automated compliance checking of construction data”, *Advanced Engineering Informatics*, vol. 60, p. 102 443, 2024. DOI: 10.1016/j.aei.2024.102443.

[8] buildingSMART Technical, *Model View Definitions (MVD) - buildingSMART Technical*, 17.10.2022. [Online]. Available: https://technical.buildingsmart.org/standards/ifc/mvd/.

[9] buildingSMART Technical, *Information Delivery Specification IDS - buildingSMART Technical*, 19.01.2024. [Online]. Available: https://technical.buildingsmart.org/projects/information-delivery-specification-ids/.

[10] L. Liu, P. Hagedorn, S. Zentgraf, M. König, M. Mellenthin-Fillardo, and J. Melzner, “A standard-based ontology network for information requirements in digital construction projects”, in *LDAC2024 - Linked Data in Architecture and Construction*, 2024.

[11] E. Prud’hommeaux and A. Seaborne, *SPARQL Query Language for RDF*, 9.10.2018. [Online]. Available: https://www.w3.org/TR/rdf-sparql-query/.

[12] H. Knublauch and D. Kontokostas, *Shapes Constraint Language (SHACL)*, 31.01.2018. [Online]. Available: https://www.w3.org/TR/shacl/.

# Deriving Fabrication Information from BIM for Automated Robotic Task Planning

Maikel Jean Silvo Brinkhoff[1] and Mohammad Reza Kolani[1]
[1]Chair of Computational Modeling and Simulation, Technical University of Munich, Arcisstraße 21, 80333 Munich, Germany
E-mail(s): maikel.brinkhoff@tum.de, mohammadreza.kolani@tum.de

**Abstract:** Construction robotics enables the integration of multiple technologies (e.g., Building Information Modelling, Artificial Intelligence and Additive Manufacturing), thus presenting an opportunity for further productivity gains for the construction industry. However, a key obstacle lies in generating fine-grained information required for robots to plan autonomous tasks. To achieve reliable robot-based construction automation, information about the product design to be built and the status of construction progress must be available to the robot systems in real time. Building Information Modeling (BIM) holds promise in converting high-level building information into the requisite level of detail for robotic operations. One approach is to enrich the data from Industry Foundation Classes (IFC) models with construction data and convert it into a robotic format for robot task planning. We propose leveraging and extending the data extracted from BIM models to integrate with Robotic Operating Systems (ROS), a prevalent framework for robot control. The framework is evaluated through robotised bricklaying realised by *MoveIt*, and visualised using *Rviz*.
*Keywords:* Building Information Modeling (BIM), Construction Robotics, Construction Simulation, Task Planning

Erschienen in Tagungsband 35. Forum Bauinformatik 2024, Hamburg, Deutschland, DOI: 10.15480/882.13543
© 2024 Das Copyright für diesen Beitrag liegt bei den Autoren. Verwendung erlaubt unter Creative Commons Lizenz Namensnennung 4.0 International.

## 1 Introduction

The Architecture Engineering and Construction (AEC) industry seeks to enhance efficiency and productivity by adopting Industry 4.0 concepts and technologies [1]. Various technologies, including data analytics, artificial intelligence, Building Information Modeling (BIM), digital twins, and (autonomous) robotics, are increasingly used during the preparation phase or off-site operations [2]. Robotics, in particular, have the distinct capability to integrate and harness these technologies on-site.

One of the prerequisites for robotics operation is providing detailed task information. Typically, robots are programmed with specific movements and actions in controlled environments like factories. This approach demands significant effort, and the tasks and their sequence are often non-reusable due to the unique and dynamic nature of construction projects. On-site operations thus cannot rely only on a predefined set of task instructions. Much attention, therefore, is paid to developing methods for

autonomous, even adaptable [3], task-planning. BIM models are becoming increasingly commonplace in practice, and the information contained within these files provides a valuable source from which the robotic operations can be derived.

The information captured in BIM is of a higher degree of abstraction. A building and its components are described as 'concrete wall, beam, column,' which is sufficient information for human labourers to perform their tasks. A robot, on the other hand, is (as of yet) unable to reason about the necessary sequence of operations for building a 'construction element.' This results in a gap between the provided information and the detailed information a robot requires. The level of detail needed also varies based on the type of robotic system (gantry, arm), construction element (wall, floor, column), and construction method (precast, in-situ, additive manufacturing). The effort to create such operational information makes it impractical for designers and engineers to manually include this level of detail in their projects. The focus of this work is therefore on converting high-level BIM information into fine-grained construction data to bridge this gap. This data is thereafter used to realise robotic task planning, exemplified by brick-laying for walls. While commercial brick-laying robots are available [4], our aim specifically targets data refinement, independent of a robot type.

Our workflow involves extracting data from IFC models to generate precise coordinates for brick placement forming overall wall structures. This process is achieved by using a BIM parsing tool for data access. The generated coordinates are based on the conversion of the wall into a boundary representation (BREP). These BREPs undergo various operations and arithmetic calculations informed by brick-laying heuristics to produce accurate brick placement coordinates. These coordinates are then transferred as inputs for the robotic motion planning, with each set of coordinates corresponding to unique actions that require their own inverse kinematics (IK) solutions to calculate movement trajectories. This method effectively translates high-level BIM data into precise construction information, enabling task planning for brick-laying scenarios. Several case studies have been conducted to test the validity and robustness of both coordinate generation and robotic motion-planning. The cases are differentiated by altering the wall's dimensions and construction method – dry-stacking or using a mortar bond.

An overview of the state-of-the-art for BIM-to-task is presented in 2. Following that, 3 addresses the data transformation from IFC to robotic task-planning. The case studies and their results are outlined in 4. The implications of the proposed procedure, as well as a conclusion and recommendations, are deliberated in 5 and 6, respectively.

## 2 Related Work

Building Information Modelling (BIM) is increasingly recognised and used in conjunction with robotics to derive task information. The information contained in the BIM file is used for tackling autonomous navigation [5], object detection [6], or to adjust a task plan based on detected material deviations [3]. Such applications target specific tasks but lack a holistic approach that includes both the tasks and the construction environment. Holistic robotic task planning requires simulation environments with detailed models of robots and assets. These environments enable safe testing, validation, and debugging of

algorithms and behaviours. Accurate construction site descriptions allow for visualisation and analysis of robotic processes before implementation.

The earliest example of such a holistic approach is by Kim et al. [7]. The authors use geometric BIM data and a predefined construction schedules for task planning, which in turn is used to generate robot motions. The construction site or objects, at least the relevant parts of it, need to be included in such holistic approaches. The researchers therefore take the geometric data, exported as an IFC schema, and convert this into a Simulation Definition Format (SDF) to set up a simulation in the Gazebo environment[1]. This step enables the authors to model the geometries in a robotic simulation environment, and accurately represent (a part of) the construction site. As the test-case is robotic painting, only walls are converted and modelled. The case study shows that the proposed method of using BIM for robot task planning can merge the fields of construction and robotics to effectively plan the operations of autonomous robots in construction projects.

Zhu et al. [8] take a different approach, where they derive the required construction information directly from the construction elements themselves. The researchers propose a method that enables task planning in a Multiple Robot Coordination (MRC) setting for prefabricated construction. IFC elements are enriched with construction status (e.g., InTransit) and required actions (e.g., NeedToTransfer) to form *Smart Construction Objects* (SCOs). The SCOs are able to communicate and update their status and requirements, which get published to the robots. Discrete Event Simulation (DES) is used to divide into the construction task in three sub-tasks (events): transport, positioning, and assembly, each assigned to a set of robots specifically suited for that task. The simulation results verified the method, and showed the benefit of using a multiple robots simultaneously.

Slepicka et al. [9] take a similar component-oriented approach for which they introduce the Fabrication Information Modelling (FIM) methodology. FIM is used to generate precise robotic execution instructions within the context of Additive Manufacturing (AM), leveraging both semantic and geometric BIM data. To ensure integration and avoid data conversion losses, the authors utilised the IFC data schema. Much like in 3D printing, an element is created by following a print path layer by layer. In similar fashion to Zhu et al. [8], the path planning process can be viewed as a discretised event within the broader task of "constructing a wall." The authors developed a software prototype that generates the print path from IFC data, which is then used by a custom script to produce the robot controls for printing a model-sized wall element.

The geometric representations and semantic information contained in BIM models provide a rich basis from which robotic operations can be derived. There are numerous formats in which BIM data can be expressed, of which the non-proprietary formats provide the most flexibility. The Industry Foundation Classes (IFC) format is most notable and prevalent, modelled on the EXPRESS modelling language. The IFC format is widely supported and accommodates various geometric representations of the same object, reflecting the diverse modelling approaches of different BIM authoring tools. IFC gets increasingly mapped onto other formats, such as the Resource Description Framework (RDF), XML, and JSON [10]. IFC and RDF follow a graph data model, whereas XML and JSON have a tree-like

[1] https://gazebosim.org

structure. Graphs differ from trees in that they provide the flexibility and expressiveness to model complex, interconnected relationships and facilitate advanced analyses. In contrast, trees offer a simpler and clearer structure for organising hierarchical data. Pauwels et al. [10] demonstrated that either data structure has the potential to enable autonomous robotic navigation.

## 3 Methodology

The workflow proposed in this work explores the conversion from high-level BIM objects into operational information suited for robotic task planning for brick walls. BIM objects and their geometric information are represented using IFC, from which target locations are generated for each brick. The targets serve as the input for the inverse kinematics (IK) solvers that finally realise the robotic movements and thus task planning. The complete methodology is presented in 2, and discussed in detail below.

The geometric information of the building elements captured in a particular building information modelling software can be stored in the IFC format. In this paper, Autodesk Revit, as one representative of BIM authoring tools, is used to generate walls and export the corresponding IFC models. To effectively process and manipulate the diverse representations that IFC accommodates, we utilise a dedicated software library that ensures robust interoperability and data handling. This library enables the parsing of IFC files and extracting and modifying necessary information. The data first needs to be preprocessed to extract relevant geometric features, after which arithmetic calculations informed by brick-laying heuristics are performed. Brick dimensions and the inclusion of a mortar gap, together with these heuristics, yield a set of coordinates to be used by the robot. The resulting set of coordinates then correspond exactly to the wall placement as modelled in the design environment.

The extracted coordinates are used to set up the robot task planning system in our simulation framework [11], which is based on the Robot Operating System (ROS)[2]. The bricklaying task consists of a sequence of actions, each corresponding to the placement of a single brick. The framework assigns an ID to each brick, and uses a task node to generate it as an entity in the scene with an initial pose (location). Upon successful placement, a new task for picking and placing a brick is added to the motion plan to generate the necessary actions for the new brick.

The framework's motion planning node receives these tasks with their IDs, divides the required motion into actions (e.g., open hand, move to pick, pick object) and sub-actions (e.g., allow collision, attach the brick to the gripper), and generates plans for the robot's gripper and arm for each stage. Arm manipulators may have multiple IK solutions per stage, achieving the same end-effector pose [12]. The simplest and fastest solution is preferred, but joint limits and collision avoidance may prevent this. We use MoveIt[3], a platform for motion planning and IK calculation, to compute the IK for every stage, providing possible and lowest-cost solutions. Optimal planning is beyond the scope of this paper and will be further investigated in future publications. This process, visualised using ROS visualisation (Rviz)[4], continues until the overarching task is complete and the wall is constructed.

[2] https://www.ros.org/
[3] https://moveit.ros.org/
[4] http://wiki.ros.org/rviz

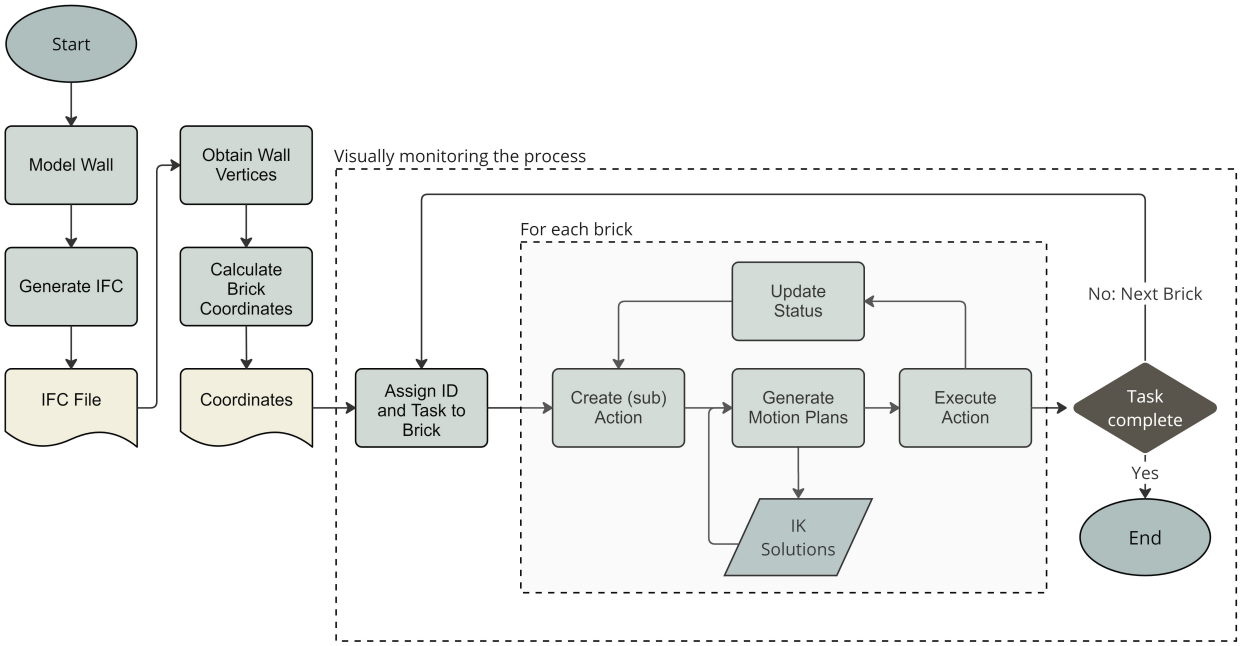


Figure 1: Flowchart of the robotic bricklaying process, from wall modelling to task execution.

## 4 Case Study

The workflow proposed in this work explores the conversion from high-level BIM objects into operational information suited for robotic task planning for brick walls. BIM objects and their geometric information are represented using IFC, from which target locations are generated for each brick. The targets serve as the input for the inverse kinematics (IK) solvers that finally realise the robotic movements and thus task planning. The complete methodology is presented in 2, and discussed in detail below.

The geometric information of the building elements captured in a particular building information modelling software can be stored in the IFC format. In this paper, Autodesk Revit, as one representative of BIM authoring tools, is used to generate walls and export the corresponding IFC models. To effectively process and manipulate the diverse representations that IFC accommodates, we utilise a dedicated software library that ensures robust interoperability and data handling. This library enables the parsing of IFC files and extracting and modifying necessary information. The data first needs to be preprocessed to extract relevant geometric features, after which arithmetic calculations informed by brick-laying heuristics are performed. Brick dimensions and the inclusion of a mortar gap, together with these heuristics, yield a set of coordinates to be used by the robot. The resulting set of coordinates then correspond exactly to the wall placement as modelled in the design environment.

The extracted coordinates are used to set up the robot task planning system in our simulation framework [11], which is based on the Robot Operating System (ROS)[5]. The bricklaying task consists of a sequence of actions, each corresponding to the placement of a single brick. The framework assigns an ID to each brick, and uses a task node to generate it as an entity in the scene with an initial

[5]https://www.ros.org/

pose (location). Upon successful placement, a new task for picking and placing a brick is added to the motion plan to generate the necessary actions for the new brick.

The framework's motion planning node receives these tasks with their IDs, divides the required motion into actions (e.g., open hand, move to pick, pick object) and sub-actions (e.g., allow collision, attach the brick to the gripper), and generates plans for the robot's gripper and arm for each stage. Arm manipulators may have multiple IK solutions per stage, achieving the same end-effector pose [12]. The simplest and fastest solution is preferred, but joint limits and collision avoidance may prevent this. We use MoveIt[6], a platform for motion planning and IK calculation, to compute the IK for every stage, providing possible and lowest-cost solutions. Optimal planning is beyond the scope of this paper and will be further investigated in future publications. This process, visualised using ROS visualisation (Rviz)[7], continues until the overarching task is complete and the wall is constructed.

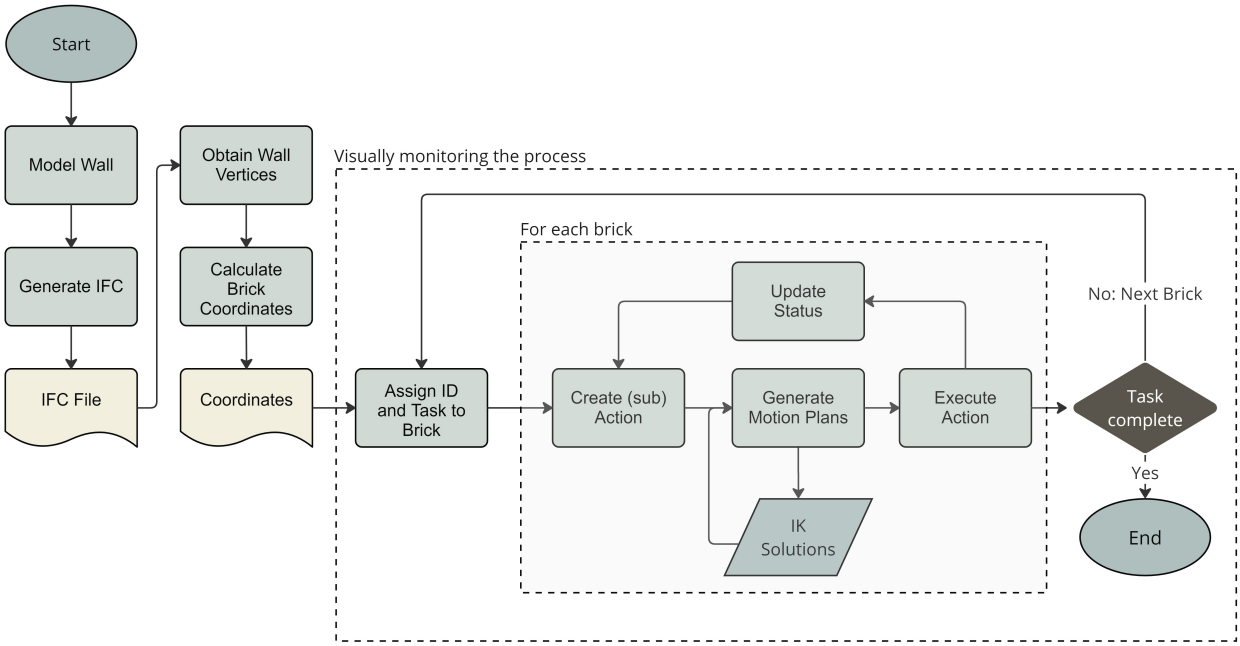


Figure 2: Flowchart of the robotic bricklaying process, from wall modelling to task execution.

## 5 Discussion

The proposed workflow generates fine-grained instructions from high-level BIM data for brick-laying. By taking the available geometric information from BIM files and fashioning a method tailored to the construction material and technique, this approach shows promise for further automation. The experiments indicate robustness and scalability in this construction method's coordinate generation and consequential task planning parts. While currently designed for brick-laying, this workflow can be extended for other construction methods and materials, such as 3D concrete printing. This extension would require generating different types of information suited to those specific methods, materials and robotic systems.

[6]https://moveit.ros.org/
[7]http://wiki.ros.org/rviz

There are several limitations still that require further development of the workflow. In the overall data flow, every conversion step from IFC to task planning requires manual effort. Using different data models, for example, graphs combined with queries, can link various data formats and streamline the process to a certain degree. More specific to the brick-laying case, details like cornerstones and cases with adjacent walls are to be included. For a more realistic simulation scenario, bricks should be placed in a material stockpile rather than spawned at a single location. In addition, the simulation revealed a practical limitation regarding the construction size; we could construct up to six rows before the inverse kinematic solutions became unfeasible without colliding with already placed bricks. This emphasises the need for incorporating robotic systems with diverse characteristics, like maximum reach, or that can cooperate to jointly overcome such challenges.

## 6 Conclusion and Future Work

This study showcases a workflow that effectively leverages the data contained in BIM files for robotised construction activities. The simulation framework utilises this enriched data for the robot's task planning system, successfully demonstrated in several case studies for robotic bricklaying. By leveraging advanced technologies such as ROS, MoveIt for motion planning and inverse kinematics calculations, and Rviz for visualisation, the framework offers a versatile platform for planning, simulating, and executing complex tasks with arm manipulators in a construction environment. Further development, including various construction methods, materials, and robotic systems, enables the generation of detailed operational information, making it possible to embed this level of detail into construction projects.

In the future, we plan to use different data models capable of capturing and linking various data representations without requiring numerous conversion steps. Specifically, we will investigate using a linked building data approach to link construction elements with the generated construction information. Analogous to that step is the incorporation of different arm manipulators and construction methods.

## Acknowledgements

The research presented in this paper has received funding from the Deutsche Forschungsgemeinschaft as part of Research Unit 5672, "Digital Backbone of Robotized Construction", in project no 517965147. In addition, the authors thank the TUM Innovation Network "CoConstruct."

## References

[1] A. Hossain and A. Nadeem, "Towards Digitizing the Construction Industry: State of the Art of Construction 4.0", *Proceedings of the ISEC*, vol. 10, 2019. DOI: 10.14455/ISEC.res.2019.184.

[2] J. M. Davila Delgado, L. Oyedele, A. Ajayi, *et al.*, "Robotics and automated systems in construction: Understanding industry-specific challenges for adoption", *Journal of Building Engineering*, vol. 26, p. 100 868, Nov. 2019. DOI: 10.1016/j.jobe.2019.100868.

[3] K. M. Lundeen, V. R. Kamat, C. C. Menassa, and W. McGee, "Autonomous motion planning and task execution in geometrically adaptive robotized construction work", *Automation in Construction*, vol. 100, pp. 24–45, Apr. 2019. DOI: 10.1016/j.autcon.2018.12.020.

[4] R. Dindorf and P. Wos, “Challenges of robotic technology in sustainable construction practice”, *Sustainability 2024, Vol. 16, Page 5500*, vol. 16, p. 5500, 13 2024. DOI: 10.3390/SU16135500.

[5] B. Xiao, C. Chen, and X. Yin, “Recent advancements of robotics in construction”, *Automation in Construction*, vol. 144, p. 104 591, 2022. DOI: 10.1016/j.autcon.2022.104591.

[6] M. Dawod and S. Hanna, “BIM-assisted object recognition for the on-site autonomous robotic assembly of discrete structures”, *Construction Robotics 2019 3:1*, vol. 3, no. 1, pp. 69–81, Aug. 2019. DOI: 10.1007/S41693-019-00021-9.

[7] S. Kim, M. Peavy, P.-C. Huang, and K. Kim, “Development of bim-integrated construction robot task planning and simulation system”, *Automation in Construction*, vol. 127, p. 103 720, 2021. DOI: 10.1016/j.autcon.2021.103720.

[8] A. Zhu, P. Pauwels, and B. De Vries, “Smart component-oriented method of construction robot coordination for prefabricated housing”, *Automation in Construction*, vol. 129, p. 103 778, 2021. DOI: 10.1016/j.autcon.2021.103778.

[9] M. Slepicka, S. Vilgertshofer, and A. Borrmann, “Fabrication information modeling: Interfacing building information modeling with digital fabrication”, *Construction Robotics*, vol. 6, no. 2, pp. 87–99, 2022. DOI: 10.1007/s41693-022-00075-2.

[10] P. Pauwels, R. de Koning, B. Hendrikx, and E. Torta, “Live semantic data from building digital twins for robot navigation: Overview of data transfer methods”, *Advanced Engineering Informatics*, vol. 56, p. 101 959, 2023. DOI: 10.1016/j.aei.2023.101959.

[11] M. R. Kolani, S. Nousias, and A. Borrmann, “Coordinating robotized construction using advanced robotic simulation: The case of collaborative brick wall assembly”, 2024. DOI: 10.48550/arXiv.2405.17171.

[12] M. Spong, S. Hutchinson, and M. Vidyasagar, *Robot modeling and control*. John Wiley & Sons, Ltd, 2020.

# A framework for using heterogenous data from digital building permits in urban mining

Marcel Heiß[1] and Timo Bittner [2]

[1] Institute of Numerical Methods and Informatics in Civil Engineering, Technical University of Darmstadt, Franziska-Braun-Str. 7, 64287 Darmstadt, Germany

[2] City of Darmstadt, Darmstadt, Germany

E-Mails: heiss@iib.tu-darmstadt.de

**Abstract:** Previous approaches to material inventories of buildings require complex surveys, complicated estimations or BIM models. The concept presented explores the use of the digital transformation of building permit in Germany to create a data collection layer for urban mining. By analysing certain aspects of building permits in Germany and using digital methods, relevant data can be extracted. Different forms of future building permits and their characteristics are defined and analysed in order to select specific digital methods such as artificial intelligence. A comparison of the different forms shows that the necessary data can be extracted from simple digitised documents and further developments of the building permit offering more potential in terms of reliability and accuracy.

*Keywords:* Urban Mining, Digital Building Permitting (DBP), Building Information Modeling (BIM)

Erschienen in Tagungsband 35. Forum Bauinformatik 2024, Hamburg, Deutschland, DOI: 10.15480/882.13528
© 2024 Das Copyright für diesen Beitrag liegt bei den Autoren. Verwendung erlaubt unter Creative Commons Lizenz Namensnennung 4.0 International.

## 1 Introduction

The built environment is society's largest resource stock and a major contributor to energy and resource demand. By reducing its high consumption, the construction sector offers considerable potential to achieve climate neutrality in Europe by 2050. Here, the recovery and reuse of building resources and components as well as their integration into a circular economy provides a significant opportunity [1]. The introduction of such concepts into the planning process of urban districts requires the coordination of material flows. This entails comprehensive knowledge of the materials in the built environment as an initial information basis for urban mining concepts. However, corresponding data is rarely available at the district level. Existing approaches require complex building surveys, costly estimations or BIM models to solve this problem. At the same time, the digital transformation is also gaining ground in many areas in Germany and machine-readable data is increasingly being generated. In the public sector, the Online Access Act facilitates digitising processes by offering administrative services electronically using digital forms and file exchange platforms. Likewise, the transition from paper-based handovers to digital exchanges also opens up opportunities to prevent data and

information disruptions and thus enables development of new technologies. An example of this is the implementation of digital building permits and the information about the built environment associated with it. The approach presented in this work explores the use of the digital transformation of building permits in Germany to create a data collection layer for urban mining. For this purpose, relevant documents, which often implicitly contain information about the building resource inventory, are analysed. Current developments for the digital transformation of building permits and material inventories of buildings are presented. Based on this, different forms of potential future digital building permits are defined incorporated into a framework for extracting and evaluating the necessary data. The framework features different pipelines for processing non-machine-readable documents with methods from the field of computer vision and artificial intelligence (AI). The integration of future machine-readable formats is then explored to collect resource data without the need for complex information extraction methods. Additionally, the use of a BIM-based building permit is examined. The results of building material inventories are evaluated regarding their use for urban mining.

## 2 Related Work and Analysis

### 2.1 Digital transformation of building permit

The use case of Digital Building Permitting (DBP) is of growing interest with the level of development varying widely in different countries around the world. It can be summarised into four distinct levels of permitting based on different degrees of automation and integration [2]. These include traditional paper-based permitting practices, electronic 2D digital data-based permitting, automated digital BIM-based permitting, and a fully automated Geo Information System (GIS)-integrated level. One of the drivers for this development are the increasing requirements for newer buildings, resulting in more extensive inspections as well as increases in workload and time to approval. The primary aim of DBP is to automate processes, thereby reducing the manual workload of the approval procedure. The electronic, 2D digital data-based permit provides a central platform for communication and data exchange, but the PDF documents submitted are often analysed manually. For this reason, most research, such as the EuroSDR GeoBIM project, suggests a high-level harmonised workflow envisaging the use of GeoBIM information to automate the building permit process [3]. The EU-funded research project BRISE [4] is examining the use of BIM and AI, particularly Natural Language Processing (NLP), in the building permit process in Vienna, Austria. In Germany electronic, 2D digital data-based permits are currently being introduced in several projects at the state level, e.g. [5]. Further research [6] includes a concept for the integration of BIM in the building permit procedure. However, the current situation in practice is different. Not all building projects are planned using BIM and are therefore not eligible for BIM-based permitting without additional work. Processes that are not BIM-based but employ digital tools and methods are therefore still valuable for handling of building permit data. There are several examples for the value of reusing and analysing this data, such as study of land development [7]. This reflects the importance and wide range of possibilities of accessible information derived from DBP.

## 2.2 Material inventory of buildings

One of the biggest challenges for society is containing the climate crisis. In order to reduce the environmental impact of the construction industry, the introduction of a circular economy offers considerable potential for savings [1]. The material inventory of individual buildings and their GIS-based representation at city level through material cadastres is necessary for the development of a knowledge-based decision-making platform. However, there is still a lack of tools that allow automated access to the data to create such inventories in form of so-called building material passports (BMP). There are several approaches that use BIM models for initial information. The research project BIMaterial [8] developed a methodology for the semi-automatic creation of a BMP by linking BIM and eco-databases. The research project BIMstocks [9] aimed to digitally record the material composition by mapping on-site recordings such as laser scans, surveys and photo documentation onto BIM models. These approaches are only applicable to buildings with a BIM model, which is not the case for most existing buildings. While BIM models tend to contain geometric information for specific components as well as superficial material names, such a database provides more in-depth properties. To improve the reliability of the process and avoid blind mapping, additional surveys and recordings are required, which need to be automatically interpreted to avoid manual intervention. One approach is using a machine learning algorithm for automated material recognition [9]. Other possibilities include automatic classification of common building materials from 3D terrestrial laser scan data [10], which is limited because only the visible layer can be estimated. On-site recording could also include laser scanning, which allows the derivation of point clouds and automated reconstruction of BIM models [11]. However, this is very time-consuming and costly, and therefore not a tool for area-wide digital capture of urban mining data. Another option is to analyse existing construction documents. While the automated analysis of plans, so called Plan2BIM approaches like CubiCasa5K [12], and further automated BIM reconstruction are well researched, the extraction of additional material data is often out of scope. When dealing with heterogeneous construction documents, the use of NLP has been proven in the application of document classification and organisation [10] and is increasingly finding its way into the processing of unstructured text data for cost estimation [13].

## 2.3 Building permit forms

In many countries, building permit information is still handled in paper-based formats or, at best, in PDF documents. Moreover, in practice, the data involved is very heterogeneous and often relatively informal. Previous research in DBP has focused strongly on the use of BIM and its Industry Foundation Classes (IFC) format in digital permits while their use is not sufficiently established. Other specific data exchange formats are rarely considered in the context of DBP. The suggested approach aims to close the research gap between digital document-based and BIM-based by introducing an additional variant of DBP. A framework for urban mining is developed using different forms of DBP, leveraging them as a data source for digital urban twins [14] and corresponding knowledge-based decision-making platforms. The concept is based on a step-by-step model for the digital transformation of the building permit. The lowest level is the analogue, paper-based approach, which is still

the most widely used in Germany and includes paper forms, documents and 2D plans. This is being replaced by the digital building permit, which often includes the same information sources in digital form submitted via an online platform, but mostly as non-machine-readable PDF documents. Little machine-readable data is captured by web forms. The intermediate step, the so-called Digital+ permit, represents a shift as most of the data is captured via machine-readable formats and files that are well-established and used in practice. The highest level of DBP+ focuses on the data provided by a BIM model in IFC format. The BIM model can replace other previous documents such as plans, as the information contained in the plans can be found in the model. The analysis of other construction documents and further semantic enrichment of BIM models is rarely researched. The work presented focuses on digital document-based, digital data-based and digital BIM-based versions as well as the enhancement of information using a developed “PerDoc2Data” framework.

# 3 Methodology

## 3.1 Material inventory processes and elements

The approach taken for the comprehensive material inventory of buildings based on DBP is a bottom-up approach. In contrast to the top-down concept commonly used, it describes the existing stock in detail and extrapolates the total quantity from these partial quantities. Using as much data as possible, the aim is to quantify resources directly and make them locally addressable. The document-, data- and BIM-based building permits introduced are starting points, as shown in Figure 1. Different steps are necessary to get the information for a material inventory for each input separately.

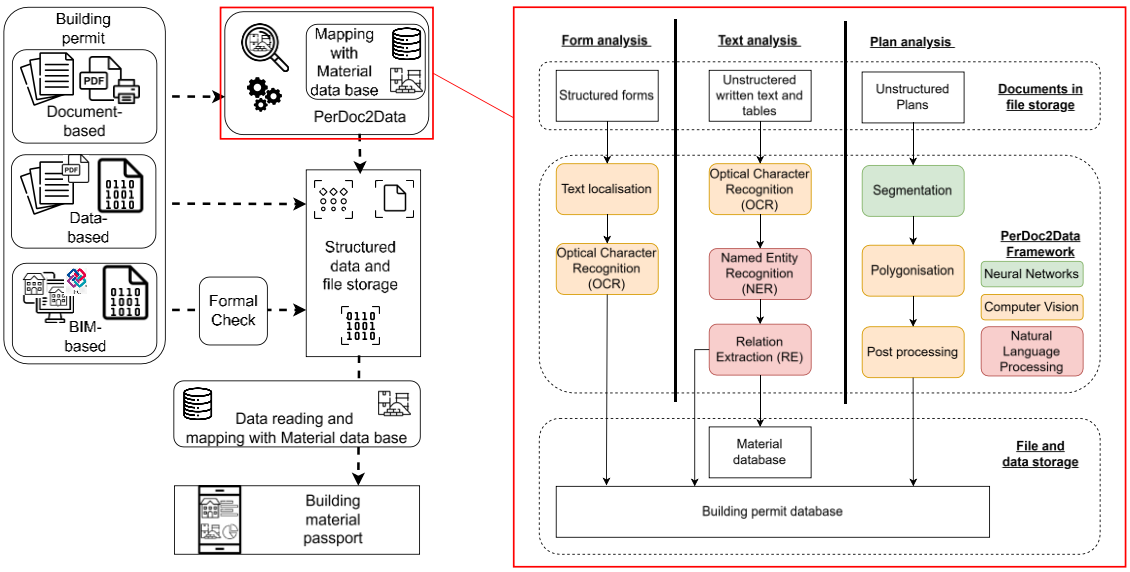


Figure 1: Material inventory processes and PerDoc2Data Framework

Similar to existing approaches, a necessary additional data source is a material database to enrich information from building permits. The structure of the database used here is based on the IFC material description, distinguishing between layered components, described by material layer sets,

and non-layered components, described by material constituent sets. Layered components consist of one or more layers of a given thickness. Unlike IFC, the material database allows more than one material to be associated with a material layer. Non-layered components with different subcomponents consist of a collection of individual materials. In order to prepare the document-based permit for automated processing and to match it with the material database, a PerDoc2Data algorithm is developed to extract structured, machine-readable data. Information extracted from PerDoc2Data is stored alongside data generated during a data-based permit, e.g., using web forms. The result is a collection of heterogeneous documents and a structured, machine-readable database for further processing. A reading and mapping process combine data from different sources such as the materials database, permit database and files. Building material passports are then generated for urban mining efforts to visualise the material inventory of a building.

## 3.2 Implementation

The development of the process pipelines was preceded by an analysis of the documents related to the current building permit in order to identify possible sources of information, revealing heterogeneous, mostly unstructured documents such as forms, descriptions and certificates depending on the building classification. Documents regarding thermal insulation, sound insulation and additional building description are particularly useful sources of data to identify the materials used. Plans are often the only source of data for component quantities. For document-based permits and the associated PerDoc2Data approach, the degree of structuring and the types of elements used within the documents are of crucial importance. Identified sources are therefore categorised according to these criteria in order to select suitable methods for data extraction. Forms with specific queries are considered structured. Unstructured forms are further separated according to the contained elements defined by written text, tables and plans. To extract data from these, three pipelines are developed shown in Figure 1. Structured forms are analysed using a text localization process and optical character recognition (OCR). The text localisation process involves scaling the input form and dividing it into subparts in order to locate specific information in a particular position. The subparts are read using OCR and transferred to a building permit database. Written text analysis starts with reading using OCR. To analyse this text, a Named Entity Recognition model is created based on a review of building permit documents with the aim of creating a knowledge base for urban mining. Through patterns and keywords, additional data such as component thicknesses, number of levels, level height, component types and construction method is recognised. Relation extraction then associates component data with material layers and thicknesses. Results are shown in Figure 2 in the middle and on the right. After selecting a material layer from the material database based on the detected component type, material and thickness value, the layer set associated with this material is linked to the component within the building permit database. For simplicity, the component types roof, external walls, internal walls, slabs and foundation are extracted. Floor plans are analysed within the plan analysis pipeline to extract quantities for component types. The CubiCasa5K neural network [12] is first used in a segmentation process to detect walls on the floor plan. In a subsequent polygonization process, the detected wall pixels are combined into polygons. A final post-processing uses computer

vision methods to differentiate between the component types slab, external and internal wall and roof. Results are shown in Figure 2 on the left. In conjunction with extracted metadata such as average level height area quantities are calculated. Fusing this quantity data and previous extracted material data allows for the determination of material inventory. Within the data-based permit, the same information on materials and component type quantities is obtained, but from different data sources. Energy performance certificates and formats for the digital provision of energy simulation models required for thermal insulation certificates play an important role. The use of these standardised, machine-readable formats such as Green Building XML and XML-based energy certificates and their combination with a material database allows the material inventory to be determined without the use of a complex framework. Compared to the other forms, the BIM-based permit uses the BIM model in IFC format as its only data source. In order to support the material mapping and data combination process and to avoid missing information, modelling guidelines and their verification are necessary. BIM models are checked for the specification of quantity data and compatibility with the material database in order to fuse with material data.

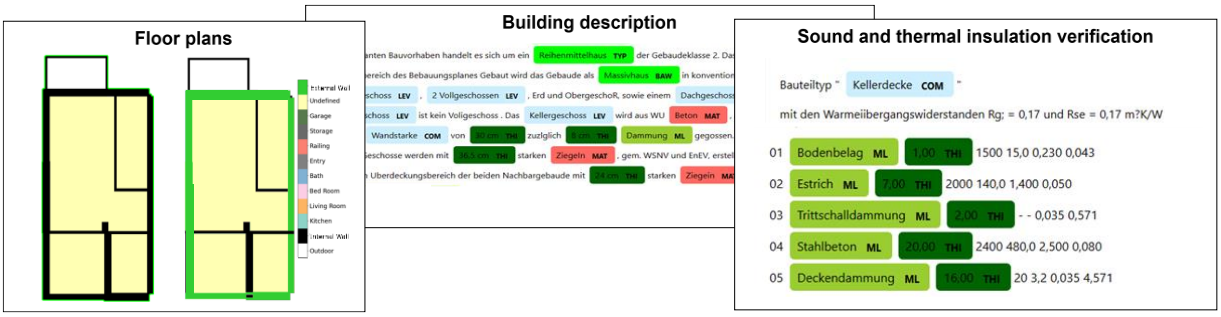


Figure 2: Results of PerDoc2Data framework

## 4 Results and Discussion

In order to compare the results of the digital and BIM-based permits, the characteristic values of the building material inventory of an example building are determined using both methods. The results, excluding window and door materials, are shown in table 1.

Table 1: Results for the material inventory of an example building

| | Digital | | BIM | | Digital | | BIM |
|---|---|---|---|---|---|---|---|
| | Total [m²] | [%] | Total [m²] | | Total [t] | [%] | Total [t] |
| Gross floor area | 279,7 | 15,1 | 243,3 | Total mass | 446,5 | 16,0 | 384,83 |
| Net floor area | 230,5 | 14,1 | 201,4 | Concrete | 231,6 | 3,9 | 222,8 |
| Exterior wall area | 196 | 43,8 | 141,7 | Metal | 87,8 | 3,9 | 84,5 |
| Interior wall area | 260,4 | 18,2 | 223,2 | Insulation | 21,44 | 21,2 | 17,69 |
| Ceiling area | 279,7 | 24,6 | 223,8 | Wood | 11,1 | -12,1 | 12,63 |
| Roof area | 279,7 | 15,1 | 243 | Gypsum | 20,71 | 49,0 | 13,9 |

A material is assigned to each component so that all masses are documented in both approaches. The aforementioned component types are considered and a standard floor height is used. The results of the Digital+BIM approach were verified through manual investigations and are consistent with them, so they are used as a baseline. The Digital+ approach was not compared with the other two concepts due to unavailable data, although its accuracy and reliability should be comparable due to the data formats used. The Digital+BIM approach results in a very accurate material inventory with deviations only occurring in conjunction with unrecorded changes during construction. The uniform deviation of area values obtained with CubiCasa5K (Digital) in one direction can be attributed to an inaccurate scaling factor when converting pixels to actual dimensions. Wall areas also show a higher deviation due to the omitted window and door openings. Consequently, deducting these openings improves the results. A similar, but less significant effect occurs for ceiling areas over openings caused by stairs and lifts. The 16% overestimation of the total amount of material can be attributed to an overestimation regarding components. A closer look at the material composition reveals some anomalies with a considerable impact on the total amount of material because of differences in bulk density. This is caused by specifications being standardised across component types, meaning that only one composition is assigned to each type, even if the actual occurrence diverges. Further improvements can be achieved by integrating the results for windows and doors from CubiCasa5k and incorporating them in the post-processing presented, allowing component quantities to be determined more accurately and door and window materials to be considered. Additional segregation of component types in terms of composition is limited by the level of detail in the approval plans, as further information on materials and layers is often not shown in the plans. More detailed plans would provide an opportunity for a more precise mapping between the aforementioned certificates and the plans, for example using machine learning methods. The use of machine learning can also add significant value when mapping between IFC or extracted data and a materials database.

## 5 Conclusion

Relevant data available in selected building permit documents provides an initial, sufficiently accurate information base for urban mining and other uses such as energy simulations. The data extracted from non-machine-readable documents is subject to a degree of uncertainty and inaccuracy, but may still be suitable for use in urban mining. For smaller and older buildings, the depth of information can be limited due to the lower requirements of previous permits, making additional data sources necessary. For larger and newer buildings, additional documentation eliminates the need for these extra sources, but the actual form might make it difficult to extract reliable data. However, certainty and accuracy will increase along with the proportion of machine-readable data, further facilitated by the possible integration of existing exchange formats and standards into the digital permit. While the reuse of materials and resources can already be assessed, the reuse of specific components requires a higher level of accuracy and information depth, often only achievable with BIM models. Here, the presented approach shows the potential of machine-readable formats and digital building permits to reliably capture relevant information for purposes such as urban mining.

## Acknowledgements

This work was funded by the German Federal Ministry of Education and Research (BMBF) within the framework of the project RessStadtQuartier2 - Urban material flow management: tools for the resource-efficient development of urban districts, funding code 033W109AN-EN.

## References

[1] R. Vogt *et al.*, “Ermittlung der Klimaschutzpotentiale in der Kreislaufwirtschaft für Deutschland und die EU,” Umweltbundesamt, 2023.

[2] K. Shahi, B. Y. McCabe, and A. Shahi, “Framework for Automated Model-Based e-Permitting System for Municipal Jurisdictions,” *J. Manag. Eng.*, vol. 35, no. 6, Nov. 2019.

[3] F. Noardo *et al.*, “EuroSDR GeoBIM project - Integrated Workflow using GeoBIM information for building permit process,” Jul. 2020, doi: 10.5281/ZENODO.3948493.

[4] (BRISE) Building Regulations Information for Submission Envolvement, Accessed: Apr. 10, 2024. [Online]. Available: https://digitales.wien.gv.at/projekt/brisevienna/

[5] Ministry of Regional Identity, Local Government, Building and Digitalization of the State of North Rhine-Westphalia, “BAUPORTAL.NRW.” Accessed: Apr. 10, 2024. [Online]. Available: https://bauportal-assistent-prod.kdvz-frechen.de/intelliform/forms/vba/vba/demo_64/index

[6] J. Tulke, M. Theiler, M. König, and A. Vonthron, “Konzept für die nahtlose Integration von Building Information Modeling (BIM) in das behördliche Bauantragsverfahren,” 2021.

[7] M. Shakro, “Tracking neighborhood development and behavioral trends with building permits in Austin, Texas,” *J. Maps*, vol. 9, no. 2, pp. 189–197, Jun. 2013.

[8] I. Kovacic *et al.*, “Prozess-Design für den „Building Information Modeling“ (BIM) basierten, materiellen Gebäudepass,” 2019.

[9] M. Honic, I. Kovacic, and D. Breitfuss, “Digital Urban Mining Platform: Assessing the material composition of building stocks through coupling of BIM to GIS,” 2023.

[10] L. Yuan, J. Guo, and Q. Wang, “Automatic classification of common building materials from 3D terrestrial laser scan data,” *Autom. Constr.*, vol. 110, p. 103017, Feb. 2020.

[11] Y. Perez-Perez, M. Golparvar-Fard, and K. El-Rayes, “Scan2BIM-NET: Deep Learning Method for Segmentation of Point Clouds for Scan-to-BIM,” *J. Constr. Eng. Manag.*, vol. 147, no. 9, p. 04021107, Sep. 2021, doi: 10.1061/(ASCE)CO.1943-7862.0002132.

[12] A. Kalervo, J. Ylioinas, M. Häikiö, A. Karhu, and J. Kannala, “CubiCasa5K: A Dataset and an Improved Multi-Task Model for Floorplan Image Analysis,” 21st SCIA 2019, Sweden, 2019,

[13] C. Gatto, A. Farina, C. Mirarchi, and A. Pavan, “Development of a framework for processing unstructured text dataset through NLP in cost estimation AEC sector,” EC3 2023 ,2023.

[14] N. Schubbe, “Urbane Digitale Zwillinge als Baukastensystem: Ein Konzept aus dem Projekt Connected Urban Twins (CUT),” *Zfv – Z. Für Geodäsie Geoinformation Landmanagement*, no. 1/2023, pp. 14–23, 2023, doi: 10.12902/zfv-0417-2022.

# Nachhaltiges Bauen durch Building Information Modeling: Eine explorative Analyse und ein methodischer Ansatz zur Verbesserung der Ökobilanzierung

Thujietha Thuraisingam[1 2], Nijanthan Mohan[1], Rolf Groß[1], Thomas Kleinow[2]
[1]Chairs of Institute of Smart Building Engineering, Fachhochschule Aachen, Bayernallee 9, 52066 Aachen
[2]PD – Berater der öffentlichen Hand GmbH, Friedrichstraße 149, 10117 Berlin

**Abstract:** Vor dem Hintergrund der zunehmenden Bedeutung von Nachhaltigkeit in der Bauwirtschaft konzentriert sich diese Studie auf den Einsatz von Building Information Modeling (BIM) Technologien zur Förderung nachhaltiger Bauprozesse. Die zentralen Forschungsfragen sind die Rolle von BIM bei der Erreichung von Nachhaltigkeitszielen, mögliche Effizienzgewinne bei der ökologischen Bewertung durch BIM sowie die damit verbundenen Chancen und Risiken. Die Studie untersucht, wie BIM die Planungsphase verbessern kann, insbesondere durch die Erleichterung des Vergleichs verschiedener Baumaterialien hinsichtlich ihrer Umweltauswirkungen. Methodisch umfasst die Studie die Erstellung eines Gebäudemodells und die Durchführung einer vorläufigen Umweltbewertung nach den Kriterien des Bewertungssystems Nachhaltiges Bauen (BNB). Die anschließende Analyse zielt darauf ab, aufkommende Chancen und potenzielle Herausforderungen zu identifizieren. Die Studie ist noch nicht abgeschlossen, aber erste Ergebnisse deuten darauf hin, dass eine Standardisierung dieser Methodik für öffentliche Bauprojekte zu einer effizienteren Planung und Bewertung zukünftiger Bauprojekte führen könnte, was einen großen Schritt in Richtung nachhaltiger Baupraktiken bedeuten würde. Diese Forschung trägt zur Entwicklung von Richtlinien für die systematische Integration von Umweltbewertungen in den BIM-Prozess bei.
*Keywords:* BIM, Nachhaltigkeit, Ökobilanzierung, Standardisierung, Bauprozesse

Erschienen in Tagungsband 35. Forum Bauinformatik 2024, Hamburg, Deutschland, DOI: 10.15480/882.13534
© 2024 Das Copyright für diesen Beitrag liegt bei den Autoren. Verwendung erlaubt unter Creative Commons Lizenz Namensnennung 4.0 International.

## 1 Einleitung

### 1.1 Status quo

In einer zunehmend globalisierten Welt steht die Menschheit vor großen Herausforderungen, die von Klimawandel und Umweltzerstörung bis hin zu sozialer Ungleichheit reichen. Diese Probleme

betreffen alle Länder und beeinflussen die Lebensqualität weltweit. Vor diesem Hintergrund hat die internationale Gemeinschaft durch die Vereinten Nationen die Agenda 2030 mit den 17 Zielen für nachhaltige Entwicklung (Sustainable Development Goals, SDGs) formuliert [1]. Diese Ziele bieten einen umfassenden Ansatz zur Lösung globaler Probleme durch die Integration sozialer, ökonomischer und ökologischer Nachhaltigkeit.

Die Bauwirtschaft spielt eine wesentliche Rolle bei der Erreichung dieser Ziele, da sie erheblich zum Ressourcenverbrauch und zu den Umweltbelastungen beiträgt. Der Sektor ist für 30-50% der globalen $CO_2$-Emissionen und 15-25% des Energieverbrauchs verantwortlich [2] [3]. Nachhaltiges Bauen, das die Prinzipien der Ökonomie, Ökologie und Soziokultur in allen Phasen eines Bauprojekts integriert, wird daher immer wichtiger. Dies umfasst die Auswahl umweltfreundlicher Baustoffe, die Reduzierung des Energiebedarfs über den gesamten Lebenszyklus eines Gebäudes und die Schaffung gesunder und behaglicher Lebensräume [4].

Die Ökobilanzierung (Life Cycle Assessment, LCA) ist ein wichtiges Werkzeug hierfür, denn damit kann ein Gebäude über seinen gesamten Lebenszyklus bewertet werden. Durch die Analyse der Umweltwirkungen von der Rohstoffgewinnung über die Nutzung bis hin zum Rückbau und Recycling kann die ökologische Leistung eines Bauwerks optimiert werden [5].

## 1.2 Rolle von Building Information Modeling

Building Information Modeling (BIM) bezeichnet eine digitale Methode, die zur Förderung nachhaltiger Bauprozesse beiträgt. BIM ermöglicht die frühzeitige Integration von Umweltdaten sowie die Visualisierung des gesamten Lebenszyklus eines Gebäudes. Dadurch wird eine ressourceneffiziente und umweltbewusste Planung und Durchführung von Bauprojekten unterstützt [6].

Die Methode BIM ermöglicht eine Reduzierung des Energiebedarfs und der $CO_2$-Emissionen durch eine optimierte Materialauswahl und Energieeffizienz bereits in der Planungsphase. Des Weiteren bietet BIM zahlreiche Vorteile gegenüber traditionellen Bauprozessen. Dazu zählen eine frühzeitige Einflussnahme auf die Projektkosten sowie die Minimierung späterer Änderungskosten. Im Betrieb eines Gebäudes ermöglicht BIM durch technisches Gebäudemonitoring und regelmäßige Soll-Ist-Vergleiche eine kontinuierliche Reduzierung des Energieverbrauchs und Materialeinsatzes. Dies resultiert in einer optimierten Gebäudeperformance, einer Reduzierung der Betriebskosten und gleichzeitig einer Minimierung der Umweltauswirkungen [7] [8].

Die Integration von LCA in BIM-Prozesse ermöglicht eine umfassende Bewertung der ökologischen Auswirkungen eines Bauwerks über dessen gesamten Lebenszyklus hinweg. Die Analyse der Umweltwirkungen erstreckt sich demnach über die gesamte Wertschöpfungskette, beginnend bei der Rohstoffgewinnung über die Nutzung bis hin zum Rückbau und Recycling. Die Verbindung von BIM und LCA ermöglicht die Identifikation von Umweltbelastungen sowie die Entwicklung von Maßnahmen zu deren Reduktion. Diese Vorgehensweise trägt zu nachhaltigeren Baupraktiken bei [9] [5].

Die vorliegende Studie untersucht den Einsatz der BIM-Methodik zur Förderung nachhaltiger Bauprozesse. Im Mittelpunkt stehen die Fragen, welche Rolle BIM bei der Erreichung von Nachhaltigkeitszielen spielt, welche Effizienzgewinne durch den Einsatz von BIM bei der ökologischen Bewertung von Bauprojekten erzielt werden können und welche Chancen und Risiken mit der Integration von BIM in nachhaltige Bauprozesse verbunden sind.

# 2 Methodik

Zur Beantwortung der im vorangegangenen Kapitel 1.2 "Rolle des Building Information Modeling" genannten Forschungsfragen wurde ein strukturierter Prozess implementiert, der die Erstellung eines BIM-Modells, die Durchführung einer thermischen Gebäudesimulation sowie eine anschließende LCA nach dem Bewertungssystem Nachhaltiges Bauen (BNB) umfasst. Dies ist im folgenden Flussdiagramm (siehe Abbildung 1) dargestellt:

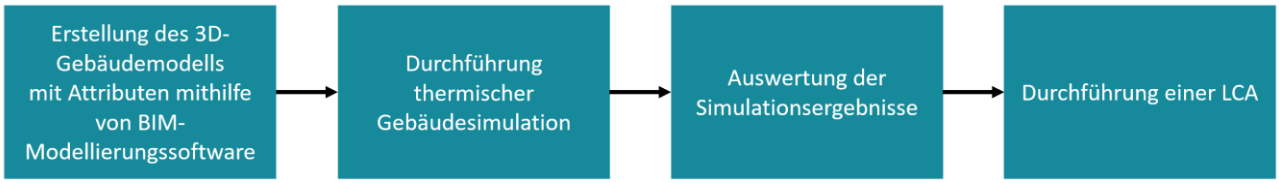


Abbildung 1: Flussdiagramm der Methodik zur Durchführung von LCA mit BIM

Die Durchführung der LCA zur Bewertung der ökologischen Auswirkungen des Gebäudes über seinen gesamten Lebenszyklus umfasst:

1. Zieldefinition: Festlegung des Umfangs und der Zielsetzungen der Umweltbewertung.
2. Sachbilanz: Sammlung und Quantifizierung aller relevanten Daten zu Material- und Energieflüssen im Lebenszyklus des Gebäudes.
3. Wirkungsabschätzung: Bewertung der potenziellen Umweltwirkungen anhand der gesammelten Daten.
4. Auswertung der Ergebnisse: Interpretation der Ergebnisse zur Identifikation von Optimierungspotenzialen und Entwicklung von Handlungsempfehlungen [10].

## 2.1 Fallbeispiel Integration von BIM und LCA

Zur praktischen Veranschaulichung des beschriebenen Prozesses dient das folgende Fallbeispiel. Das dargestellte Ablaufschema (siehe Abbildung 2) zeigt die für jeden Prozessschritt erforderlichen Inputs, die über dem jeweiligen Prozess aufgelistet sind, und die Outputs, die rechts daneben als Bilder dargestellt sind.

Zur Durchführung der LCA wurden zusätzliche Daten in die LCA-Software aufgenommen, wie z.B. die Gebäudegrundfläche und die Ergebnisse der thermischen Gebäudesimulation mit dem Energiebedarf. Es ist auch möglich, die LCA ohne die Ergebnisse der thermischen Simulation durchzuführen, indem nur die Gebäudedaten, z.B. die verwendeten Materialien, berücksichtigt werden. Für die

Bewertung wurde ein Zeitraum von 50 Jahren festgelegt und die LCA wurde nach den Kriterien der BNB erstellt.

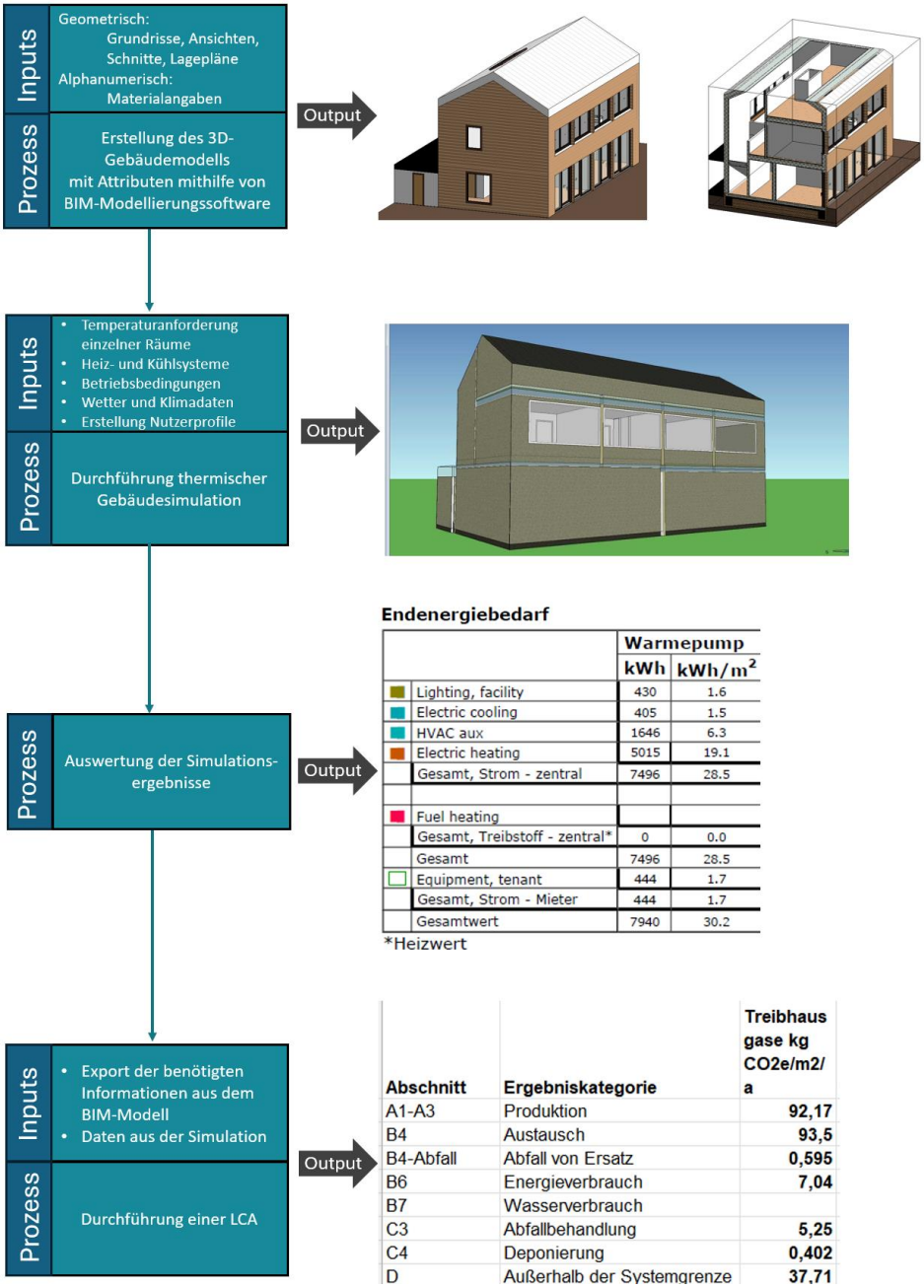


Abbildung 2: Ablaufschema für die Durchführung der LCA

Die Ergebnisse der LCA, die als letzter Output in Abbildung 2 dargestellt sind, umfassen verschiedene Umweltindikatoren, wie Treibhausgasemissionen, Versauerung, Überdüngung und Ressourcenverbrauch. Da der Schwerpunkt dieser Arbeit auf der Methodik liegt, wird auf eine detaillierte Diskussion der einzelnen Ergebnisse verzichtet. Die Analyse zeigt beispielsweise, dass die Treibhausgasemissionen während der Produktions- und Austauschphase des Gebäudes am höchsten sind. Die Ergebnisse werden differenziert nach verschiedenen Kategorien dargestellt, darunter Produktion

(A1-A3), Austausch (B4), Abfall aus Ersatz (B4-Abfall), Energieverbrauch (B6), Wasserverbrauch (B7), Abfallbehandlung (C3), Deponierung (C4) sowie Auswirkungen außerhalb der Systemgrenze (D). Diese detaillierte Aufschlüsselung ermöglicht es, spezifische Bereiche zu identifizieren, in denen Maßnahmen zur Verringerung der Umweltauswirkungen besonders wirksam sein könnten. Diese Kategorien entsprechen den Anforderungen der BNB-Zertifizierung, was für die LCA berücksichtigt werden muss [11].
Das beschriebene methodische Vorgehen bildet die Grundlage für die anschließende Analyse und Diskussion der Erkenntnisse in den folgenden Kapiteln.

# 3 Nachhaltiges Bauen mit BIM

## 3.1 Erkenntnisse aus der Studie

Die Integration von BIM und LCA bietet eine Vielfalt an Vorteilen für das nachhaltige Bauen.
Im Folgenden werden die wesentlichen Erkenntnisse dieser Studie dargelegt und teilweise mit dem aktuellen Forschungsstand oder praktischen Beispielen verglichen.

- BIM ermöglicht eine **genauere und konsistentere LCA** durch die Zusammenführung von Umwelt- und Baudaten. Im Vergleich dazu werden Umweltdaten bei herkömmlichen Methoden oft manuell erfasst und separat gespeichert, woraus ein erhöhtes Risiko von Ungenauigkeiten und Fehlern resultiert.
- Des Weiteren **reduziert** die automatisierte Datenübertragung zwischen BIM und LCA den **Aufwand und die Fehleranfälligkeit** bei der Dateneingabe. Die implementierte Plausibilitätsprüfung stellt die Konsistenz, Vollständigkeit und Genauigkeit der Daten sicher, was die Einhaltung der Zertifizierungskriterien der BNB erleichtert. Im Vergleich dazu sind manuelle Methoden fehleranfälliger und zeitaufwändiger [4].
- Darüber hinaus können **Materialien und Komponenten leicht geändert** werden, was eine umgehende Neuberechnung der LCA ermöglicht. Bei konventionellen Methoden erfordern Änderungen oft eine komplette Neuberechnung, die zeitaufwändig und ineffizient ist.
- Nicht zuletzt kann die **Energiebedarfsberechnung direkt in das BIM-Modell integriert** und automatisiert durchgeführt werden. Die Möglichkeit, verschiedene Varianten direkt zu vergleichen und ihre Auswirkungen auf den Energiebedarf und die LCA zu analysieren, ist im Zusammenhang mit der BNB-Zertifizierung besonders relevant, da der Energiebedarf eine wesentliche Rolle spielt. Manuelle Methoden erfordern oft zeitintensive Berechnungen auf der Grundlage von Bauplänen und technischen Spezifikationen [9].

## 3.2 Herausforderungen der Ökobilanzierung mittels BIM

Bei der Umsetzung dieser Methoden sind jedoch auch einige Herausforderungen zu berücksichtigen, denen mit gezielten Lösungsansätzen begegnet werden kann, wie in der folgenden Tabelle (siehe Tabelle 1) dargestellt.

Tabelle 1: Herausforderungen bei der Integration von BIM und LCA [6]

| Herausforderungen | Lösungsansätze |
|---|---|
| Komplexität und Qualität der Daten | - Regelmäßige Aktualisierung und Pflege der Daten im BIM-Modell<br>- Verwendung von standardisierten Datenformaten<br>- Einsatz von Maßnahmen zur Datenqualitätssicherung |
| Kompatibilität verschiedener Softwarelösungen | - Auswahl kompatibler Softwarelösungen<br>- Verwendung von Konvertierungstools für Datenformate<br>- Schulung des Personals in der Bedienung der Software |
| Hohe Kosten und Investitionen | - Budgetplanung für Software, Schulungen und Datenmanagement<br>- Langfristige Kosten-Nutzen-Analyse vor der Implementierung |
| Akzeptanz und Integration in der Praxis | - Schulung und Sensibilisierung der Mitarbeiter für die Vorteile von BIM und LCA<br>- Pilotprojekte zur Demonstration von Effizienz und Nutzen<br>- Einbindung von Stakeholdern in den Implementierungsprozess |

### 3.3 Auswertung - LCA mit BIM für öffentliche Bauprojekte

Durch die Verknüpfung von BIM und LCA können Bauprojekte bereits in der Planungsphase hinsichtlich ihrer Umweltauswirkungen optimiert werden. Dies umfasst die Reduzierung von Treibhausgasemissionen, Ressourcenverbrauch und Abfallentsorgung über den gesamten Lebenszyklus des Gebäudes. Ein zentraler Aspekt ist dabei die Auswahl geeigneter Materialien für das nachhaltige Bauen. BIM und die darauf aufbauende LCA nehmen hier eine wesentliche Rolle ein, da mit diesen Methoden umweltrelevante Daten, wie Materialzusammensetzung, Herkunft und Recyclingfähigkeit direkt in das Planungsmodell integriert werden können. Dadurch können verschiedene Szenarien und Materialoptionen schnell modelliert und bewertet werden. Insbesondere können diese verschiedenen Materialoptionen miteinander verglichen und sofort analysiert werden, um ihre Einflüsse auf die Umweltauswirkungen des Gebäudes zu bewerten. Diese schnelle und präzise Analysemöglichkeit trägt dazu bei, fundierte Entscheidungen über die Auswahl von Baumaterialien zu treffen, die dazu dienen, die Umweltauswirkungen gering zu halten.

Für öffentliche Gebäude gelten hinsichtlich der Nachhaltigkeit besondere Anforderungen, die durch Zertifizierungsverfahren wie z.B. die BNB-Zertifizierung sichergestellt werden müssen [12]. Eine umfassende LCA ist in diesem Zusammenhang unerlässlich, da sie eine detaillierte Analyse der Umweltauswirkungen eines Gebäudes ermöglicht.

Bei öffentlichen Bauprojekten, insbesondere bei großen Gebäudekomplexen, ist eine herkömmliche LCA mit einem erheblichen Zeitaufwand verbunden, da die manuelle Dateneingabe sowohl zeitaufwändig als auch fehleranfällig ist, wie bereits in Kapitel 3.1 " Erkenntnisse aus der Studie" beschrieben. Diese Herausforderung wird durch die Notwendigkeit verschärft, die Ergebnisse der LCA manuell mit den spezifischen Zertifizierungskriterien, wie sie für die BNB-Zertifizierung gelten, zu überprüfen und gegebenenfalls anzupassen.

Die Integration von BIM in die LCA ermöglicht nicht nur eine schnellere und genauere Modellierung

und Bewertung verschiedener Material- und Planungsoptionen, sondern auch eine direkte Überprüfung der Ergebnisse anhand der spezifischen Anforderungen der BNB-Zertifizierung. Die LCA kann beispielsweise nach den BNB-Kriterien durchgeführt werden, wie es in dieser Fallstudie praktiziert wurde. Dies vereinfacht die Analyse, ob ein Gebäude die erforderlichen Kriterien für eine Nachhaltigkeitszertifizierung erfüllt, erheblich und trägt dazu bei, den gesamten Bewertungsprozess effizienter zu gestalten.
Eine Standardisierung dieser Methodik könnte insbesondere bei öffentlichen Bauprojekten zu einer effizienteren Planung und Bewertung zukünftiger Bauprojekte führen.Trotz der Vorteile birgt die Integration von BIM und LCA Herausforderungen, wie die Komplexität und Qualität der benötigten Daten, die Kompatibilität und Schulungsbedarf für Softwarelösungen. Auch in diesem Zusammenhang kann eine Standardisierung durch einheitliche Verfahren, Richtlinien und Protokolle dazu beitragen, diese Herausforderungen zu bewältigen und die Effizienz und Zuverlässigkeit der Umweltbewertung zu verbessern.

## 4 Fazit

Das Ziel dieser Studie ist es, die Rolle von BIM bei der Förderung nachhaltiger Bauprozesse zu untersuchen und die LCA mit Hilfe von BIM zu verbessern. Insbesondere wurde untersucht, wie eine Standardisierung dieser Methodik in öffentlichen Bauprojekten zu einer effizienteren Planung und Bewertung zukünftiger Bauprojekte beitragen kann. Die Studie befindet sich noch in der Durchführung, erste Ergebnisse zeigen jedoch bereits, dass die Integration von BIM und LCA insbesondere bei öffentlichen Bauprojekten wesentliche Vorteile für nachhaltiges Bauen bietet, wie in Kapitel 3.3 "Auswertung - LCA mit BIM für öffentliche Bauprojekte" erläutert wurde.

Die methodische Verknüpfung beider Ansätze ermöglicht eine präzisere und effizientere Planung und Bewertung von Bauprojekten hinsichtlich ihrer Umweltauswirkungen. Eine Standardisierung dieser Methodik durch einheitliche Verfahren, Richtlinien und Protokolle könnte zu einer deutlichen Effizienzsteigerung führen. Zusammenfassend lässt sich feststellen, dass die Integration von BIM und LCA ein erhebliches Potenzial für die Erreichung der Nachhaltigkeitsziele öffentlicher Bauprojekte bietet. Sie ermöglicht nicht nur eine umfassende Analyse der Umweltauswirkungen eines Gebäudes, sondern auch die Durchführung der LCA direkt nach den Kriterien der BNB-Zertifizierung.
Für die Zukunft könnte eine Vertiefung der Standardisierung und Integration von BIM und LCA in öffentliche Bauprojekte von großem Interesse sein. Dies könnte die Entwicklung neuer Methoden und Richtlinien zur Vereinfachung und Optimierung der Nachhaltigkeitsbewertung umfassen. Dadurch wird nicht nur die Effizienz der Planung und Bewertung öffentlicher Bauprojekte verbessert, sondern auch ein Beitrag zur Förderung nachhaltigerer Baupraktiken auf globaler Ebene geleistet.

## Danksagung

Ein besonderer Dank gilt dem Institut für Smart Building Engineering – dem Team des Projekts DiggiTwin an der FH Aachen, gefördert durch das Ministerium für Kultur und Wissenschaft des

Landes Nordrhein-Westfalen unter dem Förderkennzeichen 005-2302-0018, Deutschland, an der FH Aachen, für ihren kooperativen Geist, der die Tiefe unserer Arbeit bereichert hat.

## Literaturverzeichnis

[1] J. M. u. W. Obenland, „Die Agenda 2030, Globale Zukunftsziele für nachhaltige Entwicklung," Global Policy Forum, Bonn /Osnabrück, 2017.

[2] United Nations Environment Programme (UNEP), "2022 Global Status Report for Buildings and Construction: Towards a zero-emission, efficient and resilient buildings and construction sector," 2022 United Nations Environment Programme, Nairobi, 2022.

[3] M. M., T. S.-P., A. Schumann, „Aktueller Überblick bei der Verwendung von nichtmetallischer Bewehrung im Neubau und beim Bauen im Bestand," Technische Universität Hamburg, Hamburg, 2024.

[4] S. T., J. H., R. W., A. M.-B., M. Z., M. Lambertz, „Ökobilanzierung und BIM im Nachhaltigen Bauen," Zukunft Bau, ein Forschungsprogramm des Bundesministeriums des Innern, für Bau und Heimat, Köln, 2019.

[5] K. Forth, „BIM-integrierte Ökobilanzierung," Technische Universität München, München, 2018.

[6] G. W., M. W., J. B., R. G., N. Mohan, „Auf dem Weg zu einem ganzheitlichen Lebenszyklusmanagement von Bauwerken für nachhaltiges Bauen: Vorschlag einer Methodik zurdigitalen Transformation durch datenbankbasierte Informationsmodelle," 34. Forum Bauinformatik, Bochum, 2023.

[7] M. K., C. K., J. B., A Borrmann, Building Information Modeling Technologische Grundlagen und industrielle Praxis, Wiesbaden: Springer Vieweg, 2021.

[8] R. G., K. M., F. T., N. Mohan, „Opportunities and Challenges in the Implementation of Building Information Modelling for Prefabrication of Heating, Ventilation and Air Conditioning Systems in Small and Medium-Sized Contracting Companies in Germany: A Case Study," WIT Transactions on The Built Environment, WIT Press, 2021.

[9] P. v. B., K. R., S. E., R. H., O. J., C. S., M. F., J. Gantner, „Ökobilanz- Integration in den Entwurfsprozess, BIM-basierte entwurfsbegleitende Ökobilanzin frühen Phasen einer Integrale Gebäudeplanung," Ernst & Sohn Verlag für Architektur und technische Wissenschaften GmbH&co.KG, Berlin, 2018.

[10] DIN EN ISO 14040, Berlin: DIN Deutsches Institut für Normung e.V., 2021.

[11] Bundesministerium für Umwelt, Naturschutz Bau und Reaktorsicherheit , „Bewertungssystem Nachhaltiges Bauen (BNB) Neubau Büro- und Verwaltungsgebäude, Bilanzierungsregeln für die Erstellung von Ökobilanzen," Bundesministerium für Umwelt, Naturschutz Bau und Reaktorsicherheit , 2015.

[12] Bundesministerium des Innern, für Bau und Heimat, „Leitfaden Nachhaltiges Bauen Büro, Zukunftsfähiges Planen, Bauen und Betreiben von Gebäude," Bundesministerium des Innern, für Bau und Heimat, 2019.

[13] H. Hülswitt, „Methodik zur Erstellung einer Gebäude-Ökobilanz entlang der BIM-Projektabwicklung," in HAWK – Hochschule für angewandte Wissenschaft und Kunst Fakultät Management, Soziale Arbeit, Bauen, Aachen, 2016.

# Nachhaltigkeitsbewertungen durch IoT-gestützte Auswertung von Nutzerverhalten im Rahmen des as-used BIM

Maximilian Gehring[1] and Yunquing Luo[1]
[1]Institut für Numerische Methoden und Informatik im Bauwesen, Technische Universität Darmstadt, Franziska-Braun-Straße 15, 64287 Darmstadt, Germany
E-mail(s): gehring@iib.tu-darmstadt.de

**Abstract:** Gebäude stellen einen wesentlichen Teil des weltweiten Energieverbrauchs und der CO2-Emissionen dar, insbesondere während ihres Betriebs. Zur Beurteilung ihrer Nachhaltigkeit und Energieeffizienz werden verschiedene Verfahren wie das ESG-Rating angewendet, vor allem im Kontext des Asset Managements großer Gebäudeportfolios. Während der Planung wird der Energiebedarf eines Gebäudes geschätzt. Da viele Gebäude ineffizient betrieben werden, ist es von großem Interesse anhand des tatsächlichen Nutzerverhaltens eine genauere Bewertung der Nachhaltigkeit zu ermöglichen. Diese Forschung wird durch den vermehrten Einsatz von IoT-Technologie unterstützt, die eine Echtzeitdatenerfassung ermöglicht. Die Integration des Building Information Model (BIM) und IoT birgt jedoch technische und datenschutzrechtliche Herausforderungen. Besonders während der Betriebsphase bleiben Daten oft isoliert und können nicht nahtlos zwischen verschiedenen Systemen ausgetauscht werden. In diesem Kontext wird ein Konzept entwickelt, das darauf abzielt die Gebäudenachhaltigkeit basierend auf dem Nutzerverhalten innerhalb von BIM unter Verwendung von IoT-Sensordaten zu bewerten. Durch eine praktische Anwendung wird dieses Konzept veranschaulicht und trägt zur weiteren Optimierung der Energieeffizienz von Gebäuden bei.
*Keywords:* IoT, as-used BIM, Nachhaltigkeitsbewertung

Erschienen in Tagungsband 35. Forum Bauinformatik 2024, Hamburg, Deutschland, DOI: 10.15480/882.13490
© 2024 Das Copyright für diesen Beitrag liegt bei den Autoren. Verwendung erlaubt unter Creative Commons Lizenz Namensnennung 4.0 International.

## 1 Einleitung

Mit der Corporate Sustainability Reporting Directive der EU sind ab 2025 Unternehmen verpflichtet neben der finanziellen Berichterstattung auch eine umfassende nichtfinanzielle Berichterstattung zu erstellen [1]. Durch diese Berichterstattung wird der Einfluss des unternehmerischen Handelns auf die Umwelt und die Gesellschaft beschrieben. Die Forderung nach einer solchen Berichterstattung spiegelt das steigende Interesse von Investoren und der Gesellschaft an sozialem Wohlergehen und der Umweltverträglichkeit des allgemeinen Handelns wider. Das gestiegene Interesse lässt sich auch auf Gebäude übertragen. So sind laut der Internationalen Energieagentur (IEA) Gebäude für 36 % des weltweiten Endenergieverbrauchs und fast 30-40 % der Kohlendioxidemissionen ($CO_2$)

verantwortlich [2]. Dabei fallen 66 % der Emissionen in der Betriebsphase des Lebenszyklus eines Gebäudes an, wodurch sie erheblich zum Klimawandel beitragen. Die Daten für die Berechnung des Energiebedarfs eines Gebäudes stammen i.d.R. aus der Planungsphase. 70 % der Gebäude werden jedoch nicht effizient betrieben [3]. Zusätzlich können sich Änderungen der Nutzung im Lebenszyklus eines Gebäudes auf den Energieverbrauch auswirken. Daher ist es wichtig zu untersuchen, wie anhand des tatsächlichen Nutzerverhaltens eine Nachhaltigkeitsbewertung genauer bestimmt werden kann. In diesem Zusammenhang wurde z.B. in der nationalen Verordnung des Vereinigten Königreichs über die Gesamtenergieeffizienz und die Kohlenstoffbilanzierung mehr Konsistenz der Gebäudeinformationen gefordert, um das $CO_2$-Emissionsziel zu erreichen [4].

Die manuelle Überwachung und Verwaltung des Energieverbrauchs kann ein zeitaufwändiger und fehleranfälliger Prozess sein. Aus diesem Grund wird die IoT-Technologie zunehmend eingesetzt, um Energieverbrauchs- und Nutzungsdaten eines Gebäudes in Echtzeit zu erfassen. Internet of Things (IoT) bezieht sich auf die Ausstattung alltäglicher physischer Objekte mit Informations- und Kommunikationstechnologien, sodass diese in ein Netzwerk integriert werden können [5]. Dabei besteht die Herausforderung die Sensordaten sinnvoll für das Gebäudemanagement aufzubereiten. In diesem Paper wird daher die Verknüpfung der Sensordaten mit Informationen aus dem Building Information Model (BIM) zu einer nachvollziehbaren und steuerbaren Nachhaltigkeitsbewertung entwickelt.

# 2 Grundlagen

## 2.1 Nachhaltigkeitsbewertung

Nachhaltigkeitsbewertungen zielen darauf ab die Entwicklung der Gesellschaft zu beeinflussen. Dabei können unterschiedliche Aspekte der gesellschaftlichen Entwicklung betrachtet werden. Die Entwicklung von Technik trägt häufig zur Entstehung von Problemen bei, kann aber auch helfen diese zu lösen. Daraus resultiert die Motivation von Nachhaltigkeitsbetrachtungen und -bewertungen, um positive wie auch problematische Entwicklungen aufzuzeigen. So werden politische Entscheider sowie Individuen bei Investitionsentscheidungen bei der Betrachtung der Nachhaltigkeit eines Objektes (Unternehmen, Gebäude, Produkt) unterstützt [6]. In der Praxis gibt es diverse nationale und europäische Gesetze (z.B. EU-Taxonomie oder Lieferkettensorgfaltspflichtgesetz), die die Anwendung einer Nachhaltigkeitsbewertung vorschreiben. Ein bekanntes Verfahren ist das ESG-Rating. ESG steht für »Environmental, Social, Governance« und meint die Untersuchung der Nachhaltigkeit eines Objektes in den genannten Bereichen. Im Bereich Umwelt werden verschiedene Faktoren zur Nachhaltigkeitsbetrachtung herangezogen, u.a. Treibhausgasemissionen, Energieverbrauch und -effizienz, Abfallerzeugung und -bewirtschaftung. [7].

Ein wichtiger Faktor, auf dem in diesem Paper der Fokus liegt, ist die Betrachtung der Treibhausgasemissionen. Im Rahmen der $CO_2$-Bilanzierung wird dazu die Auswirkung verschiedener Treibhausgase (wie Methan, Distickstoffoxid und andere) auf den Klimawandel analysiert. Dazu wird die Auswirkung einer spezifischen Emission auf eine äquivalente Menge Kohlendioxid ($CO_2$) nach Volumen normiert und so mit Emissionen anderer Objekte vergleichbar gemacht [8]. In Deutschland stellt

das Umweltbundesamt mit ProBas [9] eine Datenbank zur Verfügung, die diese Informationen zu Treibhausgasemissionen beinhaltet. So findet man dort Daten zu den $CO_2$-Äquivalenten, die zur Herstellung eines Materials wie Aluminium, eines Lebensmittels wie Milch oder die Fahrt mit einem Pkw benötigt werden.

## 2.2 Bestehende Ansätze BIM und IoT Integration

Die aktuelle Forschung beschäftigt sich mit Ansätzen zur effizienten Steuerung von Gebäuden durch die Integration von IoT-Sensoren und -Geräten. So kann bspw. die Heizung und Lüftung automatisiert [10], die Beleuchtung intelligent gesteuert [11] oder die Anwesenheit erfasst und der Raumkomfort optimiert werden [12]. Die Bedienung solcher Gebäudesysteme ist durch den fehlenden räumlichen Kontext jedoch nicht intuitiv. Daher wird die Nutzung von BIM für das Management von intelligenten Gebäuden vorgeschlagen. Dadurch wird ein räumlicher Kontext für die Funktionsweise des Systems geschaffen und eine bessere Koordinierung und Steuerung von IoT-Sensoren und -Geräten ermöglicht [13]. Bei der Integration von BIM und IoT gibt es zwei Datenquellen zu berücksichtigen:

1. BIM dient als Datenbank für die Speicherung von Kontextinformationen, zu denen in erster Linie die Gebäudegeometrie, Beschreibungen von IoT-Geräten, statische Informationen und andere funktionale Gebäudedetails wie Raumzuweisungen, Wetterinformationen, Preise, Belegungsraten usw. gehören. Die kontextuellen Informationen können entweder in einem proprietären Modellformat oder im offenen IFC-Format gespeichert werden.

2. Von Sensoren gesammelte Zeitreihendaten, die in der Regel in einer separaten relationalen Datenbank gespeichert werden und mit Hilfe der Structured Query Language (SQL) effektiv abgefragt werden können.

Die Herausforderung besteht darin diese beiden Datenquellen sinnvoll miteinander zu verknüpfen. Im folgenden sind bestehende Ansätze aufgelistet:

Tabelle 1: Bestehende Ansätze zur Verknüpfung von BIM und IoT

| Technischer Ansatz | Beschreibung | Literatur |
|---|---|---|
| Verknüpfung zweier Datenbanken | Übertragung der Daten aus dem BIM in eine (relationale) Datenbank mithilfe einer API (z.B. Revit DB Link) und Verknüpfung der Sensordaten und der BIM-Daten mithilfe eines vorher definierten Datenschemas. | [14] |
| Abfragesprache für BIM bzw. IFC Datenschema | Entwicklung einer eigenen Abfragesprache, um Daten direkt aus dem BIM, welches z.B. im IFC-Format vorliegt, abfragen zu können. | [15] |
| Nutzung von Semantic Web Technologien | Die Daten werden mittels Ontologien z.B. Resource Description Framework (RDF) und Onto-Sensor verknüpft. Dazu müssen die Daten zunächst entsprechend umgewandelt werden. Mit einer Abfragesprache (z.B. SPARQL) können die verknüpften Daten ausgelesen werden. | [16], [17] |

Ebenso gibt es bereits proprietäre Lösungen, die es ermöglichen Sensordaten in die BIM-Modelle der dazugehörigen proprietären Autorensoftware zu integrieren. Ein Beispiel dafür ist Autodesk Tandem [18].

# 3 Nutzerbasierte Nachhaltigkeitsbewertung

## 3.1 Entwickeltes Konzept

Für die Nachhaltigkeitsbewertung von Gebäuden soll das tatsächliche Nutzerverhalten verwendet werden. Dazu wird das Nutzerverhalten von IoT-Sensoren erfasst und anschließend mithilfe von gebäudebezogenen Informationen aus dem BIM die Nachhaltigkeitsbewertung angepasst. In diesem Paper wird beispielhaft die Auswirkung des Nutzerverhaltens auf die Treibhausgasemissionen durch die Heizung betrachtet. Dazu wird Sensorik, die Temperatur und Luftfeuchtigkeit im Gebäude misst, verwendet. Die Sensordaten werden dazu in eine NoSQL-Datenbank eingelesen und räumlich verortet (siehe Abbildung 1).Eine »Not Only SQL«-Datenbank (NoSQL) folgt einem nicht-relationalen Ansatz und benötigt daher keine festgelegten Tabellenschemata.

Bei der Berechnung des Wärmeenergiebedarfs eines spezifischen Raumes nach der DIN V 18599 wird die Differenz aus Außentemperatur und die standardisierte Raumsolltemperatur verwendet. Durch die Nutzung der erfassten Temperaturdaten kann somit eine nutzungsorientierte Berechnung des Wärmeenergiebedarfs erfolgen. Basierend auf dem Energiebedarf können anschließend mit einem heizungsspezifischen Emissionsfaktor die Emissionswerte für die Nachhaltigkeitsermittlung festgestellt werden.

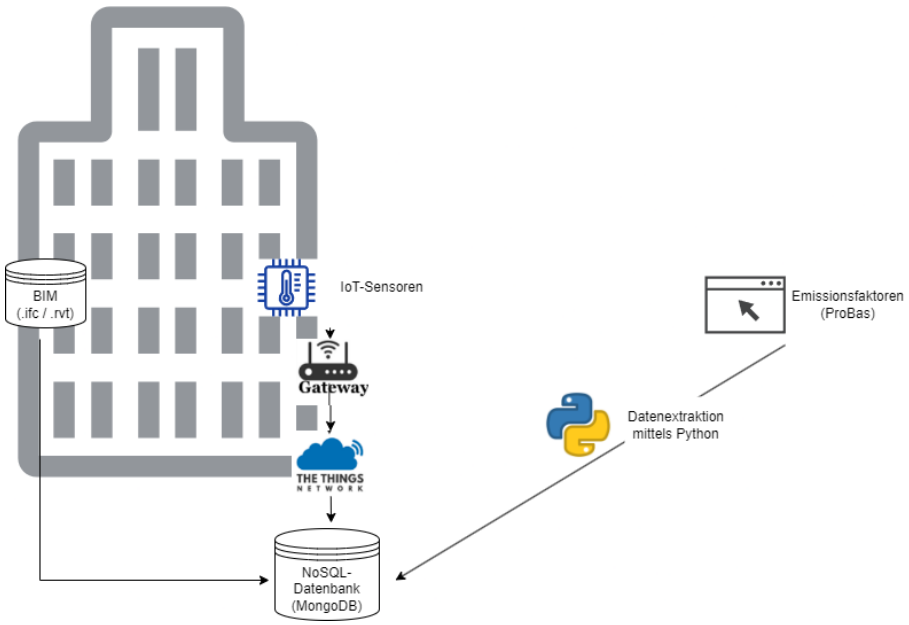


Abbildung 1: Konzept zur IoT-BIM Integration

Um den Wärmeenergiebedarf eines Raumes während der Betriebsphase zu berechnen, müssen folgende Informationen aus dem BIM extrahiert werden: Raumspezifische Details für jedes Stockwerk, einschließlich Raumnamen, eindeutige IDs, Raumfläche, Volumen und Komponenten der Raumhülle.

Zur Raumhülle gehören weiterhin die Fläche, das Volumen, die Materialien und die Dicke (für die Berechnung der U-Werte) von Wänden, Türen, Fenstern, Böden und Decken. Darüber hinaus ist es wichtig festzustellen, welche Räume eine Außenhülle haben und über Fenster verfügen. Diese Eigenschaften werden für die Berechnung der solaren Gewinne sowie den Wärmeverlust durch Lüftung und durch die Gebäudehülle benötigt. Die genannten Daten sind bereits im BIM vorhanden und werden mithilfe der proprietären Autorensoftware ausgelesen und ebenfalls in der NoSQL-Datenbank gespeichert.

Basierend auf den hinterlegten Daten können die Treibhausgasemissionen des aktuellen Heizverhaltens ermittelt und als Grundlage für eine angepasste Nachhaltigkeitsbewertung verwendet werden. Dazu werden Emissionsfaktoren aus Internetquellen importiert und ebenfalls in der NoSQL-Datenbank gespeichert.

## 3.2 Demonstrative Umsetzung

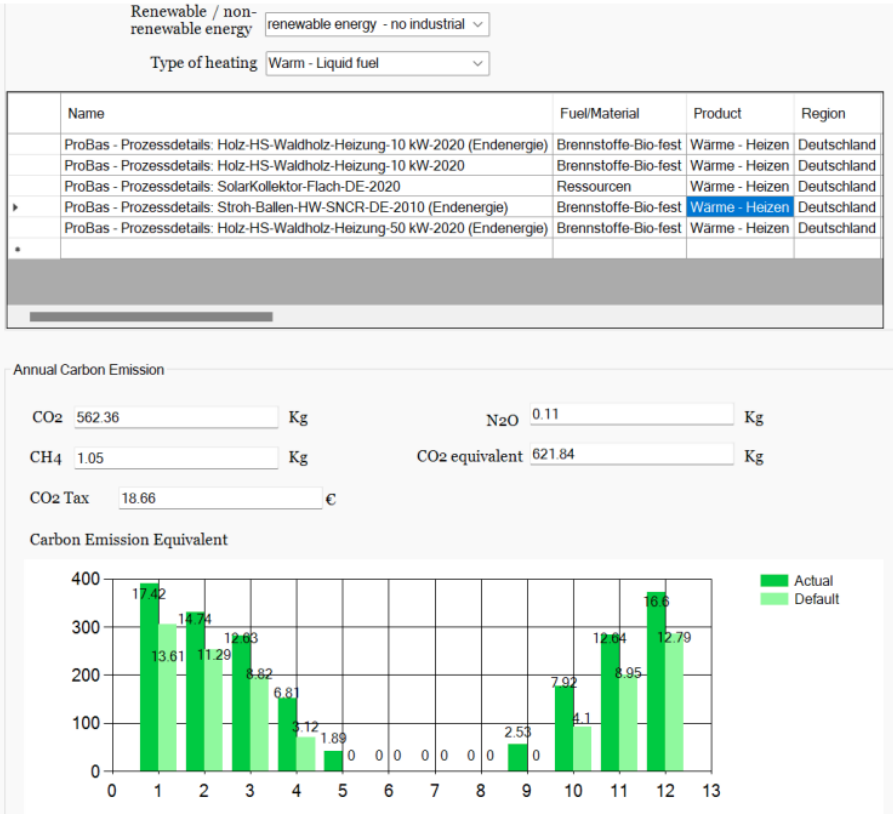


Abbildung 2: Grafische Nutzeroberfläche des Demonstrators

Um die technische Umsetzbarkeit nachzuweisen, wurde ein Demonstratorsystem entwickelt. Das Nutzerverhalten wird durch Temperatursensoren erfasst. Die Sensoren sind an einen Mikrocontroller vom Typ »Arduino Nano« mit LoRa-Modul angeschlossen. Long Range Wide Area Network (LoRaWAN) ist ein stark verbreitetes Low Power Wide Area Network (LPWAN) zur Unterstützung von IoT-Geräten und -Diensten und ermöglicht den Transfer von kleinen Datenpaketen über große Reichweiten und mit geringem Energiebedarf im Vergleich zu Bluetooth oder Wi-Fi [19]. Daher eignet es sich zur Übertragung der Daten von IoT-Sensoren ohne Netzanschluss. Über den LoRaWAN Netzwerkserver

»The Things Stack« ist es möglich die Sensordaten zu empfangen und mittels »Message Queuing Telemetry Transport«-Protokoll (MQTT) an die eingesetzte Datenbank zu übergeben.

Da die eingesetzte NoSQL-Datenbank in der Lage sein muss sowohl die Gebäudedaten als auch die Zeitreihendaten effizient zu verwalten, wurde für die demonstrative Umsetzung MongoDB gewählt [20]. Mit einen Python-Skript wurden dort zusätzlich die Außentemperaturen aus der Online-Schnittstelle »Open Meteo« [21] und Emissionsfaktoren aus der Online-Datenbank ProBas [9] importiert.

Für die Autorensoftware Autodesk Revit [22] wurde ein Add-in programmiert. Mit dem Add-in werden die Gebäudedaten in die MongoDB übertragen sowie die Emissionswerte berechnet und visualisiert. Über die Benutzeroberfläche des Add-ins wird die Zuordnung der Sensoren zu Räumen ermöglicht und die tatsächlichen Emissionswerte werden den Emissionswerten, die sich aus dem Heizbedarf nach DIN-Norm (DIN V 18599) ergeben, gegenübergestellt (siehe Abbildung 2).

## 4 Fazit und Ausblick

Dieses Paper beleuchtet die Integration von IoT-Technologie und dem Building Information Model (BIM) zur Verbesserung der Nachhaltigkeitsbewertung von Gebäuden. Angesichts der steigenden Anforderungen an Unternehmen sowohl finanzielle als auch nicht-finanzielle Berichte zu erstellen, gewinnt die präzise Erfassung und Analyse des Energieverbrauchs in Gebäuden an Bedeutung.

Durch die demonstrative Umsetzung mit einem LoRaWAN-basierten Sensornetzwerk und der Verknüpfung dieser Daten mit einem BIM wird gezeigt, wie das Heizverhalten der Nutzer erfasst und analysiert werden kann. Mit diesen Informationen können Gebäudemanager und -betreiber fundierte Entscheidungen zur Verbesserung der Energieeffizienz und Nachhaltigkeit ihrer Gebäude treffen. Insgesamt bietet die Integration von IoT und BIM eine vielversprechende Methode zur Optimierung des Gebäudemanagements und zur Förderung nachhaltiger Praktiken. Im nächsten Schritt gilt es weitere Sensoren zur Erfassung des Nutzerverhaltens zu integrieren und in einem Versuchsaufbau die erfassten Daten zu validieren.

## Literatur

[1] *Corporate sustainability reporting - European Commission*, en. Adresse: https://finance.ec.europa.eu/capital-markets-union-and-financial-markets/company-reporting-and-auditing/company-reporting/corporate-sustainability-reporting_en (besucht am 25. 06. 2024).

[2] *World Energy Outlook 2019 – Analysis*, en-GB, Nov. 2019. Adresse: https://www.iea.org/reports/world-energy-outlook-2019 (besucht am 02. 07. 2024).

[3] Z. Besenyöi, »Towards a BIM-supported facility management knowledge management system for energy efficient building operations by rule-based code compliance checking«, en, 2022. Adresse: https://depositonce.tu-berlin.de/handle/11303/17260 (besucht am 02. 07. 2024).

[4] I. Motawa und K. Carter, »Sustainable BIM-based Evaluation of Buildings«, *Procedia - Social and Behavioral Sciences*, Jg. 74, S. 419–428, 2013. DOI: https://doi.org/10.1016/j.sbspro.2013.03.015. Adresse: https://www.sciencedirect.com/science/article/pii/S1877042813004448.

[5] K. Sorri, N. Mustafee und M. Seppänen, »Revisiting IoT definitions: A framework towards comprehensive use«, *Technological Forecasting and Social Change*, Jg. 179, S. 121 623, 2022. DOI: https://doi.org/10.1016/j.techfore.2022.121623. Adresse: https://www.sciencedirect.com/science/article/pii/S004016252200155X.

[6] J. Kopfmüller, »Nachhaltigkeitsbewertung«, in *Handbuch Technikethik*, A. Grunwald und R. Hillerbrand, Hrsg. Stuttgart: J.B. Metzler, 2021, S. 482–487. DOI: 10.1007/978-3-476-04901-8_92. Adresse: https://doi.org/10.1007/978-3-476-04901-8_92.

[7] F. Mneimneh, M. Al Kodsi, M. Chamoun, M. Basharoush und S. Ramakrishna, »How Can Green Energy Technology Innovations Improve the Carbon-Related Environmental Dimension of ESG Rating?«, *Circular Economy and Sustainability*, Jg. 3, Nr. 4, S. 2183–2199, Dez. 2023. DOI: 10.1007/s43615-023-00261-6. Adresse: https://doi.org/10.1007/s43615-023-00261-6.

[8] K. Balakrishnan, J. E. Core und R. S. Verdi, »The relation between reporting quality and financing and investment: Evidence from changes in financing capacity«, *Journal of Accounting Research*, Jg. 52, Nr. 1, S. 1–36, 2014.

[9] Umweltbundesamt, *Prozessorientierte Basisdaten für Umweltmanagement-Instrumente*, 2024. Adresse: https://www.probas.umweltbundesamt.de/ (besucht am 03. 07. 2024).

[10] M. Feldmeier und J. A. Paradiso, »Personalized HVAC control system«, in *2010 Internet of Things (IOT)*, 2010, S. 1–8. DOI: 10.1109/IOT.2010.5678444.

[11] M. Jia, A. Komeily, Y. Wang und R. S. Srinivasan, »Adopting Internet of Things for the development of smart buildings: A review of enabling technologies and applications«, *Automation in Construction*, Jg. 101, S. 111–126, 2019.

[12] J. Scott, A. Bernheim Brush, J. Krumm u. a., »PreHeat: controlling home heating using occupancy prediction«, in *Proceedings of the 13th international conference on Ubiquitous computing*, 2011, S. 281–290.

[13] J. Louis und K. Rashid, »Utilizing building information models as operating systems for smart homes«, in *Proceedings of the Workshop on Human-Habitat for Health (H3): Human-Habitat Multimodal Interaction for Promoting Health and Well-Being in the Internet of Things Era*, Ser. H3 '18, Boulder, Colorado: Association for Computing Machinery, 2018. DOI: 10.1145/3279963.3281658. Adresse: https://doi.org/10.1145/3279963.3281658.

[14] M. Arslan, Z. Riaz, A. Kiani und S. Azhar, »Real-time environmental monitoring, visualization and notification system for construction H&S management«, *Journal of Information Technology in Construction (ITcon)*, Jg. 19, S. 72–91, Juni 2014.

[15] M. Alves, P. Carreira und A. A. Costa, »BIMSL: A generic approach to the integration of building information models with real-time sensor data«, *Automation in Construction*, Jg. 84, S. 304–314, 2017. DOI: https://doi.org/10.1016/j.autcon.2017.09.005. Adresse: https://www.sciencedirect.com/science/article/pii/S0926580516303648.

[16] E. Curry, J. O'Donnell, E. Corry, S. Hasan, M. Keane und S. O'Riain, »Linking building data in the cloud: Integrating cross-domain building data using linked data«, *Advanced Engineering Informatics*, Jg. 27, Nr. 2, S. 206–219, 2013. DOI: https://doi.org/10.1016/j.aei.2012.10.003. Adresse: https://www.sciencedirect.com/science/article/pii/S1474034612000961.

[17] M. Dibley, H. Li, Y. Rezgui und J. Miles, »An ontology framework for intelligent sensor-based building monitoring«, *Automation in Construction*, Jg. 28, S. 1–14, 2012. DOI: https://doi.org/10.1016/j.autcon.2012.05.018. Adresse: https://www.sciencedirect.com/science/article/pii/S0926580512001124.

[18] *Homepage*, en-US. Adresse: https://intandem.autodesk.com/ (besucht am 29. 05. 2024).

[19] *The Arduino Guide to LoRa® and LoRaWAN® | Arduino Documentation*. Adresse: https://docs.arduino.cc/learn/communication/lorawan-101/ (besucht am 03. 07. 2024).

[20] *MongoDB: Die Datenplattform Für Entwickler*, de. Adresse: https://www.mongodb.com/de-de (besucht am 22. 05. 2024).

[21] *Homepage*, en-US. Adresse: https://https://open-meteo.com/ (besucht am 29. 05. 2024).

[22] *Autodesk Revit | Preise ansehen & offizielle Revit-Software kaufen*, de-DE. Adresse: https://www.autodesk.de/products/revit/overview (besucht am 05. 07. 2024).

# Developing rule-based model checking for verifying energy properties of windows: Promoting sustainable construction practices

Janees Riyaz[1] and Emara Merna[2]
[1,2]Institut für Bauinformatik, Technical University of Dresden, Nürnberger Str. 31a, 01062 Dresden, Germany
E-mail(s): janees_riyaz.janees_riyaz@mailbox.tu-dresden.de, merna.emara@tu-dresden.de

**Abstract:** Within the Architecture, Engineering and Construction (AEC) sector, collaboration among diverse stakeholders is essential for successful construction projects. The industry is witnessing a digital transformation, characterised by the emerging advancements in technology, ensuring co-operation across the project lifecycle. This study aims to reinforce models against deviations from construction standards, focusing on energy efficiency. To achieve this, model checking methodologies are considered, involving a comprehensive examination of prevailing industry standards and regulations for buildings which ultimately results in the formulation of custom rulesets for Solibri Model Checker. The research is verified through a case study which involves enhancement of the BIM model and checking against various rulesets for verifying energy properties of windows in Solibri. Through precise verification process, the efficacy of the developed model-checking framework is assessed.This undertaking streamlines project execution, mitigates risks, and enhances compliance with energy efficiency imperatives. This contributes to refining model technologies in the AEC domain and catalyses advancements towards more sustainable and efficient construction practices.
*Keywords:* Building Information Modelling (BIM), custom rulesets, energy efficiency, model checking, sustainable design.

Erschienen in Tagungsband 35. Forum Bauinformatik 2024, Hamburg, Deutschland, DOI: 10.15480/882.13552
© 2024 Das Copyright für diesen Beitrag liegt bei den Autoren. Verwendung erlaubt unter Creative Commons Lizenz Namensnennung 4.0 International.

## 1 Introduction

In the ever-evolving field of Architecture, Engineering and Construction (AEC), the use of sustainable practices play a crucial role in enhancing environmental responsibility and operational efficiency. Building Information Modelling (BIM) represents a methodical approach that covers the generation, storage, management, sharing, and distribution of building information in a manner ensuring compatibility and reusability. This approach requires the utilization of computer-generated models to effectively imitate the various stages of a project, including planning, design, construction, and operation [1]. The adoption of Building Information Modelling (BIM) has transformed the management of projects, offering all stakeholders an intricate digital representation of physical structures. It brings various benefits such

as improved accuracy, saving of time, better design and analysis approaches, and the ability to foresee environmental and lifecycle outcomes [2]. However, with the sector's shift towards digital twins - virtual models of real-world assets, the growing necessity to put a stronger emphasis on energy efficiency within these replicas has become increasingly important. Energy efficiency is a crucial element in today's construction sector having a big influence on sustainability, cost-effectiveness and compliance with regulations. Buildings account for a significant share of global energy use and greenhouse gas emissions, making energy optimization crucial.This shift has made sure that comprehensive model checking procedures must be included in the Building Information Models to ensure compliance with energy efficiency regulations.The coming together of different stakeholders in the process and the complexity of the projects necessitates the need of a cohesive strategy.

This research encompasses a comprehensive approach towards enhancing energy efficiency in AEC projects through the development and deployment of model-checking methodologies.Windows significantly impact energy efficiency, as their inefficiency can lead to substantial heat loss and gain. Therefore, a targeted approach to assess and optimize their energy properties is crucial for enhancing building sustainability. Through examination of relevant standards for energy efficiency and developing rulesets for model checking to optimise energy usage for windows, it seeks to catalyse a paradigm shift towards greener and more resilient built environments by reducing energy costs and consequent reduction in the carbon footprint. The primary focus is on the "Förderschule Delitzsch" building as a case study where the effectiveness of the developed procedures is verified.

## 2 Methodology

This research presents an approach to enhance energy efficiency in AEC projects, with a specific focus on window optimization within Building Information Modelling (BIM) framework. The methodology encompasses several phases: Analysing standards, ruleset creation, BIM model enhancement and model checking as shown in Figure 1. The initial phase involves gathering data on energy efficiency standards and regulations pertinent to window performance. This includes reviewing existing literatures, codes, and guidelines. To ensure compliance with these standards, a comprehensive set of rules is formulated in the ruleset creation phase. These rules are based on the standards identified during the first phase and are designed to assess the energy performance of windows within the BIM model. Using the collected data, the BIM model is enhanced. The last phase involves model checking which involves running the model through the rulesets to identify any deviations from the established energy efficiency criteria. The model checking process highlights areas where windows do not meet the desired performance standards, providing specific feedback for optimization. Based on the results, iterative modifications can be made to the window properties to enhance energy efficiency. By adopting model checking techniques and rule sets derived from energy standards, the methodology provides a framework for identifying and rectifying inefficiencies in window design.

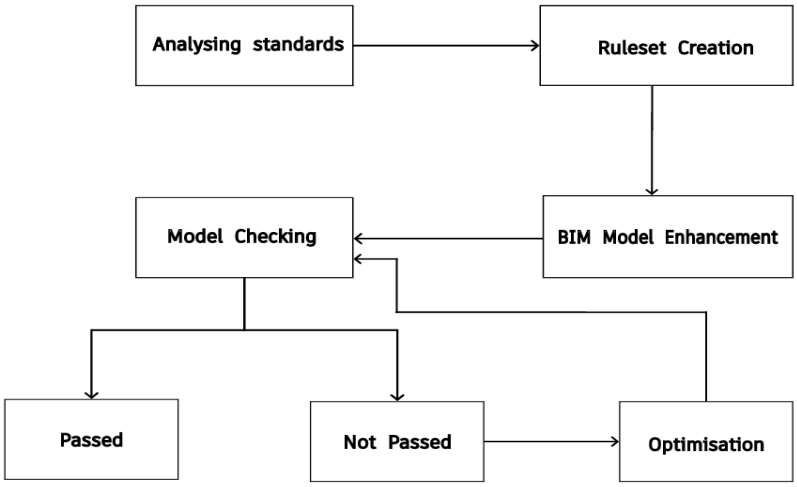


Figure 1: Methodology Overview

# 3 Implementation

## 3.1 Analysing Standards

The standard followed for verifying energy properties in windows is *Gesetz zur Einsparung von Energie und zur Nutzung erneuerbarer Energien zur Wärme- und Kälteerzeugung in Gebäuden* (Act on Energy Conservation and the Use of Renewable Energies for Heating and Cooling in Buildings) [3]. In addition to this, MVV TB - *Muster-Verwaltungsvorschrift Technische Baubestimmungen* 2023/1-part A6 (Publication of the Model Administrative Regulation Technical building regulations) [4] has been used which references various DIN codes including DIN 4108-2/2013-02 [5] and DIN 4108-7 [6] that have been used.

## 3.2 Ruleset Creation

The creation of rulesets for verification of energy properties for windows is carried out in the Ruleset Manager in Solibri. In the Libraries section, Solibri Common Rules contains multiple rule templates which can be customised as per the requirements of a specific task. For the scope of this research, Rule 203- 'Required Property Sets' was used to create all the rulesets required for verification of the case study building. According to Solibri Model Checker, this ruleset is used to verify whether a model contains required property sets and properties and that these properties contain a value or doesn't contain a value and then whether this value is acceptable or not. It consists of two component filters: Firstly, 'Checked Components'- where the rule checks whether the model contains a specific property or a value, secondly 'Property Sets'- where it checks whether the component that fulfils the first condition is fulfilling another property sets filter condition. If the properties are not fulfilling as per the criteria set in the rule, Solibri reports it as an issue [7]. The layout of the Rule 203 in the Ruleset Manager can be seen in figure 2.

The rules were created for checking the windows against all the parameters relevant for energy usage. The different codes and regulations were used to set up standard values for these properties. Gebäudeenergiegesetz provides the recommendation for the heat transfer coefficient (U value) to be

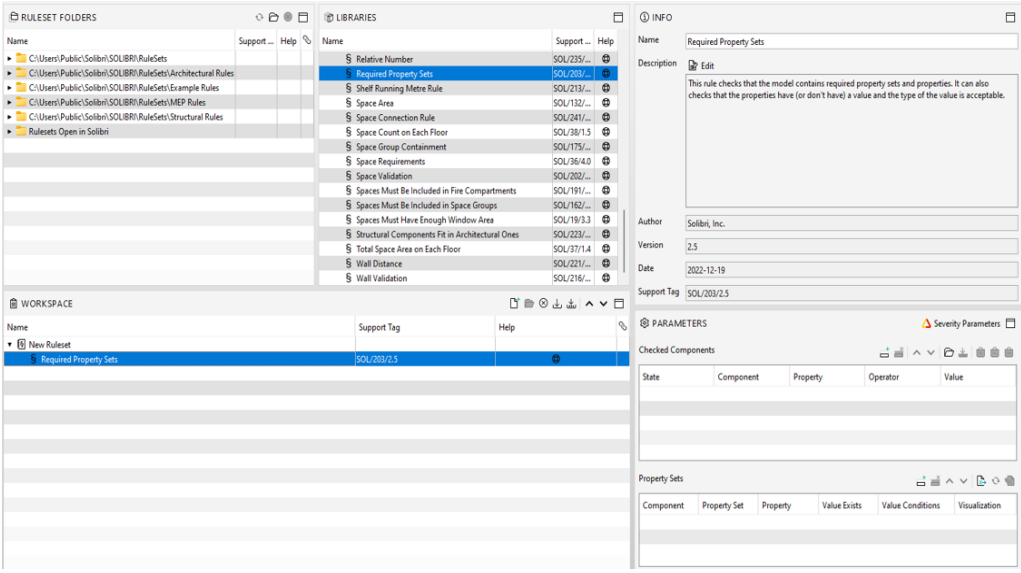


Figure 2: Solibri Common rule SOL/203/2.5

$1.3$ W/(m$^2 \cdot$ K). [3] The Heat transfer coefficient for window frames ($U_f$) should be less than or equal to $2.9$ W/(m$^2 \cdot$ K) and the Thermal resistance ($R$) should be greater than or equal to $1.2$ m$^2$ K/W as per DIN 4108-2/2013-02 [5]. Figure 3 shows the ruleset for the heat transfer coefficient. The rulesets for the Heat transfer coefficient for window frames $U_f$ and Thermal resistance $R$ were created in a similar fashion with their respective values in the Parameters Tab.

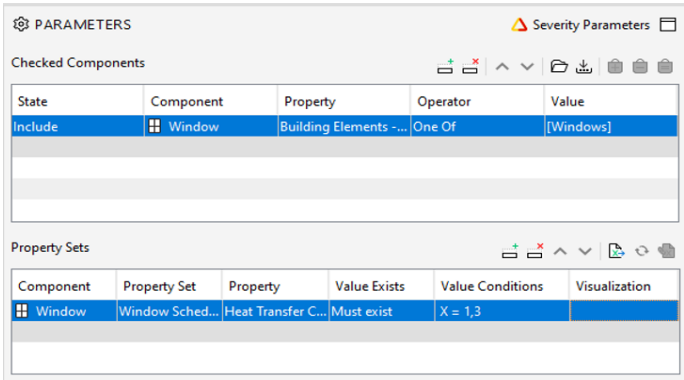


Figure 3: Ruleset for Heat Transfer Coefficient (Solibri 9.13.7)

For the creation of other rulesets viz, Visual Light Transmittance, Energy Transmittance and Daylight Supply Factor, shading was taken into consideration. Gebäudeenergiegesetz provides values for these properties depending upon whether there is sun protection or not as outlined in Table 1 [3].

Table 1: Values for properties

| Property | With sun protection | Without sun protection |
|---|---|---|
| Visual Light Transmittance | 0.62 | 0.78 |
| Energy Transmittance | 0.35 | 0.60 |
| Daylight Supply Factor | 0.15 | 0.70 |

Figure 4 shows the creation of ruleset for checking Visual light transmittance. The rule for other two properties were created in a similar way as per discussed values in Table 1.

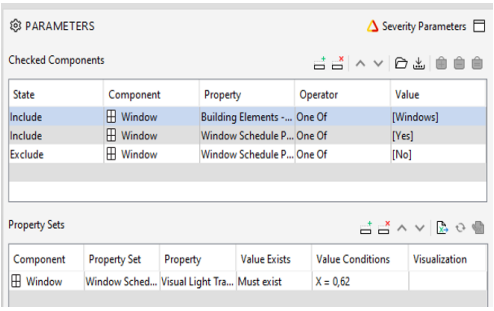


(a) With solar glazing

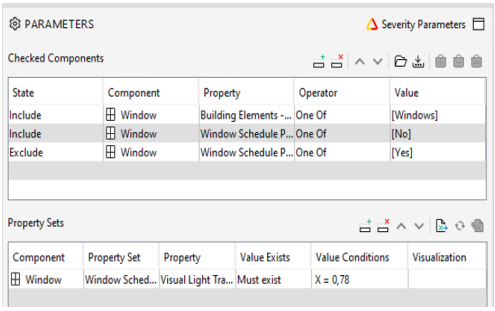


(b) Without solar glazing

Figure 4: Ruleset for Visual Light Transmittance (Solibri 9.13.7)

The ruleset created for checking the Irradiance depends upon the direction windows are facing. Accordingly, DIN 4108-2/2013-02 provides irradiance guidelines for residential and non-residential buildings and the latter have been taken into consideration. The guideline states that the value should be $150W/\mathrm{m}^2$ for windows facing North, North-East, North-west directions and $200W/\mathrm{m}^2$ for windows facing South, East and West direction [5]. Figure 5 illustrates the incorporation of the 'Orientation' parameter within Revit and the specific rules created for windows based on their orientation for windows facing North, South, East and West.

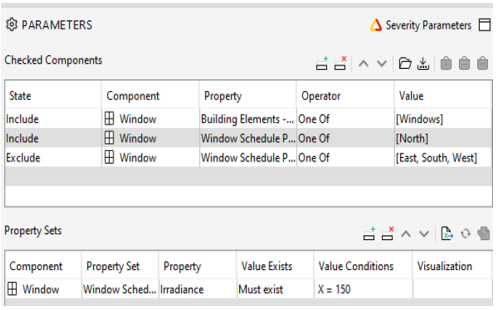


(a) For windows facing North

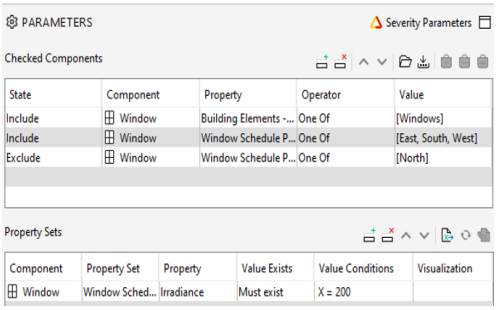


(b) For windows facing South, East and West

Figure 5: Ruleset for Irradiance Check (Solibri 9.13.7)

## 3.3 Case Study

The case study is a school building namely 'Förderschule Delitzsch' . It is built on Delitzscher Richard-Wagner-Straße. This is a new building which will accommodate two school buildings: Pestalozzi School and the Fröbel School and the capacity is for 300 students. The building is based on a modern energy concept. It is built by district of North Saxony, with an investment of 24.2 million euros [8]. The BIM model of this building shown in figure 6 is developed in Revit. The windows in this model serve as a use case for verifying energy properties. Monitoring and optimizing these properties can enhance sustainability by reducing energy costs and consequently lowering the carbon footprint.

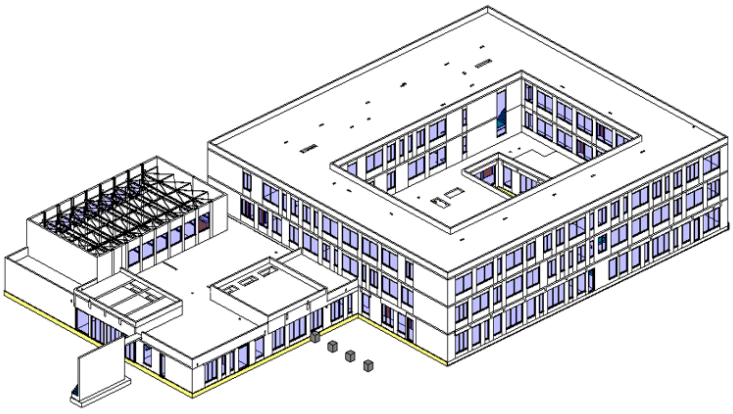

Figure 6: Case study building(Revit)

### 3.4 Enhancing the BIM Model

The Revit model for the case study building is enhanced to an appropriate level of detail, incorporating both the Level of Geometry (LOG) and the Level of Information (LOI). Once the enhancement is carried out, it is exported as an IFC file.

For having a suitable level of geometry, the modelling of windows and doors is carried out in Revit by utilizing the in-built Autodesk families. Additionally, a thorough examination of parameters associated with windows was carried out in Revit to address the information level. The type of glass selected for windows is ‘Double glazing - 1/4 in thick - clear/low-E (e = 0.05) glass’. This type was chosen due to its reputation as the best choice for school buildings in terms of sustainability taking carbon emissions and social impact into consideration. Even though a triple glazing window offers better noise reduction but that is not economical and results in higher emissions. [9]

There are two types of parameters for windows in Revit viz, default and custom. The default parameters associated with families are Visual light transmittance, Heat transfer coefficient (U) and Thermal resistance (R). The custom parameters created are Irradiance, Daylight Supply Factor, Energy Transmittance (Glazing), Shading and U-value window frame. These parameters have been created in accordance with relevant codes and regulations for windows, recognizing their crucial role in meeting standards. The values for these parameters were assigned based on previous research or practical insights in Germany with similar criteria. All the parameters were compiled in a schedule ‘Window Schedule Pset’ in Revit. The name for the schedule has "Pset" at the end rather than as a prefix, in accordance with IFC guidelines stating that the name for a user-defined property set should not include "Pset" as a prefix [10].

To enable seamless information exchange from Revit to Solibri, the model was exported as two IFC files: one for ’Structural’ and one for ’Architectural’ elements. A custom export setup was carefully configured to tailor the properties of the IFC files to specific project needs. During the export process, the project schedule was integrated as a property set, utilizing the ’Modify Setup’ tab in Revit. This

ensured that the schedule data was embedded within the 'Property Sets' of the IFC files, facilitating a more comprehensive data transfer to Solibri.

### 3.5 Model Checking Results

All the created rules were combined into a collective ruleset named 'Energy Properties of Windows Check,' which was then used to perform the checks, yielding the results shown in Figure 7.

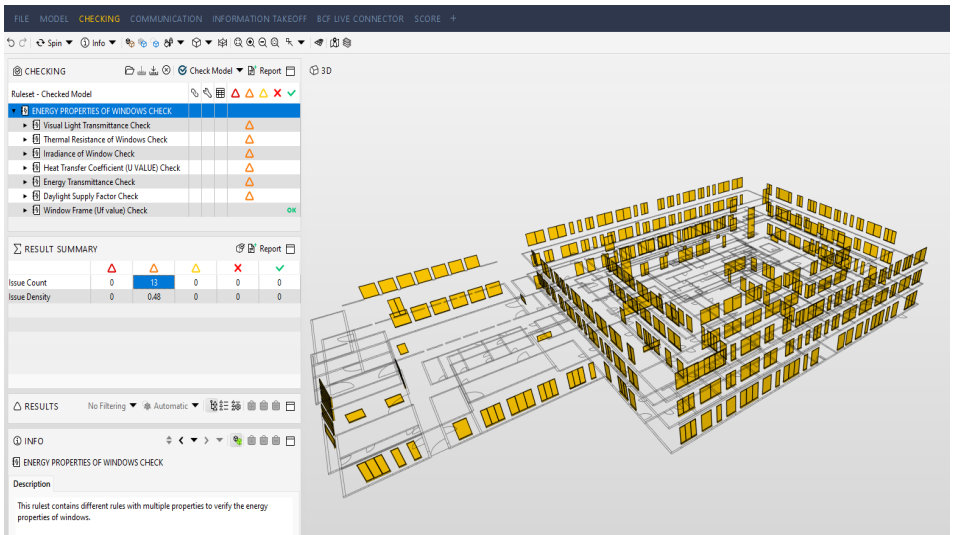


Figure 7: Ruleset checking results in Solibri

Only one ruleset namely U value for window frame passed the check as the values for all other properties were outside the acceptable range according to regulations. Hence the optimisation of window material needs to be performed for all the parameters to pass the checks and be energy efficient. The results were communicated using presentation in Solibri where all the issues are summed up and later communicated through the BIM Collaboration Format(BCF) Live Connector to the issue management platform 'BIMcollab'.

## 4 Conclusion

This research has developed a method that can be used to check a building model against deflections from industry standards keeping energy efficiency on high priority. An extensive examination of prevailing industry standards and regulations was conducted using multiple databases including DIN codes and energy standards in Germany. Using this information, the requirements related to energy efficiency for windows are laid down in terms of rulesets through model checking. The efficacy of the developed model-checking framework was rigorously assessed through a case study centered on the BIM Model of the "Förderschule Delitzsch" building. The verification through accessing the energy properties of windows result in the development of a framework utilising BIM to support efficient and effective workflow. It paves a way to have better transparency in material choices for windows and better insulation properties leading to a comfortable and greener environment through less energy consumption. In future, these created rulesets can be extended to buildings with diverse utilities and various components including doors, walls, and floors, sourced from existing codes to enhance

energy efficiency. Incorporating standards such as 'PassiveHaus Institut' can further strengthen the framework, ensuring even more rigorous energy efficiency checks. By embracing these strategies and harnessing the abundance of real-time data available, one can revolutionize the effectiveness and precision of energy efficiency checks in buildings, paving the way for a more sustainable environment.

## Acknowledgements

The publication is part of the research project entitled "iECO – Intelligence Empowerment of Construction Industry" which has received funding from Bundesministerium für Wirtschaft und Klimaschutz (BMWK) based on a resolution of the German Bundestag. The authors gratefully acknowledge the support and funding from the BMWK. The content of this publication reflects the author view only and the BMWK is not responsible for any use that may be made of the information it contains.

## References

[1] Loan Petri, Ali Hussain S Alhamami, Yacine Rezgui, and Sylvain Kubicki, "Bim for energy efficiency requirements capture", Mar. 2018.

[2] S. Beazley, E. Heffernan, and T. J. McCarthy, "Enhancing energy efficiency in residential buildings through the use of bim: The case for embedding parameters during design", *Energy Procedia*, vol. 121, pp. 57–64, 2017. DOI: 10.1016/j.egypro.2017.07.479.

[3] "Geg: Gebäudeenergiegesetz vom 8. august 2020 (bgbl. i s. 1728), das zuletzt durch artikel 1 des gesetzes vom 16. oktober 2023", Aug. 2020.

[4] "Mvv tb 2023/1, ausgabe 2: Veröffentlichung der muster-verwaltungsvorschrift technische baubestimmungen 2023/1", Apr. 2023. [Online]. Available: https://www.dibt.de/de/aktuelles/meldungen/nachricht-detail/meldung/mvv-tb-20231-veroeffentlicht.

[5] Baunormenlexikon, *Din 4108-2 | 2013-02: Thermal insulation and energy saving in buildings - part 2: Minimum requirements for thermal insulation*. [Online]. Available: https://www.baunormenlexikon.de/norm/din-4108-2/a06abee6-e691-4f50-959d-f42cce00bc7c.

[6] DIN 4108-7, *Thermal insulation and energy economy in buildings: Part 7: Air tightness of buildings*, Jan. 2011. [Online]. Available: https://nautos.de/O9G/search/item-detail/DE30042761.

[7] Solibri, *230 property rule template with component filters*. [Online]. Available: https://help.solibri.com/hc/en-us/articles/1500004738562-230-Property-Rule-Template-with-Component-Filters.

[8] *Stadt delitzsch*, Jan. 2022. [Online]. Available: https://www.delitzsch.de/portal/meldungen/landkreis-investiert-24-2-millionen-euro-in-neuen-foerderschulcampus-900001552-27640.html.

[9] A. T. Balasbaneh, D. Yeoh, and A. R. Zainal Abidin, "Life cycle sustainability assessment of window renovations in schools against noise pollution in tropical climates", *Journal of Building Engineering*, vol. 32, p. 101 784, 2020. DOI: 10.1016/j.jobe.2020.101784.

[10] IFC4_ADD2_TC1 - 4.0.2.1, *Version 4.0 - addendum 2 - technical corrigendum 1*. [Online]. Available: https://standards.buildingsmart.org/IFC/RELEASE/IFC4/ADD2_TC1/HTML/.

# Urban Tree Placement Analysis: A GIS-Based Approach for Identifying Suitable Planting Locations in Munich

Roland Reitberger[1], Nayanesh Pattnaik[2] and Ying Lu[1]
[1]Chair of Energy Efficient and Sustainable Design and Building, Technical University of Munich, Arcisstraße 21, 80333 Munich, Germany
[2]Chair for Strategic Landscape Planning and Management, Technical University of Munich, Emil-Ramann-Str. 6, 85354 Freising, Germany
E-mail(s): roland.reitberger@tum.de

**Abstract:** Trees provide various ecosystem services to humans. Therefore, increasing their number in urban areas is necessary. Identifying suitable tree planting locations is essential for cities' resource allocation. However, city-wide information, such as underground pipes, is hardly available. In this paper, we introduce a GIS-based method to identify potential tree planting locations within Munich, utilizing aboveground data. Our methodology combines imperviousness-levels with existing tree data from remote observations. This enables us to investigate tree distribution across different imperviousness levels, identifying areas unsuitable for tree planting. This approach is applied to several land use typologies, thereby identifying suitable planting distances from buildings. We perform a distance analysis for existing trees to identify the nearest neighboring tree for each individual tree. By analyzing the distribution and counts of tree-to-tree distances, a suitable distance between two trees is determined from real-world data. Our case study in Munich exemplifies the methodology. The key findings are that locations with up to 81 % imperviousness can sustain a significant probability for tree planting. Suitable planting distances vary by land use typology. The common spacing between tree pairs is 2.97 meters. The results offer insights into urban areas with a high potential for additional trees, based on above-ground data.

*Keywords:* Tree Locations, GIS Analysis, Urban Green Infrastructure, Empirical Tree Placement

Erschienen in Tagungsband 35. Forum Bauinformatik 2024, Hamburg, Deutschland, DOI: 10.15480/882.13517
© 2024 Das Copyright für diesen Beitrag liegt bei den Autoren. Verwendung erlaubt unter Creative Commons Lizenz Namensnennung 4.0 International.

## 1 Introduction

Urban trees are an important element of sustainable and resilient cities [1], [2]. However, planting areas are often limited due to restricted urban land resources, making it essential to identify suitable locations. This process is challenging due to the lack of underground infrastructure data as different institutions manage various underground utilities in cities, leading to fragmented and inconsistent information.

Additionally, street tree planting is complex and difficult to reconfigure, as several interactive constraints must be considered in the decision-making process. To address these issues, we propose a GIS-based method using available above-ground data, including existing tree locations, land use typologies, imperviousness levels, and existing building locations. This approach enables the assessment of urban areas for suitability concerning tree planting. The objective of this study is to present a data-driven methodology that facilitates the increase of urban greenery and allows the identification of suitable tree planting locations.

## 2 State of the Art

In urban environments, Geographic Information Systems (GIS) are effective tools for identifying potential tree planting sites. Wu et al. [3] developed a GIS method that uses land cover data to accurately determine these locations in a case study in Los Angeles. Their methodology enhances urban forestry planning by ensuring that new trees do not overlap with existing ones and are suitably distanced from impervious surfaces, thereby maximizing ecosystem services. However, this method demands huge computing power. Kirnbauer et al. [4] developed ArcTrees, which identifies plantable areas and suggests tree placement in urban areas. Their approach requires data on urban infrastructure, such as pipes, hydro lines, and gas lines. Buffers between existing infrastructure and new planting locations need to be defined by the user. The authors applied the approach to a case study in Ontario, Canada, and evaluated the shading from additional trees.

GIS clearly plays an important role in identifying potential planting sites and enables the quantification of increased canopy cover. However, the reliability of such methods heavily depends on the accuracy of the input data [5]. Our study proposes an improvement to the existing methods by combining several empirical rules within the GIS framework, intending to provide more accurate tree planting recommendations for urban tree managers.

## 3 Methodology

The methodology, adapted from Wu et al. [3], comprises two principal modules: 'Site Identification' and 'Tree Placement', as shown in Figure 1. The 'Site Identification' module identifies the ideal planting area, while the 'Tree Placement' module determines the most suitable locations for trees in those areas. The process starts by deriving planting criteria from the existing aboveground data. Therefore, permeable surfaces, distances between existing trees, and distances between trees and buildings are analyzed. As a result of this step, criteria for different land use typologies are developed to ensure sufficient growing space and conditions for new trees.

Subsequently, sample points in potential planting areas are generated. The 'Tree Placement' module commences with a statistical analysis of existing trees to calculate the crown radius values of the majority of trees. New trees are assumed to develop a crown radius of the 75th percentile because larger trees can provide more benefits for biodiversity and enhance ecosystem services [6]. Consequently, the minimum distance between two points is set at least twice the statistically derived radius value when generating sample points. To illustrate the efficiency of this methodology, a case study in Munich is employed to identify suitable planting locations.

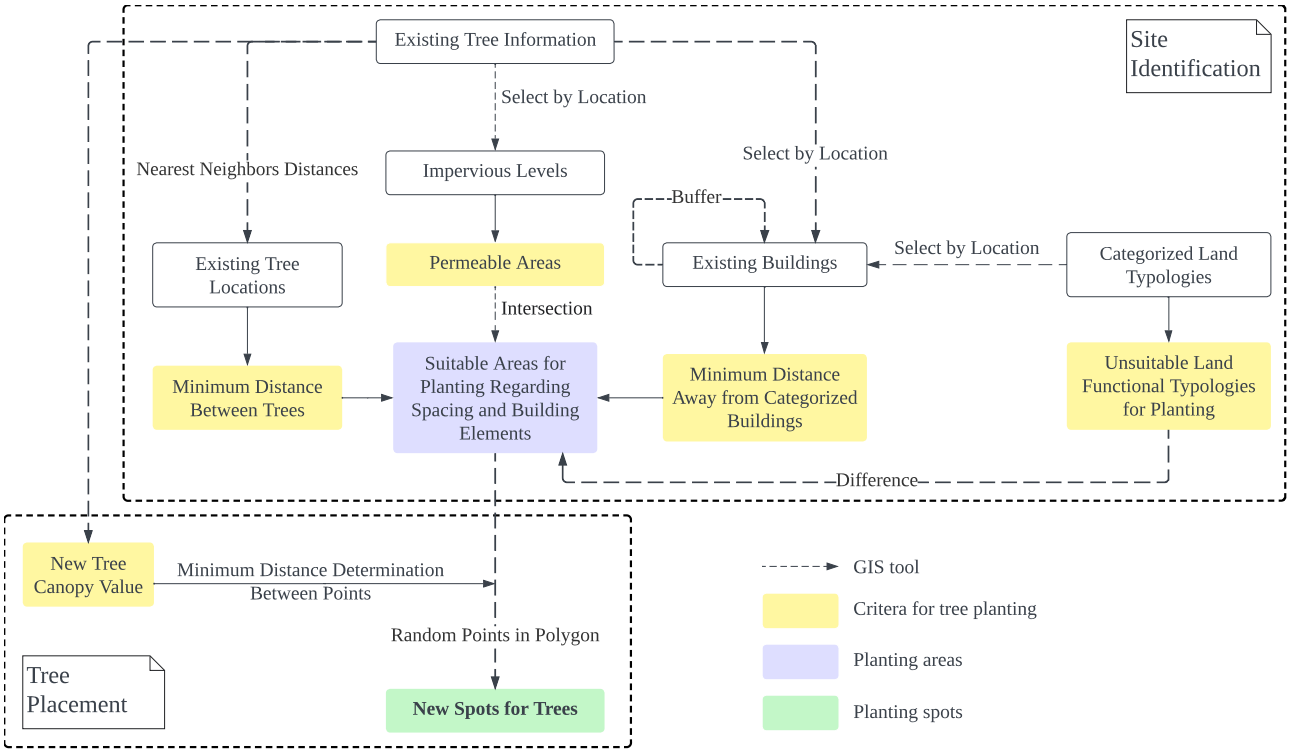


Figure 1: Flowchart of the proposed tree planting methodology

## 3.1 Data Preparation

Data is gathered and prepared involving the following steps:
(1) Existing Tree Information: Gather data on existing trees' locations and crown radii in Munich. This data is the basis for tree geometry and tree distance analysis. It is received from [7].
(2) Imperviousness Levels: Obtain data on imperviousness levels (imperviousness density) from the Copernicus website, with a resolution of 10 meters by 10 meters [8]. This data allows to integrate the extent of non-permeable surfaces in the area.
(3) Existing Buildings: Gather information on the locations of buildings for the subsequent analysis [9].
(4) Categorized Land Typologies: Collect data on different land typologies to categorize various land uses and identify functional areas unsuitable for planting. The urban typology is received from [10].

## 3.2 Spatial Analysis

### 3.2.1 Impervious Surfaces Analysis

Urban trees are surrounded by impervious surfaces, which impact their growth and function [11]. Here, the distribution of trees relative to different levels of imperviousness is assessed, providing insights into the interaction between urban greenery and non-permeable urban surfaces.

### 3.2.2 Building Proximity Analysis

The buildings are categorized by their land use typologies into four labels. A spatial join is performed between the buildings and land typologies, assigning each building the appropriate label. The details are presented in Table 1. Subsequently, buffers around each labeled building are created. The buffers

increment from 0 to 6 meters in steps of 0.01 meters. This process enables the assessment of the variation in tree density with increasing distance from buildings in different categories. The evaluation aims to identify the minimum distance from buildings for suitable tree growth.

Table 1: Tree counts by land use typology

| Label | Land Use Typology | Tree Count |
|---|---|---|
| A | Housing block trees | 295,464 |
| B | Street trees | 19,089 |
| C | Urban green spaces | 11,169 |
| D | Industrial-business trees | 4,464 |

#### 3.2.3 Tree Pair Proximity Analysis

A matrix distance analysis is performed on existing trees to identify the spatial proximity of the nearest neighboring tree for each individual tree, subsequently pairing them together. By analyzing the distribution and counts of these pairs, we aim to determine the suitable distance between two trees so that the individual tree canopies do not overlap excessively.

### 3.3 Statistical Analysis

#### 3.3.1 Impervious Surfaces Analysis

The relationship between impervious levels and tree counts is examined in Figure 2. Scatter points represent tree counts at varying impervious levels. A sixth-degree polynomial is fitted to the data points to model this relationship. Additionally, the 75th percentile of tree counts is calculated and represented by a horizontal dashed line, establishing a threshold. This threshold is employed to identify impervious levels below which the surfaces may be suitable for planting areas. Excluding data at the 0 % impervious level, the graph indicates that impervious levels below 81 % frequently occur in the existing data.

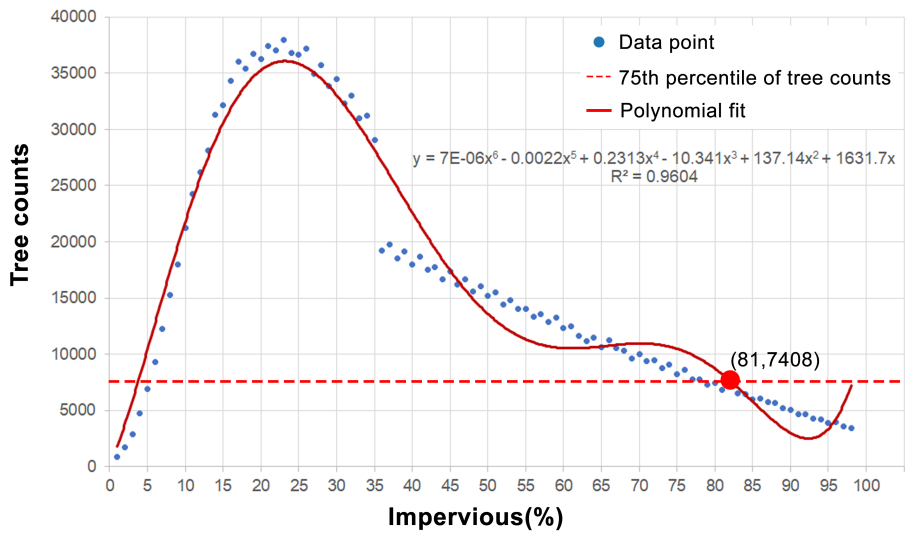


Figure 2: Tree counts in different imperviousness levels

### 3.3.2 Building Proximity Analysis

For labeled buildings, we focus on categories A, B, and D. For category A, we plot scatter points representing tree counts in each buffer ring. This shows that there is an increasing tendency in tree counts with increasing distances from the buildings, as depicted in Figure 3. To derive a threshold, we depict the rate of change in tree counts with increasing distance. Therefore, we plot the gradients between neighboring distance rings and smooth the trend of these changes, as shown in Figure 4. At a distance of approximately 0.91 meters, the rate of change in tree counts reaches a significant peak, suggesting this distance as suitable for tree planting. The same statistical methods are applied to categories B and D. For category B, the optimal distance is approximately 0.88 meters, and for category D, it is approximately 0.96 meters.

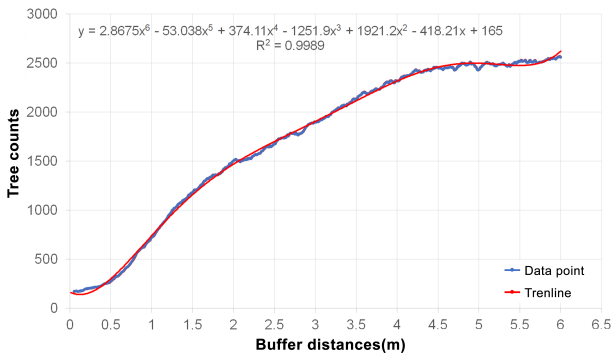


Figure 3: Incremental tree counts per 0.01 meter buffer distance for category A

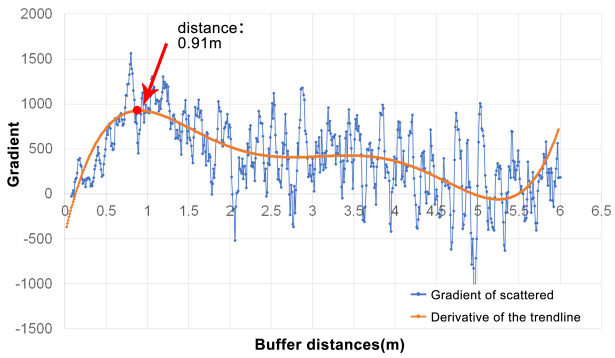


Figure 4: Gradient of tree counts change for category A

### 3.3.3 Tree Pair Proximity Analysis

To more accurately represent the relationships between tree pairs, we use the empirical cumulative distribution function (ECDF) plot (Figure 5) to describe the proportionate change as the distance between trees increases. We calculate the probability density of the ECDF (Figure 6) to identify the point of highest gradient increase. The peak probability density is observed at a distance of 2.97 meters.

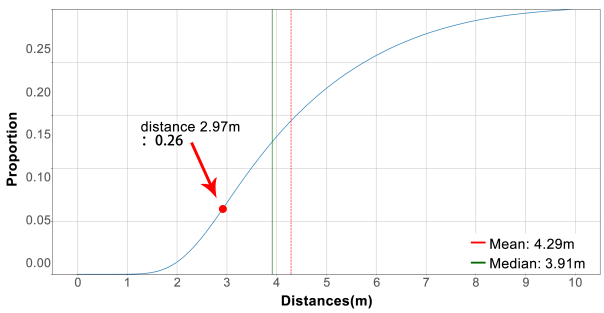


Figure 5: Distribution of nearest neighbor distances up to 10 meters

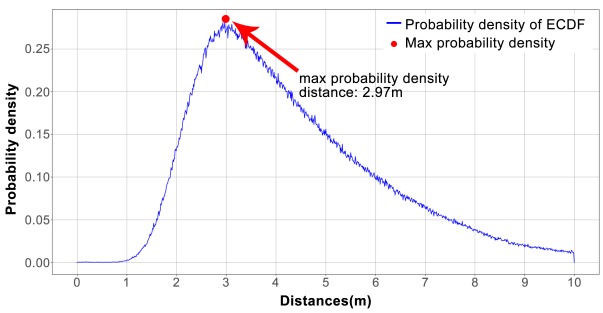


Figure 6: Probability density of nearest neighbor distance ECDF

### 3.4 Result for Site Identification

The comprehensive spatial and statistical analyses provide empirical rules for identifying potential tree planting areas. These are synthesized as follows:

- **Permeable areas**: The analysis indicates that areas with up to 81 % imperviousness can still support a significant probability for tree planting. In our case study, this threshold can serve as a criterion for identifying suitable permeable surfaces for tree planting.
- **Building proximity**: The optimal distance for tree planting varies by building categories. Overall, the ideal planting distances are between 0.88 meters (category B), 0.91 meters (A), and 0.96 meters (D). These distances help prevent damage from roots and branches while ensuring sufficient space for trees to grow [12].
- **Tree proximity**: The analysis suggests that the optimal spacing between tree pairs should be approximately 2.97 meters. This spacing ensures from a statistical perspective, that the trees in the new planting area do not overlap with the previous trees.

### 3.5 Results for Tree Planting

We apply the derived rules in an 85,000 $m^2$ study area in Munich to identify possible planting locations. For this purpose, the rules are translated into filtering functions in GIS. Additionally, it's essential to exclude certain functional typologies, such as roads, bicycle lanes, expressways, and water areas. This allows for a more accurate assessment of suitable planting locations.

To determine the expected crown radius of new trees, a statistical analysis of existing trees in Munich is conducted. The radius value at the 75th percentile is selected as the optimal choice because larger trees can provide greater benefits for biodiversity and enhance ecological functions [6]. Therefore, the resultant radius value for the new tree is standardized to 3.44 meters.

When generating sample points in potential planting areas using the GIS tool, the minimum distance between two points should be 6.88 meters. Upon completion of the above process, 103 generated points are observed. Figure 7 signifies the potential locations for tree planting within the specified case study area.

## 4 Discussion and Conclusion

This research introduced a GIS-based methodology to identify the most suitable locations for tree planting in urban areas, using Munich as a case study. The approach utilizes above-ground data, such as existing tree locations, imperviousness levels, and building locations, to avoid the common barrier of lacking detailed underground infrastructure data.

The methodology demonstrated its potential for enhancing urban greenery planning. The identified number of 103 planting locations in an area of 85,000 $m^2$ is comparable to the study of Kirnbauer et al. who found a potential of 141 and 123 large tree locations in an area of 68,500 and 55,400 $m^2$ [4]. Investigating the placement of trees based on empirical data and spatial analysis offers an extensible framework for cities aiming to expand their urban forests. Thus, urban planners should implement a practical, data-driven framework to increase canopy cover, thereby enhancing urban resilience against environmental challenges such as heat islands and air pollution [13]. This GIS-based approach provides a more precise decision-making process than alternative methodologies for identifying tree

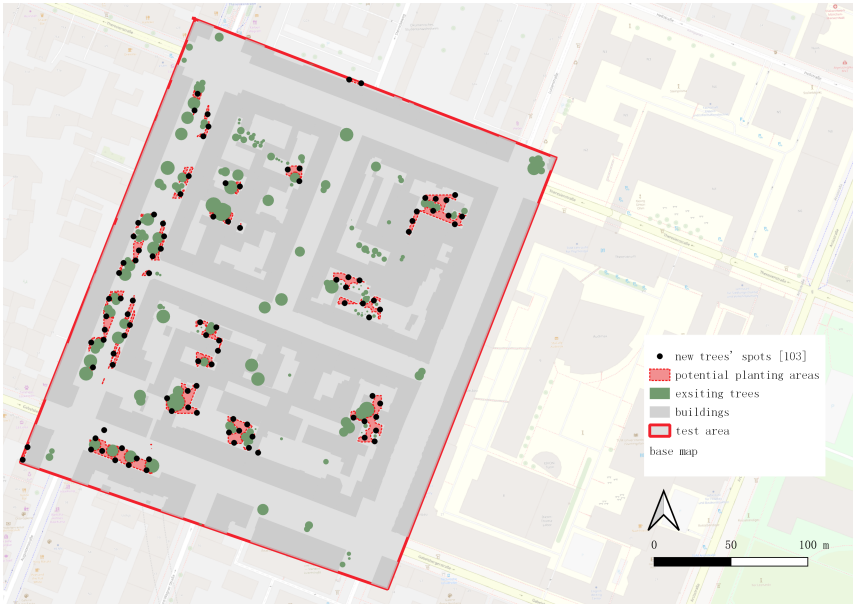


Figure 7: Identified tree locations by applying the methodology

locations that rely on underground data and user input. It uses a quantifiable and scalable method to assess the suitability of tree planting across various datasets, enhancing resource allocation and planning efficiency. However, this methodology has several limitations. It relies heavily on data availability, with the accuracy of impervious level division and land classification significantly influencing results. The accuracy level of impervious data is 10 meters, which can be large compared to the size of small districts. Inaccurate land classification could lead to misplanting trees. Additionally, only standardized trees were considered when generating sample points, ignoring different tree sizes. The reliance on existing datasets might bias the analysis towards well-surveyed areas, potentially overlooking newly urbanized regions or those with poor data coverage.

Future work should focus on integrating more multidimensional data and validating the methodology in various urban environments. Additionally, developing a more comprehensive approach tailored to different urban conditions is essential, as potential benefits provided by urban greenery heavily depend on the above and below-ground conditions in which trees are growing. Implementing machine learning models could further enhance the predictive capability of this methodology [14].

In conclusion, this study provides a framework for identifying urban areas suitable for tree planting that enhance ecosystem services while addressing the challenge of lacking underground data.

## Acknowledgements

This work was carried out within the research training group Urban Green Infrastructure, funded by the German Research Foundation under grant 437788427 - RTG 2679. The authors want to thank the State Office for Digitization, Broadband and Surveying and Leibnitz Institute for Ecological and Regional Development (Markus Münzinger) for providing the vegetation data for this study. Further, we thank Farzan Banihashemi and Hari Krishna Gadi from the chair of energy efficient and sustainable design and building for transferring the CityGML vegetation data into Geopandas.

## References

[1] E. Andersson, “Urban landscapes & sustainable cities”, *Ecology & society*, vol. 11, no. 1, 2006.

[2] R. Reitberger, N. Pattnaik, L. Parhizgar, *et al.*, “A systems perspective on the interactions between urban green infrastructure and the built environment”, *IOP Conference Series: Earth and Environmental Science*, vol. 1363, no. 012071, 2024.

[3] C. Wu, Q. Xiao, and E. G. McPherson, “A method for locating potential tree-planting sites in urban areas: A case study of Los Angeles, USA”, *Urban Forestry & Urban Greening*, vol. 7, no. 2, pp. 65–76, 2008.

[4] M. Kirnbauer, W. Kenney, C. Churchill, and B. Baetz, “A prototype decision support system for sustainable urban tree planting programs”, *Urban Forestry & Urban Greening*, vol. 8, no. 1, pp. 3–19, 2009. DOI: 10.1016/j.ufug.2008.11.002.

[5] R. Lunetta, R. Congalton, L. Fenstermaker, J. Jensen, K. Mcgwire, and L. R. Tinney, “Remote sensing and geographic information system data integration: Error sources and research issues”, *Photogrammetric engineering and remote sensing*, vol. 57, no. 6, pp. 677–687, 1991.

[6] K. Stagoll, D. B. Lindenmayer, E. Knight, J. Fischer, and A. D. Manning, “Large trees are keystone structures in urban parks”, *Conservation Letters*, vol. 5, no. 2, pp. 115–122, 2012.

[7] M. Münzinger, N. Prechtel, and M. Behnisch, “Mapping the urban forest in detail: From LiDAR point clouds to 3d tree models”, *Urban Forestry & Urban Greening*, vol. 74, no. 127637, 2022. DOI: 10.1016/j.ufug.2022.127637.

[8] E. M. Plan, *Imperviousness density 2018 (raster 10 m), europe, 3-yearly, aug. 2020*, 2018. [Online]. Available: https://land.copernicus.eu/en/products/high-resolution-layer-imperviousness/imperviousness-density-2018 (visited on 08/18/2020).

[9] *Opendata: Kostenfreie Geodaten der Bayerischen Vermessungsverwaltung*, 2024. [Online]. Available: https://geodaten.bayern.de/opengeodata/ (visited on 05/02/2024).

[10] S. Pauleit, I. Alim, M. Baghaie Poor, *et al.*, “Results brochure of the research training group urban green infrastructure – training next generation professionals for integrated urban planning research”, Tech. Rep., 2024. DOI: 10.14459/2024md1742953.

[11] N. Pattnaik, M. Honold, E. Franceschi, *et al.*, “Growth and cooling potential of urban trees across different levels of imperviousness”, *Journal of Environmental Management*, vol. 361, no. 121242, 2024. DOI: 10.1016/j.jenvman.2024.121242.

[12] G. Biddle, “Tree root damage to buildings”, in *Expansive clay soils and vegetative influence on shallow foundations*, 2001, pp. 1–23.

[13] C. P. Loughner, D. J. Allen, D.-L. Zhang, K. E. Pickering, R. R. Dickerson, and L. Landry, “Roles of urban tree canopy and buildings in urban heat island effects: Parameterization and preliminary results”, *Journal of Applied Meteorology and Climatology*, vol. 51, no. 10, pp. 1775–1793, 2012.

[14] Y. Casali, N. Y. Aydin, and T. Comes, “Machine learning for spatial analyses in urban areas: A scoping review”, *Sustainable cities and society*, vol. 85, p. 104 050, 2022.

# Integration of GIS data into 3D Space Partitioning to enhance architectural modeling

Sebastian Oswald[1] and Gresa Calliku[1]
[1]Fachgebiet für Bauinformatik, Technische Universität Berlin, Gustav-Meyer-Allee 25, 13355 Berlin, Germany
E-mail(s): s.oswald@tu-berlin.de, g.calliku@tu-berlin.de

**Abstract:** This paper explores the integration of Geographic Information System (GIS) data within a 3D unbounded space partitioning framework to enrich architectural modeling beyond conventional practices. By investigating how built environment data can be incorporated into a topologically connected 3D model, the study aims to understand its potential impacts on the design and construction phases of a project, as well as the role that integration of adjacent outer space might have, departing from the building scale to parcels, cadastral, and city development plans in the future. Space partitioning, which divides the Euclidean space into distinct nonoverlapping domains, is explored for its potential to improve modeling accuracy and efficiency. By laying the groundwork for the embedding of comprehensive spatial relationships into the modeling framework, the paper seeks to stimulate discourse on the dynamic requirements of construction projects and the transformation of iterative architectural planning practices. It outlines terrain integration as the initial phase of this exploratory and investigative approach to incorporate various scales in 3D modeling for advancement within the Architectural Engineering and Construction (AEC) industry.

*Keywords:* Space Partitioning, Topology, Architectural Design, Geometric Modeling, GIS

Erschienen in Tagungsband 35. Forum Bauinformatik 2024, Hamburg, Deutschland, DOI: 10.15480/882.13548
© 2024 Das Copyright für diesen Beitrag liegt bei den Autoren. Verwendung erlaubt unter Creative Commons Lizenz Namensnennung 4.0 International.

## 1 Introduction

Digitalization presents a significant challenge for the construction industry, necessitating improved coordination and data integration due to the participation of various disciplines in building projects. Building Information Modeling (BIM) was developed to meet these needs, facilitating transparent data integration among all stakeholders [1], [2]. Furthermore, Geographic Information Systems are crucial in construction projects in collecting, processing and visualizing geographic data, including parcel boundaries and terrain models [3]. Integrating GIS information early in the planning phase helps prevent errors and costly changes [4]. There is increasing interest in combining BIM and GIS systems to improve the execution of infrastructure projects, emphasizing the importance of accurate local terrain knowledge [5]. As these systems differ in several aspects, such as modeling paradigm and georeferencing, combining them poses a significant challenge [3]. This topic has been under

investigation for some time, and different approaches have been developed (see [3], [4]).
Given the growing complexity and diversity of data in these areas, there is an urgent need for consistent modeling techniques. The aim of this paper is therefore to present an approach for building modeling in the context of its environment while adhering to a consistent modeling technique.
In this paper, this endeavor is referred to as the integration of GIS data into a 3D unbounded space partitioning framework. The term integration emphasizes the joint representation of GIS data and the schematic 3D architectural model to visualize and evaluate both.
It is important to note that this paper sets the foundations for this approach. These foundations include clarifying the usefulness and relevance in the field of architectural modeling. Chapter 2 describes the approach to project implementation from the early service phases and explains the benefits of integrating GIS data. The chapter ends with a description of a case study that will be used in subsequent research to visualize the progress of this investigation based on real-world scenarios. Chapter 3 deals with the aspects of GIS and BIM that need to be considered in order to realize geometric integration. This includes in particular the implementation of georeferencing and the investigation of existing and usable data formats of Digital Terrain Models (DTM). Chapter 4 discusses the 3D unbounded space partitioning framework and explains how it improves consistency and supports architectural design. Finally, an outlook is given for the upcoming steps of holistic integration and the use of publicly available city models and GIS data.

# 2 GIS Data in Architectural Modeling

## 2.1 Preliminary Design Phases

The preliminary phases of an architectural project are, though of a preparatory nature, those to define the scope of the project. Depending on the tools and methods that planners use, a structure emerges with certain formal and contextual features. This structure may or may not meet or exceed its forseen design aspirations. Embarking on this journey with integrated geoinformational data [6], rather than proposing a secluded 3D model of a building, allows designers to quickly project and iterate within existing premises [7]–[10]. This approach can significantly improve project flow for planners and enable efficient project management for the contractor. An illustration of a tool that allows this integration is given in Figure 1.

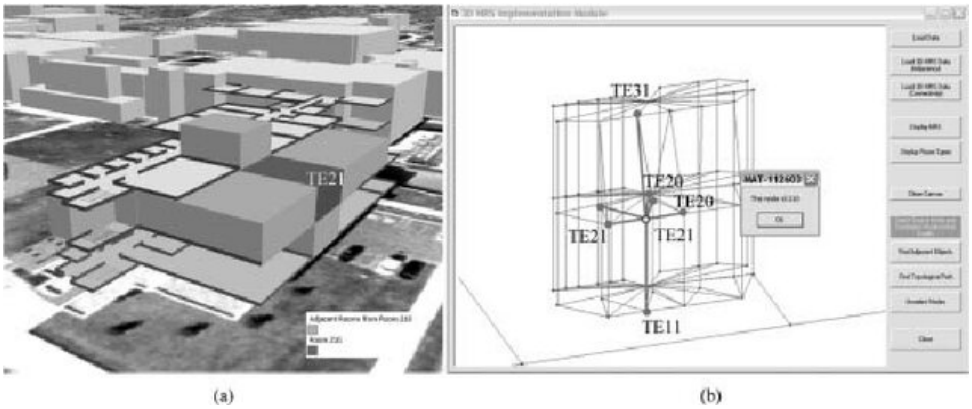


Figure 1: GIS, 3D Model and Spatial Configuration with relevant adjacencies [11]

During the Feasibility Design (FD) phase, planners conduct a comprehensive field study, which they later need for the Conceptual Design (CD) phase and the subsequent stages of the project. Site analysis provides them with vital insight into what should be designed and how to best accommodate the project demands while it guides them in making informed and effective design decisions. However, during the CD, a lot of this information is concurrently important, complex, and interrelated. Relaying solely on the planner can risk losing a significant amount of relevant data that may go flattened, as various factors often take precedence over others. Therefore, it is essential to ensure that all relevant data accumulated in the initial phases of the project is meticulously collected, documented, consistently followed, and readily accessible as needed. Data models that enable design in a consistent, connected geometric model are mentioned in Chapter 4.

## 2.2 Spatial Modeling: A Case Study

Integrating various geometric and geospatial data, each with unique scale, formats, and features, poses a challenge in creating an integrated model suited to different building typologies. Two distinct approaches to overcoming this challenge are standardization and contextualization. Standardization involves streamlining general spatial generation patterns, while contextualization would demand a tailor-made approach to each building typology. Patterns for the conceptual design of a chosen typology, in the given case an education and research facility, while assisted from space partition, are to be identified. Figure 2 illustrates how GIS data and partition modeling can be integrated into the existing data flow. When incorporating these elements into the Preliminary design phases (FD, CD), it is advisable to redefine the data intake and output processes to enhance the overall design efficiency. Case-specific guidelines determine the necessary space allocations based on the demands of academic and learning commons as well as the overall capacity. The geospatial constraints are investigated from the beginning and incorporated to generate spatial configurations that are best suited to accommodate these demands. By leveraging geometric modeling requirements such as non-convex, compact, and connected content (bounded, inner space) and context (unbounded, outer space) configurations can be designed. Through graph-based data analysis, the spatial combinations satisfying a set of requirements are iteratively to be determined.

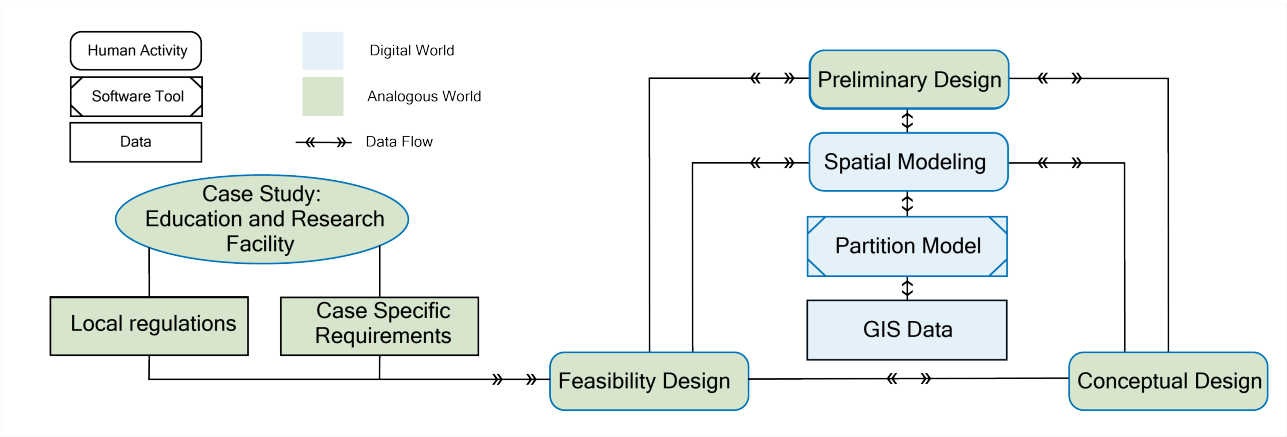


Figure 2: Spatial Design Realm

It is essential to develop an integral spatial concept before designing any building models. A widely recommended approach in research involves creating a spatial and a topological function connection, as illustrated in Figure 1b [11]. This process graphically arranges the individual units according to their functionality and interrelationships, providing an initial basis for the overall layout.
At this point, the question arises as to whether and how this concept can be implemented on the intended site. It is therefore pivotal to thoroughly evaluate the plot of land intended for development, along with its guidelines and limitations, including these considerations into the planning process. The way in which this should be done is explained in the following chapters.

# 3 GIS Models and GeoBIM

## 3.1 Georeferencing of Spatial Data

To facilitate structured planning, as discussed in chapter 2.2, construction should be modeled within its environmental context. This method, known as GeoBIM, and its implementation challenges have been explored in [12], [13].
The integration of BIM and GIS is challenging due to differences in georeferencing spatial data. Geodetic Coordinate Reference Systems (CRS) represent objects in relation to the entire Earth, whereas local Project Coordinate Systems (PCS) only describe specific buildings without considering other surroundings [3], [4].
A CRS uses a projection with known discrepancies to the real world. The Universal Transverse Mercator (UTM) projection, based on the ETRS89 reference system, is used in the European Union for the CRS representation. ETRS is a three-dimensional geodetic reference system (x, y, z) [4], [14]. The UTM projection maps the curved ellipsoidal surface of the Earth to a horizontal Cartesian plane (X, Y), which inherently involves geometric distortions, as shown in Figures 3 and 4. These figures illustrate that real lengths in the model are shortened because of these distortions.

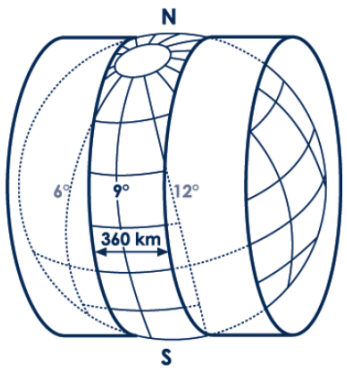


Figure 3: Universal Transverse Mercator Projektion [4]

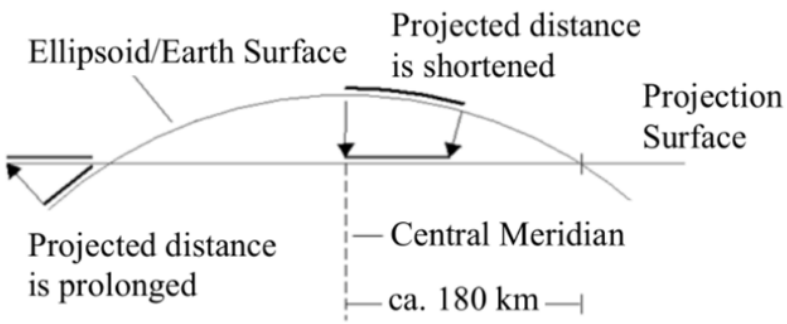


Figure 4: The distortions induced by the UTM projection [4]

To minimize distance and area distortions, strips of the ellipsoid are projected onto a cylinder with an elliptical cross section. This method is depicted in Figure 3. The approach in this paper involves modeling within a CRS. Since a CRS mapped to a UTM uses a three-dimensional Cartesian coordinate system (x, y, z), construction planning and modeling can be executed in this system. This approach,

previously described in [4], is one of three methods and is considered advantageous. For practical use, the model must be transformed back using a scale function due to distortions in the CRS dimensions. The latest version of Autodesk Revit 2025 enables the import of terrain data as point clouds in DWG, DXF, DGN and CSV formats. Georeferencing in BIM represents the current state of the art [15], [16].

### 3.2 Sources and Tools

The previous chapter determined that the modeling should be based on a CRS, requiring a DTM based on ETRS89 within Europe. These DTMs are created, quality assured, and digitally processed by surveying companies for planning and construction purposes [17]. The format of the DTM is crucial. In [17] the IfcTerrain tool was presented to convert existing DTMs into the IFC format. It seemed necessary to implement such a tool, as there are a considerable number of different formats, which are shown in Figure 5.

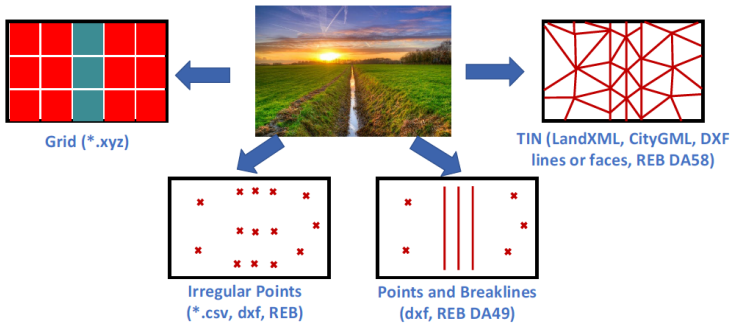


Figure 5: Different formats representing digital terrain models (DTM) [17]

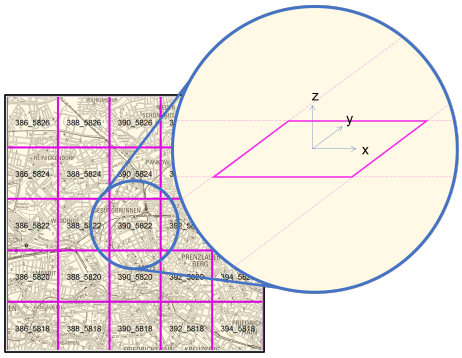


Figure 6: Visualization of an imported section. Edited image of [18]

Own investigations have shown that in Germany, DTMs are primarily available in XYZ format and geoTIFF, covering various regions or the entire country. These DTMs come in different grid sizes, from 1x1m to 1000x1000m (e.g., see [18]). Coarser grids result in less accurate elevation data as a result of linear interpolation between data points. To manage data size, the grids are divided into equally sized numbered sections (e.g. 2km x 2km). Figure 6 schematically illustrates the import of a 2 km x 2 km section of Berlin Gesundbrunnen, with the coordinate origin in the center. The dashed lines represent the unbounded planes within the three-dimensional model.
A prototype was developed to integrate DTMs into a 3D unbounded space partitioning framework [19] using point data from XYZ and geoTIFF formats to perform Delaunay triangulation, creating a Triangulated Irregular Network TIN. TINs are vector-based geographic data formed by triangulating multiple vertices into a mesh of triangles [20], [21]. Chapter 4.2 details how DTMs are imported, visualized, and modeled within the 3D framework based on a 1m grid width in a 2km x 2km section.

## 4 Space Partitioning and Data Integration

### 4.1 Partition Concept

The Partition Concept represents a paradigm shift in digital geometric modeling for applications in architecture, civil engineering, and geospatial science [22]. At its core, this concept involves dividing

the unbounded Euclidean space into discrete, clearly defined point sets, referred to as domains [19]. Unlike traditional boundary representation (BRep) methods, which often struggle with geometric errors, the Partition Concept offers a robust approach to spatial modeling [23], which organizes space into consistent and connected bounded and unbounded domains, ensuring that neighboring elements share boundaries within designated contact zones.

The concept emphasizes both topological relationships and geometric requirements, such as watertightness, non-convex and manifoldness. Topologically, it builds on constructs such as CW complexes and half-edge-based data structures to effectively manage spatial relationships. Geometrically, it ensures in every work step that the models are watertight (free from gaps or overlaps) and manifold (continuous and non-self-intersecting) [23]. A unique feature of this approach is the introduction of imaginary domains to represent unbounded spaces. By comprehensively addressing these aspects, the goal is to create consistent and interconnected geometric models by integrating GIS data and building models. It overcomes traditional modeling limitations, highlighting complex spatial relationships, and is particularly valuable for design in fields such as navigation and energy modeling, where relationships and robustness are crucial.

### 4.2 Partition Platform

The Partition Platform is an implementation of the Partition Concept, providing a practical framework for consistent spatial modeling [19]. It employs a two-fold modeling approach: a simplified user model for space divisions and a detailed core model with advanced features that include orientation, twin domains, and dihedral cycles, following GIS standards such as ISO 19107. The platform's cornerstone is its use of only two elementary work steps, split and merge, to modify adjacent domains while maintaining topological consistency. These operations are executed with strict adherence to topological rules, with work steps sorted by dimension to ensure consistency [23], offering a robust framework for consistent spatial modeling with a two-fold approach: a simplified user model for space divisions and a detailed core model with features including orientation, twin domains, and dihedral cycles.

The integration of DTMs is demonstrated as part of the modeling process. DTMs, imported using formats like `XYZ` and `geoTIFF`, are processed through Delaunay triangulation to form a TIN, providing precise elevation data for planning and construction. Georeferencing spatial data using CRS such as ETRS89 ensures that models align with real-world coordinates. The TIN splits the space model within the partition into an unbounded ground and an unbounded air cell, as well as unbounded partial neighboring surfaces. Overall, it provides a first step to a more comprehensive solution for geometric and topological integrity, which is essential for modern spatial modeling needs in the built environment.

## 5 Summary and Outlook

As described in the introduction, this paper is intended to form the foundation for the approach of modeling a building in the context of its environment while adhering to a consistent modeling technique. This paper especially focused on the architectural design iteration and the integration of DTM into a 3D unbounded space partitioning framework.

The next step is to integrate 3D city models into the framework presented. This extension makes

it possible to plan and construct buildings in relation not only to the natural environment but also to existing buildings and infrastructure. Taking into account the boundaries of the property and the existing buildings allows for more precise and comprehensive planning. This offers considerable advantages, as potential conflicts can be identified at an early stage and costly planning errors can be avoided. In addition, urban planning specifications and guidelines can be better adhered to, leading to more efficient and sustainable construction methods.
The integration of city models into the existing system represents a further significant step towards fully digitized and networked construction planning. This development opens up new opportunities for integrated and transparent collaboration between all parties involved and contributes significantly to the optimization of construction processes. Therefore, further research will be done and published to document the progress of this investigation. The case study presented in chapter 2 will continue in the following steps and will illustrate the findings and progress made.

## References

[1] J. Blankenbach, C. Clemen, and R. Becker, “Grundlagen und Informationsmanagement der BIM-Methode”, *Leitfaden Geodäsie und BIM (Version 3.2)*, 2023.

[2] R. M. Aziz, T. I. Nasreldin, and O. M. Hashem, “The role of BIM as a lean tool in design phase”, *Journal of Engineering and Applied Science*, 2024. DOI: 10.1186/s44147-023-00340-3.

[3] M. Jarosch, “BIM & GIS”, in Springer Fachmedien Wiesbaden, 2023. DOI: 10.1007/978-3-8348-2118-8_14.

[4] Š. Jaud, A. Donaubauer, O. Heunecke, and A. Borrmann, “Georeferencing in the context of building information modelling”, *Automation in Construction*, 2020. DOI: 10.1016/j.autcon.2020.103211.

[5] A. Bradley, H. Li, R. Lark, and S. Dunn, “BIM for infrastructure: An overall review and constructor perspective”, *Automation in Construction*, 2016. DOI: 10.1016/j.autcon.2016.08.019.

[6] J. Stoter and S. Zlatanova, “3D GIS, where are we standing?”, *ISPRS Joint Workshop on ’Spatial, Temporal and multi-dimensional data modelling and analysis’, Québec, October, 2003*, Jan. 2009.

[7] R. Billen and S. Zlatanova, “3D spatial relationships model: A useful concept for 3D cadastre?”, *Computers, Environment and Urban Systems*, 2003. DOI: 10.1016/S0198-9715(02)00040-6.

[8] F. Döner, R. Thompson, J. Stoter, *et al.*, “4D cadastres: First analysis of legal, organizational, and technical impact—With a case study on utility networks”, *Land Use Policy*, 2010. DOI: 10.1016/j.landusepol.2010.02.003.

[9] M. El-Mekawy, A. Östman, and I. Hijazi, “A Unified Building Model for 3D Urban GIS”, *ISPRS International Journal of Geo-Information*, 2012. DOI: 10.3390/ijgi1020120.

[10] C. A. Carrasco, I. Lombillo, and J. Sánchez-Espeso, “Methodology for the generation of 3D city models and integration of HBIM models in GIS: Case studies”, *VITRUVIO - International Journal of Architectural Technology and Sustainability*, 2022. DOI: 10.4995/vitruvio-ijats.2022.18808.

[11] J. Lee and M.-P. Kwan, “A combinatorial data model for representing topological relations among 3D geographical features in micro-spatial environments”, *International Journal of Geographical Information Science*, 2005. DOI: 10.1080/13658810500399043.

[12] F. Noardo, T. Krijnen, K. Arroyo Ohori, *et al.*, “Reference study of IFC software support: The GeoBIM benchmark 2019—Part I”, *Transactions in GIS*, 2021. DOI: 10.1111/tgis.12709.

[13] R. De Laat and L. Van Berlo, “Integration of BIM and GIS: The Development of the CityGML GeoBIM Extension”, in T. H. Kolbe, G. König, and C. Nagel, editors, Berlin, Heidelberg: Springer Berlin Heidelberg, 2011. DOI: 10.1007/978-3-642-12670-3_13.

[14] J. P. Snyder, *Map Projections: A Working Manual*. Books Express Publishing, 2012.

[15] “Autodesk revit 2025 - import von geländedaten”. (2025), [Online]. Available: https://help.autodesk.com/view/RVT/2025/ENU/?guid=GUID-A1E1DE84-29AE-4B99-B377-091C0AC45249.

[16] *DIN ISO/TR 23262:2021 – GIS (Geospatial) / BIM-Interoperabilität*, Deutsches Institut für Normung e.V. (DIN), Jan. 2022.

[17] C. Clemen, M. Schröder, T. Kaiser, and E. Romanschek, “IFCTerrain – A Free and Open Source Tool to Convert Digital Terrain Models (DTM) to OpenBIM Industry Foundation Classes (IFC)”, *ISPRS Annals of the Photogrammetry, Remote Sensing and Spatial Information Sciences*, 2021. DOI: 10.5194/isprs-annals-VIII-4-W2-2021-145-2021.

[18] Senatsverwaltung für Stadtentwicklung und Wohnen Berlin, *Geoportal Berlin - Metadaten: DGM1, Berlin (2016)*, 2016. [Online]. Available: https://gdi.berlin.de/geonetwork/srv/ger/catalog.search#/metadata/fa02f9e1-a0df-3be1-b0aa-bc624c0c7ff5.

[19] W. Huhnt, M. Sternal, and P. J. Pahl, “Modeling bounded and unbounded space with polyhedra: Topology and operators for manifold cell complexes”, en, *Advanced Engineering Informatics*, 2022. DOI: 10.1016/j.aei.2022.101790.

[20] R. Fellegara, F. Iuricich, Y. Song, and L. D. Floriani, “Terrain trees: A framework for representing, analyzing and visualizing triangulated terrains”, *GeoInformatica*, 2023. DOI: 10.1007/s10707-022-00472-3.

[21] Lund University, J. Lim, P. Pilesjö, and Lund University, “Triangular Irregular Network (TIN) Models”, *Geographic Information Science & Technology Body of Knowledge*, 2022. DOI: 10.22224/gistbok/2022.2.7.

[22] W. Huhnt, J. Z. Vetter, and M. Sternal, “Space Partitioning as a Holistic Alternative to Traditional Geometric Modeling Workflows in the AEC Industry”, in *Advances in Information Technology in Civil and Building Engineering*, 2023, pp. 415–426. DOI: 10.1007/978-3-031-32515-1_29.

[23] M. Sternal and W. Huhnt, “Robust Modeling of Polyhedral Space Partitions”, in *Advances in Information Technology in Civil and Building Engineering*, 2023, pp. 427–442. DOI: 10.1007/978-3-031-32515-1_30.

# Ein BIM-Reifegradmodell zur Messung der digitalen Transformation von Infrastrukturbehörden

Markus Boden[1,2]
[1]Professur Verkehrssystemplanung, Schwanseestraße 13, 99423 Weimar
[2]Professur Baubetrieb und Bauverfahren, Marienstraße 7a, 99423 Weimar
Bauhaus-Universität Weimar, Deutschland
E-Mail: markus.friedrich.boden@uni-weimar.de

**Abstract:** Building Information Modeling (BIM) ist eine zunehmend verbreitete Methode in der Baubranche, wird jedoch bei Behörden des Infrastrukturbaus noch nicht standardmäßig verwendet. Der Masterplan BIM Bundesfernstraßen bildet den Rahmen für die Implementierung der BIM-Methode bis 2025 bei Behörden des Bundesfernstraßenbaus. Gemäß dem Masterplan stellen BIM-Reifegradmodelle wichtige Messinstrumente für die Einhaltung der fortlaufend veröffentlichten Phasenziele dar. Die Reifegradmodelle ermöglichen die Identifikation von Organisationsbereichen mit digitalem Handlungsbedarf und die Überprüfung durchgeführter Digitalisierungsschritte. Neben den Bundesfernstraßen müssen auch der Infrastrukturbau der Länder und Kommunen durch digitale Prozesse effizienter werden. Es besteht ein Bedarf für ein frei zugängliches BIM-Reifegradmodell, das alle Verwaltungsebenen bei der BIM-Implementierung unterstützt. Dieses Paper beschreibt ein BIM-Reifegradmodell auf der Basis des Masterplans, mit angepassten Reifegradzielen entsprechend der Verwaltungsebene. Auf Grundlage einer Literaturrecherche zu (BIM-)Reifegradmodellen sowie von Normen und Richtlinien werden Dimensionen und Key Performance Indikatoren identifiziert und in einer Reifegradmatrix zusammengefasst. Die Evaluierung erfolgt durch die Anwendung bei einer Landesbaubehörde. Durch das Reifegradmodell kann der Ist-Zustand der BIM-Bereitschaft und -Fähigkeiten in verschiedenen Organisationsbereichen identifiziert und gegen den Soll-Zustand laut Masterplan abgeglichen werden. Die Berücksichtigung aller Verwaltungsebenen unterstützt die Verbreitung der BIM-Methode hin zu einem standardmäßigen Einsatz im gesamten Infrastrukturbau.
*Keywords:* BIM-Implementierung, Reifegradmodell, Infrastrukturbau, Digitale Transformation

Erschienen in Tagungsband 35. Forum Bauinformatik 2024, Hamburg, Deutschland, DOI: 10.15480/882.13509
© 2024 Das Copyright für diesen Beitrag liegt bei den Autoren. Verwendung erlaubt unter Creative Commons Lizenz Namensnennung 4.0 International.

## 1 Einleitung

In den vergangenen Jahrzehnten hat sich ein Investitionsrückstand in Milliardenhöhe in der deutschen Straßen- und Verkehrsinfrastruktur gebildet [1]. Sowohl in der öffentlichen Verwaltung als auch bei Akteuren der Bauwirtschaft besteht ein Bedarf an Digitalisierung, um den zukünftigen

Aufgaben des Infrastrukturbaus gerecht zu werden. Die Einführung der Building Information Modeling (BIM)-Methodik stellt dafür einen grundlegenden Schritt dar. Der „Stufenplan Digitales Planen und Bauen" aus dem Jahr 2015 beinhaltete das Ziel der BIM-Einführung im Infrastrukturbau bis zum Jahr 2020 [2]. Entsprechend der derzeitigen Praxis aktualisiert der Masterplan BIM Bundesfernstraßen die Ziele des Stufenplans in Form eines Phasenplans mit dem Ziel der BIM-Einführung bis zum Jahr 2025. Zur Messung und Steuerung der BIM-Einführung soll gemäß des Masterplans ein Reifegradmodell verwendet werden, welches auf den Zielvorgaben des Masterplans aufbaut und den aktuellen Implementierungsgrad identifiziert [3]. Im Rahmen eines zweiten Fachsymposiums wurden im März 2024 die Ziele der zweiten Phase des Masterplans veröffentlicht. Ein erstelltes Reifegradmodell sowie die Ergebnisse der ersten Durchführung bei Institutionen des Bundesfernstraßenbaus wurden bislang nicht veröffentlicht. Dies stellt insbesondere im Infrastrukturbau abseits der Bundesfernstraßen eine verpasste Chance dar. Es ist zu hinterfragen, ob ein Top-Down-Ansatz, bei dem der Bund die Einführung vornimmt und die Länder und Kommunen dieser folgen, den schnellsten Weg zur BIM-Einführung im gesamten Infrastrukturbau darstellt. Stattdessen wird ein frei zugängliches Reifegradmodell benötigt, welches auf den Zielen des Masterplans aufbaut, diese für die verschiedenen Verwaltungsebenen anpasst und dadurch alle Infrastrukturbehörden bei der Einführung der BIM-Methode unterstützt.

## 2 Hintergrund

Digitale Reifegradmodelle stellen eine Methode zur Messung des aktuellen Zustands einer Organisation in Bezug auf die digitale Transformation, die digitale Strategie und/oder den Einsatz von Technologie dar [4]. Der Grundgedanke der Modelle ist eine Reihe von Untersuchungen der Lücke zwischen der aktuellen und der optimalen digitalen Reife [5]. Die Einführung der ersten Reifegradmodelle führte zu einer raschen Verbreitung. Die existierende Vielzahl an digitalen Reifegradmodellen führt zu Schwierigkeiten hinsichtlich der Auffindbarkeit und Vergleichbarkeit, sodass die Suche und Auswahl geeigneter Modelle für die direkte Verwendung durch Organisationen oder als Erarbeitungsgrundlage für die wissenschaftliche Entwicklung neuer Modelle erschwert wird [6]. Aus diesem Grund erfolgt die in Kapitel 3 beschriebene Konzeption des in dieser Arbeit vorgestellten digitalen Reifegradmodells auf Grundlage des Klassifikationssystems von Mettler et al. [6] sowie der zu definierenden Bestandteile digitaler Reifegradmodelle nach Haryanti et al. [4] (Vgl. Tabelle 1).

Tabelle 1: Methodik für das Erstellen des Reifegradmodells, eigene Darstellung nach [4, 6]

| 1. Definieren der allgemeine Modellattribute | | 2. Detaillierte Beschreibungen |
|---|---|---|
| (a) Name und Akronym | (b) Anwendungsbereich | (a) Reifegrade, Dimensionen und deren Granularität |
| (c) Zielgruppe | (d) Abgrenzung zu ähnlichen Modellen/Bedarf für Neues | (b) Auswertung und Darstellung |
| (e) Wichtige Quellen & ihr Verwendungszweck | (f) Evaluierungsmethode (gesondert in Kapitel 4) | (c) Technische Implementierung |

# 3 Reifegradmodell BIM4VID

## 3.1 Definieren der allgemeine Modellattribute

Das „BIM Digital Maturity Model (DMM)-Modul für Verkehrsinfrastrukturbehörden in Deutschland“ (BIM4VID) wurde in der vorliegenden Forschungsarbeit für öffentliche Institutionen des Infrastrukturbaus in Deutschland auf Bundes-, Landes- und Kommunalebene entwickelt. Das Reifegradmodell dient der Ermittlung des Grades der Umsetzung der BIM-Methodik auf Grundlage des Masterplans „BIM Bundesfernstraßen“. Es unterstützt die Organisationen durch die Gegenüberstellung der Soll- und Ist-Zustände bei der BIM-Einführung. In der Literatur finden sich verschiedene Reifegradmodelle zur Digitalisierung von Organisationen im Bausektor. Die Reifegradziele des australischen „Strategic Framework for Digitalisation of Design and Construction“ (SFDDC) basieren auf den digitalen Zielvorgaben der Regierung von New South Wales [7]. Das Modell fokussiert sich ausschließlich auf technische Aspekte, verdeutlicht jedoch, wie staatliche Zielvorgaben die Grundlage für Reifegradmodelle darstellen und diese effektiv und praxistauglich abgefragt werden können. Die „BIM Maturity Matrix“ (BIm³) bietet ein analoges Self-Assessment bei dem Organisationen mithilfe kurzer Texte ihre Reife in verschiedenen Dimensionen einschätzen können [8]. Auch das Reifegradmodell von Siebelink et al. [9] zielt darauf ab, die BIM-Reife von Bauunternehmen zu erfassen. Es betrachtet neben technologischen Aspekten insbesondere auch nicht-technologische Dimensionen. Im Rahmen der Recherche konnte kein veröffentlichtes Reifegradmodell identifiziert werden, das auf die aktuellen Zielvorgaben deutscher Infrastrukturbehörden spezialisiert ist. Die aufgezählten Modelle dienen als Beispiele für die Einbindung von staatlichen Zielen für Reifegradmodelle sowie als Grundlage für die zu betrachtenden Dimensionen und deren Ausprägungen auf den Reifegraden.

## 3.2 Detaillierte Beschreibungen

Die Reifegrade von BIM4VID sind an die Phasen des Masterplans BIM Bundesfernstraßen angelehnt. Der Ausgangspunkt ist der Reifegrad 0, die „Initialisierung“. Dieser Reifegrad bezeichnet den Zustand, bei dem BIM noch keine Anwendung in der Organisation findet. Die weiteren Reifegrade 1-5 werden entsprechend des Masterplans „Aufgebrochen und harmonisiert“, „Ausgeweitet und professionalisiert“, „Standardisiert“, „Regelprozess“ und „Zukunftsbild“ bezeichnet. Die konkreten Zielstellungen des Masterplans wurden für eine Selbstbewertung in die drei Key Performance Indikatoren (KPI) „Implementierung der BIM-Methode“, „BIM-Projekteinsatz“ und „BIM-Anwendungsfälle“ überführt. Die Anforderungen für die Reifegrade dieser KPI korrespondieren mit den Phasenzielen des Masterplans. In der ersten Phase ist die Erstellung einer BIM-Implementierungsstrategie, die Einführung der BIM-Anwendungsfälle der Musterrichtlinie BIM Version 1 sowie die Durchführung erster Pilotprojekte erforderlich und stellen damit die Grundlage für den ersten Reifegrad „Aufgebrochen und harmonisiert“ dar. Auf dem Reifegrad 2 „Ausgeweitet und professionalisiert“ ist eine Ausweitung der BIM-Methode bei Teams in allen Niederlassungen und Abteilungen erforderlich. Die BIM-Methode soll nach Abstimmung bei Großprojekten mit hohem öffentlichem Interesse verwendet werden. Die zu implementierenden Anwendungsfälle werden durch die Version 2 der Musterrichtlinie BIM erweitert. Nach diesem Schema wurden auch die weiteren Reifegrade für die KPI der

Selbstbewertung gemäß Masterplan definiert. Die Selbstbewertung wurde daraufhin mit acht weiteren Dimensionen und insgesamt 15 KPI ausgebaut. Die Dimensionen wurden entsprechend allgemein zu betrachtender Dimensionen digitaler Reifegradmodelle nach Haryanti et al. [4] und Berghaus und Back [10] identifiziert und entsprechend der Dimensionen der weiteren Grundlagen [7–9] erweitert. Für jede Dimension wurden objektiv messbare KPI auf Basis einer Literaturrecherche sowie von Normen, Richtlinien und Empfehlungspapieren von BIM4INFRA2020 und BIM Bundesfernstraßen ausgewählt. Die nachfolgende Abbildung 1 gibt einen grafischen Überblick über alle Dimensionen und ihre KPI.

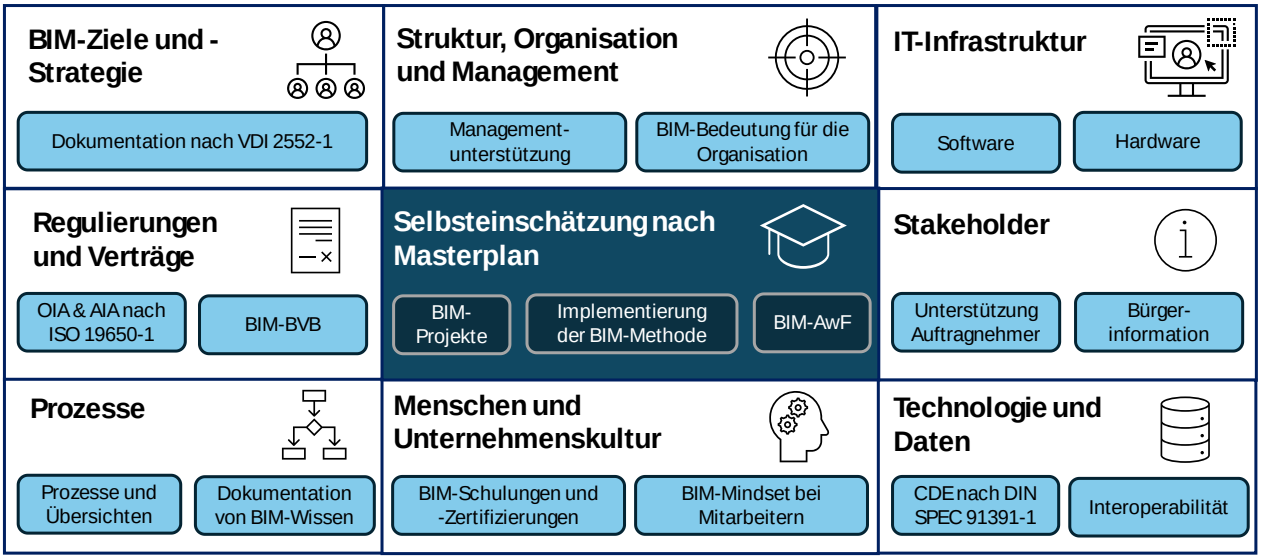


Abbildung 1: Dimensionen und KPI des Reifegradmodells BIM4VID, eigene Darstellung

Die KPI der Dimension „Regulierung und Verträge“ erfassen beispielsweise die Erstellung der organisatorischen Informationsanforderungen (OIA) und Auftraggeber-Informationsanforderungen (AIA) gemäß ISO-Standard 19650-1 sowie die Definition der Besonderen Vertragsbedingungen BIM (BIM-BVB). Die Erstellung von Informationsanforderungen stellt eine der wesentlichen Aufgaben von Auftraggebern bei BIM-Projekten dar. Für den ersten Reifegrad des KPI ist die Definition von OIA anhand von Vorlagen für die eigene Organisation erforderlich. Es ist festzuhalten, wofür die Projektinformationen kurz-, mittel- und langfristig genutzt werden sollten und welche Informationen entsprechend benötigt werden. Auf den weiteren Reifegraden wird die Nutzung von Vorlagen für die AIA und BIM-Ablaufpläne sowie deren Spezifizierung entsprechend der OIA abgefragt. Für die Erstellung von BIM-BVB sind ebenfalls Vorlagen wie die von BIM4INFRA2020 zu nutzen und auf den Reifegraden entsprechend der organisationsspezifischen Anforderungen anzupassen. Die jeweiligen Ausprägungen der Reifegrade 0–5 für die insgesamt neun Dimensionen und deren 18 KPI ergeben eine Reifegradmatrix.

Das übergeordnete Ziel des Masterplans ist das Erreichen des BIM-Regelprozesses auf Bundesfernstraßenebene ab Ende des Jahres 2025. Dementsprechend sollten ab diesem Zeitpunkt alle KPI auf Fernstraßenebene den Reifegrad 4 für eine positive Bewertung erreichen (Grün/Plus in

Abbildung 2). Liegt der gewählte Reifegrad eine Stufe unter dem Soll-Stand, so sollten in mittelbarer Zukunft Maßnahmen zur Verbesserung durchgeführt werden (Gelb/Kreis in Abbildung 2). Bei einer Wahl eines Reifegrads zwei Stufen unter dem Soll-Reifegrad sind umgehend direkte Gegenmaßnahmen zu initiieren, um die zeitlichen Ziele des Masterplans einhalten zu können (Rot/Minus in Abbildung 2). Die Soll-Zustände wurden zum einen zeitlich und zum anderen entsprechend der höchsten betreuten Straßenklasse abgestuft. Kommunen sollten damit beispielsweise ab 2025 den ersten Reifegrad erreichen, um den Entwicklungen des Bundes und der Länder folgen zu können.

| Zeit | Straßen-klasse | Reifegrad 0 Initialisierung | Reifegrad 1 Aufgebrochen und harmonisiert | Reifegrad 2 Ausgeweitet und professionalisiert | Reifegrad 3 Standardisiert | Reifegrad 4 Regelprozess | Reifegrad 5 Zukunftsbild |
|---|---|---|---|---|---|---|---|
| Bis 2025 | Fernstr. | - | ○ | + | + | + | + |
| | Landstr. | ○ | + | + | + | + | + |
| | Kreisstr. | + | + | + | + | + | + |
| Ab 2025 | Fernstr. | - | - | ○ | + | + | + |
| | Landstr. | - | ○ | + | + | + | + |
| | Kreisstr. | ○ | + | + | + | + | + |
| Ab Ende 2025 | Fernstr. | - | - | - | ○ | + | + |
| | Landstr. | - | - | ○ | + | + | + |
| | Kreisstr. | - | ○ | + | + | + | + |

Abbildung 2: Auswertungsschema von BIM4VID in Ampeldarstellung, eigene Darstellung

Die Auswertung des Reifegradmodells erfolgt durch Selektion des entsprechenden Reifegrads für jeden KPI auf Basis der beschreibenden Kurztexte der Reifegradmatrix. Zu Beginn erfolgt eine Abfrage bezüglich der höchsten betreuten Straßenklasse (Fernstraßen, Landstraßen, Kreisstraßen), um eine Einteilung gemäß des erstellten Ampelsystems vorzunehmen. Im Anschluss erfolgt ein Vergleich des Ist-Wertes mit den Soll-Werten aus Abbildung 2. Die Umsetzung des Reifegradmodells erfolgte in Form eines Web-Tools unter Verwendung der Open-Source-Bibliothek SurveyJS. Nach der Abfrage der höchsten betreuten Straßenklasse werden die Reifegrade der 18 KPI unter Verwendung der Reifegradmatrix ausgewählt (Vgl. Abbildung 3).

**Informationsanforderung nach ISO 19650-1**

| Reifegrad 0 Initialisierung | Reifegrad 1 Aufgebrochen und harmonisiert | Reifegrad 2 Ausgeweitet und professionalisiert | Reifegrad 3 Standardisiert | Reifegrad 4 Regelprozess | Reifegrad 5 Zukunftsbild |
|---|---|---|---|---|---|
| Wurden noch nicht erstellt | Organisatorische Informations-anforderungen (OIA) wurden definiert | Erste Projekte werden mit Dokumentvorlagen (AIA & BAP) durchgeführt, welche den OIA entsprechen | Die Dokumentvorlagen wurden anhand eigener Projekte evaluiert und standardisiert | Die Dokumentvorlagen werden fortlaufend auf Grundlage der Projekte optimiert | Die Dokumentvorlagen werden mit Zukunftstechnologien erweitert |

0 1 2 3 4 5

Abbildung 3: Beispielhafte Abfrage des KPI „OIA & AIA nach ISO 19650-1“ unter Verwendung der BIM4VID-Reifegradmatrix, eigene Darstellung

Die Behörden erhalten eine direkte Auswertungsübersicht mit Ampeldarstellungen für die KPI entsprechend des Soll-Ist-Vergleichs. Neben der Ampeldarstellung bietet das Web-Tool Links zu Hilfestellungen wie Online-Dokumenten und Vorlagen von BIM-Deutschland oder BIM Bundesfernstraßen (Vgl. Abbildung 4).

Abbildung 4: Ausschnitt aus der Auswertungsdarstellung im Web-Tool mit Links zu unterstützenden Web-Dokumenten, eigene Darstellung

## 4 Evaluierung

Das Reifegradmodell BIM4VID sowie dessen technische Bereitstellung wurde Vertretern einer Landesbaubehörde vorgestellt. Im Rahmen einer Pilotstudie wurde eine BIM-Reifegraderfassung durchgeführt, wobei vor, während und nach der Erfassung Interviewfragen gestellt wurden. Im Folgenden werden die Ergebnisse der Evaluierung zusammengefasst.

BIM-Reifegradmodelle werden von den Vertretern der Landesbaubehörde grundsätzlich als sinnvoll beurteilt. Die Modelle würden dazu beitragen, eine Übersicht über die zu bearbeitenden Themengebiete der BIM-Implementierung zu erhalten. Durch die wiederholte Durchführung der Evaluierung in bestimmten Zeitabständen könnten Fortschritte dokumentiert und weitere Bearbeitungsschwerpunkte sinnvoll gesetzt werden. Für die praktische Nutzbarkeit der Modelle ist insbesondere eine Übersicht der abgegebenen Antworten sowie eine direkte Auswertung durch das Reifegrad-Tool erforderlich. Die derzeitige Praxis der Reifegraderfassung des Bundes beinhaltet ein Online-Tool, das Zugriffe für die Institutionen des Bundesfernstraßenbaus vorsieht. Die jährliche Befragung erstreckt sich über einen Zeitraum von etwa einer Stunde und umfasst ausführliche Fragen zu ähnlichen Dimensionen und KPI wie das in dieser Arbeit vorgestellte Reifegradmodell BIM4VID. Innerhalb der Reifegraderfassung erfolgt eine detailliertere Abfrage von Teilbereichen wie den BIM-Anwendungsfällen. Die Ergebnisse wurden der Behörde zum Zeitpunkt der Evaluierung im Juni des Jahres 2024 noch nicht zur Verfügung gestellt. Die konkrete Auswertung und Darstellung der Ergebnisse sowie der daraus resultierende Mehrwert sind zum gegenwärtigen Zeitpunkt noch nicht abschließend geklärt. Die technische Umsetzung von BIM4VID mit freiem Zugriff und direkten Ergebnissen wird von den Vertretenden der Landesbaubehörde daher positiv wahrgenommen. In diesem Zusammenhang wurde darauf verwiesen, dass das Modell auch für verschiedene Bereiche

innerhalb der Behörde separat durchgeführt werden könnte, beispielsweise für Bundesfernstraßen, Landesstraßen oder die einzelnen Regionen der Straßenbauverwaltung. Auf diese Weise könnten die Reifegrade auch innerhalb einer Behörde differenziert und eine Diskussionsgrundlage geschaffen werden. Für die Erarbeitung detaillierter Arbeitspakete müsste das Modell ausgeweitet werden.

## 5 Diskussion

Reifegradmodelle mit direkten und übersichtlichen Auswertungen erweisen sich allgemein als hilfreich für übergeordnete Fragestellungen und Strategiebildungen. Die Abfrage von BIM4VID mittels Reifegradmatrix erfolgt schnell und zielgerichtet, könnte jedoch in einzelnen Fragen wie den Anwendungsfällen genauer definiert und beschrieben werden. Das Reifegradmodell des Bundes stellt dafür ausführliche Fragen zur Verfügung, welche eine detaillierte Erfassung des Reifegrads ermöglichen. Dessen Ergebnisse können für die Konkretisierung der Implementierungsstrategie dienen, welche auf Basis von BIM4VID erstellt wird. Insgesamt erweitert das Reifegradmodell BIM4VID das Modell des Bundes um einen schnellen und frei verfügbaren Service. Es betrachtet eine übergeordnete organisatorische Sichtweise und kann insbesondere für Länder und Kommunen abseits der BIM-Vorreiter eine Unterstützung bei der BIM-Einführung darstellen. Bei einer Veröffentlichung des bislang intern gehaltenen Reifegradmodells des Bundesfernstraßenbaus wäre es denkbar die Inhalte und Zielgebiete zu vergleichen und dadurch beide Modelle weiterzuentwickeln.

## 6 Zusammenfassung und Fazit

Die Einführung der BIM-Methode im Infrastrukturbau wird in näherer Zukunft weitere Aufmerksamkeit erhalten. Insbesondere die Unterstützung der Länder und Kommunen stellt hier eine zentrale Aufgabe dar, um die im Bereich der Bundesfernstraßen gewonnenen Erkenntnisse aufzubereiten und in die Breite zu tragen. Reifegradmodelle wie das in dieser Arbeit vorgestellte Modell BIM4VID können hierbei einen Beitrag leisten. Die Evaluierung in Zusammenarbeit mit einer Landesbaubehörde bestätigt, dass ein spezifiziertes Reifegradmodell hilft, einen Überblick über zu berücksichtigende Punkte bei dem Erstellen einer BIM-Implementierungsstrategie zu erhalten. Weiteres Forschungspotenzial besteht in der Entwicklung weiterer objektiver KPI sowie der Bereitstellung zusätzlicher Hilfeleistungen. Reifegradmodelle sollten grundsätzlich wissenschaftlich publiziert und damit dem fachlichen Diskurs geöffnet werden. Dadurch können die Modelle weiterentwickelt werden, wodurch schlussendlich sichergestellt werden kann, dass die Institutionen des Infrastrukturbaus auf allen Verwaltungsebenen ihre Implementierungsstrategien objektiv sinnvoll gestalten können.

## Datenverfügbarkeit

Die BIM4VID-Reifegradmatrix mit den neun Dimensionen sowie den jeweiligen Ausprägungen der Reifegrade je KPI und der Source-Code des Web-Tools werden über GitHub bereitgestellt unter: https://github.com/MarkusFrBoden.

## Literatur

[1] H. Scheller, "Kommunale Infrastrukturpolitik. Zwischen Konsolidierung und aktiver Gestaltung," *Bundeszentrale für politische Bildung*, 11. April 2017. Zugriff am: 24. Juni 2024. [Online.] Verfügbar: https://www.bpb.de/shop/zeitschriften/apuz/246431/kommunale-infrastrukturpolitik-zwischen-konsolidierung-und-aktiver-gestaltung/

[2] Bundesministerium für Verkehr und digitale Infrastruktur (BMVI). "Stufenplan Digitales Planen und Bauen." Zugriff am: 24. Juni 2024. [Online.] Verfügbar: https://bmdv.bund.de/SharedDocs/DE/Publikationen/DG/stufenplan-digitales-bauen.pdf?__blob=publicationFile

[3] Bundesministerium für Digitales und Verkehr (BMDV). "Masterplan BIM Bundesfernstraßen: Digitalisierung des Planens, Bauens, Erhaltens und Betreibens im Bundesfernstraßenbau." Zugriff am: 4. März 2024. [Online.] Verfügbar: https://www.bimdeutschland.de/fileadmin/media/Downloads/Download-Liste/Strasse/BIM_Masterplan_Bundesfernstrassen_barrierefrei.pdf

[4] T. Haryanti, N. A. Rakhmawati und A. P. Subriadi, "The Extended Digital Maturity Model," *BDCC*, Jg. 7, Nr. 1, S. 1–17, 2023, doi: 10.3390/bdcc7010017.

[5] C. A. Williams, D. Schallmo, K. Lang und L. Boardman, "Digital maturity models for small and medium-sized enterprises: a systematic literature review," in *ISPIM Innovation Conference – Celebrating Innovation: 500*, S. 1–15.

[6] T. Mettler, P. Rohner und R. Winter, "Towards a Classification of Maturity Models in Information Systems," in *Management of the Interconnected World: ItAIS The Italian Association for Information Systems*, A. D'Atri, Hg., Heidelberg: Physica-Verlag, 2010, S. 333–340.

[7] S. Perera, X. Jin, P. Das, K. Gunasekara und M. Samaratunga, "A strategic framework for digital maturity of design and construction through a systematic review and application," *Journal of Industrial Information Integration*, Jg. 31, S. 100413, 2023, doi: 10.1016/j.jii.2022.100413.

[8] B. Succar. "BIM Maturity Matrix - German." Zugriff am: 16. Februar 2024. [Online.] Verfügbar: https://bimexcellence.org/wp-content/uploads/301in.DE-BIM-Reifegrad-Matrix.pdf

[9] S. Siebelink, J. T. Voordijk und A. Adriaanse, "Developing and Testing a Tool to Evaluate BIM Maturity: Sectoral Analysis in the Dutch Construction Industry," *J. Constr. Eng. Manage.*, Jg. 144, Nr. 8, 2018, Art. Nr. 05018007, doi: 10.1061/(ASCE)CO.1943-7862.0001527.

[10] S. Berghaus und A. Back. "Stages in Digital Business Transformation: Results of an Empirical Maturity Study." Zugriff am: 5. April 2024. [Online.] Verfügbar: https://aisel.aisnet.org/cgi/viewcontent.cgi?article=1022&context=mcis2016

# Adding an extensive feedback loop for the creation and validation of functional requirements of BIM models

Florian M. Becker[1] and Daniel Napps[1]
[1]Chair of Computing in Engineering, Ruhr-University Bochum, Universitätsstraße 150, 44801 Bochum, Germany
E-mail(s): info@florianbecker.eu, daniel.napps@rub.de

**Abstract:** During the planning, design and permit process of buildings, various regulations must be adhered to in order to obtain a compliant building permit. Therefore formal requirements for buildings and technical rules in practice are examined and can be checked. For this purpose the open specification for checking functional requirements of a digital building model OpenBIMRL can be used. Architects or engineers may verify their BIM model with a pre-defined set of rules or entire rule-sets. This may be a set of rules for specific countries or usage (housing, commercial). In OpenBIMRL, functional requirements are formulated using a web-based platform separated from the actual rule checking engine. These rules consist of two main components: information extraction through predefined building blocks called $Nodes$, followed by the application of logical operations and comparisons. Previously, testing and verification of these rules on BIM models required a separate, non-portable program. To address this limitation, we conceived a redesign of the engine into a pure dependency structure devoid of user interaction. A server-client architecture was chosen with a RESTful endpoint. This change enables rule creators and end-users to view the outputs of defined rules and their respective $Nodes$ directly in a concise format and within the 3D model itself.

*Keywords:* Building Information Modeling (BIM), functional requirements, automation

Erschienen in Tagungsband 35. Forum Bauinformatik 2024, Hamburg, Deutschland, DOI: 10.15480/882.13550
© 2024 Das Copyright für diesen Beitrag liegt bei den Autoren. Verwendung erlaubt unter Creative Commons Lizenz Namensnennung 4.0 International.

## 1 Introduction

Securing approval for construction projects involves navigating a complex environment of regulations that must be strictly adhered to. These regulations are essential for ensuring that the final construction is safe, legal, and fits its intended purpose. The consequences of non-compliance can be significant, ranging from delays in schedule delays to potential legal implications. Building Information Modeling (BIM) is a powerful tool that is now being used by engineers, architects, and government agencies. In recent years the German federal government has begun to introduce $DigitalerBauantrag$ (digital building permit) where BIM is used extensively in the planning process. In the long term, the goal is to replace conventional paperwork completely [1].

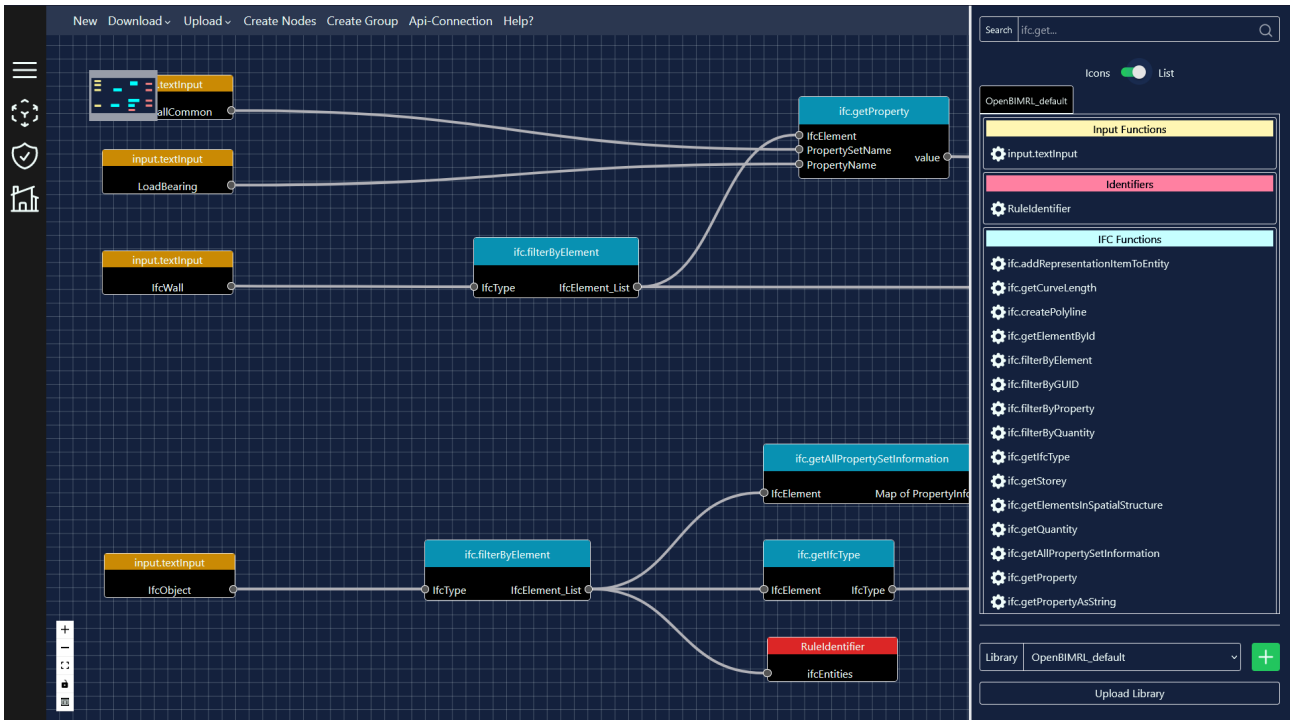


Figure 1: Example of OpenBIMRLs' graph structure.

Permitting agencies still need to verify and review the digital building model for compliance with the specific regulations. Many of these vary from state to state or country to country. BIM Rule Language (BIMRL) aims to address this complexity by defining a Domain-Specific Language (DSL) for rule checking [2]. This automated compliance checking tool is the basis of OpenBIMRL, an open format for code compliance checking of complex functional requirements which takes a different approach with a graph-based DSL [3]. OpenBIMRL, utilizing a graph-based language (see Figure 1), is considered as a low-code or no-code solution. While technical knowledge is still essential, the barrier to entry for staff without prior programming expertise (non-technical staff) is significantly reduced. The implementation was designed as a prototype or proof of concept and therefore did not take usability into account. Therefore, we decided to redesign it in order to support digitization in this area in the future.

## 2 State of the art and related works

The construction industry has long been confronted with the challenge of ensuring compliance with a multitude of regulations, standards, and building codes. The intricacy of these regulations, coupled with the dynamic nature of construction projects, necessitates the development of robust and efficient rule-checking mechanisms. Over the years, various approaches have been devised and refined in order to address these challenges. In recent times, the advent of digital technology has had a profound impact on the field of rule checking within the context of the construction industry. BIM has emerged as a crucial tool, allowing for the integration of regulatory requirements directly into the design and construction process. The research project MBO2BIM focused on preparing BIM-based inspections and creating a unified foundation for the automated verification of building code requirements using BIM-based inspection tools [4]. Another research project about occupational safety knowledge

for workplace planning deals with the digitization of regulations and the establishment of rules for workplaces e.g. checking escape routes [5]. Additional a study that examines a BIM-based method for automated code-checking of fire safety compliance in Canadian timber buildings, focusing on the National Building Code of Canada [6]. These and many other related works highlight the importance of digital code compliance checking for BIM models and the construction industry. Inspecting related works concerning rule checking BIMRL Simplified Schema (BIMRLSS) can be found in [7]. While promising some of the same aspects as OpenBIMRL and with BIMRL as both their basis (BIMRLSS and BIMRL are from the same authors) the approach to their specific DSL is different from the start. OpenBIMRL was initially designed as a graph-based language, and BIMRL(SS) has considered using a visual programming language, but there are no open source implementations yet. [8]. Their program structure also differs. As for the state of the art the comparison of rule-based checking systems by Solihin, Dimyadi, and Lee [8] highlights several key factors that distinguish different approaches to BIM-based automated rule checking. Their analysis, includes criteria such as language openness, practical applicability, and integration capabilities. According to their findings, OpenBIMRL stands out for its modular design and ease of integration with other software systems (Table 1). As to be explained in detail, our revised solution can be integrated into existing code bases in a variety of ways.

Table 1: Eleven-criteria metrics assessment. Modified according to [8].

| **Language or tool** | **1. Formal or standard schema for the rule definition** | **2. Language expressiveness** | **3. Ease of defining rules** | **4. Minimum logic or programming constructs** | **5. Minimum domain knowledge required** | **6. Support for complex rules** | **7. Integrated geometry engine** | **8. Performance indication** | **9. Openness** | **10. Interface to other languages and systems** | **11. Level of maturity** |
|---|---|---|---|---|---|---|---|---|---|---|---|
| NLP | N.A. | N.A. | N.A. | - | - | - | N.A. | ? | - | - | - |
| [...] | | | | | | | | | | | |
| BIMRL | N.A. | + | + | + | + | O | O | + | + | O | O |
| [...] | | | | | | | | | | | |
| Dynamo + Revit | N.A. | - | + | O | - | O | O | O | O | - | + |
| [...] | | | | | | | | | | | |
| [a]Solibri Model Checker (SMC) | N.A. | N.A. | N.A. | N.A. | O | O | + | + | N.A. | N.A. | + |
| OpenBIMRL | + | O | + | + | - | + | + | - | + | + | O |
| [b]BIM.Permit | O | - | + | O | - | + | + | + | + | O | + |

Legend:

| | |
|---|---|
| - | Low |
| O | Moderate |
| + | High |
| N.A. | Not Applicable |
| ? | Unknown |

[a]SMC is included here due its popularity even though it is not strictly language-based rule checking system

[b]BIM.Permit uses the OpenBIMRL

# 3 Methodology

Since this project employs an open format and implementation, the entire development process is accessible and can be reviewed on GitHub[1].

## 3.1 The reference Implementation

The reference implementation consisted of a non open source Industry Foundation Classes (IFC) viewer called *apstex IFC Framework* which as of the time of writing did not receive an update in over four years and does not comply to the latest IFC standards, specifically $IFC4.3ADD2$ [9], [10]. Portability was also not considered for the initial draft and users with different Operating Systems (OS) experienced difficulties using the software in their respective environments.

## 3.2 General Design

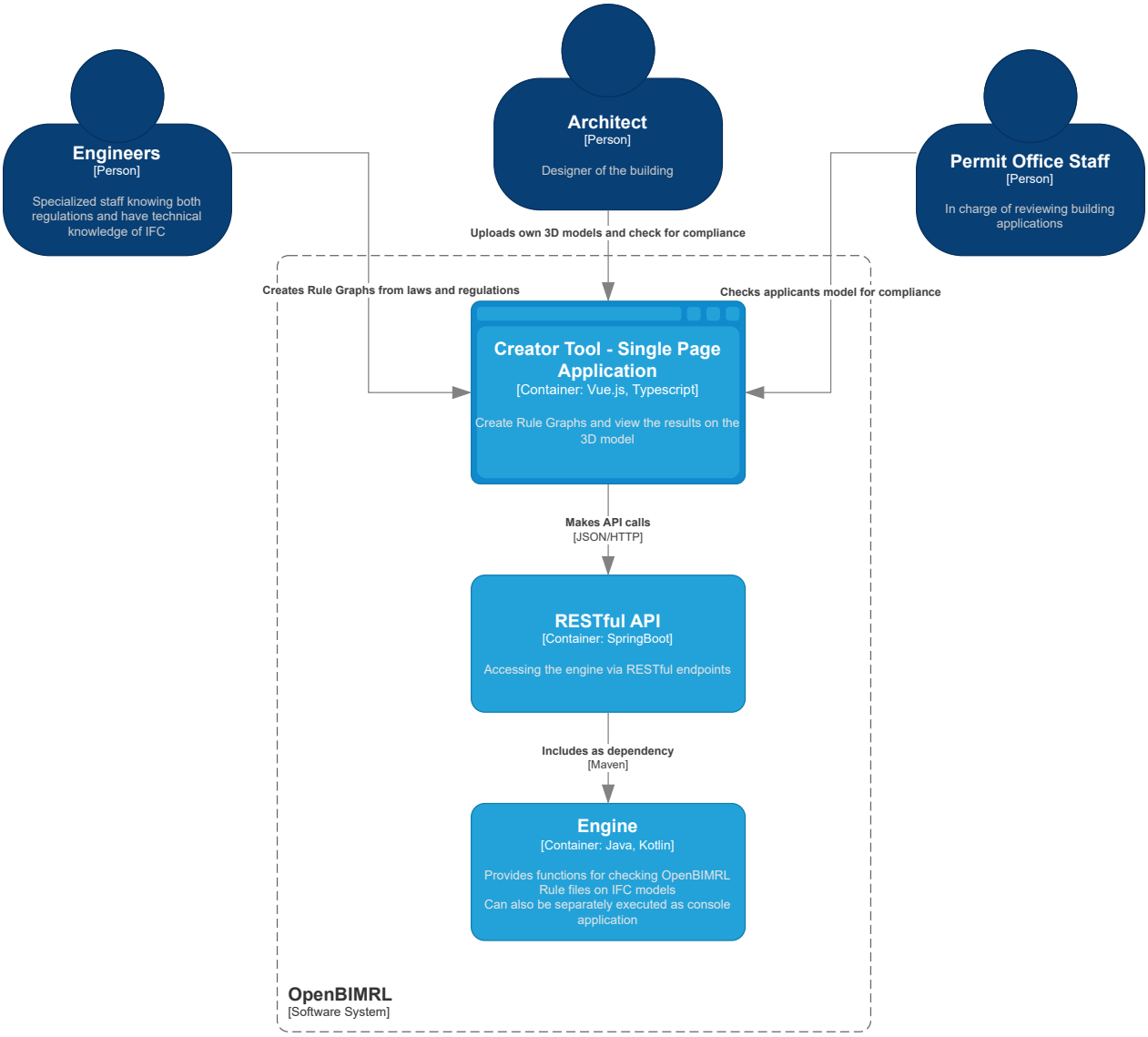


Figure 2: C4 Container diagram of OpenBIMRL.

[1] https://github.com/OpenBimRL/

We have opted for a containerized application with a web-frontend (Creator-Tool) shown in Figure 2, for two main reasons: First, containerization addresses the previously mentioned issue of operating system differences by encapsulating the application and its dependencies within containers, so that a consistent runtime environment across various OS is ensured. This guarantees that our OpenBIMRL implementation operates uniformly regardless the underlying OS. Second, containerization significantly enhances reproducibility. Packaging the application along with its complete environment in containers ensures that the exact setup can be recreated across different systems and by different user(-groups) regardless the previous configuration of their system. This approach not only enhances the reliability but also supports a broader audience by providing an instantaneous repeatable and verifiable environment. For Graphical User Interface (GUI) we chose a web-frontend (client) which is a common choice when using a RESTful API on the backend (server). There are many benefits when targeting the browser as GUI due to the long and ongoing process of standardising ECMAScript (also known as JavaScript), HTML and CSS across all platforms (e.g. mobile, PC, Mac, ...). While some inconsistencies remain, the majority of feature are widely available. With these design choices it is possible for any user to use our software without installing anything[2] while the backend may be deployed by organisations without any prior configuration. Per design the website is not tied to the backend with the intention of choosing a compatible backend. Any system that provides the needed endpoint is a valid option as well as any website, calling these endpoints may display and process given data their way, making not only OpenBIMRL an open standard but also not limiting the user to any of our design implementations. Also the actual rule checking engine has a separate code base to the RESTful API. This is by design to minimise the hurdle of integrating OpenBIMRL into an existing project as it may be included via a dependency management system.

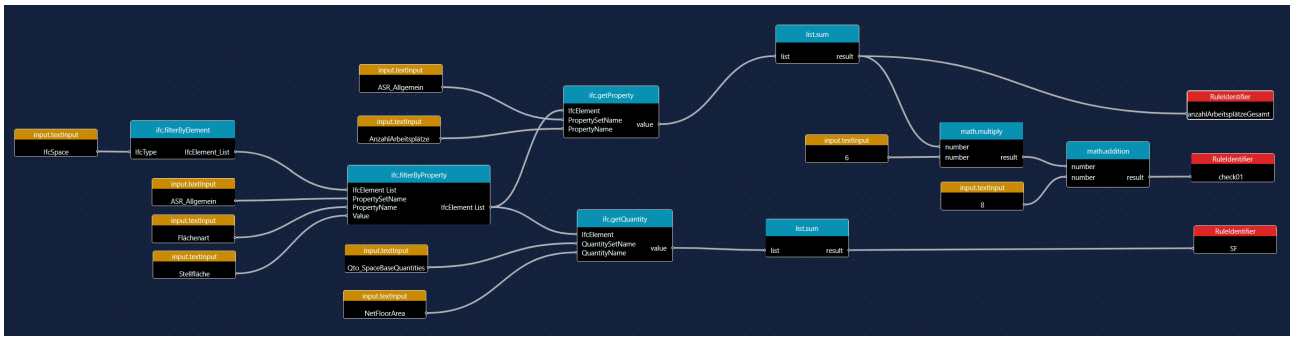


Figure 3: Implementation of a rule set from ASR A1.2 in OpenBIMRL.

When explained, rules can be considered logical but getting to a final result as demonstrated in Figure 3, proved to be a difficult task in terms of debugging. When writing code a so called debugger gives crucial insight into a programs inner workings by exposing changes in values after each operation. The absence of such features can be a significant disadvantage, requiring substantial guesswork, especially when dealing with an unfamiliar DSL. This is where the new implemted feedback loop becomes essential. With the new reference implementation the outputs are displayed ordered by node as a JSON e.g. Algorithm 1. Also the IFC elements can he highlighted in the result viewer.

[2]browser not included but is pre-installed on most devices

Algorithm 1: Output of a rule check.

```
{
  nodes:{
    ifc.getAllPropertySetInformation:{...},
    input.textInput:{...},
    ifc.getProperty:{...},
    ifc.filterByElement:{
      inputs:[...],
      outputs:[
        0:[
          0:{
            type:"IfcSite",
            guid:"20FpTZCqJy2vhVJYtjuIce",
            properties:{...},
            quantities:{...},
          },
          1:{...},
          ...,
        }
      },
    ...
```

## 4 Empirical Study

To see where OpenBIMRL is best used is to look at the application of Germanys' "Technische Regeln für Arbeitsstätten" (technical regulations for workplaces) or ASR for short. For example the rule for checking the ASR A1.2 which regulates the size of office spaces for a given amount of work spaces BAuA [11], may be automated with the graph visualized in Figure 3. While looking intimidating at first, this graph boils down to four steps:

1. Fetching all IfcSpace elements from the BIM model and filtering them for allocated office spaces.
2. At this point the graph splits into two paths. One retrieving the property $AnzahlArbeitspl\cup tze$ (number of work spaces) in the property group $ASR_Allgemein$ (ASR general) which is a IfcProperty specially set for ASR A1.2.
3. The second path retrieves the IfcQuantity $NetFloorArea$ in the quantity group $Qto_SpaceBaseQuantities$ which is a quantity defined in the Ifc specification [12, ch. 5.4.5.6].
4. At the end there are some calculations done to match the space requirements of given work spaces.

The graph is able to perform these steps. Once the graph is done executing there are checks done to verify the results. In this case the check in Figure 4 compares each workplaces' space requirement against their actual floor area and produces a list of Boolean values (e.g.: [true, false, ...]) which are then again reduced to a final check result. This is done by defining the underlying group check

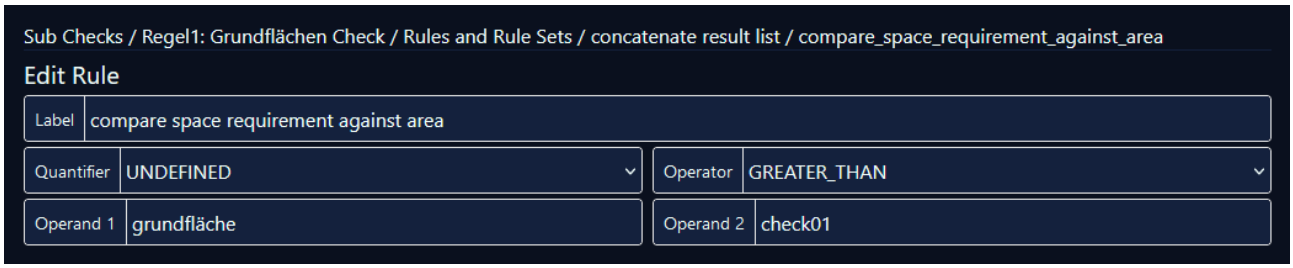


Figure 4: Checking the result of check01 against the floor area.

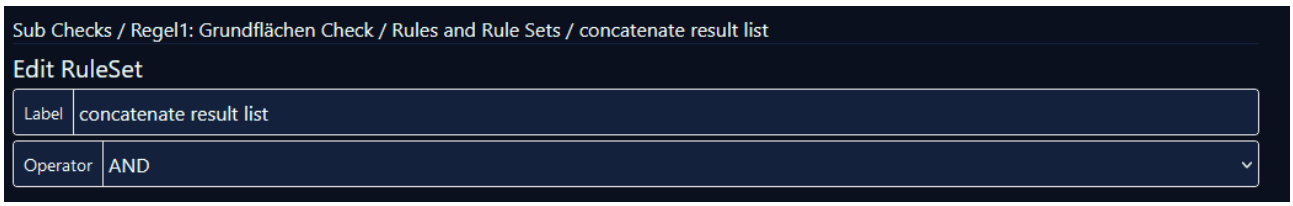


Figure 5: Defining logical operator for result sets.

and setting the concatenation operator to $AND$ as seen in Figure 5 which logically applies the $AND$ operation to all elements of the list.

## 5 Discussion

OpenBIMRL is not at all finished. Limitations include: Currently, OpenBIMRL is not dynamic in terms of graph nodes. All nodes currently available had to be implemented one by one and are static in their behavior.This lack of dynamism limits the flexibility and adaptability of the system, which can be a significant drawback in complex and evolving projects. Large graphs become quite difficult to navigate with no option to group related nodes together.This can lead to confusion and inefficiencies, as users struggle to maintain a clear overview of the project structure. Furthermore, the current system has a critical flaw in data persistence. When the creator page is reloaded, all the work is lost since it is not stored unless manually saved. To improve OpenBIMRL, it is essential to address these issues.

## 6 Conclusion and future work

In a nutshell the process of adapting new rules has been streamlined and the feedback now provided enables everyone using the new reference implementation of OpenBIMRL to better understand the inner workings of the system. Furthermore, the newly introduced modularity facilitates the seamless integration of OpenBIMRL into other software systems. Addressing the limitations, one thing currently on our bucket list are groups. Much like Unreal Engines Blueprint DSL Nodes may be visually clustered as distinct groups or act as one Node with their inputs and outputs inherited from the grouped Nodes they call Macros [13]. Another limitation - the lack of dynamic behaviour of nodes - can be elevated by allowing the creation of "code nodes". These nodes, ideally sand-boxed, capable of executing arbitrary code in a general-purpose programming language, would allow extendability without modifying the core system's source code.

## References

[1] Jesco Denzel for the German federal government, *Planungsbeschleunigung, digitalisierung und wärmewende*, https://www.bmwsb.bund.de/SharedDocs/kurzmeldungen/Webs/BMWSB/DE/2023/03/meseberg.html, 2023.

[2] J. Dimyadi, W. Solihin, C. Eastman, and R. Amor, "Integrating the bim rule language into compliant design audit processes", Nov. 2016.

[3] M. Stepien, A. Vonthron, and M. König, "Openbimrl – an open format for code compliance checking of complex functional requirements from a regulation to the bim model", Jul. 2023.

[4] Chair of Computing in Engineering of the Ruhr-University Bochum, "Digitalisierung der Musterbauordnung (MBO2BIM)", Tech. Rep.

[5] Bundesanstalt für Arbeitsschutz und Arbeitsmedizin (BAuA) [Federal Institute for Occupational Safety and Health], "Arbeitsschutzwissen für die Arbeitsstättenplanung - Neue Planungsinstrumente zur Unterstützung einer arbeitsschutzgerechten Gestaltung bei der Bau-Planung von Arbeitsstätten durch eine bauteilorientierte und maschinenausführbare Aufbereitung des Arbeitsstättenrechts", Tech. Rep.

[6] K. Kincelova, C. Boton, P. Blanchet, and C. Dagenais, "Fire safety in tall timber building: A bim-based automated code-checking approach", *Buildings*, vol. 10, no. 7, 2020. DOI: 10.3390/buildings10070121. [Online]. Available: https://www.mdpi.com/2075-5309/10/7/121.

[7] W. Solihin, J. Dimyadi, Y.-C. Lee, C. Eastman, and R. Amor, "Simplified schema queries for supporting bim-based rule-checking applications", *Automation in Construction*, vol. 117, 2020. DOI: 10.1016/j.autcon.2020.103248. [Online]. Available: https://www.scopus.com/inward/record.uri?eid=2-s2.0-85084290727&doi=10.1016%2fj.autcon.2020.103248&partnerID=40&md5=6aa7679ba4b23d1fe8c745a2ecc99587.

[8] W. Solihin, J. Dimyadi, and Y.-C. Lee, "In search of open and practical language-driven bim-based automated rule checking systems", in *Advances in Informatics and Computing in Civil and Construction Engineering*, I. Mutis and T. Hartmann, editors, Cham: Springer International Publishing, 2019, pp. 577–584.

[9] *apstex IFC Framework*, https://www.apstex.com/.

[10] *IFC schema specifications*, https://technical.buildingsmart.org/standards/ifc/ifc-schema-specifications/.

[11] Bundesanstalt für Arbeitsschutz und Arbeitsmedizin (BAuA) [Federal Institute for Occupational Safety and Health], "Bek. v. 1.3.22, Bekanntmachung von Technischen Regeln; ASR A1.2 „Raumabmessungen und Bewegungsflächen"", *Gemeinsames Ministerialblatt*, p. 241, 2022.

[12] *IFC4x3ADD2 Schema Specifications*, buildingSMART International, Ltd., 2023, ch. 5.4.5.6,

[13] *Unreal engine 4.27 documentation*, Epic Games, Inc., Macro Library UI.

# Semi-automated assessment in fundamental BIM pedagogy for large cohorts

Jiabin Wu[1], Sebastian Esser[1], Kasimir Forth[1], Ainur Kairlapova[1] and Julian Gerstner[1]
[1]Chair of Computational Modeling and Simulation, Technical University Munich, Arcisstr. 21, 80333 Munich, Germany
E-mail(s): j.wu@tum.de, sebastian.esser@tum.de, kasimir.forth@tum.de, ainur.kairlapova@tum.de, julian.gerstner@tum.de

**Abstract:** Due to the increasing relevance of Building Information Modeling (BIM) in students' curricula, BIM courses are increasingly in demand. Hence, to advance the quality of teaching and practical application, the Technical University of Munich split BIM teaching into four consecutive parts: BIM.fundamentals, BIM.project, BIM.advanced, and BIM.infra. For the fundamental BIM course, we use graded assignments in the fields of geometric and semantic modeling, model checking, and rendering, which add to voluntary exercise tutorials. However, individual support and evaluation of the assignments cannot be offered for large cohorts exceeding more than 400 students but requires means to streamline feedback provision. We developed a semi-automated workflow for practical assignments using State-of-the-Art digital methods to efficiently evaluate these individually and fairly, even for large numbers of students. To support the objective of geometric and semantic modeling using open BIM technology, we utilize semi-automated, rule-based model-checking approaches. Additionally, based on parametric design generation, we provide individual IFC models to enhance the object of exercising BIM collaboration tasks, such as clash detection and BCF-based communication. To evaluate the use case implementation of model visualization, we aim to use Computer Vision techniques to semi-automatically assess the rendering quality.
*Keywords:* Building Information Modeling (BIM), Industry Foundation Classes (IFC), Model Checking, Engineering Pedagogy

Erschienen in Tagungsband 35. Forum Bauinformatik 2024, Hamburg, Deutschland, DOI: 10.15480/882.13493
© 2024 Das Copyright für diesen Beitrag liegt bei den Autoren. Verwendung erlaubt unter Creative Commons Lizenz Namensnennung 4.0 International.

## 1 Introduction

Traditionally, computational methods for the built environment have attracted a few students enrolled in engineering study programs (e.g., civil or environmental engineering). Participants sometimes hesitated to enroll due to the extensive computer science concepts involved in related teaching modules. Nowadays, an increasing number of students use digital methods to design and construct built facilities, particularly with the growing interest in Building Information Modeling (BIM). This has led to a significant rising demand for BIM courses. At the same time, motivation and average performance

among participants appear to decrease due to the complex interdisciplinary knowledge and the variety of software applications required. Conventional lectures comprised of theoretical introductions and software exercises lack systematic enhancement methods to effectively guide and motivate participants. Designing suitable learning materials with comprehensive feedback support requires significant curriculum rearrangement, but this is necessary.

Model checking techniques have been extensively studied to facilitate the evaluation of building designs against established building codes [1]. Given the varying levels of complexity [2], a theoretically infinite number of rules can be defined to assess whether a BIM model meets or fails specific requirements. In a similar vein, automated assessment approaches can be integrated to streamline the evaluation of student works in fundamental BIM education. This integration promises to enhance the evaluation efficiency and facilitate the effective implementation of pedagogical strategies for a growing student population. Hence, this study seeks to address the question of how advanced BIM technologies can be leveraged to enhance teaching methods and evaluate performance improvements in fundamental BIM pedagogy for large cohorts.

# 2 Context

Challenges in offering effective BIM courses by universities hinder the preparation of students for a digital future in the construction sector [3]. Designing the learning material for the rapidly changing field of BIM has proven difficult and requires significant effort. Integrating BIM into higher education necessitates several key components to reach its full potential for training future engineers. For example, participants are supposed to learn relevant industry software and understand various roles in collaborative work. Appropriate teaching methods are essential to offer up-to-date fundamental knowledge and practical exercises, helping students document and communicate their ideas, incorporating elements such as collaborative curricula, industry relevance, and technical skills [4]. Educators typically use tutorials, exercises, assignments, and supporting exercises in such modules [5].

BuildingSMART International standardized a four-level professional certification, differentiating between entry, foundation, management, and practitioner knowledge [6]. The entry level is a self-learning offer, while the foundation level is also suitable for students, and management and practitioner levels with its openBIM management and openBIM coordination offers are available for professionals with industry experience. In German university teaching, the German Association of Computing in Civil Engineering defined BIM-related topics for teaching in Master's degree programs [7]. Besides general motivation and digital modeling of buildings and infrastructure, the main topics are geometry representation, data exchange, data management, digital modeling of processes, and BIM use cases.

# 3 Methodology

## 3.1 Overview of BIM teaching at Technical University of Munich

Figure 1 illustrates the modules at TUM. The course *BIM.fundamentals* focuses on the basic principles of BIM. The module aims to equip students with the ability to understand and apply Building Information Modeling (BIM) in the planning process, identify and solve potential issues within BIM processes, and critically evaluate commercial software options for BIM-based planning. Our students learn to

appropriately select and utilize digital analysis and simulation tools, analyze BIM technologies through case studies, comprehend BIM data formats, and effectively utilize data exchange mechanisms. The course content covers various aspects, including digital technology introduction, BIM concepts and terminology, use cases, BIM systems, geometric modeling, collaborative workflows, and BIM-GIS integration. Teaching methods include lectures for theoretical understanding and tutorials with software examples and exercises to reinforce practical skills.
Following the essential foundations taught in BIM.fundamentals, several additional modules can be selected to gain additional skills in this topic. *BIM.project* is a seminar coursework. In this module, students team up in groups of five and perform joint project work. Besides creating BIM models in dedicated authoring tools, students perform coordination and other simulations across different disciplines.

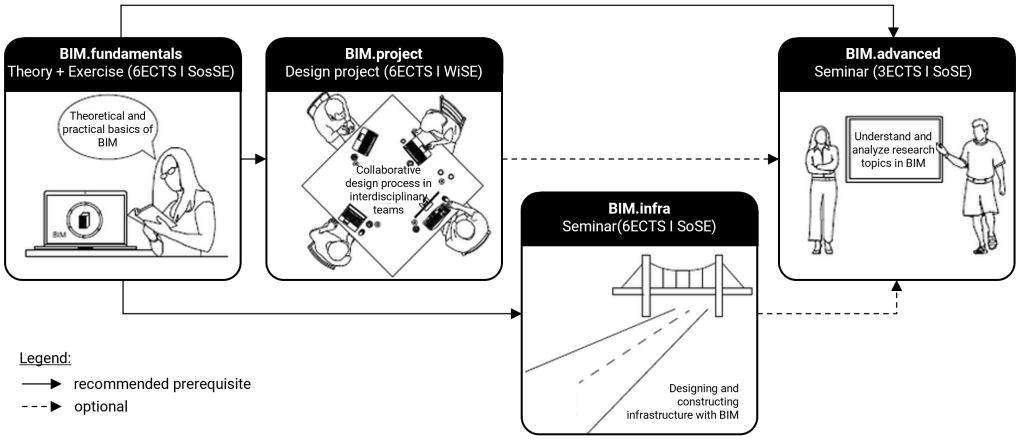


Figure 1: BIM Courses offered at TUM

To deepen the understanding of how BIM is adopted in the industry, the module *BIM.advanced* is a lecture series where practitioners present how they utilize BIM and other digital methods in the design and construction process. In addition to that, the students investigate a technological or scientific topic in-depth and summarize their findings in a written report. Upon completing the *BIM.infra* module, students will possess a comprehensive understanding of creating and evaluating client information requirements and BIM execution plans in transport infrastructure construction projects, along with proficiency in classifying specific discipline requirements within the scope of infrastructure projects. They will also acquire practical knowledge of industry-standard data exchange formats and software products, enabling them to effectively utilize these tools to develop solutions for BIM-based planning tasks in traffic route construction.

### 3.2 Overall teaching approach for basic BIM knowledge

The *BIM.fundamentals* course is available for Master's students of different study programs, such as architecture, civil and structural engineering, sustainability, and more. As shown in Figure 2, the course is structured in theoretical lectures, covering the topics of geometric and parametric modeling, data management and collaboration, model checking, data exchange and interoperability, project

execution, and BIM use cases such as Quantity Take-offs, documentation, sustainability analyses, or BIM and GIS.

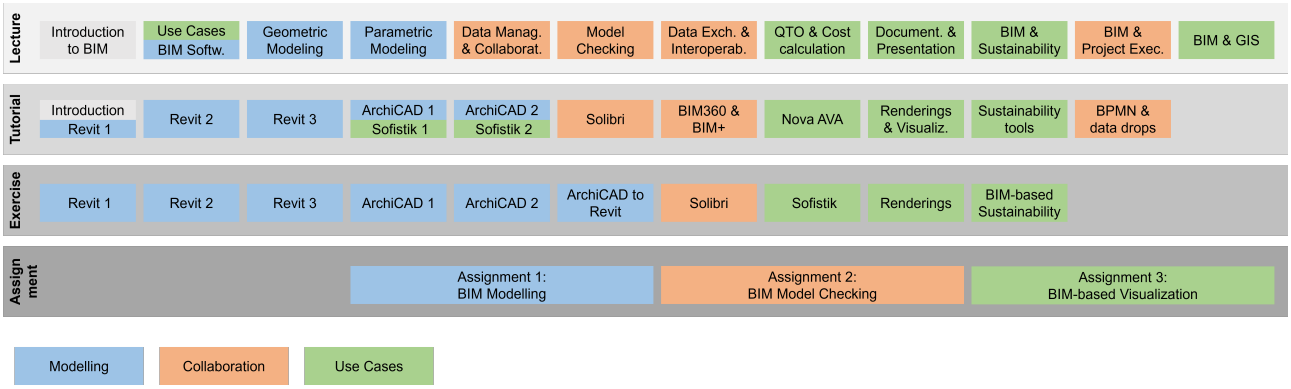


Figure 2: Overview of different blocks and content of the BIM.fundamentals module at Technical University of Munich

Practical tutorials follow the lectures to apply the theoretical concepts in class using different software products introduced by tutors. Afterward, the students are encouraged to do self-studying blocks using exercise sheets for deepening the learned content in the field of BIM model authoring, IFC export, BIM-based structural analyses, or several BIM-based sustainability assessments, such as solar radiation studies, daylight and complete building energy simulation, and life cycle assessment. To increase the students' motivation for practice and to check the learning outcome of the tutorials and exercise sheets, we introduced three voluntary assignments, which were corrected and included in the grading process. The assignments cover the topics of model authoring, model checking and the use case of visualization, which will be introduced in the following sections.

### 3.2.1 BIM modeling with authoring tools

The model authoring assignment focuses on BIM-based modeling, enabling participants to produce OpenBIM models that adhere to specified semantic, geometric, and exchange requirements. Participants are free to choose their preferred authoring software, including but not limited to Autodesk Revit, Graphisoft ArchiCAD, and Allplan, to develop a model representing either a residential or office building.

The building outline shapes, geometric parameters, and dimensional specifications are individually generated for each participant by the organizers. Essential building objects such as walls, windows, columns, doors, beams, roofs, slabs, and stairs must be included, with a sufficient variety of object types. Specific emphasis must be spent on the semantics of load-bearing building elements, as well as the accurate designation of internal and external walls and doors. Furthermore, the assignment mandates space objects with descriptive names and realistically sized areas for their intended use. The final deliverable must adhere to the IFC 4 Reference View standards to enhance participants' understanding of the collaborative design process. The model authoring assignment aims to help participants enhance their BIM and IFC proficiency and develop skills to integrate architectural and structural considerations into a functional model.

### 3.2.2 Model Checking

The model checking assignment involves examining an IFC model of a three-story office building to identify and communicate design issues in accordance with specified requirements with the Solibri Office model checker. This assignment includes several space-related architectural checks, such as window-to-space area ratios, minimum room areas, and space accessibility. It also involves checking door clearance for clashes with furniture and detecting incorrectly assigned properties, like internal walls mistakenly marked as external.
To communicate the model checking results for each task, participants must briefly describe the detected issues, provide a textual proposal for resolution, and attach a highlighted view that includes the affected building parts. Additional information, such as coordination and responsibilities, is optional but recommended. The final deliverable is a bcfzip file adhering to the BCF Report v2.0 format. This assignment aims to familiarize participants with the OpenBIM workflow including models and issue communication means to enhance their skills in model quality control.

### 3.2.3 Visualization

To perform a thorough downstream application without required domain-specific knowledge, the scope of the third assignment is the creation of BIM-based renderings. Therefore, two visualizations are requested from the students, one each from the interior and exterior of the student's model of the first assignment. Several requirements are set for the renderings and used for grading, such as clear and consistent lighting, materials settings including intended textures and reflection, surroundings and people, and realistic sky and weather conditions.

# 4 Implementation

Students hand in their solutions via a Moodle platform hosted by TUM. The course instructors then use Moodle's batch download options to import all submissions into the checking platform. Due to the specific demands and the variety of data of the three different assignments, a dedicated checking platform has been implemented to streamline the evaluation process of all three assignments. The platform itself is developed in Python and offers a web-based user interface. It further utilizes additional software packages described in the following paragraphs.

## 4.1 Automated model quality checking

To effectively evaluate the large number of assignments submitted for the first assignment, we automated the process of checking the IFC models. Tasks in the assignment outline the concrete requirements that have to be reached in a model by students. Each requirement is graded with specific points depending on the delivered quality. Hence, the threshold of these criteria played an important role in the fair assessment of the models. Figure 3 represents the workflow performed from the parametrization of assignment tasks up to the grading process using the model checking Solibri software. The ruleset, as well as information take-off (ITO) templates, were created to retrieve the relevant parameters of the model. To address the number of submitted models, the Solibri Autorun extension tool is utilized to be able to process them in a batch. Later, the results are fed into the checking platform, where previously set thresholds are applied to grade the students accordingly.

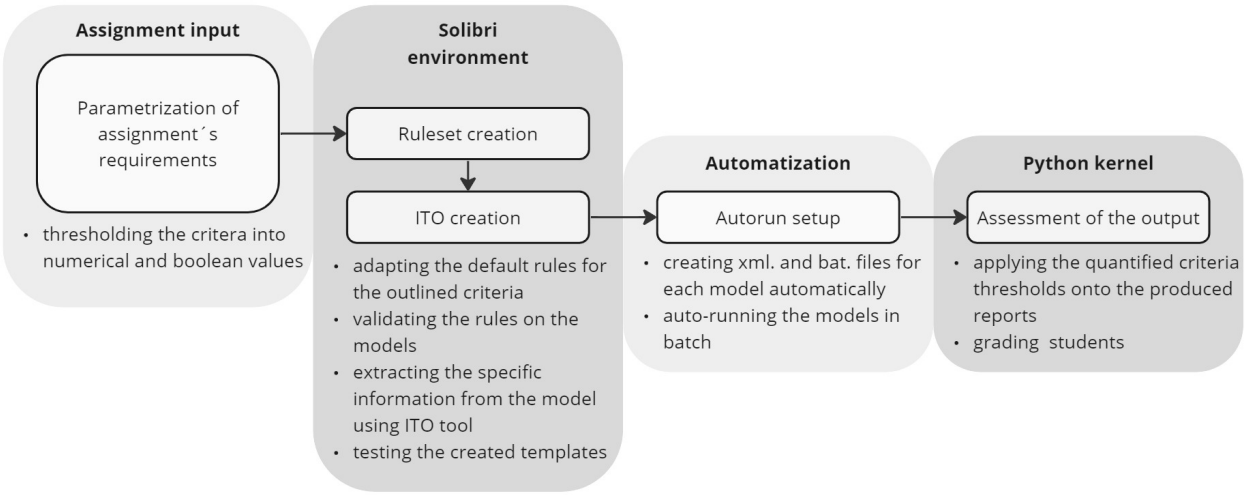


Figure 3: Automated model quality checking workflow

## 4.2 BCF parsing of model checking

To ensure robust evaluation, we use parametric modeling to create unique models with different issues for each participant. For example, space accessibility errors are introduced by randomly removing doors from internal spaces, while internal and external property errors are created by mislabeling internal walls as external. By varying a basic model of a three-story office building and refreshing all IFC GUIDs, we provide unique IFC files for each participant to complete the model checking assignment. This approach offers different architectural issues and enables an automated assessment process based on parametrically pre-defined design errors each participant must identify.

Based on these custom models, each student performs model checking and submits a bcfzip file containing the identified deficiencies. Each issue must include the task title, descriptions, authorship details, and snapshots. The instructors evaluate the textual description and resolution proposal of the detected issues manually. Additionally, the referenced elements in the snapshot are extracted from viewpoint files. We automatically check if the identified components carry the correct IFC GUIDs and comply with the expected values originating from the parametric model generation. The approach taken facilitates the evaluation process and efficiently helps prevent plagiarism in large cohorts.

## 4.3 Visual quality checking of Renderings

Figure 4 exemplarily shows the platform for manually grading the rendering quality of the exterior in the third assignment. In total, 10 points can be achieved for both interior and exterior rendering. For every criterion, the grading step is 0.5 points with one point maximum each for exterior and interior light conditions, people, aesthetics, and perspectives for the exterior and interior renderings, and half a point for exterior and interior materials, exterior ground, and sky conditions.

A practical study was conducted to find a means of semi-automating the visual quality checking of the renderings submitted by students. The goal was to find a ready-made deep-learning model to semantically understand the renderings and output individual scores in all ten categories. This output can then aid the examiners by providing a rough grading preview. Deep-learning models of the types "Visual Question Answering" and "Image Text to Text" provide the most promising results out of the

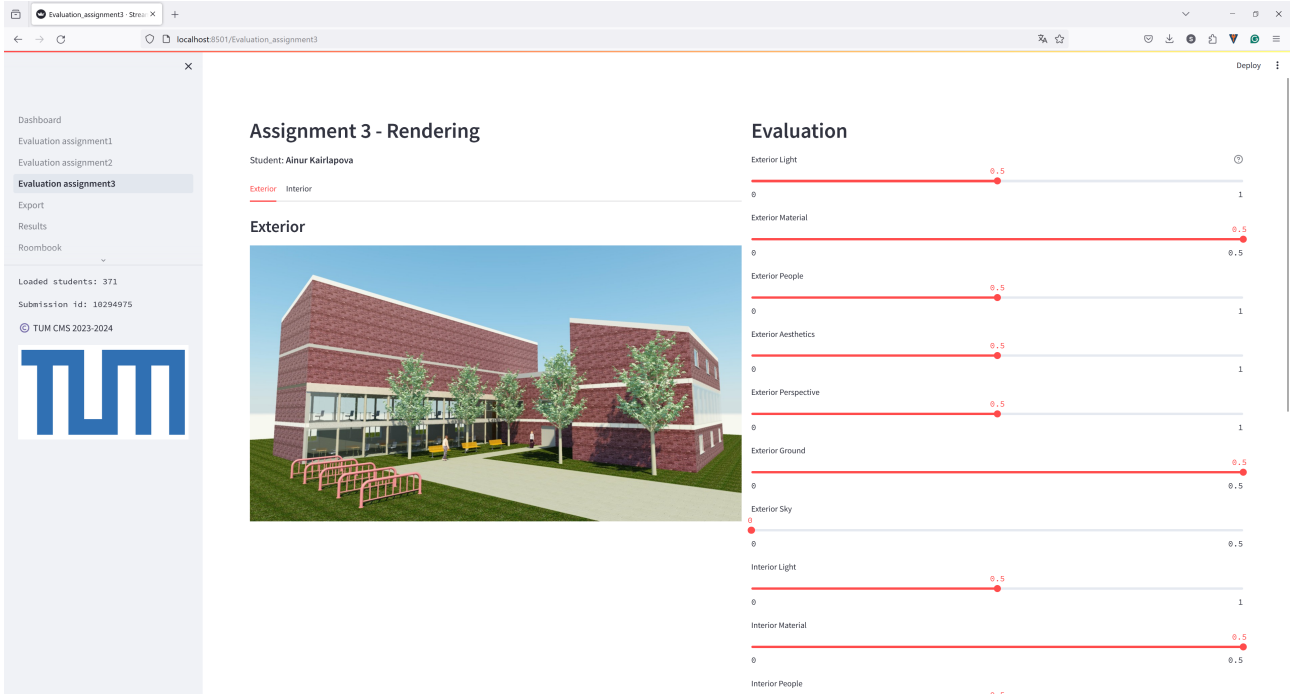


Figure 4: Manual grading of exterior rendering as the third assignment

box. The best model tested is Google's PaliGemma 3B Mix 224 [8], an open vision-language model. While not able to output structured data representations, it can output "yes" or "no" when specific questions for the respective categories are prompted. The accuracy, computed as the number of correct predictions divided by the number of all predictions, of the model's predictions was asserted by comparing the model predictions to the ground truth grading for all images and all categories from a previous semester. The category "Exterior Sky" shows the lowest accuracy of 71.68%. The highest accuracy is achieved for the category "Interior Material", with a value of 95.33%. This binary prediction does not yet allow for the more fine-grained grading of the categories that can receive a score of 0, 0.5, or 1. Further testing and possibly transfer learning must be done for the model to be used for fully automated quality checking of the renderings.

## 5 Conclusion and Outlook

The semi-automated assessment method presented in this paper enables efficient evaluation of large cohorts of students. This method checks the quality of OpenBIM models and extracts the core elements in design issue communication files in an automated manner, significantly reducing the time and effort required in manual evaluation. It also facilitates the visual quality assessment of renderings and has the potential to leverage machine learning for more efficient evaluations. This automated evaluation allows course participants to receive more timely and consistent feedback, enhancing their theoretical BIM knowledge and supporting systematic practices of BIM-related skills.

We envision this system as a continuous support mechanism where participants can upload their assignments and receive instant feedback. Furthermore, the current checking kernel could be improved to accommodate larger IFC files, enabling the evaluation of more complex exercises. Furthermore, we

envision incorporating the checking system into the Moodle platform to enable students to check their models already during the assignment preparation. Such an integration would allow even more direct individual feedback to the students.
Besides this, further investigations are planned to enhance the quality checking of submitted renderings. Given the visual grading of architectural renderings is more subjective than the technical grading of an IFC model, predicting the renderings' scores roughly as an aid to the examiners may be sufficient. This is already possible with the above-mentioned accuracy achieved with the pre-trained model. We will report on this matter in future publications.

## Acknowledgements

We would like to express our appreciation for our student assistants' support in implementing our checking kernel. Namely, we want to thank Kai Dietmair, Tomas Curti Spielmann, and Nepomuk Wolf for their work during the initial prototyping phase.

## References

[1] C. Eastman, J.-m. Lee, Y.-s. Jeong, and J.-k. Lee, "Automatic rule-based checking of building designs", *Automation in Construction*, vol. 18, pp. 1011–1033, 8 Dec. 2009. DOI: 10.1016/j.autcon.2009.07.002.

[2] W. Solihin and C. Eastman, "Classification of rules for automated bim rule checking development", *Automation in Construction*, vol. 53, pp. 69–82, May 2015. DOI: 10.1016/j.autcon.2015.03.003.

[3] O. Casasayas, M. R. Hosseini, D. J. Edwards, S. Shuchi, and M. Chowdhury, "Integrating BIM in Higher Education Programs: Barriers and Remedial Solutions in Australia", *Journal of Architectural Engineering*, vol. 27, no. 1, pp. 1–11, 2021. DOI: 10.1061/(asce)ae.1943-5568.0000444.

[4] M. Shelbourn, J. Macdonald, T. McCuen, and S. Lee, "Students' perceptions of BIM education in the higher education sector: A UK and US perspective", *Industry and Higher Education*, vol. 31, no. 5, pp. 293–304, 2017. DOI: 10.1177/0950422217725962.

[5] M. Hu, "BIM-Enabled Pedagogy Approach: Using BIM as an Instructional Tool in Technology Courses", *Journal of Professional Issues in Engineering Education and Practice*, vol. 145, no. 1, pp. 1–9, 2019. DOI: 10.1061/(ASCE)EI.1943-5541.0000398.

[6] buildingSMART Professional Certification, *Our Program - buildingSMART Professional Certification*, 2024. [Online]. Available: https://education.buildingsmart.org/our-program/ (visited on 05/24/2024).

[7] GACCE, *Building Information Modeling: BIM in university teaching for the subject of building informatics*, German Association of Computing in Civil Engineering, editor, 2024. [Online]. Available: https://gacce.de/bim/ (visited on 05/24/2024).

[8] G. Research, *Google Research Big Vision PaliGemma*, Google Reasearch, editor, 2024. [Online]. Available: https://github.com/google-research/big_vision/tree/main/big_vision/configs/proj/paligemma (visited on 05/24/2024).

# Simplification of Polygons from Point Cloud Data for Automated Floorplan Generation

Antonio Carlone[1] and Felix Gabler[1]
[1]Fachgebiet für Bauinformatik, Technische Universität Berlin, Gustav-Meyer-Allee 25, 13355 Berlin, Germany
E-mail(s): carlone@tu-berlin.de, f.gabler@tu-berlin.de

**Abstract:** This paper investigates methodologies for identifying significant edges in polygons, with a particular focus on applications in floor plan analysis. The primary objective is to develop and evaluate an algorithm that can accurately simplify and refine polygonal representations of rooms, ensuring that key structural details are preserved. The study introduces a novel simplification algorithm that combines holistic filtering, regression techniques, and a mechanism for closing polygons. This algorithm is designed to address the shortcomings of existing methods by providing a more comprehensive approach to reducing complexity while maintaining essential geometric features. The algorithm is validated through testing on two datasets of floor plans derived from real laser scans. The findings contribute to the field of automated floor plan generation, offering a scale-independent solution for simplifying redundant polygonal data while preserving spatial accuracy.
*Keywords:* indoor environment, polygon simplification, automated floorplan generation, scan-to-BIM

Erschienen in Tagungsband 35. Forum Bauinformatik 2024, Hamburg, Deutschland, DOI: 10.15480/882.13546
© 2024 Das Copyright für diesen Beitrag liegt bei den Autoren. Verwendung erlaubt unter Creative Commons Lizenz Namensnennung 4.0 International.

## 1 Introduction

As digitalization continues to transform the Architecture, Engineering, Construction, and Operations (AECO) industry, floor plans have evolved from hand-drawn sketches to derivations from digital BIM models. Automation has become integral to various processes, including the creation of Indoor Floor Plans (IFPs). IFPs are crucial in fields such as architectural design, indoor navigation, and safety assessment. However, the creation of IFPs is not only of relevance during the planning phase of new buildings, but is also essential for depicting existing buildings and as-built documentation. Traditionally, the manual creation of IFPs is labor-intensive and time-consuming, leading to a growing interest in their automatic generation. Consequently, scan-to-BIM approaches have emerged as a popular solution [1]. Creating floor plans from laser scans allows for the recreation of existing building layouts, often resulting in models that are more accurate than the original plans due to potential building inaccuracies [2].

## 2 Related Research

To automate IFP creation and ensure their consistency with original indoor layouts, many methods for generating IFPs from indoor 3D point clouds have been proposed. [3]
There are several sources of inaccuracies for room polygons compared to the planned building model. Inaccuracies occur during the construction phase but can also be caused by measurement errors and the standard deviation of laser scanners [2], [4]. In the worst case, these errors accumulate. The major challenges in dealing with inaccuracies in 2D floor plans involves handling corners and more vertices within a polygon than necessary [5], [6].
Existing approaches that could provide a solution are the Douglas-Peucker algorithm [7], the RANSAC algorithm [8], the alpha shapes algorithm [9], the Line Segment Detector (LSD) [10], and the algorithm proposed by Phan, Huynh, and Truong-Hong [11].
The Douglas-Peucker algorithm is a line reduction algorithm that takes a polygonal chain as input. It detects significant vertices and connects them to a new polygonal chain [7]. This algorithm cannot repair corners that are not represented by a vertex, because it cannot generate new vertices. Bad representations of corners often occur in measured room polygons and hence the algorithm is not suitable for simplification after pre-processing [6].
The RANSAC algorithm is used to perform a regression on a set of data points omitting points of gross errors. It can be applied in 2D and 3D, but does not aim to simplify the data points to exactly one point per corner and therefore may not simplify it to the desired degree [8].
The alpha shape algorithm proposed by Edelsbrunner, Kirkpatrick, and Seidel [9] finds a closed polygonal chain in a set of points that encloses every point of the set. Varying the alpha value of the algorithm defines the degree of fineness. This approach does not simplify the polygon to a degree where only the clear corners are represented by a vertex and therefore is not suitable here while still being used for pre-processing.
The LSD works in the field of line recognition in pictures, therefore is not suitable to simplify room polygons [10]. Nevertheless, principle steps of this algorithm can be adopted to the current problem.
Phan, Huynh, and Truong-Hong [11] use the RANSAC and alpha shapes algorithm to generate 2D floor plans from 3D point clouds. Their simplification of the room polygons needs an absolute length value whereas our approach works with percentages relative to the room polygons perimeter, making it scalable.

## 3 Simplification Algorithm

In this chapter, a new algorithm is presented to simplify a polygon representing a room in a floor plan. First, the research objectives are defined in Section 3.1 followed by the definition of the input data in Section 3.2. Next the processing stages are explained in Section 3.3 and finally, examples and limitations are discussed in Section 3.4.

### 3.1 Objectives

While point cloud data naturally consists of a large number of points, polygons benefit from as less points as needed. The description of the footprint of a room usually only requires one vertex per

corner and a linear connection between them. Figure 1 shows two polygons in different simplification stages of the same room. The polygon depicted in Figure 1a represents the concave hull derived from a segmented and sliced point cloud, consisting of 1192 vertices. The polygon in Figure 1b represents the same room. It has been modelled using a CAD-tool and consists of only 8 vertices.

The polygons in Figure 1 are divided into regions (r1 to r8) and corners (e.g. r1/r2) between them. While the region r4 is represented by exactly one edge for the modelled polygon, the region r4 of the left polygon consists of multiple. Corners however, see corner r4/r5 for the left polygon, may show diagonal characteristics and may not be clearly presented. Depending on which information is of interest, e.g. the area of the polygon/room, additional vertices do not contribute to information enrichment.

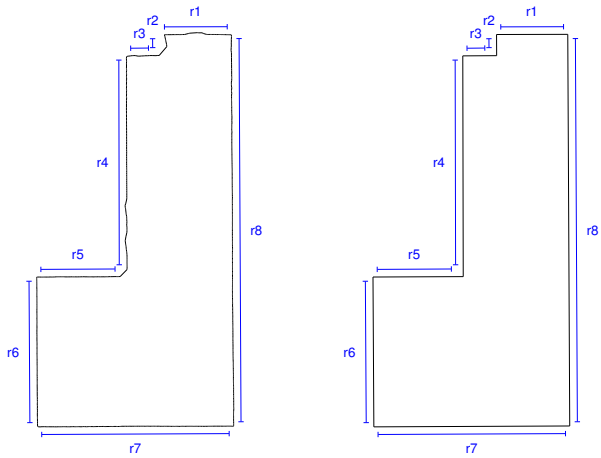


(a) Polygon from point cloud with 1192 vertices.

(b) The same polygon modelled with 8 vertices.

Figure 1: Comparison of two room polygons in different quality stages.

This paper aims to offer a solution to the simplification of closed planar polygons derived from point clouds. The main focus is on reducing the number of vertices while sharpening corners at the same time. Limiting the field of application to indoor situations of the built environment allows focusing on typical room geometries. Floor plans with exclusively one straight line per region as area boundaries are classified as typical room geometries while occurrences of arcs or diagonal lines are referred to as irregularities [12]. While the simplest room geometry is a rectangle, more complicated polygons may occur. Considering the possibility of slanted walls means that we are not restricted to the manhattan world assumption. Taking building elements such as columns into consideration, room polygons may have protrusions. Niches however, may be created by recesses. It is assumed that combinations of these features cover the majority of room geometries.

### 3.2 Preliminaries

Polygons are the input of our algorithm. They must neither be self-intersecting nor self-touching. However, polygons may have holes. Therefore polygons must consist of one exterior boundary and may have none to multiple intersecting-free interior boundaries. As interior and exterior boundaries,

both are closed edge-loops, they will be treated equally. Each single polygonal chain is processed individually and is referred to as polygon in the following.

## 3.3 Processing Stages

Our algorithm consists of three processing stages, as shown in the first column of Table 1. The first stage, the Holistic Filter, receives a closed polygon as input and involves the most important step of the algorithm, the identification of significant edges. The result of the Holistic Filter, a collection of significant edges, is further processed by a Regression on Sectors. Resulting line segments are then connected to achieve a closed polygonal chain.

Table 1: Processing Stages and Parameter Configuration of the Simplification Algorithm determined from the two datasets.

| Processing Stage | Parameter | Value |
|---|---|---|
| Holistic Filter | angle threshold<br>length threshold | 2.7°<br>10% of the perimeter |
| Regression on Sectors | sector angle threshold<br>on edge threshold | 45°<br>0.787% of the perimeter |
| Connecting Representatives | distance margin<br>complete threshold | 10% of the perimeter<br>90% of the edge |

### 3.3.1 Holistic Filter

The Holistic Filter represents the core of the presented approach. Its function is to identify and collect significant edges of the polygon. It is assumed that a subset of edges is sufficient to approximately represent the polygon while preserving geometric information such as the area. The input is a closed polygon and its output is a set of edges. We define them as *significant edges*. However, the original order of the vertices is preserved for the last step of our algorithm.
In a first step, for each edge a group of supporting edges including itself is identified. All edges whose angle to the examined edge is smaller than a specific angle threshold are members of this group. Using an angle threshold of 2.7° (see table 1) showed the best results for the test data. In a second step, the accumulated length of the resulting sets of edges is evaluated. If a length of a group is greater than 10% of the perimeter of the original polygon, the corresponding edge is a *significant edge*. Filtering edges by its group length instead of its individual edge length ensures the identification of protrusion edges as *significant edges*. It is assumed, that protrusion edges have a similar orientation as other edges. The set of *significant edges* is passed to the next step.

### 3.3.2 Regression on Sectors

The second step of our algorithm groups the significant edges to *sectors* and calculates a representative edge per *sector*. *Significant edges* belong to the same *sector* if two conditions are met: First, the distance of the vertices of two edges must be below a defined threshold (see *on edge threshold* in table 1), relative to the perimeter of the polygon. Second, the angle between the two edges, must be less than the defined *sector angle threshold* of 45°.
For each *sector*, a weighted regression, considering the length of each edge, is performed. The result of each regression is one edge: the *representative* of the corresponding *sector*. Consequently, in case

of multiple edges per *sector*, the number of edges is reduced to one. The result of this processing step is a number of *sectors*, each represented by a single edge, the *representative*.

### 3.3.3 Connecting Representatives

The result of the previous processing step is approximately representing the original polygon. However, the edges must be connected to form a closed polygonal chain. This step is executed here. For each pair of adjacent *representatives*, defined by the order in the list, an intersection point is calculated and evaluated for its validity (see Figure 2). A major problem for existing algorithms lies in identifying rooms with missing or unsatisfactory measurement data for certain walls [5]. This approach will be able to handle such an example if the surrounding walls are properly represented by measurement data.
A region may consist solely of edges that do not collect enough group length to pass the Holistic Filter. The resulting *sector* of these regions will not have a *representative* (see r2 in the polygon of Figure 3c). This issue is detected in this approach if two neighbouring *sectors* form a too tight inside angle (see Figure 2b) or if a wall edge is shortened by the intersection point (considering a specific threshold, referred to as complete threshold see Figure 2c and Table 1). A very tight inner angle of a corner is considered to be an unusual feature of a floor plan (see Chapter 3.1) and is detected if the intersection point lies outside of the polygon by a distance margin times the perimeter of the polygon (see Table 1). The second criterion is employed, because we assume, there is no wall, that starts in the middle of another wall.

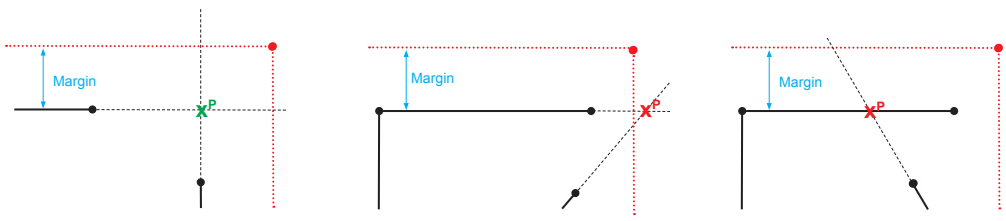


(a) Valid (b) Invalid: Outside of margin (c) Invalid: Intersecting significant edge

Figure 2: Possible cases of intersection points.

If a missing *representative* is detected, it is recreated. This is done by connecting the last vertex of the prior *representative* to the first vertex of the following *representative*. The resulting connecting line e is rotated to the angle of the *representative*, whose angle differs the least from the angle of e. This can be done under the assumption of parallel walls.

## 3.4 Examples and Limitations

The proposed algorithm has been tested using real-life data provided by ReconTOP project partner Elsafty [13]. The point cloud data captured with a terrestrial laser scanner has been preprocessed into two test datasets. The preprocessing involves the registration, segmentation, and planar slicing of the point cloud data. Our input polygons are the concave hulls of point sets per room, using the Alpha shape algorithm [9]. The provided data consists of 27 room polygons from 5 different apartments. The polygons of the first dataset, consisting of 1000 to 2000 vertices, have been simplified using again the

Alpha shape algorithm. The polygons of the second dataset consist of 15 to 50 vertices. Taking the two different quality stages of the room polygons into account, we tested our algorithm on 54 different polygons. Throughout this chapter, the selected polygon in Figure 1a will be used in its simplified version as input to demonstrate the progress of the algorithm. The simplified version is chosen for the demonstration as its longer edges are easier to see for the reader. This polygon has multiple corners in r2/r3, r3/r4 and r4/r5 that connect regions with diagonal edges. That means, the polygon has more vertices than would be necessary to properly represent its geometry.
The following example illustrates how the Holistic Filter ensures the representation of protrusions. The pink edge in the polygon of Figure 3a shows an edge from a protrusion that is short and therefore would be filtered by every plain length filtering. The accumulated length of the pink and every similarly oriented edge (green edges of the polygon shown in Figure 3a) though, is longer than the specified length threshold and therefore the pink edge is not filtered by the Holistic Filter. The polygon after the Holistic Filter is shown in Figure 3b. It shows an open polygon which has no diagonal connections of corners opposed to the input polygon in Figure 1a.
The polygon in Figure 3c shows the combined edges of the Holistic Filter after the Regression on Sectors and the polygon in Figure 3d shows the resulting closed polygon with the recreated edge in r2 after Connecting Representatives.

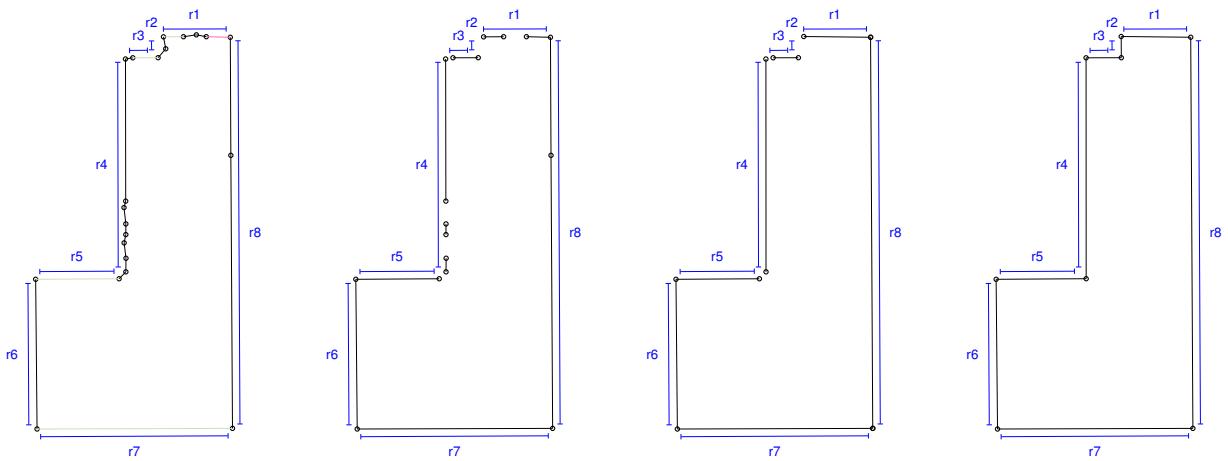


(a) Protrusion edge in pink (top right), similar edges in green.

(b) Polygon after Holistic Filter.

(c) Polygon after Regression on Sectors.

(d) Polygon after Closing.

Figure 3: Different processing stages of the example room polygon.

The main limitation of the methodology occurs if two or more neighbouring *sectors* lack a *representative*, meaning all their edges got filtered out by the Holistic Filter (see Figure 4b). The algorithm recognises that two or more neighbouring *sectors* are missing after first noticing that one *sector* is missing. If either the start or end point of this *sectors* recreated *representative* lies outside of the distance margin (see Figure 2b) it is detected that both neighbouring *sectors* are missing. Subsequently the polygon is closed by connecting the neighbouring available *representatives* of the empty *sectors* as shown in orange in Figure 4c. The resulting polygon may then deviate from the expected outcome and be unsatisfactory. This only occurred on an example of the further simplified polygon data set.

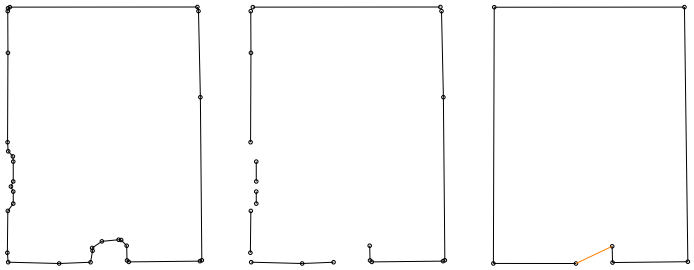

(a) The input polygon.

(b) A missing pair of *sectors* (bottom center).

(c) Result polygon with provisional edge.

Figure 4: The processing stages of the polygon from the dataset, for which the algorithm does not find a satisfactory solution.

## 4 Conclusion and Outlook

A solution for the simplification of closed 2D floor plan polygons, with a particular focus on corners and the reduction of vertices is proposed. The room polygons are divided into their exterior and interior boundaries, meaning that each boundary is considered independently rather than in relation to the entire polygon. In 9 out of 54 polygons unrepresented *sectors* were identified and artificially recreated. 8 of those 9 polygons have only one missing representative in a row and are closed in a satisfactory manner. The polygon shown in Figure 4 is the only polygon that lacks a representative edge in two neighbouring *sectors*. The polygon is closed by an edge connecting the *sectors* before and after the two empty *sectors*. However, this result is unsatisfactory because, despite significant vertex reduction prior to processing, the original shape of the room was lost. In conclusion a total of 54 polygons of varying number of vertices per region were processed using this approach and using different parameter configurations. A parameter configuration that satisfactorily processed the 27 not further simplified polygons in a satisfactory manner has been found (see column "values" of Table 1), fine tuning initial assumptions for the values in a case study. This is a promising result and shows that the algorithm should be used for polygons with as much information (high number of vertices) as possible rather than polygons being preprocessed by another algorithm. The goal of our approach is to find a parameter configuration that works for every polygon representing a room in a floor plan. The user is not ought to adjust the parameters himself but rather get presented a finished algorithm. To achieve this, further research on a larger dataset of room polygons is necessary. Future developments of this algorithm could expand its application to entire floor plans or extend to 3D space, using concave hulls consisting of faces rather than edges.

## Acknowledgements

Special thanks to A. Elsafty from the ReconTOP research project for providing the preprocessed point clouds. The ReconTOP research project is a joint research project executed together with Prof. Georg Suter, TU Wien, Austria, Prof. Timo Hartmann, TU Berlin, and the Bauinformatik group at TU Berlin. ReconTOP is funded by the Austrian Science Fund (FWF - Project number I 5171-N) and by the German Research Foundation (DFG - Project number 454008779).

The research presented in this paper results from the student research project conducted by Antonio Carlone [14] and is closely linked to the ReconTOP research project.

## References

[1] F. Gabler and W. Huhnt, “Where is the end of the wall: Decomposition of air and material into spaces and building components”, in Aug. 2023. DOI: 10.1007/978-3-031-32515-1_27.

[2] S. Yang, M. Hou, and S. Li, “Three-dimensional point cloud semantic segmentation for cultural heritage: A comprehensive review”, *Remote Sensing*, vol. 15, no. 3, p. 548, 2023. DOI: https://doi.org/10.3390/rs15030548.

[3] X. Gao, R. Yang, J. Tan, and Y. Liu, “Floor plan reconstruction from indoor 3d point clouds using iterative ransac line segmentation”, *Journal of Building Engineering*, vol. 89, 2024. DOI: https://doi.org/10.1016/j.jobe.2024.109238.

[4] .

[5] H. Fang, F. Lafarge, C. Pan, and H. Huang, “Floorplan generation from 3d point clouds: A space partitioning approach”, *ISPRS Journal of Photogrammetry and Remote Sensing*, vol. 175, pp. 44–55, 2021. DOI: https://doi.org/10.1016/j.isprsjprs.2021.02.012.

[6] J.-P. Bauchet, R. Sulzer, F. Lafarge, and Y. Tarabalka, “Simplicity: Reconstructing buildings with simple regularized 3d models”, *arXiv preprint arXiv:2404.08104*, 2024. DOI: https://doi.org/10.48550/arXiv.2404.08104.

[7] D. H. Douglas and T. K. Peucker, “Algorithms for the reduction of the number of points required to represent a digitized line or its caricature”, *Cartographica: The International Journal for Geographic Information and Geovisualization*, vol. 10, no. 2, pp. 112–122, 1973. DOI: 10.3138/FM57-6770-U75U-7727.

[8] R. C. Bolles and M. A. Fischler, “A ransac-based approach to model fitting and its application to finding cylinders in range data”, in *International Joint Conference on Artificial Intelligence*, 1981.

[9] H. Edelsbrunner, D. Kirkpatrick, and R. Seidel, “On the shape of a set of points in the plane”, *IEEE Transactions on Information Theory*, vol. 29, no. 4, pp. 551–559, 1983. DOI: 10.1109/TIT.1983.1056714.

[10] R. Gioi, J. Jakubowicz, J.-M. Morel, and G. Randall, “Lsd: A line segment detector”, *Image Processing On Line*, vol. 2, pp. 35–55, Mar. 2012. DOI: 10.5201/ipol.2012.gjmr-lsd.

[11] A. T. Phan, T. Huynh, and L. Truong-Hong, “Generating 2d building floors from 3d point clouds”, in Dec. 2023, pp. 1660–1668. DOI: 10.1007/978-981-99-7434-4_179.

[12] Z. Lu, T. Wang, J. Guo, *et al.*, “Data-driven floor plan understanding in rural residential buildings via deep recognition”, *Information Sciences*, vol. 567, pp. 58–74, 2021. DOI: https://doi.org/10.1016/j.ins.2021.03.032.

[13] A. Elsafty, Room Point Clouds, Feb. 2024.

[14] A. Carlone, “Identification of significant edges in polygons”, Student Research Project, Technische Universität Berlin, May 2024.

# Incremental model updates in BIM: a critical analysis of the collaboration platform Speckle

Kai Dietmair[1], Sebastian Esser[1] and Benedict Harder[1]
[1]Chair of Computational Modeling and Simulation, Technical University of Munich, Arcisstraße 21, 80333 Munich, Germany
E-mail(s): kai.dietmair@tum.de, sebastian.esser@tum.de, benedict.harder@tum.de

**Abstract:** Current practice and international standards implement BIM collaboration based on domain model federation, which leads to repetitive exchange of model versions as monolithic files. Subsequently, stakeholders receiving new model versions must manually check them to identify potential impacts on their own disciplines, which is labor-intensive and error-prone. These limitations can be overcome by implementing incremental update procedures. This way, only the information about the modified objects is transmitted in the event of model changes. In this paper, we examine the collaboration platform Speckle and critically assess its approach to implementing incremental model updates. Speckle provides an open and vendor-neutral data format and is known for its extensibility. We address several issues that were identified in Speckle's hierarchical data structure concerning the insertion and removal of model objects. An improved data structure inspired by Labeled Property Graphs will be presented, enabling more intuitive updates of BIM models and facilitating more accurate version control by maintaining object relationships.

*Keywords:* Speckle, incremental model updates, version control, BIG Open BIM

Erschienen in Tagungsband 35. Forum Bauinformatik 2024, Hamburg, Deutschland, DOI: 10.15480/882.13542
© 2024 Das Copyright für diesen Beitrag liegt bei den Autoren. Verwendung erlaubt unter Creative Commons Lizenz Namensnennung 4.0 International.

## 1 Introduction

The planning of the built environment is characterized by a large number of involved engineers from different disciplines. Collaboration and communication are essential to achieve an overall consistent design. In the last two decades, the traditional exchange of information in the form of printed plans and documents has increasingly been replaced by model-based approaches from the field of Building Information Modeling (BIM) [1]. A BIM model contains geometric and semantic information about a building and can be encoded in various file formats [2]. Due to the iterative nature of planning processes, models are often subject to changes after they have already been exchanged with other project participants. Today's common practice is to share the modified model as a new monolithic file with other stakeholders. They have to check the new model for any changes applied and to identify inconsistencies with their own models, which is labor-intensive and error-prone. This situation can be

improved by using incremental update procedures, in which only the information about the modified objects is transferred in the event of a change.

In this paper, we critically assess the approach pursued by the collaboration Platform Speckle [3] when incrementally updating BIM models. To this end, the design of the Speckle platform is summarized, and case studies are conducted to evaluate its power. Subsequently, we address several issues concerning the insertion and deletion of model objects that were identified in Speckle's data structure and present an improved structure inspired by graph-based methodologies. We aim to explore how Speckle's hierarchical data structure can be enhanced to address current limitations, ultimately providing more robust and intuitive version control for BIM models.

The paper is organized as follows. Section 1 presents our motivation and the problem statement. Section 2 briefly summarizes related work. Section 3 critically reviews Speckle's current data model, identifies issues within it, and proposes a solution to the identified issues afterward. Section 4 discusses the proposed approach and lists its advantages and limitations compared to the traditional hierarchic way of structuring increments. Section 5 concludes this paper and outlines potential directions for future research.

## 2 Related Works

Version control and associated techniques to transfer incremental changes have been subject to a wide variety of investigations in different industries. Very prominent examples are version control systems for source code, which are in common use today. In contrast to purely textual representations, however, BIM models appear as highly networked structures that contain information about objects and relations across these objects. Such interconnected structures are required to reflect the complexity of the built environment in a sufficient computer-interpretable representation. Over the past ten years, several concepts have been developed that address the challenge of version control for BIM models.

Back in 2005, Firmenich, Koch, Richter, *et al.* [4] developed an approach that took up the concept of textual version control, which was already established in software development at the time and was intended to replace the exchange of entire files in the event of planning changes. They developed a procedure for serializing object sets and storing them in a text-based Version Control System (VCS). This allowed them to make use of existing VCS functions.

Some of the ideas of that time have been taken up by Speckle [3]. Speckle arose from the need of large planning and engineering offices for the coupling of models for data integration between specialist applications [5]. Speckle is an open-source vendor-neutral collaboration platform for planning the built environment, designed to facilitate collaboration between the various parties involved in a construction project. It was originally developed in 2016 at University College London by Dimitrie Stefanescu as part of the InnoChain project [6]. Speckle's main objectives are version control, creating compatibility between different domain-specific software products, storing authorship, and minimizing the amount of data to be transferred. The latter is realized by transferring only the modified model components in case of a model change and structuring them hierarchically.

In addition to Speckle there are also other open and vendor-neutral exchange formats for BIM models. One of them is represented by Industry Foundation Classes (IFC) [7], which is already widely supported by market-leading BIM software vendors. In this context, Shi, Liu, Gao, *et al.* [8] proposed IFCdiff, a content-based automatic comparison approach for IFC files based on a similarity metric. Unlike traditional methods for comparing IFC files that rely on manual inspection or simplistic attribute checks, IFCdiff's approach reduces computational time and space requirements. Thus making it suitable for incremental backup of BIM data. IFCdiff constructs hierarchical structures that eliminate redundant instances for each of the two IFC files to be compared. Afterward, it calculates a similarity score using a recursive depth-first search. However, the calculated score is a mere scalar value that does not provide a deeper understanding of the actual changes applied to the model.

Esser, Vilgertshofer, and Borrmann [9] have developed an alternative approach to enable incremental updates of BIM models. Their central idea is to represent BIM models in the form of Labeled Property Graphs (LPG), which aim to represent complex and interconnected object structures better than text-based approaches. Similar ideas are also documented in Zhu, Wu, and Lei [10] or Ismail, Nahar, and Scherer [11]. Changes applied to a model are determined based on the graph representations of two IFC model versions. Subsequently, the derived changes are stored as graph transformation rules and exchanged with other project stakeholders. They can then apply the transformation to its outdated version of the graph and thus end up with the most recent model version.

With several incremental update methods for BIM models, the question arises as to which of them is the most suitable for today's construction practice and what the advantages and limitations of the respective methods are. In this paper, we critically look at Speckle's incremental update approach for BIM models and explore alternative ways of organizing the increments to be transferred. We draw inspiration from the graph-based approach in [9] to make suggestions for improving the hierarchic Speckle approach.

# 3 Critical Assessment

In this section, after a brief summary of Speckle's basic approach to incremental updates, we will identify problems in Speckle's way of organizing the increments to be transferred. Subsequently, we will present an approach to resolve the identified problems.

## 3.1 Speckle's Data Model

Speckle is an object-based platform, meaning that data is not stored as monolithic files but as individual objects. The platform can be divided into two main components: the server and the connectors. The connectors are plug-ins for popular software products in the Architecture, Engineering, and Construction (AEC) industry. As of June 2024, Speckle offers 28 different connectors. When sending objects to the Speckle server, the connectors create so-called commits, which are essentially snapshots of the selected design data at a specific point in time. Each time objects are sent to the server, the corresponding connector converts the objects from their original software-specific format into Speckle's software-neutral format and serializes them into JSON format. When receiving objects

from the server, the same conversion takes place in the opposite direction. This enables data to be transferred between different software products.

When a Speckle object is created, the corresponding connector assigns it a unique Speckle ID. This Speckle ID is then mapped to the object's native ID in the application where it was created. The native IDs of all new objects created when receiving the Speckle object are also mapped to this Speckle ID. This mapping can be stored in various repositories, such as the Speckle server or SQLite databases. When receiving a commit from the server, the connector compares the native IDs mapped to the received Speckle objects with the native IDs of the objects currently present in the model and updates the native objects accordingly. This ID-based comparison is Speckle's basic approach to incremental updates.

Collections are the most generic objects in Speckle and are used universally by all connectors to hierarchically structure the objects contained in a commit. Collections possess an attribute called "elements", which represents a container for other Speckle objects. This means collections can contain further collections, leading to a nesting of Speckle objects. For example, the Revit connector automatically creates collections for all objects according to their Revit categories. Like collections, built objects are structured hierarchically in Speckle. Hosted Objects, such as doors or windows, are elements of their host objects and are, therefore, part of the host object's collection when committed to the server. Hosted objects are only assigned to a separate collection if their corresponding host objects are not included in the commit. An example case of this concept, where walls are used as host objects and doors as hosted objects, is depicted in fig. 1 and fig. 2. The BIM model used in this example was created within the BIM authoring software Autodesk Revit (version 2024.1). Selected model objects were then included in commits and sent to the Speckle server using the Revit Connector (version 2.17.0).

### 3.2 Problem Identification

In many cases, Speckle successfully implements incremental updates of BIM models, especially if the transferred increments consist of moving and dimensioning existing model objects [12]. However, particularly during the insertion and deletion of objects hosted by other objects, the Speckle connectors frequently encounter issues or fail to produce the expected results. As a cause for these issues, we identified a data model problem and additional requirements with the hierarchical structure of built objects and the strict separation of collections described in section 3.1.

The Revit connector creates commits in which host objects reference their elements via corresponding IDs. However, referencing in the opposite direction from the hosted object to the host object does not occur. For example, an element in the door collection cannot access its host wall. As a result, a newly created door committed as a single increment is not inserted into the model when received back from the server. Instead, to successfully insert the door, its host wall must also be included in the commit, which is not intuitive for the end user (cf. fig. 3).

The limitations of Speckle's current data model are apparent not only when inserting hosted objects but also when deleting objects. A Speckle commit can only contain objects. It is impossible to commit

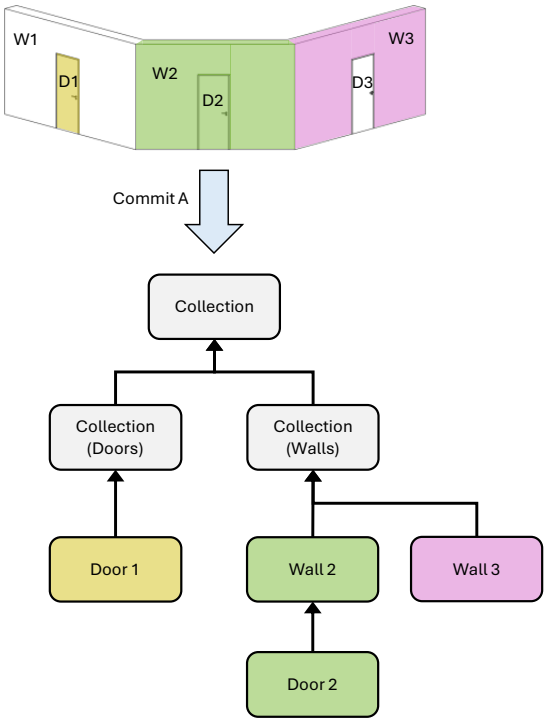


Figure 1: Commit A

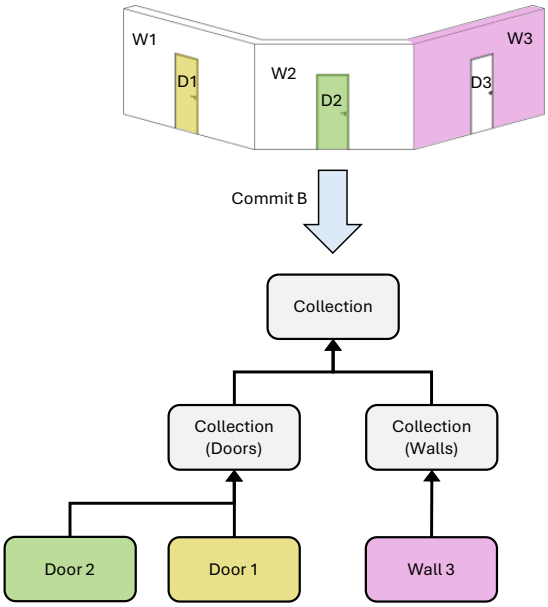


Figure 2: Commit B

a "delete command" to remove an object when pulling the commit into another version of the model. Instead, to successfully remove an object from a Revit model, a commit must be received that contains at least two objects. If, for example, a door is to be removed from a model, it is not enough to simply receive its empty host wall into the model. Instead, the commit must contain at least one object besides the wall, such as a window (cf. fig. 4).

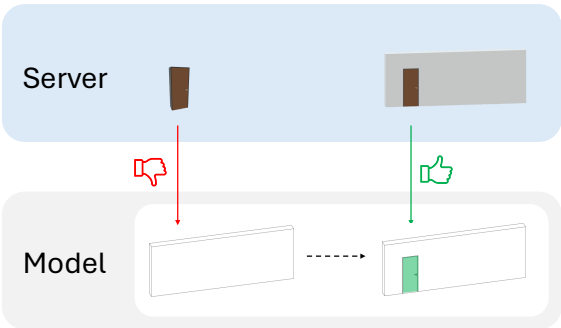


Figure 3: Inserting a door via Revit connector

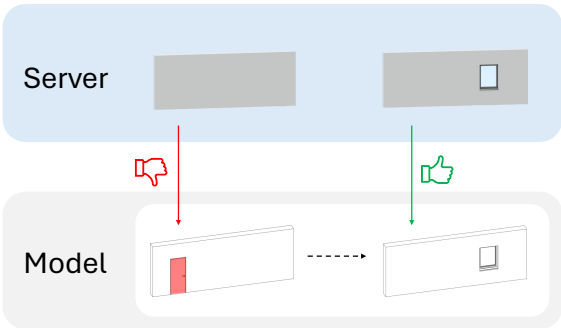


Figure 4: Deleting a door via Revit connector

### 3.3 Proposal to overcome identified issues

This section presents the developed solution to the problem specified in section 3.2. The central idea is to abolish the hierarchical structuring of the built objects and the strict separation of collections from each other. Instead, the individual Speckle objects are now sorted into homogeneous collections, which only contain objects that actually belong to the same component category. For example, a door that is committed together with its host wall is no longer regarded as an element in the wall collection

but as a separate object in the door collection. However, these homogeneous collections are not strictly separated from each other, but the individual Speckle objects they contain can be linked to each other. Here we fall back on the concepts used by Esser, Vilgertshofer, and Borrmann [9] when creating LPGs. The objects and collections are represented as nodes, and the connections between the individual nodes as labeled directed edges. A strict hierarchy between objects, therefore, no longer exists, as these edges are also formed across collections. For example, hosted objects reference their respective hosts via directed inter-collectional edges labeled as "fills". As a result, the collections and objects contained in a Speckle commit no longer form a hierarchical tree structure but a graph structure. Another important component of the proposed solution is the virtuality of nodes and edges. Even if a hosted object is committed without its host object, the edge between the two persists virtually by connecting the hosted object to a virtual instance of its host. An example case of this concept is depicted as a Graph Meta Model in fig. 5 and fig. 6, taking up the example for Speckle's commit structure shown in fig. 1 and fig. 2.

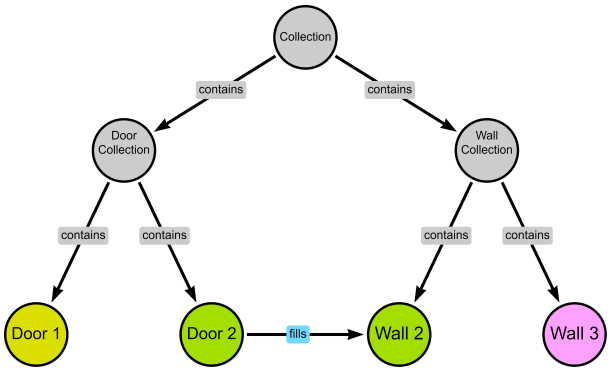


Figure 5: Commit A Graph proposal

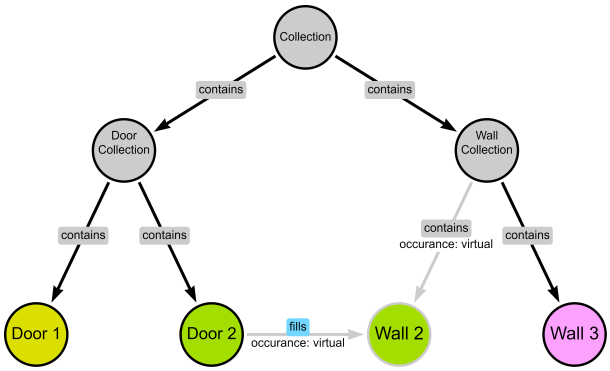


Figure 6: Commit B Graph Proposal

With this method, a newly inserted hosted object can be intuitively committed as a single object, retaining its reference to the host object. As a result, it can be inserted into all previous model versions containing the host object by receiving the commit back from the server. This way, the problem with inserting hosted objects mentioned in section 3.2 is resolved.

The proposed approach also improves the way objects are incrementally deleted from BIM models when receiving a Speckle commit. If a user removes objects hosted by another object, this former host object has no "fills" relationships when it is committed to the server. Therefore, all previously hosted objects are deleted when the former host object is received into an old model version. This resolves the issue of a commit containing only one object not being able to delete objects from a BIM model.

The proposal could be implemented into Speckle's existing system by adding an additional attribute to the JSON serialization of hosted objects. By storing the IDs of the host objects in attributes of the corresponding hosted objects as references, it is possible to integrate the graph-based approach seamlessly into Speckle's current way of transferring increments. This modification would ensure that hosted objects retain their references to host objects, facilitating accurate and intuitive incremental updates.

# 4 Discussion

The hierarchical structuring of objects and collections offers a straightforward way to incrementally update BIM models, especially when using hierarchical exchange formats, such as JSON. However, our investigation identifies drawbacks in Speckle's hierarchical method, particularly in handling the insertion and deletion of model objects. The proposed solution, which involves transitioning from a hierarchical tree-like structure to a graph-based structure, offers a promising alternative. By leveraging the concepts of LPGs, our approach allows for more flexible and robust handling of object relationships. Homogeneous collections and directed inter-collectional edges facilitate better representation of object dependencies and ensure that hosted objects maintain their references even when committed independently from their respective hosts.

However, the proposed concept of virtual nodes and edges has its limitations. While it addresses the issue of incremental deletions and insertions of hosted objects by allowing the representation of objects not explicitly included in the commit, it also increases the amount of data that needs to be transferred. The goal should be to keep the transferred increments as small as possible and only as large as necessary. This trade-off between maintaining accurate object relationships and minimizing data transfer must be carefully considered in practical applications. Furthermore, the implementation of the proposed solution has not been realized yet. However, Speckle's architecture can be extended to meet such requirements.

# 5 Conclusion and Outlook

We have critically evaluated some of the Speckle functions currently available in June 2024. Issues about the separation and hierarchical structure of collections have been identified as presented in section 3.2. The proposed improved data model from section 3.3 addresses these issues by transitioning from a hierarchical tree-like structure to a graph-based structure with homogenous collections connected by inter-collectional edges. Thus, the flexibility and robustness of object relationships when transferring incremental updates of BIM models are enhanced, ultimately improving the user experience and efficiency in managing construction projects. A preliminary solution for implementing the proposed concepts is to add ID-based attributes to the hierarchical serialization of model objects. However, further research and development are needed to realize the potential of the proposed solution fully. Future work could focus on the practical implementation and testing of the proposed model within Speckle and other BIM platforms. This includes evaluating the performance and scalability of the approach in real-world projects, as well as exploring additional features and optimizations that could further enhance its utility.

Overall, the proposed graph-based approach could significantly enhance Speckle's incremental update capabilities, addressing the identified issues and providing a more flexible, intuitive, and efficient data management framework for the AEC industry.

## References

[1] S.-E. Schapke, J. Beetz, M. König, C. Koch, and A. Borrmann, “Prinzipien und Techniken der modellgestützten Zusammenarbeit”, in *Building Information Modeling*, Springer, 2021, pp. 309–333. DOI: 10.1007/978-3-658-33361-4_15.

[2] M. Oh, J. Lee, S. W. Hong, and Y. Jeong, “Integrated system for BIM-based collaborative design”, in *Automation in Construction*, vol. 58, 2015, pp. 196–206. DOI: 10.1016/j.autcon.2015.07.015.

[3] *Speckle*, 2024. [Online]. Available: https://speckle.systems/ (visited on 02/07/2024).

[4] B. Firmenich, C. Koch, T. Richter, and D. Beer, “Versioning structured object sets using text based Version Control Systems”, in *Proceedings of the 22nd CIB-W78 Conference on Information Technology in Construction*, 2005, pp. 105–112.

[5] D. Mondino, “BIM im architektonischen Entwurf”, in *Building Information Modeling*, Springer, 2021, pp. 381–391. DOI: 10.1007/978-3-658-33361-4_19.

[6] P. Poinet, D. Stefanescu, and E. Papadonikolaki, “Collaborative Workflows and Version Control Through Open-Source and Distributed Common Data Environment”, in *Proceedings of the 18th International Conference on Computing in Civil and Building Engineering*, 2020, pp. 228–247.

[7] *BuildingSMART, Industry Foundation Classes (IFC)*, 2024. [Online]. Available: https://www.buildingsmart.org/standards/bsi-standards/industry-foundation-classes/ (visited on 04/07/2024).

[8] X. Shi, Y.-S. Liu, G. Gao, M. Gu, and H. Li, “IFCdiff: A content-based automatic comparison approach for IFC files”, in *Automation in Construction*, vol. 86, 2018, pp. 53–68. DOI: 10.1016/j.autcon.2017.10.013.

[9] S. Esser, S. Vilgertshofer, and A. Borrmann, “Graph-based version control for asynchronous BIM collaboration”, in *Advanced Engineering Informatics*, vol. 53, 2022, p. 101 664. DOI: 10.1016/j.aei.2022.101664.

[10] J. Zhu, P. Wu, and X. Lei, “IFC-graph for facilitating building information access and query”, in *Automation in Construction*, vol. 148, 2023, p. 104 778. DOI: 10.1016/j.autcon.2023.104778.

[11] A. Ismail, A. Nahar, and R. Scherer, “Application of graph databases and graph theory concepts for advanced analysing of BIM models based on IFC standard”, in *24th International Workshop on Intelligent Computing in Engineering (EG-ICE 2017)*, 2017.

[12] K. Dietmair, “Analyse der Kollaborationsplattform Speckle im Hinblick auf inkrementelle Updates von BIM-Modellen”, Bachelor’s thesis, Technische Universität München, 2024.

# Automated IFC-based mesh refinement and quality control for indoor airflow simulations using OpenFOAM

Anna Hochberger[1] and Veronika Elisabeth Richter[1]
[1]Institute of Energy Efficiency and Sustainable Building (E3D), RWTH Aachen University, Mathieustraße 30, 52074 Aachen, Germany
E-mail(s): anna.hochberger@rwth-aachen.de, richter@e3d.rwth-aachen.de

**Abstract:** Computational fluid dynamics (CFD) simulations are an essential tool for indoor airflow simulations and in the design process of energy-efficient buildings. Setting up CFD models typically demands considerable manual effort, including the modeling of geometry, defining boundary conditions, and meshing. This complex and labor-intensive process can be streamlined by automatically generating indoor CFD models from IFC-based Building Information Modeling (BIM) models. To integrate this CFD model setup in an existing tool, a plugin for the IFC-based multi-domain *bim2sim* simulation environment with the open-source CFD library *OpenFOAM* was developed, including automated meshing and refinements. As the accuracy of simulation results highly depends on the mesh quality, the mesh must satisfy specific quality criteria. Furthermore, balancing a sufficiently detailed solution provided by finer grids and reasonable runtimes is a persistent challenge in CFD. This paper presents algorithms for automatic IFC-based mesh refinement for interior elements like radiators and air terminals. These algorithms are evaluated by refinement studies and a mesh quality analysis in a case study of a single office. The proposed optimal grid refinements can be used in further research to automatically set up CFD simulations for IFC-based thermal comfort analysis.
*Keywords:* BIM, IFC, CFD, OpenFOAM, Meshing

Erschienen in Tagungsband 35. Forum Bauinformatik 2024, Hamburg, Deutschland, DOI: 10.15480/882.13503
© 2024 Das Copyright für diesen Beitrag liegt bei den Autoren. Verwendung erlaubt unter Creative Commons Lizenz Namensnennung 4.0 International.

## 1 Introduction

Computational Fluid Dynamics (CFD) simulations are a crucial tool for analyzing indoor airflow, heat distribution, and thermal comfort in buildings. Although CFD simulation results can be beneficial in the early stages of the building design process, setting up CFD models is not as straightforward as anticipated by companies within the construction industry [1]. The missing interface to open exchange formats for semantic building data is one of the existing challenges. Building Information Modeling (BIM) data can be represented using the Industry Foundation Classes (IFC), which are an open international standard for data exchange in BIM [2]. The IFC format provides a structure for storing building data, including space boundaries that can form an airtight room, which is needed for

performing CFD simulations. Unfortunately, most CFD tools, particularly those that are open-source, are not equipped to import this data format, especially its latest standard, IFC4 [1, Tab. 7.3].
To address parts of this complex problem, the open-source *bim2sim* library (https://github.com/BIM2SIM/bim2sim) was designed as a multi-domain building simulation tool that automates the simulation model setup based on IFC. For geometry processing, *bim2sim* uses the open-source geometry kernel *OpenCascade* (https://dev.opencascade.org/). The *bim2sim* tool provides plugins for multiple approaches like Building Performance and System Simulation, Life Cycle Assessments, and CFD simulations. Within the *bim2sim* tool, a CFD plugin has been developed using the open-source CFD kernel *OpenFOAM* (https://www.openfoam.com/) [3]. The goal of the *PluginOpenFOAM* is to automatically mesh, set up, and run CFD simulations for a room extracted from an IFC file. Here, automating the meshing process is one of the central challenges since the mesh quality also significantly impacts the quality of the simulation results. Therefore, this paper focuses on evaluating and enhancing the generated mesh within the plugin.

# 2 Related Research

Within the *bim2sim* project [1], initial investigations of IFC-based CFD-simulations have been conducted using the commercial software *ANSYS* (https://www.ansys.com/). Even though it was also implemented as a plugin for *bim2sim*, the automatic meshing and setup of boundary conditions has not been developed within this project. Despite *ANSYS* providing a variety of meshing tools, the new *PluginOpenFOAM* builds upon the *OpenFOAM*-kernel to align with the goal of creating open-source software. In this context, *OpenFOAM* also provides the advantages of being usable without a graphical user interface and its seamless integration into the codebase of *bim2sim*.
A lot of research has been conducted regarding mesh quality and improvement. Fundamentals can be found in Knupp et al. [4], who presented a mathematical derivation for a variety of mesh quality assessment criteria based on the Jacobi matrix, which have been implemented similarly in the *OpenFOAM* functionality `checkMesh`. A selection of these criteria can also be found in many commercial and open-source simulation tools (e.g. ANSYS, SimScale, MATLAB). However, in related research, no extensive investigation of full *OpenFOAM*-generated meshes has been conducted, and methods for automatically adjusting refinement levels and regions for geometric constructions like a room with furniture can hardly be found. Lee et al. [5] presented BIM-based CFD simulation setups with slightly simplified geometries. They discussed grid optimization with the focus on improving the mesh cell quality and finding an overall optimal grid size using improved grid independence tests [6]. However, their research implies that the cell quality is an indicator of overall mesh quality. It neglects the option of creating accurate meshes based on geometric and physical aspects of individual objects in the model (e.g., boundaries, air terminals, heaters, furniture), which is discussed in this paper.

# 3 Methodology

## 3.1 Object-based Meshing in OpenFOAM

The *PluginOpenFOAM* meshing process utilizes the geometry of the room including furniture combined with IFC-based semantic information, e.g., on surface types. For this, first a `blockMesh` of a specified

grid size $\Delta x_{bM}$ is created, which divides the whole domain into a uniform grid. In a second step, `snappyHexMesh` refines this uniform grid using refinement levels at the object surfaces and in specified refinement regions.

One refinement level corresponds to halving the current cell width. Hence, the new grid size $\Delta x_{new}$ [m] at refinement level $l$ can be computed from the `blockMesh` size $\Delta x_{bM}$ [m] as:

$$\Delta x_{new} = \frac{\Delta x_{bM}}{2^l}. \tag{1}$$

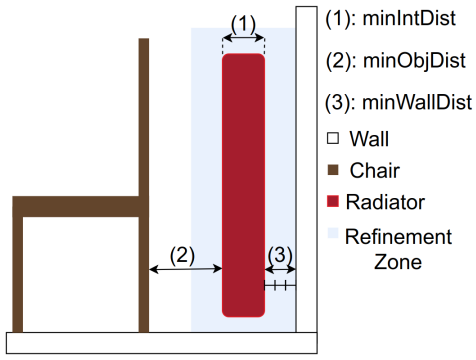


Figure 1: Relevant distances for automatic refinement.

Introducing automatic refinement is especially important closer to the walls, around objects, and at complex object geometries. For this, the three distances shown in Figure 1 become of relevance: (1) the smallest distance between two vertices inside an object (`minIntDist`), (2) the smallest non-zero meshing distance between an object and the closest room surface (`minWallDist`), and (3) the smallest meshing distance between an object and any other object inside the room (`minObjDist`). Refinement levels $refLevel$ are defined through an upper and a lower limit $l$, where the upper limit is chosen as $l + 2$. According to the desired final cell size, the $refLevels$ can be computed from the up-rounded Equation 1:

$$refLevel(minDist, \Delta x_{bM}) = [l, l+2], \text{ where } l = \left\lceil \frac{log(\frac{\Delta x_{bM}}{minDist})}{log(2)} \right\rceil. \tag{2}$$

### 3.2 Evaluating Mesh Quality

The overall quality of a mesh must be evaluated regarding the quality of the single cells and regarding its geometric correctness and completeness. For the evaluation on cell level, *OpenFOAM* provides the `checkMesh` functionality, which states the maximum value for four widely used criteria in comparison between all mesh cells. *Cell Openness* describes the ratio between the cell's volume and the volume of the smallest enclosing box (Upper Limit (UL): 1e-06). The *Aspect Ratio* is the ratio between shortest to longest edge of the cell (UL: 20). *Non-Orthogonality* relates to the angle between the vector connecting two neighboring cell centers and the vector normal to the connecting face (UL: 70). *Skewness* describes the cell's deformation compared to the ideal reference cell. This is usually normalized to a maximum of 1 but *OpenFOAM* does not perform normalization. Thus, an *OpenFOAM* user guide [7] states an UL of 8 for skewness.

A general mesh check based on correctness and completeness is not pre-implemented in *OpenFOAM* and is hard to generalize. In the proposed setup, the general mesh check focuses on identifying holes in the mesh. For this purpose, a method for validating the mesh volume is introduced. Here, the sum of all cell volumes $V_{discrete}$ is compared to the volume of the actual geometry $V_{geometric}$ in the form of the relative error: $\frac{\|V_{geometric} - V_{discrete}\|}{V_{geometric}} < tolerance$.

# 4 Implementation

For the volume validation, the volume $V_{geometric}$ of a closed model is computed from the provided STL files extracted from the IFC geometry using a built-in function from the Python STL package. Detected holes are fixed by adjusting the corresponding refinement zones and levels.

Regarding automatic refinement for complex geometries such as an air diffuser, the `minIntDist` is the most important distance. The vertices of an object are obtained from their geometry, e.g., a) using their `TopoDSShape`, which is the *OpenCascade* representation of an object internally used in *bim2sim*, or b) using the corresponding STL file. Based on these object vertices, the minimal distance between any two vertices within this object is identified.

Since objects in the code are only available in the triangulated form, Algorithm 1 removes the triangulation before computing the `minIntDist`. To only obtain the border vertices of the geometry, first, all edges connected to more than one triangle are removed. Second, collinear and coincident vertices are removed based on an algorithm introduced by Richter et al. [8].

The other two external distances can be computed using an in-built method from *OpenCascade* using their `TopoDSShape` representation or by converting corresponding STL files into this datatype using the `STLAPIReader`. The resulting distances, either the `minWallDist` or the `minObjDist`, must be divided by 3 to obtain the minimum distance `minExtDist`, which is further used to compute the resulting region refinement levels. This additional division ensures that there are always three cells in between two assigned boundary conditions.

For a typical diffuser, for example, Algorithm 2 determines the surface refinement level $l_s$ based on the `minIntDist`, and the refinement level of the corresponding refinement region is set to $[0, l_s]$. For other object types, including simplified radiators, Algorithm 2 determines surface and region refinements using the `minExtDist`.

Algorithm 1: Detriangulation.

```
input: mesh; output: vertices
faces = getFacesFromMesh(mesh)
edges = getEdgesFromMesh(mesh)
outerEdges = []
for edge in edges:
    if edge not ∈ > 1 face:
        outerEdges.append(edge)
outerVertices = set([getVertices(edge) for edge
    in edges])
outerVertices = removeCoincidentVertices(
    outerVertices)
vertices = removeCollinearVertices(outerVertices)
```

Algorithm 2: Object Refinement Levels.

```
input: object, otherObjects, space, Δx_bM
output: surfaceRefinement, regionRefinement
intDist = minIntDist(object.vertices)
wallDist = minExtDist(object, space)
objDist = wallDist
for object2 in otherObjects:
    newDist = minExtDist(object, object2)
    objDist = min(objDist, newDist)
extDist = min(wallDist, objDist)
regionRefinement = refLevel(extDist, Δx_bM)
if intDist < extDist:
    surfaceRefinement = refLevel(intDist, Δx_bM)
else surfaceRefinement = regionRefinement
```

When performing CFD simulations that include turbulence and viscosity, it can be necessary to increase the refinement near walls. The wall refinement depends on the placement of the first cell at the wall within the boundary layer. The model implemented in the *OpenFOAM* plugin is based on the `omegaWallFunction`, which switches automatically between the so-called viscous and the logarithmic layer. Hence, no wall refinement is necessary from a physical perspective. However, fully omitting wall refinements results in a mesh with blunt edges, and a wall refinement level of [1, 2] was kept.

# 5 Results

## 5.1 Setup

Figure 2 shows the general setup of the use case. While this paper only discusses this specific example, the plugin generally supports creating models based on any given IFC space. Models typically include air conditioning consisting of air inlets and outlets, and radiators. The main challenges regarding the meshing of this setup lie in the complex diffuser air terminal geometry and the short distance of the radiator to the wall.

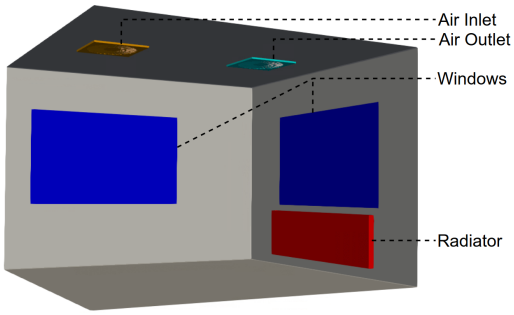


Figure 2: Room setup (Floor area: $12.95\,\mathrm{m}^2$, Height: $2.5\,\mathrm{m}$, two ext. walls).

## 5.2 Volume Validation

The most noticeable issue regarding correctness of the resulting mesh volume appears for meshes with $\Delta x_{bM} >= 0.14\,\mathrm{m}$ with a computed surface and region refinement level of [4, 6] for the radiator. The wall behind the heater is malformed (Figure 3a) and a deviation of $0.082\,\mathrm{m}^3$ ($0.25\,\%$ of total space volume) was computed. Even though the radiator's refinement region was computed according to Algorithm 2, fixing this hole mainly requires a wall refinement (WR) adaption of increasing the WR by one step as displayed in Figure 3b.

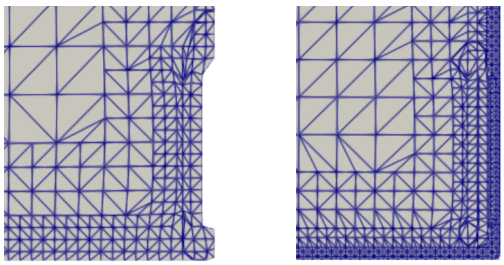

(a) Malformed mesh, WR = [1, 2].

(b) Fixed mesh, WR = [2, 3].

Figure 3: Meshing at radiator ($\Delta x_{bM} = 0.15\,\mathrm{m}$).

Table 1: Mesh cell quality evaluation of a set of 13 tested meshes of the use case.

| Criterion | Minimum | Maximum | Limit |
|---|---|---|---|
| Cell Openness | 3.06e-16 | 4.29e-16 | 1e-06 |
| Aspect Ratio | 5.83 | 14.52 | 20 |
| Non-Orthog. | 49.55 | 60.00 | 70 |
| Skewness | 1.23 | 3.72 | 8 |

For other holes and gaps in the mesh, a clear difference in volume was computed and they were fixed by increasing corresponding refinement levels. Among the comparison of multiple complete meshes, the maximum deviation of $0.047\,\mathrm{m}^3$ ($0.145\,\%$) was observed for $\Delta x_{bM} = 0.1\,\mathrm{m}$ and WR = [1, 2]. Following these completeness checks, Figure 1 presents the evaluation results of the cell quality using *OpenFOAM*'s `checkMesh` functionality. These meshes range from $0.01\,\mathrm{m} \leq \Delta x_{bM} \leq 0.2\,\mathrm{m}$ including different types of air terminals, where some of these meshes contained holes. All results are well below the proposed limits and no mesh stands out as particularly good or bad. There also does not seem to be any kind of tendency, as coarser meshes did not show a worse cell quality.

## 5.3 Accuracy of Automatic Refinements

The level of mesh refinement of diffusers directly affects the quality of the shape representation. If the diffuser is not well refined (Figure 4b), some gaps between blades cannot be preserved and the air

stream is disturbed. Compared to a much finer meshed diffuser (Figure 4d) the velocity distribution is less uniform. From Algorithm 1, the minimal distance in the diffuser is determined to be $1.37\,\mathrm{mm}$, leading to a refinement level of [7, 9] for $\Delta x_{bM} = 0.1\,\mathrm{m}$. For this improved refinement, differences of $0.01$ - $0.05\mathrm{m\,s^{-1}}$ can be observed over the full room, with base velocities ranging from $0$ - $1\mathrm{m\,s^{-1}}$.

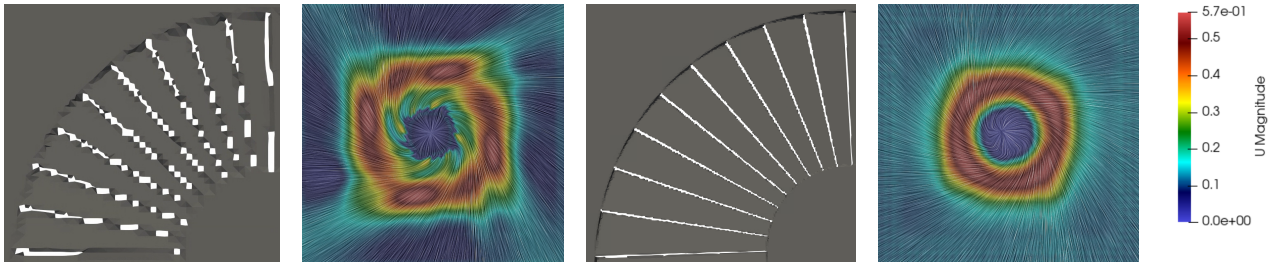


(a) Coarse mesh ([4, 6]). (b) Coarse stream. (c) Fine mesh ([7, 9]). (d) Fine stream. (e)

Figure 4: Top view of parts of a meshed diffuser and its stream using different mesh resolutions.

## 5.4 Meshing Performance Evaluation

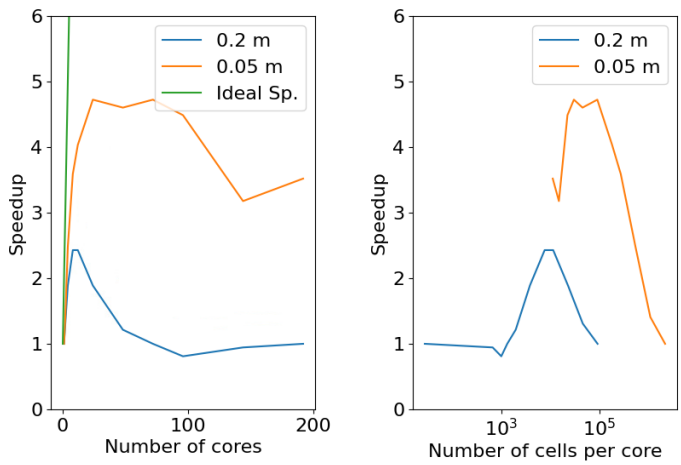


(a) Speedup over cores. (b) Speedup over cells.

Figure 5: *OpenFOAM* meshing process including mesh de- and reconstruction.

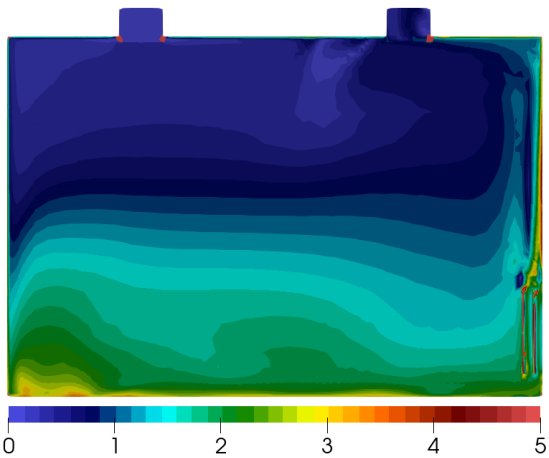


Figure 6: Root Mean-Squared Error of temperature between coarse and fine mesh (slice through air terminals (top) and radiator (right)).

To evaluate the performance of the meshing process in *OpenFOAM*, an analysis of a coarser mesh of $\Delta x_{bM} = 0.2\,\mathrm{m}$ with a total of $0.47 \cdot 10^6$ vertices and a finer mesh of $\Delta x_{bM} = 0.05\,\mathrm{m}$ with $2.6 \cdot 10^6$ vertices is presented. Figure 5a shows the speedup from 1 to 192 cores on the RWTH Computing Cluster CLAIX-23 for both meshes. It is noticeable, that the speedup only increases for a very small number of cores in both cases. Even though the speedup for the coarser mesh is a lot lower ($17\,\mathrm{s}$ for 1 core) than the one of the finer mesh ($359\,\mathrm{s}$ for 1 core), both stagnate or decrease for more than 24 cores. Figure 5b shows that the speedup peak not only depends on the number of cells per core but also on the total mesh size due to increased communication for a higher number of cells.

Figure 6 presents the temperature error between the two meshes, referring to an absolute temperature range from $285$ - $310\,\mathrm{K}$ calculated as a baseline using the fine mesh. Differences of $1$ - $3\,\mathrm{K}$ are visible in huge parts of the room. Around and above the radiator, the differences are even higher. For the air

velocity, ranging from $0$ - $1.02\,\mathrm{m\,s^{-1}}$, differences of $0$ - $0.15\,\mathrm{m\,s^{-1}}$ are distributed over the full room. Additionally, an investigation of the Grid Convergence Index (GCI) could have been very informative as a verification that the results converge to the analytical solution with decreasing grid size. Unfortunately, the GCI sets relatively high demands on the grids, especially regarding the number of vertices, which could not be fulfilled in this setup. However, the evaluation of the GCI might become more feasible when investigating larger room models.

## 6 Discussion & Limitations

Overall, the cell quality of all meshes is in a good range and does not seem to be a potential source of errors for the evaluated setups. The selection of criteria that the `checkMesh` functionality provides includes the most important evaluation criteria, which could also be provided by other tools. However, the observed well-formedness of the cells could change as soon as furniture or other objects with a more complex geometry are included in the CFD model. While the algorithmic validation of the completeness of the mesh gave very clear results, two problems remain. First of all, the limit for the deviation of the volumes is not set yet. Even for complete meshes, the deviation is not constant and it remains unclear, how well only a few missing cells could be detected by this algorithm. Secondly, it is important to identify the location of holes or missing cells automatically, to be able to specify the region that needs to be refined. As of now, fixing holes therefore remains a mainly manual process that requires more extensive research.

Regarding the accuracy of the mesh refinements, the proposed algorithms provide an effective framework for automatically detecting relevant refinement sizes. Since this framework can be based on STL files, it can also be applied outside the *bim2sim* environment. Figure 4 shows that the meshing on individual elements can have an impact on the full room and therefore proved the importance of geometrically accurate meshing. However, the holes in Figure 3a showed that it might be necessary to extend Algorithm 2 to also adapt the wall refinements in the future.

Independent of determining the desired refinement levels, meshes often did not turn out as expected. Even though a diffuser surface refinement level of [6, 8] gave great results for $\Delta x_{bM} = 0.1\,\mathrm{m}$, these results could not be reproduced for finer meshes, especially with $\Delta x_{bM} < 0.08\,\mathrm{m}$. For both, higher and lower refinement levels and variations in the refinement region size, the diffuser came out very coarsely meshed. The reasons for this are unresolved since there was no observable pattern throughout a variety of tests and this issue continues to exist for further research. Additionally, other meshing tools (e.g., SALOME, CFMesh) should be evaluated regarding a more reliable mesh quality.

The meshing performance evaluation highlighted that parallelization is not very efficient for meshing, mostly due to the high overhead from distributing the relatively small room onto many processes. It may therefore be useful to check the runtimes again when performing simulations of larger rooms. Generally, the runtimes of the meshing are relatively small compared to the actual simulation times and should not be given too much weight when making parallelization decisions. The mean-squared error proved that the mesh size has a significant influence on overall simulation results. While it is usually the case that finer meshes provide more accurate solutions, this still needs verification in the future, e.g., using the GCI or grid independence tests as adapted by Lee et al. [6].

# 7 Conclusion

This paper presented a basis for setting up automatic object refinements and evaluating IFC-based meshes using *OpenFOAM* within the *bim2sim* simulation environment. Besides classic cell quality criteria, a method for checking the completeness of a mesh was introduced. Automatic refinement was introduced for surface and region refinements based on the minimal internal distance of a detriangulized object and the minimal distance to any other surface in the room. Though these algorithms form a widely usable framework for automatically improving meshes in the context of BIM, they still require more extensive testing to guarantee stability which are subject of further research.

# Acknowledgements

This research was funded by the Federal Ministry for Economic Affairs and Climate Action within the project “BIM2Praxis” (grant number 3EN1050A). Simulations were performed with computing resources granted by RWTH Aachen University under project thes1667.

# References

[1] D. Müller, D. P. Jansen, C. A. van Treeck, *et al.*, *BIM2SIM - Methodenentwicklung zur Erstellung von Simulationsmodellen aus Daten des Building Information Modeling : gemeinsamer Endbericht*. 2021. DOI: 10.2314/KXP:1819319997.

[2] ISO 16739-1, *Industry Foundation Classes (IFC) for data sharing in the construction and facility management industries - Part 1: Data schema.* 2018.

[3] V. Richter, C. van Treeck, and J. Frisch, “Extending an ifc-based framework to include an automated cfd-setup using pre-computed boundary conditions”, in *Proceedings of BauSIM Conference 2024*, ser. BauSIM Conference, Wien, Austria: IBPSA DACH, 2024.

[4] P. M. Knupp, “Algebraic mesh quality metrics”, *SIAM Journal on Scientific Computing*, vol. 23, no. 1, pp. 193–218, 2001. DOI: 10.1137/S1064827500371499.

[5] M. Lee, G. Park, H. Jang, and C. Kim, “Development of building cfd model design process based on bim”, *Applied Sciences*, vol. 11, no. 3, p. 1252, Jan. 2021. DOI: 10.3390/app11031252.

[6] M. Lee, G. Park, C. Park, and C. Kim, “Improvement of grid independence test for computational fluid dynamics model of building based on grid resolution”, *Advances in Civil Engineering*, vol. 2020, W. Tangchirapat, editor, pp. 1–11, Dec. 2020. DOI: 10.1155/2020/8827936.

[7] WolfDynamics, *Advanced meshing using openfoam technology: Cfmesh*.

[8] V. Richter, A. Malhotra, E. Fichter, A. Hochberger, J. Frisch, and C. van Treeck, “Validation of ifc-based geometric input for building energy performance simulation”, in *Proceedings of the 2022 Building Performance Analysis Conference and SimBuild*, ser. ASHRAE/IBPSA-USA Building Simulation Conference, ASHRAE and IBPSA-USA, 2022. DOI: 10.26868/25746308.2022.C033.

# iDesignArch: Chatbot-supported architectural requirements management for inspiring building designs

Jan H. Heinbach[1] and Daniel Napps[1]
[1]Chair of Computing in Engineering, Ruhr Universität Bochum, Universitätsstrasse 150, 44801 Bochum, Germany
E-mail(s): Jan.Heinbach@ruhr-uni-bochum.de, Daniel.Napps@ruhr-uni-bochum.de

**Abstract:** Describing buildings and their internal structures is a complex architectural task. Nevertheless, a precise description is essential, especially if the description should enable the search for suitable building designs among existing models. Building Information Modelling (BIM), floor or zone plans simplify the description by providing a standardized format for mainly geometric information in different levels of detail. However, creating building representations for utilization as search input is time consuming and should be carried out by experienced users only. Therefore, this paper introduces a tool that enables architects and other stakeholders to gather relevant information by answering specific project related questions posed by the tool. It generates questions based on a developed decision tree and processes the answers, to gather as much information for an upcoming building project as possible. The resulting description is subsequently used as input for identifying similar digital building models from a database. This intelligent solution, which also allows inexperienced users to use it, offers an efficient and user-friendly way of recording and modifying building requirements in order to gain inspiration from existing similar buildings for the design, conversion or modernization of a building or part of a building.

*Keywords:* Building Information Modeling (BIM), Decision Tree, Design Automation, Project Requirements

Erschienen in Tagungsband 35. Forum Bauinformatik 2024, Hamburg, Deutschland, DOI: 10.15480/882.13513
© 2024 Das Copyright für diesen Beitrag liegt bei den Autoren. Verwendung erlaubt unter Creative Commons Lizenz Namensnennung 4.0 International.

## 1 Introduction

The current building design process has evolved significantly, integrating technologies like Building Information Modeling (BIM) and Industry Foundation Classes (IFC) to improve efficiency and accuracy. This transformation is driven by the need to improve project outcomes, reduce costs, evaluate alternative designs and mitigate mistakes. Early design decisions are crucial, as they impact the whole project lifecycle. Decisions made during these early stages can have a great impact on project success, affecting everything from aesthetics, cost and schedule to sustainability and operational energy and efficiency [1]. BIM has proven to be a critical component of modern building design,

facilitating collaboration by providing a shared digital model, improving visualization, coordination, and decision-making. Using BIM in the design process ensures that potential issues are identified and resolved early, reducing the likelihood of costly changes and delays during construction [2]. IFC is an open standard for a loss free data exchange of models in the architecture, engineering, and construction (AEC) industry. It enables seamless interoperability between disparate software applications, ensuring interchangeability and effective use of information. By using IFC in the design process, communications and collaboration are improved by ensuring that everyone is working with accurate and up-to-date information [3]. However, the lack of a centralized model database hampers efficiency, as each new project requires time-consuming (and often redundant) designs from scratch. This absence limits the ability to reference or utilize previous similar building designs, complicating efforts to streamline and optimize new projects [4]. In fact, in addition to a centralized database, the reuse of existing models requires a way to search systematically. Enabling a systematic search itself requires a possibility of effective and structured input of project parameters, limits and objectives to search for. This work focusses on the development and implementation of such an user-friendly and efficient method that captures the multitude of possible design decisions and their potential building parameters.

## 2 Background

To address the problem of starting designs from scratch and the lack of a centralized model database, previous research has developed a framework to overcome the limitations and support the architects in the early design phases with inspiration for new projects. The methodology used is based on the Case-Based Reasoning (CBR) concept, which enables problem-solving and learning by using past experiences or so called cases to understand and solve new problems. This approach allows for multiple input parameters in the comparison process, enabling specific user queries to be matched against the database [5]. Initially, the method was developed to compare BIM models. These models are exported as IFC files and transformed into a graph representation. The structural alignment of a knowledge graph with a graph from the database is performed using graph pattern matching. The graphs are analyzed for common subsets, and if a structural match is found, various similarity algorithms are then applied to compare the semantic information in the respective nodes and edges. The nodes in these graphs represent IfcEntities, such as $IfcWall$ or $IfcDoor$, and the edges represent IfcRelationships. In the first step, for instance, an $IfcWall$ is matched with another $IfcWall$, and selected semantic and geometric information of the entities are compared. This comprehensive method calculates the overall similarity, considering both structural and detailed semantic aspects [6]. Subsequent research has extended the approach to allow for multiple input parameters in the comparison process, so that specific user queries can be matched against the database and also include other analytical result in the calculation, such as cost estimation [7], the detailing of the specific elements [8] and even capture subjective criteria for design decisions [9]. The presented tool should be integrated in this framework to enable more effective search input.

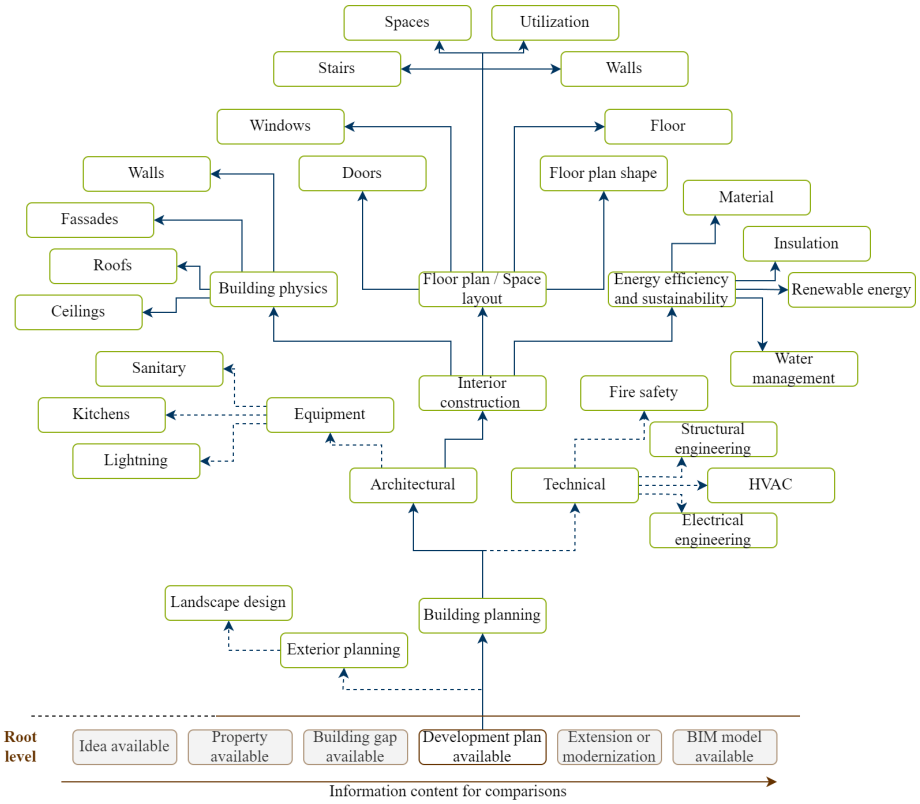


Figure 1: The developed iDesignArch decision tree for input with available development plan.

# 3 Methodology

The methodology of this work aims to provide architects with an structured alternative to the currently difficult and unstructured method of building descriptions making it easier to subsequently use it for searching in a database.

## 3.1 Requirements

Matching information from BIM models, represented by IFC, allows for a very structured process and captures detailed information requirements. The goal of getting away from required BIM models as search input, while preserving the possible information amount, is challenging. Especially specific parameters for new projects — such as plot size, usage type, or the number of certain units or rooms — are significantly increasing the complexity of the retrieval process. This abundance of potential information makes it nearly impossible to manage effectively.

For this reason, potential levels for possible input accuracy are differentiated on root level of the developed decision tree. This distinction considers whether the architect has only a rough idea for a new project (Idea available) or if there is already an existing plot of land, a development plan, or even a BIM model. The decision tree in Figure 1 illustrates an example in case of the existence of a specific development plan for a new project and the possible requirements that an architect can capture to match them with a suitable BIM building from the database (searching for models). This work focuses on the solid line, describing the possibilities of architectural design for a building.

Nevertheless, capturing information from the other branches of the tree (dashed line) is also feasible. Thus, the architectural decisions focus on the internal structure, building design, floor plan, and energy efficiency. The information becomes increasingly detailed down to the leaves of the tree (e.g., Walls and Windows). It should be noted that these leaf nodes do not represent the end of the tree, as further details such as materiality or other properties are stored for each of them. The tree is structured to cover the most crucial decisive information in architecture that have a crucial impact on the building's lifecycle and are available during design phase.

## 3.2 iDesignArch

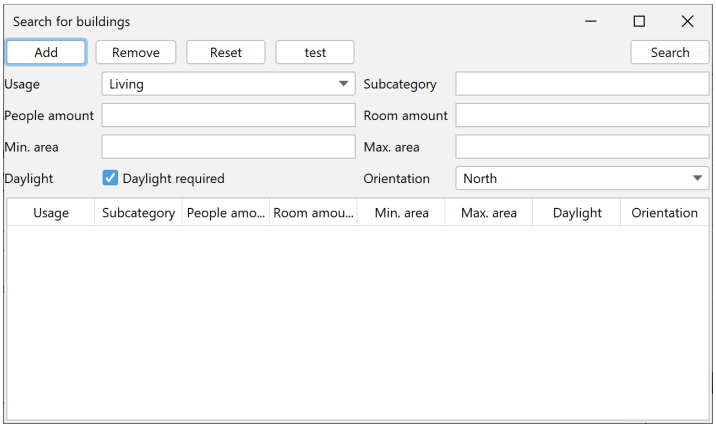


Figure 2: The sub-GUI for room details from the first approach.

The developed structured, innovative, and user-friendly tool is introduced as iDesignArch. This abbreviation stands for Intelligence Design-Decision-Making for Architects. The basis of iDesignArch is the discussed and carefully crafted decision tree for decision-making in early design phases.

### 3.2.1 Previous Approach

In a first approach, a Graphical User Interface (GUI) for gathering the information described in Section 3.1 was developed. However, due to the complexity of the input data the GUI is unintuitive, complex and confusing. It consist of a lot of different sub GUIs, of which an example for room details can be seen in Figure 2. In contrast to creating a simple schematic BIM model, this approach involves numerous detailed steps. Additionally this approach is less flexible.

### 3.2.2 Decision Tree

The search input needs to be structured according to the required parameters for the building search. Some of the information, which is very complex to enter, is not even required for the actual search. Therefore the input possibilities can be filtered and reduced according to their importance for good search results.

A closer look on the relevant information reveals dependencies between the different search parameters. These dependencies are sometimes obvious (e.g. details about the rooms are required before wall details can be added) from the context of building physics, but sometimes they purely arise from the search design itself (e.g. requiring floor plan shape before adding room details). These dependencies result in the fact, that some information, which was entered in a complicated way,

could not be used for a search due to missing additional information it depends on. Combining these dependencies and the insight, that some parameters are more important than others, a decision tree was developed. In fact there are multiple decision trees, as the information basis (e.g. only idea available, property known, development plan available or BIM model available) highly effects the required information and their importance. This paper sets the focus on the availability of an existing development plan. The resulting decision tree for that case is visible in Figure 3.

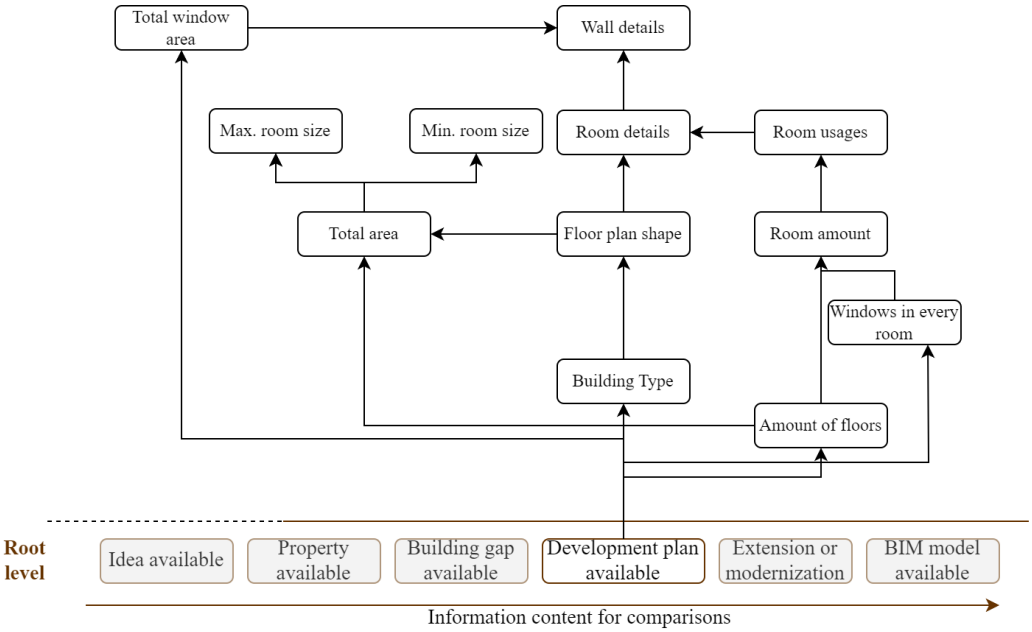


Figure 3: The developed iDesignArch decision tree for specific input data with available development plan.

The decision tree represents a structured way to gather the required information. A node is considered as *fulfilled*, if the information, represented by a node is available and all parent nodes are *fulfilled* as well. Based on Figure 3, the *total area* node is *fulfilled*, if the total area of the building is provided (available information), as well as the *Floor plan shape* and *Amount of floors* nodes are *fulfilled* (*fulfilled* parents). An example input will be discussed in Section 5.2. The root node of each decision tree is the initial information basis, which in this case is the available development plan. As long as a node is not *fulfilled*, the corresponding information can not be used for a search until additional information is provided. The decision tree is used to identify these required information.

## 4 Implementation

The decision tree approach developed in Section 3 is used to develop an interactive input method which enables user friendly and fast input of information without requiring a schematic BIM model. An initial approach uses sequential input (Subsection 4.1), while the final approach uses a Large Language Model (LLM) to enable free text input and increase usability (Subsection 4.2).

### 4.1 Sequential Input

To use the decision tree in an actual input, the tree need to be available in a machine readable way. In addition to that, every node is associated with a string, containing a human understandable question for the corresponding parameter. The input program will process the decision tree sequentially. Starting at the root node asking the user the corresponding question level by level. As visible in Figure 4, the user than enters the relevant information. However the total amount of project information gathered by the tool is drastically reduced, as the input is limited to search relevant questions.

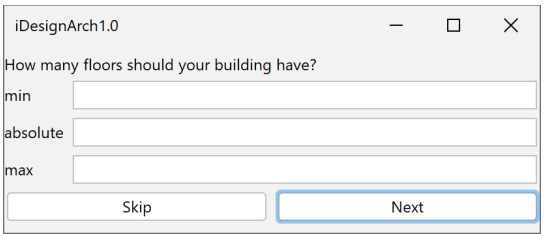


Figure 4: The sequential input window from iDesignArch. Input for *Amount of floors* node.

### 4.2 Large Language Model Input

To combine the advantages of the GUI and the sequential approach, as well as to increase usability, a LLM — in our case customized ChatGPT [10] — is used to process user input. The customized ChatGPT enables the user to freely describe the searched building and then subsequently answer queries, raised according to the decision tree, which are crucial to the search quality. More detailed, the user need to answer questions until all nodes, for which information was provided, are *fulfilled*. Afterwards the user is asked to optionally provide information about nodes on the next level in the decision tree.

The LLM is used only for processing user input and generating questions. The actual search or data processing happens outside of ChatGPT. Therefore iDesignArch does not have to use ChatGPT. The implementation need to be understood as a proof of concept. Information matching one of the nodes in the decision tree is passed to the search tool, and all other information is captured as project information.

## 5 Demonstration

This section describes an exemplarily usage of iDesignArch with LLM (Subsection 4.2).

### 5.1 Setup

For demonstration purposes, an office worker with no background in building or construction industry, should search for a new building for his department. We briefly explained the information available from the development plan (e.g. property dimensions and height regulations) but did not prescribe any other properties. Due to the scope of this paper, we manually summarized the input in Table 1. The summary was created by a human, reading the input provided by the office worker and extracting the properties. The original input started with : "Hello. I want to build a new office building. I need 3 to 5 stories with at least 35 offices. I need 5 conference rooms..."

Table 1: Manual summary of input requirements.

| | | |
|---|---|---|
| office Building | 3 to 5 floors | min. 35 offices |
| 5 conference rooms | 2 bathrooms per floor | 5 additional rooms |
| large room on ground floor | smart home functions | air conditioning |

## 5.2 Results

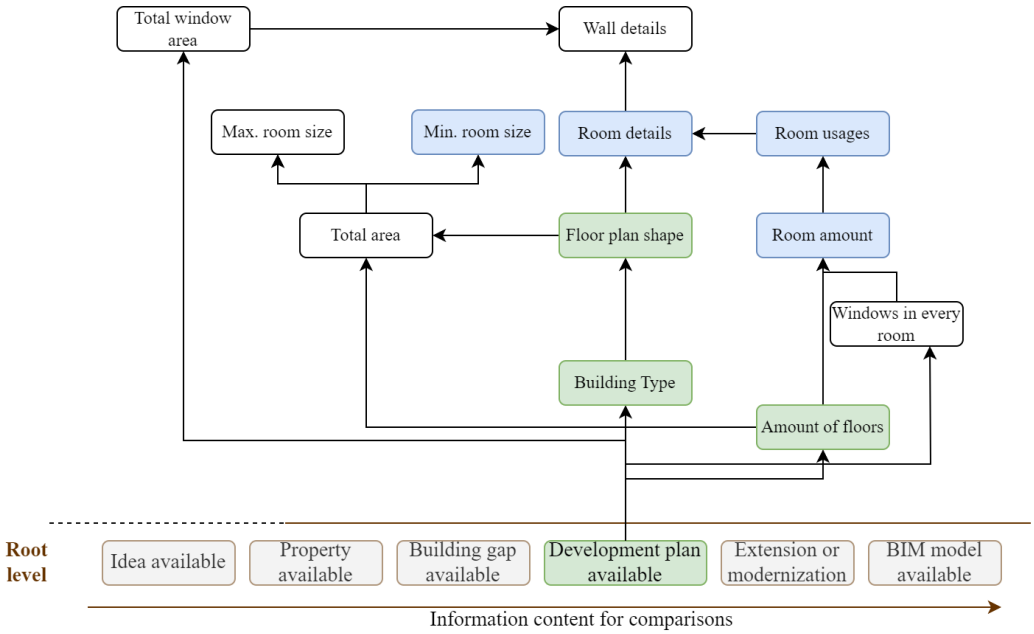


Figure 5: The iDesignArch decision tree after initial input. Nodes highlighted in blue if information is provided, green if *fulfilled*. For white nodes there is no information provided.

As visualized in Figure 5, some nodes have provided information, without being fulfilled (blue). For example the room amount was specified. The node *Room amount* on the top right has two parents: *Amount of floors* and *Windows in every room*. While one of them is *fulfilled* (green), there is no information about *Windows in every room*. Therefore, *Room amount* and all children can not be *fulfilled*.

Accordingly, ChatGPT asks for the missing information to *fulfil* all blue nodes. In our example the prompt is "Would you like all the rooms in your office building, including the offices, conference rooms, and additional rooms, to have windows?" [1].

Subsequently to the input phase the data to is extracted from ChatGPT as JSON and passed on to the search tool. This is where current limits of the demonstration application become clear, as ChatGPT did not always use the correct JSON identifiers required for the search input. In the same way there is no guarantee that ChatGPT (or any other LLM) interprets user input correctly. Additionally there is no guarantee how wrong user input is handled. Therefore, future work, especially reducing these issues, is required.

[1] Generated by ChatGPT [10]

## 6 Conclusion

The presented iDesignArch approach uses current technologies — more precisely LLMs — to enhance and simplify the user input for capturing project data. Together with search algorithms from previous research, it enables the search for similar buildings, even with input from inexperienced users. To ensure the transparency, reproducibility and modularity of the approach, the LLM is used only to handle the user input. Despite promising performance, there are still some challenges regarding the LLM to be overcome. Actual search and information processing is handled without them. This ensures that if not available or requested, the LLM can be replaced by iDesignArch GUIs, another LLM or other input possibilities.

## References

[1] Y.-W. Song, M. Herzog, and B. Bender, "Understanding the initial requirements definition in early design phases", en, *Proceedings of the Design Society: International Conference on Engineering Design*, vol. 1, no. 1, pp. 3751–3760, Jul. 2019. DOI: 10.1017/dsi.2019.382.

[2] M. K. Najjar, K. Figueiredo, A. C. J. Evangelista, A. W. A. Hammad, V. W. Y. Tam, and A. Haddad, "Life cycle assessment methodology integrated with bim as a decision-making tool at early-stages of building design", *International Journal of Construction Management*, vol. 22, no. 4, pp. 541–555, Mar. 2022. DOI: 10.1080/15623599.2019.1637098.

[3] 14:00-17:00, *Iso 16739-1:2024*, en. [Online]. Available: https://www.iso.org/standard/84123.html.

[4] C. J. Hopfe and R. S. McLeod, "Enhancing resilient community decision-making using building performance simulation", *Building and Environment*, vol. 188, p. 107 398, Jan. 2021. DOI: 10.1016/j.buildenv.2020.107398.

[5] A. Aamodt and E. Plaza, "Case-based reasoning: Foundational issues, methodological variations, and system approaches", en, *AI Communications*, vol. 7, no. 1, pp. 39–59, 1994. DOI: 10.3233/AIC-1994-7104.

[6] D. Napps, D. Pawlowski, and M. König, "Bim-based variant retrieval of building designs using case-based reasoning and pattern matching", en-US, *ISARC Proceedings*, pp. 435–442, Nov. 2021.

[7] D. Napps, J. Maibaum, and M. König, "Identifying cost-efficient alternatives to building designs based on building regulations", en,

[8] D. Napps and M. König, "Consideration of detailing in the graph-based retrieval of design variants", in *ECPPM 2022 - eWork and eBusiness in Architecture, Engineering and Construction 2022*. CRC Press, 2023.

[9] D. Napps, A. Zahedi, M. König, and F. Petzold, "Visualisation and graph-based storage of customised changes in early design phases", en-US, *ISARC Proceedings*, pp. 191–198, Jul. 2022.

[10] OpenAI, *Chatgpt: A large language model based on gpt-4 architecture*, 2024. [Online]. Available: https://www.openai.com/research/chatgpt.

# Ensuring Compliance in Construction: A Deep Dive into BIM Model Checking and Automated Code Verification

Mohamed Helmy Ammar[1] and Merna Emara[1]
[1]Institute of Construction Informatics, Dresden University of Technology, Helmholtzstraße 10, 01069 Dresden, Germany
E-Mails: mohamed.ammar@mailbox.tu-dresden.de, merna.emara@tu-dresden.de

**Abstract:** The paper examines code compliance of energy efficiency in building design through (BIM) tools, particularly the BIMQ – Solibri rule plugin and a custom-created Solibri ruleset. It aims to simplify the validation of thermal transmittance (U-value) for architectural components such as doors, slabs, walls, and windows, ensuring these elements fulfil the established energy efficiency standards. The BIMQ plugin in Solibri Model Checker (SMC) effectively assigns and confirms thermal transmittance values across different components while identifying errors in the BIM model in Autodesk Revit. Furthermore, the model checking with the custom ruleset facilitates the assessment of components against energy efficiency rule criteria in the paper by pointing out the components that need adjustments to improve the whole building's performance and their exact locations. Using an Excel template to export the results from (SMC) makes analyzing the data simpler for stakeholders. The project highlights the significant importance of BIM in the construction sector especially in achieving energy efficiency objectives and it sets the foundational basis for future improvements in BIM technologies to further improve the consistency and efficiency with the AEC industry while acknowledging challenges and inaccuracies in component classification in the model that require further improvement.

*Keywords:* Code Compliance, Energy Efficiency, BIM, BIMQ, Solibri Model Checker, EIR

Erschienen in Tagungsband 35. Forum Bauinformatik 2024, Hamburg, Deutschland, DOI: 10.15480/882.13538
© 2024 Das Copyright für diesen Beitrag liegt bei den Autoren. Verwendung erlaubt unter Creative Commons Lizenz Namensnennung 4.0 International.

## 1 Introduction

The construction industry faces the challenge of ensuring that buildings comply with strict standards, often slowed down by manual and error-prone compliance methods, leading to costly delays. Implementing a systematic and precise approach, particularly within Building Information Modeling (BIM), is crucial to enhance project outcomes, safety, and regulation. Despite both BIM's methods and processes efficiency, adapting to evolving compliance requirements remains a barrier. This

paper aims to address this by developing an Automated Code Compliance Checking (ACCC) solution to facilitate BIM model verification and code compliance. The main objective of the study is to establish an automated code checking focusing on construction projects. The primary objectives are to identify and locate the relevant rules from the standards and regulations that influence the thermal resistance of building components. Following this, the Employer's Information Requirements (EIR) are created using BIMQ and digitally transfer it into BIM software. The Revit model is then reviewed and adjusted according to these standards. Afterwards, the model is exported into an IFC file to facilitate its transformation into Solibri. Finally, the model is checked in Solibri to ensure that the information and values are accurate, thereby guaranteeing the building's energy efficiency. The methodology consists of seven steps: examining standards and regulations to extract energy efficiency rules, creating EIR using BIMQ, adjusting the model to comply with standards, conducting a compliance check on each building component, transferring EIR workflows to Solibri for further analysis, creating custom rules in Solibri to evaluate model compliance, and analyzing workflows and proposing enhancements for optimal outcomes. By bridging traditional gaps, the proposed ACCC solution promises safer, more efficient, and sustainable construction practices, essential for dealing with various requirements.

## 2 Literature Review

Automated code compliance checking within Building Information Modelling (BIM) has garnered significant attention in recent research. This rapidly expanding field delves into various aspects of rule-based checking systems, the integration of artificial intelligence (AI), and automation model verification to ensure compliance with building regulations, supported by an extensive literature review. [1] outlines the evolution of rule-based checking systems, highlighting the potential of advanced tools to support design and compliance tasks effectively. [2] underscored the pivotal role of AI in enhancing automated code compliance by minimizing human error and improving the accuracy of BIM models. Meanwhile, [3] proposed a methodological approach to automate code-checking processes within BIM frameworks, utilizing computer-readable language rules and software tools like Dynamo and Python scripting. Additionally, scholars like [4] and [5] contributed by providing conceptual frameworks and identifying inefficiencies in manual compliance procedures, highlighting the potential of BIM to streamline the process. [6] addressed the challenges inherent in automating rule checking, proposing a classification system to facilitate the process. [7] focused on automating model checking in building design, aiming to develop methods for specifying and evaluating building rules within BIM contexts. Collectively, these studies underscore the growing importance and potential of automated code compliance checking within BIM environments, offering valuable insights into its implementation, challenges, and future directions.

# 3 Methodology

This section outlines the plan for implementing automatic code compliance checking in a construction project in Germany. Based on the framework proposed by [1], the approach includes five main phases. The methodology involves a comprehensive approach to implementing automatic code compliance checking for energy efficiency in construction projects using Building Information Modeling (BIM). The process begins with rule interpretation, where relevant standards and regulations, particularly focusing on thermal transmittance (U-value), are extracted and formatted for software processing. Next, the Employer's Information Requirements (EIR) are prepared, detailing the necessary information and Level of Geometry (LOG) for various architectural components. The building model is then developed using Autodesk Revit 2023, incorporating essential elements like windows, doors, slabs, and walls, all selected for their compliance with energy efficiency standards. Following this, the compliance check is executed using the BIMQ – Solibri rule plugin and a custom-created Solibri ruleset, which identifies building components, that violate the energy efficiency criteria. The results are systematically reported, highlighting compliant components and those needing adjustments. This detailed reporting ensures compliance with energy efficiency standards, thereby enhancing the overall building performance and consistency. This structured approach not only simplifies the validation process but also highlights the significant role of BIM in achieving energy efficiency in the construction sector. Figure 1 below summarizes the whole process of code compliance checking.

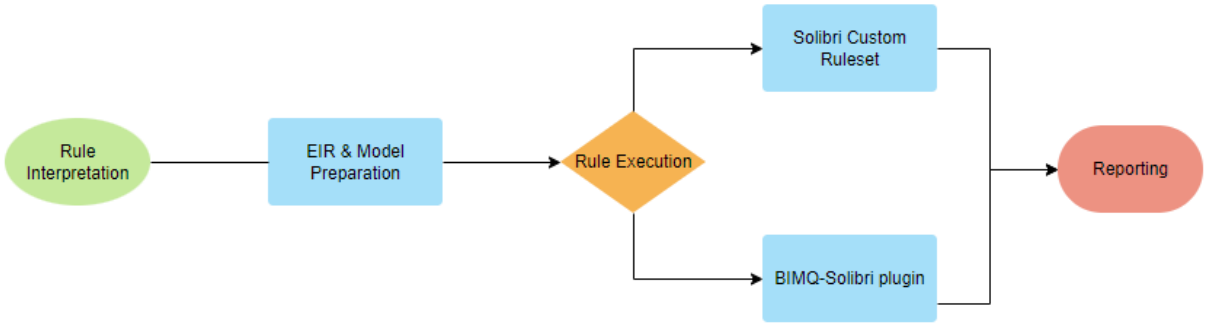


Figure 1: Process for Checking Compliance.

# 4 Implementation

This section details the practical application of the automatic code compliance checking framework, showcasing the operational phases and outcomes of the implemented methodology.

## 4.1 Rule Interpretation

This step begins by extracting and converting energy efficiency rules from relevant standards and regulations. By going through an in-depth examination of the Muster-Verwaltungsvorschrift Technische Baubestimmungen (MVV TB) that was published by the German Institute of Civil

Engineering [8]. The focus lies on thermal resistance and transmittance. Key rules extracted from DIN standards are summarized in Table 1.

Table 1: Extracted Rules from DIN Standards for Building Components

| Standard | Reference | Element | Description |
|---|---|---|---|
| DIN 4108-2 | Table (3) – Minimum values for thermal resistance of components, R-value | Walls | The Thermal Resistance of walls should be R-value ≥ 1.20 m²·K/W, (or **U-value ≤ 0.84 W/m²·K**) |
| DIN 4108-2 | Table (3) – Minimum values for thermal resistance of components, R-value | Slabs | The Thermal Resistance of slabs should be R-value ≥ 0.90 m²·K/W, (or **U-value ≤ 1.2 W/m²·K**) |
| DIN 4108-4 | Table (7) – Heat transfer coefficient of external doors, U-value **Or** Section (5.1.4) in DIN 4108-2 | Doors | The Thermal Transmittance of doors should be **U-value ≤ 2.90 W/m²·K** |
| DIN 4108-4 | Table (10) – Heat transfer coefficient, U-value | Windows | The Thermal Transmittance of windows should be **U-value ≤ 2.00 W/m²·K** |

## 4.2 EIR Preparation

The next step involves creating the Employer's Information Requirements (EIR) using BIMQ, a crucial process that ensures the accuracy of the BIM model for subsequent energy efficiency evaluation. This process includes defining key actors, such as the architect and other stakeholders, assigning discipline models, and exporting the EIR report for further analysis. The EIR preparation process precisely defines the extracted rules from the standards to be included in the BIM model, ensuring that all project requirements are met. This includes specifying the Level of Geometry (LOG) for different architectural components, such as walls, slabs, doors, and windows. For instance, walls and slabs are assigned a LOG of 300, while doors and windows are assigned a LOG of 350, providing a high level of detail for precise compliance checking. Additionally, the EIR outlines the Level of Information (LOI) required, which includes data such as material specifications and thermal transmittance values (U-values). The process involves accurate checks to verify that each component meets the required standards. Once the EIR is prepared, it is exported as a detailed PDF report for further analysis. This report includes comprehensive information requirements for each component, ensuring that the BIM model includes all necessary data for compliance checking and

project execution. By using BIMQ, the process facilitates more efficient communication and collaboration among project stakeholders, ensuring that all parties are aligned with the project goals and requirements. This structured approach enhances the BIM model quality, ensuring compliance with energy efficiency standards.

## 4.3 Building Model Preparation

A school project (Förderschule) in Delitzsch, Germany, serves as the case study, prepared using Autodesk Revit 2023. Initially, the model lacked windows and doors, which were then integrated, as shown in Figure 2. Specifications for these elements were selected to comply with energy efficiency standards, focusing on materials with suitable thermal properties. Revit derives the R-value and U-value, ensuring compliance with DIN standards. According to [9], the building model data should be formatted to be compatible with the code-checking process. After modification, the model data was prepared for export to an IFC file to ensure compatibility with Solibri Model Checker (SMC). This required specific adjustments in Revit's export settings to guarantee accurate data transformation and inclusion for reliable code compliance checking.

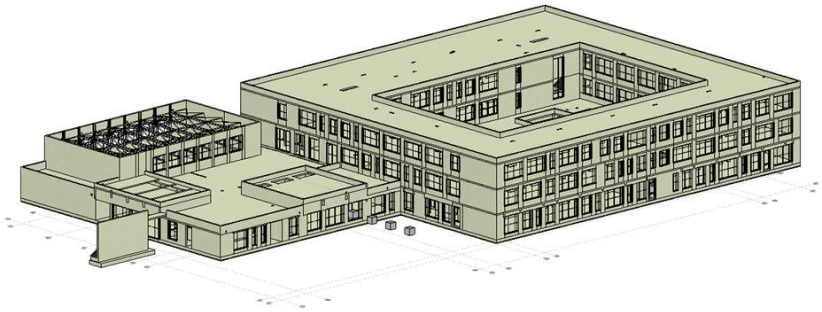

Figure 2: Model After Adding Windows and Doors.

## 4.4 Rule Execution Overview

The rule execution process is divided into two stages: the initial compliance check using the BIMQ-Solibri plugin, followed by a custom ruleset in Solibri for detailed evaluation.

### 4.4.1 BIMQ Plug-in Checking

The compliance checking process begins with the BIMQ-Solibri plugin within Solibri, which verifies that the thermal transmittance (U-value) was correctly assigned to all specified architectural components such as doors, slabs, windows, and walls in the Revit model, ensuring the fulfilment of energy efficiency standards. The plugin imports requirements from BIMQ and loads the IFC file from Revit into Solibri for verification. A new ruleset is created in Solibri based on BIMQ guidelines. During the check, a critical error is identified with the stair component, incorrectly defined as IfcSlab in Revit. This was corrected by redefining it as IfcStairs and re-exporting the model. Upon rechecking, all components had the correct U-values, and the model passed all compliance checks. Figure 3 shows the BIMQ requirements view and results of the BIMQ rule.

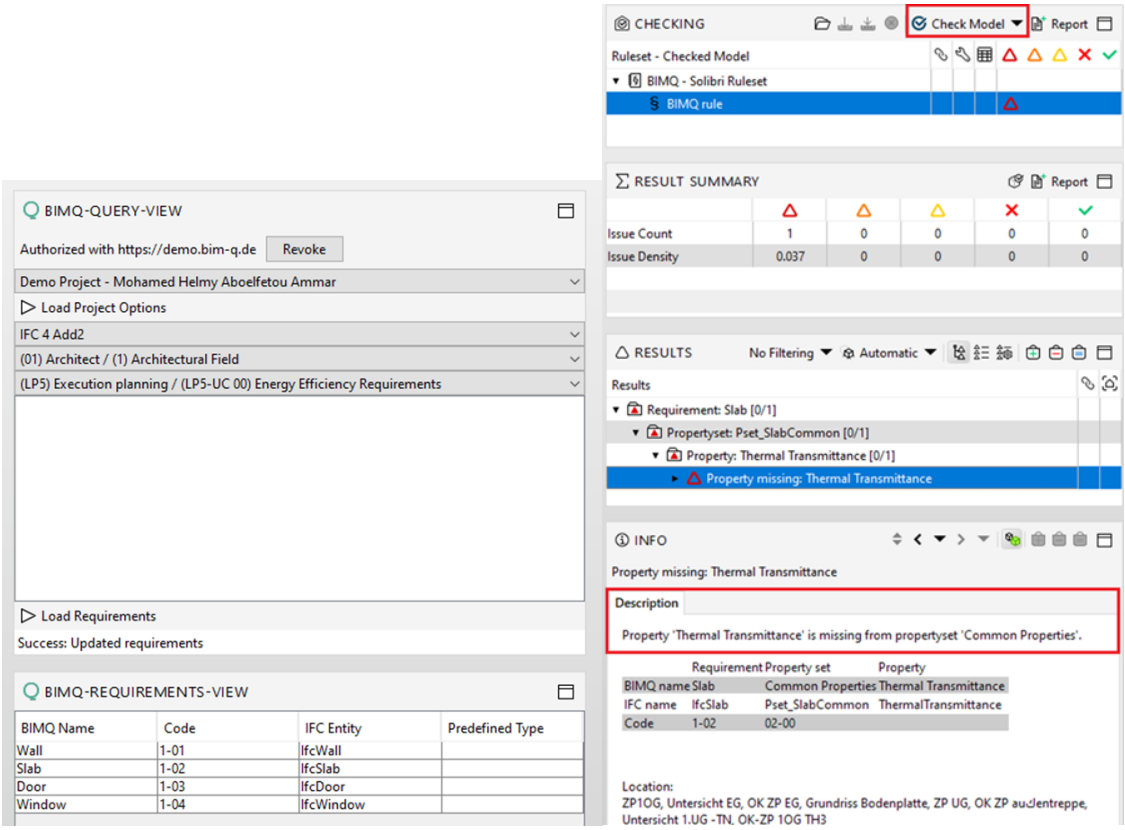


Figure 3: BIMQ Query and Requirements View, and Results of BIMQ Rule.

### 4.4.2 Solibri Created Ruleset

The compliance checking process with a custom Solibri ruleset involves exporting the Revit model as an IFC file to ensure compatibility. This ruleset assesses thermal transmittance values (U-values) for components like doors, slabs, walls, and windows against DIN standards. The ruleset checks if these components meet the U-value criteria: ≤ 2.90 W/m²K for doors, ≤ 1.20 W/m²K for slabs, ≤ 0.84 W/m²K for walls, and ≤ 2.0 W/m²K for windows. Components exceeding these limits are flagged as not energy efficient. The results highlight areas where the building design fails to meet energy efficiency standards, with detailed feedback highlighting issues as illustrated in Figure 4.

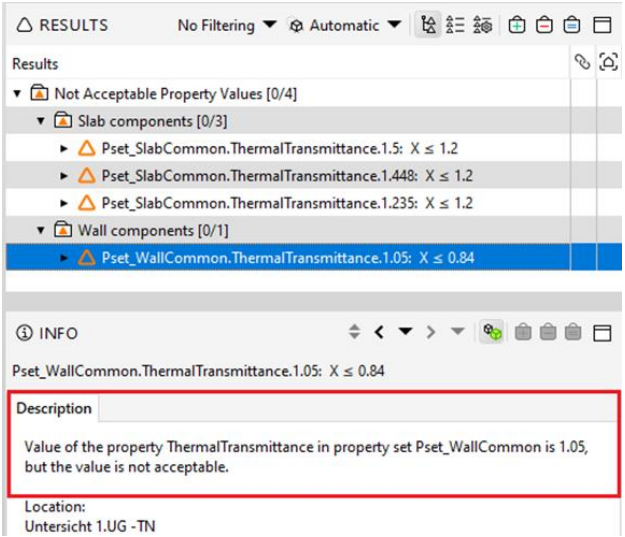


Figure 4: Detailed Results of Wall Components Exceeding U-value Limit.

### 4.5 Rule Checking Results

The rule-checking process utilized the BIMQ – Solibri plugin and a custom Solibri ruleset to validate that thermal transmittance values were correctly assigned, ensuring compliance with energy efficiency standards for architectural building components. The BIMQ plugin verified that doors, slabs, walls, and windows had assigned thermal transmittance (U-values), revealing an initial error with the misclassification of stair components in Revit, which is corrected by redefining it as IfcStairs. Subsequent checks confirmed component compliance. The customized ruleset checked these components against DIN standards, identifying areas where slabs and walls failed to meet the specified U-values. Detailed feedback from Solibri highlighted non-compliant components, allowing for precise adjustments. Reports summarizing these checks were exported to Excel for easier analysis and understanding.

## 5 Conclusion and Limitations

This research underscores the pivotal role of Building Information Modeling (BIM) tools, particularly the integration of the BIMQ – Solibri plugin and a custom Solibri ruleset, in improving the verification process for energy efficiency in building components. By effectively allocating and validating thermal transmittance values, these tools ensure compliance with energy efficiency standards by correcting inconsistencies within the BIM model. The custom ruleset offers specialized evaluations, identifying components that violate the standards and allowing for focused enhancements. Exporting results into an Excel template enhances data analysis accessibility, emphasizing BIM's critical importance in achieving energy efficiency objectives and facilitating future advancements in sustainable construction design. Due to BIMQ – Solibri plugin limitations in only checking for U-value assignments without verifying compliance with standards, a custom Solibri ruleset was developed

for component compliance, improving BIM-based compliance checking and promoting more sustainable building practices.

## Acknowledgement

The publication is part of the research project entitled “iECO – Intelligence Empowerment of Construction Industry” which has received funding from Bun-desministerium für Wirtschaft und Klimaschutz (BMWK) based on a resolution of the German Bundestag. The authors gratefully acknowledge the support and funding from the BMWK. The content of this publication reflects the author's view only and the BMWK is not responsible for any use that may be made of the information it contains.

## References

[1] Eastman, C., Lee, J. min, Jeong, Y. suk, & Lee, J. kook. (2009). Automatic rule-based checking of building designs. Automation in Construction, 18(8), 1011–1033. https://doi.org/10.1016/j.autcon.2009.07.002

[2] Sun, H., & Kim, I. (2022). Applying Ai Technology To Recognize Bim Objects and Visible Properties for Achieving Automated Code Compliance Checking. Journal of Civil Engineering and Management, 28(6), 497–508. https://doi.org/10.3846/jcem.2022.16994

[3] Di Giuda, G. M., Boseggia, A. B., & Francesco, P. (2021). Development of a rule-based system for automated BIM code-checking. Proceedings of International Structural Engineering and Construction, 8(1). https://doi.org/10.14455/ISEC.2021.8(1).AAE-08

[4] Hjelseth, E. (2016). Classification of BIM-based Model checking concepts. Journal of Information Technology in Construction, 21(CIB W78 2015), 354–369. http://www.itcon.org/2016/23

[5] Ismail, A. S., Ali, K. N., & Iahad, N. A. (2017). A Review on BIM-based automated code compliance checking system. International Conference on Research and Innovation in Information Systems, ICRIIS, 1–6. https://doi.org/10.1109/ICRIIS.2017.8002486

[6] Solihin, W., & Eastman, C. (2015). Classification of rules for automated BIM rule checking development. Automation in Construction, 53, 69–82. https://doi.org/10.1016/j.autcon.2015.03.003

[7] Sydora, C., & Stroulia, E. (2019). Towards rule-based model checking of building information models. Proceedings of the 36th International Symposium on Automation and Robotics in Construction, ISARC 2019, Isarc, 1327–1333. https://doi.org/10.22260/isarc2019/0178

[8] DIBt. (2023). Publication of the Model Administrative Provisions – Technical Building Rules. MVVTB_2023-1. Deutsches Institut für Bautechnik, 1(2), 352. https://www.dibt.de/de/aktuelles/meldungen/nachricht-detail/meldung/mvv-tb-20231-veroeffentlicht

[9] Andrich, W., Daniotti, B., Pavan, A., & Mirarchi, C. (2022). Check and Validation of Building Information Models in Detailed Design Phase: A Check Flow to Pave the Way for BIM Based Renovation and Construction Processes. Buildings, 12(2). https://doi.org/10.3390/buildings12020154

# Teil IV

# Computer Vision

# Kombination von Thermographie und Laserscanning zur Erfassung und Visualisierung von Störstellen mittels BIM

Melanie Müßle[1]

[1]Institut für Technologie und Management im Baubetrieb, Karlsruher Institut für Technologie, Gotthard-Franz-Str. 3, 76131 Karlsruhe, Deutschland

E-Mail: melanie.muessle@kit.edu

**Abstract:** Die Thermographie ist ein wichtiges Verfahren zur Analyse von Bestandsbauten. Mit dieser zerstörungsfreien Prüfmethode können z. B. Schadensinspektionen durchgeführt oder Wärmebrücken an Gebäuden aufgespürt werden. Standardwärmebildkameras liefern zweidimensionale Thermogramme ohne räumlichen Bezug. Zur besseren Interpretierbarkeit und räumlichen Verortung der Wärmebilder ist es notwendig, diese mit einem dreidimensionalen Modell des Gebäudes zu verknüpfen. Die Gebäudestruktur kann z. B. mithilfe eines Laserscanners erfasst und als dreidimensionale Punktwolke dargestellt werden, welche als Grundlage für das BIM-Modell dient. In diesem Beitrag wird ein Überblick über Methoden zur Kombination von Wärmebildern und 3D-Punktwolken gegeben und diese miteinander verglichen. Es zeigt sich, dass die automatisierte Interpretation und BIM-Integration der kombinierten Daten aktuell noch in den Kinderschuhen steckt und weiter Gegenstand zukünftiger Forschung sein wird. Als Fallbeispiel wird die aktive Thermographie zur Erfassung von visuell nicht sichtbaren metallischen Störstellen beim Rückbau von Kernkraftwerken eingesetzt. Diese in den Betonflächen der Gebäude eingebauten Objekte sind zur Planung des Rückbaus exakt zu erfassen und innerhalb der Gebäudeflächen zu lokalisieren. Die Eignung der vorgestellten Methoden für die beschriebene kerntechnische Anwendung wird diskutiert und ein aus 3 Schritten bestehendes Verfahren zur BIM-Integration der Ankerplatten vorgeschlagen.

*Keywords:* Building information modeling (BIM), Bestandserfassung, Thermographie, Datenfusion

Erschienen in Tagungsband 35. Forum Bauinformatik 2024, Hamburg, Deutschland, DOI: 10.15480/882.13496
© 2024 Das Copyright für diesen Beitrag liegt bei den Autoren. Verwendung erlaubt unter Creative Commons Lizenz Namensnennung 4.0 International.

## 1 Einleitung

Als Grundlage für die Planung von Sanierungen, Umbauten, Erweiterungen oder dem Rückbau bestehender Gebäude und Infrastrukturen wird häufig ein digitales Bestandsmodell erstellt. Voraussetzung ist die 3D-Bestandserfassung des Bauwerks. Als Ergebnis wird dabei eine Punktwolke erzeugt, anhand derer ein dreidimensionales Modell des Bauwerks abgeleitet werden

kann, welches die Grundlage für die Anwendung der BIM-Methodik bildet. Insbesondere zur Planung von Sanierungsmaßnahmen werden zusätzliche Informationen über den Zustand eines Bauwerks benötigt, welche mit optischen Methoden wie z. B. dem Laserscanner nicht erkennbar sind. Hier kommt die bildgebende Thermographie ins Spiel. Mit dieser zerstörungsfreien Prüfmethode können z. B. Schäden inspiziert oder Wärmebrücken an Gebäuden aufgespürt werden [1]. Das Ergebnis ist ein Wärmebild, also eine zweidimensionale farblich oder in Grauwerten codierte Darstellung der Temperaturverteilung auf der Oberfläche der abgebildeten Objekte. Wärmebilder lassen sich ohne Hintergrundwissen über die abgebildeten Objekte und Strukturen oft nur schwer interpretieren [1]. Für viele Anwendungen ist es daher von Vorteil, die Informationen der Wärmebilder mit einer dreidimensionalen Darstellung des entsprechenden Bauwerks zu verknüpfen, so dass diese Informationen eindeutig lokalisiert und im Zusammenhang betrachtet werden können [1], [2]. Um die Thermaldaten räumlich verorten zu können, muss eine Fusion der Wärmebilder mit der Punktwolke sowie eine Integration der Informationen in das BIM-Modell stattfinden.

In der Literatur lassen sich zwei wesentliche Ansätze zur Kombination von Thermographie- und 3D-Messdaten unterscheiden [3], je nachdem, ob der Fokus auf der kombinierten Messdurchführung der unterschiedlichen Sensoren liegt oder auf der Zusammenführung der unabhängig voneinander erfassten Daten. In allen untersuchten wissenschaftlichen Artikeln zum Thema wird entweder der erste oder der zweite Ansatz verfolgt. Dieser Beitrag liefert dahingegen einen Überblick und Vergleich beider Ansätze (Kapitel 2). Kapitel 3 gibt einen Überblick über die BIM-Integration der kombinierten Daten. In Kapitel 4 wird ein Fallbeispiel aus dem kerntechnischen Rückbau vorgestellt und die Eignung der Verfahren dafür diskutiert. Abschließend erfolgt in Kapitel 5 ein Fazit.

# 2 Kombination von Wärmebildern und Punktwolken

Unabhängig vom gewählten Ansatz sollte die Wärmebildkamera vor dem Einsatz geometrisch (siehe z. B. [1], [4]) und – sofern absolute Temperaturwerte von Interesse sind – auch radiometrisch (z. B. [2]) kalibriert werden, um die Qualität der Ergebnisse zu steigern und zu validieren [2].

## 2.1 Sensorgetriebene Fusion

### 2.1.1 Kombiniertes Messsystem

Für diesen Ansatz zur Kombination von Thermal- und 3D-Daten ist der Aufbau eines Messsystems wesentlich, das eine gemeinsame Durchführung und Zuordnung der Messungen ermöglicht. Im besten Fall existiert ein mobiles Multisensorsystem [5], bestehend aus mindestens einem Sensor zur 3D-Datenerfassung (z. B. Laserscanner, 360°-Kamera oder RGB-Stereokamerasystem) sowie einer (360°-)Wärmebildkamera. Die Sensoren sind in einem festen Abstand auf einer (mobilen) Plattform montiert. Die relative Position und Ausrichtung der Sensoren untereinander kann im Rahmen einer gemeinsamen gegenseitigen Kalibrierung vor Beginn der eigentlichen Aufnahmen ermittelt werden [5], [6]. Mithilfe der dabei bestimmten Transformationsparameter können die Lage und Ausrichtung der Wärmebildkamera im dreidimensionalen Koordinatensystem der Punktwolke

aus der 3D-Vermessung zu jedem Aufnahmezeitpunkt berechnet werden [6]. Sofern die Sensoren keinen festen Abstand zueinander haben, kann der sensorgetriebene Ansatz trotzdem realisiert werden, indem Lage und Ausrichtung der Wärmebildkamera z. B. mittels eines Tracking-Systems zu jedem Messzeitpunkt exakt erfasst werden. Beispiele dafür finden sich in [7] und [8].

### 2.1.2 Thermale Texturierung der Punktwolke

Sind Position und Ausrichtung der Wärmebildkamera relativ zum 3D-Messsystem bekannt, kann eine korrekte Registrierung der Wärmebilder auf die 3D-Punktwolke mittels Ray-Tracing ermöglicht werden [6], [7]. Dabei wird für jeden Punkt der Punktwolke der Verbindungsstrahl vom Messzentrum des Laserscanners (bzw. vom Referenzpunkt des entsprechenden RGB-(Stereo-)Kamerasystems) zum entsprechenden 3D-Punkt hinsichtlich eines Schnittes mit der Bildebene der Wärmebildkamera zum Zeitpunkt der jeweiligen Aufnahme untersucht. Existiert ein solcher Schnittpunkt, wird der Wert des Wärmebildes an dieser Stelle interpoliert und auf den 3D-Punkt des jeweiligen Verbindungsstrahls übertragen, so dass nach und nach die gesamte Punktwolke mit Thermalwerten texturiert wird. Der entsprechende Algorithmus wird insbesondere in [7] ausführlich erläutert.

## 2.2 Datengetriebene Fusion

In vielen Fällen existiert kein kombiniertes Messsystem, d. h. 3D-Vermessung und Thermographie werden unabhängig voneinander durchgeführt, oft auch zu unterschiedlichen Zeitpunkten. Die Positionen der Sensoren zum Aufnahmezeitpunkt sind hierbei nicht genau bekannt. Die Verortung der Wärmebilder in der Punktwolke muss nachträglich durch eine rein datenbasierte Fusion erfolgen.

### 2.2.1 Kombination von 2D- und 3D-Thermaldaten mit den Daten der 3D-Vermessung

Im Standardfall geht es darum, zweidimensionale Wärmebilder mit einer dreidimensionalen Punktwolke zu kombinieren. Die räumliche Verortung der Wärmebilder in der Punktwolke wird in diesem Fall über die Zuordnung abgebildeter Objekte durchgeführt, welche sich sowohl in den Wärmebildern als auch in der Punktwolke eindeutig identifizieren lassen. Die Herausforderung dabei liegt in der relativ niedrigen räumlichen Auflösung von Wärmebildkameras sowie in der Tatsache, dass sich viele Objekte in Wärmebildern deutlich schwerer identifizieren lassen als in RGB-Bildern oder Laserscans [9]. Dafür enthalten Wärmebilder wiederum auch Strukturen, die in RGB-Bildern überhaupt nicht sichtbar sind. Manche Wärmebildkameras bieten die Möglichkeit, gleichzeitig Thermal- und RGB-Bilder aufzunehmen. Obwohl es sich um ein und dasselbe Gerät handelt, sind die Objektive und Bildebenen der beiden Kamerasensoren nicht identisch. Analog zur gegenseitigen Kalibrierung der einzelnen Messgeräte eines Multisensorsystems muss auch hier die relative Orientierung der beiden Kamerasensoren vorab bestimmt werden, wie z. B. in [9] erläutert. Sofern die Abweichung rechnerisch berücksichtigt wird, kann die Identifizierung der markanten Objekte daraufhin in den RGB-Bildern anstelle der Wärmebilder vorgenommen werden [9], wofür bereits Algorithmen zur automatisierten Zuordnung erprobt sind. Ein Spezialfall des datengetriebenen Ansatzes beruht auf der Kombination von direkt dreidimensional erfassten Thermographiedaten mit einer dreidimensionalen Punktwolke aus der 3D-Vermessung. Die 3D-Thermographie kann auf

verschiedene Wege realisiert werden: In [11] wurde ein Panoramakopf entwickelt, auf welchem eine Wärmebildkamera in zwei verschiedenen Höhen angebracht und horizontal sowie vertikal rotiert werden kann. Durch Kombination der Bilder aus beiden Höhen lassen sich nach dem Prinzip der Stereophotogrammetrie [11] dreidimensionale Koordinaten berechnen. Eine Erweiterung dieses Prinzips der 3D-Rekonstruktion auf Multi-View-Stereo sowie eine Zuordnung mehrerer sich überlappender Wärmebilder mittels Structure from Motion (SfM) wird z. B. in [12] durchgeführt. In [13] dagegen werden direkt thermale Punktwolken von Indoor- und Outdoor-Szenen mithilfe einer 360°-Wärmebildkamera erzeugt. Nachteile der dreidimensionalen Thermographie, wie die relativ niedrige räumliche Auflösung und Genauigkeit, lassen sich gemäß [3] und [11] durch eine Kombination mit einer höher aufgelösten Punktwolke aus der 3D-Vermessung ausgleichen.

### 2.2.2 Transformation der Thermaldaten in die Punktwolke über identische Punkte

Für die räumliche Transformation eines Bildes an die richtige Position in der Punktwolke sind mindestens sechs identische Punkte erforderlich [4]. Oft (u. a. in [4] und [9]) wird die Auswahl und Zuordnung dieser Punkte, z. B. markanter Objektecken, händisch vorgenommen. Anhand der Koordinaten der Punkte im jeweiligen Koordinatensystem werden für jedes Bild die Transformationsparameter berechnet und die Bilder transformiert. Im nächsten Schritt muss die Punktwolke wie in Abschnitt 2.1.2 mit den Wärmebilddaten texturiert werden [4], [9]. Ansätze zur automatisierten Zuordnung identischer Objekte zwischen Wärmebildern und RGB-Daten existieren ebenfalls: In [10] erfolgt die Zuordnung über automatisch segmentierte Linien. In [1] wird der sog. RIFT-Algorithmus vorgestellt, der eine automatisierte Zuordnung von Bildern unterschiedlicher Spektralbereiche ermöglicht. Auch 3D-Thermaldaten können anhand von identischen Objekten in die Punktwolke der 3D-Vermessung transformiert werden. Darauf aufbauend wird jeder Punkt der höher aufgelösten Punktwolke mit dem nächstgelegenen Temperaturwert der thermalen Punktwolke texturiert [1].

## 2.3 Vergleich

Abbildung 1 zeigt eine Übersicht der geschilderten Kombinationsmöglichkeiten. Der in Abschnitt 2.1 beschriebene sensorgetriebene Ansatz zur Kombination von bildgebender Thermographie und 3D-Vermessung beruht auf einer kombinierten Durchführung der verschiedenen Messungen. Dabei liegen Informationen zu den einzelnen Sensoren und deren relativer Position und Ausrichtung bereits während der Messung vor oder werden in Echtzeit erfasst. Dies erfordert einen erhöhten Aufwand für den Aufbau des Messsystems und die Vorbereitung der Messungen. Der in Abschnitt 2.2 geschilderte Ansatz dagegen beinhaltet eine rein datenbasierte Fusion. Hierbei können die Messungen unabhängig voneinander erfolgen und die Zusammenführung von Punktwolke und Thermaldaten wird allein auf Grundlage der erfassten Daten durchgeführt, was einen erhöhten Auswerteaufwand bedeutet. Die Qualität des datenbasierten Ansatzes hängt im Wesentlichen davon ab, wie viele gemeinsame Strukturen in den unterschiedlichen Datensätzen identifiziert und wie genau diese zugeordnet werden können. Dieser Ansatz kann nur gewählt werden, wenn die erfassten Objekte eine eindeutige Zuordnung erlauben. Die Genauigkeit des ersten Ansatzes dagegen wird im Wesentlichen durch die Genauigkeit der gegenseitigen Kalibrierung bzw. der

Positionsbestimmung festgelegt. Dieser Ansatz ist vor allem dann zu wählen, wenn die Zuordnung unabhängig von den erfassten Objekten erfolgreich sein soll. Wiederholte Wärmebildaufnahmen können beim zweiten Ansatz auf demselben Wege wie die Erstaufnahme integriert werden. Die Datenmenge ist relativ gering, insbesondere wenn Wärmebilder nur punktuell von einzelnen zu inspizierenden Objekten oder Gebäudeteilen benötigt werden. Der erste Ansatz dagegen erfordert jedesmal eine parallele 3D-Vermessung, was zu einer großen Menge an redundanten Daten führt.

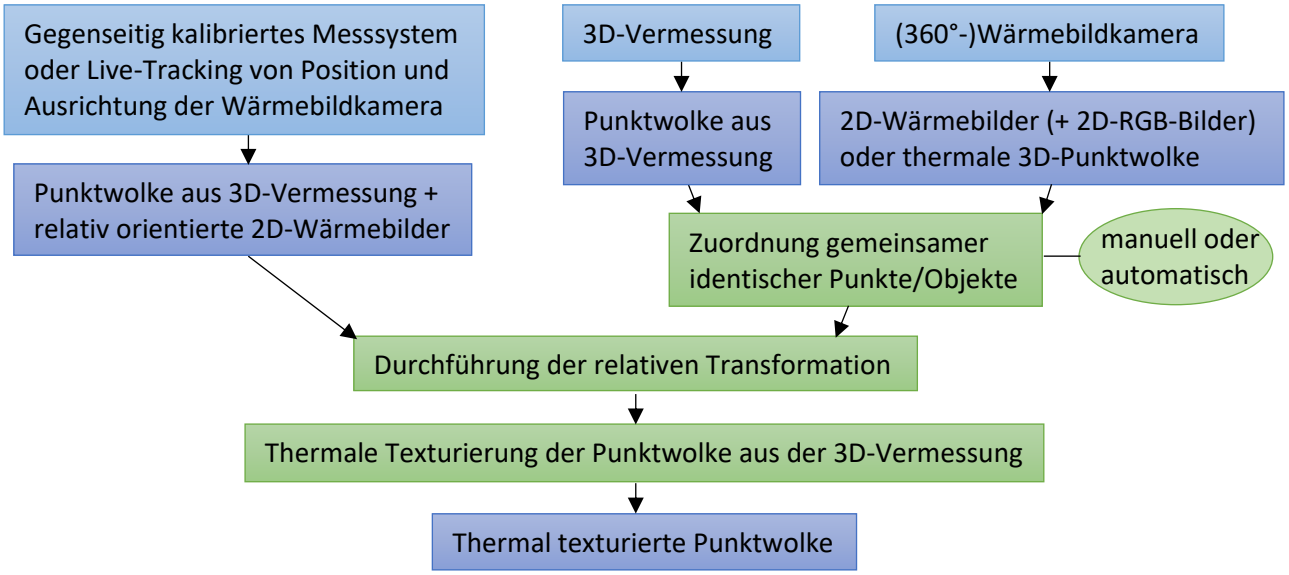


Abbildung 1: Übersicht über Kombinationsmöglichkeiten

# 3 BIM-Integration der Thermaldaten

Der Schwerpunkt in der Literatur liegt eindeutig auf der Erzeugung von thermal texturierten Punktwolken. Nur wenige Artikel behandeln die BIM-Integration dieser kombinierten Daten oder davon abgeleiteter Informationen. Ausgewählte Verfahren werden in diesem Kapitel vorgestellt.

## 3.1 Grafische Integration von Thermaldaten ins BIM als zusätzlicher Layer

Eine grafische Integration und Visualisierung kann z. B. durch Projektion der Thermaldaten auf das zugehörige Gebäudemodell umgesetzt werden, wie in [6] für weitere Untersuchungen vorgeschlagen wird. Eine Umsetzung erfolgt z. B. in [12], wo manuell ein grobes Gebäudemodell erstellt wird, auf welches die thermal texturierte Punktwolke orthogonal projiziert und das Orthothermogramm in Form eines Zusatzlayers zum Modell in der BIM-Software abgespeichert wird.

## 3.2 Semantische Integration von Thermaldaten ins BIM

Auch für die semantische Integration von Thermaldaten werden in vielen Fällen Orthothermogramme für einzelne Gebäudeteile berechnet. Diese werden jedoch nicht grafisch ins Modell integriert. Stattdessen wird daraus z. B. die Durchschnittstemperatur des Objekts [13] oder für Wände eine bauphysikalische Kenngröße [14], [15] (in der Regel R- oder U-Wert)

teilautomatisiert ermittelt und dem jeweiligen BIM-Objekt tabellarisch zugeordnet. Die Geometriedaten sowie die jeweilige thermale Kenngröße werden in den genannten Beiträgen in einer sogenannten gbXML-Datei zusammengefasst, einem Standard zum Austausch von BIM-Daten, welcher vor allem zur energetischen Analyse von Gebäuden eingesetzt wird.

### 3.3 BIM-Integration von extrahierten Objekten aus der thermalen Punktwolke

Die Ableitung von Informationen aus den dreidimensionalen Thermaldaten findet oftmals manuell statt [2]. Es finden sich nur wenige Beispiele, bei denen automatisiert Strukturen in thermalen Punktwolken segmentiert werden, z. B. [16] und noch weniger, in denen daraus BIM-Objekte erzeugt werden, z. B. [17]. Hier werden sowohl die wärmsten als auch die kältesten Bereiche einer Decke selektiert und mithilfe eines Clustering-Algorithmus gruppiert und zu Bauteilen zusammengefasst.

## 4 Praktische Anwendung beim Rückbau kerntechnischer Anlagen

Für den Rückbau eines Kernkraftwerks müssen sämtliche Betonflächen des Gebäudes erfasst und freigemessen werden, um nachzuweisen, dass die Aktivität unterhalb des Freigabegrenzwerts gemäß der Strahlenschutzverordnung liegt. Vor der Freimessung sind alle in den Betonflächen oberflächennah enthaltenen Objekte, wie z. B. (Rohr-)Durchführungen oder Ankerplatten exakt zu erfassen und zu lokalisieren, da diese bei der Messung und deren Auswertung separat zu betrachten sind. Eine Herausforderung liegt darin, Ankerplatten zu detektieren, die völlig plan in den Betonflächen liegen und gleichzeitig mit einer mehrere Millimeter dicken Dekontaminationsschicht überdeckt sind (Abbildung 2 links). Diese Platten sind in der Punktwolke nicht sichtbar, aber nach aktiver Erwärmung thermographisch erfassbar (Abbildung 2 rechts). Ziel ist es, diese Ankerplatten an richtiger Position in das BIM-Modell zu integrieren. In einer Fallstudie wurden 5 Räume mit insgesamt 35 Gebäudeflächen untersucht, wovon knapp 20% verdeckte Ankerplatten enthalten, die thermographisch zu erfassen sind. Zur Integration der Ankerplatten in das BIM-Modell sind 3 Schritte notwendig: Der 1. Schritt ist die Transformation der Wärmebilder in die Punktwolke. Um die Zahl der notwendigen identischen Punkte zu reduzieren, wird alternativ eine Transformation in die gemäß [18] erzeugten RGB-Orthobilder der Gebäudeflächen durchgeführt. Es zeigt sich, dass die meisten Gebäudeflächen viele zuordenbare Strukturen (Öffnungen oder sichtbare Metallteile) enthalten, was einer datenbasierten Kombination förderlich ist oder so klein sind, dass die Flächen komplett mit einer Aufnahme erfasst werden können, was eine Zuordnung über die Eckpunkte ermöglicht. Etwa ein Drittel der Flächen dagegen enthält nur verdeckte Ankerplatten und wenige sichtbare Strukturen. Da gleiche Strukturen in der Punktwolke und im Wärmebild zudem oft unterschiedlich aussehen, würde eine Wärmebildkamera mit integriertem RGB-Sensor (wie in Abschnitt 2.2.1) die Zuordnung deutlich erleichtern. Ob sich die Anschaffung eines Multisensorsystems lohnt, wäre anhand von Genauigkeitsuntersuchungen zu evaluieren und wirtschaftlich abzuwägen. Ansonsten wäre für unstrukturierte Flächen auch die Anbringung von thermographisch und optisch sichtbaren Markierungen als Passpunkte denkbar. In Schritt 2 der BIM-Integration müssen die einzelnen Ankerplatten aus den transformierten Wärmebildern extrahiert werden. Hier zeigt der Clustering-

Algorithmus aus Abschnitt 3.3 erste vielversprechende Ergebnisse. Um die exakten Ränder zu erkennen, muss zusätzlich eine Kantendetektion erfolgen. Auch ist eine Unterscheidung zwischen Öffnungen und Ankerplatten vorzunehmen, da sich diese im Wärmebild ähnlich dunkel darstellen (siehe Abbildung 2 rechts). In Schritt 3 soll schließlich ein entsprechendes BIM-Objekt an richtiger Position im Gebäudemodell platziert werden. Hier können analog zu [18] mit der visuellen Programmiersprache Dynamo in der Software Autodesk Revit entsprechende Bauteile erzeugt und anhand der Raumkoordinaten der detektierten Ankerplatten ins Gebäudemodell eingefügt werden.

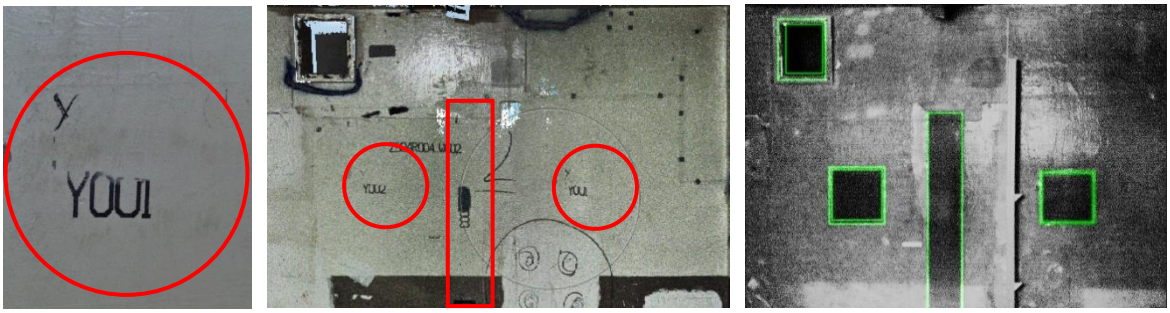


Abbildung 2: beschichtete Ankerplatten in RGB-Großaufnahme, Punktwolke und Wärmebild

## 5 Fazit

Die meisten Beiträge in der wissenschaftlichen Literatur beschäftigen sich nur mit der Kombination von Punktwolken und Wärmebildern zur Erzeugung von thermal texturierten Punktwolken. Dafür existieren verschiedene Verfahren, deren Auswahl je nach Anwendung abzuwägen ist. Für den beschriebene Fall im kerntechnischen Rückbau wäre entweder ein kombiniertes Messsystem oder eine Wärmebildkamera mit integriertem RGB-Sensor zielführend. Eine BIM-Integration von Thermaldaten findet sich in der Literatur laut [2] nur in sehr wenigen Fällen. Hier besteht noch großer Forschungsbedarf, vor allem hinsichtlich einer automatisierten Extraktion von relevanten Strukturen oder Informationen aus den Thermaldaten und deren Darstellung im BIM-Modell. Zur Erkennung der Ankerplatten in den Thermaldaten stellt sich eine Kombination aus Clustering und Kantendetektion als vielversprechend heraus. Für die BIM-Integration der detektierten Platten wird eine Erzeugung und Platzierung entsprechender Bauteile mit visueller Programmierung in Dynamo vorgeschlagen.

## Danksagungen

Das Forschungsprojekt “ViSDeMe – Visualisierung von Störstellen für Dekontaminationsarbeiten und Entscheidungsmessungen mit Hilfe von BIM” wird vom Bundesministerium für Bildung und Forschung im Rahmen des Förderprogramms FORKA (FKZ: 15S9435A) gefördert. Die gezeigten Bilder wurden mit Genehmigung der RWE Nuclear GmbH im Kernkraftwerk Mülheim-Kärlich erfasst.

## Literaturverzeichnis

[1] J. Zhu et al.: “Generation of thermal point clouds from uncalibrated thermal infrared image sequences and mobile laser scans”, IEEE Trans. on Instr. and Measurement, Band 72, 2023.

[2] A. Ramón et al.: “Thermal point clouds of buildings: A review”, Energy and Buildings, Band 274, Elsevier, Amsterdam, 2022.

[3] L. Hoegner et al.: “Fusion of 3D point clouds with TIR images for indoor scene reconstruction”, ISPRS-Archives, Band XLII-1, 2018.

[4] S. Lagüela et al.: “Energy efficiency studies through 3D laser scanning and thermographic technologies”, Energy and Buildings, Band 43, Ausgabe 6, Elsevier, Amsterdam, 2011.

[5] F. Collins et al.: “360-Degree Tri-Modal Scanning: Engineering a Modular Multi-Sensor Platform for Semantic Enrichment of BIM Models”, ISPRS-Archives, Band X-1-2024, 2024.

[6] A. Schischmanow et al.: “Seamless Navigation, 3D Reconstruction, Thermographic and Semantic Mapping for Building Inspection”, Sensors 2022, 22, 4745, 2022.

[7] A. Chromy, O. Klima: “A 3D Scan Model and Thermal Image Data Fusion Algorithms for 3D Thermography in Medicine”, Journal of Healthcare Engineering, Band 2017, 2017.

[8] C. Maierhofer et al.: „Kombination der aktiven Thermografie mit laserbasierten Verfahren zur Erfassung von 3D-Geometrien in der Denkmalpflege “, Fachtagung Bauwerksdiagnose, 2010.

[9] H. Macher, T. Landes: “Combining TIR images and point clouds for urban scenes modelling”, ISPRS-Archives, Band XLIII-B2-2022, 2022.

[10] E. Coiras et al.: “Segment-based registration technique for visual-infrared images”, Optical Engineering Band 39, S. 282–289, 2000.

[11] S. Fiedler et al.: „DT360: Digital Thermography 360° – Projekt »ThermoHead« “, zfv 2/2022, 147. Jahrgang, DVW-Schriftenreihe, Wißner-Verlag, Augsburg, 2022.

[12] M. Angelosanti et al.: “Combination of Building Information Modeling and Infrared Point Cloud for Nondestructive Evaluation”, IEEE Intern. Workshop on Metrology for Living Env., 2022.

[13] V. Pérez-Andreu et al.: “Thermal Characterization of Buildings with as-is Thermal-Building Information Modelling”, Buildings 2023, 13, 972, 2023.

[14] C. Wang and Y. K. Cho: “Automated gbXML-Based Building Model Creation for Thermal Building Simulation” in Proc. - 2014 Int. Conf. 3D Vis. Work. 3DV 2014, pp. 111–117, 2015.

[15] Y. Ham et al.: “Mapping actual thermal properties to building elements in gbXML-based BIM for reliable building energy performance modeling,” in Autom. Constr., Band 49, S. 214–224, 2015.

[16] A. Adán et al.: “Temporal-Clustering Based Technique for Identifying Thermal Regions in Buildings” in Lect. Notes in Computer Science, Band 12002, S. 290–301, 2020.

[17] P. Kim et al.: “Building element recognition with thermal-mapped point clouds” in ISARC 2017 - Proceedings of the 34th Intern. Symp. on Autom. and Robotics in Constr., S. 872–878, 2017.

[18] M. Müßle: “Scan2BIM: Automatisierte Detektion von Störobjekten in Wänden in Punktwolken und Visualisierung mit Hilfe von BIM” in Tagungsband 34. Forum Bauinformatik, Bochum, 2023.

# Automatic Detection of Shaft Locations in Site Plans

Timo Santehanser[1] and Phillip Schönfelder[2]
[1]Department of Computer Science, Ruhr University Bochum,
Universitätsstraße 150, 44801 Bochum, Germany
[2]Department of Civil and Environmental Engineering, Ruhr University Bochum,
Universitätsstraße 150, 44801 Bochum, Germany
E-mail(s): timo.santehanser@rub.de, phillip.schoenfelder@rub.de

**Abstract:** Site plans play a crucial role in construction projects, providing detailed layouts of structures and infrastructure components. Extracting specific information, such as sewage system details including shafts and pipeline routes, from these plans is essential for accurate cost estimation. However, it remains a labor-intensive task, especially for pixel-based drawings lacking machine-interpretable vector geometries and machine-readable text elements. In this study, we conceptualize an automated method to streamline this process, leveraging object detection and optical character recognition (OCR) techniques. The proposed approach involves three main steps: (1) locating the legend region in which the shaft symbol is specified using a specialized OCR method, (2) identifying the relevant shaft symbol from the plan's legend, and (3) detecting shaft locations within site plans using state-of-the-art object detection algorithms. Developing this method aims to significantly increase efficiency in construction cost estimation by automating the tedious task of extracting and analyzing site plan data. The preliminary results included in this study demonstrate candidate techniques for symbol processing in site plans.
*Keywords:* site plan, automation, computer vision, deep learning, drawing analysis

Erschienen in Tagungsband 35. Forum Bauinformatik 2024, Hamburg, Deutschland, DOI: 10.15480/882.13530
© 2024 Das Copyright für diesen Beitrag liegt bei den Autoren. Verwendung erlaubt unter Creative Commons Lizenz Namensnennung 4.0 International.

## 1 Introduction

Site plans constitute a central component of building applications in Germany, in accordance with the building code regulations [1]. They consist of a written and a graphical section, with this work focusing on the latter. The graphical section provides a scaled top-down view of the planned object, typically at 1:500 in densely built areas and 1:1000 in sparsely built areas [2]. In particular, site plans depict pipelines, including utility lines (water, gas, electrical), as well as phone and internet cables. The visualization of pipelines adheres to DIN 2425 [2], which defines symbols and line types to denote different pipeline types, directions, and functions. Site plans also depict shafts, which are structural elements typically embedded in the ground, serving various functions such as the intake and/or discharge of water, as well as providing access to underground pipelines. The visualization

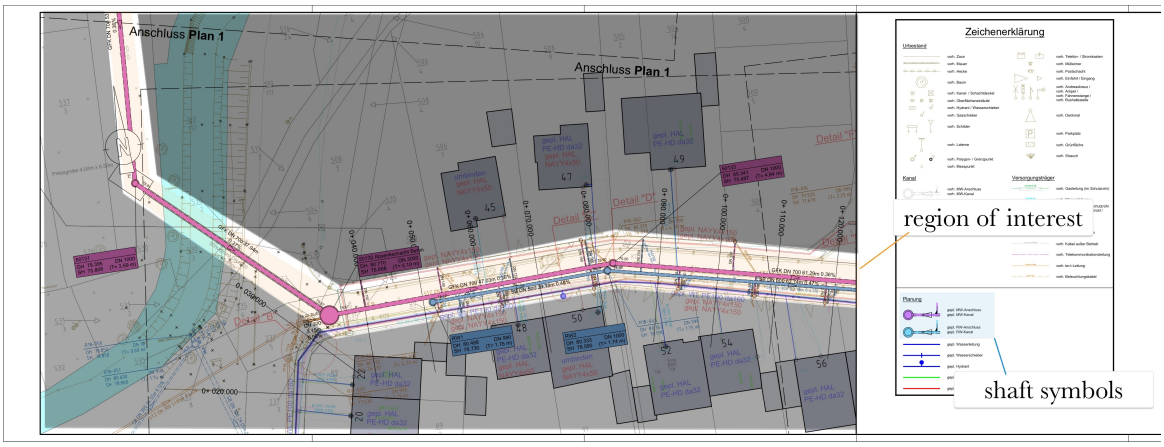


Figure 1: An example site plan, with highlighted areas for shaft symbols within the legend, as well as the region of interest containing planned shafts and pipelines

of shafts typically includes additional details like depth, dimensions, and connections to other shafts within the plan. An example site plan is shown in Figure 1.

Extracting information about sewage systems, including the routes of pipelines and locations of shafts, is beneficial for multiple reasons. First, this information is essential for accurate quantity estimation, and, thus, for the cost calculation during a project's planning phase. Second, in the construction phase, this information can be useful for creating 3D models of the construction site, which can help coordinate construction machinery to avoid conflicts with existing components through smart visualization systems. Third, such 3D models can be used in the later stages of a building's life-cycle as well, for instance, for scheduling maintenance tasks or planning adjacent buildings.

However, actually extracting the information from the plans remains a labor-intensive task, especially for pixel-based drawings that lack machine-interpretable vector geometries and machine-readable text elements. Currently, human experts manually retrace pipeline routes and locate shafts in the original plans to reconstruct the geometry. Although specialized software can aid this process, it is still time-consuming and highlights the need for an automated solution.

Therefore, in this study, we aim to conceptualize an automated system for extracting and interpreting information from site plans. The three main steps of the proposed system notably leverage recent advancements in the symbol recognition research for spatial diagrams, e.g., regarding specialized Optical Character Recognition (OCR) and legend processing [3], [4] as well as shafts and symbol detection [5], [6]. The system is meant to automatically process a scanned site plan, thereby streamlining the digitization process and improving the efficiency and accuracy of construction planning and management.

The remainder of this paper is organized as follows: Section 2 revisits previously proposed methods for diagram processing, addressing their strengths and limitations. Section 3 presents details on the proposed system. Section 4 reflects on the implications and shortcomings of this study. Finally, Section 5 concludes the paper.

# 2 Related Work

The current method for extracting pipeline route information from site plans heavily relies on human interaction with the document. Specifically, individual shafts are identified manually, and the pipeline routes are reconstructed by connecting these shafts. Additionally, details such as the depth of the shafts must be recognized in a separate section of the site plan and manually evaluated. This approach is not only time-consuming but also prone to errors [7]. Consequently, the capture and analysis of data from site plans require a high level of manual effort and expertise.

Previous works on automating similar symbol recognition tasks have shown that existing methods often require a predefined set of symbols, particularly when using neural network-based computer vision approaches [6], [8], [9]. This requirement stems from the learning phase of neural networks, which necessitates an annotated training dataset and, thus, a predefined list of symbols to be detected. This dependency limits the applicability of such methods to site plans, where symbol representations can vary due to factors such as the creator, the standards followed, or other contextual differences. This limitation highlights the need for more flexible and adaptive approaches. Few-Shot Learning (FSL) offers a potential solution to the problem of large variety in real site plan collections. FSL refers to a model's ability to learn new tasks or classes from only a few examples. The goal is for the model to generalize quickly from these few examples. [10]

One common method in FSL is the use of prototypical networks, which calculate a prototype in the feature space for each class and classify new examples based on their similarity to these prototypes. [11] Another popular approach is Model-Agnostic Meta-Learning (MAML), which aims to initialize a model so that it can be optimized for new tasks with minimal adjustment steps. [12] One-Shot Learning is a specialization of FSL where the model requires only a single example per class to recognize that class successfully. This approach is particularly challenging, as it demands extreme efficiency in transfer learning and generalization. [13] Techniques used in One-Shot Learning are often similar to those in Few-Shot Learning but impose even stricter constraints on the number of available examples. A recently developed method by Gupta et al. [14] describes how symbols in Piping and Instrumentation Diagrams (P&IDs) can be recognized using FSL. In this method, first, all symbols in the diagrams are detected, and, second, the symbols are classified using a Siamese network. This approach demonstrates the effectiveness of FSL in scenarios where annotated training data is limited and symbols may vary, underscoring its potential for application to site plans where symbol variability and limited training data are common challenges as well.

# 3 Method

## 3.1 Overall Concept

Since site plan symbols might not be known a priori, the automatic extraction of shaft symbols and pipelines on site plans must be divided into two stages: (1) extracting shaft symbol classes from the legend and (2) locating their respective positions on the site plan itself. Addressing both stages, we propose a concept for an automated site plan analysis method, which is illustrated in Figure 2. First, text detection is performed on the site plans using a pretrained YOLOv8 [15] model. The detected text

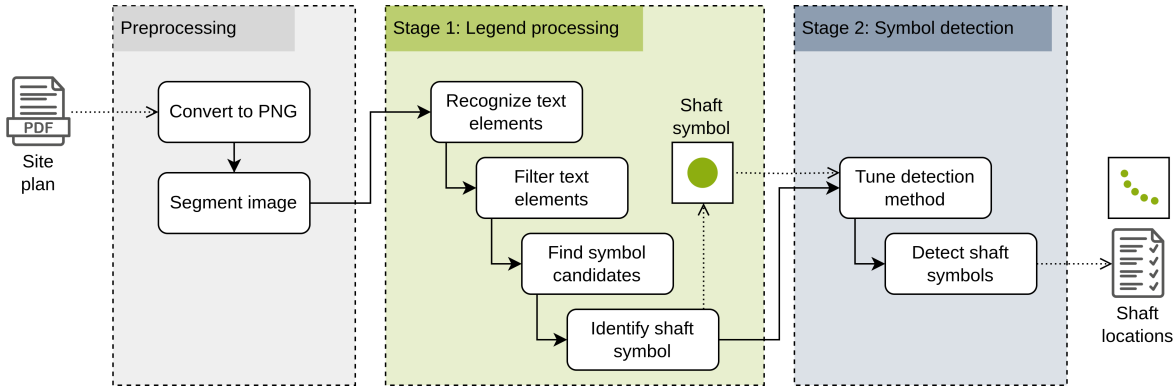


Figure 2: Proposed shaft localization concept.

Figure 3: Examples of shaft representations in site plans.

objects are then converted to strings using Tesseract OCR [16], and filtered for keywords to locate the legend and identify the shaft symbols within it. Using morphological operations, nearby candidate symbols are found to select one of them as the shaft symbol. Implementation details of this stage are given in Section 3.3. Second, these symbols are then used to find the shaft symbols in the site plan, determine the pipelines, and calculate the positions of the shafts. For this stage, preliminary results suggest which methods are suitable for the final development, as detailed in Section 3.4. Additionally, preprocessing steps are outlined in Section 3.2.

## 3.2 Preprocessing

Site plans possess certain characteristics that necessitate preprocessing. First, in the data at hand, they are available as PDF files, requiring conversion to a format suitable for image processing, e.g., by Convolutional Neural Networks (CNN). Therefore, the files are converted to PNG. Second, since the YOLOv8 architecture was developed for images of size up to 1280 pixels in side length, this site plan images are segmented to into several smaller images. To ensure that segmentation boundaries do not render parts of the site plan unreadable, which could lead to missed symbols, segments are created with a 40% overlap with their neighboring segments.

## 3.3 Symbol detection in legends

Due to the various symbols for shafts on plans, with some examples depicted in Figure 3, training a learning-based model for automated symbol detection presents difficulties. The national DIN standard [2] does not specify how shafts must be represented, so the symbols' appearances are largely up to the plan's draftsman or company standard. However, since the symbols for the documented shafts are always indicated in a legend on the plan, the proposed concept involves recognizing the symbols for shafts in the legend and then identifying these in the plan's graphical section, indicated as region of interest in 3.

Symbol class recognition is achieved through the following steps:

1. *Text detection.* To perform text detection on the site plan, a YOLOv8 model pretrained by Schönfelder et al. [3] is employed. Originally trained on floorplan drawings, it is expected to generalize to site plans, as the characteristic text element features are similar.

2. *Text recognition.* To convert the text regions to strings, Tesseract OCR is applied to the identified regions. It offers fast processing and shows high performance on good quality site plan images. To safely include the entire text element, the detected regions are extended by a two pixel margin.

3. *String matching.* The recognized strings are searched for key terms like `Shaft` and `Connector`, to identify the relevant regions in the legend.

4. *Horizontal cropping.* The image is cropped to the region where the corresponding symbol is assumed to be located, which is the smallest rectangle containing the text region, and spanning the entire width of the image segment. This decreases the likelyhood of false positive matches.

5. *Morphological processing.* With the exception of the text region itself, the crop undergoes several processing steps, including binary thresholding and contour approximation to identify symbol region candidates.

6. *Symbol identification*. The symbol is finally identified by selecting the candidate region that is closest to the text region, while also being larger than 10x10 pixels.

The described steps, in particular the choice of key terms and the symbol identification step parameters, are validated with a set of 50 (German) example site plans.

## 3.4 Symbol detection in the graphical section

This section discusses some approaches for symbol recognition outside of the legend on the site plan that are evaluated in the course of this study.

### 3.4.1 Template matching

Template matching relies on the symbol template as provided by the legend, and includes a brute-force search of this template in the entire image. While this offers a potential solution to the symbol detection steps, it is found to be impractical for two main reasons. First, symbols might be partially occluded by other lines, rendering the symbol undetectable for symbol matching, which requires a near perfect match with the template. Second, the symbols in the plan might have been subject to affine transformations, and appear rotated or scaled. Even in the case of axisymmetric symbols, this necessitates an unreasonably large number of additional templates to include rotated and scaled templates to the search, which proves computationally extensive while still often inaccurate. Therefore, one should rather focus on techniques invariant to scale and rotation, like homography finding or CNNs.

### 3.4.2 Homography finding

With regards to homography finding, cv2 implements the `findHomography` function, which computes a 3x3 homography matrix describing a perspective transformation between two images. This matrix

allows for the projection of points from one image into another, considering perspective differences, inluding rotation and scaling. The homography matrix $H$ is a 3x3 matrix describing the relationship between the homogeneous coordinates of the template symbol in the legend and the candidate symbol in a plan segment. It is defined as

$$s \begin{bmatrix} x' \\ y' \\ 1 \end{bmatrix} = H \begin{bmatrix} x \\ y \\ 1 \end{bmatrix}, \tag{1}$$

where $(x, y)$ are the template symbol's coordinates, $(x', y')$ are the coordinates of the candidate symbol, and $s$ is a scaling factor. To compute $H$, at least four point correspondences between the two symbols are needed. In our implementation, we use the Scale-Invariant Feature Transform (SIFT) to extract keypoints and descriptors from both the template symbols and the sliding windows within the plan segments. To match the keypoints between the template and candidate symbols, we employ a FLANN-based matcher (Fast Library for Approximate Nearest Neighbors), optimized for fast and efficient high-dimensional feature matching. Lowe's ratio test is applied to filter out weak matches, retaining only those with a significantly better best match, thereby reducing false positives.

Once the matches are identified, the RANSAC algorithm within the `findHomography` function is used to compute the homography matrix $H$. RANSAC iteratively selects random subsets of matches to estimate the homography and evaluates the number of inliers—points that fit well with the estimated transformation. The number of inliers serves as a metric for match strength, with valid matches exceeding a predefined threshold. This process is applied across sliding windows in the plan, with the best homography matrix for each window selected based on the highest number of inliers, ensuring robustness even under rotation, scaling, or minor distortions.

By combining SIFT for feature extraction, FLANN for efficient matching, and RANSAC for robust homography estimation, our method achieves accurate and reliable symbol detection across complex plan images, with a precision of 82% and a recall of 78%.

## 4 Discussion

The extraction of shaft symbols from the legend is an effective solution for the non-uniform symbols in the plans, which make training a dedicated model difficult. While this approach is effective for the data sample at hand, it might however require algorithmic adjustment for plans that exhibit unseen formats. However, the fundamental process is expected to remain functional for most legend formats. In our evaluation of the FSL approach as demonstrated by the recent study of Gupta et al. [14], we found that while the method shows promise in the context of P&IDs, it does not generalize to the domain of site plans. One of the primary challenges is that, unlike P&IDs, where symbols typically exist in isolation without overlapping with other elements like pipelines, site plans present a more complex environment. In site plans, symbols often overlap with various other content, including pipelines, structures, and roads, making reliable symbol detection significantly more challenging.

Regarding the learning-free attempts towards symbol detection in the graphical section of the plan, implementations of template finding show poor results in the sample dataset. Especially the large image sizes of the site plans and the potential rotation and scaling of the symbols increases the runtime by multiple orders of magnitude. The investigated homography matching approach successfully identified the majority of symbols extracted from the legend within the site plans. However, challenges remain, particularly with low-contrast symbols, such as yellow symbols on a white background. These cases may require further optimization or the application of pre-processing filters to enhance symbol visibility and improve detection accuracy. Another significant challenge arises with the recognition of less complex, symmetric symbols, such as simple geometric shapes or symbols with uniform color distributions. The homography-based approach, while effective for more detailed and feature-rich symbols, struggles to detect these simpler symbols due to the lack of distinctive keypoints.To address this limitation, a hybrid approach could be a viable solution. Such an approach would combine the strengths of different methods to ensure robust symbol detection across a variety of symbol types. For instance, the process could begin with SIFT-based keypoint detection for complex symbols, followed by template matching for simpler, geometric symbols that lack sufficient keypoints.

## 5 Conclusion

As a first step towards the automatic extraction of shaft locations and pipeline routes in site plans, this study achieves (1) a concept for and end-to-end extraction method for shaft symbols, (2) a proof-of-concept for a legend processing method that enables extraction of plan-specific symbol class templates, and (3) considerations about candidate techniques for symbol detection on site plans with few available training examples. In terms of learning-free symbol detection, a homography-based approach shows promising in accurately detecting symbols within the provided site plans, even though the symbols are subjected to variations in scale and orientation. However, it is important to note that parameter optimization remains a critical step in this pipeline, requiring further fine-tuning to maximize detection accuracy. Additionally, the performance of this approach on symbols with suboptimal contrast ratios remains an area that needs further development. Symbols that blend with the background, such as those with low contrast, present challenges that necessitate the application of advanced pre-processing techniques or adjusted detection parameters to improve reliability. Overall, while the homography-based method has shown substantial potential, ongoing refinement is necessary to fully address the nuances of symbol detection in diverse site plan contexts.

## Acknowledgments

The authors would like to express their gratitude to isl-kocher GmbH and IB Becker for providing the sample dataset used in this study.

## References

[1] Bauministerkonferenz, *Musterbauordnung (MBO), zuletzt geändert durch Beschluss vom 23.09.2022*. [Online]. Available: https://www.dibt.de/fileadmin/dibt-website/Dokumente/Rechtsgrundlagen/MBO.PDF (visited on 07/07/2024).

[2] *DIN 2425-4:2022-11, Planwerke für die Versorgungswirtschaft, die Wasserwirtschaft und für Fernleitungen_- Teil_4: Entwässerungssysteme außerhalb von Gebäuden*. DOI: 10.31030/3384593.

[3] P. Schönfelder, F. Stebel, N. Andreou, and M. König, "Deep learning-based text detection and recognition on architectural floor plans", *Automation in Construction*, vol. 157, p. 105 156, 2024. DOI: 10.1016/j.autcon.2023.105156.

[4] T. Hassan, J. Verges-Llahi, and A. Gonzalez, "High-Performance Preprocessing of Architectural Drawings for Legend Metadata Extraction via OCR", in *Proceedings of the 2017 ACM Symposium on Document Engineering*, 2017, pp. 197–200. DOI: 10.1145/3103010.3121042.

[5] S. Sarkar, P. Pandey, and S. Kar, "Automatic Detection and Classification of Symbols in Engineering Drawings", *arXiv*, 2022. DOI: 10.48550/arXiv.2204.13277.

[6] A. Rezvanifar, M. Cote, and A. B. Albu, "Symbol Spotting on Digital Architectural Floor Plans Using a Deep Learning-based Framework", in *Proceedings of the 2020 IEEE/CVF Conference on Computer Vision and Pattern Recognition Workshops (CVPRW)*, 2020, pp. 2419–2428. DOI: 10.1109/CVPRW50498.2020.00292.

[7] S. Paliwal, A. Jain, M. Sharma, and L. Vig, "Digitize-PID: Automatic Digitization of Piping and Instrumentation Diagrams", in *Proceedings of the 2021 Pacific-Asia Conference on Knowledge Discovery and Data Mining*, 2021, pp. 168–180. DOI: 10.1007/978-3-030-75015-2_17.

[8] L. Jamieson, C. Francisco Moreno-García, and E. Elyan, "A review of deep learning methods for digitisation of complex documents and engineering diagrams", *Artificial Intelligence Review*, vol. 57, no. 6, p. 136, 2024. DOI: 10.1007/s10462-024-10779-2.

[9] E. Elyan, L. Jamieson, and A. Ali-Gombe, "Deep learning for symbols detection and classification in engineering drawings", *Neural Networks*, vol. 129, pp. 91–102, 2020. DOI: 10.1016/j.neunet.2020.05.025.

[10] X. Li, Z. Sun, J.-H. Xue, and Z. Ma, "A concise review of recent few-shot meta-learning methods", *Neurocomputing*, vol. 456, pp. 463–468, 2021. DOI: 10.1016/j.neucom.2020.05.114.

[11] J. Snell, K. Swersky, and R. S. Zemel, "Prototypical Networks for Few-shot Learning", in *Proceedings of the 31st International Conference on Neural Information Processing Systems*, 2017, pp. 4080–4090. [Online]. Available: https://dl.acm.org/doi/abs/10.5555/3294996.3295163#.

[12] C. Finn, P. Abbeel, and S. Levine, "Model-Agnostic Meta-Learning for Fast Adaptation of Deep Networks", in *Proceedings of the 34th International Conference on Machine Learning - Volume 70*, 2017, pp. 1126–1135. [Online]. Available: https://dl.acm.org/doi/10.5555/3305381.3305498.

[13] Y. Wang, Q. Yao, J. T. Kwok, and L. M. Ni, "Generalizing from a few examples: A survey on few-shot learning", *ACM Computing Surveys*, vol. 53, no. 3, p. 63, 2020.

[14] M. Gupta, C. Wei, and T. Czerniawski, "Semi-supervised symbol detection for piping and instrumentation drawings", *Automation in Construction*, vol. 159, p. 105 260, 2024. DOI: 10.1016/j.autcon.2023.105260.

[15] G. Jocher, A. Chaurasia, and J. Qiu, *YOLOv8*, 2024. [Online]. Available: https://github.com/ultralytics/ultralytics (visited on 07/07/2024).

[16] R. Smith, "An Overview of the Tesseract OCR Engine", in *Proceedings of the 9th International Conference on Document Analysis and Recognition (ICDAR)*, 2007, pp. 629–633. DOI: 10.1109/ICDAR.2007.4376991.

# Automated Inspection of Obstructed Fire Extinguishers Using Amodal Instance Segmentation

Jan H. Heinbach[1] and Angelina Aziz[1]
[1]Chair of Computing in Engineering, Ruhr Universität Bochum, Universitätsstrasse 150, 44801 Bochum, Germany
E-mail(s): Jan.Heinbach@ruhr-uni-bochum.de, Angelina.Aziz@ruhr-uni-bochum.de

**Abstract:** Fire safety inspections are essential to ensure the safety of occupants during a fire outbreak. These inspections involve checking various items, such as fire safety equipment (FSE), to ensure they are unobstructed and fully functional. Recent research has highlighted the potential of machine learning and computer vision in automating and enhancing fire safety inspection processes using image analysis. However, identifying obstacles or potential obstructions in front of fire extinguishers effectively remains a challenge. The research focuses on reviewing documented images to identify instances where extinguishers are obstructed, either partially or fully. This study proposes a novel approach to address this challenge by combining modal and amodal instance segmentation models to evaluate the level of obstruction. One conducts classical (modal) instance segmentation of visible fire extinguisher parts, while the other performs amodal segmentation. Additionally, the annotation and dataset creation for amodal segmentation tasks is addressed. The study generates obstacles on images from both open-source and self-created datasets containing (unblocked) fire extinguishers. This approach requires only one modal annotation iteration to generate modal and amodal annotation data. Results demonstrate the effectiveness of the proposed approach in detecting covered or partially blocked extinguishers. Future research aims to refine amodal mask results and extend the approach to other FSE components, further enhancing fire safety inspection processes.

*Keywords:* Computer Vision, Instance Segmentation, Amodal Segmentation, Fire Safety Equipment

Erschienen in Tagungsband 35. Forum Bauinformatik 2024, Hamburg, Deutschland, DOI: 10.15480/882.13512
© 2024 Das Copyright für diesen Beitrag liegt bei den Autoren. Verwendung erlaubt unter Creative Commons Lizenz Namensnennung 4.0 International.

## 1 Introduction

Preventive fire protection is an essential component of construction and building management. Its main goal is to prevent fires and, in the event of a fire, to minimize the spread of fire and smoke to protect people and property. This begins in the planning phase, where the selection of appropriate materials and designs reduces the risk of fire. In building management and maintenance, preventive fire protection includes regular maintenance and inspections of fire safety equipment (FSE) — such as fire extinguishers — as well as training for residents and staff. Due to its importance, preventive

fire protection and especially the fire safety inspections, which include inspection and maintenance of FSE, are mandatory in every building [1].

Fire safety inspections are essential to ensure the functionality and the visibility of FSE in case of a fire and therefore to ensure the security of occupants in the building. However, especially the inspection is a time consuming task. During a typical on-site fire safety inspection, a fire safety manager walks through the building while processing a checklist (e.g. [2]). Most of the inspection tasks are done by physical or visual review manually conducted by the fire safety manager. The inspections results are written down by hand or manually maintained with software support. In addition to the time consumption, this approach is prone to errors.

A crucial aspect of the inspection is to check whether FSE is blocked. As the fire safety manager often documents his inspection with images of the inspected FSE, the use of Artificial Intelligence (AI) to perform inspections based on these images is the most obvious approach. Computer vision methods can be used to inspect FSE on these images and detect blocked ones. Previous work from [3], can inspect simple FSE using visual object detection to detect obstacles in front of FSE. However, this approach has a limited amount of obstacles that could be detected, as each obstacle require training data to be detected as an individual class. As it is unrealistic to consider every possible obstacle as a single class, further work is required to enable the inspection of more complex objects.

In this paper, we want to improve the inspection and detection rate of fire extinguishers and be able to estimate blocked FSE behind any obstacle using trained (amodal) segmentation models, even if only a small part of the asset is visible.

# 2 Related Background

## 2.1 Digitalization of FSE inspections

Due to the huge potential of automation, there is a lot of research going on to support during FSE inspections [4]–[8], as well as to increase the level of automation in the context of preventive fire protection in general [9], [10]. Due to the fact that the use of visual object recognition enables immediate deployment in existing and new buildings, computer vision methods are a widely used approach. Oh et al. [8] create an approach to use object recognition on augmented reality glasses to support the fire prevention officer during the fire safety inspection or even allow general public to contribute to the fire safety inspection. Similar to that approach, Bayer and Aziz [4] as well as Corneli et al. [6] enable and evaluate real-time detection of different FSE inside buildings, while Kumar et al. [7] detect FSE at construction sites. More enhanced approaches, as from Alayed et al. [5] or previous work from us [3], use the detection of FSE to perform actual inspections. Alayed et al. [5] are inspecting fire extinguishers using object detection to classify if a certain inspection criteria is met. In [3], object detection is used to detect FSE and obstacles to identify obstacles that block FSE.

## 2.2 Amodal Object Detection

Recent work in computer vision aims to develop a new computer vision technique besides classification, detection with bounding boxes and classical instance segmentation: Amodal segmentation [11], [12].

Classification, as the simplest task, aims to classify a whole image to predefined classes. Object detection with bounding boxes, aims to identify and locate objects in images using bounding boxes. Among others, R-CNN [13], the You Only Look Once (YOLO) [14] architecture series with YOLOv8 [15] as a current state of the art version, are capable of both tasks. Classical instance segmentation, hereafter referred to as modal segmentation, aims to not only locate the object but identifies each pixel belonging to the object. Exemplarily, Mask R-CNN [16] and YOLOv8 [15] are modal segmentation approaches. The difference from modal to amodal segmentation is visualized in Figure 1. While modal segmentation aims to identify the visible part of an instance (visible on the right), an amodal segmentation aims to identify both the visible and the occluded parts of an instance (visible on the left). [11], [17]

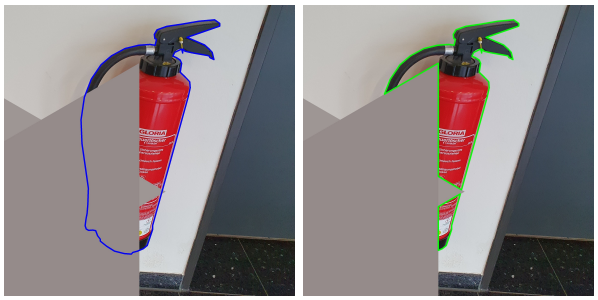

Figure 1: Amodal segmentation annotation (left, blue) and (well known) modal segmentation annotation (right, green). In the modal segmentation the mask is split up in two parts.

While this might be an solvable task to a human [18], the computational amodal segmentation is still subject of current research [12], [19], [20]. A lot of different approaches are studied in this context. The method from Li and Malik [11] uses R-CNN [13] modal segmentation results as a basis to perform a bounding box expansion. *SharpMask* [21] is an Convolutional Network [22], specially for amodal segmentation. In contrast to that, some approaches just use state of the art modal segmentation solutions with new training data [12].

# 3 Methodology

Since amodal segmentation is still subject of current research and — to the best of our knowledge — there is no state-of-the-art amodal segmentation solution available, we use a straight forward approach and create amodal training data to train YOLOv8 [15] modal segmentation models as amodal ones.

## 3.1 Amodal Annotation

The creation of amodal segmentation data is challenging, as the generation of annotations is complicated. In contrast to modal segmentation, where the modal segmentation mask can be definitely determined by humans based on images, parts of the amodal mask are invisible (see Figure 1). Therefore, these human annotations are inaccurate and might not be the ground truth [11].

For this reason, we collect images with completely visible fire extinguishers, create modal annotations and generate artificial obstacles. Subsequently, the previously modal annotation can be used as amodal annotation, as the fire extinguisher was completely visible before. The new modal annotation

can be calculated by calculating the difference between the fire extinguisher and the artificially generated obstacles. No manual amodal annotation is required and the amodal annotation definitely represents the ground truth.

Figure 2: Generated artificial obstacles. *Type 1* (monochrome simple shapes) on the left and *Type 2* (rectangles, filled with patterns) on the right.

We generated two different types of obstacles, exemplarily seen in Figure 2. The first type are different simple geometric shapes in the average pixel colour value of the image (*Type 1*). The second obstacle type are rectangles, filled with different patterns (*Type 2*).

### 3.2 Data

To start the amodal annotation mentioned before, data from various sources is collected. More precisely, out of 888 different images, 388 are real world images, mostly self-made in a mixture of buildings in Germany (primarily university related buildings and fire stations) and from the FireNet dataset from University College in London [23]. The remaining 500 images are synthetically created.

Based on these original images (without obstacles), three different amodal datasets are generated. 876 images with *Type 1* obstacles and 862 images with *Type 2* obstacles are generated. The resulting datasets are listed in Table 1. According to Subsection 3.1, each dataset contains two labels, one with modal annotation and one with amodal annotations.

Table 1: Overview about created amodal datasets.

| Dataset name | Contained obstacles | Total Image amount |
|---|---|---|
| *Shape Obstacles* | *Type1*, original | 1764 |
| *Pattern Obstacles* | *Type2*, original | 1750 |
| *Shape and Pattern Obstacles* | *Type1*, *Type2*, original | 2626 |

### 3.3 YOLOv8 Training

Each of the created datasets from Table 1 is used to train two different YOLOv8 [15] segmentation models. For this purpose, the datasets are separated in 70% training (*train*), 20% validation (*val*) and

10% test (*test*) data. In a first iteration, the modal (classic) annotations are used to train YOLOv8 [15] models for modal instance segmentation. The second training iteration uses the amodal annotations in the same YOLOv8 training setup, aiming to create an YOLOv8 amodal segmentation model. All trainings are performed on 6 NVIDIA A100-SXM4-40GB GPUs with the same setup. The used YOLOv8 parameters [1] are IMGSZ set to 640, BATCH set to 72 and PATIENCE set to 50. All other parameters are default values. The PATIENCE parameter allows to terminate training if no progress is made in 50 epochs. Table 2 list the effective training epochs of the trained YOLOv8 models and the short names of the models.

Table 2: Effective training epochs of the different YOLOv8 models.

| Model | Training Epochs |
|---|---|
| Shape Amodal (SA) | 352 |
| Shape Modal (SM) | 414 |
| Pattern Amodal (PA) | 416 |
| Pattern Modal (PM) | 282 |
| Shape Pattern Amodal (SPA) | 345 |
| Shape Pattern Modal (SPM) | 492 |

## 4 Evaluation

Subsequently, the trained models are evaluated. As evaluation metric the mean Intersection over Union (mIoU), which is the average IoU over all images, is used. If the mask of a fire extinguisher was divided by an obstacle, the two resulting modal segmentations are considered together as one when calculating the IoU. In addition to the evaluation, the *occlusion rate* is calculated. The *occlusion rate* indicates how much of an extinguisher (the amodal segmentation) is hidden (missing in the modal segmentation). We suggest a threshold of 0.05 for considering the fire extinguisher as blocked, but further work is required here. The detailed evaluation results and exemplarily detection results can be found in Table 3. The modal models (SM, PM, SPM) show good results. Reviewing the amodal models (SA, PA, SPA), the PA and SPA model perform better than the SA model (only *Type 1* obstacles), clearly visible when reviewing Example 2. In total, it definitely points out, that the amodal segmentation of fire extinguishers performs surprisingly good.

## 5 Conclusion

The paper presents a promising approach to improve the automation of FSE inspections, using amodal segmentation. The straight forward approach to train YOLOv8 models — which originally perform modal segmentations — with amodal training data works amazingly well. The amodal annotation strategy ensures that annotations present the ground truth. Future work aims to integrate the models in an inspection tool (as proposed in [3]) to further support the fire safety manager by detecting blocked FSE regardless of the blocking object. It could be extended to multiple different FSE or other inspection tasks, possibly in combination with mobile robots as in [24].

[1] All parameters can be found here: https://docs.ultralytics.com/modes/train

Furthermore, the amodal segmentation approach, as well as the amodal annotation strategy, can be used to detect and predict hidden parts of objects in multiple different areas, not only in building an construction industry, as amodal segmentation is a current research topic.

## References

[1] Bundesministerium für Arbeit und Soziales (BMAS), *Technische Regeln für Arbeitsstätten: Maßnahmen gegen Brände (ASR A2.2)*, German, GMBI, 2018.

[2] Bundesministerium des Innern, für Bau und Heimat (BMI), *Brandschutzleitfaden für Gebäude des Bundes*, Arbeitskreis Brandschutzleitfaden, editor, Jun. 2019.

[3] J.-H. Heinbach and A. Aziz, "Visual partial inspection of fire safety equipment using machine learning", en, in *34th Forum Bauinformatik / 34. Forum Bauinformatik*. Bochum: Ruhr-Universität Bochum, 2023, pp. 324–331. DOI: 10.13154/294-10096. [Online]. Available: https://hss-opus.ub.ruhr-uni-bochum.de/opus4/10096.

[4] H. Bayer and A. Aziz, "Object detection of fire safety equipment in images and videos using yolov5 neural network", en, in *Proceedings of 33. Forum Bauinformatik*, München, 2022.

[5] A. Alayed, R. Alidrisi, E. Feras, S. Aboukozzana, and A. Alomayri, "Real-time inspection of fire safety equipment using computer vision and deep learning", en, *Engineering, Technology & Applied Science Research*, vol. 14, no. 22, pp. 13 290–13 298, Apr. 2024. DOI: 10.48084/etasr.6753.

[6] A. Corneli, B. Naticchia, M. Vaccarini, F. Bosché, and A. Carbonari, "Training of yolo neural network for the detection of fire emergency assets", in *ISARC. Proceedings of the International Symposium on Automation and Robotics in Construction*, vol. 37, IAARC Publications, 2020, pp. 836–843.

[7] S. Kumar, H. Gupta, D. Yadav, I. A. Ansari, and O. P. Verma, "Yolov4 algorithm for the real-time detection of fire and personal protective equipments at construction sites", *Multimedia Tools and Applications*, vol. 81, no. 16, pp. 22 163–22 183, 2022.

[8] D.-S. Oh, J. H. Jeon, J.-K. Kim, K. B. Lee, and S. G. Hong, "Inspection system of firefighting facilities based on yolov4 using augmented reality glass", in *2022 13th International Conference on Information and Communication Technology Convergence (ICTC)*, IEEE, 2022, pp. 1604–1608.

[9] F. M. Talaat and H. ZainEldin, "An improved fire detection approach based on yolo-v8 for smart cities", en, *Neural Computing and Applications*, vol. 35, no. 28, pp. 20 939–20 954, Oct. 2023. DOI: 10.1007/s00521-023-08809-1.

[10] Y.-J. Chen, Y.-S. Lai, and Y.-H. Lin, "Bim-based augmented reality inspection and maintenance of fire safety equipment", *Automation in Construction*, vol. 110, p. 103 041, Feb. 2020. DOI: 10.1016/j.autcon.2019.103041.

[11] K. Li and J. Malik, "Amodal instance segmentation", en, in *Computer Vision – ECCV 2016*, B. Leibe, J. Matas, N. Sebe, and M. Welling, editors, Cham: Springer International Publishing, 2016, pp. 677–693. DOI: 10.1007/978-3-319-46475-6_42.

[12] J. Ao, Q. Ke, and K. A. Ehinger, “Image amodal completion: A survey”, *Computer Vision and Image Understanding*, vol. 229, p. 103 661, Mar. 2023. DOI: 10.1016/j.cviu.2023.103661.

[13] R. Girshick, J. Donahue, T. Darrell, and J. Malik, “Rich feature hierarchies for accurate object detection and semantic segmentation”, in *Proceedings of the IEEE conference on computer vision and pattern recognition*, 2014, pp. 580–587.

[14] J. Redmon, S. Divvala, R. Girshick, and A. Farhadi, “You only look once: Unified, real-time object detection”, 2016, pp. 779–788. [Online]. Available: https://www.cv-foundation.org/openaccess/content_cvpr_2016/html/Redmon_You_Only_Look_CVPR_2016_paper.html.

[15] G. Jocher, A. Chaurasia, and J. Qiu, *Ultralytics yolov8*, version 8.0.0, 2023. [Online]. Available: https://github.com/ultralytics/ultralytics.

[16] K. He, G. Gkioxari, P. Dollar, and R. Girshick, “Mask r-cnn”, 2017, pp. 2961–2969. [Online]. Available: https://openaccess.thecvf.com/content_iccv_2017/html/He_Mask_R-CNN_ICCV_2017_paper.html.

[17] Y. Zhu, Y. Tian, D. Metaxas, and P. Dollar, “Semantic amodal segmentation”, en, in *2017 IEEE Conference on Computer Vision and Pattern Recognition (CVPR)*, Honolulu, HI: IEEE, Jul. 2017, pp. 3001–3009. DOI: 10.1109/CVPR.2017.320. [Online]. Available: http://ieeexplore.ieee.org/document/8099803/.

[18] G. Kanizsa, “Organization in vision: Essays on gestalt perception”, en, *(No Title)*, [Online]. Available: https://cir.nii.ac.jp/crid/1130000796894898688.

[19] P. O. Pinheiro, R. Collobert, and P. Dollar, “Learning to segment object candidates”, no. arXiv:1506.06204, Sep. 2015. DOI: 10.48550/arXiv.1506.06204. [Online]. Available: http://arxiv.org/abs/1506.06204.

[20] K. Xu, L. Zhang, and J. Shi, “Amodal completion via progressive mixed context diffusion”, en, no. arXiv:2312.15540, Dec. 2023. [Online]. Available: http://arxiv.org/abs/2312.15540.

[21] P. O. Pinheiro, T.-Y. Lin, R. Collobert, and P. Dollàr, “Learning to refine object segments”, no. arXiv:1603.08695, Jul. 2016. DOI: 10.48550/arXiv.1603.08695. [Online]. Available: http://arxiv.org/abs/1603.08695.

[22] Y. Lecun, L. Bottou, Y. Bengio, and P. Haffner, “Gradient-based learning applied to document recognition”, en, *Proceedings of the IEEE*, vol. 86, no. 11, pp. 2278–2324, Nov. 1998. DOI: 10.1109/5.726791.

[23] J. Boehm, F. Panella, and V. Melatti, *Firenet*, Jul. 2019. DOI: 10.5522/04/9137798.v1. [Online]. Available: https://rdr.ucl.ac.uk/articles/dataset/FireNet/9137798.

[24] A. Aziz, P. Herbers, H. Bayer, and M. König, “Fully autonomous fire safety equipment inspection missions on a legged robot”, EN, pp. 804–812, Jan. 2024. DOI: 10.1061/9780784485224.097.

Table 3: Evaluation data of the trained YOLOv8 models (full names : Table 2). Left : Amodal Segmentation models, Right : modal segmentation models. The mIoU is the average IoU over *test*, *train*, *val* and full dataset. Example 1 out of *test* dataset, Example 2, 3 : real world images (not part of the dataset). Red : Segmentation masks, Green : amodal ground truth, Blue : modal ground truth. Rotations only for visualization.

| Model | mIoU | Example 1 | Example 2 | Example 3 |
|---|---|---|---|---|
| SA | *train:* 0.86<br>*test:* 0.82<br>*val:* 0.85<br>*total:* 0.85 | | | |
| PA | *train:* 0.88<br>*test:* 0.85<br>*val:* 0.83<br>*total:* 0.86 | | | |
| SPA | *train:* 0.91<br>*test:* 0.88<br>*val:* 0.88<br>*total:* 0.89 | 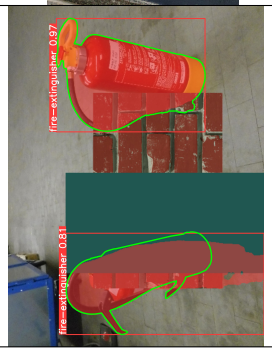 | | |

| Model | mIoU | Example 1 |
|---|---|---|
| SM | *train:* 0.85<br>*test:* 0.81<br>*val:* 0.84<br>*total:* 0.85 | 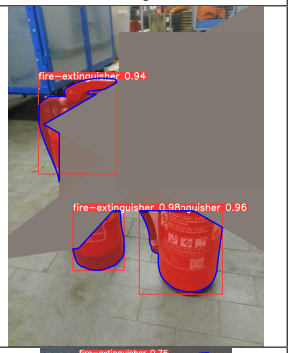 |
| PM | *train:* 0.87<br>*test:* 0.80<br>*val:* 0.80<br>*total:* 0.84 | |
| SPM | *train:* 0.90<br>*test:* 0.88<br>*val:* 0.86<br>*total:* 0.88 | 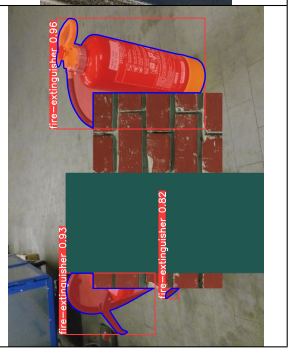 |

# Exploring Explainable AI for Symbol Detection in Construction Drawings

Jan Michalak[1] and Benedikt Faltin[1]
[1]Chair of Computing in Engineering, Ruhr-Universität Bochum, Universitätsstraße 150, 44801 Bochum, Germany
E-mail(s): jan.michalak@rub.de, benedikt.faltin@rub.de

**Abstract:** Having information in a digitally accessible format can significantly improve the efficiency of processes by enabling automation. In the construction industry, however, much building-related information is only available in analog form, mainly paper-based drawings, which hinders the introduction of digital processes. Artificial intelligence offers a practical approach for converting these analog construction drawings into digital information. Neural networks, such as the YOLO object detection model, can efficiently identify and extract crucial information from the drawings on a large scale. However, these models operate as "black boxes," making it challenging to understand the basis of their decisions. To address this problem, this study applies techniques from explainable artificial intelligence to gain insight into the inner workings of a neural network. In particular, YOLOv8 is trained to detect symbols in pixel-based drawings, and the Eigen-CAM visualization method is utilized to shed light on the network's internal decision-making processes. With the acquired knowledge about the inner decisions of the trained network during symbol detection, the training data set is refined to enhance the model's overall performance, leading to an improvement in the detection of $mAP_{50}$ 10 points.

*Keywords:* XAI, Machine Learning, Symbol Detection, YOLO, Eigen-CAM

Erschienen in Tagungsband 35. Forum Bauinformatik 2024, Hamburg, Deutschland, DOI: 10.15480/882.13499
© 2024 Das Copyright für diesen Beitrag liegt bei den Autoren. Verwendung erlaubt unter Creative Commons Lizenz Namensnennung 4.0 International.

## 1 Introduction

Digital transformation is a crucial objective for today's society. Transforming analog processes into digital ones has the potential to make processes more efficient by unlocking automation. This task is particularly crucial for the construction industry. Since many buildings were erected before computers existed, thousands of documents containing critical aspects about the structures are still archived in analog form. However, extracting this information and transforming it into a digital building model can enhance the efficiency of maintenance management [1]. To make the information contained digitally accessible is a massive task.

A solution to this challenge may lie in artificial intelligence (AI). In the last decade, the capabilities of AI have advanced rapidly to a human degree and, in some cases, even surpassed it [2]. AI is already

being successfully deployed in various fields, such as medicine, autonomous driving, engineering, and transportation. As a result, using AI to convert information from analog documents in the construction industry is an area of research attracting much attention. However, many state-of-the-art AI models operate as "black boxes," and how decisions are made remains unknown. This lack of transparency leads to distrust among users and, therefore, to less acceptance from society to use these new tools - especially in sensitive work fields with a big influence on human life (e.g., medicine, finance, and construction) [3]. Explainable AI (XAI) can be used to gain insight into the model, making the "black box" more transparent and trustworthy while enabling the model to be improved by refinement of the training data set. Flaws in the training data could be directly observed and fixed, as demonstrated in work from the Fraunhofer Heinrich-Hertz-Institut [4]. This study employs XAI to gain insights into an object detection model trained to identify symbols in engineering drawings. By examining the model's internal mechanisms, the training data set can be refined to address weaknesses in the trained model. After retraining with the improved dataset, changes in detection accuracy are compared and evaluated.

## 2 Related Literature

The amount of research on symbol detection in technical drawings using object detection models is limited [5]. In the work by Zhao et al. [6] the object detection method YOLOv1 was used to efficiently and accurately detect structural components in scanned structural drawings. The same authors later published a further improved method in which they used R-CNN to get a more precise extraction of information for reconstructing digital building models [7].

Lu et al. [8] propose a different approach based on images and CAD drawings. This semi-automatic method reconstructs a digital model from images and CAD drawings. First, a circle Hough transform detects symbols in floorplan drawings, which is then combined with textual information extracted using OCR. In addition, a neuro-fuzzy network detects the building component class in images and identifies the material of the component surface. By integrating all this information, the building geometry is reconstructed and translated into an IFC-based model.

While some approaches utilize symbol detection methods for technical drawings, to the best of the author's knowledge, no research on applying explainable AI methods in this area exists. Consequently, the current state of XAI methods has been examined.

SHapley Additive exPlanation (SHAP) [9] is a method rooted in game-theory where each feature relevant to a decision is modeled as a player in a coalition game. This provides a measure of importance known as the Shapley value. Interpretations derived from SHAP can be both local and global and are consistent with each other. However, feature dependencies pose a challenge in SHAP since it assumes feature independence.

Class activation maps (CAMs) can only be applicable with Convolutional Neural Networks (CNNs) [10]. In CAMs the per-class weighted linear sum of visual patterns is used to localize features in a picture. However, CAMs have a drawback in that they cannot be applied to pretrained networks, and to networks, which do not consist of a CNN-based architecture.

Therefore, Selvaraju et al [11] introduce a gradient-weighted schema to the CAM approach (Grad-CAM) to extend its applicability to pretrained neural network architecture. However, it produces noisy visualizations and does not perform well with multiple instances of the same object in an image.

To overcome this issue, Chattopadhay et al. [12] smooth the visualizations by pixel-wise weighting the gradients (Grad-CAM++). Additionally, Grad-CAM++ can also work with multiple instances of the same feature in an image. The drawback of Grad-CAM and Grad-CAM++, is that both methods implement backpropagation and therefore assume that classifiers decide correctly.
In the work of Muhammad and Yeasin [13] this issue is addressed with their method Eigen-CAM. Eigen-CAM computes the principle components of the learned features of the network from its respective convolutional layer as shown in Section 3.2.

# 3 Methodology

In this study, the object detection model YOLOv8 [14] is combined with Eigen-CAM to investigate the network's inner decision-making when applied to the task of symbol detection. YOLOv8 was chosen because of its high accuracy among the available models and because it is well documented. The overall procedure is illustrated in Figure 1.

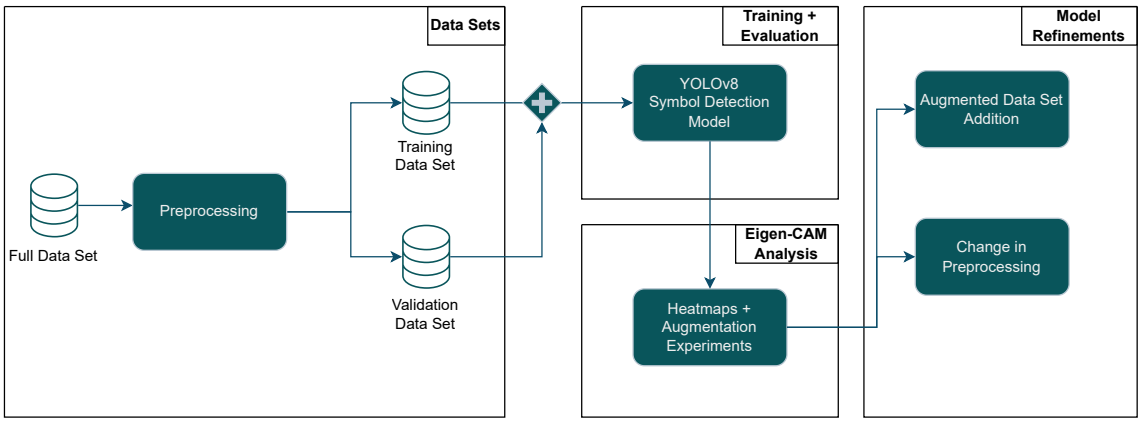


Figure 1: Overview of the structure of the study.

First, a data set consisting of 53 bridge construction drawings is collected and manually annotated as described in Section 3.1. This data is used for training YOLOv8. By utilizing Eigen-CAM, as detailed in Section 3.2, the performance of the trained YOLOv8 model is examined in Section 4. Based on these findings, the training data is extended to address the identified weaknesses of the model. The model is then retrained, and its performance is compared to the original results.

## 3.1 Data set

A data set of 53 drawings is collected to train and validate the object detection model. These drawings were provided by various industry partners. The data set identified four distinct significant symbol classes: axis symbols, section symbols, gradient symbols, and elevation symbols, as shown in Figure 2. These symbols were manually labeled, resulting in a total of 4,787 labeled instances. Given the relatively small size of these symbols compared to the overall drawings, the images were divided into smaller patches as proposed by Faltin et al. [15]. This method aligns with the findings presented in [16], which demonstrated that tiling large images enhances the detection rate of small objects. Finally, the annotations are exported using the Datumaro library[1] in the YOLO format, making them

[1] https://github.com/openvinotoolkit/datumaro (Accessed: 06 July 2024)

compatible with the YOLOv8 network. The data set is further divided into training and validation data sets. The training data set comprised 14,000 images containing 4,432 instances, while the evaluation set included 1,080 images with 345 instances.

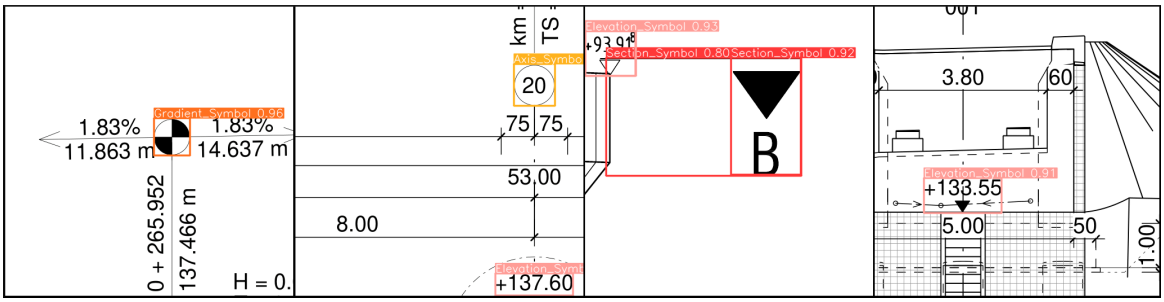


Figure 2: Exemplary representation of typical symbols contained in construction drawings. From left to right: gradient symbol, axis symbol, section symbol, and elevation symbol.

### 3.2 Eigen-CAM

The XAI method Eigen-CAM is utilized to gain insight into the patterns the YOLOv8 network is learning for symbol detection. The central idea of Eigen-CAM is to identify the principal components of the individual layers in the CNN, as illustrated in Figure 3, and visualize them based on an input image. For the $k$th-layer the output $O_k$ for an input image $I$ is determined by the combined weight matrix $W_k$, as described by the following equation

$$O_k = W_k^T I \tag{1}$$

By singular value decomposition (SVD), the principal components of $O_k$ can be calculated with

$$O_{L=k} = U \Sigma V^T \tag{2}$$

Here, matrix $U$ is an orthogonal matrix, with its columns representing the left singular vectors. The diagonal matrix $\Sigma$ contains the singular values along its main diagonal. Matrix $V$ is also orthogonal, with its columns forming the right singular vectors.
The class activation map, $L$ is given by the projection of $O_k$ onto the first eigenvector, as expressed by

$$L = O_k V_1 \tag{3}$$

Here, $V_1$ represents the first eigenvector in the matrix $V$. The visualization is achieved through a normalized heatmap highlighting areas in the image representing saliency features learned by the object detection model.

Applying this technique to the symbol detection network, it is possible to determine which pixels/features have the greatest impact on the predictions. The training data can be improved by analyzing errors in the predictions to mitigate these effects.

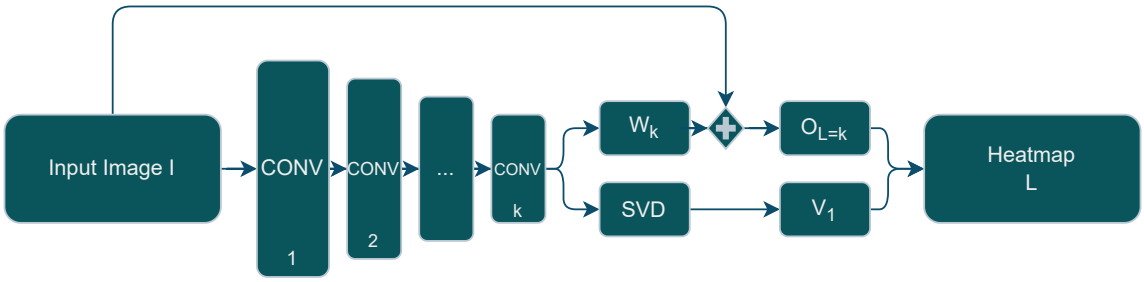


Figure 3: The input image $I$ is processed by multiple convolutional layers $CONV_i$. Eigen-CAM visualizes the pixels of highest importance for the prediction by calculating the eigenvalues of the target layer $k$ using SVD and using the projection of $O_k$ onto $V_1$.

Table 1: Performance comparison after Eigen-CAM Analysis.

| | $mAP_{50}$ | Precision | Recall |
|---|---|---|---|
| Pre Eigen-CAM Analysis | 82.93 | 91.40 | 86.42 |
| Synthetic Data Set Addition | 85.21 | 85.77 | 85.21 |
| Change in Preprocessing (Overlap) | 92.28 | 92.40 | 90.58 |

## 4 Results and Discussion

The state-of-the-art object detection model YOLOv8 is trained using a NVIDIA A100 SXM4 40 GB graphics card. A batch size of 128 was utilized for training, with a maximum of 100 epochs. The backpropagation process employed the AdamW optimizer with a learning rate of 0.001 and a momentum of 0.9 for the first 10,000 iterations. For more iterations the SGD optimizer with a learning rate of 0.01 and a momentum of 0.9 is used. The trained network achieves a high $mAP_{50}$ as shown in Table 1 for symbol detection in the construction drawings.

To gain further insight into the detection model, the Eigen-CAM method is used to visualize the areas the model considers for predicting the different symbols, as shown in Figure 4.

The class activation map for the axis symbols, gradient symbols and elevation symbols shows that the model's attentive area is larger than the symbol itself. The results indicate that the model predicts symbols by focusing on their surrounding context. For instance, the text around the gradient symbol typically describes the gradient parameters. The model, therefore, searches for parameter texts in the region of the potential gradient symbol and makes a positive prediction if this context information is present.
The interpretation for the section symbol is not as straight forward. Counterintuitively, the detection

Table 2: Performance comparison after Eigen-CAM Analysis of elevation symbol detections. True positive and false positive values as instances and normalized values.

| | TP (inst.) | TP (norm.) | FP (inst.) | FP (norm.) |
|---|---|---|---|---|
| Pre Eigen-CAM Analysis | 273 | 0.87 | 42 | 0.93 |
| Synthetic Data Set Addition | 282 | 0.90 | 56 | 0.98 |
| Change in Preprocessing (Overlap) | 326 | 0.93 | 7 | 0.87 |

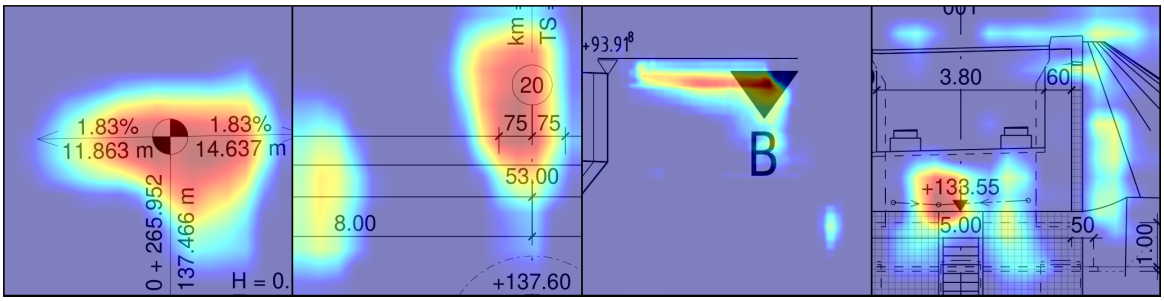


Figure 4: Exemplary illustration of the Eigen-CAM heatmaps for the layer 21 of the detection seen in 2. The red-colored parts mark highly significant parts, while the blue-colored parts are insignificant for the prediction.

head for small objects shows a fitting heatmap for the section symbol, even though its size is relatively large compared to other symbols. This can be explained by the distinctive geometrical features of the section marker, which are less dependent on the context of the image.

To enhance the detection model, the focus was shifted to the elevation symbol due to its high occurrence in the dataset. It had the lowest true positive detection rate and the highest false positive rate, as shown in Table 2. Often dimension symbols are incorrectly classified as an elevation symbol. This may be due to the tiling process in which a part of the elevation symbol is cut off. This leaves a geometric structure that could be mistaken for the dimension symbol. Due to the tiling process, the accuracy of predictions can decrease for symbols with nondistinctive geometric forms.

By analyzing the Eigen-CAM heatmaps, it is concluded that the elevation marker's false positive detections are mainly due to a larger field of attention, which also contains a significant amount of white space. Two different approaches are implemented to refine the model's field of attention: First, synthetic training data was created by copying tiles containing elevation symbols, then partially hiding parts of the images with white space and rearranging the elevation symbols into new positions. Second, the preprocessing of the drawings is modified, by including a overlap of 50 pt in the tiling of the construction plans. While the first approach shows no significant improvements, as illustrated in Table 1, the second approach significantly improves detection accuracy. The inclusion of a overlap lead to a increase of the accuracy by 10 points. Furthermore, this change is evident in the heatmaps, as shown in Figure 5. The model's field of attention is smaller for each symbol compared to the attention fields before the preprocessing change.

## 5 Conclusion and Outlook

The proposed study utilized the XAI method Eigen-CAM to analyze how the YOLOv8 network makes decisions when detecting symbols in bridge construction drawings. While YOLOv8 performed well in detecting symbols, Eigen-CAM provided insights into its decision-making process, particularly highlighting issues with uncertain or incorrect predictions. This information guided adjustments to the data set, improving the network's performance. Retraining on the expanded data set resulted in an approximately 11% improvement in $mAP_{50}$, showcasing the potential of XAI methods to enhance symbol detection accuracy.

Despite these promising findings, further research is needed. Normalization should be applied to

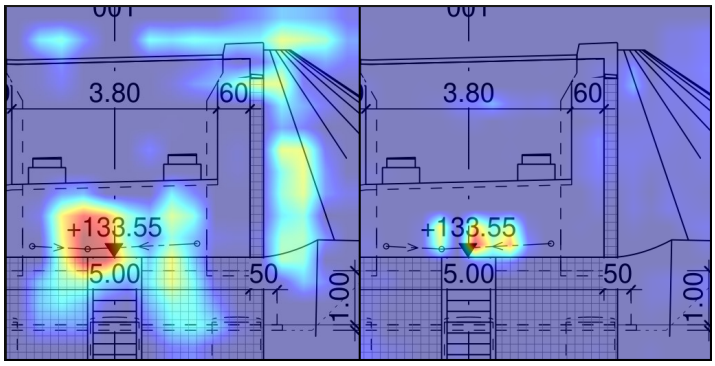


Figure 5: Comparison of Eigen-CAM heatmaps: Model without overlap (left) and with overlap (right) in tiling of the pictures in data preprocessing.

Eigen-CAM visualizations to ensure better heatmap comparability across different layers and images. Concatenating normalized Eigen-CAM activation maps globally may yield additional valuable insights. Moreover, exploring optimal tile overlap in relation to XAI methods such as Eigen-CAM could further enhance detection metrics, as demonstrated in this study's use of a tiled approach with overlap.

## References

[1] R. Sacks, A. Kedar, A. Borrmann, *et al.*, "Seebridge as next generation bridge inspection: Overview, information delivery manual and model view definition", *Automation in Construction*, vol. 90, pp. 134–145, 2018. DOI: https://doi.org/10.1016/j.autcon.2018.02.033. [Online]. Available: https://www.sciencedirect.com/science/article/pii/S0926580517303977.

[2] Y. LeCun, Y. Bengio, and G. Hinton, "Deep learning", *Nature*, vol. 521, no. 7553, pp. 436–444, May 28, 2015. DOI: 10.1038/nature14539. [Online]. Available: https://www.nature.com/articles/nature14539 (visited on 11/18/2023).

[3] R. Confalonieri, L. Coba, B. Wagner, and T. R. Besold, "A historical perspective of explainable artificial intelligence", *WIREs Data Mining and Knowledge Discovery*, vol. 11, no. 1, e1391, Jan. 2021. DOI: 10.1002/widm.1391. [Online]. Available: https://wires.onlinelibrary.wiley.com/doi/10.1002/widm.1391 (visited on 11/17/2023).

[4] A. Rommel and W. Samek, *Cebit 2017: Analyse-software für neuronale netze – dem computer beim denken zuschauen*, 2017. [Online]. Available: https://www.hhi.fraunhofer.de/fileadmin/PDF/CC/PM/2017/PI_FraunhoferHHI_Dem_Computer_beim_Denken_zuschauen_CeBIT_d.pdf.

[5] C. F. Moreno-García, E. Elyan, and C. Jayne, "New trends on digitisation of complex engineering drawings", *Neural Computing and Applications*, vol. 31, no. 6, pp. 1695–1712, Jun. 2018. DOI: 10.1007/s00521-018-3583-1. [Online]. Available: http://dx.doi.org/10.1007/s00521-018-3583-1.

[6] Y. Zhao, X. Deng, and H. Lai, "A deep learning-based method to detect components from scanned structural drawings for reconstructing 3d models", *Applied Sciences*, vol. 10, no. 6, 2020. DOI: 10.3390/app10062066. [Online]. Available: https://www.mdpi.com/2076-3417/10/6/2066.

[7] Y. Zhao, X. Deng, and H. Lai, “Reconstructing bim from 2d structural drawings for existing buildings”, *Automation in Construction*, vol. 128, p. 103 750, 2021. [Online]. Available: https://api.semanticscholar.org/CorpusID:236240776.

[8] Q. Lu, L. Chen, S. Li, and M. Pitt, “Semi-automatic geometric digital twinning for existing buildings based on images and cad drawings”, *Automation in Construction*, vol. 115, p. 103 183, 2020. DOI: https://doi.org/10.1016/j.autcon.2020.103183. [Online]. Available: https://www.sciencedirect.com/science/article/pii/S0926580519315079.

[9] S. M. Lundberg and S. Lee, “A unified approach to interpreting model predictions”, *CoRR*, vol. abs/1705.07874, 2017. arXiv: 1705.07874. [Online]. Available: http://arxiv.org/abs/1705.07874.

[10] B. Zhou, A. Khosla, À. Lapedriza, A. Oliva, and A. Torralba, “Learning deep features for discriminative localization”, *CoRR*, vol. abs/1512.04150, 2015. arXiv: 1512.04150. [Online]. Available: http://arxiv.org/abs/1512.04150.

[11] R. R. Selvaraju, M. Cogswell, A. Das, R. Vedantam, D. Parikh, and D. Batra, “Grad-cam: Visual explanations from deep networks via gradient-based localization”, in *2017 IEEE International Conference on Computer Vision (ICCV)*, 2017, pp. 618–626. DOI: 10.1109/ICCV.2017.74.

[12] A. Chattopadhay, A. Sarkar, P. Howlader, and V. N. Balasubramanian, “Grad-CAM++: Generalized gradient-based visual explanations for deep convolutional networks”, in *2018 IEEE Winter Conference on Applications of Computer Vision (WACV)*, Lake Tahoe, NV: IEEE, Mar. 2018, pp. 839–847. DOI: 10.1109/WACV.2018.00097. [Online]. Available: https://ieeexplore.ieee.org/document/8354201/ (visited on 11/17/2023).

[13] M. B. Muhammad and M. Yeasin, “Eigen-CAM: Class activation map using principal components”, in *2020 International Joint Conference on Neural Networks (IJCNN)*, Glasgow, United Kingdom: IEEE, Jul. 2020, pp. 1–7. DOI: 10.1109/IJCNN48605.2020.9206626. [Online]. Available: https://ieeexplore.ieee.org/document/9206626/ (visited on 11/29/2023).

[14] G. Jocher, A. Chaurasia, and J. Qiu, *Ultralytics yolov8*, version 8.0.0, 2023. [Online]. Available: https://github.com/ultralytics/ultralytics.

[15] B. Faltin, P. Schönfelder, and M. König, “Inferring interconnections of construction drawings for bridges using deep learning-based methods”, in *ECPPM 2022 - eWork and eBusiness in Architecture, Engineering and Construction 2022*, 1st ed., London: CRC Press, Mar. 8, 2023, pp. 343–350. DOI: 10.1201/9781003354222-44. [Online]. Available: https://www.taylorfrancis.com/books/9781003354222/chapters/10.1201/9781003354222-44 (visited on 04/06/2024).

[16] F. O. Unel, B. O. Özkalayci, and C. Çigla, “The power of tiling for small object detection”, *2019 IEEE/CVF Conference on Computer Vision and Pattern Recognition Workshops (CVPRW)*, pp. 582–591, 2019. [Online]. Available: https://api.semanticscholar.org/CorpusID:198903617.

# Comparison of Tracking Methods for Augmented Reality-Supported Damage Mapping of Grid Shell Structures

Christian Rosenkranz[1] and Pascal Mosler[2]

[1]Studienbereich Computational Engineering, Technische Universität Darmstadt, Dolivostraße 15, 64293 Darmstadt, Germany

[2]Institut für Numerische Methoden und Informatik im Bauwesen, Technische Universität Darmstadt, Franziska-Braun-Str. 7, 64287 Darmstadt, Germany

E-Mails: cr-ing@t-online.de, mosler@iib.tu-darmstadt.de

**Abstract:** As powerful mobile devices become available and robust tracking methods are further developed, Augmented Reality (AR) becomes increasingly suitable for use on construction sites. For the renovation of the Mannheim *Multihalle*, the world's largest free-form timber grid shell structure, various AR tracking methods are examined for their suitability for carrying out damage mapping: manual initialization (four points or vector input) and localization by cloud anchors. As the uniform grid of the grid shell makes orientation difficult during manual damage mapping, using a smartphone AR application to correctly recognize the laths and nodes is promising. Three key test criteria were used to compare the methods: the correct assignment of the laths, the smallest computationally recognized error and sufficient stability, meaning the absence of drift. In addition, the effort required for preparation and handling during use was considered. For the use case of damage mapping using a smartphone, the tests showed that although manual initialization using vector input is the most suitable method, even this method is not satisfactory. Therefore, in the outlook, measures to facilitate optical tracking and the use of differential GPS and synchronization with point cloud data are discussed.

*Keywords:* Augmented Reality (AR), Damage Mapping, Tracking, SLAM Systems, Cloud Anchors

Erschienen in Tagungsband 35. Forum Bauinformatik 2024, Hamburg, Deutschland, DOI: 10.15480/882.13491
© 2024 Das Copyright für diesen Beitrag liegt bei den Autoren. Verwendung erlaubt unter Creative Commons Lizenz Namensnennung 4.0 International.

## 1 Introduction

During damage mapping of buildings, damages are recorded manually or digitally in order to plan structural changes to the building and to upgrade the structure based on the structural assessment. Augmented Reality offers the possibility of overlaying the real building with a virtual model of the structure during the survey. The *Multihalle* in Mannheim (see Figure 1) is the world's largest free-

form timber grid shell designed by Pritzker Prize winner Frei Otto for Germany's National Garden Show of 1975. The experimental structure is considered an outstanding example of lightweight architecture and was classified as a cultural monument of special significance. The laths of the grid shell form a regular grid with a mesh size of 50 cm. As part of the upcoming renovation of the *Multihalle*, damages need to be repaired and the structure reinforced [1]. As it is difficult to orientate in the uniform grid of the lattice shell, mapping the damage is to be supported by overlaying it with a wireframe model in AR. The aim of digitally capturing the damages on a smartphone or tablet is to improve collaboration between planners and contractors and to make mapping more efficient by eliminating intermediate steps of sketching damage onto 2D paper drawings.

The tracking method is crucial for the correct superimposition of reality and virtual objects. For this purpose, various methods were tested on-site under field conditions. Based on on-site conditions and the constraints of the renovation concept, criteria for selecting the tracking methods were established for the use case and a pre-selection was made. In preliminary field tests, various optical methods were tested with "Simultaneous Localization and Mapping" (SLAM) systems for which sufficient visual features could be detected on the timber structure. Two manual initialization methods and localization via cloud anchors were selected for implementation in a demonstration application.

Figure 1: Entrance area of the *Multihalle* in Mannheim (Source: Fast + Epp).

## 2 Related Work

Previous approaches to AR in the construction industry can be found primarily in the visualization of planning. In other use cases, such as construction, operations and maintenance, development is mainly at the initial trial stage [2]. At the Technical University of Vienna, several approaches to AR are being pursued in which Building Information Modeling (BIM) is seen as a driving factor in advancing digitalization in the construction industry. Schranz et al. [3] summarized various possible applications, including applications in construction work and documentation, to support consultations, as well as for maintenance work and training. Gerger et al. [4] and Schranz et al. [5] describe possible use cases during the approval process in more detail.

Changing light conditions, large monochrome surfaces, repetitive patterns and moving objects pose particular challenges for tracking on construction sites. Urban et al. [6] analyzed commercially available AR systems with regard to their suitability for use on construction sites. They tested tracking

with an infrared depth sensor at different lighting levels and investigated the influence of room size and the number of features in optical tracking.

Initialization is necessary for SLAM systems unless a previously recorded map can be used. Gehring and Mosler [7] as well as Marino et al. [8] used QR codes for initial tracking, with additional markers to reduce drift. Schranz et al. [9] identified four possible initialization methods. A comparison with QR codes proved to be the most error-prone. In the second option, in the course of a vector input, a point and a direction vector are marked by the user. The third option is to mark three orthogonal planes, which are taken from a BIM model. The authors have not yet tested the fourth option of carrying out the localization freely in the environment without markers. The previous investigations were mainly limited to use in solid construction. In this paper, the initialization methods are further developed with the aim of using them in the wooden grid shell of the *Multihalle*.

# 3 Method

To correctly superimpose reality and virtual objects, a total of six degrees of freedom (translation in three directions and rotation around three axes) must be determined by tracking. Not all methods can be used to determine all degrees of freedom. In addition, the tracking methods vary in their accuracy. As AR systems are mobile applications, they generally rely on the sensors built into the devices. Equipping the environment with additional sensors is not practical, especially in large environments.

## 3.1 Boundary conditions for tracking

To find the appropriate tracking method, the boundary conditions of the use case were considered. Initially, the local conditions of the grid shell were taken into account.

- Lighting conditions: The translucent membrane results in a predominantly uniform, diffuse light on the inside of the hall. Artificial lighting is necessary in the darker months of the year.
- Weather conditions: The hall has an open-sided roof. Fluctuations in temperature, air pressure and humidity are to be expected. Cold temperatures reduce battery life.
- Surface structure: The wooden laths provide a structured surface. However, the pattern is repetitive.
- Installation of markers: Possible in principle, but these may have to be repositioned after replacing individual building components.
- Structural changes, occlusions: Birdcage scaffold will be erected during the renovation.

Further constraints result from the functional requirements of the software application for damage mapping. The accuracy of the tracking is key for being able to assign damages to individual building components such as laths and nodes. The deviation should be less than half the mesh size of the grid, ideally no more than 15 cm. Simple handling is important for the continuous use and acceptance

of digital damage mapping on the construction site. The application was implemented using the Unity Game Engine and license-free software development kits (SDKs). For the on-site tests, an Android smartphone was used.

### 3.2 Preselection of tracking methods and preliminary investigations

Based on the described boundary conditions, a preselection of potentially suitable tracking methods was made (see Figure 2). In preliminary investigations, scanning a single marker proved to be too inaccurate for localization, especially with regard to rotation. With the *AR Foundation* sample app [10], however, sufficient features could be recognized on-site for markerless tracking. However, geometric planes were recognized quite arbitrarily. The depth information of the LiDAR sensor was discarded due to the short range of the sensor in the test device. Although SLAM is generally suitable, tests with the SDKs from *Immersal* [11] and *Easy AR* [12], which use pre-recorded point clouds, did not provide sufficient accuracy. With the *Immersal* mapper, point clouds can be generated by taking overlapping photos. During tests on site, deviations of up to 70 cm could be observed, which is significantly more than one mesh size. With *Easy AR*, the point cloud recorded in an AR session can be saved on a server together with virtual objects created by the user. Virtual objects added in the tests were sometimes displayed at a different location later or jumped to a different location during display. Both SDKs do not offer any customization options to improve precision.

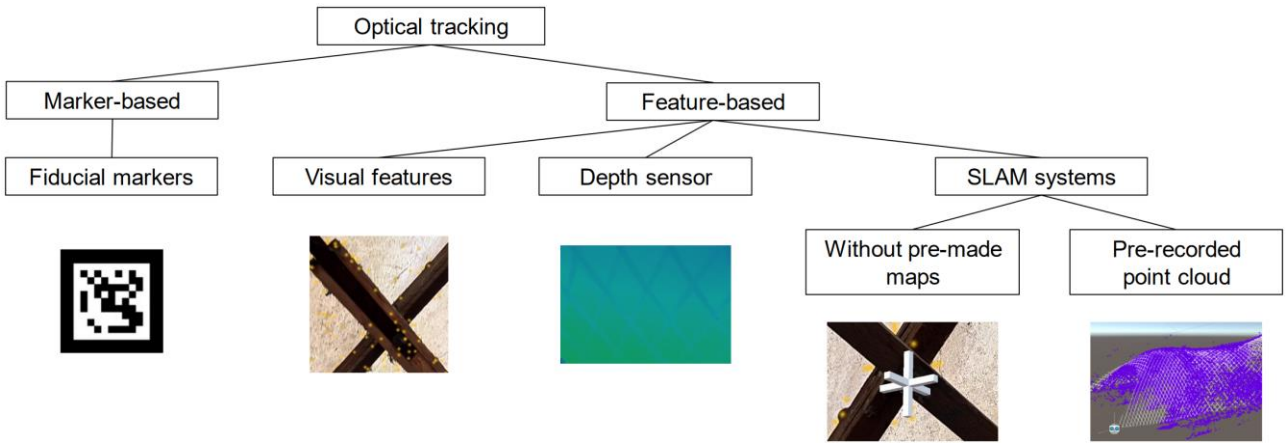


Figure 2: Overview of the tracking methods analyzed in preliminary tests.

### 3.3 Implemented tracking methods

During implementation, attention was paid to the adaptability of the methods to improve accuracy. The methods implemented in the demonstration application are shown in Figure 3.

- Manual initialization using four points: The user marks four points on the grid shell to determine the transformation between the world coordinate system and the local coordinate system of the AR application. Theoretically, the coordinates of three points would be sufficient to locate a model in space. However, as the points cannot be expected to match exactly, an approximate calculation is carried out for which at least four points are required.

- Manual initialization via vector input: The user only marks one point as the origin and one horizontal direction. As the smartphone's inertial sensors have already detected the orientation to the earth's surface, this information is sufficient.
- Localization via *Google* cloud anchors [13]: The cloud anchors are marked in advance. For hosting, the point cloud around the anchors is captured from all sides. An indicator shows the quality of the point cloud. When sufficient quality is achieved, the point cloud is transferred to the server. As it is difficult to correctly record the rotation of the cloud anchors on the grid shell, only the position of the cloud anchors is evaluated during tracking. As with manual initialization, at least four anchors are required. These must be evenly distributed and must not lie approximately on a line. For localization, the user walks along the walls of the grid shell until enough anchors have been found. It is also possible to continue the search for cloud anchors after the model has been localized and to update the position of the model later. The calculation used provides a computational error of the individual anchors. If the deviation of an anchor is too large, it is excluded from the calculation. Figure 4a shows the result of a successful superimposition.

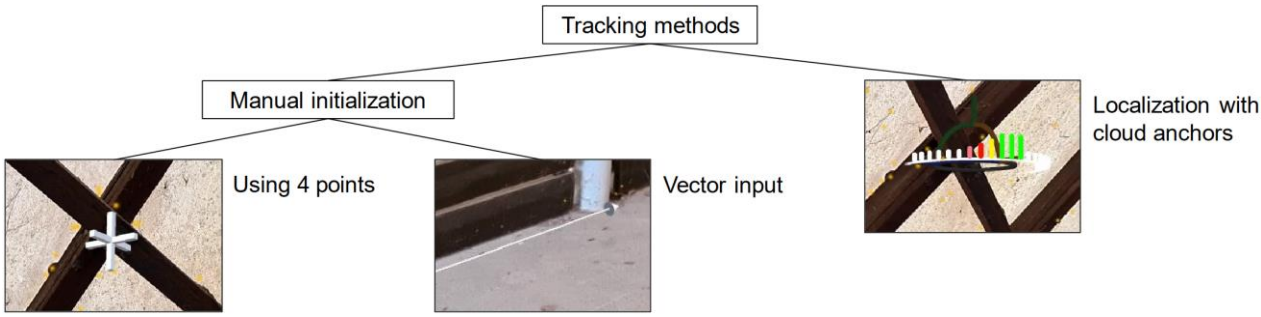


Figure 3: Tracking procedures implemented in the demonstration application for damage mapping.

After initializing the tracking, the user can select one or more components on the grid shell and enter a description of the damage using a menu (see Figure 4b). Additionally, it is possible to take photos for documentation purposes. Damage can be directly flagged for repair or marked for approval.

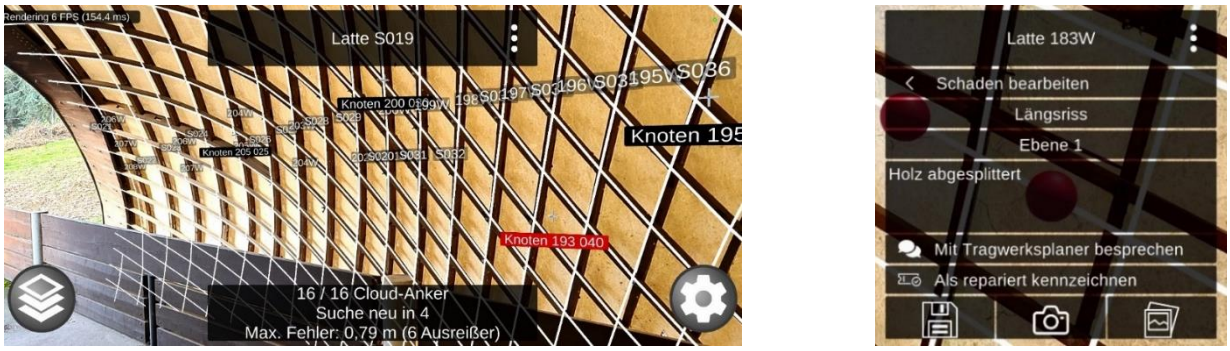


(a) Superimposition with 16 cloud anchors (outliers marked red). (b) Menu for mapping.

Figure 4: On-site use of the damage mapping application.

# 4 Experiments and Results

To evaluate the tracking methods, they were tested in a final on-site test under standardized boundary conditions. Three test criteria were defined for this test:

- Clear assignment of the individual lath sections
- Largest recognized computational error of an anchor point after positioning
- Time in which the superimposition remains stable until drift is detected

The tests were carried out over a maximum period of two minutes. For manual initialization, positioning using four points and vector input were tested. For localization via cloud anchors, variants with four anchors without updating and with eight and sixteen anchors with continuous updating were tested. Ten runs were carried out for each method. The results are summarized in Figure 5.

| 10 runs per method | Manual Initialization | | Cloud Anchors | | |
|---|---|---|---|---|---|
| | 4 Points | Vector input | No updating | With continuous updating | |
| | | | 4 anchors | 8 anchors | 16 anchors |
| **Frequency of precise allocation** | 10% ●○○○○○○○○○○ | 90% ●●●●●●●●●○ | 40% ●●●●○○○○○○ | 40% ●●●●○○○○○○ | 50% ●●●●●○○○○○ |
| **Average maximum alignment error** | 0,31 m | Not applicable | 0,24 m* | 0,24 m | 0,47 m |
| **Stable superimposition** (measured in 10 second intervals over 2 minutes) 0% 50% 100% | | | | | |

* Only runs with a maximum deviation of 1 m were taken into account

Figure 5: Results of the comparative test.

In the comparative test, manual initialization via vector input achieved the best results with a success rate of 90%. However, in only one third of the cases the superimposition remained stable for at least two minutes. After a loss of tracking, it was possible to resume tracking after returning to the initial location. When marking four nodes, drift already occurred during initialization. When using cloud anchors, some anchors were detected incorrectly. This influenced the alignment of the model so that only 40%–50% of the runs achieved sufficient accuracy for damage mapping. The overlay was less stable for the variants with continuous updating, which is due to the fact that localization can also become less accurate when adding additional anchors with a larger deviation during updating.

# 5 Discussion

Precision is the most important factor for damage mapping. Only if the components can be clearly assigned, it is possible to carry out the mapping reliably with the application. If laths are mixed up, this can lead to a repair being carried out in the wrong place. The vector input achieves an almost

exact overlay. The precision of localization using cloud anchors is impaired by the fact that individual cloud anchors are recognized in the wrong position. The manual initialization using four points is not pursued further due to its low success rate. To ensure the usability and efficiency of the mapping, it is also important that the overlay remains stable for as long as possible. The SLAM systems used still need to be improved for this purpose.

Another criterion is the preparation effort. For manual initialization, only the coordinates of the points to be marked need to be stored in the application. These can be easily replaced in case of changes. For localization via cloud anchors, they first have to be captured. The accuracy and lighting conditions when hosting the anchors are essential for how reliably they can subsequently be resolved. Creating a sufficiently dense network of cloud anchors for the *Multihalle* would take around six working days. However, a new network would have to be created, if the local conditions change.

To compete with manual mapping, the application needs to be robust and user-friendly. In practice, the need to repeat the initialization when tracking is lost, could result in frustration outweighing the increase in efficiency through digital mapping. The advantage of using cloud anchors is that scanning takes place automatically in the background. Nevertheless, the precision and drift are still too high for a reliable application for damage mapping, making further optimization necessary.

## 6 Conclusion

For damage mapping in the *Multihalle*, a high degree of accuracy in the range of 15 cm–20 cm is required to ensure the correct recording of damages. A reliable, stable overlay and simple handling are required for practical use. The methods tested do not yet fulfil these requirements. However, the accuracy would be sufficient for other purposes such as indoor navigation or a digital tour.

To improve tracking, point clouds created from survey data could be analyzed further. Using point clouds created from terrestrial laser scanning data is expected to result in higher accuracy. By comparing point clouds across a large area, tracking could also be more stable in terms of occlusions, as only small areas would be covered at any given time.

Furthermore, positioning using cloud anchors could be optimized by means of a parameter study. The number of anchors to be used for localization could be limited and optimized depending on the distance between the anchors on the structure. Another option would be to use cloud anchors only in a certain radius around the position of the user.

As an alternative to optical methods, tracking using differential GPS could also be investigated. However, as this requires an unobstructed line of sight to several satellites, it is only suitable for outdoor use. The extent to which the quality of the signal is reduced even by light roofing, as in the *Multihalle*, to enable precise localization inside would have to be tested. However, this process would be feasible for the use on the exterior of the lattice shell.

The tests carried out show the need for further research into mobile tracking methods to open up further uses for AR in the construction industry with high precision requirements.

## Acknowledgements

The authors would like to thank *Fast + Epp* and the City of Mannheim for their support.

## References

[1] J. Stahl and C. Rosenkranz, “Rehabilitation of the Mannheim Multihalle,” *Journal of the International Association for Shell and Spatial Structures*, vol. 65, no. 2, 2024.

[2] J. M. D. Delgado, L. Oyedele, P. Demian, and T. Beach, “A research agenda for augmented and virtual reality in architecture, engineering and construction,” *Advanced Engineering Informatics*, no. 45, 2020.

[3] C. Schranz, A. Gerger, and H. Urban, „Augmented Reality im Bauwesen: Teil 1 – Anwendungs- und Anforderungsanalyse,“ *Bauingenieur*, vol. 95, no. 10, pp. 379–388, 2020.

[4] A. Gerger, H. Urban, and C. Schranz, “Augmented Reality for Building Authorities: A Use Case Study in Austria,” *Buildings*, vol. 13, no. 6, 2023.

[5] C. Schranz, H. Urban, and A. Gerger, “Potentials of Augmented Reality in a BIM based building submission process,” *ITcon*, vol. 26, pp. 441–457, 2021.

[6] H. Urban, T. Irschik, C. Schranz, and C. Schönauer, „Augmented Reality im Bauwesen: Teil 2 – Baustellentaugliches Trackingsystem,“ *Bauingenieur*, vol. 95, no. 12, pp. 501–508, 2020.

[7] M. Gehring and P. Mosler, “Indoor Navigation with Augmented Reality and BIM: A Marker-Based Approach for Locating Logistics Areas on Construction Sites,” in *Proceedings of 33. Forum Bauinformatik*, München, Germany, 2022, pp. 199–206.

[8] E. Marino, L. Barbieri, B. Colacino, A. K. Fleri, and F. Bruno, “An Augmented Reality inspection tool to support workers in Industry 4.0 environments,” *Computers in Industry*, no. 127, 2021.

[9] C. Schranz *et al.,* „Einsatz von Augmented Reality zur Abnahme und Qualitätssicherung auf Baustellen: AR-AQ-Bau,“ Bundesministerium für Klimaschutz, Umwelt, Energie, Mobilität, Innovation und Technologie (BMK), Berichte aus Energie- und Umweltforschung 5/2022.

[10] GitHub, *Unity-Technologies/arfoundation-samples: Example content for Unity projects based on AR Foundation.* Accessed on: Jun. 17, 2023. [Online]. Available: https://github.com/Unity-Technologies/arfoundation-samples

[11] Immersal, *Innovative VPS Solutions for AR Developers.* Accessed on: Jun. 23, 2023. [Online]. Available: https://immersal.com/developers

[12] EasyAR, *EasyAR Product Overview.* Accessed on: Jul. 1, 2023. [Online]. Available: https://www.easyar.com/price.html

[13] Google for Developers, *Cloud Anchors allow different users to share AR experiences.* Accessed on: Jan. 6, 2024. [Online]. Available: https://developers.google.com/ar/develop/cloud-anchors

# Enabling Component-Based Progress Monitoring on Construction Sites Through Image-Based Computer Vision

Felix Friedl[1] and Fabian Pfitzner[1]
[1]Chair of Computational Modeling and Simulation, Technical University of Munich, Arcisstraße 21, 80333 Munich, Germany
E-mail(s): felix.friedl@tum.de, fabian.pfitzner@tum.de

**Abstract:** Vision-based construction monitoring methods have improved on-site transparency. However, many point cloud-based techniques are complex and often involve an image-dependent reconstruction step, making them prone to uncertainties. Additionally, few address productivity insights at the construction activity level. This paper presents a novel computer vision approach for automating construction progress monitoring, extracting information directly from image data enhanced through as-built details. A PIDNet Semantic segmentation model was trained to identify cast-in-place concrete walls, columns, and slabs during panel, rebar, and concrete phases. The detected components were processed using averaging techniques to monitor element-specific progress. The resulting data was integrated with as-built models through geometric projections, forming the basis for a digital twin construction. Our method was deployed on two-month construction data, providing detailed progress information and demonstrating its robustness. Compared to previous methods, this approach effectively merges existing as-built models with comprehensive as-performed image data.
*Keywords:* Construction Monitoring, Computer Vision, Semantic Segmentation, As-built geometry

Erschienen in Tagungsband 35. Forum Bauinformatik 2024, Hamburg, Deutschland, DOI: 10.15480/882.13520
© 2024 Das Copyright für diesen Beitrag liegt bei den Autoren. Verwendung erlaubt unter Creative Commons Lizenz Namensnennung 4.0 International.

## 1 Introduction

There have been few increases in productivity and digitization during the last decades in the construction sector despite the recent developments towards Industry 4.0 [1]. Specifically, project management and progress monitoring are often carried out manually, comparing the status of building elements against a construction schedule. This tedious and error-prone process results in frequent cost and time overruns [2]. Novel approaches towards site monitoring need to be developed that aim at the digital twin idea [3] supporting management in everyday construction projects.
However, recent approaches lack monitoring functionalities for cast-in-place concrete elements (e.g. columns, walls and slabs) [4]. The authors aim to close this gap by providing a new approach for semantic segmentation based progress data collection on these elements' panel, rebar, and con-

crete phases. The potential of our approach is highlighted by demonstrating improved workflows for extracting and coupling element-specific progress data with a BIM model.

## 2 Related Work

The monitoring approach proposed by this paper relies on automating the visual understanding of construction environments with the help of 2D semantic segmentation. This computer vision discipline allows the detection of specific objects in images by partitioning them into multiple segments with matching characteristics and assigning a categorical label from a predefined set of classes to each one. Convolutional Neural Networks (CNNs) use learnable convolutional kernels to efficiently process image data and perform this task autonomously [5]. However, as most models retain the problem of generality, curated datasets with annotated ground truths tailored to the specific research problem are required for training.

Many applications of computer vision and digital twinning pose significant benefits to the construction sector. In this context, a digital twin is a virtual replica of a building that uses real-time data to simulate, monitor, and optimize the performance of the structure throughout its lifecycle [6]. Computer Vision techniques are used to evaluate productivity and progress monitoring on an activity-level in construction operations [7] or in smaller areas of application like crack detection in reinforced concrete structures [8].

Progress monitoring is fundamental for digital twins in construction by extending as-planned data with as-performed data [3]. To fully leverage the digital twin construction, it's essential to gather and organize vast data for various assessments [6]. Pfitzner, Braun, and Borrmann [9], for example, enable extracting precise construction metrics through knowledge graph-based methods. Despite extensive research in vision-based construction monitoring, significant gaps remain. Existing work, such as that described in [10], primarily focuses on tracking single elements like pre-cast walls, which limits the scope of progress monitoring. Expanding existing datasets to include additional elements like slabs and pillars could provide a more comprehensive understanding of the construction process. Moreover, approaches as demonstrated by [8] are limited by uncertainties in unordered photographs, which can be mitigated through advanced averaging algorithms to enhance data reliability. Additionally, while [7] demonstrates detailed activity-level monitoring, it involves complex processing steps limiting reproducibility. Therefore, there is a need for a more efficient and accurate approach that can expand the range of elements monitored, enhance tracking precision, and simplify the monitoring process.

This study aims to enhance vision-based techniques for monitoring construction progress by addressing existing limitations. Specifically, it focuses on expanding the scope of monitored elements, enabling in-depth progress tracking, and streamlining the overall monitoring process. By leveraging state-of-the-art semantic segmentation networks, the proposed method intends to reduce the time and effort required for effective monitoring while maintaining the accuracy and comprehensiveness of the tracking.

# 3 Method

Our approach provides a semantic segmentation-based pipeline towards automating construction progress monitoring by detecting element-specific construction progress timestamps. The generated information is coupled with an as-built model.

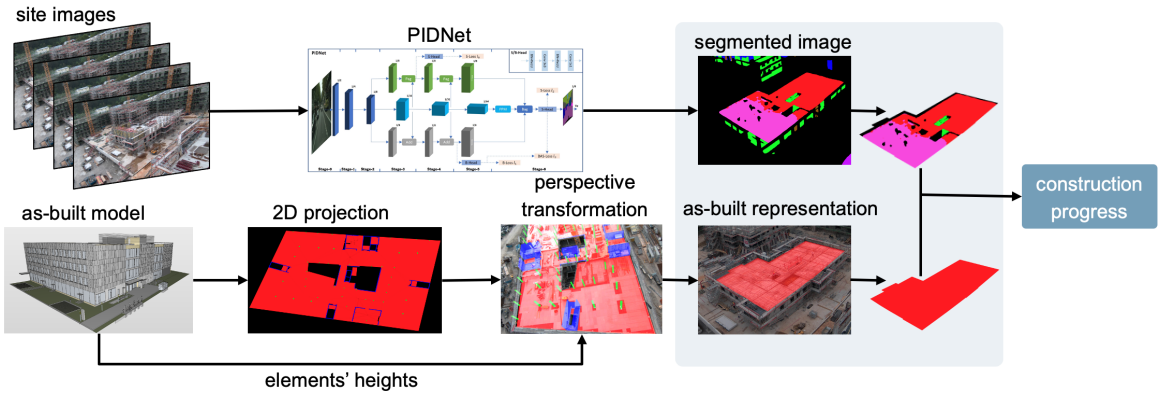


Figure 1: Method overview

Pretrained semantic segmentation models [11] are used to generate predictions from the site images. Our work focuses on cast-in-place slabs, walls and columns. The detected classes include three different construction stages: panel, rebar and concrete.

Figure 1 shows the proposed pipeline: In the first step, crane-mounted cameras with a fixed viewpoint capture a continuous stream of site images. These images are then processed by the semantic segmentation model PIDNet [12]. Finally, element-wise construction progress is extracted from the resulting prediction files.

The integration of the as-built data is done as follows: First, the elements' geometry is extracted from the BIM model and then plotted element-wise in a top-down perspective. These geometries are then represented in a simplified, top-down view image where each element's ground floor area is highlighted in red against a black background, as illustrated Fig. 1. The orientation of each element is aligned with the actual building directions using rotation based on the as-built model. To match the camera's percepective, the as-built representations are converted using perspective transformation. Per building floor and camera, a transformation matrix is computed using a direct linear transformation algorithm [13] and point picking. The resulting matrix is applied to each pixel of an element's as-built representation. A vector computation determining the elements' heights was applied to overcome the 2D limitation of the perspective transformation approach. A vanishing point, predefined on two parallel lines, determines the z-direction of a building component. The element height extracted from the as-built representation and the vector computation is converted into pixels and projected onto the image. The element-wise as-built representations are ultimately passed back to the progress monitoring pipeline, fusing the resulting data.

A percentage value indicating the components progress is computed based on the overlapping area. Two thresholds per construction state are assumed: 10%: the start of a panel, rebar, or concreting phase and 80%: the end. To reduce the number of computations and minimize outliers, all entries within a specified *averaging interval* are aggregated to compute the mean pixel count for each class.

# 4 Case Study

## 4.1 Data and Setup

A custom dataset of site images [9] containing cast-in-place concrete elements of real-world site environments was prepared to showcase our method. The annotated dataset contains 390 samples. The segmentation model *PIDNet-S* was used within the computation pipeline.
Two examples were investigated thoroughly to determine the in-depth accuracy of the proposed method. All cast-in-place types (*rebar, slab, concrete*) were included. The gap between both timestamps was used to measure the framework's accuracy. In the following tables, a negative error indicates the derived timestamp is earlier than the actual, while a positive error means it's later.
Various averaging techniques were tested by adjusting starting and ending thresholds from 0% to 50% and from 50% to 100%, respectively, in 5% increments.
In total, 121 combinations were analyzed for averaging intervals from 0 to 30 minutes in one-minute intervals for each camera. The total error over all evaluated timestamps was recorded. However, only the best-scoring combinations of threshold and averaging interval parameters were further evaluated to enable precise monitoring.
All as-built representations were compared against manually drawn annotations as shown in Figure 3, 4 and 5. Common pixels are coloured in red, pixels missing from model-generated ones in green and pixels missing from the model-generated pictures in blue. The combined error value was calculated as a fraction of wrong to correct pixels in percent.
Lastly, the entire pipeline was tested on one construction site using images from two cameras over two months. The as-built representations were generated for all building elements from the first and second floors, resulting in 290 elements. Considering only concrete slabs, walls and columns, all elements were monitored over the whole two-month timespan using a parameter configuration of an averaging interval of 7 minutes and thresholds of 75% and 10%, respectively. The detected construction progress was analyzed further by comparing it to manually derived as-built timestamps for 8 elements.

## 4.2 Results

The segmentation model *PIDNet-S* was trained on a specific dataset consisting of 390 annotated images from two different construction sites and achieved a mean average precision (mAP) of 74.20%, demonstrating sufficient precision and performance. The test results shown in Table 1 indicate sufficient performance across all classes. Yet, a lower mAP was achieved for wall or column elements in the rebar phase presumably due to lacking features. However, to achieve higher generalisability of the model, additional training data is required. A comprehensive investigation of the semantic training and testing process was carried out in the authors' prior work [11].
The monitoring results for a specific wall element are shown in Figure 2 with a negative error indicating, that the derived timestamp is earlier than the actual, while a positive error means it's later. These results illustrate, that precise results can be achieved when using different averaging intervals for singular cameras and by averaging the monitoring results over multiple cameras.
Including this wall example, six elements were closer investigated to establish a best suited combination of top-level parameters being the length of the averaging interval and the upper and lower threshold

Table 1: Results for the PIDNet-S model - mAP [%]

| class | background | column | | | slab | | | wall | | |
|---|---|---|---|---|---|---|---|---|---|---|
| | | concrete | panel | rebar | concrete | panel | rebar | concrete | panel | rebar |
| mAP [%] | 98.34 | 63.60 | 72.60 | 22.59 | 66.88 | 93.95 | 94.00 | 83.02 | 79.90 | 67.12 |

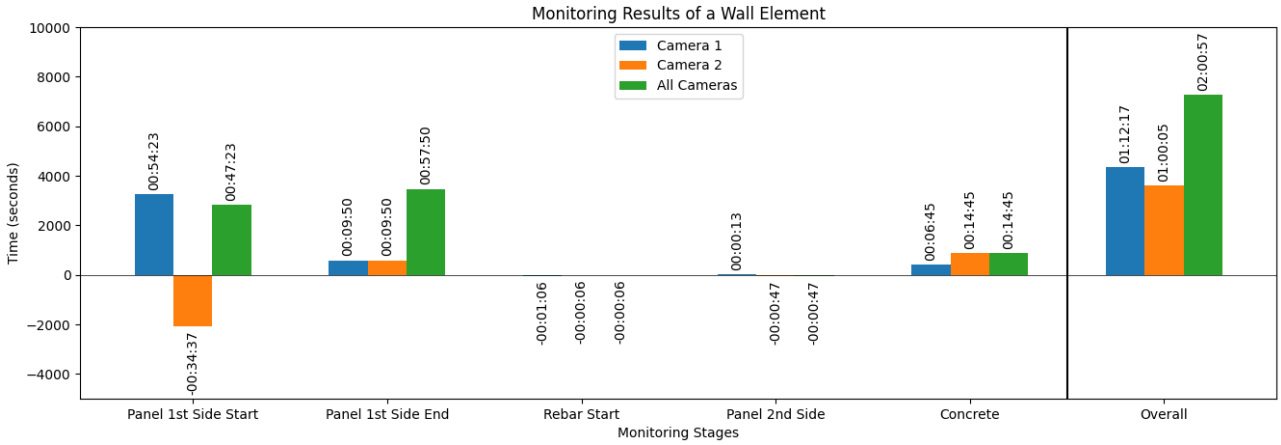


Figure 2: In-depth monitoring results of a wall element

used for detecting element specific progress milestones. The element-wise best suited upper threshold varied highly: Especially for partially occluded elements, a conservative threshold like the median of all examples of 75% seemed practical. However, most studied examples generated precise results with a minor lower threshold of 5%-10%. Over all samples, a smaller averaging interval of 5 to 10 minutes generated the best results as errors could be compensated, and a certain level of accuracy was maintained. This configuration of parameters poses a likely combination to work for monitoring arbitrary construction elements and is used in the following studies.

The generated as-built representations for slabs showed very high accuracy of 96.47% correctly colored pixels. It must be pointed out that one stairwell platform rendered insufficient results because of its different base height.

An tolerable error of 18.51% was achieved for the wall elements. This was primarily due to the fact that in the model-generated images, some elements that should be at the bottom appeared higher due to the limitations in pixel precision.

Higher errors of 61.12% for column elements were encountered as a result of the height conversion problem and the column's smaller mask area.

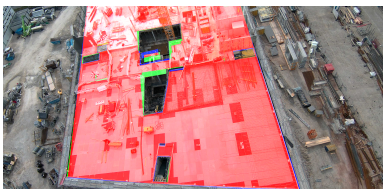

Figure 3: Slab elements

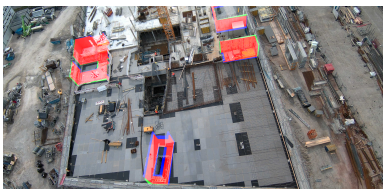

Figure 4: Wall elements

Figure 5: Column elements

The resulting differences between detected and as-built timestamps for the eight closer investigated elements passed through the end-end pipeline are shown in Table 2. A positive value indicates the

detected event occurring earlier than the actual one. Additionally, all samples are color-coded with entries below 15 minutes appearing in green, below 24 hours in orange and higher than 24 hours in red. Unsuccessful tests are shown with a grey background.

Table 2: Examples for determining the accuracy

| Event | Slab 1 | Slab 2 | Wall 1 | Wall 2 | Wall 3 | Column 1 | Column 2 | Column3 |
|---|---|---|---|---|---|---|---|---|
| Panel Start | 00:11:13 | 00:00:00 | >1day | >1day | 03:50:08 | >1day | -23:57:45 | -01:43:36 |
| Panel End | -14:36:13 | >1day | 00:01:06 | -00:08:45 | 00:57:50 | - | 00:15:35 | >1day |
| Rebar Start | >1day | 03:07:34 | - | - | -00:01:06 | -00:00:13 | 00:06:02 | 02:06:20 |
| Rebar End | -00:08:40 | -22:39:57 | - | - | -20:26:46 | - | - | - |
| Concrete Start | >1day | 01:40:40 | >1day | >1day | >1day | -00:00:41 | -00:00:44 | -00:01:48 |
| Concrete End | 00:00:10 | - | 00:00:40 | 00:07:43 | 00:14:15 | - | - | - |

Unlike the positive outcomes depicted in Figure 2, challenges were encountered in identifying the completion times for the rebar stages of wall elements and both rebar and concrete completion events for column elements. Timestamps for panel phases, however, were detected more accurately. Similar observations were made for all examined elements despite using fixed parameters based on identical thresholds and averaging intervals. The underlying reasons and possible fixes for these inaccuracies are discussed below.

## 5 Discussion

Our method demonstrated sufficient results in precisely measuring fine-granular phases of construction progress using sequential on-site images and fusing it with as-built data. While the overall performance of this approach proved to be promising, some limitations were noted:

The elaborated monitoring methodology could not detect the completion of rebar works correctly. As the segmentation-based approach identifies an area as 100% completed once a single layer has been installed, the two necessary directional layers per side could not be monitored. Additionally, the completion of concreting for walls and columns is only detected once the formwork is removed and concrete-labeled pixels are visible in the proposed camera setup. Prior limitations can be addressed by exploring additional monitoring techniques increasing the level of detail [4], [14]. The perspective transformation method's inaccuracies can be approached using referenced on-site markers. A future investigation of this method sourced from laser-scanning [15] and its application to semantic segmentation would be desirable.

Figure 6 highlights noisy results stemming from a slab with detected *panel*, *rebar*, or *concrete* timestamps at the same time in different sections of the element. These noisy results were caused by a lack of details in the as-built model, e.g., missing reinforcement sections. Specific modeling rules are necessary to represent the element accurately in all phases.

Finally, inaccuracies coming from bad lighting conditions and occlusions could not be compensated for small elements. Moreover, camera sway from crane movements affected detection accuracy. On-site markers for dynamic perspective transformation could mitigate this issue.

While there has been exhaustive work in construction progress monitoring, our approach differs from existing work as follows: In contrast to [10], progress tracking beyond one element (pre-cast walls) is demonstrated here. The in-depth analysis of slabs and pillars highlighted additional challenges and

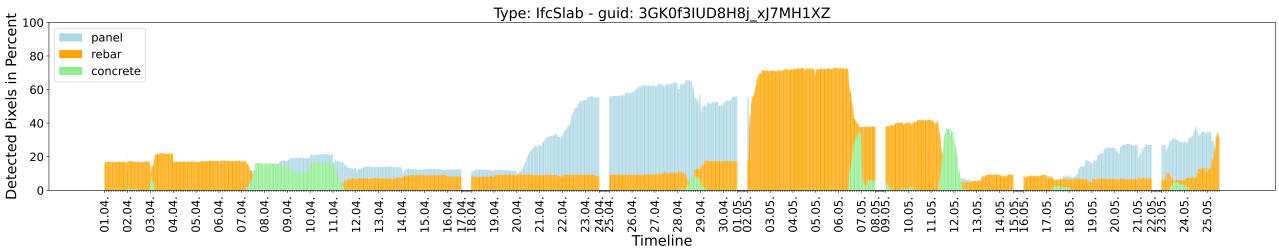


Figure 6: Evaluation of a slab in the second building floor with noisy results

requirements for precise monitoring. Fine-granular monitoring allowed a comprehensive understanding of the construction process, necessary for efficient and effective on-site resource allocation. This approach overcomes the uncertainties that arise from unordered photographs [8] through the use of an averaging algorithm. This algorithm not only smooths out the variations in the data but also provides a more accurate representation of the overall progress, enhancing the reliability of our results. While [7] has shown an innovative approach to monitor not only the construction progress but also the activity-level progress details, a lot of processing steps and computational resources were necessary to achieve these details. We demonstrate that similar results can be gained using a much simpler prediction pipeline based on image level. This underscores the need for further exploration of diverse monitoring methodologies to identify practical approaches for the task at hand.

## 6 Conclusion

This paper presented a novel approach to automating progress monitoring of cast-in-place concrete slabs, walls, and columns, extracting information directly from image data and enhancing it through as-built details. For this task, algorithms for evaluating element-specific construction progress timestamps and procedures for coupling the obtained information with as-built models have been proposed. With the integration of different averaging approaches, robust performance with high precision was proven in case studies concerning the specific parts of the elaborated framework and the whole end-to-end approach. In contrast to many other studies, the suitability of the proposed methodology on real-world construction sites has been thoroughly analyzed. In conclusion, the approach demonstrated practical applicability and potential for supporting on-site management toward higher productivity.

## Acknowledgements

We thankfully acknowledge Innovationsmanagement Bau GmbH for their financial support and for providing us access to multiple construction sites to collect valuable data.

## References

[1] R. Agarwal, S. Chandrasekaran, and M. Sridhar, *Imagining construcion's digital future*, Singapur, Jun. 2016. [Online]. Available: https://www.mckinsey.com/~/media/mckinsey/business%20functions/operations/our%20insights/imagining%20constructions%20digital%20future/imagining-constructions-digital-future.pdf.

[2] K. Mostafa and T. Hegazy, “Review of image-based analysis and applications in construction”, *Automation in Construction*, vol. 122, 2021. DOI: 10.1016/j.autcon.2020.103516.

[3] R. Sacks, I. Brilakis, E. Pikas, H. S. Xie, and M. Girolami, “Construction with digital twin information systems”, *Data-Centric Engineering*, vol. 1, 2020. DOI: 10.1017/dce.2020.16.

[4] J. Yang, M.-W. Park, P. A. Vela, and M. Golparvar-Fard, “Construction performance monitoring via still images, time-lapse photos, and video streams: Now, tomorrow, and the future”, *Advanced Engineering Informatics*, vol. 29, no. 2, pp. 211–224, 2015. DOI: 10.1016/j.aei.2015.01.011.

[5] S. Ghosh, N. Das, I. Das, and U. Maulik, “Understanding deep learning techniques for image segmentation”, *ACM Computing Surveys*, vol. 52, no. 4, pp. 1–35, 2020. DOI: 10.1145/3329784.

[6] J. Schlenger, F. Pfitzner, A. Braun, S. Vilgertshofer, and A. Borrmann, “Digitaler zwilling baustelle – baustellenüberwachung zur automatisierten zeit– und kostenkontrolle”, *Bautechnik*, vol. 100, no. 4, pp. 190–197, 2023. DOI: 10.1002/bate.202300005.

[7] A. Pal, J. J. Lin, S.-H. Hsieh, and M. Golparvar-Fard, “Activity-level construction progress monitoring through semantic segmentation of 3d-informed orthographic images”, *Automation in Construction*, vol. 157, 2024. DOI: 10.1016/j.autcon.2023.105157.

[8] K. C. Laxman, N. Tabassum, L. Ai, C. Cole, and P. Ziehl, “Automated crack detection and crack depth prediction for reinforced concrete structures using deep learning”, *Construction and Building Materials*, vol. 370, 2023. DOI: 10.1016/j.conbuildmat.2023.130709.

[9] F. Pfitzner, A. Braun, and A. Borrmann, “From data to knowledge: Construction process analysis through continuous image capturing, object detection, and knowledge graph creation”, *Automation in Construction*, vol. 164, Aug. 2024. DOI: 10.1016/j.autcon.2024.105451.

[10] Z. Wang, Q. Zhang, B. Yang, *et al.*, “Vision-based framework for automatic progress monitoring of precast walls by using surveillance videos during the construction phase”, *Journal of Computing in Civil Engineering*, vol. 35, no. 1, 2021. DOI: 10.1061/(ASCE)CP.1943-5487.0000933.

[11] F. Friedl, “Bim-based progress monitoring using 2d semantic segmentation”, M.S. thesis, Technische Universität München, Apr. 2024.

[12] J. Xu, Z. Xiong, and S. P. Bhattacharyya, *Pidnet: A real-time semantic segmentation network inspired by pid controllers*, 2023. arXiv: 2206.02066. [Online]. Available: https://arxiv.org/abs/2206.02066.

[13] D. A. Forsyth and J. Ponce, *Computer Vision: A Modern Approach*, 2. Auflage. Harlow: Pearson Education, 2012.

[14] F. Pfitzner, A. Braun, and A. Borrmann, “Object detection-based knowledge graph creation: Enabling insight into construction processes”, in *Computing in Civil Engineering 2023*, Y. Turkan, J. Louis, F. Leite, and S. Ergan, editors, Reston: American Society of Civil Engineers, 2024, pp. 186–193. DOI: 10.1061/9780784485224.023.

[15] L. Cheng, S. Chen, X. Liu, *et al.*, “Registration of laser scanning point clouds: A review”, *Sensors (Basel, Switzerland)*, vol. 18, no. 5, 2018. DOI: 10.3390/s18051641.

# Teil V

# Organization, Management, & Linked Builing Data

# Berücksichtigung von Nutzeranforderungen bei der Planung von ÖPNV-Trassen: Eine Methode zur objektiven Bewertung und Empfehlungen im Kontext von Haltestellenstandorten

Helena Hamann[1], Felix Petre[2]; Martin Wogan[1, 3]

[1]B/M Consult, Lampestraße 3, 38114 Braunschweig, Germany

[2]Institut für Verkehr und Stadtbauwesen, TU Braunschweig, Hermann-Blenk-straße 42, 38108 Braunschweig, Germany

[3]Institut für Bauinformatik, TU Dresden, Nürnberger Str. 31a, 01187 Dresden, Germany

E-Mails: martin.wogan@bmconsult.de

**Abstract:** Die Planung von ÖPNV-Trassen im urbanen Raum unterliegt einer Vielzahl von technischen und gesetzlichen Rahmenbedingungen. Zusätzlich müssen Anforderungen der zukünftigen Nutzer über den gesamten Projektablauf berücksichtigt werden, auch wenn diese nicht durch Regelwerke und Gesetze klar definiert sind. Die Aufgabe des Ingenieurs besteht darin, alle an das Projekt gestellten Anforderungen zu ordnen, zu bewerten und Handlungsempfehlungen z. B. in Form von Plänen, Modellen, Berichten und Präsentationen für den Auftraggeber und in allgemeinverständliche Form für die zukünftigen Nutzer zu formulieren. Die Berücksichtigung einer Vielzahl von Nutzergruppen mit unterschiedlichen Anforderungen bei der Bewertung ist hierbei ein nicht zu vernachlässigender Bearbeitungsschritt. In dieser Arbeit wurden dafür die Standortbestimmungen von ÖPNV-Haltestellen im Kontext von Nutzergruppen untersucht und eine Methode entwickelt, um objektive Bewertungen und Handlungsempfehlungen für die Platzierung zu erzeugen. Das langfristige Ziel der Autoren ist es, eine individuell anpassbare Mobilitätsbewertungsplattform (MBPF) zu entwickeln. Die MBPF ist dabei eine Plattform, die es ermöglicht, an einem beliebigen Standort die Erreichbarkeit von Zielorten (Points of Interest, POI) zu berechnen und zu bewerten.

Keywords: Mobilitätsbewertungsplattform (MBPF), OpenStreetMap, Synthetische Population, ÖPNV, Point of Interest (POI)

Erschienen in Tagungsband 35. Forum Bauinformatik 2024, Hamburg, Deutschland, DOI: 10.15480/882.13495
© 2024 Das Copyright für diesen Beitrag liegt bei den Autoren. Verwendung erlaubt unter Creative Commons Lizenz Namensnennung 4.0 International.

# 1 Einleitung

Der öffentliche Personennahverkehr (ÖPNV) wird als Basis einer nachhaltigen innerstädtischen Mobilität angesehen, da dieser anderen Verkehrsmitteln hinsichtlich Leistungsfähigkeit (Transportkapazität) und Umweltbilanz, bei guter Auslastung, deutlich überlegen ist [1]. Eine nachhaltige Verkehrswende gelingt daher nur mit einem attraktiven und qualitativ hochwertigen ÖPNV [2]. Die Attraktivität und Qualität des ÖPNV-Angebots bedarf einer gezielten Förderung [3, 4] um eine gezielte Erweiterung zur Aufrechterhaltung und Verbesserung des aktuellen Angebotes [3] zu erreichen. Damit die Qualität und Attraktivität für unterschiedliche Nutzergruppen bereits in der Planung sichergestellt werden kann, fehlt es den Planern aus Sicht der Autoren aktuell an einer Methode, die nutzergruppenspezifische Anforderungen (nsA) an den ÖPNV zu berücksichtigt.

Die Mobilität ist ein Grundbedürfnis jedes Einzelnen. Mobilität ist hierbei der physische Bewegungsvorgang zwischen verschiedenen Standorten [5]. Jeder möchte über den Tag verschiedene Ziele, im Weiteren Points of Interest (POIs) genannt, erreichen, woraus sich individuelle Wegeketten jedes Einzelnen über einen betrachteten Zeitraum zusammensetzen [6]. Eine besondere Bedeutung haben hierbei die Umsteigeknoten in den Wegeketten, die Haltestellen des ÖPNV. Diese gilt es attraktiv und komfortabel z. B. durch Schutz vor Hitze oder Regen [7] zu gestalten, aber auch in ihrer Lokalität optimal zu verorten [8]. Die nsA bilden die Grundlage zur Bestimmung von Wegeketten und deren Optimierung im Kontext von Haltestellengestaltung, -platzierung und optimalen ÖPNV-Routen [9].

Die vorgestellte Methode ist ein Baustein für die Entwicklung einer Mobilitätsbewertungsplattform (MBPF). In der MBPF sollen zukünftig die im Planungsprozess von Infrastrukturprojekten zu berücksichtigenden nsA zusammengefasst werden und zur Verbesserung der Planungsergebnisse führen [10].

Um die nsA der verschiedenen Nutzergruppen in der MBPF abzubilden, müssen detaillierte Eigenschaften der Bevölkerung im Untersuchungsraum bekannt sein. Diese Daten sind jedoch in der Regel nur stark aggregiert verfügbar. Eine Methode zur disaggregierten Rekonstruktion dieser Daten, die teilweise bei agentenbasierten Verkehrsmodellen genutzt wird [11], ist die Erstellung einer synthetischen Bevölkerung. Hierbei werden verschiedene Informationsquellen kombiniert, um eine repräsentative Bevölkerung auf Haushaltsebene zu erstellen, die für weitere Berechnungen verwendet werden kann. Ein fortschrittlicher Population Synthesizer ist das Tool "PopulationSim", eine Programmbibliothek, die als Teil des ActivitySim Verkehrsnachfragemodells entwickelt wurde [12]. Hierbei werden Kontrollmerkmale wie Alter und Geschlecht verwendet, um die Eigenschaften der Bevölkerung in einem bestimmten geographischen Rahmen widerzuspiegeln. Die Verbindung von POIs, synthetischer Population und nsA sind im Kontext der Mobilitätsbewertung (Abbildung 1) neu und wurden bisher nicht genutzt, beinhalten aber ein großes Potentiale für die Planung.

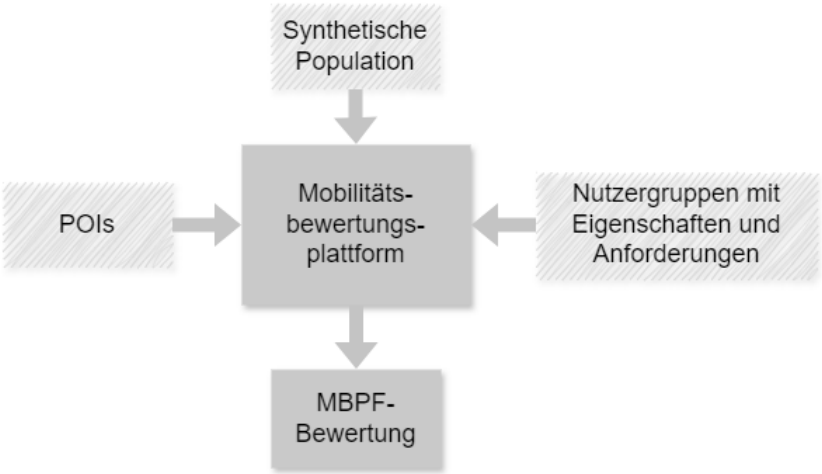


Abbildung 1: Überblick MBPF Schema

# 2 Stand der Praxis

Für die ÖPNV-Planung gelten verschiedene Gesetze, Verordnungen und Empfehlungen. Aus den hier wichtigsten Regelwerken ergeben sich folgende Vorgaben für die ÖPNV-Haltestellen und deren Platzierung:

- Sicherer und ordnungsgemäßer Betrieb muss gewährleistet sein [13,14, 15, 16]
- Kurze, ansprechende Zugangs- und Reisezeiten sowie eine Minimierung externer Störungseinflüsse (bestimmen Attraktivität und Qualität) [1]
- Barrierefreiheit ist bei der ÖPNV-Planung verpflichtend [1, 17]
- Haltestellen als „Visitenkarte des ÖPNV“ [1]
- Haltestellenabstand für optimale Reisegeschwindigkeit (wichtige Anforderung) [1]
- Es hat sich bewährt, Haltestellen an Kreuzungen/Knotenpunkten anzuordnen [1]
- In der Regel werden Haltestellenkaps empfohlen (Ausnahmen: Pausenzeiten, Schülerverkehr (Sicherheit) oder Abwarten von Anschlüssen vorgesehen) [1]

Eine Unterscheidung in verschiedene Nutzergruppen sowie eine detaillierte Betrachtung der nsA findet in den Regelwerken, abgesehen von der Sicherheit von Schülern und der Barrierefreiheit für Menschen mit Mobilitätseinschränkungen, keine Erwähnung. Die nsA von Fahrgästen werden nur allgemein benannt und bieten keine hinreichende Grundlage für die MBPF.

## 2.1 Unterscheidung von Bewertungsverfahren von Haltestellen

### 2.1.1 Haltestellenqualitäts-Bewertungsverfahren

Die Verfahren zur Bewertung von Haltestellen unterscheiden sich zwischen den jeweiligen Infrastrukturanbietern und basieren auf einem vergleichbaren Muster. In den meisten Bewertungsverfahren wird der Bestand bei einer Vorortbesichtigung auf einer Punkteskala bewertet und anschließend

mit Gewichtungen verrechnet. Daraus errechnet sich eine Gesamtnote, die sich aus einer unterschiedlichen Anzahl von Teilnoten ergeben kann. Hierbei werden z. B. die Sauberkeit der Haltestelle, die vorhandenen Einrichtungen wie Uhren und Infotafel sowie deren Zustand erfasst. Es findet somit nur eine Bewertung des Ist-Zustandes statt, der helfen soll, einen optimalen Ist-Zustand zu erreichen bzw. zu erhalten. [18]

### 2.1.2 Standort-Bewertungsverfahren

Eine Vorgabe zur Bewertung der Haltestellenstandorte konnte in der Recherche nicht gefunden werden. In den Gesetzen, Verordnungen und Empfehlungen für den ÖPNV, werden die Interessen von Fahrgästen im Kontext von Haltestellen nur in allgemeiner Form und ohne die Betrachtung unterschiedlicher Nutzergruppen berücksichtigt. Es werden keine konkreten Vorgaben zur Platzierung von Haltestellen gemacht, sondern nur eine Empfehlung zur Platzierung an Kreuzungen ausgesprochen [1].

## 3 Methode

Die Wegekette eines Nutzers setzt sich aus POIs zusammen, die je nach nsA unterschiedlich oft frequentiert werden. Eine Ansammlung von POIs, die möglichst viele nsA bedienen, könnte somit einen guten Standort für eine Haltestelle darstellen. Gleichzeitig wird angenommen, dass auch ein POI der in vielen nsA erwähnt wird, ein guter Haltestellenstandort sein könnte, da viele unterschiedliche Personengruppen den POI erreichen wollen. Es gilt somit POIs, nsAs und Wegeketten zu kombinieren und auszuwerten, um Rückschlüsse auf optimale Haltestellenstandorte zu erhalten. In vorherigen Untersuchungen hat sich gezeigt, dass die nsA und damit verbunden individuellen Wegeketten schwer zu ermitteln sind. Es mussten daher Annahmen in Bezug auf die Benutzergruppen getroffen werden, die es weiter zu verifizieren gilt. Hierfür wurde eine Basismatrix auf Grundlage von Expertengesprächen und Vor-Ort-Beobachtungen entwickelt. Diese Basismatrix wird fortlaufend durch z. B. Befragungen bei Bürgerbeteiligungen um nsAs, POIs und den entsprechenden Knotenverbindungen ergänzt. Implementierungen in Graphen und Ontologien sind in Arbeit.

### 3.1 Mobilitätsbewertungsplattform (MBPF)

Die konzeptionellen Ursprünge einer MBPF wurden im Rahmen der Veröffentlichung Hasselberg et al. [19] entwickelt. Dabei ging es um die Fragestellung, ob anhand von POIs die Fahrradtauglichkeit für die innerstädtische Verkehrsplanung basierend auf OpenStreetMap (OSM) Datensätzen analysiert und mittels Web-Visualisierung Planern (Abbildung 2) zur Verbesserung des Planungsprozess und somit von Planungsergebnissen genutzt werden kann. Die technische Machbarkeit konnte in der Veröffentlichung gezeigt werden. Als Weiterentwicklungsmöglichkeiten wurde die Einbeziehung der nsA identifiziert. Zudem wurde die Entwicklung eines zusätzlichen Moduls zur Bewertung von ÖPNV-Haltestellen angeregt.

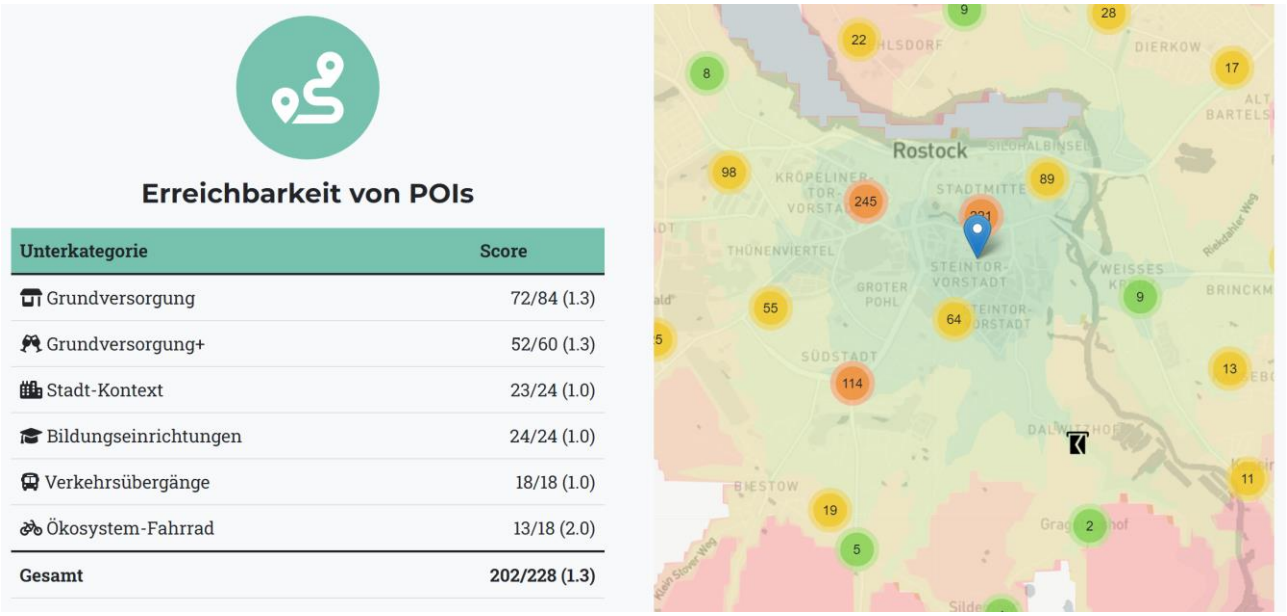

**Erreichbarkeit von POIs**

| Unterkategorie | Score |
|---|---|
| Grundversorgung | 72/84 (1.3) |
| Grundversorgung+ | 52/60 (1.3) |
| Stadt-Kontext | 23/24 (1.0) |
| Bildungseinrichtungen | 24/24 (1.0) |
| Verkehrsübergänge | 18/18 (1.0) |
| Ökosystem-Fahrrad | 13/18 (2.0) |
| **Gesamt** | **202/228 (1.3)** |



Abbildung 2: Erreichbarkeit von POIs nach Hasselberg

## 3.2 Nutzergruppen / POIs

Eine Berücksichtigung von Nutzergruppen sowie der nsA wird als wichtig erachtet, da nur eine effektivere und inklusive Transportplanung durch eine transparente und methodisch fundierte Erfassung von Nutzerbedürfnissen erreicht werden kann, was letztlich zu einem besseren, an die tatsächlichen Bedürfnisse der Nutzer angepassten ÖPNV führen wird [8].

Die betrachteten ÖPNV-Nutzergruppen sind, angelehnt an [20], in Abbildung 3 dargestellt. Diese Darstellung beinhaltet nur einen kleinen Ausschnitt der Nutzergruppen und eine exemplarische Auswahl an Verbindungen zwischen Nutzergruppen und potenziell häufig besuchter POIs. Eine Erweiterung auf eine unbegrenzte Anzahl von Nutzergruppen sowie die Faktoren der Vermischung (Nutzer ist morgens Arbeitnehmer, nachmittags Freizeitnutzer) wurden in der MBPF berücksichtig.

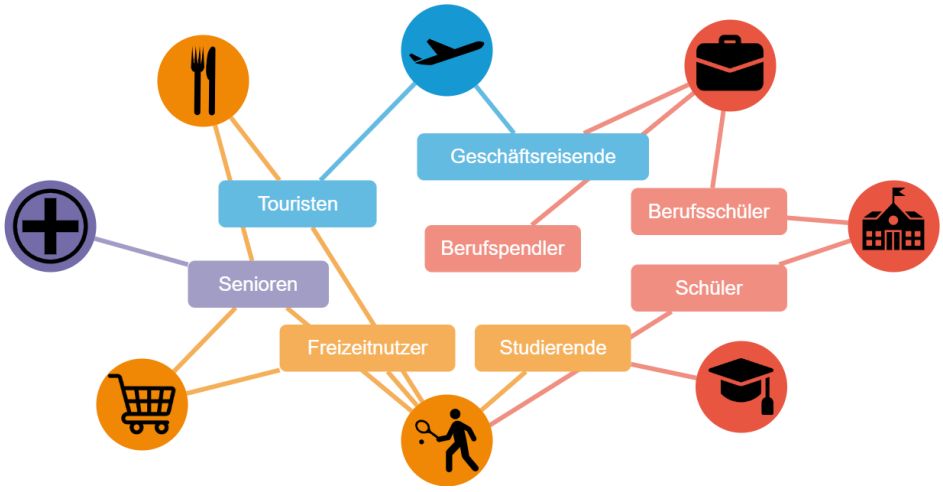



Abbildung 3: Exemplarische POIs für unterschiedliche Nutzergruppen

### 3.3 Synthetische Bevölkerung

Zur Erstellung der synthetischen Bevölkerung nutzt die MBPF den population synthesizer “PopulationSim”. Da PopulationSim alleinstehend sehr aufwändig und komplex nutzbar ist, wurde ein “preprocessor” entwickelt, der die Nutzung weitestgehend automatisiert. Als Grundlage wird hier der Zensus, die “Mobilität in Deutschland” (MiD), und öffentlich verfügbare stadtteil- und stadtweite Daten genutzt. Die entwickelte Methodik liefert eine sehr gute Abbildung der Bevölkerung, insofern Daten in ausreichender Qualität vorliegen [21].

Mithilfe des hier genutzten Ansatzes können Modellbevölkerungen für einen beliebigen Planungsraum in Deutschland flexibel und leicht anpassbar auf die jeweilige Datenverfügbarkeit erstellt werden und so Nutzergruppen zuverlässig erfasst werden.

### 3.4 Haltestellenstandortbewertung

Die Grundlage der Methode bildet die Bewertung auf Basis von realen fußläufigen Entfernungen. Dies konnte bereits in der von Hasselberg [19] beschriebenen Plattform automatisiert durchgeführt werden. Mit geringem Aufwand kann so die reale fußläufige Entfernung inklusive Topografie in der Einheit Minuten bestimmt werden. Bei der Methode wird bewusst auf die Nutzung von Scores verzichtet, weil diese Rohdaten "verschatten", indem sie wichtige Details verdecken. Außerdem führt eine Gewichtung der Daten zu Verzerrungen und einem möglichen Bias. Aufgearbeitete Rohdaten hingegen bieten in der Praxis einen viel größeren Nutzen, da sie eine detaillierte und präzise Analyse ermöglichen, die zu fundierteren Entscheidungen führt. Außerdem werden folgende Faktoren berücksichtigt:

- Einbindung von Bevölkerungsdaten und demografischer Entwicklung (Synthetische Bevölkerung)
- Differenzierung von verschiedenen Nutzergruppen und deren Ansprüchen (nsA)
- Berücksichtigung von lokalen Besonderheiten durch Nutzung von POIs aus OSM
- Kontinuierliches Lernen aus Nutzereingaben (z. B. Beliebtheit von POIs)

Als Ergebnis werden dem Nutzer aufbereitete, standortabhängige Daten wie die Reisedauer zu verschiedenen POIs, die Zuwegedauer zu Haltestellenstandorten für verschiedene Nutzergruppen ausgegeben. Insbesondere das Empfinden über die Erreichbarkeit aufgrund einer Wegstrecke ist hochgradig subjektiv und muss somit auf nsA hin untersucht und unterschieden werden. Aktuell beruhen die Berechnungen auf standardisierten Annahmen für die Gehgeschwindigkeit, perspektivisch lässt sich diese aber nutzergruppenspezifisch abbilden.

## 4 Zusammenfassung / Ausblick

Im Hinblick auf das Thema Planungstransparenz kann die MBPF einen wichtigen Beitrag leisten. Durch die Möglichkeit einer Plattform sinkt die Wahrscheinlichkeit, dass Nutzergruppen „vergessen” werden oder besondere nsA von Planern ungewollt „übersehen” werden.

Im nächsten Schritt muss die Methode weiter verfeinert und in einfach nutzbaren Softwareapplikationen umgesetzt werden. Eine Anbindung des Prototypen an weitere Datenbanken ist in Bearbeitung und soll es zukünftig ermöglichen, durch offene Schnittstellen weiter an Intelligenz zu gewinnen. Weiter fehlt es dem Prototypen noch an Untersuchungen zur Usability, einer potentiellen Plattformumgebung sowie einer visuellen Aufbereitung, die allgemeinverständlich von allen Nutzern verständlich ist.

Aktuell wird an der Entwicklung von weiteren Features wie die Einbindung von verkehrsmittelübergreifenden Wegeketten gearbeitet. Perspektivisch soll eine direkte Anbindung an Planungstools erfolgen. Dies soll zukünftig die beschriebene sofortige Auswertung und Ergebnisanzeige im Planungsprozess liefern, ohne über Drittsoftware den Arbeitsprozess unterbrechen zu müssen.

## Referenzen

[1] Forschungsgesellschaft für Straßen- und Verkehrswesen. Empfehlungen für Anlagen des öffentlichen Personennahverkehrs: EAÖ. Bd. 289. FGSV. Köln: Forschungsgesellschaft für Straßen- und Verkehrswesen, op. 2013.

[2] Verkehrsverbund Rhein-Ruhr (VRR), Hrsg. Gemeinsam. Nachhaltig. Mobil. https://www.vrr.de/de/der-vrr/nachhaltigkeitsagenda/, [Letzter Zugriff: 20.05.2024].

[3] Umweltbundesamt, Hrsg. Klimaschutz im Verkehr. https://www.umweltbundesamt.de/themen/verkehr/klimaschutz-im-verkehr#umweltverbund, [Letzter Zugriff: 25.05.2024].

[4] Bundesministerium für Digitales und Verkehr, Hrsg. Überblick: Klimaschutz im Verkehr.https://bmdv.bund.de/DE/Themen/Mobilitaet/Klimaschutz-im-Verkehr/Ueberblick/ueberblick.html, [Letzter Zugriff: 25.04.2024].

[5] Handwörterbuch der Raumforschung und Raumordnung. 4., neu bearb. Aufl. Hannover: Akademie für Raumforschung, 2005, S. 655.

[6] Arbeitsgruppe Verkehrsplanung. Multi- und Intermodalität: Hinweise zur Umsetzung und Wirkung von Maßnahmen im Personenverkehr. Hrsg. von Forschungsgesellschaft für Straßen- und Verkehrswesen. https://www.fgsv.de/fileadmin/gremien/ak_128/Teilpapier_1_Definitionen.pdf, [Letzter Zugriff: 15.04.2024].

[7] F. Körner, N. Sievers, and B. Ehrenholz, „ÖPNV-Haltestellen an Extremwetterereignisse anpassen − Erarbeitung eines Konzepts," Der Nahverkehr, vol. 09/2023, pp. 12-14, 2023.

[8] R. Hrelja and H. Antonson, 'Handling user needs: methods for knowledge creation in Swedish transport planning', Eur. Transp. Res. Rev., vol. 4, no. 3, pp. 115–123, Sep. 2012.

[9] J. M. A. M. Ramos, V. G. J. Almeida, H. S. Santana, T. R. M. Braga Silva, and F. A. Silva, 'User-centered analysis of a safe bus routing strategy', JISA, vol. 14, no. 1, pp. 84–94, Jun. 2023.

[10] O. Manambelona, 'Anwendungsorientierte Prüfung der interaktiven parameterbasierten Planung und Bewertung von Radwegen in urbanen Räumen'. Oct. 23, 2023.

[11] B. Fabrice Yaméogo, P. Gastineau, P. Hankach, und P.-O. Vandanjon, „Comparing Methods for Generating a Two-Layered Synthetic Population“, Transp. Res. Rec. J. Transp. Res. Board, Bd. 2675, Nr. 1, S. 136–147, Jan. 2021.

[12] B. M. Paul, J. Doyle, B.Stabler, J Freedman, and A. Bettinardi, “Multi-level Population Synthesis Using Entropy Maximization-Based Simultaneous List Balancing,” *Transportation Research Board 97th Annual MeetingTransportation Research Board,* 2018.

[13] Allgemeines Eisenbahngesetz: AEG, https://www.gesetze-im-internet.de/aeg_1994/AEG.pdf, [Letzter Zugriff: 01.04.2024], 1993.

[14] Eisenbahn-Bau- und Betriebsordnung: EBO, https://www.gesetze-im-internet.de/ebo/EBO.pdf, [Letzter Zugriff: 01.04.2024], 1967.

[15] Verordnung über den Bau und Betrieb der Straßenbahnen: BOStrab, https://www.gesetze-im-internet.de/bgg/BGG.pdf, [Letzter Zugriff: 01.04.2024] 1987.

[16] Verordnung über den Betrieb von Kraftfahrunternehmen im Personenverkehr: BOKraft, https://www.gesetze- im- internet.de/bokraft_1975/BOKraft.pdf, [Letzter Zugriff: 01.04.2024] 1975.

[17] Personenbeförderungsgesetz: PBefG, https://www.gesetze- im- internet.de/pbefg/PBefG.pdf, [Letzter Zugriff: 01.04.2024] 1961.

[18] S. Jagdhuhn, “35. Qualitatskontrolle an den Bahnstationen in Schleswig-Holstein: Ergebnisbericht Winter 2018/2019”, In: (2019) https://www.nah.sh/assets/downloads/Bericht-QK35-Winter-2018.pdf, [Letzter Zugriff: 24.05.2024], S. 2–25.

[19] J. Hasselberg, M. Berger, and M. Wogan, *Microservice-basierte Analyse und Web-Visualisierung zur Fahrradtauglichkeit für die innerstädtische Verkehrsplanung*. DE: Wichmann Verlag, 2023. Accessed: Dec. 11, 2023. [Online]. Available: https://doi.org/10.14627/537742013.

[20] J. Zwiers, S. Behrendt, L Büttner, I. Kollosche, C. Scherf, S. Mader, and W. Schade, Wandel des öffentlichen Verkehrs in Deutschland: Veränderung der Wertschöpfungsstrukturen durch neue Mobilitätsdienstleistungen : eine Transformationsanalyse aus der Multi-Level-Perspektive. Bd. Nr. 451 (Januar 2021). Study/ Hans-Böckler-Stiftung. Düsseldorf: Hans-Böckler-Stiftung, 2021, S. 37.

[21] F. Bigi, T. H. Rashidi, F. Viti, Synthetic Population: A Reliable Framework for Analysis for Agent-Based Modeling in Mobility. Transportation Research Record, 2024, Available: https://doi.org/10.1177/03611981241239656

# Integration of Multi-Criteria Decision-Making in Heritage Building Information Management

Laura Fernandez Resta[1]
[1]Professorship for Design and Analysis of Structures, HafenCity University Hamburg,
Henning-Voscherau-Platz 1, 20457 Hamburg, Germany
E-mail(s): laura.resta@hcu-hamburg.de

**Abstract:** This paper proposes a theoretical framework that integrates Heritage Building Information Management (HBIM) with Multi-Criteria Decision-Making (MCDM) techniques, to improve decision-making processes in the field of heritage conservation. The proposed framework employs the detailed semantic and geometric data provided by HBIM to evaluate and prioritize conservation strategies based on multiple criteria, including historical significance, architectural integrity, economic viability, social relevance, and environmental impact. The combination of both methodologies has the potential to not only technically improve heritage conservation but also facilitate informed and transparent decision-making processes by allowing stakeholder participation, balancing competing priorities, and achieving sustainable conservation outcomes. This study lays the foundation for a comprehensive, dynamic, and adaptive decision-making workflow that addresses the complicated challenges of heritage conservation.

*Keywords:* HBIM, MCDM, decision-making, heritage preservation

Erschienen in Tagungsband 35. Forum Bauinformatik 2024, Hamburg, Deutschland, DOI: 10.15480/882.13488
© 2024 Das Copyright für diesen Beitrag liegt bei den Autoren. Verwendung erlaubt unter Creative Commons Lizenz Namensnennung 4.0 International.

## 1 Introduction

Heritage sites hold significant value in terms of history, education, and science, as they provide insight into human ingenuity, craftsmanship, and cultural integrity. Heritage conservation is increasingly regarded as a component of sustainable development [1], in alignment with the principles of the circular economy. This is achieved through the responsible conservation and adaptation of historic structures, which entails maintaining their physical integrity and ensuring the preservation of their cultural and historical significance. In comparison to new construction, heritage conservation often has a lower environmental impact [2].

Effective heritage conservation necessitates a multidisciplinary approach that engages various stakeholders [2], [3], including conservationists, architects, historians, and the local community [4]. This collaborative process must consider historical, cultural, social, and environmental factors while navigating uncertainties and balancing competing interests to achieve long-term conservation goals [5],

[6]. However, decision-making in this context is often constrained by the complexity and diversity of the factors involved.

This paper explores the integration of Heritage Building Information Management (HBIM) [7] and Multi-Criteria Decision-Making (MCDM) techniques to enhance decision-making processes in heritage conservation. While HBIM offers a dynamic representation of historic buildings, MCDM provides the tools to evaluate different conservation strategies based on various criteria. This integration creates a comprehensive framework to optimize heritage conservation decisions, facilitate collaboration between stakeholders, and promote transparency in the decision-making process.

## 2 State-of-the-Art

The conservation of historic buildings has traditionally been approached through a process of option prioritization and efficient resource allocation, with a reliance on expert judgment and qualitative assessments. However, in recent years, there has been a growing interest in the integration of quantitative approaches, such as MCDM [8], which is seen as offering the potential to systematize and streamline the decision-making process [9].

MCDM techniques have been employed in various fields, including engineering, environmental science, and public policy, for the evaluation of alternatives based on multiple criteria [8]. In the field of heritage conservation, MCDM has been employed to evaluate the significance of historic buildings, select adaptive reuse options, and assess the impact of interventions [9]. Studies have demonstrated the efficacy of MCDM in facilitating transparent and informed decision-making, balancing competing objectives, and promoting stakeholder involvement [2], [4].

In the construction industry, Building Information Modeling (BIM) has become a cornerstone for improving project outcomes through enhanced visualization, collaboration, and data management. However, as the scope of BIM has expanded to encompass a broader range of functions, many in the field now refer to it as Building Information Management [10]. Recent developments in integrating MCDM with BIM [11] have further facilitated decision-making processes in construction activities, risk management, and sustainability assessment [6]. The evolution of BIM towards HBIM, specifically tailored for heritage buildings, has opened new avenues for applying MCDM to heritage conservation. HBIM models provide a digital representation of historic buildings, capturing both their physical and historical attributes [1], [3], [5], [11], which can be analyzed using MCDM techniques to evaluate conservation alternatives.

The integration of MCDM with HBIM is still in its early stages, with most existing research focusing on limited applications. Studies have highlighted the benefits of this integration, including the assessment of the sustainability of rehabilitation interventions with an emphasis on environmental, economic, and social criteria [3], as well as the ranking of retrofit alternatives for heritage buildings with a focus on economic and functional aspects [12]. However, these approaches concentrate on a narrow set of criteria and very specific decision-making scenarios and do not address the management of data complexity within the HBIM models. Despite promising developments, further research is required to

address the challenges of integrating MCDM with HBIM, particularly concerning data management, criteria selection, and stakeholder engagement.

## 3 MCDM and HBIM Approach

In the field of historic preservation, decision-makers must reconcile the competing demands of historic integrity with modern functionality and sustainability. Integrating MCDM techniques with HBIM offers a holistic approach to preserving cultural heritage and adapting it for contemporary use. When making decisions related to historic heritage, it is essential to consider multiple factors. MCDM provides a structured framework for evaluating and prioritizing these factors.

In the context of MCDM applied to heritage buildings, a series of decisions must be made, i.e., the selection of alternative uses, the prioritization of renovation efforts, the assessment of significance, the evaluation of solutions, the estimation of service life, and the choice of contractors. These decisions are guided by several criteria dimensions, such as:

- Historic [3], [9], [13]: The distinctive stories, uniqueness, and historical significance of the building, including its heritage and archaeological value, period details, and construction techniques.
- Architectural [4], [9], [13]: The visual appearance and unique design, which serve to highlight the artistic and architectural significance and authenticity of the building.
- Economic [2]–[4], [9]: Financial aspects, including funding opportunities, conservation costs, tourism potential, and long-term economic benefits.
- Social [2]–[4], [9], [13]: The relevance and utility of the building to the local community, including political considerations and its role in fostering community identity and cohesion.
- Cultural [2], [4], [9], [13]: The contribution of the building to the cultural heritage and identity of the community, with particular emphasis on its educational value, cultural significance, and the preservation of traditions and practices.
- Managerial [4], [9]: Administrative and logistical considerations, such as personnel management, spatial organization, storage needs, and urban planning.
- Technological [3], [4], [9]: The building's capacity to fulfill current requirements, including accessibility, fire safety, environmental controls, and protection from the natural elements.
- Structural [4], [9], [14]: The condition and stability of the physical structure of the building, including its integrity, load-bearing capacity, risk management, and signs of damage affecting its longevity.
- Environmental [2]–[4], [9]: The ecological impact of the building, with a focus on sustainability, energy efficiency, and the minimization of the environmental footprint of maintenance and occupancy.

- Functional [2], [4], [9]: The current usability of the building and its future adaptability, ensuring that it remains usable and relevant. This is achieved by taking into account the occupancy, practical use, and continuity of purpose.

The HBIM application can integrate MCDM criteria and methodologies into three-dimensional models [6] of heritage sites, facilitating stakeholder interaction. This digital representation collects comprehensive information about heritage buildings, including structural components and historical annotations, enabling MCDM analysis. Stakeholders can assign weights to the various criteria in real-time and directly compare renovation options within the HBIM model [6], with visual representations of each choice. HBIM also permits the simulation of various conservation scenarios, which are evaluated using MCDM to assist decision-makers in selecting sustainable options [14]. The interactive nature of HBIM involves stakeholders, with sensitivity analysis and expert validation ensuring alignment with real-world preferences and constraints.

## 4 Methodology

The HBIM and MCDM approach employs a structured, iterative process comprising distinct phases. These include the understanding of historic buildings, the collection of accurate data, and the application of decision-making techniques. This approach involves all stakeholders and ensures transparency and alignment with preservation goals and current needs. Figure 1 shows schematically the iterative decision-making process using the HBIM-MCDM approach.

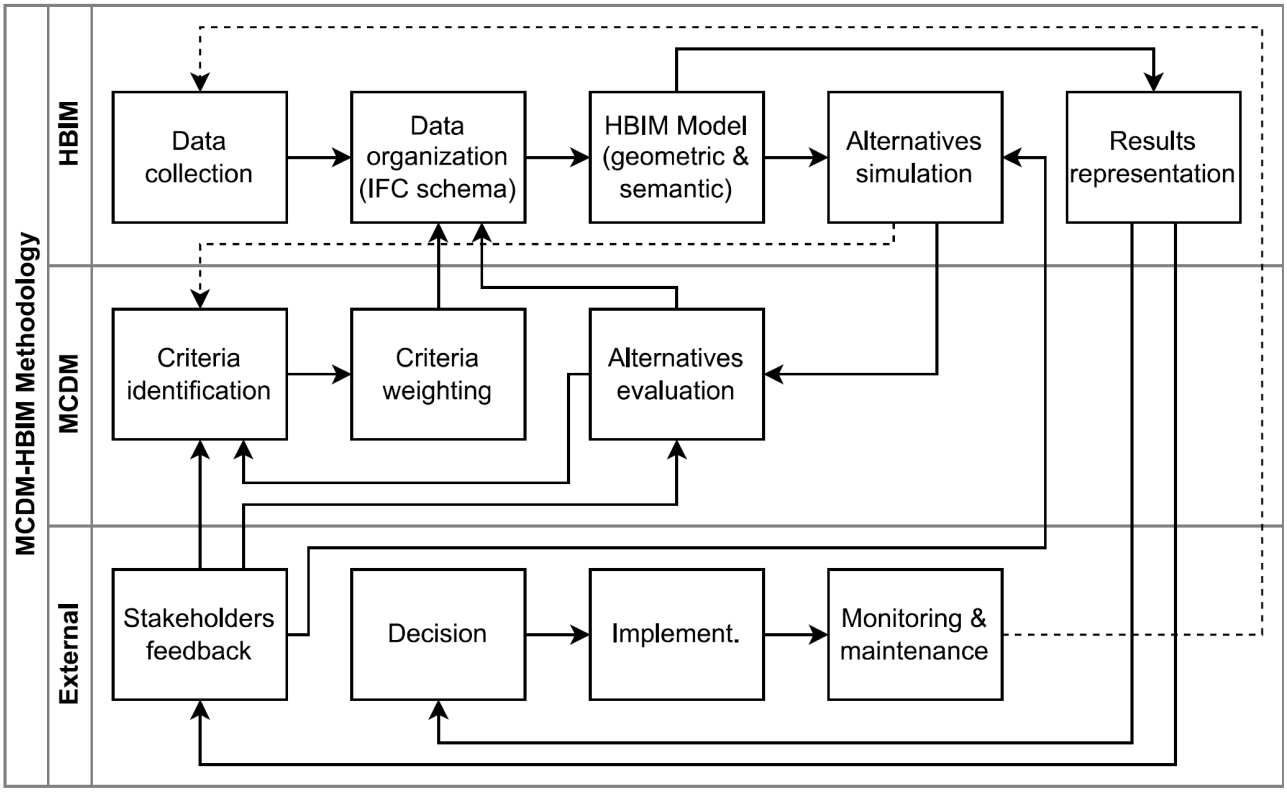


Figure 1: Methodology schema *(dashed lines are used when two arrows cross)*

### 4.1 Data Collection and HBIM Model Development

The initial phase of the process involves the collection of data essential to the development of the HBIM model. This includes historical research, on-site inspections, and materials analysis [1]. To gather the necessary data, various techniques are employed, such as the retrieval of historical documents, archival records, and previous surveys [14]; the use of laser scanning, photogrammetry, and manual measurements to conduct on-site inspections [11]; and the documentation of construction and restoration materials. Once the data has been collected, it is organized and integrated into the Industry Foundation Classes (IFC) schema defined by buildingSMART International (bSI) to create the HBIM model.

### 4.2 Criteria Identification and Weighting for MCDM

In parallel with the creation of the HBIM model, and having previously defined the final objectives of the decision to be made, a set of criteria for decision-making in heritage conservation is identified and classified into dimensions encompassing historic, architectural, economic, social, cultural, managerial, technological, structural, environmental, and functional considerations. Each criterion is assigned a weight that reflects its relative importance concerning the final objectives, determined by techniques such as stakeholder or expert consensus [6], [8].

### 4.3 Integration of MCDM Techniques with HBIM

The integration of MCDM techniques with the HBIM model involves several steps [4]. The first step is the assignment of criteria. This involves the incorporation of criteria and their respective weights into the HBIM model by associating them with specific elements and properties within the IFC schema. The second step is the simulation of alternatives. This is the use of the HBIM model to simulate various alternatives and evaluate their effects on the criteria [6]. The third step is the evaluation of alternatives. This is the application of MCDM techniques to rank the alternatives and calculate scores based on weighted criteria [6]. Finally, the fourth and final step is the integration of results. The alternative rankings are incorporated into the HBIM model by associating them with elements and properties within the IFC schema.

### 4.4 Decision Support

To facilitate decision-making, the results of the MCDM analysis are presented visually to stakeholders. This allows for the different scenarios, rankings, criteria scores, and key areas of interest to be displayed in the HBIM models. A feedback mechanism enables stakeholders to provide input on the scenarios, thereby refining the criteria, alternatives, or rankings iteratively.

### 4.5 Implementation and Monitoring

Once a decision has been made, the selected strategy is applied to the building, and the HBIM model serves as the central repository for ongoing monitoring and evaluation [11]. Regular updates of the HBIM model with new data from inspections, maintenance activities, and post-intervention evaluations ensure its effectiveness in long-term monitoring and support for future decision-making [1], [5], [14].

# 5 Discussion and Outlook

The HBIM and MCDM framework presents significant advantages, but its practical implementation is constrained by some key challenges. These include clustering and modeling decision factors, ensuring data accuracy, managing uncertainty, fostering effective communication and consensus among stakeholders, updating HBIM models, unifying decision-making processes into a cohesive system, and adapting users to new workflows.

Future research should prioritize a comprehensive understanding of stakeholder requirements and perspectives through qualitative interviews and content analysis. This understanding will inform the establishment of formal heritage conservation criteria.

Once these criteria have been clearly defined, they should be integrated, along with their weighting, into the HBIM model. This integration should ensure that the criteria are linked to relevant model elements and property sets (criteria groups). Following this, efforts should be directed towards optimizing the representation and regular updating of these criteria. In addition, defined responsibilities should be assigned to stakeholders, modelers, or collaborative teams.

It would be beneficial to explore intuitive and user-oriented methods for presenting and ranking alternatives within the HBIM model, considering whether MCDM processes should be conducted internally or externally. Establishing clear protocols for evaluating and ranking alternatives will enhance transparency and stakeholder engagement. An iterative workflow should be implemented to facilitate continuous updates, allowing the HBIM model to evolve in response to new data, changing requirements, and the outcomes of alternative evaluations.

Ultimately, the HBIM-MCDM framework must be validated through both theoretical and practical case studies to ensure it meets the necessary standards and effectively supports heritage conservation in real-world applications.

# 6 Conclusion

This approach shows the potential of integrating Heritage Building Information Management (HBIM) and Multi-Criteria Decision-Making (MCDM) techniques to enhance the preservation and adaptive reuse of historic buildings. By leveraging the digital modeling capabilities of HBIM and the structured decision-making processes of MCDM, stakeholders can achieve a more holistic and transparent approach to heritage conservation decision-making.

The integration of HBIM and MCDM addresses the multifaceted nature of heritage conservation by providing a framework that takes into account several factors, including historical significance, architectural integrity, economic viability, social relevance, and environmental impact. This approach facilitates informed decision-making, promotes stakeholder involvement, and ensures that conservation strategies are aligned with both contemporary needs and cultural heritage preservation.

Nevertheless, the successful implementation of this integrated approach necessitates the overcoming of several challenges. The accurate collection of data, effective communication among stakeholders,

and the management of complex technical processes are essential for the creation of reliable HBIM models and the execution of MCDM techniques. Furthermore, the implementation of continuous updates and long-term monitoring is necessary to maintain the relevance and accuracy of conservation strategies.

Future research should focus on further developing the integration of HBIM and MCDM. This can be achieved by developing uniform criteria for heritage conservation and exploring methods for data representation and stakeholder interaction. To this end, a case study on a listed building in Hamburg will be conducted. This will involve collaboration with various stakeholders to identify and prioritize conservation strategies, which will facilitate the validation and refinement of the framework in a real-world context.

## Acknowledgements

I would like to express my gratitude to Prof. Dr. Annette Bögle and Prof. Daniel Mondino for their invaluable guidance, support, and advice.

## References

[1] F. Calcerano, S. Thravalou, L. Martinelli, K. Alexandrou, G. Artopoulos, and E. Gigliarelli, “Energy and environmental improvement of built heritage: HBIM simulation-based approach applied to nine mediterranean case-studies”, *Building Research & Information*, pp. 1–23, 2023. DOI: 10.1080/09613218.2023.2204417.

[2] Y. Li, L. Zhao, J. Huang, and A. Law, “Research Frameworks, Methodologies, and Assessment Methods Concerning the Adaptive Reuse of Architectural Heritage: A Review”, *Built Heritage*, vol. 5, no. 1, p. 6, 2021. DOI: 10.1186/s43238-021-00025-x.

[3] S. Santini, V. Borghese, and C. Baggio, “HBIM-based decision-making approach for sustainable diagnosis and conservation of historical timber structures”, *Sustainability*, vol. 15, no. 4, p. 3003, 2023. DOI: 10.3390/su15043003.

[4] B. O. Vehbi, K. Günçe, and A. Iranmanesh, “Multi-Criteria Assessment for Defining Compatible New Use: Old Administrative Hospital, Kyrenia, Cyprus”, *Sustainability*, vol. 13, no. 4, p. 1922, 2021. DOI: 10.3390/su13041922.

[5] P. Clini, C. Mariotti, R. Angeloni, and J. Muñoz Cádiz, “Architectural Heritage Digital Representations for Conservation Strategies”, in *The International Archives of the Photogrammetry, Remote Sensing and Spatial Information Sciences*, 2024, pp. 111–118. DOI: 10.5194/isprs-archives-XLVIII-2-W4-2024-111-2024.

[6] S. Yarramsetty, M. Faheem, and S. K. Mvn, “An integrated approach to building planning using the multi-criteria decision method (MCDM) and BIM”, *International Journal of Sustainable Construction Engineering and Technology*, vol. 14, no. 4, pp. 49–63, 2024. DOI: 10.30880/ijscet.2023.14.04.005.

[7] M. Murphy, E. McGovern, and S. Pavia, “Historic Building Information Modelling (HBIM)”, *Structural Survey*, vol. 27, no. 4, pp. 311–327, 2009.

[8] H. Taherdoost and M. Madanchian, “Multi-criteria decision making (MCDM) methods and concepts”, *Encyclopedia*, vol. 3, no. 1, pp. 77–87, 2023. DOI: 10.3390/encyclopedia3010006.

[9] R. R. Nadkarni and B. Puthuvayi, “A Comprehensive Literature Review of Multi-Criteria Decision Making Methods in Heritage Buildings”, *Journal of Building Engineering*, vol. 32, p. 101 814, 2020. DOI: 10.1016/j.jobe.2020.101814.

[10] M. Bolpagni, “Building Information Modelling and Information Management”, in *Industry 4.0 for the Built Environment* (Structural Integrity), M. Bolpagni, R. Gavina, and D. Ribeiro, editors, Structural Integrity. Cham: Springer International Publishing, 2022, vol. 20, pp. 29–54. DOI: 10.1007/978-3-030-82430-3_2.

[11] T. Tan, G. Mills, E. Papadonikolaki, and Z. Liu, “Combining Multi-Criteria Decision Making (MCDM) Methods with Building Information Modelling (BIM): A Review”, *Automation in Construction*, vol. 121, p. 103 451, 2021. DOI: 10.1016/j.autcon.2020.103451.

[12] M. Pavlovskis, D. Migilinskas, J. Antucheviciene, and V. Kutut, “Ranking of Heritage Building Conversion Alternatives by Applying BIM and MCDM: A Case of Sapieha Palace in Vilnius”, *Symmetry*, vol. 11, no. 8, p. 973, 2019. DOI: 10.3390/sym11080973.

[13] K. Bansal and P. Chhabra, “Values-based decision-making for conserving built heritage”, in *2022 International Conference on Decision Aid Sciences and Applications (DASA)*, 2022, pp. 1770–1774. DOI: 10.1109/DASA54658.2022.9765068.

[14] N. Makoond, L. Pelà, and C. Molins, “A Risk Index for the Structural Diagnosis of Masonry Heritage (RISDiMaH)”, *Construction and Building Materials*, vol. 284, p. 122 433, 2021. DOI: 10.1016/j.conbuildmat.2021.122433.

# Automatisierte projektabhängige Filterung von technischen Regeln mit IDS

Lennard Buttgereit[1,2,3] and Merna Emara[1]
[1]Institut für Bauinformatik, Technische Universität Dresden, Nürnberger Str. 31a, 01062 Dresden
[2]Schüßler-Plan Digital GmbH, Grafenberger Allee 293, 40237 Düsseldorf
[3]IPROconsult GmbH, Schnorrstraße 70, 01069 Dresden
E-mail(s): lennard.buttgereit@gmail.com, merna.emara@tu-dresden.de

**Abstract:** Die deutsche Bauindustrie ist geprägt von einem komplexen Gefüge an technischen Regeln und Regularien. Am Bau Beteiligte müssen in der Regel eigenständig identifizieren, was davon auf sie in einem konkreten Bauprojekt zutrifft und was vernachlässigt werden kann. Dies, in Kombination mit der hohen Dynamik in Regelwerkentwicklung und -aktualisierung kann zu Unstimmigkeiten mit Behörden und langwierigen Genehmigungsverhandlungen führen. Vor allem trägt es aber auch zu einer empfundenen Überregulierung bei. Die nachfolgende Arbeit stellt ein Konzept für einen Dienst vor, der auf Grundlage von konkreten Projektinformationen automatisiert filtern kann, welche technischen Regeln, als ein Teil der Regulierung, zu beachten sind. Es basiert auf einem Register an Informationsanforderungen im Format von buildingSMARTs Information Delivery Specification, bei dem jeder Anwendungsbereich einer Regel eine eigene Informationsanforderung darstellt. Der Umfang des Registers ist aktuell auf die in der Musterverwaltungsvorschrift Technische Baubestimmungen gelisteten technischen Regeln festgelegt.
*Keywords:* Building Information Modeling (BIM), Code Compliance, Technische Regeln, Technische Baubestimmungen

Erschienen in Tagungsband 35. Forum Bauinformatik 2024, Hamburg, Deutschland, DOI: 10.15480/882.13541
© 2024 Das Copyright für diesen Beitrag liegt bei den Autoren. Verwendung erlaubt unter Creative Commons Lizenz Namensnennung 4.0 International.

## 1 Welche technischen Regeln sind rechtlich bindend?

Das Deutsche Institut für Normung (DIN) führt ca. 3900 technische Regeln mit Relevanz für das Bauwesen [1]. Vom DIN herausgegebene Normen oder technische Regeln müssen jedoch nicht automatisch beachtet werden. In Deutschland ist das Bauordnungsrecht maßgebend, also die jeweilige Bauordnung eines Landes (LBO). Im Nachfolgenden wird vereinfacht auf die standardisierende Musterbauordnung (MBO) Bezug genommen. Die dort in § 3 niedergeschriebenen allgemeinen Anforderungen an Anlagen können nach § 85a Abs. 1 Satz 1 durch sogenannte technische Baubestimmungen konkretisiert werden [2]. Dabei handelt es sich um technische Regeln, die aufgrund der Verkündung im Rahmen des Bauordnungsrechts zu beachten sind. Zu eigenständigen Rechtsnormen werden sie durch die Verweisung nicht [3].

Um welche technischen Regeln es sich konkret handelt, wird von der obersten Bauaufsichtsbehörde eines jeweiligen Landes bekannt gemacht. Analog zur MBO besteht in der Muster-Verwaltungsvorschrift Technische Baubestimmungen (MVV TB) eine für die 16 Länder homogenisierende Version. Sie wird vom Deutschen Institut für Bautechnik jährlich aktualisiert bzw. veröffentlicht und umfasst für den maßgebenden Abschnitt A in der Version 2023/01 nur 216 Verweise auf technische Regeln [4]. Die MVV TB und davon abgeleitete Landesverwaltungsvorschriften werden ausschließlich als PDF veröffentlicht (Stand 2024).

In der Theorie können am Bau Beteiligte das digitale Dokument sichten und die relevanten technischen Regeln identifizieren. In der Praxis ist dieses Vorgehen jedoch wenig realistisch. Zumeist wird auf das eigene Wissen, das erfahrener Kolleginnen und Kollegen zurückgegriffen oder im Zweifelsfall angenommen, dass alle technischen Regeln mit Bezug zum Projekt beachtet werden müssen. Im ersten Fall wird eine gewisse Fehleranfälligkeit und im zweiten Fall eine Überregulierung in Kauf genommen. Eine Möglichkeit, dies zu umgehen, wäre ein Dienst, der anhand konkreter Projektdaten automatisiert schlussfolgert, welche technischen Regeln für das Projekt gelten und welche vernachlässigt werden können. Im Grunde könnte ein solcher Dienst auch als Veröffentlichung der MVV TB in einem maschineninterpretierbaren Format interpretiert werden. Im Nachfolgenden wird ein solcher Dienst konzeptioniert.

## 2 Konzept zur projektabhängigen Filterung von technischen Regeln

Zunächst wird geklärt, welche Form die Projektdaten für den Dienst aufweisen sollen. Im Bestreben nach Transparenz kommt das offene Datenmodell der Industry Foundation Classes (IFC) zum Einsatz. Abhängig von der Serialisierung ergeben sich im Anschluss unterschiedliche Möglichkeiten, ein konkretes Bauwerkinformationsmodell gegen Anwendungsbereiche von technischen Regeln zu prüfen.

Für Modelle nach ifcOWL im Resource Description Framework (RDF) bieten sich die standardisierten Sprachen SPARQL und SHACL an, um entweder benötigte Komponenten abzufragen oder sie als vergleichbare Datenformen (Shapes) vorzugeben. Liegt ein Modell als STEP Physical File (IFC-SPF) vor, besteht in der Information Delivery Specification (IDS) ebenfalls eine standardisierte Technologie, um zu erfüllende Datenmuster vorzugeben.

Da für den vorliegenden Anwendungsfall keine zusätzlich benötigten Funktionen über die von IDS hinaus identifiziert werden konnten, wird aus Praxisgründen das Vorgehen mit IDS umgesetzt (Abbildung 1). So können Umformungsschritte des häufiger genutzten IFC-SPF zu einer RDF-Serialisierung gespart und ggfs. die Anwendung des Konzepts erleichtert werden.

Zur digitalen Weiterverarbeitung sollen die Ergebnisse anschließend in einem maschinenlesbaren bzw. -verarbeitbaren Format erfolgen. Eine Möglichkeit hierfür ist die Übergabe eines Information Container for linked Document Delivery (ICDD) nach DIN EN ISO 21597. Die im Rahmen des Beitrags umgesetzte Alternative sieht eine IFC-basierte Modellanreicherung vor. Das IFC-Schema umfasst bereits benötigte Entitäten und Beziehungen, die es ermöglichen, eine technische Regel mit den Komponenten des Projekts zu verknüpfen (Abbildung 2).

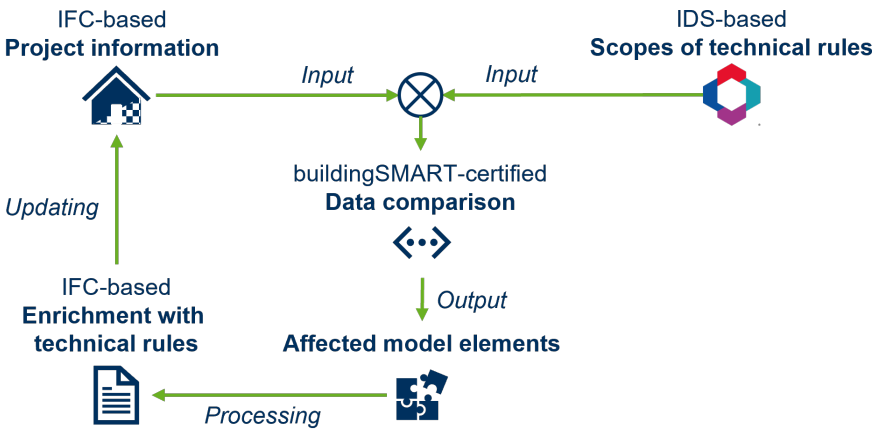


Abbildung 1: Konzept zur projektabhängigen Filterung von technischen Regeln als Prozessschema

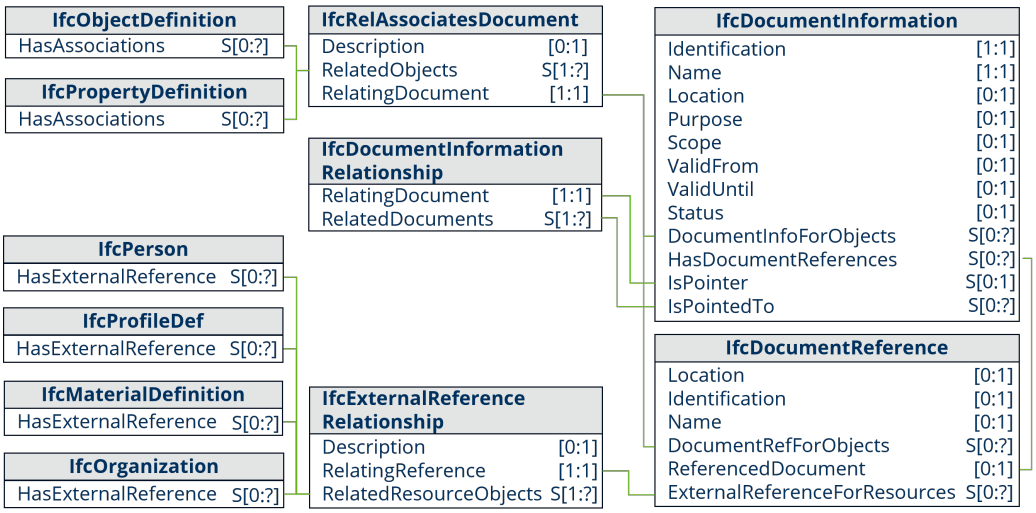


Abbildung 2: Ergebnisausgabe als IFC-basierte Modellanreicherung

# 3 Implementierung eines Prototypen

Für eine Implementierung des Konzepts gilt es zunächst, die Anwendungsbereiche der technischen Regeln auf IDS abzubilden. Im Rahmen des Prototypen wird dies für die 216 technischen Regeln der MVV TB durchgeführt. Bei einer händischen Sichtung der Anwendungsbereiche konnten vier Kriterien ausgemacht werden, mit Hilfe derer nahezu sämtliche Anforderungen abgebildet werden können: (1) Leistungsbeschreibung, (2) Anlagentyp, (3) Verwendete Baumaterialien und (4) Dokumentabhängigkeit.

## 3.1 Homogenisierung häufig auftretender Kriterien

Neben der Identifizierung der vier Kriterien muss festgestellt werden, dass die Beschreibungssprache und verwendete Begrifflichkeiten in den Anwendungsbereichen stark variieren. Dadurch könnte es bei Abgleich mit den Bezeichnungen innerhalb eines Bauprojektes zu Verwirrung und unvollständigen Ergebnissen kommen. Der Vorschlag lautet stattdessen, für den Dienst einheitliche, auf Standards fußende Bezeichnungen zu verwenden.

Das Kriterium „Leistungsbeschreibung“ wird als eine Kombination aus Leistungsbild und Leistungsphase (LPH) nach der Verordnung über die Honorare für Architekten- und Ingenieurleistungen (HOAI) umgesetzt. Demnach ergeben sich für ein Leistungsbild in einer bestimmten LPH regelmäßige zu erbringende Grundleistungen [5]. Für den Anlagentyp können mit den Objektlisten ebenfalls Definitionen der HOAI genutzt werden. Die Materialeinordnung orientiert sich an der Europäischen Bauprodukteverordnung (EU-BauPVO) und den darin enthaltenen 35 Produktbereichen [6].

### 3.2 Abbildung der homogenisierten Kriterien auf IFC4.0.2.1

Für den ersten Teil der Leistungsbeschreibung, das Leistungsbild, wird der Entitätstyp IfcActorRole eingesetzt. Standardmäßig ist das Attribut *Role* und ein Eintrag der entsprechenden IfcActorRoleEnum zur Wertebelegung zu verwenden. Da es hierbei aber wieder zu Unstimmigkeiten mit der HOAI käme, wird die Behilfslösung mit dem Wert *USERDEFINED* und dem Attribut *UserDefinedRole* stattdessen umgesetzt. Die HOAI-LPHs können mit IfcTask und dem Attribut *Identification* deklariert werden. Über das Attribut *Status* ist zudem hinterlegbar, welche LPHs aktuell laufen, welche bereits abgeschlossen oder noch nicht angefangen sind.

Den Anlagentyp, also die Einträge der HOAI-Objektlisten abzubilden, ist weniger eindeutig. Grob teilt die HOAI in Gebäude, Innenräume, Freianlagen, Ingenieurbauwerke, Verkehrsanlagen und Fachplanungs- bzw. Beratungsleistungen ein. Letztes sind vor allem Tragwerksplanung und Technische Ausrüstung. Für Gebäude wird IfcBuilding, für Innenräume IfcSpace, für Tragwerke IfcStructuralAnalysisModel und für technische Ausrüstung IfcDistributionSystem jeweils mit dem Attribut *ObjectType* verwendet. Bei Freianlagen, Ingenieurbauwerken und Verkehrsanlagen hingegen ist in IFC 4.0.2.1 kein ideales Pendant zu finden. Möglich sind Entitäten für einzelne Objekte wie IfcGeographicElement und IfcCivilElement oder ein System aus den genannten als IfcSpatialZone. Mit der bereits offiziellen Anerkennung von IFC 4.3 als ISO-Standard entstehen neue Möglichkeiten zur Abbildung, die Bestandteil einer zukünftigen Erweiterung des Prototypen sind.

Das dritte Kriterium umfasst die verwendeten Materialien, was in IFC mit IfcMaterial abgebildet wird. Zur Wertebelegung eignet sich das Attribut *Category*. Die Dokumentabhängigkeit wird nicht als IDS-Anforderung abgebildet und bedarf daher nicht zwingend einer IFC-Abbildung. Stattdessen erfolgt die Umsetzung darunter fallender technischer Regeln im Rahmen der Ergebnisausgabe. Ist die übergeordnete technische Regel anzuwenden, so ist es die davon abhängige ebenfalls und wird dem Modell hinzugefügt.

### 3.3 Abbildung der Anwendungsbereiche auf IDS 1.0

Das Vorgehen wird exemplarisch anhand des Eurocodes 3 Teil 1-1 erläutert:

> EN 1993-1-1 enthält Regeln für den **Entwurf**, die **Berechnung** und **Bemessung** von **Tragwerken** aus **Stahl**. Zusätzlich werden Anwendungsregeln für den **Hochbau** angegeben.

Die Kriterien werden identifiziert (fett hervorgehoben), den Kategorien zugeordnet, dann auf die standardisierten Werte und IFC-Definitionen abgebildet und daraus eine IDS-Formulierung abgeleitet.

Im Rahmen des Prototypen erfolgte die Abbildung der individuellen Begriffe auf die standardisierten Werte manuell über einen Textabgleich der Bezeichnungen mit der HOAI bzw. der EU-BauPVO. Die Ergebnisse werden tabellarisch festgehalten (Tabelle 1).

Tabelle 1: Übersicht der aus dem Anwendungsbereich extrahierten Informationen

| Begriff | Kategorie | | HOAI/EU-BauPVO | IFC Entität.Attribut |
|---|---|---|---|---|
| Entwurf<br>Berechnung<br>Bemessung | Leistungs-bschreibung | Leistungsbild | Architektur,<br>Ingenieurwesen,<br>Tragwerksplanung | IfcActorRole.UserDefinedRole<br>(+ Role) |
| | | LPH | 1, 2, 3, 4, 5 | IfcTask.Identification<br>(+ Status) |
| Tragwerk | Anlagentyp | | Tragwerksplanung | IfcStructuralAnalysisModel.ObjectType |
| Hochbau | Anlagentyp | | Gebäude | IfcBuilding.ObjectType |
| Stahl | Material | | Metallbauprodukte<br>und Zubehörteile | IfcMaterial.Category |

Für den Prototypen wurden die 216 technischen Regeln der MVV TB analysiert und deren Anwendungsbereiche anhand der vier Kriterien festgehalten. Die Transformation zu IDS-Formulierungen erfolgt über einen Python-Algorithmus mit Hilfe des IfcTester-Packages als Teil von IfcOpenShell [7].

Für jede technische Regel entsteht ein IDS-Dokument mit je einer *specification* pro Kriterium. Jede *specification* besteht wiederum aus einem Bereich der *applicability* und einem der *requirements*. Das Kriterium LPH innerhalb der Leistungsbeschreibung im Beispiel oben hat beispielsweise alle Instanzen von IfcTask als *applicability* und die *requirements* sind, dass das Attribut *Identification* einen der Werte (LPH 1 bis LPH 5) annehmen muss (Quelltext 1).

Algorithm 1: Auszug aus einer IDS-Spezifikation für die Leistungsphase nach HOAI.

```
<specification name="LPH␣nach␣HOAI" ifcVersion="IFC4" minOccurs="1" maxOccurs="
    unbounded">
    <applicability>
        <entity>
            <name> <simpleValue>IFCTASK</simpleValue> </name>
        </entity>
    </applicability>
    <requirements>
        <attribute>
            <name> <simpleValue>Identification</simpleValue> </name>
            <value>
                <xs:restriction base="xs:string">
                    <xs:enumeration value="LPH␣1"/>
                    <xs:enumeration value="LPH␣2"/>
                    ...
                </xs:restriction>
            </value>
        </attribute>
    </requirements>
</specification>
```

### 3.4 Abgleich mit Bauwerkinformationsmodellen und Ergebnisausgabe

Mit IfcTester können Bauwerkinformationsmodelle als IFC-SPF in einer Python-Programmierumgebung automatisiert gegen IDS-Dateien geprüft werden [7]. Das Ergebnis umfasst für jede Spezifikation der IDS, welche Modellkomponenten überprüft wurden, welche davon die Bedingungen erfüllen und davon abgeleitet auch, welche dies nicht tun. Im Rahmen des Beitrags erfolgt die Ergebnisausgabe als IFC-basierte Modellanreichung.

Dabei wird zunächst ein Dokumentobjekt für die MVV TB allgemein erstellt. Trifft eine technische Regel daraus auf die Projektkonfiguration zu, wird sie dem Modell als Dokumentinformation hinzugefügt und erhält eine Beziehung zum MVV TB Objekt, um den rechtlichen Charakter zu deklarieren. Davon wird eine tatsächliche Referenz mit Hilfe einer aktuellen URL abgeleitet, die wiederum mit den Modellkomponenten verlinkt wird, auf die sich die technische Regel bezieht (Abbildung 3).

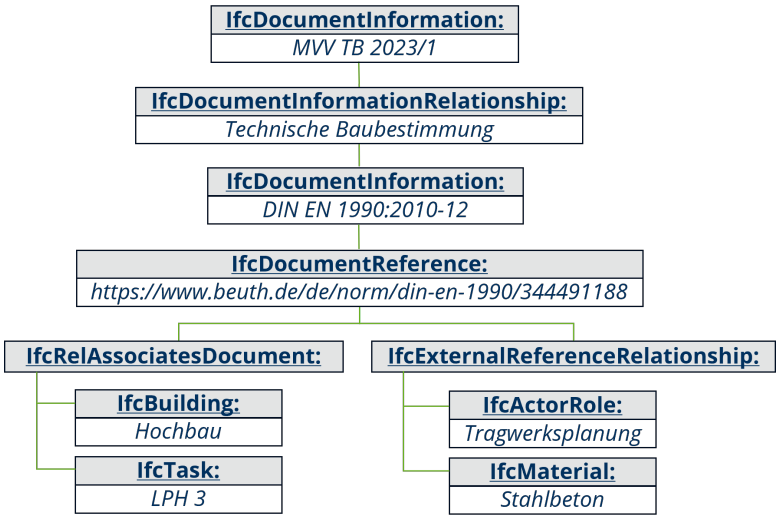


Abbildung 3: Vereinfachte Darstellung der Ergebnisausgabe als IFC-basierte Modellanreicherung

## 4 Auswertung

Die Auswertung erfolgt anhand eines Beispielprojekts. Gegeben sei eine zu planende Industriehalle, die als Holz-Beton-Verbund hergestellt werden soll. Ein Planungsbüro bewirbt sich mit einem Architekturentwurf und möchte sicher gehen, dass die technischen Regeln zur allgemeinen Gestaltung beachtetet wurden. Sie nutzen den konzeptionierten Prototyp, um nur die für ihr Projekt relevanten Regeln zu filtern. Dafür ist es im ersten Schritt notwendig, die Projektinformationen IFC-konform und entsprechend der HOAI bzw. der EU-BauPVO anzulegen, sofern nicht eh geschehen (Quelltext 2). Mit der Instanz von IfcBuilding und dem *ObjectType* „Gewerbe/Industrie/Landwirtschaft“ wird deklariert, dass es sich um einen Industriebau nach HOAI Anlage 10.2 handelt (Quelltext 2, #2). Der aktuelle Projektfortschritt ist durch eine IfcTask-Instanz und hier den Wert „LPH 2“, also Vorplanung, angegeben (Quelltext 2, #4). Als involvierte Rollen nach den HOAI-Leistungsbildern wird in diesem Szenario nur das allgemeine Leistungsbild „Architektur“ angenommen (Quelltext 2, #3). Zum Schluss werden auch die verwendeten Hauptmaterialien deklariert. Die Bezeichnungen entsprechen den Produktbereichen 1 (Beton) und 13 (Bauholz) (Quelltext 2, #5-6).

Algorithm 2: Auszug Beispielprojekt nach Ergebnisausgabe als angereichertes IFC-SPF

```
DATA;
\#1=IFCPROJECT('23TUNhvP12PxBm8uH3kFOb',$,'Beispielprojekt',$,$,$,$,$,$);
\#2=IFCBUILDING('2fQJ9reTz6IRdKjcw2G$wX',$,$,$,'Gewerbe/Industrie/Landwirtschaft
    ',$,$,$,$,$,$,$);
\#3=IFCACTORROLE(.USERDEFINED.,'Architektur',$);
\#4=IFCTASK('3kLdI5xGLCkuwA2vNcyL4S',$,$,$,$,'LPH 2',$,'Begonnen',$,$,$,$,$);
\#5=IFCMATERIAL($,$,'PRODUKTE AUS BAUHOLZ FUER TRAGENDE ZWECKE UND
    HOLZVERBINDUNGSMITTEL');
\#6=IFCMATERIAL($,$,'PRODUKTE AUS VORGEFERTIGTEM NORMAL-, LEICHT- ODER
    PORENBETON');
\#7=IFCDOCUMENTINFORMATION('DIN 68800-1:2011-10','Holzschutz - Teil 1:
    Allgemeines',$,$,$,$,$,$,\#25,$,$,$,$,$,$,$,$);
\#8=IFCDOCUMENTREFERENCE('https://www.dinmedia.de/de/norm/din
    -68800-1/144627702','DIN 68800-1:2011-10',$,$,\#7);
\#9=IFCEXTERNALREFERENCERELATIONSHIP($,$,\#8,(\#5));
...
ENDSEC;
```

Für eine solche Projektkonfiguration ergibt sich nach Abgleich mit den IDS-Spezifizierungen der 216 technischen Regeln der MVV TB, dass nur 16 davon zum aktuellen Zeitpunkt relevant sind. Sie werden als Metadatenobjekte dem Initialmodell beigefügt und mit den verantwortlichen Komponenten verknüpft. Über die Objektbeziehung Die DIN 68800-1 (Holzschutz) steht dann z.B. in einem Verhältnis zum Material Bauholz (Quelltext 2, #9). Analog werden auch die restlichen 15 technischen Regeln automatisch hinzugefügt. Anschließend kann das Modell beispielsweise über eine Programmierschnittstelle wieder analysiert und die relevanten Regeln ausgelesen werden. Dabei ist es möglich, entweder für eine Modellkomponente, bspw. ein Material, die zu beachtenden Regeln zu filtern oder andersherum von der Regel ausgehend alle Komponenten zu filtern, auf die sie sich bezieht.

## 5 Zusammenfassung und Ausblick

In dem Prototypen besteht grundsätzlich die Validierung eines Konzepts zur automatisierten Auswahl projektspezifischer technischer Regeln in Abhängigkeit eines Bauwerkinformationsmodells. Es muss allerdings festgestellt werden, dass die Voraussetzungen für den Dienst eine große Hürde darstellen. Nicht nur müssen allgemeine Projektinformationen IFC-gerecht modelliert sein, sondern sich in ihrer Ausprägung auch noch an den ausgewählten Standards orientieren.

Ist dies der Fall, liegen die Ergebnisse mit dem vorgeschlagenen Konzept anschließend grundsätzlich strukturiert und maschinenlesbar vor. Es besteht aber noch kein etablierter Dienst, mit dem in IFC modellierte Dokumente und insbesondere deren Verlinkungen sinnvoll ausgewertet werden könnten. Für das ICDD-Konzept hingegen gibt es bereits fortgeschrittene Konzepte und Dienste zu einer solchen Plattform. Eine Abänderung der bisherigen Ergebnisausgabe auf einen ICDD sollte daher ernsthaft erwägt werden. Darüber hinaus kann auch ein zusätzlicher Report für mehr Klarheit sorgen.

Als letztes stellt sich die Frage, inwiefern davon ausgegangen werden darf, dass tatsächlich nur die in der MVV TB, respektive Landesversion, gelisteten technischen Regeln anzuwenden sind.

Bauvertragliche Abmachungen darüber hinaus oder Abweichungen bei gleichbleibender Erfüllung der allgemeinen Anforderungen sind erlaubt und häufig vorzufinden. Der noch immmer geltende Anspruch darauf, dass Anlagen nach den 'anerkannten Regeln der Technik' angeordnet, errichtet, geändert und instand gehalten sind ist ein Problem für die hier klar vorgenommene Abgrenzung von *relevant* zu *irrelevant*. Der vorgestellte Dienst darf damit wieder nur als Hilfestellung interpretiert werden.

## Acknowledgements

The publication is part of the research project entitled "iECO – Intelligent Empowerment of Construction Industry" which has received funding from Bundesministerium für Wirtschaft und Klimaschutz (BMWK) based on a resolution of the German Bundestag. The authors gratefully acknowledge the support and funding from the BMWK. The content of this publication reflects the author view only and the BMWK is not responsible for any use that may be made of the information it contains.

## Literatur

[1] T. Steidl, »Teures Bauen: Bremst sich die Branche mit Normen und Standards selbst aus?«, *Verband Beratender Ingenieure - VBI*, 4.01.2024. Adresse: https://www.vbi.de/aktuelles/news/teures-bauen-bremst-sich-die-branche-mit-normen-und-standards-selbst-aus/.

[2] Bauministerkonferenz, *Musterbauordnung: MBO*, 23.11.2023. Adresse: https://www.dibt.de/fileadmin/dibt-website/Dokumente/Rechtsgrundlagen/MBO.pdf.

[3] M. Kment, K. Finkelnburg und K.-M. Ortloff, *Öffentliches Baurecht* (JuS-Schriftenreihe), 8., neu bearbeitete Auflage 2022. München: C.H.Beck, 2022, Bd. 107. DOI: 10.17104/9783406783333.

[4] Deutsches Institut für Bautechnik, *Muster-Verwaltungsvorschrift Technische Baubestimmungen (MVV TB)*, Berlin, 2023. Adresse: https://www.dibt.de/fileadmin/dibt-website/Dokumente/Referat/P5/Technische_Bestimmungen/MVVTB_2023-1.pdf.

[5] Bundesregierung, *Verordnung über die Honorare für Architekten- und Ingenieurleistungen: HOAI*, 2002. Adresse: https://www.hoai.de/hoai/volltext/hoai-2021/.

[6] Europäisches Parlament und Europäischer Rat (ER): *Verordnung (EU) Nr. 305/2011 des Europäischen Parlaments und des Rates vom 9. März 2011 zur Festlegung harmonisierter Bedingungen für die Vermarktung von Bauprodukten und zur Aufhebung der Richtlinie 89/106/EWG des Rates Text von Bedeutung für den EWR: EU-BauPVO*, 2011. Adresse: https://eur-lex.europa.eu/legal-content/DE/TXT/?uri=celex%3A32011R0305.

[7] T. Krijnen und R. Schultz, *IfcOpenShell*, 2023. Adresse: https://ifcopenshell.org/.

# Geometric rule check with Answer Set Programming for barrier-free navigation

Marian Kurzawa
Construction Informatics, University of Kassel, Mönchebergstraße 7, 34125 Kassel, Germany
E-mail(s): m.kurzawa@uni-kassel.de

**Abstract:** The topic of rule-based navigation within buildings is an area of current research. The objective to make a public building accessible for all user groups requires the implementation of complex geometric rule checks. This paper defines exemplary rules based on the German building code DIN 18040-1 and implements rule checks using a declarative programming approach (Answer Set Programming). The results indicate that the declarative implementation has some significant limitations in terms of complexity (linear solver). However, it also offers a promising approach to constraint-based geometric rule checking, which could be a valuable contribution to future research.
*Keywords:* Rule check, Declarative Programming, Algorithms

Erschienen in Tagungsband 35. Forum Bauinformatik 2024, Hamburg, Deutschland, DOI: 10.15480/882.13504
© 2024 Das Copyright für diesen Beitrag liegt bei den Autoren. Verwendung erlaubt unter Creative Commons Lizenz Namensnennung 4.0 International.

## 1 Introduction

In the light of recent developments concerning indoor navigation, the topic of accessibility has assumed greater significance. A number of countries have expressed a desire to ensure, that public buildings are accessible to all user groups. The requirements for such accessibility can be derived from the relevant building codes (in Germany DIN 18040-1 [1]). The range of complexity for such requirements varies considerably, from relatively simple to highly sophisticated and detailed. For instance, the required minimum width of a door is a relatively straightforward confirmation. While the verification of unobstructed maneuvering spaces in front of doors or other points of egress may be straightforward in practice, the formulation of an algorithmic representation of such requirements for a general case is more complex. Consequently, this paper explores the current state of conceptualization for geometric rule checks. In this context, a „rule“ refers to a set of requirements prescribed by the building codes. Rule checks for different complexity classes are developed with a declarative programming approach (Answer Set Programming). Limitations of the used approach are identified, and possibilities for future research in the domain of declarative programming and geometric rule checking are proposed.

### 1.1 Related work

A number of authors have addressed the definition of rules. Métral, Daponte, Caselli, *et al.* [2] specify rule expressions with mathematical operators and limiting values. The rules can be evaluated for models expressed in RDF, using SHACL or SPARQL. Another approach is presented by Pauwels,

Deursen, Verstraeten, *et al.* [3]. The authors utilize a rule ontology to verify semantic properties, such as the room height, and more complex calculations to assess the acoustic performance of a building. The aforementioned concepts are primarily concerned with semantics. In their work, Eastman, Lee, Jeong, *et al.* [4] present a process for rule definition and discuss example rules on accessibility rule checking. These include the wheelchair turning space in Solibri Office (formerly Solibri Model Checker). Similar checks are conducted by Andrich, Daniotti, Pavan, *et al.* [5], also with Solibri Office. The concepts already incorporate geometric tests. However, as Solibri Office is a proprietary software, there is no publicly available rule definition for such geometric tests. The traversability of spaces is discussed by Bandi and Thalmann [6]. The passability of a space can be determined by discretizing the indoor space into regular rectangular grids. Literature also contains complex discretizations using Voronoi-Diagrams or hexagonal grids [7]-[8]. A more complex approach is developed by Diakité and Zlatanova [9] with the Flexible Space Subdivision (FSS). Spaces are classified into O(bject)-spaces, F(unctional)-spaces and R(emaining free)-spaces, with only the R-spaces beeing considered passable, if there is sufficient space for an A(gent)-space to traverse it. Without respect to navigation Akanmu, Olayiwola, and Olatunji [10] apply a game engine to render geometric tests for maintenance workers. They verify the correct positioning of a ladder at a specific location within the building, taking into account the height of the floor and the ground of the ladder (with a Bounding Box). The majority of the introduced methods can be assigned to imperative object-oriented programming (focus on control flow). Literature lacks declarative implementations (focus on output) for complex geometric rule checking. One of the few declarative approaches to execute rule checks on a building models is presented by Arias, TÖRMÄ, Carro, *et al.* [11]. The authors employ Answer Set Programming (ASP) to filter a building model, using logic expressions. In this approach, the „answers“, which fulfill all given constraints, are collected in answer sets. In addition to verifying a sufficient width of windows within a particular room type, the authors also employ Boolean operations on shapes. Their concept is founded on logical principles, but operates on geometric models. Consequently, it can be extended to check complex geometric rules.

### 1.2 Methodology

As the known concepts for geometric rule checking focus on imperative programming, the objective of this paper is to test the usability of complex geometric rule checks, using a declarative programming approach. Therefore, the implementation of Arias, TÖRMÄ, Carro, *et al.* [11] is extended to check geometric rules. Exemplary, checkable requirements with different complexity are collected from the German building code DIN 18040-1 [1]. Based on the resulting codes, benefits and limits to the used approach are stated, followed by potentials for future development in this area.

## 2 Checkable Rules

The following sections present the implementation of inclusive navigation requirements using Answer Set Programming. The checkable rules are derived from building codes. For the tests, different rules with varying degree of complexity are employed. As a definition for the complexity of those rules, this paper refers to Solihin and Eastman [12]. The authors define four complexity classes: rules that require a single or small number of explicit data (class 1), rules that require simple derived attribute

values (class 2), rules that require an extended data structure (class 3), and rules that require a „proof of solution“ (class 4). Based on these classes, different rules are to be tested, which correspond to requirements demanded by the building codes. As discussed by Kurzawa and Kirchner [13], the building codes of several countries exhibit certain similarities. One of those is the clear space in front of a door. The following rules are abstracted from common requirements of the building codes.

### 2.1 Minimum door width (class 2)

The first checkable rule assumes, that a door must be at least 1.0 m wide, in order to be traversable by a wheelchair user (based on DIN 18040-1). This rule can be classified as class 1, if the width of the door is stored in an object attribute. In this example, the width is derived from the geometry. Consequently, the rule is considered to be class 2.

### 2.2 Clear door spaces (class 3)

A more complex issue is to ascertain, whether there is sufficient turning space for a wheelchair in front of a door. In this test, a free space of 1.5 x 1.5 m in front of both sides of the door is required (based on DIN 18040-1). In order to maintain the simplicity of the checks, it is assumed that the space is placed in the center in front of the door. In order to ascertain whether the space in front of the door is unobstructed, it is necessary to utilize an auxiliary object for the door space. For a compliant door, the corresponding auxiliary door space should not clash with other objects (in this case walls). The test is classified class 3.

### 2.3 Accessibility of doors in room (class 4)

The accessibility check of doors from a specific room is considered to be class 4. A rule check entails determining, whether there are any obstructions in the path to the door. For the sake of simplicity, only the straight path from the center of the door space to the center of a room with a convex footprint is considered. In accordance with the provisions of DIN 18040-1, the minimum width of the passageway is 1.2 m. However, the complexity of this rule significantly increases, if concave rooms are taken into account.

## 3 Answer Set Programming

In this section, the aforementioned rules (see Chapter 2) are implemented, using Answer Set Programming. The spatial reasoner proposed by Arias, TÖRMÄ, Carro, *et al.* [11] serves as the foundation for the tests. The fundamental objective is to identify all volumetric bodies, that comply with predefined constraints without contradictions. The concept employs a linear constraint solver. In the case of orthogonally aligned examples, mathematical operations such as „intersection(...)“ can be evaluated by formulating constraints like $X < X_a$ and $X > X_b$ as intervals and then shifting the borders of the interval of $X$. However, volumetric bodies are only approximated as the union of convex shapes that are parallel to axes of coordinates. This approach does not consider non-orthogonally aligned examples. The used datasets store the shapes of physical objects by three points. The initial two points delineate intervals along the coordinate axes (see https://gitlab.software.imdea.org/joaquin.arias/spatial/-/tree/master/examples). Similarly, doors and windows are defined by the opening space within a wall. In the orthogonally aligned model, the

third point of the dataset is not used and it is unclear, how this point is defined. Typically, the third point defines the orientation of the volumetric body. In the given examples the third point is situated in proximity to the centroid of the shape. In conclusion non-orthogonally aligned examples result in defective geometries, as illustrated in Figure 1. In the example, an input file containing rotated points is utilized. Although the solver is unable to process non-orthogonally aligned examples, the following rule checks should be applicable to a general non-orthogonally aligned example as well. For these tests, the third point is corrected either as (1,0,0) or (0,1,0). In the subsequent sections, only code snippets are shown and explained. The revised input files, along with the comprehensive developed code, are accessible on https://gitlab.com/designforall/geometric-rule-checking.

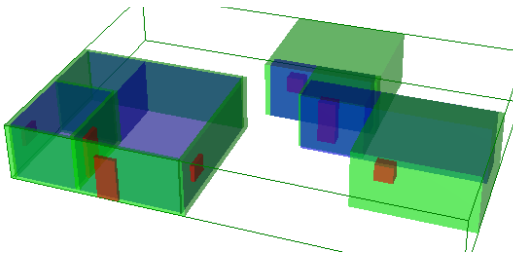

Figure 1: Left: original; right: 45° rotated

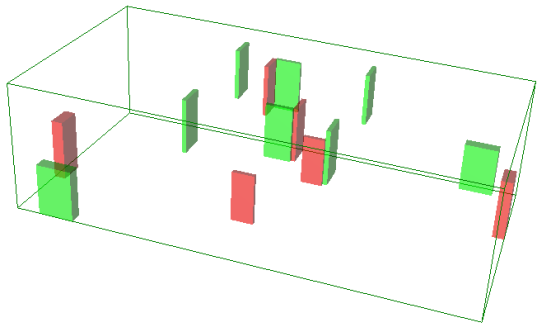

Figure 2: Evaluation of the existing door openings

### 3.1 Minimum door width (class 2)

In order to ascertain the width of the doors, in a first step the doors have to be filtered (compare Algorithm 1). The width of the door can then be derived from the geometry of the door. As the third point defines the direction of the door, the depth of the door can be determined using the Hesse normal form and coordinate form of a plane. The plane is defined by the first given point $p_1$ and the directional vector $n$ (here $p_3$). The width of the door opening is obtained by rotating the directional vector $n$ by 90 degrees. With the rotated direction vector the distance between $p_2$ and the plane with $p_1$ the outcome of the equation is the door width between the two points normalized with $L$ (compare Algorithm 1).

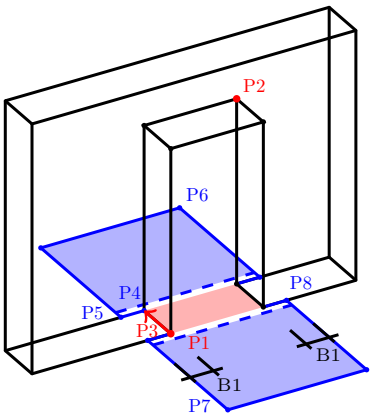


Figure 3: Door space definition via orientation vectors

Algorithm 1: Check of the width of the door openings

```
check_doorwidth :-
    findall(Sh,(
        object('IfcDoor', _, (X1, Y1, Z1), (X2,
            Y2, Z2), (X3, Y3, Z3)),
        L is sqrt(X3 * X3 + Y3 * Y3),
        Width is abs(-Y3*(X2-X1)+X3*(Y2-Y1))/L,
        Width >= 1.0,
        box_shape(point(X1, Y1, Z1), point(X2, Y2
            , Z2), Sh)),
    GoodDoors),
    output([par(GoodDoors,green)]).
```

These mathematical calculations must be evaluated for the geometry of each filtered object. All answers $Sh$ that satisfy the condition ($Width \geq 1.0$) are included in the answer set *GoodDoors*, answers that violate the rule can be gathered analogously in an answer set *BadDoors*. The results are visualized in a X3D file. The objects are colored according to the result of the rule (compare Figure 2).

### 3.2 Clear door spaces (class 3)

To check door spaces, auxiliary objects must be defined. These are computed based on the direction of the door $p_3$ ($X_3$, $Y_3$). The depth $D$ and the width $W$ of the door opening are to be charged similarly to Chapter 3.1. Subsequently, the points $P_4$ to $P_8$ are estimated by translating the given points according to the orientation of the door (see Figure 3 and Algorithm 2). The door spaces from $P_5$ to $P_6$ and $P_7$ to $P_8$ are returned (see Figure 4). The points $P_5$ and $P_8$ are additionally translated by 2 cm away from the door in order to avoid clashes between the door spaces and the door hosting wall.

Algorithm 2: Create door spaces based on direction vectors

```
door_space(X1, Y1, Z1, X2, Y2, Z2, X3, Y3, Sh) :-
    L is sqrt(X3 * X3 + Y3 * Y3),
    D is (X3*(X2-X1)+Y3*(Y2-Y1))/L,      W is abs(-Y3*(X2-X1)+X3*(Y2-Y1))/L,
    B1 is (1.5 - W) / 2,
    Px4 is X1 + D*X3,
    Py4 is Y1 + D*Y3,
    L2 is sqrt((X2-Px4) * (X2-Px4) + (Y2-Py4) * (Y2-Py4)),
    Px5 is Px4 - B1*(X2-Px4)/L2 + 0.02*X3/L,
    Py5 is Py4 - B1*(Y2-Py4)/L2 + 0.02*Y3/L,
    Px6 is X2 + 1.5*X3/L + B1*(X2-Px4)/L2,
    Py6 is Y2 + 1.5*Y3/L + B1*(Y2-Py4)/L2,
    Px7 is Px5 - (1.5+D)*X3/L,
    Py7 is Py5 - (1.5+D)*Y3/L,
    Px8 is X2 - (D+0.02)*X3/L + B1*(X2-Px4)/L2,
    Py8 is Y2 - (D+0.02)*Y3/L + B1*(Y2-Py4)/L2,
    (box_shape(point(Px5, Py5, Z1), point(Px6, Py6, Z2), Sh);
    box_shape(point(Px7, Py7, Z1), point(Px8, Py8, Z2), Sh)).
```

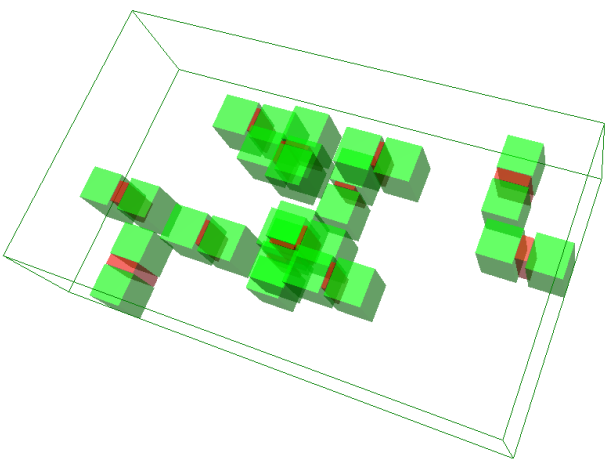

Figure 4: Red: doors, green: door spaces

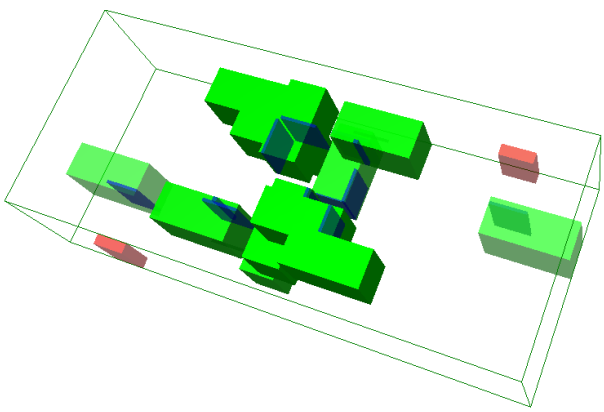

Figure 5: Red: doors with sufficient door spaces, green: simplified door spaces with intersections, blue: intersections with walls

In another query all doors with clashes between door spaces and existing walls are computed. The method *shape_intersect(...)* is described by Arias, TÖRMÄ, Carro, *et al.* [11]. In this example, the evaluation can be executed in a single query, rendering this step unnecessary. The doors that contravene the rule, can be identified, by computing the intersection of the door spaces with walls. If the intersecting area is empty, the door is returned (compare Algorithm 3).
If the identification of the violating objects requires multiple queries, the valid doors can also be identified through the application of mathematical calculations. After computing the intersections of the door spaces with walls (see Figure 5 in blue), corresponding simplified door spaces (one box using solely the points $P_5$ and $P_8$, shown in Figure 5 in green) can be determined. The intersection of the simplified door spaces with the doors yields the rule-violating doors. If no intersection between one door and any of the computed simplified door spaces exists, the door passes the test (shown in Figure 5 in red). As illustrated by this example, the approach proposed by Arias, TÖRMÄ, Carro, *et al.* [11] does not yield the bounding values themselves within a box shape. Instead, it provides constraints that define the boundaries of the shape (box shape: [X,Y,Z]; $X>X_a$, $X<X_b$, etc.). Consequently, it is not straightforward to access the door to the intersecting door space. In the case of multiple queries it is advisable to include the boundaries of the volumetric body within the return of the method *box_shape(...)*. This facilitates their use in subsequent computations.

Algorithm 3: Detection of doors without sufficient maneuvering space

```
findall(Door,(
    object('IfcWall', _, (Xa, Ya, Za), (Xb, Yb, Zb), _),
    box_shape(point(Xa, Ya, Za), point(Xb, Yb, Zb), Walls),
    object('IfcDoor', _, (X1, Y1, Z1), (X2, Y2, Z2), (X3, Y3, Z3)),
    door_space(X1,Y1,Z1, X2,Y2,Z2, X3,Y3, Doorspace),
    shape_intersect([Walls], [Doorspace], Inter), Inter \= [],
    box_shape(point(X1, Y1, Z1), point(X2, Y2, Z2), Door)),
ProblematicDoors),
```

### 3.3 Accessibility of doors in room (class 4)

To ascertain whether a door is directly accessible from the center of a space, even orthogonally aligned building objects lead to non-orthogonally aligned paths between the two considered objects. When considering only convex spaces, the path can be computed with two orthogonally aligned cuboids (compare Figure 6). The query is defined for one space. First, walls, doors and spaces are filtered similarly to the implementation in Chapter 3.1. For the selected space and for the door spaces of each door, the two-dimensional centroids are computed. In this orthogonally aligned example with convex spaces, the path from the center of the space to the door space can be computed using two cuboids (see Figure 6). Algorithm 4 illustrates the code to implement a path (first in the x-, then in the y-direction). A second path (first in the y-, then in the x-direction) can be defined analogously. For a door to be accessible from the center of the room, it is necessary that at least one of the two paths (*PathPartA*, *PathPartB*) does not intersect with any walls (compare Algorithm 5).

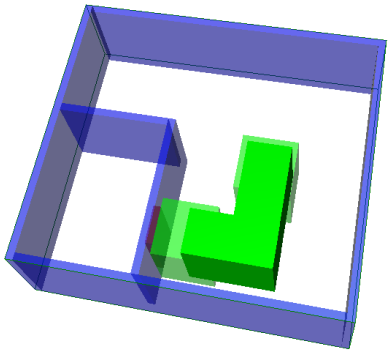

Figure 6: One possible path (*Path1(...)*, green) from the center of the room to the door (red)

Algorithm 4: Compute orthogonally aligned path

```
path1(X1, Y1, Z1, X2, Y2, Sh) :-
    Z2 is Z1+2.1,          B is 1.2,
    Y1l is Y1-B/2,         Y1r is Y1+B/2,
    X2l is X2-B/2,         X2r is X2+B/2,
    Y2r is Y2+B/2,
    (box_shape(point(X1, Y1l, Z1),
        point(X2r, Y1r, Z2), Sh);
    box_shape(point(X2l, Y1l, Z1),
        point(X2r, Y2r, Z2), Sh)).
```

Algorithm 5: Compute, whether an orthogonally aligned path intersects any wall

```
path1(Xm2,Ym2,Z1, Xm,Ym, PathPartA), path2(Xm3,Ym3,Z1, Xm,Ym, PathPartB),
((\+ ( member(Wall, Walls),
    shape_intersect([PathPartA], [Wall], Intersection), Intersection\=[]));
(\+ ( member(Wall, Walls),
    shape_intersect([PathPartB], [Wall], Intersection), Intersection\=[])))
```

## 4 Discussion

This paper provides a concise overview of current developments in rule checking. The literature offers several object-oriented approaches that utilize semantics. In addition to space discretization geometric tests are less frequently recorded. This paper presents a declarative implementation based on Answer Set Programming, which is derived from the work of Arias, TÖRMÄ, Carro, *et al.* [11]. The constraint-based concept facilitates mathematical operations similar to Constructive Solid Geometry for cuboids. Based on the German building code, three rules for accessibility of paths with different complexity are introduced and implemented. The examples demonstrate that complex geometric rules can be checked using declarative programming. Yet the used implementations reveal significant shortcomings. For instance, the linear solver lacks definitions for non-orthogonally aligned shapes. The assumption of orthogonally aligned volumetric bodies significantly simplifies the complexity of the solver, as there are fewer special cases to be considered and mathematical operations are easier to evaluate. However, as the third example (Chapter 3.3) indicates, navigation problems often require non-orthogonally aligned paths. Therefore, the solver implementation is considered too specific for complex geometric navigation testing.

The definition of a rotation angle of the object would be more appropriate. In general, the declarative approach presents certain challenges. For instance, after filtering all door spaces, the access of the underlying door object within a subsequent query (without geometric calculations) is not supported (see example 2 in Chapter 3.2). Nevertheless, the constraint-based concept of describing volumetric bodies and querying computed intersections is promising for future research. A solver with constraint logic for non-orthogonally aligned geometries (comparable to CSG-transformations) would be advantageous to define more complex shapes.

## References

[1] DIN Deutsches Institut für Normung e.V., *DIN 18040-1: Barrierefreies Bauen - Planungsgrundlagen - Teil 1: Öffentlich zugängliche Gebäude*. Berlin: Beuth Verlag, 2010.

[2] C. Métral, V. Daponte, A. Caselli, G. Di Marzo Serugendo, and G. Falquet, "ONTOLOGY-BASED RULE COMPLIANCE CHECKING FOR SUBSURFACE OBJECTS", *ISPRS - International Archives of the Photogrammetry, Remote Sensing and Spatial Information Sciences*, vol. XLIV-4/W1-2020, pp. 91–94, 2020. DOI: 10.5194/isprs-archives-XLIV-4-W1-2020-91-2020.

[3] P. Pauwels, D. V. Deursen, R. Verstraeten, *et al.*, "A semantic rule checking environment for building performance checking", *Automation in Construction*, vol. 20, no. 5, pp. 506–518, 2011. DOI: https://doi.org/10.1016/j.autcon.2010.11.017.

[4] C. Eastman, J.-m. Lee, Y.-s. Jeong, and J.-k. Lee, "Automatic rule-based checking of building designs", *Automation in Construction*, vol. 18, no. 8, pp. 1011–1033, 2009. DOI: https://doi.org/10.1016/j.autcon.2009.07.002.

[5] W. Andrich, B. Daniotti, A. Pavan, and C. Mirarchi, "Check and Validation of Building Information Models in Detailed Design Phase: A Check Flow to Pave the Way for BIM Based Renovation and Construction Processes", *Buildings*, vol. 12, no. 2, 2022. DOI: 10.3390/buildings12020154.

[6] S. Bandi and D. Thalmann, "Space Discretization for Efficient Human Navigation", *Computer Graphics Forum*, vol. 17, no. 3, pp. 195–206, 1998. DOI: 10.1111/1467-8659.00267.

[7] I. Afyouni, C. Ray, and C. Claramunt, "Spatial models for context-aware indoor navigation systems: A survey", *Journal of Spatial Information Science*, vol. 4, 2012. DOI: 10.5311/JOSIS.2012.4.73.

[8] J. O. Wallgrün, "Autonomous Construction of Hierarchical Voronoi-Based Route Graph Representations", in *Lecture Notes in Artificial Intelligence (Subseries of Lecture Notes in Computer Science)*, vol. 3343, 2004, pp. 413–433. DOI: 10.1007/978-3-540-32255-9_23.

[9] A. A. Diakité and S. Zlatanova, "Spatial subdivision of complex indoor environments for 3D indoor navigation", *International Journal of Geographical Information Science*, vol. 32, no. 2, pp. 213–235, 2018. DOI: 10.1080/13658816.2017.1376066.

[10] A. A. Akanmu, J. Olayiwola, and O. A. Olatunji, "Automated checking of building component accessibility for maintenance", *Automation in Construction*, vol. 114, p. 103 196, 2020. DOI: https://doi.org/10.1016/j.autcon.2020.103196.

[11] J. Arias, S. TÖRMÄ, M. Carro, and G. Gupta, "Building Information Modeling Using Constraint Logic Programming", *Theory and Practice of Logic Programming*, vol. 22, pp. 1–16, 2022. DOI: 10.1017/S1471068422000138.

[12] W. Solihin and C. Eastman, "Classification of rules for automated BIM rule checking development", *Automation in Construction*, vol. 53, pp. 69–82, 2015. DOI: 10.1016/j.autcon.2015.03.003.

[13] M. Kurzawa and J. Kirchner, "Extension of accessibility ontologies by requirements for inclusive indoor navigation", *EG-ICE 2024 conference held on July 3-5, at Universidade de Vigo*, 2024.

# Informationsintegration in der Betriebsphase von Bauwerken: Eine diagnostikspezifische Ontologie im ICDD

Paul-Christian Schuler[1], Yannic Stark[2] and Mahsa Mirboland[1]
[1]Professur Intelligentes Technisches Design, Bauhaus-Universität Weimar, Coudraystraße 13A, 99423 Weimar
[2]Marx Krontal Partner GmbH, Zum Hospitalgraben 2, 99425 Weimar
E-mail(s): paul-christian.schuler@uni-weimar.de, yannic.stark@marxkrontal.com, mahsa.mirboland@uni-weimar.de

**Abstract:** Während der Entwurfs-, Bau- und Betriebsphasen eines Bauwerks werden Daten in verschiedenen Formaten und Versionen produziert und zwischen den beteiligten Akteuren ausgetauscht. In der Betriebsphase ist es entscheidend, einen robusten und nachhaltigen Ansatz zur Integration und Speicherung von Daten zu haben. Linked-Data-Container (LDC) können genutzt werden, um Verbindungen und Beziehungen zwischen verschiedenen Datenquellen und Prozessen auf strukturierte und standardisierte Weise herzustellen. Das Ziel dieser Studie ist es, einen umfassenden Projektablauf durch die Entwicklung und Implementierung einer spezifischen Ontologie für Diagnostikprojekte zu modellieren und in einen LDC zu integrieren. Die vorgestellte Ontologie mit dem Namen Structural Information (SI)-Ontologie wurde auf Basis der diagnostischen Anforderungen an Datenerfassung -bereitstellung und -integration sowie der erforderlichen Informationsstrukturen in Bezug auf Prozessabläufe und die daraus resultierenden Daten konzipiert. Ein entwickeltes Framework ermöglicht die Integration dieser Ontologie in den Information Container for linked Document Delivery (ICDD) gemäß den bestehenden ISO 21597-Standards. Durch die Verlinkung von Dokumenten wird eine effiziente Nutzung der Ontologieinstanzen als Informationsgrundlage ermöglicht. Abschließend werden potenzielle Anwendungsbereiche diskutiert. Es wird aufgezeigt, wie bestehende Ontologien im Bauwesen sinnvoll an die entwickelte SI-Ontologie angegliedert werden können, um die Datenintegration und -nutzung weiter zu optimieren und zugänglicher zu machen.

*Keywords:* Building Information Modeling, Semantic Web, Linked Building Data, Building Diagnostics, Digital Twin

Erschienen in Tagungsband 35. Forum Bauinformatik 2024, Hamburg, Deutschland, DOI: 10.15480/882.13514
© 2024 Das Copyright für diesen Beitrag liegt bei den Autoren. Verwendung erlaubt unter Creative Commons Lizenz Namensnennung 4.0 International.

# 1 Einleitung

Die Erhaltung und Überwachung von Brückenbauwerken stellt eine zentrale Aufgabe im Ingenieurwesen dar. Sie erfordert die Durchführung von regelmäßigen visuellen Inspektionen, diagnostischen Untersuchungen und Monitoring-Techniken. Die Anwendung der Building Information Modeling (BIM)-Methodik, für die eine Digitalisierung der Structural Information (SI)-Daten erforderlich ist, bietet bedeutende Möglichkeiten. Diese Technologien ermöglichen eine effizientere Erfassung, Verarbeitung und Analyse der Daten sowie eine fundierte Entscheidungsfindung bezüglich der Instandhaltungsmaßnahmen. Die fortlaufende Weiterentwicklung und Anpassung dieser Technologien und Methoden sind entscheidend, um die Langlebigkeit und Sicherheit von Brückenkonstruktionen während ihres gesamten Lebenszyklus zu gewährleisten und zu optimieren. Aus diesem Grund befasst sich diese Arbeit mit der Integration der Daten, die während diagnostischer Untersuchungen erhoben werden.

# 2 Forschungsgrundlage

## 2.1 Instandhaltungsmanagement

Ingenieurbauwerke wie Brücken sind für eine Nutzungsdauer von bis zu 100 Jahren ausgelegt, wobei strukturelle Veränderungen langsam erfolgen. Um ihre Sicherheit und Funktionstüchtigkeit sicherzustellen, sind gemäß DIN 1076 [1] regelmäßige Inspektionen alle 3 bis 6 Jahre notwendig. Diese Inspektionen, meist visuell, dokumentieren sichtbare Schäden und Mängel, die zur Zustandsbewertung des Bauwerks herangezogen werden [2]. Ein definierter Algorithmus ermittelt daraus eine Zustandsnote, die für die Planung von Instandhaltungsmaßnahmen entscheidend ist. Bei gravierenden Schäden werden weiterführende Untersuchungen wie Monitoringsysteme und diagnostische Verfahren eingesetzt. BIM unterstützt die digitale Transformation der Bauindustrie durch digitale Darstellungen der physischen und funktionalen Eigenschaften eines Bauwerks. Während Standards für BIM im Neubau etabliert sind, fehlen spezifische Anforderungen für die Integration von SI-Daten aus Bauwerksuntersuchungen zur Bestandsbewertung. Bauwerksdiagnostische Untersuchungen, die beispielsweise den inneren Aufbau und Materialeigenschaften eines Bauwerks liefern, sind entscheidend für die Erhaltung bestehender Infrastrukturen und werden mittels zerstörungsfreier und zerstörungsarmer Prüfverfahren durchgeführt. Derzeit werden diese Informationen meist analog verarbeitet und in Berichtsform bereitgestellt, was zu einer fragmentierten Datenhaltung führt. Diagnostische Untersuchungen gehen über visuelle Inspektionen hinaus und nutzen verschiedene Methoden und Messverfahren zur Ermittlung realitätsnaher Zustandsinformationen. Sie werden anlassbezogen durchgeführt, um spezifische Fragestellungen zu klären oder umfassende Bestandsaufnahmen zu erstellen. Die Digitalisierung dieser Diagnostikdaten und deren Integration in ein BIM-Modell können die Bewertung und Planung von Instandhaltungsmaßnahmen erheblich verbessern [3].

## 2.2 Ontologien und Wissensgraphen

Ontologien stellen eine entscheidende Komponente in der modernen Informationswissenschaft sowie im semantischen Web dar. Sie sind nicht nur Instrumente zur systematischen Erfassung und Organisation von Wissen, sondern auch wesentliche Komponenten für die Interoperabilität zwischen verschiedenen Wissensdomänen. Die Definition von Klassen und Beziehungen innerhalb eines spe-

zifischen Gegenstandsbereichs erlaubt die Schaffung einer einheitlichen Terminologie, wodurch Ontologien die Grundlage für eine gemeinsame Sprache schaffen. Dies fördert die Auffindbarkeit und Wiederverwendung von Informationen und unterstützt die Datenintegration durch Bereitstellung eines gemeinsamen Verständnisses der Datenkategorien und -beziehungen.

Im Kontext des semantischen Webs ermöglichen Ontologien Computern die Verarbeitung und das Verständnis von Inhalten. Dieses Verständnis basiert auf der Fähigkeit, komplexe Zusammenhänge zu erkennen und automatisierte Schlüsse zu ziehen. Die Instanziierung von Ontologien resultiert in der Bildung von Wissensgraphen, welche Wissen in einer vernetzten Form darstellen und somit neue Einsichten und Entdeckungen ermöglichen.

Die Darstellung von Bauwerksmodellen als Wissensgraphen erweist sich als sinnvoll. Dies betrifft auch Ingenieurbauwerke, insbesondere Brücken [4], [5]. Forschende entwickeln Verfahren zur Verknüpfung von Structural Health Monitoring (SHM)-Daten mit Ontologien, wobei der Schwerpunkt auf der Integration kontinuierlicher Messungen an Bauwerken liegt [6], [7].

## 2.3 Linked Data Container (LDC)

Die wachsende Vielfalt digitaler Informationen in der Baubranche hat verstärkte Forschungsanstrengungen im Bereich der LDCs hervorgerufen. LDCs verknüpfen und integrieren Daten aus verschiedenen Quellen, um sie leichter auffindbar, zugänglich und nutzbar zu machen [8]. Sie ermöglichen die Zusammenführung von Informationen aus verschiedenen Lebenszyklusphasen eines Gebäudes und erleichtern die Interoperabilität zwischen verschiedenen Informationsquellen und Datenformaten, was die Zusammenarbeit im Bauprozess unterstützt. LDCs basieren auf dem Linked-Data-Konzept, das durch Standards wie Resource Description Framework (RDF) und SPARQL Protocol And RDF Query Language (SPARQL) den semantischen Informationsaustausch ermöglicht [8]. Zwei Hauptausprägungen von LDCs im Bauwesen sind der Information Container for Linked Document Delivery (ICDD), auf Grundlage eines internationalen Standards nach ISO 21597 [9], [10], und der Multi-Model-Container nach DIN 18290 [11].

Der ICDD verwendet das komprimierte ZIP-Format (*.icdd) und enthält eine *Index.rdf*-Datei, die alle zu verlinkenden Dateien beschreibt. Der ICDD-Container nutzt zwei RDF-basierte Ontologie-Ressourcen:

- Die Container-Ontologie definiert die Struktur und Metadaten des Containers.
- Die Linkset-Ontologie definiert die semantischen Verknüpfungen zwischen den eingebetteten Dokumenten und Daten.

Die ISO 21597-1 [9] definiert die ICDD-Struktur, bestehend aus einer *Index.rdf*-Datei und drei spezifischen Ordnern:

- Ontology resources: Enthält alle im Container genutzten Ontologien.
- Payload documents: Speichert die von Nutzern erstellten Dokumente.
- Payload triples: Enthält die erzeugten Instanzen basierend auf den verfügbaren Ontologien.

Diese Struktur ermöglicht Verknüpfungen auf subdokumentarer Ebene, etwa von Objektattributen innerhalb einer IFC-Datei. Im Rahmen der Forschungstätigkeiten zum ICDD wird zunehmend dessen Anwendbarkeit im Bauwesen untersucht. Dies führte zu Erkenntnissen, die auch für die visuellen Brückeninspektionen und Straßenerhaltungsplanung von Nutzen sind [12].

# 3 Methodologie

Dieses Kapitel beschreibt die Methodik zur Implementierung eines graphbasierten Datenaustauschs in diagnostischen Projekten. Ziel ist die Erhebung, Speicherung und langfristige Bereitstellung von Informationen. Über die Lebensdauer von Bauwerken erzeugen und verarbeiten verschiedene Akteure zahlreiche Informationen. Ein wiederverwendbarer und maschinenlesbarer Datenstandard ist daher unerlässlich. Dieser Standard ermöglicht effiziente Erfassung und zukünftige Bereitstellung der Informationen. Diagnostische Untersuchungen an Bauwerken nutzen diverse Methoden, deren Ergebnisse in Form, Informationsgehalt und Nutzbarkeit variieren. Diese Studie zielt darauf ab, diese Informationen in einer Ontologie abzubilden, um sie langfristig nutzen zu können. Die Integration der Ontologie in den ICDD ermöglicht die Nutzung der standardisierten Dateistruktur und Verlinkungsmöglichkeiten. Es wird die Structural Information (SI)-Ontologie mit ihrer modularen Konstruktion und den implementierten diagnostischen Verfahren vorgestellt. Ein Framework zeigt die Einbindung in den ICDD, illustriert durch ein praxisbezogenes Anwendungsbeispiel. Abschließend erfolgt eine kritische Bewertung des Systems und die Darstellung möglicher Limitationen für zukünftige Verbesserungen. Diese Methodik bietet einen umfassenden Ansatz zur Implementierung eines graphbasierten Datenaustauschsystems für diagnostische Projekte, um Informationen effizient und langfristig zu verwalten.

# 4 Implementierung

Das System entstand aus der Notwendigkeit, heterogene Daten zwischen Fachplaner*innen während eines diagnostischen Projekts auszutauschen und diese langfristig nutzbar zu machen. Der ICDD nach ISO 21597 [9], [10] bildet eine gute Grundlage. Daher ist die Erstellung einer spezifischen Ontologie zur Speicherung von Informationen aus diagnostischen Projekten und deren Einbindung in den ICDD der nächste sinnvolle Schritt.

## 4.1 Ontologie

Der Aufbau einer Ontologie umfasst die präzise Definition des Anwendungsbereichs und der Ziele, einschließlich der Domäne und des Umfangs. Eine Ontologie besteht aus Klassen, deren Beziehungen und Attribute durch Datentypen definiert werden. Die in Abbildung 1 dargestellte Ontologie zeigt Klassen und deren Beziehungen. Sie gliedert sich in drei Hauptbereiche: projektspezifische Klassen, Klassen zur Verortung der Untersuchung und Klassen für die Untersuchungsverfahren. Dank der definierten Beziehungen in der Ontologie kann eine Untersuchung einem spezifischen Ort innerhalb eines Bauwerks zugeordnet werden. Jede Untersuchung enthält Informationen über den Durchführungsort, das Projekt und das Ziel. Eine Instanz der Klasse „Untersuchungsverfahren“ beinhaltet Details zur Zugehörigkeit des Durchführungsorts, des Projekts und zur Zusammenfassung von Instanzen in einem Untersuchungsbereich.

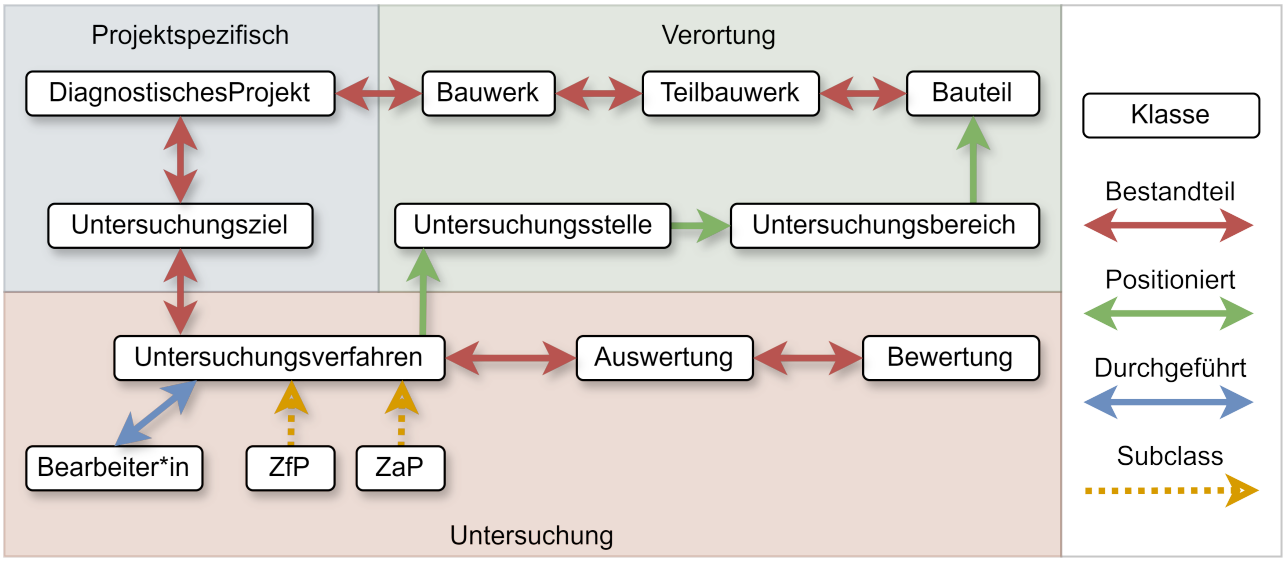


Abbildung 1: Übersicht des Strukturmodells der Ontologie

Die Untersuchungsverfahren sind als Subklassen modelliert und den Klassen zerstörungsfreie Prüfung (ZfP) und zerstörungsarme Prüfung (ZaP) zugeordnet. Bereits modellierte Klassen sind Bohrung (untergliedert in Spiral- und Kernbohrung), Endoskopie, Sondierungsöffnung und Ultraschalluntersuchung. Laboruntersuchungen, welche zum Teil direkt am Bauwerk und zum Teil im Labor durchgeführt werden, bilden eine Unterklasse der Untersuchungsverfahren und sind in den einzelnen Verfahren weiter untergliedert. Dazu gehören derzeit die Chloridanalyse, die Carbonatisierungstiefenbestimmung, die Druckfestigkeitsprüfung, die Rohdichtebestimmung sowie die E-Modulbestimmung. Weitere Verfahren können als Subklassen hinzugefügt werden. Die Auswertungsklasse ist mit der Untersuchungsverfahren-Klasse verknüpft, sodass verschiedene Ergebnisse aggregiert werden können.

## 4.2 Anbindung an ICDD

Die zuvor vorgestellte Ontologie bietet ein Schema, um alle notwendigen Informationen, die bei einer diagnostischen Untersuchung entstehen, systematisch zu erfassen. Dies ermöglicht es, sowohl die Untersuchung selbst als auch die daraus gewonnenen Erkenntnisse jederzeit nachverfolgen zu können. Dennoch bleibt es teilweise erforderlich, mit Dateien in verschiedenen Datenformaten zu arbeiten. Diese sollen nicht nur über die *Linkset.rdf*-Ontologie miteinander verknüpft werden, sondern bei Bedarf auch mit indizierten Objekten der SI-Ontologie.

Die SI-Ontologie wird im Ordner *Ontology resources* abgelegt, während der durch die Instanziierung der Ontologie entstehende Knowledge Graph im Ordner *Payload triples* gespeichert wird. Alle anderen Dateien werden gemäß der ISO 21597 [9], [10] in einer geeigneten Struktur im Ordner *Payload documents* abgelegt.

Die Datei *Index.rdf* definiert den Inhalt des Containers und initiiert alle vorhandenen Dokumente, sodass diese durch eine Uniform Resource Identifier (URI) eindeutig identifizierbar sind. Um aus Klassen der SI-Ontologie Verlinkungen zu Dateien herzustellen, wird wie in der Abbildung 2 dargestellt

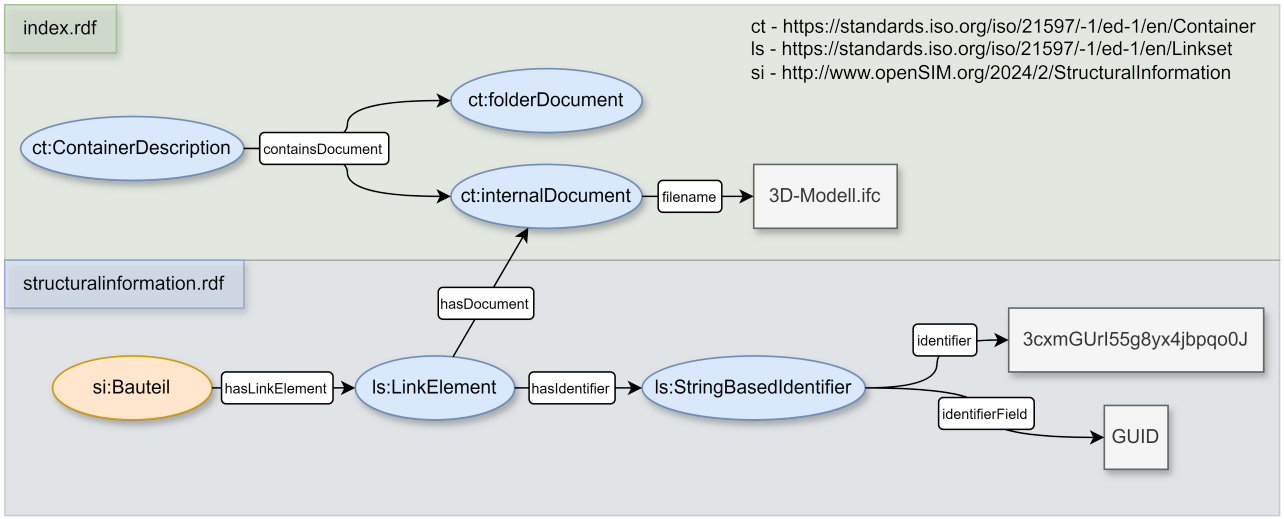


Abbildung 2: Darstellung der Anbindung der SI-Ontologie an den ICDD

das Objektattribut *hasLinkElement* verwendet, welches auf ein LinkElement-Objekt verweist. Die darauf folgende Struktur entspricht dem Schema, das in der ISO 21597 [9], [10] beschrieben ist.

## 5 Anwendungsbeispiel

Das Schema wurde in einem diagnostischen Projekt erprobt, das Bohrkernentnahme und Druckfestigkeitsprüfung einer Stahlbetonbrücke umfasste. Der Auftraggeber (AG) erstellt einen ICDD mit allen relevanten Dateien zum Bauwerk und zur Projektdurchführung. Bei einem vorhandenen Gebäudemodell können Bauwerks- und Teilbauwerksklasse aus der SI-Ontologie instanziiert und mit Dateien verknüpft werden (Abbildung 3a). Der vom AG erzeugte Container dient im Vergabeverfahren als Kalkulationsgrundlage und zur Einreichung von Bewerbungsunterlagen (Abbildung 3a/b).

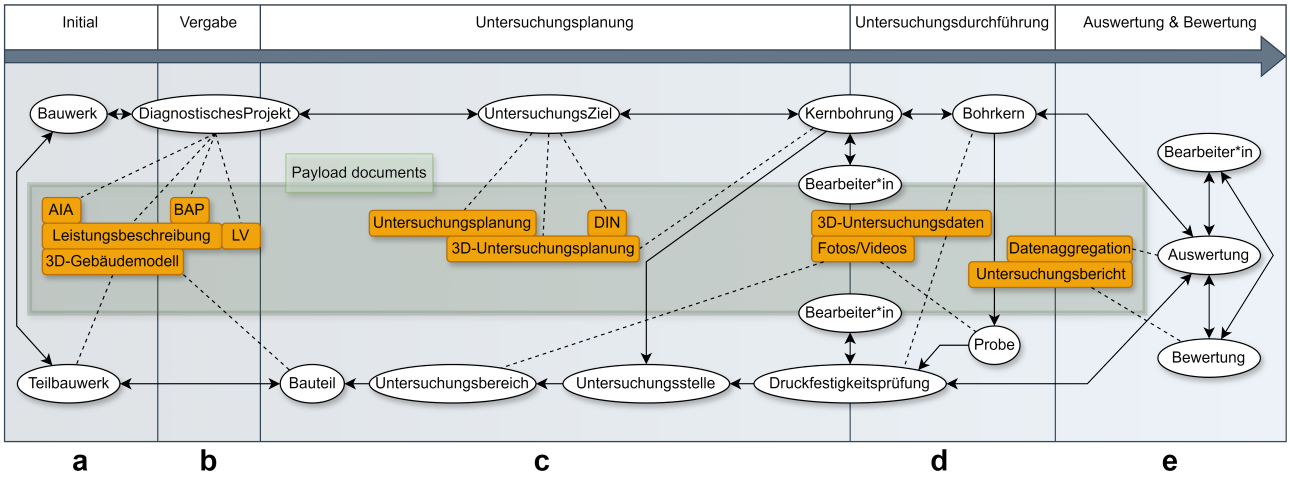


Abbildung 3: Integration von SI-Daten anhand der Bestimmung der Druckfestigkeit von Bohrkernen

Nach Vertragsabschluss erstellen Diagnostik-Fachplaner*innen eine Untersuchungsplanung aus der die in Abbildung 3c dargestellten SI-Klassen zur Abstimmung mit allen Fachplaner*innen instanziiert werden und Verknüpfungen zu Dokumenten entstehen können. Nach der Freigabe der Planung führen

Diagnostiker*innen die Untersuchungen durch, wobei gewonnene Informationen als Attribute den Entitäten in Abbildung 3d zugeordnet werden. Abweichungen in der Versuchsdurchführung können auftreten und anhand der Entitäten in Abbildung 3c/d dokumentiert werden. Nach Auswertung und Bewertung der Untersuchungen (Abbildung 3e) entstehen Textdokumente, die mit Objekten verknüpft und dem AG sowie Fachplaner*innen als Arbeitsgrundlage dienen. Die abschließende Übergabe des Containers stellt die Nachvollziehbarkeit des Projektverlaufs sicher und macht alle Informationen langfristig nutzbar.

## 6 Diskussion & Ausblick

Die SI-Ontologie ist eine spezialisierte Ontologie zur Strukturierung und Darstellung von zerstörungsfreien und zerstörungsarmen Prüfverfahren bei Brückenbauwerken. Sie umfasst projektspezifische Klassen und Attribute, die sowohl das Bauwerk als auch die diagnostischen Aspekte beschreiben. Diese Strukturierung ermöglicht die systematische Erfassung, nachvollziehbare Speicherung und Analyse detaillierter Untersuchungsinformationen. Die Integration der SI-Ontologie in den ICDD schafft eine solide Datengrundlage für Fachplaner*innen, wodurch alle Projektbeteiligten den aktuellen Stand eines Projektes einsehen können. Die Verlinkung von Dateien, die nicht als semantische Tripel dargestellt werden, ermöglicht eine kontextbezogene Interpretation. Ein wesentlicher Vorteil dieses Verfahrens besteht darin, dass neben dem Bericht auch alle notwendigen Details übermittelt werden, was zu einer zentralen Sammlung detaillierter Informationen führt. Langfristig ist jedoch eine Integration in eine Datenbank erforderlich, da separierte Container keine dauerhafte Lösung zur Datenhaltung darstellen. Zudem ist die Nutzung des ICDD durch verfügbare Anwendungen zum Schreiben und Lesen der Container sowie durch die Integration in Common Data Environments begrenzt. Zukünftig werden der SI-Ontologie weitere Untersuchungsverfahren hinzugefügt, um ein breiteres Spektrum der Fachdomäne Bauwerksdiagnostik abzudecken. Zudem wird geprüft, wie die SI-Ontologie mit anderen Ontologien verknüpft werden kann, um robuste Knowledge Graphs pro Bauwerk zu erstellen, einschließlich der verlustfreien Integration verschiedener Koordinatenreferenzsysteme. Der vorgeschlagene Workflow und die entwickelte Ontologie führen zu einer übersichtlicheren und nachvollziehbareren Bearbeitung diagnostischer Projekte. Die Erstellung solcher Container ermöglicht die semantische Anreicherung und langfristige Speicherung großer heterogener Datenmengen, was für zukünftige Vorhaben wie die Erstellung eines Digitalen Zwillings von großer Bedeutung ist.

## Acknowledgements

Die vorliegende Studie wurde im Rahmen des OpenSIM-Forschungsprojekts durchgeführt, welches durch die mFUND-Initiative des Bundesministeriums für Digitales und Verkehr (BMDV) unter dem Förderkennzeichen 19F2217F gefördert wurde.

## Literatur

[1] »DIN 1076:2024-02, Ingenieurbauwerke im Zuge von Straßen und Wegen –Überwachung und Prüfung«,

[2] B. für Digitales und Verkehr (BMDV), *Digitaler Zwilling von Brücken - Beitrag zum Masterplan Digitaler Zwilling Bundesfernstraßen*. Berlin: Eigenverlag, 2023.

[3] C. Fritsch, C. Voigt, J. Burkhardt, R. Arndt und S. Marx, »Digitale Bauwerksdiagnose–ein Projekt zur digitalen Transformation«, *Bautechnik*, 2024.

[4] J. Beetz, J. v. Leeuwen und B. d. Vries, »IfcOWL: A case of transforming EXPRESS schemas into ontologies«, *AI EDAM*, Jg. 23, Nr. 1, S. 89–101, Feb. 2009. DOI: 10.1017/S0890060409000122.

[5] A. Göbels und J. Beetz, »Conversion of legacy domain models into ontologies for infrastructure maintenance«, *Proceedings of the 9th Linked Data in Architecture and Construction Workshop*, S. 20–31, 2021. DOI: 10.18154/RWTH-2021-07330.

[6] G. P. Tsialiamanis, D. J. Wagg, I. Antoniadou und K. Worden, »An Ontological Approach to Structural Health Monitoring«, in *Topics in Modal Analysis & Testing, Volume 8*, B. Dilworth und M. Mains, Hrsg., Cham: Springer International Publishing, 2021, S. 51–59. DOI: 10.1007/978-3-030-47717-2_6.

[7] R. Li, T. Mo, J. Yang, S. Jiang, T. Li und Y. Liu, »Ontologies-Based Domain Knowledge Modeling and Heterogeneous Sensor Data Integration for Bridge Health Monitoring Systems«, *IEEE Transactions on Industrial Informatics*, Jg. 17, Nr. 1, S. 321–332, Jan. 2021. DOI: 10.1109/TII.2020.2967561.

[8] J. Beetz, P. Pauwels, K. McGlinn und S. Tormä, »Linked Data im Bauwesen«, in *Building Information Modeling: Technologische Grundlagen und industrielle Praxis*, A. Borrmann, M. König, C. Koch und J. Beetz, Hrsg., Wiesbaden: Springer Fachmedien, 2021, S. 223–242. DOI: 10.1007/978-3-658-33361-4_11.

[9] »DIN EN ISO 21597-1:2021-07, Informationscontainer zur Datenübergabe_- Austausch-Spezifikation_- Teil_1: Container (ISO_21597-1:2020); Deutsche Fassung EN_ISO_21597-1:2020«, Beuth Verlag GmbH, Techn. Ber. DOI: 10.31030/3137795.

[10] »DIN EN ISO 21597-2:2021-07, Informationscontainer zur Datenübergabe_- Austausch-Spezifikation_- Teil_2: Dynamische Semantik (ISO_21597-2:2020); Deutsche Fassung EN_ISO_21597-2:2020«, Beuth Verlag GmbH, Techn. Ber. DOI: 10.31030/3192763.

[11] R. J. Scherer und S.-E. Schapke, Hrsg., *Informationssysteme im Bauwesen 1: Modelle, Methoden und Prozesse*. Berlin, Heidelberg: Springer Berlin Heidelberg, 2014. DOI: 10.1007/978-3-642-40883-0.

[12] A.-H. Hamdan, *Ein ontologiebasiertes Verfahren zur automatisierten Bewertung von Bauwerksschäden in einer digitalen Datenumgebung* (Berichte des Instituts für Bauinformatik Heft 19), 1. Auflage. Dresden: Institut für Bauinformatik, Fakultät Bauingenieurwesen, TU Dresden, 2023.

# Enabling Circular Construction: Evaluating ICDD for Effective Deconstruction Processes

Victoria Jung[1]
[1]Chair of Individualized Production, RWTH Aachen University, Campus-Boulevard 30, Aachen, Germany
E-mail(s): jung@ip.rwth-aachen.de

**Abstract:** The construction industry faces significant challenges related to information loss, from pre-production, assembly and operation through to eventual deconstruction. Furthermore, the urgent need to decarbonise the construction sector demands the reuse of building materials. The use of existing building materials as secondary resources can make a significant contribution to sustainability goals. However, many deconstruction and material reuse initiatives are hindered by insufficient information available from the planning, manufacturing, and operational phases. In response to these challenges and aiming to maximise material reusability, this paper evaluates the Information Container for Linked Document Delivery (ICDD) as a long-term data storage solution for supporting circular construction practices. The study investigates how ICDD can mitigate information loss during transitions from pre-production, on-site assembly, and operation to deconstruction by archiving relevant deconstruction information. It identifies key deconstruction data requirements and information preservation standards. The application of the ICDD framework is demonstrated through a case study on the deconstruction of an assembled steel girder.

*Keywords:* ICDD, Circular Construction, Linked Data, Information Continuity, Material Reusability

Erschienen in Tagungsband 35. Forum Bauinformatik 2024, Hamburg, Deutschland, DOI: 10.15480/882.13525
© 2024 Das Copyright für diesen Beitrag liegt bei den Autoren. Verwendung erlaubt unter Creative Commons Lizenz Namensnennung 4.0 International.

## 1 Introduction

The construction industry is characterised by numerous stakeholders and complex projects [1], leading to significant challenges in achieving interoperability among diverse data sources and in linking various process information to the same element. At the same time, there is an increasing demand for material reuse to mitigate rising $CO^2$ emissions, landfill usage, and material shortages [1], as the construction industry is contributing 5-12 % of the greenhouse gas emissions [2]. Construction materials are typically designed for a lifespan of 50-100 years [3]; nevertheless, they are frequently demolished prematurely. This premature demolition highlights the potential for reusing these materials, thereby addressing challenges related to sustainability and resource efficiency. However, current deconstruction and material reuse efforts often fail due to insufficient information from the planning, manufacturing, and operation phases [4]. In this context, Linked Data provides a robust framework

for creating a more connected, accessible and interoperable data environment [5]. Concurrently, the integration and application of Linked Data in construction, as Linked Building Data (LBD) is on the rise. In accordance to these concepts the Information Container for Linked Document Delivery (ICDD) was developed and defined in the DIN EN ISO 21597 [6], [7] to overcome the limitations of existing frameworks for exchanging diverse and distributed building data [8]. This paper assesses the ICDD as a persistent data storage solution for enabling circular construction. It evaluates whether the industry's challenges of information loss from pre-production and on-site assembly to the deconstruction phase can be addressed by archiving all deconstruction-relevant information within the ICDD to support deconstruction processes.

# 2 State of the Art

## 2.1 Circular Construction

The demand for circular construction has increased in recent years, aiming to transform materials and components from having an 'end-of-life' to being reused, recycled, or recovered [9]. Benefits of circular construction include waste minimisation, cost efficiency, reduced energy requirements, and lower emissions. However, barriers to its implementation exist, categorised into economic, sociological, environmental, technical, organisational, and political challenges [10]. Transitioning to circularity requires changes in the value chain, early design for disassembly, and recognising waste as a resource, with data availability being crucial for informed decision-making across the life cycle and among stakeholders [4]. Various tools like Life Cycle Assessment (LCA), Energy Certificates, Material Flow Analysis (MFA), and Material Passports (MP) support data-based sustainable construction [11]. Recent studies focus on integrating MP into Building Information Modelling (BIM) to manage building materials throughout their life cycle [12]. Other emphasise the relevance of a total view of the life cycle process (TLCP) of a building. The use of database-based information models (DIM) and the standardised description of the information requirements of the various phases on the basis of the Level of Information Need (LOIN) for the structured recording, exchange and management of project-relevant information is recommended [13]. However, a more holistic approach to storing information about building elements beyond material properties and Information Delivery Manual are essential to address existing challenges in the deconstruction process.

## 2.2 Semantic Web and Linked Data

The concept of Linked Data originates from the World Wide Web, invented by Tim Berners-Lee and Robert Cailliau at CERN in 1990 [14]. Initially, the web aimed to enhance data exchange among scientists and facilitate the referencing of information regardless of location. Berners-Lee emphasised the need to address distributed information, incompatible file formats, and evolving information requirements [15], leading to the development of the Semantic Web and Linked Data. These principles are highly relevant for the construction industry, characterised by separate systems, multiple stakeholders, and continuous changes. Linked Data can facilitate seamless information exchange, enabling stakeholders to maintain their formats and systems while accessing linked information and referring to the same construction element.

A key component of leveraging Linked Data in construction is the use of ontologies and the standardised description of elements and processes. Ontologies, as formal representations of concepts, their relationships, and attributes [16], are crucial for creating consistent descriptions of construction elements and processes. Recently, developing ontologies for specific domain structures has become increasingly common, particularly in construction, where they address project complexities and enhance interoperability across systems and stakeholders [17].

### 2.3 Collaboration and Storage - ICDD

Currently, Building Information Modelling (BIM) establishes common definitions for construction elements and processes and serves as the leading digital tool for information sharing in the construction industry. While current research focuses on BIM-based information management during the design phase, applying these practices to the construction and maintenance phases can significantly enhance information flow, efficiency, and reusability in circular construction [18]. However, to fully leverage digital tools in the construction industry, it is essential to go beyond BIM by incorporating Linked Data principles. The biggest challenges are the vendor-neutral exchange of heterogeneous, distributed building data as well as the long-term storage and access to the data. The Information Container for Linked Document Delivery (ICDD) was released in 2020 to provide a standardised format for exchanging and sharing of construction-related documents and data. The ISO 21597 provides an open and structured container format for different types of shared information, such as building models, documents and other relevant data and most important, their relationship [6], [7]. In order to guarantee conformity to the container schema and the links between the files within the ICDD, recent research has concentrated on semantic rule checking using Shapes Constraint Language (SHACL) [19]. Moreover, the utilisation of the ICDD can be evidenced as an effective deployment of an exchange platform for diverse stakeholder activites pertaining to asset management during the operational phase [20]. The chapter 3.4 examines the various components of the ICDD structure with regard to the possibility of using the containers as persistent storage of construction data for deconstruction and ensuring access to the data.

## 3 Linked Data for Circular Construction

### 3.1 Methodology

This paper evaluates the ICDD as a data storage solution for circular construction by assessing its ability to address knowledge loss in transitions from pre-production, assembly and operation to deconstruction. It focuses on deconstruction data requirements and the information preservation standard, demonstrated through a case study on steel girder deconstruction.

### 3.2 Construction Requirements

The construction industry is characterised by multiple stakeholders, each with their proprietary systems, and long-lasting project durations encompassing planning, pre-fabrication, on-site assembly, operation, maintenance, and eventual deconstruction. In all phases a variety of data that is produced, requested and enriched throughout the lifecycle of a building. Standardised structuring, effective management and linking of this data is critical to optimising processes and ensuring sustainability. For the planning

phase of the deconstruction process, it is of great benefit to categorise the required data according to the specific requirements of different deconstruction activities. Consistent pre-structuring and linking of data will ensure that all necessary information is systematically organised and readily accessible to support efficient and effective deconstruction efforts. Key categories of data required may include:

Table 1: Required data at deconstruction stage

| Category | Data and Usage |
|---|---|
| Planning and Design | Material, Structural and Design Data |
| Carbon Footprint Assessment | Location of Both Sites and Transport Emissions |
| Testing and Validation | Type and Result of Material Testing |
| (Robotic) Deconstruction Process | Installation Location, Weight, Size, Assembly Data |
| Authorisations and Legal Requirements | Deconstruction Authorisations and Legal Documents |
| Logistics | Assembly, Weight, Structural Data and Transport Data |
| Time Plan | Detailed Schedule and Structured Workflow with Responsibilities |
| Technical Equipment | Availability of Necessary Machinery and Equipment |
| Administration | Responsibility and Contact Data |

### 3.3 Requirements for the Implementation of Information Preservation Standards

Implementing information preservation standards in construction requires a comprehensive approach with the following key requirements:

- Standardised data structure to ensure completeness of required data at deconstruction phase
- Enable proprietary systems but linked data of individual stakeholder at construction project
- Enable the addition of information throughout the lifecycle of the structure
- Enable collaboration during planning, construction and deconstruction phase
- Ensure comprehension of data
- Ensure data availability in 30-50 years
- Overcome current boundaries of data ownership and authorisation

### 3.4 Application ICDD as Data Storage

The following section evaluates the application of the ICDD as a data storage solution for enabling deconstruction, specifically addressing the key requirements outlined in 3.3. Triple stores as the central data storage facilitate data access and specific querying for information during the construction project. However, it is also crucial to not only have structured individual data, but also to link different documents within a construction project. The ICDD offers a solution for creating these document links. The container comprises three components: an ontology folder containing the file schema, a linkset folder with the links, and a payloads folder containing the documents [6], [7]. Proposing the ICDD for data storage to enable circular construction may extend its use beyond merely publishing the ICDD in the Common Data Environment (CDE) as a virtual repository for collecting and managing construction projects. The concept would follow this procedure:

- **Ensure Completeness of Index File:** It covers the completeness and unique identification of meta-information of the file, e.g. which project information are contained
- **Ensuring Completeness of Ontology Folder:** It covers the structure of the construction and collaboration data of the project, so users (machine and human) can interpret the data at a later point, e.g. using the *dstv* ontology to explain how fabrication data for steel elements is modelled
- **Ensuring Completeness of Linkset Folder:** It includes the consistent and complete link of documents, e.g. link of fabrication data and onsite assembly documentation data
- **Ensuring Holistic Data in Payloads Folder:** It includes all the relevant data and files itself, e.g. the architectural model, delivery notes, quality documents, etc.
- **Exporting ICDD at Point in Time:** Once it is ensured that all relevant data and files are stored within the container, it can be exported as a *Zip file at a specified time, e.g. when the building is handed over to the client
- **Save ICDD File:** The file must be stored in a location that ensures long-term access and availability. Since the container includes all relevant information, incompleteness is not an issue. However, challenges remain regarding storage locations, such as local versus cloud servers (including copies), as well as data ownership and authorisation.

### 3.5 Use Case

Referring to Table 1 and the proposed ICDD procedure, the following use case demonstrates the theoretical application of ICDD as a data repository for the deconstruction of an assembled steel girder (see Figure 1).

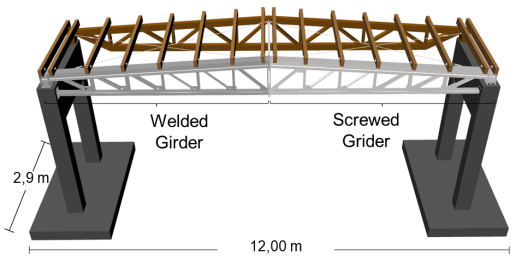


Figure 1: Assembled steel girder, Reference to IoC demonstator [21]

Within Linked Data, ontologies ensure a standardised data structure tailored to each specific domain. For construction, and specifically the reuse of a steel girder, initial approaches for an ontology in steel construction have been developed [22]. This allows for the storage and linking of domain-specific information, such as holistic and unified manufacturing details (e.g. the diameter or position of a hole) and process feedback (e.g. the machine used and time of manufacture). Defining a Uniform Resource Identifier (URI) at the project's outset ensures that all information added by different stakeholders, using their specific software, links to the same element. This unique connection and collaboration are maintained throughout the life cycle, whether in manufacturing, logistics, or on-site assembly.

For evaluating the theoretical application of ICDD as a data repository, it is assumed that the steel girder will be robotically deconstructed following its initial use in a building. The deconstruction

process necessitates several essential pieces of information: the girder's location within the building for accurate robot positioning, the weight of the girder to ensure machine capacity and availability, detailed specifications for effective gripper placement, and the type of connections and assembly details to enable the robot to disassemble the components accurately.

One of the key advantages of Linked Data is that it is both human-readable and machine-readable. This requires that information is explicitly defined to cater to different uses and interpretations. For example, while a human can intuitively understand that a part of the steel beam is screwed and thus easier to dismantle, a robot requires this information to be clearly encoded to interpret and execute the task effectively.

Referring to the ICDD, all required information for the deconstruction process should be contained in the *Zip file. In this case, the ontology folder contains the *dstv* ontology, which maps the fabrication processes in steel construction. The robot can retrieve information about the different elements, their connections, and assembly details to disconnect the screwed parts. From the payloads folder, the robot can determine the screws' locations and the force with which they are tightened, enabling it to separate the elements. The linkset folder integrates two distinct documents—fabrication information, which specifies the placement of the threaded hole on the beam, and on-site assembly documentation, which records the final position and force used to tighten the screws—facilitating the deconstruction process.

## 4 Results and Outlook

The paper introduced an approach utilising Linked Data concepts and ICDD as storage for preserving information, enabling deconstruction processes and Circular Construction. As demonstrated in 3.5, the structured ICDD and Linked Data can address the necessary information outlined in 3.2, providing a comprehensive database for accessing relevant data. However, further research is required to validate the approach and apply it to real-world scenarios. One significant challenge arises when utilising the ICDD file exported at a single point in time, particularly in managing information related to building operation and maintenance. This challenge encompasses determining how to add new data to the container and ensuring the completeness of information, along with addressing issues of data ownership, responsibility, and access authority.

The current methodology primarily focuses on newly constructed buildings for information preservation, overlooking challenges related to accessing information from existing structures for secondary material resources. Solutions can be drawn from recent research on data preservation, maintenance, and digitisation of built cultural heritage [23]. Like built cultural heritage, construction projects face challenges of heterogeneous data, diverse domain experts, and standards. Storing 3D point cloud data representing the built environment and linking it to new data for deconstruction processes can address this challenge.

Linked Data enables collaboration, information querying, process optimisation, and preserves process and project knowledge, benefiting future projects by promoting the reuse of processes and information across similar endeavors. This approach ensures that construction projects are not seen as singular

efforts but as part of a continuum, enhancing efficiency and continuity. Moreover, this approach is applicable beyond steel construction and can be extended to various construction processes and projects, including concrete and timber production, infrastructure, and special engineering projects.

## Acknowledgements

This work is part of the research project EConoM funded by the Federal Ministry for Digital and Transport of Germany within the initiative InnoNT (funding number 19OI22009F). It was supported within the TARGET-X framework, a project funded by the Smart Networks and Services Joint Undertaking (SNS JU) under Horizon Europe (funding number 101096614). The author is responsible for the content.

## References

[1] P. Santos, G. C. Cervantes, A. Zaragoza-Benzal, *et al.*, "Circular material usage strategies and principles in buildings: A review", *Buildings*, vol. 14, no. 1, 2024. DOI: 10.3390/buildings14010281.

[2] United Nations Environment Programme, *2022 global status report for buildings and construction: Towards*, Nairobi, 2022.

[3] S. Ji, B. Lee, and M. Y. Yi, "Building life-span prediction for life cycle assessment and life cycle cost using machine learning: A big data approach", *Building and Environment*, vol. 205, 2021. DOI: 10.1016/j.buildenv.2021.108267.

[4] R. Carvalho Machado, H. Artur de Souza, and G. de Souza Veríssimo, "Analysis of guidelines and identification of characteristics influencing the deconstruction potential of buildings", *Sustainability*, vol. 10, no. 8, 2018. DOI: 10.3390/su10082604.

[5] T. Heath and C. Bizer, *Linked Data*. Cham: Springer International Publishing, 2011. DOI: 10.1007/978-3-031-79432-2.

[6] *Din en iso 21597-1:2021-07, informationscontainer zur datenübergabe_- austausch-spezifikation_-teil_1: Container (iso_21597-1:2020);* Berlin. DOI: 10.31030/3137795.

[7] *Din en iso 21597-2:2021-07, informationscontainer zur datenübergabe_- austausch-spezifikation_-teil_2: Dynamische semantik (iso_21597-2:2020);* Berlin. DOI: 10.31030/3192763.

[8] P. Hagedorn, M. Senthilvel, H. Schevers, and L. B. Verhelst, *Towards usable icdd containers for ontology-driven*, Matera, Italy, 2023.

[9] S. H. Ghaffar, M. Salman, and M. Chougan, "The circular construction industry", in *Innovation in Construction: A Practical Guide to Transforming the Construction Industry*, S. H. Ghaffar, P. Mullett, E. Pei, and J. Roberts, editors, Cham: Springer International Publishing, 2022. DOI: 10.1007/978-3-030-95798-8_4.

[10] R. Charef, J.-C. Morel, and K. Rakhshan, "Barriers to implementing the circular economy in the construction industry: A critical review", *Sustainability*, vol. 13, no. 23, 2021. DOI: 10.3390/su132312989.

[11] M. Honic, I. Kovacic, P. Aschenbrenner, and A. Ragossnig, “Material passports for the end-of-life stage of buildings: Challenges and potentials”, *Journal of Cleaner Production*, vol. 319, 2021. DOI: 10.1016/j.jclepro.2021.128702.

[12] I. Atta, E. S. Bakhoum, and M. M. Marzouk, “Digitizing material passport for sustainable construction projects using bim”, *Journal of Building Engineering*, vol. 43, 2021. DOI: 10.1016/j.jobe.2021.103233.

[13] N. Mohan, G. Wolf, M. Wogan, J. Beilfuß, and R. Groß, “Auf dem weg zu einem ganzheitlichen lebenszyklusmanagement von bauwerken für nachhaltiges bauen: Vorschlag einer methodik zur digitalen transformation durch datenbankbasierte informationsmodelle”, 2023.

[14] T. Berners-Lee, *Weaving the Web: The Original Design and Ultimate Destiny of the World Wide Web*. 2000.

[15] R. Guns, “Tracing the origins of the semantic web”, *Journal of the American Society for Information Science and Technology*, vol. 64, no. 10, 2013. DOI: 10.1002/asi.22907.

[16] T. R. Gruber, “A translation approach to portable ontology specifications”, *Knowledge Acquisition*, vol. 5, no. 2, 1993. DOI: 10.1006/knac.1993.1008.

[17] Z. Zhou, Y. M. Goh, and L. Shen, “Overview and analysis of ontology studies supporting development of the construction industry”, *Journal of Computing in Civil Engineering*, vol. 30, no. 6, 2016. DOI: 10.1061/(ASCE)CP.1943-5487.0000594.

[18] D.-G. Lee, J.-Y. Park, S.-H. Song, and S. K. Shukla, “Bim-based construction information management framework for site information management”, *Advances in Civil Engineering*, vol. 2018, 2018. DOI: 10.1155/2018/5249548.

[19] P. Hagedorn, P. Pauwels, and M. König, “Semantic rule checking of cross-domain building data in information containers for linked document delivery using the shapes constraint language”, *Automation in Construction*, vol. 156, p. 105 106, 2023. DOI: 10.1016/j.autcon.2023.105106.

[20] P. Hagedorn, L. Liu, M. König, *et al.*, “Bim-enabled infrastructure asset management using information containers and semantic web”, *Journal of Computing in Civil Engineering*, vol. 37, no. 1, 2023. DOI: 10.1061/(ASCE)CP.1943-5487.0001051.

[21] T. Adams, S. Brell-Cokcan, P. R. Wildemann, *et al.*, “Ioc-demonstrator zur digitalisierung und automatisierung unternehmensübergreifender bauprozesse”, in *IoC - Internet of Construction : Informationsnetzwerke zur unternehmensübergreifenden Kollaboration in den Fertigungsketten des Bauwesens*, S. Brell-Cokcan and R. H. Schmitt, editors, Wiesbaden: Springer Fachmedien Wiesbaden, 2024. DOI: 10.1007/978-3-658-42544-9_7.

[22] L. Kirner, J. Oraskari, V. Jung, and S. Brell-Çokcan, “Dstv: An ontology-based extension of the dstv-nc standard for the use of linked data in the automation of steel construction”, in *LDAC*, 2023. [Online]. Available: https://api.semanticscholar.org/CorpusID:260708060.

[23] S. Noor, L. Shah, M. Adil, *et al.*, “Modeling and representation of built cultural heritage data using semantic web technologies and building information model”, *Computational and Mathematical Organization Theory*, vol. 25, no. 3, 2019. DOI: 10.1007/s10588-018-09285-y.

# Teil VI

# Sustainability

# How can development plans promote the sustainability of construction projects?

Jan Luther[1] and Jonas Maibaum[1]
[1]Chair of Computing in Engineering, Ruhr University Bochum, Universitaetsstrasse 150, 44801 Bochum, Germany
E-mail(s): jan.luther@rub.de, jonas.maibaum@rub.de

**Abstract:** The increasing demands on sustainability require a reorientation in neighborhood and building planning that takes into account various criteria from different areas. Early planning decisions in particular have a significant influence on the later sustainability performance of construction projects. Development plans are a suitable instrument for considering and ultimately defining tangible sustainability requirements for future neighborhood quarters and buildings at municipal level. A multi-layered model-based approach was developed for this purpose, which can be seen as a link between municipal neighborhood development and the subsequent building planning. Based on identified development plan parameters, a two-stage semi-automated process is used to perform a multi-criteria (ecological, economic and social) sustainability assessment. Initially, the parametric building envelope is generated based on the assumed development plans boundary conditions. In the second step, this is linked with component assemblies, materials, social, cost and environmental parameters. This process is repeated for various compliant scenarios and the results are then compared to determine the Pareto optimum for various criteria. In this way, the potential of the sustainability requirements defined in development plans can be clarified and the influence of early consideration and comparison of different scenarios for municipal urban and neighborhood development can be demonstrated. Advancing standardization (system, management and technical standards) and digitalization (data availability) in the field of neighbourhood planning and development will allow the potential to be further exploited in the future.

*Keywords:* Building information modeling (BIM), design automation, algorithms, energy simulation

Erschienen in Tagungsband 35. Forum Bauinformatik 2024, Hamburg, Deutschland, DOI: 10.15480/882.13524
© 2024 Das Copyright für diesen Beitrag liegt bei den Autoren. Verwendung erlaubt unter Creative Commons Lizenz Namensnennung 4.0 International.

## 1 Introduction and research framework

The realization of construction projects requires highly demanded primary resources and consumes huge amounts of energy. In addition, especially the extraction of raw materials and the manufacturing of construction products have a considerable impact on the environment [1].

Because of this, various goals have been defined that increase sustainability and thus should lead to a more circular economy. The main goals are to reduce the use of primary raw materials, close

material cycles, increase durability and reuse and exploit the potential of digital technologies such as BIM [2]. In order to implement this, it is necessary to identify the relevant levers (laws, guidelines and planning tools) for demanding and promoting greater sustainability and to provide construction-related information in a transparent, structured form to enable the use of standardized methods for calculating sustainability metrics.

The municipality can play an essential role in the solution here, as it is the planner and decision-maker in the creation and adaptation of land use planning and the subsequent planning and implementation of specific construction measures [3]. Municipal decision-makers have the opportunity to define various boundary conditions in context of sustainability for a construction project through the tendering process and land use planning. In Germany, the development plan in particular offers the opportunity to integrate sustainability aspects in a legally binding manner at an early stage.

With this area in mind, the characteristics of the development plan and the benefits of early BIM application are first presented before existing approaches in the context of sustainability calculation and optimization are outlined. Based on this, the developed optimization approach is introduced step by step and evaluated and finally classified using an implementation example.

## 1.1 Development plan and early BIM

Development (de: Bebauungsplan (BPlan)) and land use (de: Flächennutzungsplan) plans are an essential tool of urban land use planning. The land use plan is serving as a preparatory guide for the land usage of a municipality and the development plan as a binding urban instrument, that controls land use and urban development within specific areas of the municipality. According to the German Building Code (de: Baugesetzbuch), the development plan consists of two parts: the plan drawing, which graphically depicts the spatial arrangement and use of the land, and the text description, which describes the stipulations in detail. The objectives of the development plan are to ensure orderly urban development, sustainable land use and the creation of a legal basis for construction projects. However, the creation or adaptation of development plans is a time-consuming and complex procedure and can sometimes take several years.

Digitalization, particularly through the use of Building Information Modeling (BIM), significantly enhances the effectiveness and quality of building planning and construction processes. It facilitates early project evaluation, minimizes errors, and enables the pre-calculation of costs, environmental impacts and other aspects [4]. As part of linking the development plan and early planning phases with the help of BIM, the approach of Emamgholian et al. illustrate how development plan requirements can be integrated into the 3D environment in the form of rule validation and approval control. In addition, Borkowski et al. demonstrate that different environmental (GIS) and building information (BIM) can be merged and introduce the LIM (Land Information Model) for this purpose [5], [6].

## 1.2 Multi-criteria sustainability assessment

A sustainability assessment system typically involves data gathering, impact assessment for decision-making, and preparation for monitoring and reporting. It relies on established standards, iterative data refinement, and standardized procedures, with regulations being crucial for effective implementation [3]. The underlying environmental sustainability assessment method is the four-step (goal definition,

life cycle inventory, life cycle impact assessment and evaluation) LCA (life cycle assessment), which is standardised according to ISO 14040/44 [7], [8]. The LCC (life cycle cost assessment) and SLCA (social life cycle assessment) assessment follow a similar pattern to LCA and can be aggregated to the overall LCSA (life cycle sustainability assessment). In the context of LCSA, Wortmann et al. demonstrate that both the selection of materials (micro) and the urban or neighborhood morphology (macro) influence the various environmental impact directly [9]. It can be stated that for an object (material to urban scale) with the greatest possible sustainability, elements of micro, meso (building) and macro levels should be taken into account.

A current notable challenge within LCSA involves inconsistent utilization and insufficient clarity concerning the underlying data and key assumptions [10].

For linking BIM and LCSA at the building and neighborhood level, there exist various theoretical and practical integration approaches and numerous case studies with different scopes (level of detail (information and geometry), life cycle phases and number of parameters considered) [11]–[13]. Furthermore, it is apparent that BIM-LCSA integration is increasingly being shifted to the early planning phases [14]. However, both the integration of urban environment parameters and the consideration of sustainability during the preparation of development plans as part of municipal urban planning are currently only considered to a limited extent.

The linking of scenario modeling and sustainability assessment procedures within the scope of the possibilities of the development plan therefore appears to be appropriate and is described subsequently.

## 2 Development plan based LCSA using BIM

In the context of the challenge described, the three areas of development plan, BIM and LCSA should be merged. A multi-layer approach is used for this, which can be broken down into the three layers of data, application and user. As Figure 1 illustrates, data from various sources is collected, processed, analyzed and made available to the user for decision-making. For the concept developed for this purpose, first the substantive procedure and then the technical implementation are explained.

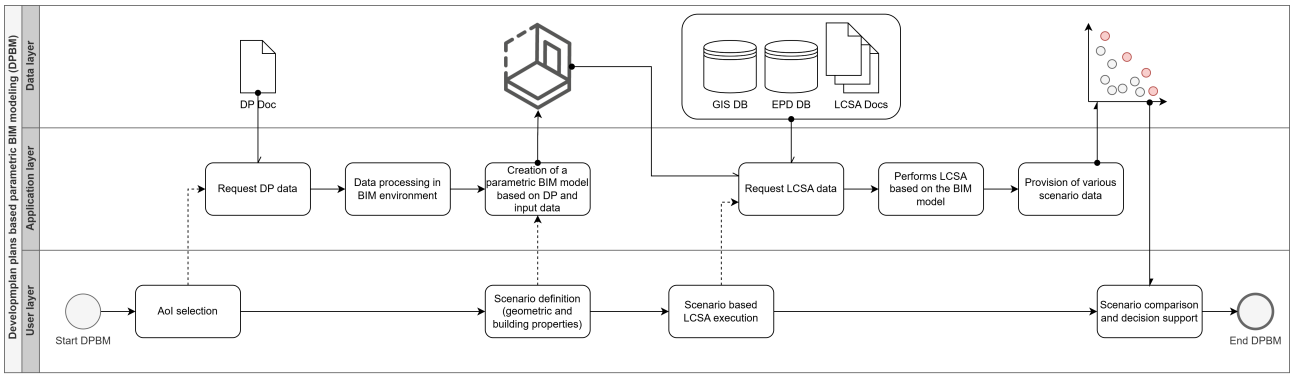


Figure 1: Concept overview, broken down by user, application and data layer (DPBM = Development Plan based BIM Modeling; DP = Development Plan; GIS DB = Geodata from GIS (e.g. OpenStreetMap); EPD DB = DataBase for Environmental Product Declarations (e.g. Oekobaudat); Doc(s) = Document(s))

## 2.1 Concept

For the application essentially two optimization points were identified: Development plan preparation (taking sustainability criteria into account) and sustainability-conscious neighborhood/building planning in compliance with development plan specifications. Both areas, the preparation of the development plan and the final implementation of the specifications and consideration of sustainability goals in accordance with regulations, are therefore very time-consuming and complex.

In order to take sustainability requirements into account and identify resource and environmental hotspots when creating development plans, various scenarios are formed for specific development plan areas (Area of Interest - AoI). Ecologic (environmental impacts), economic (costs) and social (comfort and environmental analysis) data are retrieved from LCA databases, literature values and geo-reference data, and linked with each other on a model and rule basis. The generic and average values used are suitable for the uncertainty that still exists at the time of application of the approach with regard to costs, environmental impact and building design aspects. Using this approach, an combined analysis of these criteria can be carried out for different types of neighborhood and the resulting values can be used as a decision-making support for parameter variation and definition in the development plan creation and neighborhood/building planning process. During the planning phase, sustainability reference values can initially be specified and then checked for compliance by running numerous possible general scenarios.

The data for the analysis comes from two main sources: user input by a decision-maker or planner of the development plan in the municipal service and deposited data from databases and literature values. The user input relates primarily to the geometry of the object and the selected construction type. The stored data for the overall life cycle assessment (e.g. GWP - global warming potential) comes from the German EPD database (Ökobaudat), whose generic data sets are supported by scientific studies. GWP is used as an LCA indicator in the case study as an example. All LCA levels (A1-C4 + recycling potential) are aggregated to calculate the total value for the entire service life of the building component. The cost data comes from the BKI cost catalogue (de: BKI Kostenkatelog) and the geo-referenced environmental data is retrieved via the Overpass API, which can be used to access OpenStreetMap data. With this data, a uniform scenario database for the further calculations is created. Pareto Optimum (cf. Figure 3) can then be formed from the data of the LCSAs in orderto determine the most suitable configuration for the defined priority of sustainability. A modelling approach has therefore been developed that combines the various areas of development plan preparation, BIM and LCSA in a simple way to enable municipal decision-makers to demand and promote sustainability requirements through informative scenario creation and analysis.

## 2.2 Technical implementation

For the technical implementation, existing software architecture was used. Both the BIM authoring software Revit and the Dynamo extension, which is already natively integrated in Revit, were used for this purpose. Revit is only used for the geometric representation and evaluation basis of the 3D BIM models created. Dynamo is an open source extension for Revit that serves as a program interface between the created program code and the Revit model in order to implement automatic processes. By starting the developed Dynamo application, decision makers can select different parameters for the

modeling to simulate different scenarios. This is done via an user interface in which parameters such as the number, height and roof shape of the objects can be selected. As part of the modeling process, the development plan is first converted into a format that can be interpreted by CAD systems. Then, a sub-area of the entire development plan is selected (AoI, see Figure 2a) and the relevant development plan parameters are identified (building line, distance area, type and extent of building use, construction method, maximum and minimum dimensions, etc.). The area of interest is subdivided into smaller plots depending on the type of development selected. This serves as the basis for cubature modeling, which generates the floor levels, the exterior walls and the roof. The roof then adapts to the last floor and is generated ontop of it. Finally, a geometry is created for the interior walls, which supports various apartment layouts. Depending on the floor area and the chosen parameters, it gets divided into one or more sub-areas, in which the parametrically pre-defined apartment plans of the individual apartments are integrated (cf. Figure 2b). The floor plans used are based on a range of standard apartment layouts and can be choosen by the user.
Four different construction types serve as the basis for the layout of the different parts (outer- and inner walls, roof, floor): Brick, Concrete, Wood and PreCast-Concrete. Each of these construction types not only defines the general cross-sectional geometry of the respective building parts but also categorizes the materials used for environmental impact calculations. The data addressed for this purpose comes from an EDP data bank (Oekobaudat) and is requested at runtime using an API and linked to the intended model elements. In this step, the material data available as XML is processed using Python code within the Dynamo framework. The total GWP for each material is calculated, linked with the dedicated material category for each part and then, the sum between every material from each category is formed, to get every possible combination of parts.
The social indicator is determined by the size of the living area per person, access to public transport and the distances to various social infrastructure facilities such as schools or hospitals. This geodata is requested and processed using an API to the geodata database Overpass by comparing the coordinates of the object area with the stored data from Overpass. The social indicator is then determined from this data, with a high index being classified as good. A breakdown and weighting of the various social criteria would also be possible.
The results from the BIM model are saved as a CSV file that contains all relevant information (e.g. number of floors, GWP, apartment size, etc.). Various model data can then be analyzed and compared using a Python script. For this purpose, a multidimensional (3D) Pareto front is created from the parameters cost, GWP and social of the various created objects and compared with each other. The Pareto front (cf. fig. 3) considers all factors simultaneously and evaluates them without neglecting any other factor. It is also possible to only analyze the models in regards to one or two of the parameters, if needed. Both the different geometries and the types of construction used are taken into account.

## 3 Use Case

The approach developed is implemented as part of an application example. The relevant information (development plan parameters) is extracted for a development plan sub-area (AoI) and automated neighborhood modeling is carried out. The preliminary process of semantic acquisition of development plan information is explained in Schönfelder et al. [15].

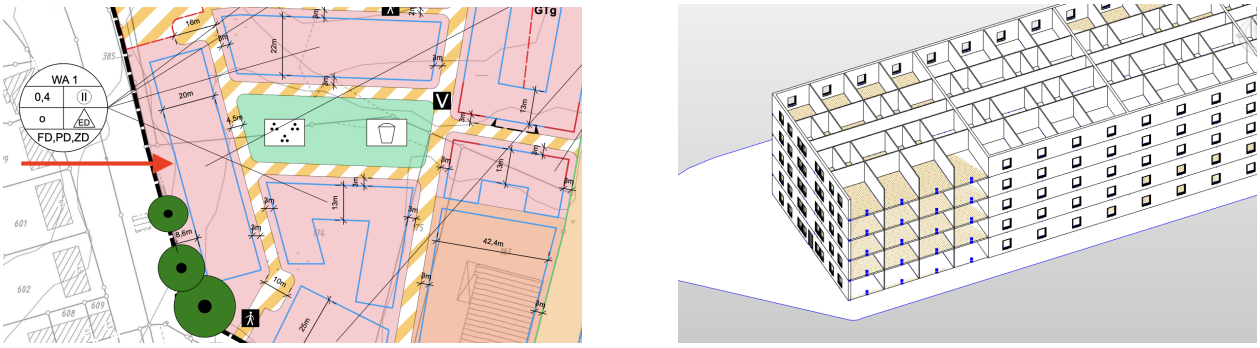


(a) (b)

Figure 2: (a) Cutout of existing Development Plan (DP), (b) Cutout of DP-based BIM-Model

For the use-case, a sub-area from a development plan located in Witten, Germany is used as a template. Decision-making for the selectable parameters is simulated. For this purpose, several buildings with different geometries and construction methods are modeled for the property and then analyzed.
The size, number of residents and type of property are varied in order to capture and compare as many building types as possible. To be able to compare the results with each other, the respective data is normalized to the per person value. Detached apartment buildings, terraced houses and individual residential units were simulated as building types. Different roof shapes, apartment layouts and building materials were used. In addition, the retrieved and subsequently calculated LCSA data is visualised in a 3D Pareto front. This reflects the trade-offs between the three sustainability criteria assessed. The Pareto front provides information about the most efficient solutions where an improvement in one criteria is not possible without worsening the performance of another. Solutions that lie on the 3D Pareto front represent the best trade-offs and offer the most efficient options in terms of GWP, costs and social. For the three-dimensional visualisation, one criteria from each sustainability area was compared. A dedicated comparison is also possible. This information is helpful for decision making when selecting the optimal neighborhood or building design for certain circumstances and objectives.

The results of the case study based on an existing development plan show advantageous values for the used material wood and prefabricated concrete, due to their low CO2 emissions. In addition, the construction of terraced houses and apartment buildings is favored, as they offer a higher level of living comfort (cf. Figure 3). In the Pareto front, the best results for the different categories can be seen: Precast concrete apartment building is the most economical, wooden apartment building the most ecological and the multi-family-house has the highest social-indicator. The wooden multi-family-house performs the best among all three aspects.

## 4 Conclusions

The main focus was on the creation of a modeling approach for the integration of urban planning requirements from development plans, environmental parameters (e.g. accessibility) and the multi-

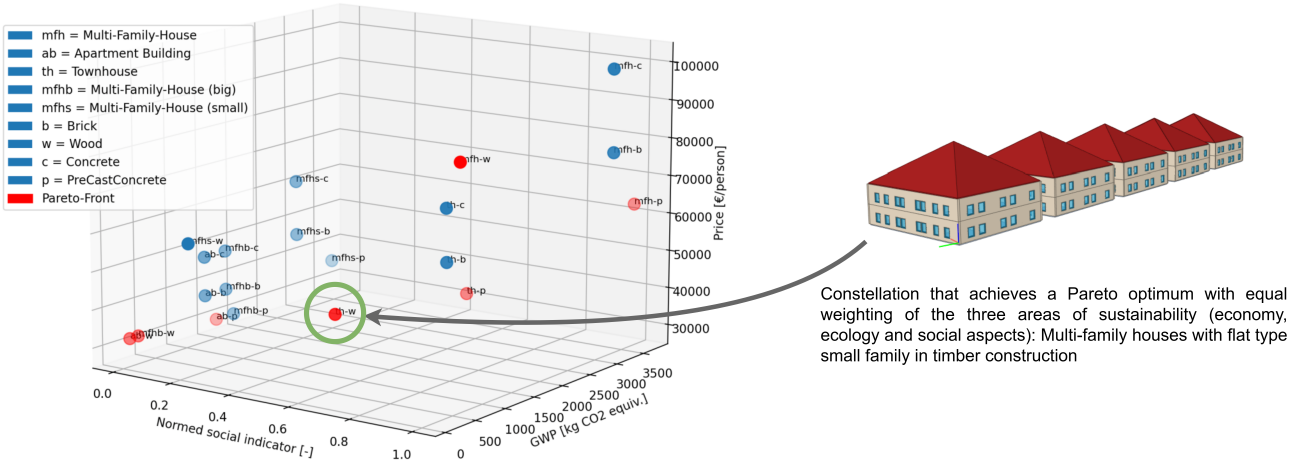


Figure 3: Left: Pareto Optimums for multi-criterial LCSA; Right: Pareto Optimum equal weighting of the three areas of sustainability

criteria sustainability assessment in combination with BIM. Depending on the sustainability priorities of a municipality, different scenarios can be created and compared. Ultimately the most suitable one can be selected for further neighborhood planning. By calculating the Pareto optimum, it is possible to determine and visualise these priorities. Using multi-stage modeling, relevant geometric and semantic parameters were retrieved, linked and used for sustainability assessments. For the scenarios considered in a case study, it was demonstrated that by determining the Pareto optimum for various sustainability criteria, a basis for decision-making was created that does not focus solely on the cost criteria, as is often the case in current practice. The authors conclude that this early consideration of sustainability on the basis of development plan parameters as part of neighborhood planning can improve the later sustainability performance of constructions

The approach currently focuses on greenfield sites and new buildings. Additional potential can be exploited by considering existing buildings and adding further sustainability approaches such as climate and soil analyses. To furthermore strengthen the results and make the analysis more precise, additional factors could be taken into account, such as access to natural light, noise pollution, usage of recycled material and cost values for different parts and life cycle stages. Especially for the social aspects, a broader research basis for linking specific living parameters with the perception of their residents would be advantageous.

In general, as also demanded by the Roadmap Circular Econmoy, more standardization for sustainability calculation methods and data collection, and a uniform mandatory database for environmental, product, component and material data would be desirable. The establishment of a standardised level of information need would be the objective for this.

## References

[1] United Nations Environment Programme', "2022 global status report for buildings and construction: Towards a zero-emission, efficient and resilient buildings and construction sector", 2022.

[2] Bundesministerium für Umwelt, Naturschutz, nukleare Sicherheit und Verbraucherschutz and www.bmuv.de, "Entwurf einer nationalen kreislaufwirtschaftsstrategie (nkws) (en: Draft national circular economy strategy", 2024.

[3] DIN, DEA, VDI and BMVU, "Standardization roadmap circular economy", 2023.

[4] A. Borrmann, M. König, C. Koch, and J. Beetz, *Building Information Modeling*. Springer Fachmedien Wiesbaden, 2021. DOI: 10.1007/978-3-658-33361-4.

[5] S. Emamgholian, J. Pouliot, and D. Shojaei, "3d citylur: Modelling 3d city land-use regulations to support issuing a planning permit", *ISPRS Annals of the Photogrammetry, Remote Sensing and Spatial Information Sciences*, 2021. DOI: 10.5194/isprs-annals-VIII-4-W2-2021-113-2021.

[6] A. Borkowski, Ł. Kochański, and M. Wyszomirski, "A case study on building information (bim) and land information (lim) models including geospatial data", *Geomatics and Environmental Engineering*, 2022. DOI: 10.7494/geom.2023.17.1.19.

[7] ISOa, "Iso 14044 - environmental management — life cycle assessment — principles and framework", 2022.

[8] ISOb, "Iso 14044 - environmental management — life cycle assessment — requirements and guidelines", 2022.

[9] F. De Luca, J. Natanian, and T. Wortmann, "Ten questions concerning environmental architectural design exploration", *Building and Environment*, 2024. DOI: 10.1016/j.buildenv.2024.111697.

[10] J. G. Backes and M. Traverso, "Application of life cycle sustainability assessment in the construction sector: A systematic literature review", *Processes*, 2021. DOI: 10.3390/pr9071248.

[11] L. Wastiels and R. Decuypere, "Identification and comparison of lca-bim integration strategies", *IOP Conference Series: Earth and Environmental Science*, 2019. DOI: 10.1088/1755-1315/323/1/012101.

[12] J. P. Carvalho, I. Alecrim, L. Bragança, and R. Mateus, "Integrating bim-based lca and building sustainability assessment", *Sustainability*, 2020. DOI: 10.3390/su12187468.

[13] R. K. Zimmermann, S. Bruhn, and H. Birgisdóttir, "Bim-based life cycle assessment of buildings—an investigation of industry practice and needs", *Sustainability*, 2021. DOI: 10.3390/su13105455.

[14] T. Potrč Obrecht, M. Röck, E. Hoxha, and A. Passer, "Bim and lca integration: A systematic literature review", *Sustainability*, 2020. DOI: 10.3390/su12145534.

[15] P. Schönfelder, H. Duski, J. Maibaum, and M. König, "Image segmentation for enhanced visualization and accessibility of historical municipal development plans", *ICCCBE, Montreal*, 2024.

# Distance-based Loss Function for Machine Learning in Image Segmentation of Concrete Cracks

Baris Özcan and Fabian Alexander Schmiedecke
Geodetic Institute and Chair for Computing in Civil Engineering & Geo Information Systems,
RWTH Aachen University, Mies-van-der-Rohe-Str. 1, 52074 Aachen, Germany
E-Mail: oezcan@gia.rwth-aachen.de

**Abstract:** Crack detection is essential for maintaining the integrity and safety of infrastructure such as bridges, roads, and buildings. Traditional manual inspection methods are labor-intensive and error-prone, which underscores the need for automated solutions. Advances in machine learning have shown promise in automating this task, but further improvements are necessary to address specific challenges, such as the thin and elongated nature of cracks, varying lighting conditions, and background noise. This paper presents a refined loss function designed to enhance the performance of machine learning models in detecting fine-structured concrete cracks. This loss function considers the spatial distances between predicted and actual crack locations, penalizing false positives that are far from true crack positions. In this way, our approach emphasizes the thin nature and continuity of cracks, ensuring that even the smallest features are accurately detected. Our initial experiments demonstrate that this strategy offers a more accurate and reliable solution to crack detection.
*Keywords:* Concrete Crack Detection, Computer Vision, Machine Learning, Image Segmentation, Loss Functions

Erschienen in Tagungsband 35. Forum Bauinformatik 2024, Hamburg, Deutschland, DOI: 10.15480/882.13533
© 2024 Das Copyright für diesen Beitrag liegt bei den Autoren. Verwendung erlaubt unter Creative Commons Lizenz Namensnennung 4.0 International.

## 1 Introduction

Crack detection is crucial in civil engineering and infrastructure maintenance, ensuring the safety and longevity of structures like bridges, roads, and buildings. Early detection and timely repair of cracks can prevent catastrophic failures, making crack detection a critical task. Traditional methods rely on manual inspection, which is labor-intensive, time-consuming, and prone to human error. Consequently, automated crack detection using advanced

image processing and machine learning techniques has seen significant attention in recent years.

In automated crack detection, deep learning models, particularly convolutional neural networks (CNNs), have demonstrated remarkable performance improvements. These models can learn complex patterns and features from large image datasets, enabling highly accurate detection of cracks. Despite these advancements, there are several challenges. One primary challenge is that traditional loss functions and evaluation metrics often fail to adequately capture and consider the thin, elongated nature and continuity of cracks, as well as account for varying lighting conditions and background noise.

This research proposes a distance-based loss function customized for detecting fine structures, such as cracks, in images using machine learning. The proposed loss function enhances the performance of crack detection models by penalizing false positives that are far from the true crack locations, thereby improving the detection and continuity of cracks. By focusing on the spatial distance between predicted and actual crack locations, this loss function effectively addresses the challenges associated with the thin and elongated nature of cracks, leading to more complete, precise and reliable automated crack detection.

The remainder of this paper is organized as follows: Section 2 reviews crack detection techniques and loss functions in machine learning contexts. Section 3 outlines our methodology, including the data preparation and the proposed loss function. Section 4 describes the experimental setup, including model architecture and training protocol. Section 5 presents our preliminary results and Section 6 provides a discussion of the results. Finally, Section 7 concludes the paper and suggests directions for future research.

## 2 State-of-the-art

### 2.1 Crack Detection Techniques

Early automated methods for crack detection [1] focused on image processing techniques, such as edge detection algorithms (e.g., Canny, Sobel), thresholding methods, and morphological operations. While these techniques showed some success, they were often limited by their sensitivity to noise, lighting variations, and the complexity of the background.

The emergence of machine learning, particularly deep learning, has revolutionized crack detection. Convolutional neural networks (CNNs) have been widely adopted due to their ability to automatically learn and extract hierarchical features from images. Several studies demonstrated the efficiency of CNNs in detecting cracks in various materials and conditions

[2]. However, these models, however, still often face challenges in accurately detecting fine, elongated cracks and differentiating them from similar patterns in the background.

### 2.2 Loss Functions in Image Segmentation

The choice of loss function is crucial in training deep learning models, as it directly impacts the ability of the model to learn from the data. In the context of image segmentation, several loss functions have been employed.

**Cross-Entropy Loss**: Commonly used in classification tasks, cross-entropy loss has also been applied to crack detection. However, it may not be the most effective for segmenting thin and elongated cracks due to its focus on pixel-wise classification without considering spatial arrangement or continuity.

**Dice Loss**: Dice loss is particularly useful for segmentation tasks, as it maximizes the overlap between the predicted and ground truth masks. This loss function often shows better performance in crack detection tasks compared to cross-entropy loss [3], particularly because it is less sensitive to class imbalance and better suited for cases where the object of interest occupies a small area relative to the background, such as thin cracks.

**Intersection over Union (IoU) Loss**: IoU loss measures the overlap between predicted and ground truth masks relative to their union. While similar to Dice loss in its focus on overlap, IoU loss provides a different perspective by emphasizing the union of the predicted and ground truth areas, which can be beneficial when minimizing false positives is crucial.

However, while these loss functions are effective in many scenarios, they may still face challenges in fully capturing the thin and continuous nature of cracks, particularly when spatial continuity and elongation are critical. Without further customization, machine learning models might produce fragmented or incomplete detections, potentially reducing their effectiveness in practical applications. Therefore, tailored loss functions are often necessary to enhance segmentation performance and ensure reliable automated crack detection.

## 3 Methodology

This section outlines the methodology of our research, including the data preparation and the loss function tailored for crack detection.

### 3.1 Data Preparation

For this study, we utilized a publicly available dataset comprising images of various surfaces with annotated cracks, accessible at Kaggle [4]. This dataset is a compilation of 12 publicly available crack segmentation datasets, containing approximately 11,200 images. All images

in the dataset has been resized to a resolution of 448 x 448 pixels. The dataset includes images from diverse environments, ensuring variability in crack appearance due to different lighting conditions, materials, and background noise. However, inaccurate labels in the dataset were identified and manually removed to maintain reliability in model training and evaluation. Some sample images of this dataset is shown in Figure 1.

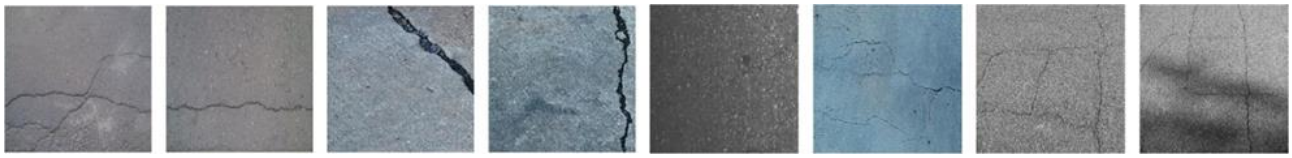

Figure 1: Sample images of the crack dataset.

To enhance the robustness and generalizability of the model, data augmentation techniques were applied. These techniques include rotation and flipping to introduce geometric variability, adjustments on brightness and contrast to simulate different lighting conditions and addition of Gaussian noise to make the model more resilient to real-world image noise.

Further preprocessing steps included resizing images to a uniform size of 128 x 128 Pixel with bicubic interpolation and normalizing pixel values.

### 3.2 Distance-based Loss

The Distance-based Loss function (DL) is designed to emphasize the continuity of cracks and prevent the prediction of background noise as separate cracks. This loss function integrates a distance map for each image, where every pixel is assigned a normalized value, depending on its distance to the nearest crack pixel priors to penalize FP predictions that are further away from the cracks in the predicted crack segments. The mathematical formulation is as follows:

$$\mathcal{L}_{DL} = \mathcal{L}_{Dice} \cdot (1 + \mathcal{L}_{Dist} \cdot (\alpha - 1)) \tag{1}$$

where $\mathcal{L}_{Dice}$ is the Dice loss ensuring overlap maximization, and $\mathcal{L}_{Dist}$ is a term that penalizes false positives based on their distance from the nearest crack pixel. The parameter $\alpha$ controls the balance between the two components.

$$\mathcal{L}_{Dice} = \frac{2 \cdot \mathrm{TP}}{2 \cdot TP + FP + FN} \tag{2}$$

$$\mathcal{L}_{Dist} = \frac{1}{N_{FP}} \sum_{i=1}^{N_{FP}} ND(FPI(i)) \tag{3}$$

with

$N_{FP}$: Number of False Positives

$ND$: Normalized Distance from Nearest Crack Pixel

$FPI$: False Positive Index

# 4 Experimental Setup

This chapter describes the experimental setup used to evaluate the proposed loss function for crack detection, including details about the model architecture and the training protocol.

## 4.1 Model Architecture

For our experiments, we used the U-Net architecture [5], a state-of-the-art CNN known for its effectiveness in image segmentation tasks. We specifically chose U-Net due to its proven performance in medical image segmentation, which shares similarities with crack detection in terms of requiring precise localization and boundary delineation. U-Net's encoder-decoder structure with skip connections allows for combining high-resolution features from the encoder with upsampled features from the decoder, capturing both fine details and contextual information. The encoder consists of convolutional and max-pooling layers, reducing spatial dimensions while increasing feature maps. The decoder includes upsampling and convolutional layers, restoring spatial dimensions and integrating features through skip connections, crucial for accurate crack detection.

## 4.2 Training Protocol

We split our dataset into 80% training, 10% validation, and 10% test sets to ensure comprehensive training and evaluation. The model was trained with the Adam optimizer (learning rate $5 \times 10^{-4}$, a batch size of 25, and for 50 epochs). We used the proposed Distance-based Loss function with the parameter $\alpha = 4.0$. To prevent overfitting and improve generalization, dropout layers with a rate of 0.3 were used in the decoder and encoder, and extensive data augmentation techniques such as rotation, flipping, brightness and contrast adjustment, and noise addition were employed.

# 5 Results

In this section, we present the results of our experiments for the proposed loss function for crack detection and compare it with standard loss functions.

### 5.1 Quantitative Results

We evaluated our model trained with the proposed loss function using five common metrics and compared it with two models trained with standard loss functions (Binary Cross-Entropy and Dice Loss). The results are summarized in Table 1.

Table 1: Performance comparison of our proposed loss function with two standard loss functions based on several metrics.

| Metric | Binary Cross-Entropy Loss | Dice Loss | Distance-based Loss |
|---|---|---|---|
| Precision | 0.4771 | 0.5202 | 0.5856 |
| Recall | 0.2336 | 0.7407 | 0.7707 |
| F1 Score | 0.2860 | 0.6001 | 0.6589 |
| IoU | 0.2147 | 0.3824 | 0.5027 |
| Dice | 0.3000 | 0.5609 | 0.6078 |

### 5.2 Qualitative Results

Additionally, the visual results for the predicted image masks of the cracks offer a more detailed evaluation of the model's performance. Figure 2 illustrates a comparison of crack detection outcomes using the three different loss functions, together with the original input images and the ground truth masks.

## 6 Discussion

Our initial experiments show that the model trained with the proposed Distance-based Loss function outperforms those using traditional loss functions. The proposed loss function led to better results for all evaluation metrics, indicating superior performance in the segmentation of cracks. Additionally, visual results show that the Distance-based loss function produces more accurate and continuous crack detections compared to traditional loss functions.

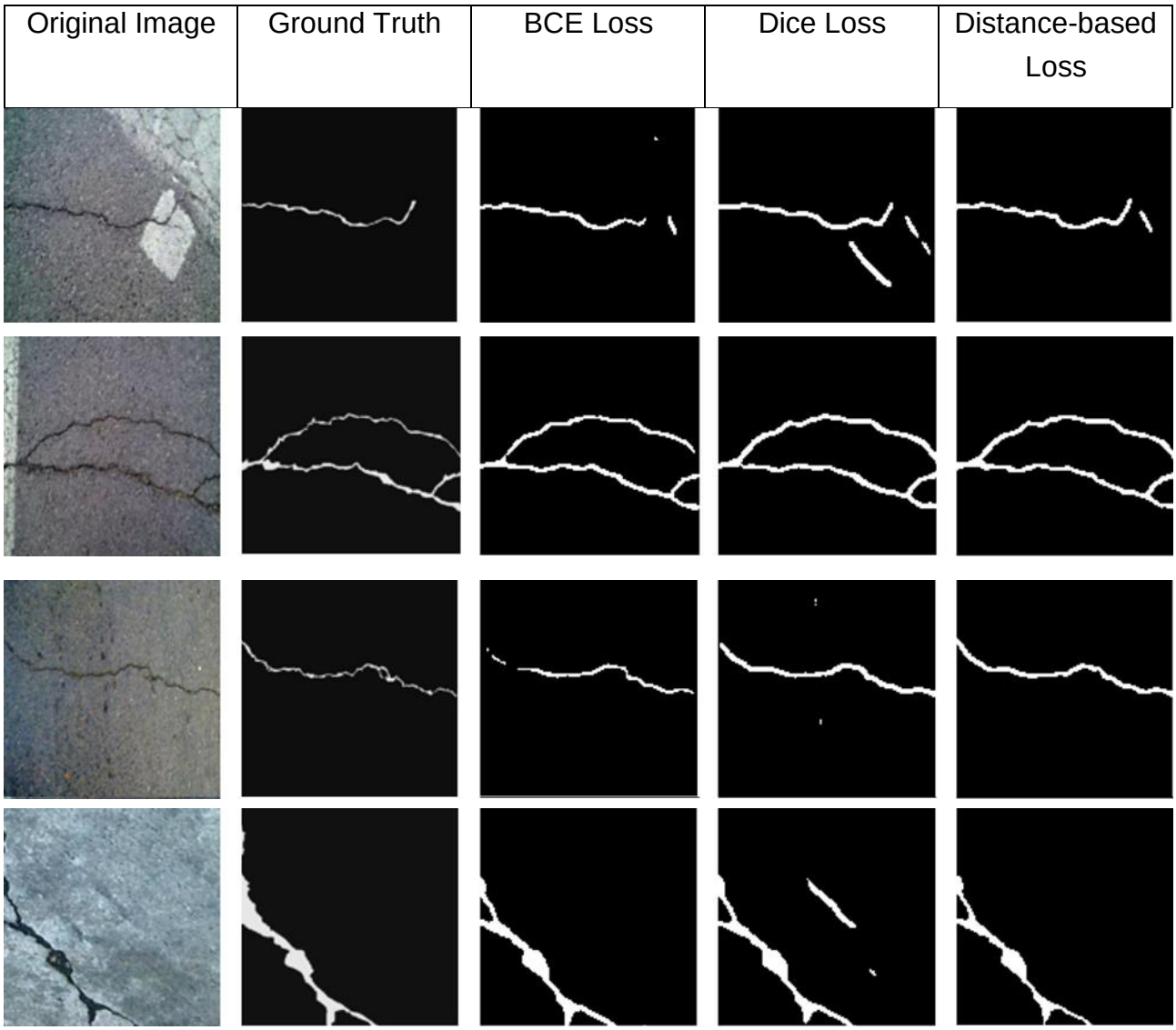


Figure 2: Crack detection results, from left to right: Original image, Ground Truth, Binary Cross-Entropy Loss, Dice Loss, and Distance Loss

The improved performance of the distance-based loss function comes from its ability to penalize false positives that are spatially distant from the true crack locations. This added spatial dimension reduces inaccuracies by focusing on the spatial relationship between the predicted and actual crack locations, unlike traditional loss functions that treat each pixel independently. Furthermore, the Distance-based loss function facilitates the model to detect cracks as continuous entities rather than seperated segments by emphasizing the spatial distance between connected components. This approach promotes spatial coherence, leading to smoother and more continuous predictions. Moreover, by focusing on the spatial consistency of cracks, the loss function helps the model differentiate between true crack signals

and random noise, leading to more reliable crack detection in the presence of image noise. Additionally, handling class imbalance more effectively, the distance-based loss function prioritizes the accurate identification of crack pixels, improving detection performance in imbalanced datasets where non-crack pixels dominate. Also, the spatial relationships in the loss function helps the model learn more generalized features of cracks, making it more robust to different types of cracks and variations in new datasets. Lastly, the loss function aligns predicted cracks with human perception by ensuring that detected cracks are continuous and structured, which makes the results more intuitive.

## 7 Conclusion

In this paper, we proposed a Distance-based loss function customized for crack detection to address the limitations of traditional loss functions. This loss function penalizes false positives that are far from the true crack locations, improving the continuity and accuracy of detected cracks. Our initial experiments demonstrated that this approach outperforms traditional loss functions.

Future work will focus on integrating additional loss functions and evaluation metrics to further enhance crack detection models. Building on our proposed Distance-based loss function, we aim to develop and incorporate more such functions and evaluation metrics that better capture the structures and nuances of cracks. This approach will help refining models for crack dectection, making them more robust and effective in practical applications.

## References

[1] A. Mohan and S. Poobal, "Crack detection using image processing: A critical review and analysis," Alexandria Engineering Journal, vol. 57, no. 2, pp. 787-798, June 2018.

[2] Y. Hamishebahar, H. Guan, S. So, and J. Jo, "A Comprehensive Review of Deep Learning-Based Crack Detection Approaches," Applied Sciences, vol. 12, no. 3, 2022.

[3] Q. D. Nguyen and H.-T. Thai, "Crack segmentation of imbalanced data: The role of loss functions," *Engineering Structures*, vol. 297, 2023.

[4] L. Middha, "Crack Segmentation Dataset," Kaggle, 2024. Accessed on: Aug. 23, 2024. [Online]. Available: https://www.kaggle.com/datasets/lakshaymiddha/crack-segmentation-dataset.

[5] O. Ronneberger, P. Fischer, and T. Brox, "U-Net: Convolutional networks for biomedical image segmentation," in Proc. Medical Image Computing and Computer-Assisted Intervention (MICCAI), Munich, Germany, 2015.

# Robotic Disassembly and Window Upgrading

Begum Aktas[1] and Mehrzad Esmaeili Charkhab[2]
[1]Civil System Engineering, Technical University of Berlin, Straße des 17. Juni 135, Berlin, Germany
[2]Robot-Assisted Manufacturing of the Built Environment,Technical University of Berlin, Straße des 17. Juni 135, Berlin, Germany
E-Mails: b.aktas@tu-berlin.de (corresponding author)

**Abstract:** Regular renovation of the built environment is essential for regulatory compliance and environmental impact reduction, with window upgrades significantly improving energy efficiency and reducing carbon footprints. Upgrading involves disassembling windows for repair or replacement and extending their life through reuse, repair, and remanufacturing. A Disassembly Map guides this process, showing different routes toward the end-of-life (EoL) for window components, ensuring efficient disassembly, repair, or replacement, thereby minimizing environmental impact. The 'Right to Repair' proposal in the EU promotes sustainable consumption, emphasizing the need for detailed disassembly planning. Robots can enhance disassembly efficiency, reduce costs, and decrease energy use. This study introduces a methodology for robotic window disassembly, focusing on an aluminum frame window to validate the method for upgrading window components. It includes a virtual simulation stage using RoboDk software and a demonstration stage with a UR10e robotic arm, emphasizing the critical role of Disassembly Maps in guiding efficient and sustainable upgrades.
*Keywords:* Windows Disassembly, Robotic Disassembly, Upgrading, Disassembly Map

Erschienen in Tagungsband 35. Forum Bauinformatik 2024, Hamburg, Deutschland, DOI: 10.15480/882.13535
© 2024 Das Copyright für diesen Beitrag liegt bei den Autoren. Verwendung erlaubt unter Creative Commons Lizenz Namensnennung 4.0 International.

## 1 Introduction

Regular renovation of the built environment is crucial for complying with regulations and minimizing the environmental impact of buildings. A significant aspect of these renovations is the upgrading of building components, especially windows, which plays a vital role in enhancing energy efficiency and reducing carbon footprints. Upgrading windows involves disassembling their components for repair, replacement, or recycling, thus extending their lifespan and aligning within the New Consumer Agenda and the Circular Economy Action Plan, which aim to overcome barriers to repair and promote sustainability, contributing to the goal of making Europe the first climate-neutral continent by 2050.

Disassembly, therefore, is essential not only for extending the lifecycle of construction components but also for reducing waste through material recovery options such as reuse, remanufacturing, and

recycling. A Disassembly Map plays a critical role in this process by outlining the sequences and process to minimize environmental impact. However, most windows are designed and manufactured without considering EoL and disassembly, which significantly increases their environmental burden. Given the complexity of windows and other building components, detailed EoL scenarios must be developed to enhance sustainability.

Effective disassembly planning requires a high level of detail regarding the physical interfaces among building components to identify physical constraints and sequence the necessary steps for dismantling [1]. This process defines and logically orders the deconstruction activities. Factors such as the joint type, material type, required performance, and target automation level are crucial in disassembly planning [2]. Disassembly planning and sequencing further formalize this process by illustrating the geometrical and technical features involved. Typically, precedence relations of components are represented graphically, where disassembly graph planning which can be defined as Disassembly Map, is treated as a tree search problem. This method begins from the assembled state and searches for a sequence of actions until a fully disassembled state is achieved, which can then be automated using robotics [3].

## 1.1 Research Gap and Contribution

Disassembly often requires intensive manual labor, which can limit material recovery options. However, robots, with their ability to perform precise, repetitive movements consistently, offer a significant advantage in reducing material waste. Robots in product disassembly can lead to semi-automated, intelligent production that enhances disassembly efficiency, reduces operational costs, decreases energy consumption, optimizes cycle time, and increases flexibility. In this context, Disassembly Maps play a crucial role by defining the motion sequences necessary for the robotic disassembly of windows, ensuring a systematic and efficient process. These maps provide essential details such as a minimum set of parts, the order of disassembly, and the directions for part removal.

This study makes two key contributions to the field. First, it develops an innovative methodology for disassembling building components, specifically focusing on upgrading and remanufacturing windows to comply with current regulations and reduce environmental impacts. This methodology includes detailed procedures and techniques designed to ensure both efficiency and sustainability. Second, the study introduces a comprehensive systematic framework for the robotic disassembly of windows, emphasizing the critical role of Disassembly Maps. These maps, a key component of the framework, guide the disassembly process by providing detailed instructions and pathways, enhancing the precision and effectiveness of the upgrading process, and facilitating material recovery options at the end of the window's life cycle. By doing so, the study promotes sustainability in the built environment, aligning with broader goals of reducing environmental impact and improving resource efficiency.

## 2 Disassembly Modelling, Planning, and Sequencing

Disassembly is a process of dismantling and separating EoL products into its components and sub-assemblies prior to reconditioning operations that restore EoL products to or nearly to original equipment manufacturer standards through an ordered set of parts and disassembly directions [4, 5, 6,]. Determining an optimal disassembly sequence is a critical decision within disassembly operations and may change based on the quality of an EoL product [7]. Disassembly planning, a crucial and impactful process, involves systematically determining the sequence of operations for disassembling complex objects into their constituent components [6]. A visual representation of the disassembly process is a powerful tool for design decisions [8] and disassembly map representation. The Disassembly Map is an intuitive design repair tool suitable for product designers, architects, engineers, design consultants, and researchers [8]. The Disassembly Map, a key component of this process, is crucial in guiding design decisions. Such diagrams help designers navigate the disassembly process, identify difficulties, focus on cost-driving tasks, pinpoint defect-prone steps, and find solutions [9]. However, building component disassembly planning needs standardized methods and defined characteristics [1], which still limits the disassembly approach for building components. Previous studies of disassembly maps have not dealt with developing disassembly maps for building components. Most studies in the field have focused on the disassembly map development of the product, particularly for the early design phase of the product, and utilizing the disassembly approach as a tool for design decisions.

Disassembly is performed with the scope of isolating (i) hazardous components that should not enter the de- and remanufacturing flow, (ii) reusable parts with high residual value, and (iii) parts that need to go through a dedicated process chain [2]. The performance and the level of disassembly should be considered before the disassembly process, which is crucial for the disassembly planning process. Three main types of disassembly levels exist: complete, partial, and selective disassembly. Selective disassembly is the optimal order of operations that disassembles a specific component and regarding the remaining components, saving disassembly time and increasing disassembly profit [7, 10]. Selective disassembly is generally used to repair and maintain a product or end-of-life disassembly [11]. Therefore, we utilized selective disassembly to perform with the scope of reusable parts with high residual value through selective disassembly level to upgrade the windows to extend their lifecycle.

## 3 Robotic Disassembly for Window Upgrading Process

Upgrading construction products through robotic disassembly adds value by extending the life of building products and reducing waste. According to the level of independence and exchangeability of building components, all building structures can be grouped into three categories: category 1 has a low disassembly potential of 30%, and category 2 has a medium disassembly potential of 30-70%. Category 3 is a high disassembly potential where both indicators of transformation (independence and exchangeability) have more than 70% of their best values. This category is made of integrated structural, mechanical, electrical, envelope, and partitioning systems in a way that will stimulate their

independence and exchangeability in different phases of the building's life cycle [12]. Also, typically, windows last about 20-25 years and must be updated to meet technological advancements and regulatory requirements [13]. In that sense, although windows are arguably the most complex systems in any building that frame, exterior finishes, glazing, etc., ıs needed to be changed for repair or appearance every 25 years, they are also in category three with the highest independence and exchangeability. That explains why windows are important for this study in developing disassembly maps for robotic disassembly automation.

In the literature, windows reduce energy consumption, carbon emissions, and waste while maintaining building value, which can be achieved by upcycling the window parts or components by replacing single-glazed windows with double or triple-glazed ones, significantly saving energy. Aluminum windows are stable and suitable for large surfaces and heavy-duty buildings [14]. The current study adopts a case study approach in that a 1.3mX1.3m aluminum frame window, which is a common dimension of the aluminum window in Germany and thus representative of a significant portion of the market, is scaled to 0.4mx0.4m to validate the disassembly map methodology for upgrading window components through robotic disassembly. The configurational space of the robotic arm (UR20) and the working field of the 3D printer (Prusa) determined the aluminum window dimension of 0.4mx0.4m.

In the built environment, many windows are designed and manufactured without considering the EoL and material recovery options at the end of the window's life to minimize the disposal and maximize the amount of material and component recovery where disassembly plays a crucial role. A major problem with disassembly map development is the need for detailed geometrical documentation and, if possible, a three-dimensional window model to define the precedence relations, which is hard to get before dismantling the window from the building or studying it at the warehouse. However, construction documents such as drawings and specifications, which are highly detailed, are a necessity before constructing the building. On the other hand, construction documents are also challenging to get for many buildings and window types. Therefore, the first step of this case study is to search for the aluminum windows section drawing to model it and define the geometrical precedence and constraints before defining the disassembly map. The two-dimensional section drawing is converted into a three-dimensional model using 1:1 section detail as a starting point, which is required for stages one and two. Then, a 3D window model is 3D printed and disassembled in the second stage to evaluate the disassembly map methodology. This study has two stages: 1) a simulation in the virtual environment and 2) Demonstration with a robotic arm.

### 3.1 Stage 1: Virtual Simulation

The disassembly map is formulated as a tree search problem, beginning from the assembled state and identifying a sequence of actions to reach the disassembled state for 0.4mx0.4m aluminum-framed single-glazed window units. (Figure 1). The 3D model of the window, which is also the assembled window model, is utilized for disassembly map development to investigate geometrical preferences, fastener locations, and details following a disassembly-by-assembly approach. This

process defines each step of robotic automation by disassembly motion sequences. The outer aluminum profiles were planned to be disassembled individually for the four edges. Subsequently, the gasket would be removed and recycled, and the single-glazed flat glass would be removed and replaced with double or triple-glazed ones.

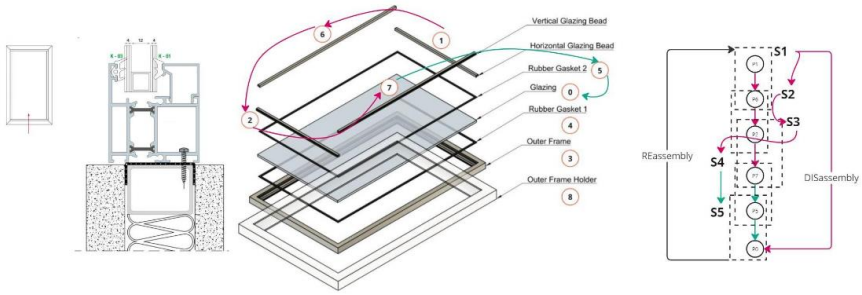


Figure 1: Aluminum-framed window section and axonometric decomposition of the parts, including disassembly planning graph for aluminum-framed window upgrading

The disassembly map allows us to get the disassembly planning and sequences to simulate the sequence in the virtual environment. The simulation was performed using RoboDK software. In the virtual environment, the window model is broken into components and exporting them as .igs files, with their original positions and spatial coordinates preserved. Window component models are preprocessed in the RoboDK environment by converting .stl files to .igs data format and identifying frames for each component import. These files were then imported into RoboDK, a versatile offline programming and simulation software for industrial robots (Figure 2).

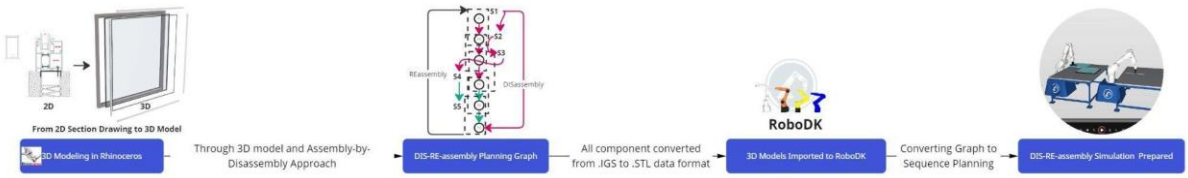


Figure 2: Workflow of Rootic Disassembly for Aluminum-framed Single-Glazed Window

The disassembly planning graph plays a crucial role in defining the sequence plan of the robot in RoboDK software, allowing for the determination of each step, or 'target,' in the simulation environment. The sequence plan was generated by creating a path through the disassembly planning graph, enabling a complete disassembly simulation. An ID-to-component map was used to obtain target coordinates in the world coordinate system. The disassembly path moves multiple parts from the assembled state on Table 1 to the target-disassembled state on Table 2, with the initial disassembly of outer frames following the sequence: {P1, P6, P2, P7}. After disassembling the outer frames and gaskets, the glazing beads {P5} are removed in a predetermined sequence. The single-glazed glass is then dismantled on Table 1 and upgraded to double-glazed glass as {P0} (Figure 3).

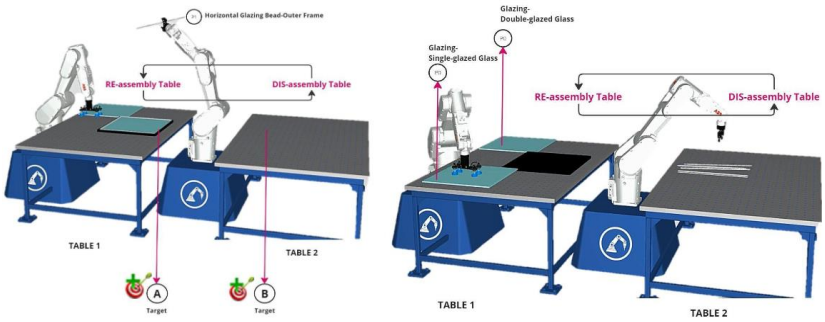


Figure 3: Left: Disassembly path between RE-assembly - DIS-assembly Tables for P1
Right: Upgrading single-glazed glass to double-glazed glass on table 1

### 3.2 Stage 2: Demonstration with robotic arm

The demonstration with a UR10e robotic arm used a custom-designed and 3D-printed end-effector tool. This end-effector, a parallel gripper manufactured using PLA, features a spur gear mechanism driven by a servo motor for precise parallel movement of the rack-connected finger. Its seamless integration and operation, controlled by an Arduino Nano, reassure its compatibility with the robotic arm. The necessity for this custom build arose to meet specific project requirements and enhance flexibility, allowing future upgrades, such as incorporating a screwdriver with minimal modifications to the base structure. After that, demonstration with the robotic arm by following the disassembly map to motion planning for the robotic arm at URScript. Then, a robotic arm is demonstrated, which is not gone as it is simulated (Figure 4). Currently, it is noted that gripping the outer aluminum profiles by custom-designed end-effector is where required improvement both in design and material choice of it.

Figure 4: Robotic window disassembly demonstration

## 4 Conclusion

This study presents a two-stage approach to upgrading building components, specifically focusing on windows, through robotic disassembly. The first stage involved a virtual simulation through a 3D model of an aluminum-framed single-glazed window. A disassembly map, formulated as a tree search problem, was developed to define the sequence of actions for robotic automation. A UR10e

robotic arm was employed in the second stage to demonstrate the physical disassembly process through a custom-designed and 3D-printed end-effector tool. The study highlighted the critical role of the Disassembly Map in defining disassembly path planning and motion sequences, ensuring an efficient and systematic process for manual and robotic disassembly through section drawings of the windows at the EoL stage. This research contributes to the field by developing a methodology for upgrading building components to meet regulatory requirements and reduce environmental impacts. Emphasizing the use of disassembly maps not only ensures the precision but also the effectiveness of the upgrading process, promoting sustainability in the built environment.

## Acknowledgements

We would like to thank Cemal Hekim from TU Berlin for supporting robotic automation. We gratefully acknowledge support from the European Union's Horizon Europe research and innovation program under grant agreement No.101056773 for funding this work under the Reincarnate project.

## References

[1] Sanchez, B., Herthogs, P., & Stouffs, R. (2023). Identifying key parameters for BIM-based disassembly planning. In ISARC. Proceedings of the International Symposium on Automation and Robotics in Construction (Vol. 40, pp. 32-39). IAARC Publications.9.

[2] Tolio, T., Bernard, A., Colledani, M., Kara, S., Seliger, G., Duflou, J., Battaïa, O., & Takata, S. (2017). Design, management and control of demanufacturing and remanufacturing systems. CIRP Annals, 66(2), 585–609. https://doi.org/10.1016/j.cirp.2017.05.001

[3] Esmaeili, M. C., Liu, Y., Belousov, B., Peters, J., Tessmann, O. (2023). Designing for robotic (Dis-)Assembly. Advances in architectural geometry 2023.

[4] Smith, S., Hsu, L., & Smith, G. C. (2016). Partial disassembly sequence planning based on cost-benefit analysis. Journal of Cleaner Production, 139, 729–739.

[5] Wurster, M., Michel, M., May, M. C., Kuhnle, A., Stricker, N., & Lanza, G. (2022). Modeling and condition-based control of a flexible and hybrid disassembly system with manual and autonomous workstations using reinforcement learning. Journal of Intelligent Manufacturing, 33(2), 575–591. https://doi.org/10.1007/s10845-021-01863-3

[6] Tabar, R. S., Magnanini, M. C., Stamer, F., May, M. C., Lanza, G., Wärmefjord, K., & Söderberg, R. (2024). Selective disassembly planning considering process capability and component quality utilizing reinforcement learning. Procedia CIRP, 121, 1–6.

[7] Rickli, J. L., & Camelio, J. A. (2014). Partial disassembly sequencing considering acquired end-of-life product age distributions. International Journal of Production Research, 52(24), 7496–7512. https://doi.org/10.1080/00207543.2014.939237

[8] De Fazio, F., Bakker, C., Flipsen, B., & Balkenende, R. (2021). The Disassembly Map: A new method to enhance design for product repairability. Journal of Cleaner Production, 320.

[9] Ishii, K., & Lee, B. H. (1996, August). Reverse fishbone diagram: a tool in aid of design for product retirement. In International Design Engineering Technical Conferences and Computers and Information in Engineering Conference (Vol. 80494, p. V001T01A008). American Society of Mechanical Engineers.

[10] Zhao, X., Li, C., Tang, Y., & Cui, J. (2021). Reinforcement Learning-Based selective disassembly sequence planning for the End-of-Life products with structure uncertainty. IEEE Robotics and Automation Letters, 6(4), 7807–7814. https://doi.org/10.1109/lra.2021.3098248

[11] Lambert, A., & Gupta, S. M. (2004). Disassembly modeling for assembly, maintenance, reuse and recycling. In CRC Press eBooks. https://doi.org/10.1201/9780203487174

[12] Durmisevic, E., Ciftcioglu, Ő., & Anumba, C. J. (2003, May). Knowledge model for assessing disassembly potential of structures. In Deconstruction and Materials Reuse Proceedings of the 11th Rinker International Conference.

[13] Guy, B. (2008). Design for disassembly in the built environment: a guide to closed-loop design and building. In University Park, Penn.

[14] “Save more energy with new windows,” 2017. Available: https://www.window.de/fileadmin/redaktion_window/vff/Shop_pdfs/VFF-BF_Study_Save_more_energy_with_new_windows_2017-09.pdf

# Teil VII

# Digital Twins

# DiggiTwin: End-to-end use of digital twins to realize a climate-neutral building stock

Sriram Badri[1,2], Nijanthan Mohan[1,2], Marc Oyen[2], Lukas Schnittcher[2]
[1]Institut Smart Building Engineering (ISBE), [2]FH Aachen - University of Applied Sciences, Germany
E-Mail: badri@fh-aachen.de

**Abstract:** The construction sector is one of the most resource-intensive sectors and responsible for a considerable share of energy consumption and greenhouse gas emissions. In order to achieve the sector targets of the German government's climate protection plan, the planning, construction, operation, maintenance and dismantling of buildings must be completely rethought and reassessed. This paper proposes an end-to-end digital method which captures the entire life cycle of a building. An interdisciplinary work that combines expertise from the fields of computer science, electrical, civil and energy engineering and tests the method on existing buildings at Aachen University of Applied Science with a main focus on optimising the building's energy consumption. The digital twin is created using methods from the field of Building Information Modelling and linked with sensor technology, data analysis and artificial intelligence in order to identify anomalies in energy consumption. With the availability of geometric, functional and real-time data from the sensors, one can identify key performance indicators relevant to the respective use cases and simulate "what if" scenarios by making predictions to achieve optimum results in terms of sustainability.

*Keywords*: Simulation, Digital Twin, Monitoring & Optimisation, IoT, Anomaly Detection

Erschienen in Tagungsband 35. Forum Bauinformatik 2024, Hamburg, Deutschland, DOI: 10.15480/882.13536
© 2024 Das Copyright für diesen Beitrag liegt bei den Autoren. Verwendung erlaubt unter Creative Commons Lizenz Namensnennung 4.0 International.

## 1 Introduction

In the European Union (EU), energy production and use are responsible for 80% of all greenhouse gas (GHG) emissions. Buildings account for about 40% of EU's final energy and 36% of $CO_2$ emissions, consequently associated with a significant untapped energy saving potential [1]. Building Information Modelling (BIM) is one of the most recognized and rapidly increasing technologies to minimise building energy use in recent years [2]. However, there have been many challenges in utilising BIM during asset operations, which have hindered asset owners from deriving value from their initial investments. The Architecture, Engineering and Construction (AEC) industry is struggling with the transition of BIM-based deliverables from the design and construction phases to the operations and use phase. This may be due to the divergent nature between these phases in terms of the aims,

objectives and scope of operations [3]. It is therefore crucial that the models not only cover the planning phase, but also the entire life cycle of a building in order to identify potential energy savings and ensure sustainable building operation. A key feature of BIM is the 3D model commonly referred to as the BIM model which is realised with object-oriented software. However, the BIM model is limited in providing dynamic real-time data of the physical environment. Yet, construction projects and assets are both implemented within a dynamic physical environment generating a vast amount of non-geometric data. The emerging concept of the digital twin (DT) offers an opportunity to address the limitations of BIM [4]. The integration of the physical and digital worlds by adding dynamic real-time data to a static BIM model is now known as DT. Due to the lack of standardisation and misconceptions about the definitions of DTs, developing a standardised DT framework for information management processes regarding construction assets is essential [5]. With regard to the climate targets of the Federal Republic of Germany, this paper focuses on sustainable building optimisation using DTs. The basis for holistic building monitoring and optimisation is digitalisation and automation in the sense of a smart building. This paper examines the most popular and promising BIM to life cycle assessment (LCA) tools according to the German assessment system "Bewertungssystem Nachhaltiges Bauen" (BNB). Additionally, it explores strategies for detecting operational anomalies using IoT (Internet of Things) sensor technology to enhance energy-efficient building operations. The focus is on precise monitoring and anomaly detection of critical building data to identify and utilize untapped energy-saving potential. As DTs in the built environment are still in nascent stages, a novel end-to-end process chain is proposed, starting from the design and construction phase up to the operational phase for energy efficient renovation of a university building located in the western part of Germany.

## 2 State of the Art

In this section, the PRISMA method [6] for collecting data is applied to identify, evaluate and synthesize the existing body of knowledge on the topics of digital tools and strategies implemented for sustainable building optimization.

### 2.1 BIM-To-LCA

In order to achieve a holistically sustainable building design, expertise on environmental assessment has to be offered to stakeholders to reduce the life-cycle related GHG emissions of buildings [7]. Recently, LCA is increasingly applied for assessing the environmental performance of buildings not only in research, but also in practice in the form of a post-design evaluation for sustainability certification purposes. Digital tools based on BIM provide the potential to decrease the additional effort for LCA and speed up the process [8]. Three research questions were posed to facilitate the understanding of previous studies that supported the idea of BIM based LCA tools.
Q1: What are the available open-source and commercial tools for assessing building life-cycle?
Q2: What are the LCA databases for buildings in Germany?
Q3: Which certification schemes support BIM-based submission of LCA results?

Web of Science, Scopus and Scholar were used as databases for this review and Boolean operators were used in the 'Title, Abstract and Keywords' fields to search articles using the keywords "BIM software", "LCA tools", "Open-source tools & Databases", "BNB", "Dynamic LCA", "Building lifecycle" & "Systematic literature review". Thus, according to the PRISMA methodology, 360 articles were found to be published within last 5 years. The most prominently used German environmental database is Ökobau.dat, developed in 2012 from Bundesinstitut für Bau-, Stadt- und Raumforschung (BBSR). eLCA, also developed by BBSR, is a reliable open source web-based LCA tool which supports assessment of only office and administration buildings. Generis [9], CAALA, LEGEP and Umberto NXT are some of the commercially available tools which support BIM-based submission of LCA results for BNB and DGNB certification.

## 2.2 Operational Anomaly detection

The building's consumption data is available as a time series. For the purposes of pattern and anomaly detection, a decision must be made first whether this should be based on the time series or on characteristics derived from them, such as cumulative or average consumption. Furthermore, there are different types of anomalies, which are shown in Figure 1.

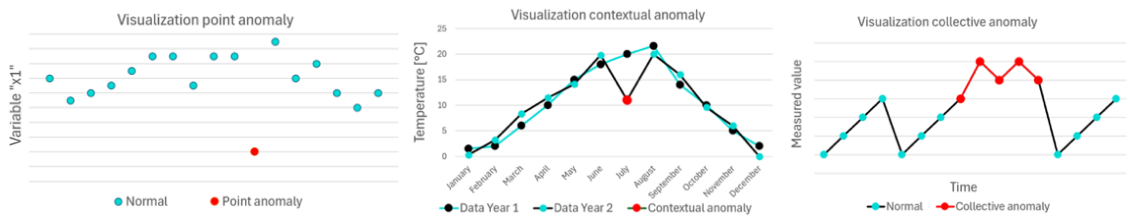


(a) (b) (c)

Figure 1 Visualization of a (a) point anomaly (b) contextual anomaly (c) collective anomaly

Point anomalies (Figure 1a) are the easiest anomalies to recognise. They can be caused by an outlier which occur when a data point significantly deviates from the range of values of the other data points. Examples of point anomalies are measurement errors or a sudden drop in energy consumption due to a technical failure. Since point anomalies occur independently of context, they can be detected in univariate data. This is different for contextual anomalies. An anomaly is called contextual if its value differs significantly from the value of other data points in the same context. Figure 1b illustrates this using the example of a temperature curve: the low temperature in the context of the month of July is anomalous. It is important to note that data points can be classified as abnormal in one context but normal in another context. A third type of anomaly is described by the collective anomaly (Figure 1c). Such an anomaly describes a subset of data points within a data set. It is not the individual data points themselves that are anomalous, but their joint occurrence. Examples of collective anomalies are unusual sequences in a time series, as shown in Figure 1c. Further details about anomalies in time series can be found in the work by [10].

# 3 Methodology

Effective information transfer is crucial for the success of AEC projects, yet it often presents significant challenges due to the multifaceted nature of project requirements and stakeholder involvement. As all project participants have different starting points, it is essential to have a defined digital knowledge transfer to ensure accurate and transparent information transfer. The core of the proposed end-to-end process chain is an Information Transfer Matrix (ITM). According to Mohan et. al. standardised ITM must be created based on specific use cases to optimise the digital twin for specific applications. These should be used in all phases of planning, construction and operation to ensure the bi-directional transfer of relevant data between the actors and the digital twin [11]. As shown in Figure 2, first a BIM model of the building under consideration is created. This is using the scan2BIM methodology where a 3D representation of the building is created using a LIDAR point cloud reconstructed in Revit. The BIM model forms the basis for the digital twin of the building based on the which refurbishment concepts can be created and evaluated.

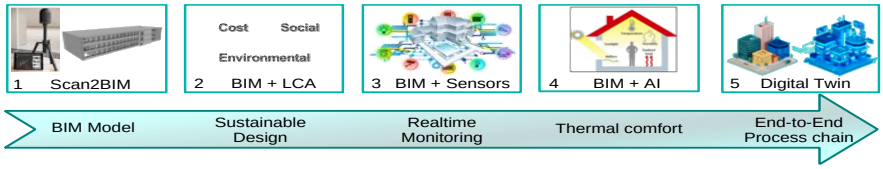


Figure 2: Digital Twin for energy efficient renovation

Kylili et al. [12], reviewed previous studies that employed the key performance indicators (KPIs) approach in sustainable building renovation and identified eight generic KPI categories related to economic, environmental, social, technological, time, quality, disputes and project administration aspects. In the next step suitable sensors are specifically chosen to gather real time data relevant for the selected KPIs. All data recorded using the selected sensors, are initially stored centrally on an external data storage / cloud storage system. The stored data is continuously analysed to identify consumption patterns and anomalies ensuring the building can be used energy-efficiently during operation and identify optimisation potential. This is based on pattern and anomaly recognition methods from the field of machine learning. For reliable functioning of these algorithms, a lot of training data is necessary [13]. After collecting enough data, pre-trained models are tested and evaluated.

## 3.1 Design and Construction phase

### 3.1.1 BIM-To-LCA

The general workflow of BIM based LCA is summarised in Figure 3. The building element templates specific to the project are first created on the basis of Environmental Product Declarations (EPDs) and generic datasets (Ökobau.dat) and assigned to the respective cost groups according to DIN 276 in the eLCA software, generating the IDs for each of the element templates. Both cost groups and the eLCA element-ID, are now stored as attributes for the corresponding elements of the BIM model. With the extension of the element properties, the BIM model can then either be exported directly in the vendor-neutral IFC file format or a component list can be created and exported as CSV. When

using the IFC interface, the IFC file is transferred to the eLCA program automatically and evaluated. When using the CSV interface, however, the component list is manually linked with the corresponding attributes generated in the first step and then imported into eLCA for evaluation.

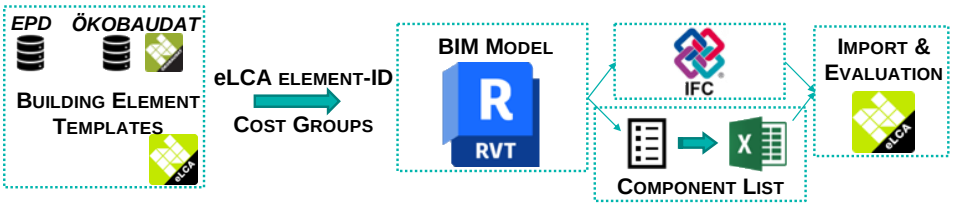


Figure 3: Process for calculation of embodied impacts based on BIM

## 3.2 Operations and Use phase

### 3.2.1 Communication protocols for monitoring

The centralized storage is crucial, as it allows for efficient data management and accessibility for subsequent processing stages. State-of-the-art communication protocols like LoraWAN [14], Enocean [15] and Thread [16] can transmit data from sensors wirelessly over long distances and in an energy-efficient manner. These protocols ensure reliable and long-range communication and ensure that sensors that rely on batteries are guaranteed a long service life, making them ideal for various IoT applications. The data collected by the IoT sensors is integrated into an open-source IoT automation framework, Home-Assistant [17]. This platform is responsible for gathering, processing, and storing the data in a centralised database.

### 3.2.2 BIM-To-SIM

Some of the KPIs relevant to the respective use case in the current project are: 1) Life Cycle Costs (EUR/m$^2$), 2) Indoor Air Quality ($CO_2$ concentration ppm), 3) Thermal comfort (temperature range in °C), 4) Climate change ($CO_2$ eq. emissions), 5) Energy consumption (kWh/m$^2$a) and 6) Onsite energy ratio (%) [18]. As a higher goal, for the selected building, initial KPIs that are planned to be measured and evaluated are energy loss in the building and thermal comfort [20] defined in the European norm EN ISO 7730 [21]. The decision on which sensors and actuators to use depends on the requirements a room must fulfill (e.g. an auditorium has different requirements than a boiler room). The input comprises of diverse datasets from different rooms, providing a comprehensive overview of the building's environment. When the anomaly detection system identifies an anomaly, detailed output specifying the start and end times of the detected anomaly, the specific room where the anomaly occurred, and an estimation of the suspected problem's nature is made available to the user. Figure 4 shows the data acquisition and processing of data captured from the sensors. The sensors continuously gather a wide range of data, capturing multivariate time series information. The collected data is then transmitted through intermediary devices known as gateways and securely stored in an external database designed to handle large volumes of complex sensor data.

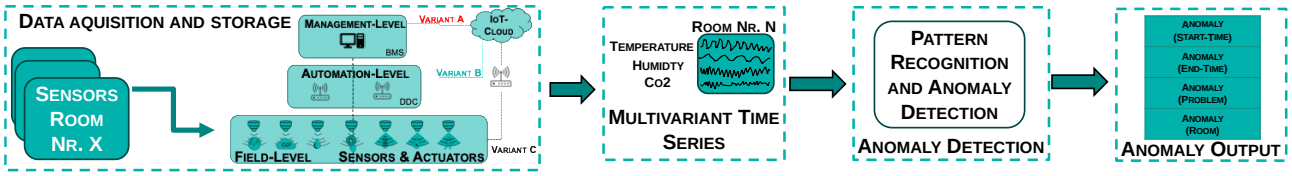


Figure 4: Process diagram for data acquisition and processing.

Energy modeling tools like IDA ICE can be used to predict energy consumption and evaluate optimal parameters in the energy renovation process. However, often discrepancies can be observed between the actual usage and predicted performance due to the uncertainties in the data input, namely assumptions of the U-values, system efficiencies factors that were not possible to determine on the job site, randomness and variability of the weather data and occupancy input [22]. In this method the real time data gathered using the different sensors take into account these discrepancies and help model an accurate DT. The DT consequently aids in developing reliable building energy models (BEMs) to simulate different scenarios (by varying occupancy, system failure, weather etc.) in turn predicting energy consumption and help evaluate suitable renovation strategies.

## 4 Experiment & Results

The selected building for testing of the methodology is the FH Aachen campus building located in Bayernallee, Aachen. A commercial LIDAR scanner – Leica BLK360 Generation 1 is used to capture the building as point cloud and commercial software Revit is used to create the BIM model. The BIM model consisting of 5 wings was developed with the help of point cloud data which was prepared with approximately 1200 individual scans. The LCA analysis in this paper will be limited to the third wing (Department of Civil Engineering). The building, which dates back to 1962 has a net floor area ("Nettogrundfläche" NGF) of 3262 $m^2$. The environmental impacts of the building's life cycle are normalised to one year and one $m^2$ NGF. While the gas requirement for the building is 190.3 $kWh/m^2a$, 7.3 $kWh/m^2a$ is the electricity requirement. From Table 1 it can be seen that the operation stage (B6 – energy use) has been highlighted as the main contributor to the Global Warming Potential (GWP).

Table 1: GWP values [kg $CO_2$-eqv.] according to life cycle module

| Total (INCL. A1 - A3, B6, C3, C4) | A1-A3 | B6 | C3 | C4 | Maintenance and repair (INCL. A1-3, C3, C4) |
|---|---|---|---|---|---|
| 44.37 | 0 | 41.63 | 0.1 | 0.41 | 2.236 |

Six different rooms are fitted with sensors to gather real time information about the building operation namely, Auditorium, Office room, Computer Lab, Architecture Studio, Boiler Room and Toilet. They are selected in order to reduce the DT as individual control rooms to create simple BEM which when extrapolated would represent the entire building.

# 5 Conclusion

This paper presents a methodology for end-to-end use of digital twins to realise a climate-neutral building stock. The suggested methodology is tested for developing a renovation strategy for a university building which consists of 6 different types of rooms depending on their usage. The sensors employed in this research along with the necessary anomaly detection strategies will be published subsequently discussing the potentials of using DT for optimising building operational energy. Although there are different BIM based LCA tools available for achieving a holistically sustainable building design, the only open-source tool is eLCA that is available for submitting results for certification in accordance with the German assessment system (BNB). Even eLCA does not fully support vendor neutral IFC format which again promotes the use of commercial tools. The presented methodology can further be expanded to include other types of buildings which promotes the standardised framework for applying DTs for building monitoring by asset and facility managers.

## Acknowledgements

We would like to thank the Ministry of Culture and Science of the State of North Rhine-Westphalia, which is financially supporting the project "DiggiTwin - The path to climate-neutral building stock through the use of digital twins" under the funding code 005-2302-0018. Further thanks go to the Institute for Smart Building Engineering at Aachen University of Applied Sciences.

## References

[1] M. Economidou, V. Todeschi, P. Bertoldi, D. D'Agostino, P. Zangheri, and L. Castellazzi. "Review of 50 years of EU energy efficiency policies for buildings." Energy and buildings 225 (2020): 110322.

[2] F. Alkhatib, A. M. Alawag, and A. Daris. "Building information modelling (BIM) and energy performance of building-A review." Journal of Applied Artificial Intelligence 2, no. 1 (2021): 22-31.

[3] M. Munir, A. Kiviniemi, S. Jones, and S. Finnegan. "BIM business value for asset owners: key issues and challenges." International Journal of Building Pathology and Adaptation 39, no. 1 (2021): 135-151.

[4] Valerian Vanessa Tuhaise, Joseph Handibry Mbatu Tah, and Fonbeyin Henry Abanda. "Technologies for digital twin applications in construction." Automation in Construction 152 (2023): 104931.

[5] Mohamed Nour El-Din, Pedro F. Pereira, João Poças Martins, and Nuno MM Ramos. "Digital twins for construction assets using BIM standard specifications." Buildings 12, no. 12 (2022): 2155.

[6] David Moher, Alessandro Liberati, Jennifer Tetzlaff, Douglas G. Altman, and T. PRISMA Group*. "Preferred reporting items for systematic reviews and meta-analyses: the PRISMA statement." Annals of internal medicine 151, no. 4 (2009): 264-269.

[7] O. Jorgji, R. Di Bari, R. Horn, and D. Chuchra. "Facilitating buildings' life cycle assessment through flexible lca tools."

[8] Alexander Hollberg, Gianluca Genova, and Guillaume Habert. "Evaluation of BIM-based LCA results for building design." Automation in construction 109 (2020): 102972.

[9] Rafael Horn, Sebastian Ebertshäuser, Roberta Di Bari, Olivia Jorgji, René Traunspurger, and Petra von Both. "The BIM2LCA approach: An industry foundation classes (IFC)-based interface to integrate life cycle assessment in integral planning." Sustainability 12, no. 16 (2020): 6558.

[10] A. Blázquez-García, A. Conde, U. Cortés, and I. Lozano, "A review on outlier/anomaly detection in time series data", ACM Comput. Surv., vol. 54, no. 3, pp. 1–33, 2021. DOI: 10.1145/3444690.

[11] Nijanthan Mohan, Gertraud Wolf, Martin Wogan, Jan Beilfuß, and Rolf Groß. "Auf dem Weg zu einem ganzheitlichen Lebenszyklusmanagement von Bauwerken für nachhaltiges Bauen." (2023).

[12] Angeliki Kylili, Paris A. Fokaides, and Petra Amparo Lopez Jimenez. "Key Performance Indicators (KPIs) approach in buildings renovation for the sustainability of the built environment: A review." Renewable and Sustainable Energy Reviews 56 (2016): 906-915.

[13] T. Schmidl and F. Naumann, "Anomaly detection for schema and data using approximate functional dependencies", in Proceedings of the 25th International Conference on Extending Database Technology (EDBT), 2022.

[14] H. U. Rahman, M. Ahmad, H. Ahmad, and M. A. Habib, "Lorawan: State of the art, challenges, protocols and research issues", in 2020 IEEE 23rd International Multitopic Conference (INMIC), 2020, pp. 1–6. DOI: 10.1109/INMIC50486.2020.9318170.

[15] Alliance, Enocean. "EnOcean–The World of Energy Harvesting Wireless Technology." EnOcean Technology Whitepaper (2015).

[16] I. Unwala, Z. Taqvi, and J. Lu, "Thread: An iot protocol", in 2018 IEEE Green Technologies Conference (GreenTech), 2018, pp. 161–167. DOI: 10.1109/GreenTech.2018.00037.

[17] Home Assistant, Home assistant, Accessed: 2024-06-10, 2024. [Online].

[18] Krzysztof Klobut, Tarja Mäkeläinen, Aapo Huovila, Juha Hyvärinen, and Jari Shemeikka. "KPI framework for energy efficient buildings and neighbourhoods." In eWork and eBusiness in Architecture, Engineering and Construction: ECPPM 2016, pp. 309-314. CRC Press, 2017.

[19] Assessment system for sustainable building (BNB), Online & Comfort parameters, Online, Accessed on: June 10, 2024.

[21] ISO 7730, https://www.dinmedia.de/de/norm/din-en-iso-7730/89417255, Accessed on: June 10, 2024.

[22] Socorro Järvistö. "Renovation strategies for the energy consumption of a 1954 single-family house using IDA-ICE." (2023).

# Presentation of an optimized process for generating analysis models in structural engineering using Graph Neural Networks

Toni Nabrotzky[1]

[1]IHBB | Institut für Hochbau, Baukonstruktion und Bauphysik, Leipzig University of Applied Sciences, Karl-Liebknecht-Straße 143, 04277 Leipzig, Germany

E-mail(s): toni.nabrotzky@htwk-leipzig.de

**Abstract:** Building Information Modeling (BIM) methodology is increasingly used in the construction industry. When this method is utilized for the structural integrity analysis of architectural models, these models must be converted into finite element models. However, automated processes of model conversion are prone to errors, as relevant connections between BIM objects are often missing. Hence, structural engineers often prefer the manual creation of the analysis model in practice. The aim of this paper is to introduce new methods for an efficient and collaborative workflow for automated model conversion. To this end, the use of an AI system in the form of a Graph Neural Network (GNN) is proposed. This system aims to recognize the load-bearing components in a BIM model through semantic enrichment and to establish their relationships based on load transfer in the form of a graph model. Incorrect connections or missing links between building elements are identified using a GNN approach to repair these issues and create correct and computationally efficient structural analysis models. Through these optimized processes, the need for individuall model adaption is expected to be reduced in the future.

*Keywords:* Building Information Modeling (BIM), Industry Foundation Classes (IFC), structural engineering, machine learning

Erschienen in Tagungsband 35. Forum Bauinformatik 2024, Hamburg, Deutschland, DOI: 10.15480/882.13522
© 2024 Das Copyright für diesen Beitrag liegt bei den Autoren. Verwendung erlaubt unter Creative Commons Lizenz Namensnennung 4.0 International.

## 1 Introduction

The ongoing development of Building Information Modeling (BIM) in the construction industry is reshaping work processes and tools employed therein. While conventional practices often rely on 2D plans for the exchange of project-specific information, BIM offers the capability to utilize enriched 3D models for collaboration within a project [1]. This transition to digital planning and construction introduces a range of novel benefits, as it integrates both geometric and alphanumeric data into the model. Consequently, BIM models can be directly leveraged for various analysis and computational tools [2]–[4].

One application area is structural analysis. Currently data exchange is limited due to the different geometric representations of the architectural model and the analysis model. Conversion is achieved through hardcoded rules, which require significant manual effort to create. The resulting rule sets are often tailored to specific structures and are difficult to apply to other projects without risking errors in translation. Sibenik et al. [5] developed the program *redDim*, which interprets the geometry of a structure and transforms it into an analysis model by reducing its dimensionality. Additionally, Jia et al. [6] proposed a method for automatically generating Finite Element Models from BIM models. This method extracts necessary information from the BIM model and constructs the corresponding element types using an automatic decision-making mechanism.

However, the methods published so far do not allow for fully automatic transformations of the models and still require the manual creation of construction rules for interpreting the ontology. Additionally, some methods are designed for calculations with volumetric models (three-dimensional elements such as tetrahedrons and hexahedrons) and are not, or only partially, suited for the analysis of 1D and 2D elements. In the construction industry, however, efficient methods that are as fully automated as possible and utilize simplified calculation procedures with abstracted components are economically advantageous.

Artificial Intelligence (AI) has significant potential for improving on these methods. By training on large datasets, AI algorithms can identify patterns and trends that humans may overlook or require more time to recognize [7]. Therefore, advanced techniques such as Deep Learning (DL) and Machine Learning (ML) are employed for various purposes, including predicting analysis calculations [8], [9] and automating routine tasks [10]. For instance, Bloch et al. [11] investigated the use of graph-based learning algorithms instead of hardcoded rules for automated structural inspections. Their research demonstrates that graph-based models generally outperform classical ML models in classifying structural elements. They recommend incorporating not only geometric but also topological information into the models [12].

In this paper we develop a new AI-powered workflow to further advance data exchange between structural design and architectural design. This AI-assisted approach aims to simplify the model transformation from the architectural model to the analysis model for structural design. Particularly in early planning phases, this methodology supports data exchange, as a large number of models can be automatically converted and analyzed, for example, in variant studies. It should be noted that this paper aims to present the conceptual design. A comprehensive analysis of the accuracy of the AI system and the parameters to be selected for AI training is still pending and will be addressed in future work. This new workflow can be divided into three phases (see Figure 1):

**Extract Information:** The basic concept of the new workflow involves extracting all load-bearing structural elements from an IFC model along with their metadata. In this context, metadata includes all non-structural information.

**Graph Construction:** Subsequently, this feature list is used to create a spatial property graph, with each structural element represented as a node. The extracted metadata is attached to these nodes as

node features. Using the concept of link prediction, a Graph Neural Network (GNN) is employed to predict which elements can transfer loads to each other and represent this relationship as an edge.

**Repair of analysis model:** With the understanding of which elements interact with each other during load transfer, this knowledge base is utilized to repair the associated analysis model if not all beam and surface elements are seamlessly connected. For this workflow, it is assumed that the analysis model is not in a proprietary format but in matrix format or in tabular form, such as the SAF format [13]. Therefore, a matching algorithm assigns the structural elements to the nodes in the graph. By linking the entities, it can then verify whether the nodes and edges of those elements are related to each other are on a common level. If this is not the case, it adjusts the positions of the elements accordingly.

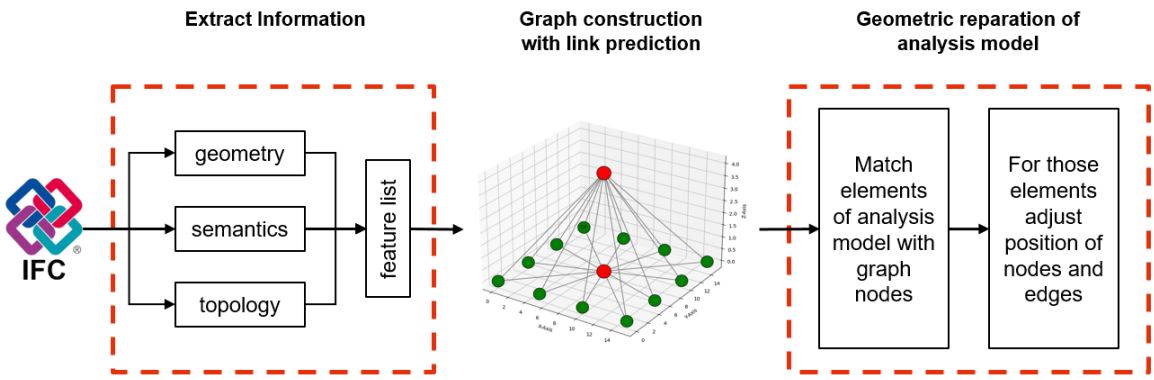


Figure 1: Presentation of the optimized workflow of the proposed framework. First, extract necessary information. Second, employ a Graph Neural Network (GNN) to identify relationships between the building elements. Third, align the nodes with your analysis model to correct the position and alignment of the model.

# 2 Framework for optimizing analysis models

## 2.1 Creating a database

Since a large number of labeled models is not available, we propose the use of parametrically generated models. Different value ranges can be defined for individual parameters, which are then combined into a parameter set. This allows for the automated creation of a large database comprising several hundred models. By further dividing the models into submodels, the existing quantity of training data can be maximized. However, this approach is only useful within certain limits, as the parametric construction of the building results in many similar models within the database. This poses the risk of overfitting, where the AI system becomes too closely adapted to the training data and fails to learn the systematics behind its actual task. To counteract this, it is recommended to augment the training data with synthetically generated data, as successfully implemented by Bloch et al. in their experiments [11].

For the upcoming training of the AI system, a parametric training model, as shown in Figure 2 will be utilized. This model consists of a simple structure composed of slabs and columns, which was programmed using Rhino and the visual programming environment Grasshopper with the Visual-ARQ plugin [14]. The following parameters will be varied:

- Dimensions in the x and y directions
- Floor height
- Number of floors
- Number of columns per floor
- Position of columns per floor

After conducting the initial training runs, the dataset used must be checked for overfitting. If overfitting is detected, the proportion of the parametric model in the training data needs to be reduced. Simultaneously, the dataset must be expanded to include additional models with different geometries, materials, and usage types. To achieve this goal, the parametric example model can be extended to include additional component types (walls, beams, etc.) and additional floors. Other models that should be included as training data can be real projects from industry partners who provide some IFC models for training the AI system.

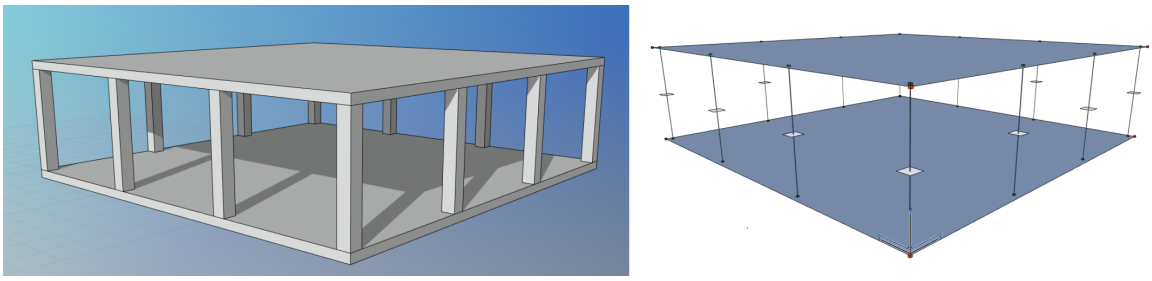

Figure 2: Parametric example model for generating training data. The structural model, displaying all load-bearing elements, is shown on the left. The analysis model is presented on the right.

## 2.2 Selection of relevant information

Before beginning the extraction of metadata from the IFC model, the relevant information for this purpose must be determined. In addition to alphanumeric attributes, the basis for training an ML model includes geometric data, material data, loading data, physical data, or the intended use and functionality. Since this workflow is primarily intended for application in early planning phases (1-3), it cannot be assumed that data on loads, stresses, and internal forces are already present in the model. Further data, such as building physics parameters or fire protection information, play a subordinate role in determining and analyzing the load-bearing elements. Therefore, for the extraction of metadata, the focus initially lies on an information set consisting of three essential aspects:

- Alphanumeric attributes
- Geometric information
- Material data

**Alphanumeric attributes** are used to describe each building element. In the base class 'IfcRoot', the attributes 'GUID' (IfcGloballyUniqueId) and 'Name' are created and inherited by all subclasses. All components with a physical or functional representation are described by the class 'IfcProduct'. At a deeper implementation level, these components are then assigned an abstract 'IfcType,' such as 'IfcWallStandardCase' or 'IfcSlab'. This 'IfcType' is also extracted.

**Geometric information** is essential for forming the structural system. It describes, for example, the position (the origin coordinate) of the element or its extent in the x, y and z directions. Orientation and rotation are indicated by direction vectors, showing the direction in which a component is aligned. References to both global and local coordinate systems can be established. Additionally, symmetry or shape can be described under this category, indicating whether the cross-section is square, circular, or otherwise defined. Spatial distances to other components, which are important for collision checks, for example, can also be derived from the model.
**Material data** serves to identify the type of material present. Examples of these materials include concrete, steel, wood, and masonry. Additional physical properties are not included in the training. However, in future training sessions of the ML system, it should be investigated what influence these properties have on link prediction. It may be conceivable to expand the database to include material density, thermal conductivity, fire resistance, or ecological data.

## 2.3 Extraxtion of data

This section describes the algorithm for this process step. We will use the Python program library *ifcopenshell* [15] for parsing the IFC data. With this library, all entities with the class IfcProduct and an existing physical representation will first be filtered. Next, the property sets of these elements will be read and checked to see if the respective component has the property 'LoadBearing' = 'True'. If so, the attributes described above will be extracted.

Since a physical building element in an IFC model can be described by different representations, such as 'Brep', 'MappedRepresentation' or 'SweptSolid', we will initially make the simplified assumption that all components are horizontally or vertically oriented. This allows us to describe the entities using their bounding box. The exact determination of all vertices can be implemented at a later stage when the training data includes more complex models. For material data, we will initially only query which material type was defined for the element. Subsequently, the collected information will be saved as a JSON file.

## 2.4 Graph Neural Network

**Graph Structure:** The proposed graph shall be designed in form of a spatial property graph. This type of graph integrates spatial data with traditional graph properties, enabling the representation and analysis of both attribute-based and spatial relationships. Formally it can be described as: $G = (N, E, C, M)$ where:

- $N$ is the set of nodes (vertices) in the graph
- $E$ is the set of edges (links) connecting the nodes
- $C$ is the set of coordinates, representing the origin coordinates (spatial position) of the nodes
- $M$ is the set of metadata (properties) associated with the nodes and edges.

The aim of this workflow is for a GNN to automatically generate and represent spatial property graphs precisely. To achieve the goal of accurate predictions, consideration must be given to how the structure of the graph should look and how the GNN should ideally be trained. The proposed graph comprises all load-bearing elements as nodes, their interaction in load transfer as edges, their spatial origin as

coordinates and their metadata as node features. Using the program library *networkx* [16], an empty undirected graph will be initialized. Information about nodes and their respective node features can then be extracted from the JSON file. It is important to note that the data from the JSON file must first be converted into numerical feature vectors for a GNN to process the extracted information. Using the methodology of Link Prediction, the GNN should then predict the relationships between the nodes. Subsequently, the predicted connections between the nodes by the GNN can be implemented as well.

In Figure 3 the process of data extraction from the IFC model and the subsequent initialization of the graph is depicted. It illustrates the detailed processes of the first two steps 'Extraxt information' and 'Graph construction with link prediction' from Figure 1. First it shows how each element in an IFC file is examined. If the requirements that it is a physically present component defined as 'load-bearing' are met, the relevant information is extracted and stored in a JSON file. These data are then extracted, and the graph with its nodes and node features is created. The GNN completes this graph by predicting the connections. This graph serves as the working basis for the next step in the process, the geometric error correction of the analysis model.

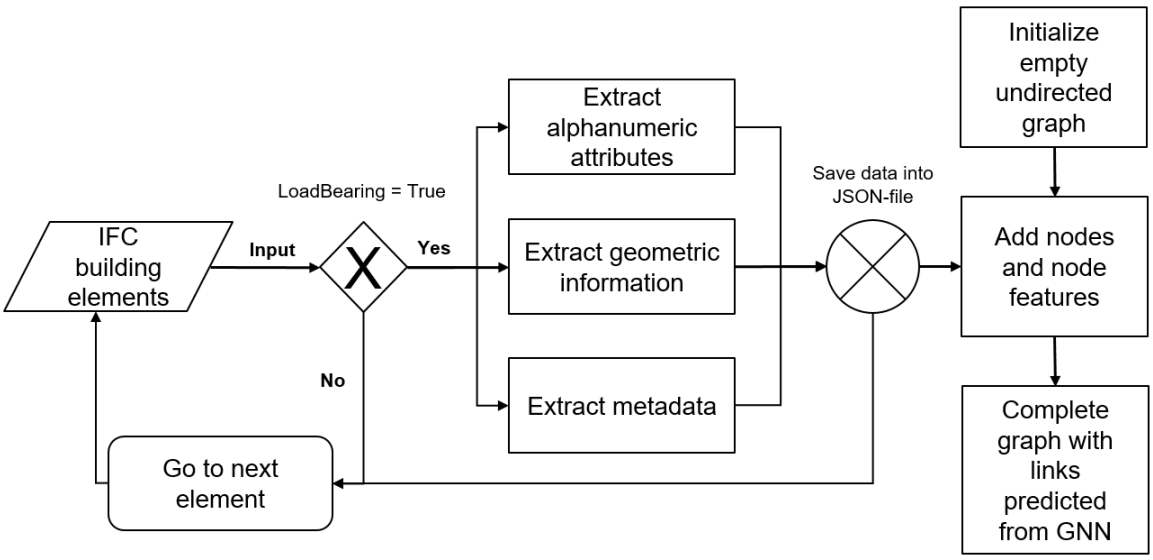


Figure 3: Process of creating spatial graph

**Training the GNN:** The planned GNN will be coded using the program libraries *PyTorch* and *PyTorch Geometric* [17], [18]. It will use the empty graph filled in with the information from the JSON files as input data, which need to be converted into an appropriate structure. The generated training data must be divided into training, validation, and test sets. Typical models for training GNNs include Graph Convolutional Networks (GCNs) or Graph Attention Networks (GATs). At this point, no methodology has been established on how the GNN should be trained. In later experimental phases, both architectures will be applied and tested to decide on one of the two variants.

In some IFC models, relationships are already stored using 'IfcRelationship'. It is important to note that some relationships may be redundant from the perspective of structural engineering, which could potentially confuse the GNN during the learning process. Therefore, it is necessary to investigate

whether training for efficient link prediction could benefit from the use of these data if they are available. In the application of this framework later on, it is conceivable that the existing connections are already integrated into the graph, and the GNN merely examines their plausibility and removes unnecessary connections besides its actual task of the classical link prediction.

### 2.5 Repair of the analysis model

The graph completed by the GNN forms the basis for the next steps, aimed at repairing an existing analysis model. A matching algorithm then determines the similarities between the elements from the analysis model and the nodes from the graph. The knowledge of the relationship between multiple elements is then used to repair geometric errors in the analysis model. This involves examining whether the nodes and edges of elements from the analysis model that are connected in the graph are on a common plane. If not, the coordinates of the affected points need to be adjusted. In the case of the example model, no errors occur due to the rule-based derivation, given its low complexity. However, when evaluating the effectiveness of the workflow in future work, the matrices of the analysis models will need to be manually manipulated to introduce errors at this stage. In further experiments with more complex models, this step will no longer be necessary, as the analysis models will not be directly computable as finite element models.

## 3 Outlook

The workflow presented in this paper is particularly intended for early planning phases, where structural engineering often does not yet have its own specialized model but needs to explore many design variants using the 3D model. In future experimental runs, it will be examined whether the selected relevant information is suitable for training the AI system and whether additional information should be included. However, only information that is typically available in the early planning stages should be integrated. Additionally, it needs to be validated how existing data from 'IfcRelationship' influences the training of the GNN. For the adjustment of elements, new sets of rules must be created. It is conceivable that components could be assigned specific priorities. When multiple elements need to be aligned, an algorithm could designate components with the highest priority as the fixed point to which all elements with lower priorities are adjusted. The workflow can then be examined for its functionality and effectiveness. It should be considered effective if the revised analysis models exhibit fewer errors than before and result in a computable finite element model.

## Literature

[1] A. Borrmann, M. König, C. Koch, and J. Beetz, *Building Information Modeling: Technologische Grundlagen und industrielle Praxis*. Springer-Verlag, 2015.

[2] S. Azhar, "Building information modeling (BIM): Trends, benefits, risks, and challenges for the aec industry", *Leadership and Management in Engineering*, vol. 11, no. 3, pp. 241–252, 2011. [Online]. Available: https://ascelibrary.org/doi/abs/10.1061/%28ASCE%29LM.1943-5630.0000127.

[3] P. Bynum, R. R. A. Issa, and S. Olbina, “Building information modeling in support of sustainable design and construction”, *Journal of Construction Engineering and Management*, vol. 139, no. 1, pp. 24–34, Jan. 2013. [Online]. Available: https://ascelibrary.org/doi/abs/10.1061/%28ASCE%29CO.1943-7862.0000560.

[4] E. Krygiel and B. Nies, *Green BIM: Successful Sustainable Design with Building Information Modeling*, 1st ed. Wiley, 2008.

[5] G. Sibenik, I. Kovacic, V. Petrinas, and W. Sprenger, “Implementation of open data exchange between architectural design and structural analysis models”, *Buildings*, vol. 11, no. 605, 2021. [Online]. Available: https://www.mdpi.com/2075-5309/11/12/605.

[6] J. Jia, J. Gao, W. Wang, L. Ma, J. Li, and Z. Zhang, “An automatic generation method of finite element model based on bim and ontology”, *Buildings*, vol. 12, no. 11, 2022. [Online]. Available: https://www.mdpi.com/2075-5309/12/11/1949.

[7] S. Haghsheno, G. Satzger, S. Lauble, and M. Vössing, *Künstliche Intelligenz im Bauwesen*, 1st ed. Springer Vieweg Wiesbaden, 2024.

[8] R. E. Meethal, A. Kodakkal, M. Khalil, *et al.*, “Finite element method-enhanced neural network for forward and inverse problems”, *Advanced Modeling and Simulation in Engineering Sciences*, vol. 10, no. 1, p. 6, 2023. [Online]. Available: https://doi.org/10.1186/s40323-023-00243-1.

[9] D. Roznowicz, G. Stabile, N. Demo, D. Fransos, and G. Rozza, “Large-scale graph-machine-learning surrogate models for 3d-flowfield prediction in external aerodynamics”, *Advanced Modeling and Simulation in Engineering Sciences*, vol. 11, no. 1, p. 6, 2024. [Online]. Available: https://doi.org/10.1186/s40323-024-00259-1.

[10] A. Buruzs, M. Šipetić, B. Blank-Landeshammer, and G. Zucker, “Ifc bim model enrichment with space function information using graph neural networks”, *Energies*, vol. 15, no. 8, 2022. [Online]. Available: https://www.mdpi.com/1996-1073/15/8/2937.

[11] T. Bloch, A. Borrmann, and P. Pauwels, “Graph-based learning for automated code checking - exploring the application of graph neural networks for design review”, *Advanced Engineering Informatics*, vol. 58, p. 102 137, 2023. [Online]. Available: https://www.sciencedirect.com/science/article/pii/S1474034623002653.

[12] G. Austern, T. Bloch, and Y. Abulafia, “Incorporating context into bim-derived data - leveraging graph neural networks for building element classification”, *Buildings*, vol. 14, 2024. [Online]. Available: https://www.mdpi.com/2075-5309/14/2/527.

[13] SAF-Documentation. (2024), [Online]. Available: https://www.saf.guide/en/stable/.

[14] VisualARQ. (2024), [Online]. Available: https://www.visualarq.com/de/.

[15] IfcOpenShell-Community. (2024), [Online]. Available: https://ifcopenshell.org/.

[16] NetworkX. (2024), [Online]. Available: https://networkx.org/.

[17] PyTorch. (2024), [Online]. Available: https://pytorch.org/.

[18] PyTorchGeometric. (2024), [Online]. Available: https://www.pyg.org/.

# Automatic conversion of real-world data from a German road infrastructure management system into a labelled property graph

Ina Heise[1]
[1]Chair of Computational Modeling, Technical University of Munich, 80333 Munich, Germany
E-mail(s): ina.heise@tum.de

**Abstract:** Maintenance of road infrastructure in many countries, including Germany, is carried out by various specialised institutions. These institutions use separate systems that often rely on relational databases. As a result, it becomes nearly impossible to conduct a comprehensive analysis of road infrastructure data. To address this challenge, graph-based representations are commonly used to enable more flexible and comprehensive data linking. This paper introduces an approach to represent geospatial data as a labelled property graph (LPG). The standardization of geospatial data provision through Web Feature Services is leveraged to develop a universal concept for creating the graph representation of geospatial data. The resulting LPG enables a more flexible evaluation of road management data stored in established GIS-based systems, facilitating integration into comprehensive systems. Real-world data from the road management system in Bavaria, a state in Germany, is transformed into an LPG to validate the concept, and an example of a comprehensive query is provided.

*Keywords:* road infrastructure, labelled property graphs, GIS, GML, digital twin

Erschienen in Tagungsband 35. Forum Bauinformatik 2024, Hamburg, Deutschland, DOI: 10.15480/882.13523
© 2024 Das Copyright für diesen Beitrag liegt bei den Autoren. Verwendung erlaubt unter Creative Commons Lizenz Namensnennung 4.0 International.

## 1 Introduction

Road infrastructure is crucial for society, making its management and maintenance exceptionally important. The sheer size and complexity of the system pose significant challenges. According to [1], digital twins, which accurately represent physical systems in their current state, are considered an effective tool for enhancing the operation of road infrastructure. These digital twins serve as comprehensive databases, facilitating in-depth data analysis and providing a basis for decision support.

A comprehensive infrastructure management system based on a digital twin differs significantly from the current practice of managing road infrastructure. Various aspects of road infrastructure are managed in separate, unconnected systems, mostly based on relational databases. The dispersed data management in place requires significant manual effort to conduct comprehensive data analysis, if possible at all. Therefore, the consideration of road infrastructure as a system consisting of different

interacting subsystems is not feasible.
Graph-based approaches are commonly used to facilitate flexible and comprehensive evaluations of (highly) connected data. As a result, graph-based representations of legacy data are frequently employed to incorporate legacy data into digital twins. Existing approaches commonly use ontologies describing the legacy data structures for this purpose. Subsequently, representations based on RDF graphs can be established. However, these approaches depend on the availability of the underlying data structure, which may not always be publicly accessible, such as in the case of Bavarian road data. Additionally, RDF graphs may not always provide the most compact information representation
Hence, this paper presents an alternative method for transforming existing infrastructure data into graph-based representations. The suggested concept focuses on a general approach for converting geospatial data provided through a Web Feature Service (WFS) into a graph. The selected graph model is the labelled property graph (LPG) model, which offers a more concise representation. Moreover, the underlying schemaless approach provides advantages when converting data with unknown data structures.
The result is an approach allowing the evaluation of data contained in GIS systems much more flexibly and integrating it with other data sources in a digital representation of a digital twin. The method was tested using the GIS system utilised in Bavaria for road infrastructure management. This system provides geospatial data on Bavarian infrastructure through a WFS. The geospatial data retrieved is automatically converted into an LPG. By inspecting the metamodel of the LPG in neo4j, the graph structure obtained could be derived, allowing the formulation of comprehensive queries as road conditions in conjunction with road cross-section data for all Bavarian roads.

## 2 Related Research

The research on digital twins in road infrastructure carried out by Taherkhani, Ashtari, and Aziminezhad [2] underscores their potential and the challenges posed by different existing systems. The major challenges identified include poor data quality and insufficient consideration of the overall infrastructure. Heise [3] discusses the existence of data silos in German infrastructure management and compares the available data in distributed systems with potential use cases, highlighting the necessity for comprehensive data evaluation. This emphasises the potential of a cross-system approach while revealing that existing relational database systems lack the necessary flexibility to conduct data evaluations for these use cases effectively. Consequently, the suggested solution is to employ graph-based representations of the legacy data instead.
Existing research already provides approaches for the creation of graph-based representations. Ismail, Strug, and Ślusarczyk [4] discuss a solution for generating graph representations of IFC models. However, the approach presented focuses more on buildings rather than infrastructure structures. Another approach, presented in [5], deals directly with the data of the system used in Germany for infrastructure asset management. The introduced ASB-ING ontology covers the data structure underlying the infrastructure asset management system, and an RDF graph is generated as a graph representation by instantiating this ontology with data from the legacy system. Beetz, Amann, and Borrmann [6] apply the same approach for road data corresponding to the OKSTRA-schema by introducing and instantiating okstraOWL. However, these concepts were developed based on the

knowledge of the underlying structure of the instance data. Furthermore, the focus was on establishing one-directional data conversion due to the existing interfaces of the systems under consideration. In the case of existing GIS systems for road data, there are already systems providing interfaces with implemented web services that theoretically facilitate connections to overarching digital twin systems. A graph-based representation would, therefore, serve as an extension, enabling semantic analyses and contextual linking of GIS data with other systems data. Hence, this paper outlines the development of a concept for creating a graph representation that serves as an extension by representing geodata, which can be queried via these web services. Unlike the previously presented approaches that used RDF graphs, this concept utilises LPGs, which offer benefits in terms of a more compact structure. Furthermore, LPGs are better suited for representing data whose data structure is not entirely known in advance. In this case, a schemaless approach, when combined with the use of self-describing database systems like neo4j, is particularly advantageous because the graph representation could be used additionally for their analysis of the data structure.

## 3 Background

Geospatial data from GIS systems is typically provided through Web Services, which adhere to standards set by the Open Geospatial Consortium (OGC). The choice of web service specifications needed depends on the geospatial data that needs to be accessed. When integrating geospatial data into a digital twin and connecting it to other infrastructure data sources, the primary emphasis is on the semantics. Therefore, the WFS, standardised by the OGC, is crucial. Although WFS provides extensive functionality beyond file-based geospatial data provision, its main purpose is to make vector data accessible. This functionality is utilised to create the graph-based representation. To retrieve data, an HTML request in accordance with the web service definition needs to be sent to the respective server endpoint. The returned data is typically formatted in XML and follows the Geography Markup Language (GML) Encoding Standard, which is also defined by the OGC.
According to the Spatial Data on the Web Best Practices by W3C, geospatial data is typically described using *Features* defined in DIN EN ISO 19101. According to DIN EN ISO 19101, Features are "abstractions of real-world phenomena" and mainly describe geographical units. The use of *Features* is rooted in the General Feature Model (GFM), standardised by DIN EN ISO 19109. The GFM defines *FeatureTypes* and *FeatureInstances*. Similar to class definitions in object-oriented programming, *FeatureTypes* outline generalisations, while *FeatureInstances* describe specific objects. *FeatureTypes* can have properties. These properties are described using *PropertyTypes*. While *PropertyTypes* define the characteristics of *FeatureTypes*, they are modelled separately. This separation results in a *FeatureType* not being defined by its properties. The subclasses of *PropertyType* include different types of properties: *AttributeType* for static properties, *Operation* for dynamic properties represented by function calls, and *FeatureAssociationRole* for characterising types of associations. The connection between *PropertyTypes* and *FeatureTypes* is defined by *ValueAssignments* and their subclasses, which also encompass *Operation*. Additionally, there may be associations or inheritance relationships between *FeatureTypes*. These associations are further delineated by *FeatureAssociationRole*, while the inheritance relationship is represented using *InheritanceRelation*. In summary, the geospatial data accessible via a WFS is described by instances of *FeatureTypes*. *FeatureTypes* may possess various

properties and relationships with each other, but they are not defined by these.
In contrast, there is the labelled property graph model, as defined, for instance, in [7]. Information is depicted as nodes linked by edges, which can be directional. Both nodes and edges are assigned labels and may possess other attributes. The significant advantage of using graphs for storing data is their effectiveness in representing interconnected information. Furthermore, by allowing attributes to be directly assigned to nodes and edges, LPGs offer a much more concise representation of information compared to RDF graphs.

# 4 Concept

## 4.1 Proposed graph structure for representing FeatureInstances

When geospatial data is represented as LPG, the main objective is to improve the capability to analyse relationships within data and link it to other data sources. Therefore, the emphasis is on capturing the semantics inherent in the geospatial data, and it is assumed that the graph representation supplements the WFS without entirely replacing it. This means that not all information available from the WFS needs to be explicitly represented in the graph.
In the LPG, all *FeatureInstances* are represented as nodes with their associated *FeatureTypes* as labels. When it comes to representing the properties of individual *FeatureInstances*, a distinction is made between *AttributeType*, *Operation*, and *FeatureAssociationRole* properties. Static properties (excluding attributes for describing geometry) are stored as properties at the *FeatureInstance* nodes. The attribute name serves as the property name, and the value is assigned accordingly. Moreover, the ID of a respective *FeatureInstance* is stored in a property, named following the schema `label name_ID`. For attributes that describe geometry or have dynamically changing values, we propose that the original data source (the WFS) be referred back to. One way to implement this reference is by storing the HTML request for the corresponding resource as a string in the respective property value. In the case of attributes with changing values, this approach helps prevent inconsistencies between the graph representation and the geodata. Regarding geometric attributes it ensures that the graph is not burdened with geometric information that may not be necessary for the semantic linking.
Relationships between different *FeatureInstances* are depicted through edges, utilising labels to describe the relationship type. Additionally, the option to assign properties to edges in LPGs allows for the potential modelling of other relationship properties. Figure 1 illustrates the proposed graph structure, depicting the representation of two *FeatureInstances* in relation to each other.

## 4.2 Creation of the graph representation

With a system depicted in Figure 2, the LPG can be created. The primary component is a Python script that initially retrieves geospatial data by sending an HTML request to the WFS server, followed by the interpretation of the returned GML data and generation of the graph by sending queries to a graph database server instance. Since neo4j was chosen as the graph storage system, CYPHER queries have to be used. In order to generalise the graph creation process, an object-oriented data structure is defined, as depicted in Figure 3, comprising three classes: *ConversionObject*, *ConversionLink*, and *ConversionProperty*. Instances of the *ConversionObject* class must have an *ObjectID* storing the unique *FeatureInstance*-ID and an *ObjectType* holding the associated *FeatureType* to enable clear

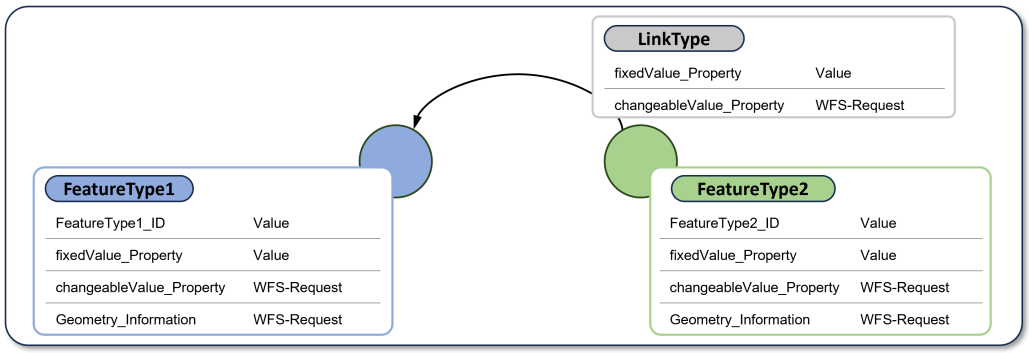


Figure 1: Graph structure of the resulting LPG, displayed using two example instances

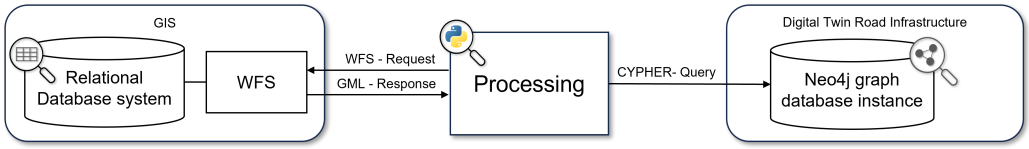


Figure 2: Prototype system for the conversion of geodata into LPG using the WFS of a GIS system

identification of the described *FeatureInstance* in the original data. Additionally, *ConversionObject* instances can possess a list of *ConversionLink* and *ConversionProperty* instances. *ConversionLink* instances store the relationship to another *FeatureInstance* through *LinkType*, which specifies the type of link, and *LinkedObjectType* and *LinkedObjectID* attributes, describing the target object of the link by specifying its *ObjectType* and *ObjectID*. *ConversionProperty* instances detail the attributes of the respective *FeatureInstance* with *PropertyType*, *PropertyName* and *PropertyValue*.

To generate the graph based on the list of instances of *ConversionObject*, it is important to ensure that all nodes representing specific *FeatureInstances* are uniquely identifiable. Therefore, property existence and property uniqueness constraints are set up for nodes with the respective label before the node itself is created. For generating the nodes, the *MERGE* clause is used to check whether a node with the corresponding label and ID already exists. If so, the remaining attributes stored in *ObjectProperties* are appended to it; otherwise, a new node with associated properties is generated. When creating the edges to represent the links, it's important to consider that edges can only be established between two existing nodes. Thus, if the 'target node' of the link doesn't exist when the edge is being created, a 'placeholder node' is required. This 'placeholder node' serves as a temporary representation of the target node, allowing the edge to be established. After the 'placeholder node' is generated using the information from the *ConversionLink* instance regarding the target node (label and ID), the edge can be established. The remaining information is then added to the 'target node' later during the conversion of the associated *FeatureInstance*, as it can be uniquely identified by its label and ID.

This approach allows for the automatic construction of the graph representation by iterating over the list of all *ConversionObject* instances. However, how the *ConversionObject* instances are to be generated may vary slightly depending on the underlying application schema in the WFS implementation.

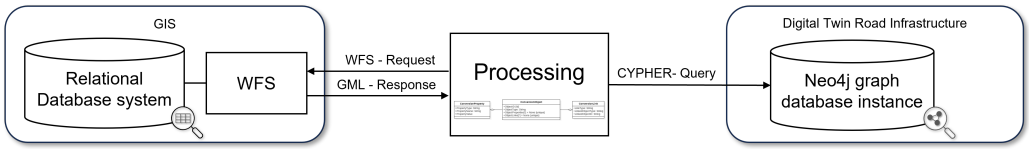


Figure 3: Object oriented datastructure used for parsing

## 5 Application Bavarian road data

The approach presented is implemented for BAYSIS, the road management system used in Bavaria. BAYSIS relies on ttSIB, a GIS system developed by novasib. The data stored in ttSIB's relational database system can be accessed through a WFS. However, neither the data structure in the database system nor the application schema used to create the complex features for WFS provision are publicly available. Consequently, the general structure of the returned XML files was deduced by querying and inspecting several example files. Subsequently, a Python script was created to automatically instantiate the conversation classes mentioned above.

First, the XML sub-elements that describe the individual *FeatureInstances* have to be identified since the hierarchy level of these instances within the XML tree is unknown. The script iterates through sub-elements and uses the existence of a unique ID to identify the relevant XML elements. The result is the information on the hierarchy level of the *FeatureInstances*, allowing the generation of a list of XML elements representing single *FeatureInstances*, which can be iterated over in the next step.

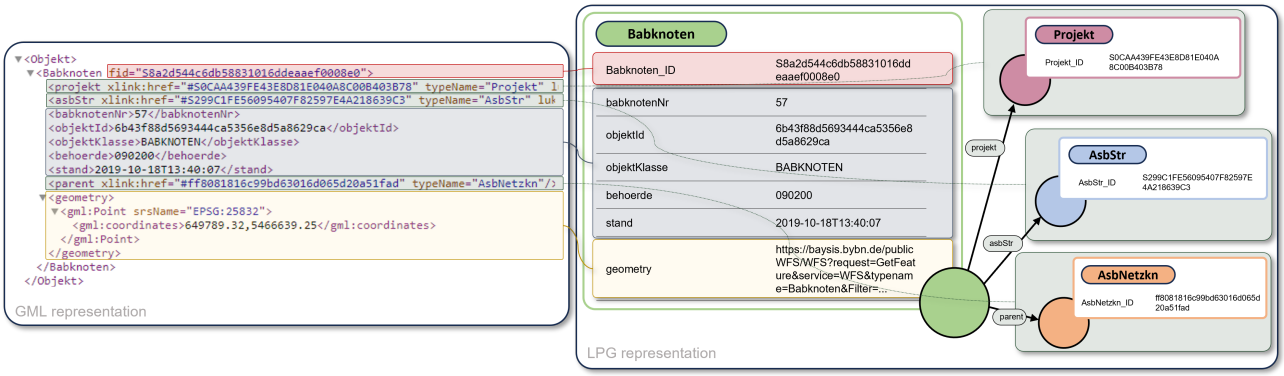


Figure 4: Representation of an example *FeatureInstance* in the GML file and in the LPG

Every XML element belonging to a *FeatureInstance* is searched for attributes and links to other *FeatureInstances*. Properties and links are stored as either subelements of the XML element or as attributes of the XML element, also visible in an excerpt of an example instance shown in Figure 4. The structure of the XML elements and subelements is analysed further to determine whether the information contained within is to be saved as a property, link, or geometry information. All direct attributes of the *FeatureInstance* XML element are considered properties. Direct subelements of the *FeatureInstance*-element are categorised based on their own subelements. If a subelement has no further subelements and no attributes of its own, it is considered a property, and the tag is used as the property name, while the content of the subelement is used as the property value. The remaining sub-elements are further divided into sub-elements holding information on links to other instances

of other *FeatureTypes* or geometric information, again based on their structure. If a subelement has more than one attribute but no other subelements, it is assumed to be describing a link. Then the tag name is interpreted as the name of the link. The attribute *href* with the http://www.w3.org/1999/xlink namespace is used to extract the referenced instance, since per the XLINK-schema definition, this attribute contains the IRI or URI of the referenced object. However, upon examining sample data, it was observed that the link objects in the GML data provided by the ttSIB WFS only contain the ID of the referred *FeatureInstance*, which must be interpreted in conjunction with another attribute containing the name of the *FeatureType*.
An additional property instance is created for attributes recognised as describing geometry, where the tag name is used as the property name, and a generated string containing a WFS query for the source resource is used as the attribute value. The list of *ConversionObject* instances created in this way is used to create the LPG according to the procedure described in section 4.2. Upon examining the metamodel of the generated LPG, it was feasible to discern the data structure that underlies the data and to construct comprehensive queries based on it. One possible query is showcased in Figure 5 on the right, where all road conditions are queried in conjunction with the road cross-section elements at the corresponding positions.

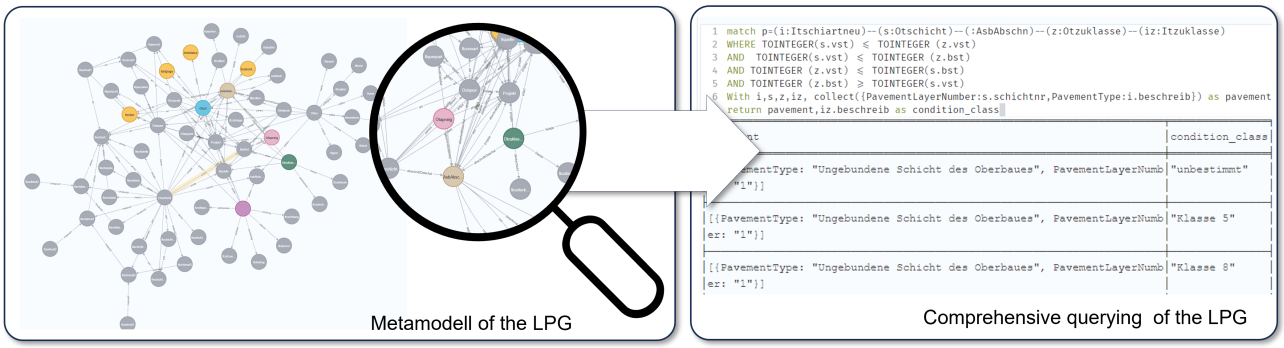


Figure 5: Metamodel of the LPG of Bavarian road data and a possible comprehensive query

## 6 Results and Discussion

This paper proposes a methodology to generate an LPG representation of geospatial data provided through a WFS using the example of the Bavarian road management system. Each individual *FeatureInstance*, along with its properties, is depicted as a node with the associated *FeatureType* as a label and its corresponding properties. Links between *FeatureInstances* are represented as edges between the respective nodes. Rather than explicitly encompassing geometry attributes and variable attribute values, they are integrated through a reference to the WFS.
Upon analysing the metamodel of the resulting LPG, it is possible to examine the data structure of the represented geospatial data. Using this information, a query was formulated to correlate road conditions to data about the road cross-section throughout the entire dataset. This serves as an example of the comprehensive data analysis that the LPG facilitates within the road data.
Future studies will seek to explore the potential linkage between road data represented by graphs and other infrastructure data, specifically structural data. This will involve integrating historical data

from existing infrastructure asset management systems and consideration of IFC models within the framework of BIM-GIS integration.
The approach presented has limitations, as it has not conclusively addressed the question of ensuring consistency between the original data and its graph representation. The possibility of changing attribute values in the representation of non-static properties is taken into account by using a reference to the original data. Although it's relatively easy to perform a consistency check for individual *FeatureInstances* using the information on *FeatureType* and ID stored at the node, how newly added or deleted *FeatureInstances* can be quickly and effectively detected in the original data in order to update the graph remains unclear.

## Acknowledgements

The presented research has been funded by the Bavarian Ministry for Housing, Construction, and Transport in the frame of the project "Digital twin for operating road infrastructure".

## References

[1] E. VanDerHorn and S. Mahadevan, "Digital twin: Generalization, characterization and implementation", *Decision Support Systems*, vol. 145, Jun. 2021. DOI: 10.1016/j.dss.2021.113524.

[2] R. Taherkhani, M. A. Ashtari, and M. Aziminezhad, "Digital twin-enabled infrastructures: A bibliometric analysis-based review", *Journal of Infrastructure Systems*, vol. 30, 1 Mar. 2024. DOI: 10.1061/JITSE4.ISENG-2323/SUPPL_FILE/SUPPLEMENTAL.

[3] I. Heise, "Requirements analysis for a digital road infrastructure twin", *Proceedings of the 34. Forum Bauinformatik*, 2023. DOI: 10.13154/294-10105.

[4] A. Ismail, B. Strug, and G. Ślusarczyk, "Building knowledge extraction from bim/ifc data for analysis in graph databases", pp. 652–664, 2018. DOI: 10.1007/978-3-319-91262-2_57.

[5] A. Göbels, "Conversion of infrastructure inspection data into linked data models", *32. Forum Bauinformatik*, 2021. DOI: 10.18154/RWTH-2021-07268.

[6] J. Beetz, J. Amann, and A. Borrmann, "Analysis of application possibilities of linked information (Linked Data) and ontologies and related technologies (Semantic Web) in the road sector", Bundesanstalt für Straßenwesen (BASt), Abschlussbericht, 2018. [Online]. Available: https://mediatum.ub.tum.de/doc/1451874/xq8ya8ljdktao3vzqcf3wus0p.2018_Borrmann_EGICE.pdf (visited on 07/01/2024).

[7] R. Angles, "The property graph database model", *AMW*, 2018. [Online]. Available: https://ceur-ws.org/Vol-2100/paper26.pdf (visited on 07/01/2024).

# Model-Based-Systems-Engineering for bridges: Representing modular precast bridges with SysML

Benedict Harder[1] and Sebastian Esser[1]

[1]Chair of Computational Modeling and Simulation, Technical University of Munich, Arcisstraße 21, 80333 Munich, Germany

E-mail(s): benedict.harder@tum.de, sebastian.esser@tum.de

**Abstract:** Model-Based-Systems-Engineering (MBSE) and its corresponding modeling language, SysML, have been widely used in mechanical and systems engineering. While its underlying structure was designed with systems engineering in mind, buildings in the AEC domain can also be represented using the same principles of structure, behavior, requirements, and parametrics. Specifically, bridge constructions can benefit from representation through clearly defined constraints and specifications. This paper focuses on developing a concept to adapt system engineering principles to the modular precast bridge construction space, resulting in a preliminary method of representing bridges with the system modeling language. SysML diagrams representing the core functions of an exemplary bridge were created to showcase the viability of using MBSE and the necessary modifications to be appropriately adapted into the AEC domain.

*Keywords:* Design Automation, MBSE, SysML, BIM

Erschienen in Tagungsband 35. Forum Bauinformatik 2024, Hamburg, Deutschland, DOI: 10.15480/882.13505
© 2024 Das Copyright für diesen Beitrag liegt bei den Autoren. Verwendung erlaubt unter Creative Commons Lizenz Namensnennung 4.0 International.

## 1 Introduction

In recent years, construction projects have started to transition from document-based information management, such as 2D plans and specifications, to model-based information management. The method of choice for this new approach is Building Information Modeling (BIM), which aims to reduce costs and errors, as well as provide a suitable base for modeling data adhering to paradigms such as *single-source-of-truth* [1]. Meanwhile, a similar paradigm shift has happened in the field of systems engineering. Model-Based-Systems-Engineering (MBSE) promises similar advantages as BIM by eliminating the need for document-based system specifications.

Naturally, there are stark differences between BIM and MBSE. BIM is designed to manage all the necessary information concerning planning, construction, operation, and demolition [1] accurately and consistently. In contrast, MBSE was created with precise, time-critical system procedures and complex component interactions in mind. Thus, the tools created to assist in the design process of

systems on the one hand (such as the Systems Modeling Language, SysML) and buildings on the other focused on differing aspects.

The fundamental differences between these two perspectives are difficult to overcome, and implementing MBSE concepts in the construction sector is anything but simple. Yet, MBSE's emphasis on interactions, data flow, and time-sensitive behavior can prove useful for specialized construction subdomains. Cyber-Physical-Systems (CPS) aim to bridge the gap between the digital world of data and the physical world of manufacturing and installation. With the help of clearly defined interfaces between the data models and authoring tools on the one hand and fabrication/installation systems on the other, feedback loops can be created that optimize processes for Design for Manufacturing and Assembly (DfMA) and the propagation of changes for design automation. Modeling this system with all its necessary components, ranging from the general structure of the building to the fabrication machinery and various sensors, can prove to be complicated. While BIM aims to primarily describe what the model *is*, MBSE primarily describes how it *behaves*, and thus offers the tools necessary to model such a CPS. This paper attempts to develop a method of representing built structures such as bridges by means of an appropriate system modeling language.

# 2 Related Works

## 2.1 Model-Based Systems Engineering

Model-Based Systems Engineering is the practice of utilizing a central *system model* to design a system, as opposed to using a conventional *document-based* approach [2]. In detail, this means that the system model stores all necessary components and associations while employing paradigms such as *single-source-of-truth*. Contrary to the conventional approach, where system specifications are spread across various documents ranging from PDFs, spreadsheets, and diagrams, the system model manages all data in a single place, with human interface views (such as diagrams) being automatically generated based on the model. This way, changes to a single component can be immediately updated in all views, ensuring consistency and mitigating human error. Changes in one part of the system are immediately propagated to all other corresponding parts.

## 2.2 The Systems Modeling Language

While MBSE is the underlying concept, including necessary paradigms and best practices, it does not offer a concrete design method or provide the necessary tools to develop the said model. This is where modeling languages, such as SysML, fill the gap. SysML was developed from the ground up with MBSE in mind and employs those same paradigms while additionally clearly defining diagram types with which it is possible to model a system in a human-readable manner. Being a dialect of UML, it makes use of various diagram types to define the system architecture, such as the block definition diagram (*bdd*), requirements diagram (*req*), use case diagram (*uc*), and more. These diagram types are either reused or extended from the UML 2.0 specification [3]. In Figure 1, an example of a block definition diagram can be seen. It includes multiple elements already known from UML, such as blocks (classes), associations, generalizations, and compositions.

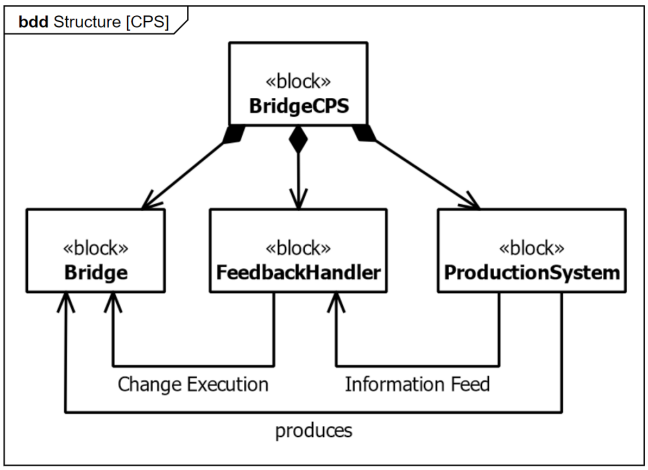


Figure 1: Example of a SysML Block Definition Diagram (*bdd*)

While SysML specifies an ontology as to what possible elements we can add to our diagrams, it does not directly create a system model. Since it is only a language, the underlying model creation is the job of the various pieces of software that implement the SysML specification and, based on the user-defined diagrams, build the model.

## 2.3 Cyber-Physical-Systems

Cyber-physical systems bridge the gap between the physical components of a system, such as machines, and the digital software that operates them. CPSs are tightly integrated and often embedded directly within physical components, such as sensors, but can also integrate more big-picture systems, such as directly relating planning and design tools to the physical hardware that executes upon that data. To stay in the Architecture, Engineering, and Construction (AEC) context, CPS can strongly link the planning and design software, such as BIM authoring tools, to the manufacturing and assembling machinery, thus creating a more robust data delivery between components and the possibility of intelligent feedback loops for iterative design improvements, based on real-world data [4]. To design these systems, a modeling method such as the earlier mentioned MBSE is suitable.

## 2.4 Specific Related Research Contributions

The adoption of MBSE in the AEC domain has been explored scientifically in numerous contexts. Many application areas make systems engineering an attractive way of describing and designing highly complex systems and designs that conglomerate different disciplines into one project. The AEC domain has many of these potential use cases, each differing from the next. A select few research articles will be presented below.

Nasserdine et al. explore the general transformative potential of adopting a model-centric approach in the AEC industry. Specifically, they establish concrete objectives and concepts that the industry needs to abide by to ensure a successful and advantageous transition, such as *single-source-of-truth*. The industry can achieve significant improvements by shifting to a model-centric approach, where digital models serve as the central repository of information throughout the project lifecycle. In Detail, these possible improvements include better collaboration possibilities among stakeholders, enhanced

and more nuanced decision-making based on integrated data, greater productivity, and the resulting cost and time savings. Numerous case studies and practical examples are provided to illustrate the successful implementation and positive outcomes of model-centric practices in real-world projects [5].

Philipp Geyer focuses on applying systems modeling to enhance the sustainability of building designs. He emphasizes the complex nature of sustainable building design, which requires balancing multiple criteria such as energy efficiency, environmental impact, and cost-effectiveness. Geyer proposes a systems modeling approach using SysML to evaluate and optimize building design performance holistically. By employing this approach, designers can better understand the interdependencies between different building components and make more informed decisions to achieve sustainability goals. Specifically, block definition diagrams (*bdd*), requirement diagrams (*req*), use case diagrams (*uc*), and activity diagrams (*act*) are created in the context of a residential building as a case study to explore the potential challenges and possibilities of systems engineering in the AEC domain poses. The study demonstrates the effectiveness of systems modeling through case studies, highlighting its potential to improve design outcomes and support the development of sustainable buildings [6].

O. Badreddin et al. introduce fSysML, an extension of the Systems Modeling Language (SysML) tailored specifically for modeling cyber-physical systems (CPS) to manage their complexity and ensure reliable performance robustly. The authors present fSysML as a foundational and executable version of SysML, designed to enhance the expressiveness and precision of models used in CPS development. fSysML incorporates formal semantics to enable the execution of models, facilitating early verification and validation of system behavior. This executable capability allows for simulation and testing of the interactions between the cyber and physical components of the system in a virtual environment. The paper outlines the architecture and features of fSysML, illustrating how it can be used to model various aspects of CPS, such as control systems, communication networks, and physical processes. Cast studies such as a monitoring system from the healthcare domain demonstrate the practical application and benefits of fSysML, highlighting its potential to improve the design, analysis, and implementation of complex cyber-physical systems [7].

### 2.5 Identified Research Gap

In general, it can be said that the transition to model-centric methods has numerous benefits. Yet, real-world attempts have been made to adopt methods such as MBSE into the AEC domain. While this is partially due to BIM filling that role, there are use cases where other established modeling methods and languages, such as SysML, can prove advantageous, specifically when confronted with situations with numerous in- and outputs and complex behavior. The SysML extension fSysML also introduces the idea of executable and simulatable system models. This paper attempts to model a basic bridge structure fabricated by the likes of a concrete printing robot with multiple interconnected levels of detail. A prototype model, including product structure representing the bridge, fabrication systems, and sensor groups, will be modeled using SysML to use MBSE principles. This example model will provide the necessary basis for answering the following research questions: (1) How can model structures of a bridge be combined with those of a fabrication system with the help of SysML? (2) Can the resulting model be used to perform model analysis?

# 3 Modeling a CPS through SysML diagrams

To make use of SysML as our modeling language, we must first analyze the possibilities and capabilities the language offers for our use case. Crucial to our bridge-CPS example are diagram types that concern (1) the necessary requirements, such as structural integrity, (2) the intended behavior, such as the production of modules, (3) the general structure of the bridge. With this in mind, sample diagrams of the requirements of the type and use case (*req*,*uc*), block definition (*bdd*), and activity (*act*) attempting to model the previously mentioned points will be created.

## 3.1 Structure

To begin, the general structure of a bridge and its corresponding CPS is modeled. SysML allows for multiple diagrams of the same type to exist in parallel, such as the block definition diagram. This is convenient when wanting to adequately separate different aspects of the same system. Nonetheless, components can be a part of multiple diagrams, even though the underlying unit stays the same. This allows the modeling of associations between different parts of the system without defining unnecessary details in a certain diagram view - these details can be described in a different diagram. To explain this further, let us have a look at a high-level basic representation of our bridge CPS:

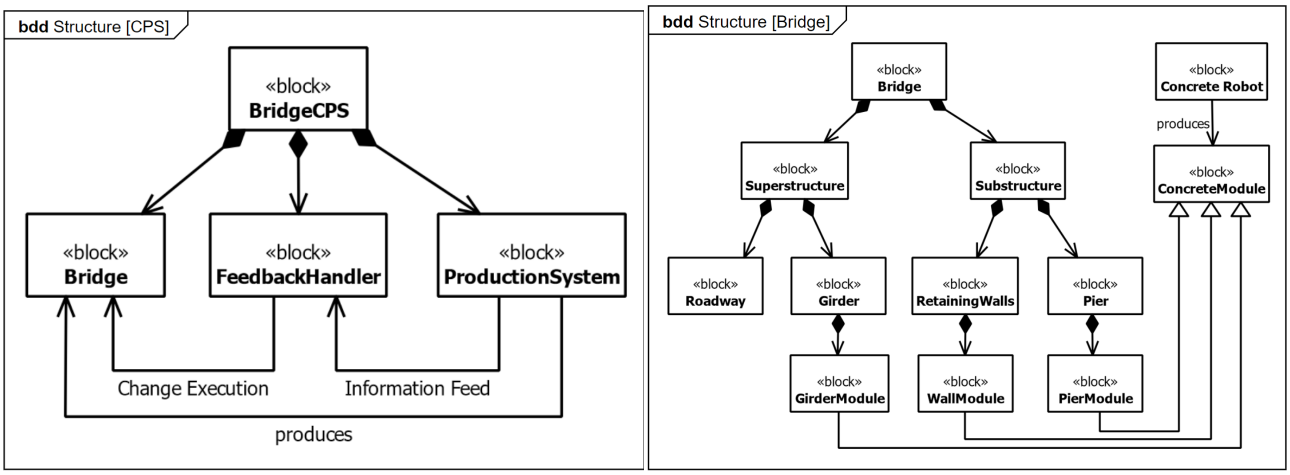


(a) (b)

Figure 2: Two examples of a block-definition-diagram. (a) shows the high-level structure of the CPS through *blocks*( (rectangles), *compositions* (black diamond) and *associations* (arrows). (b) details the structure of the bridge component in more detail through more granular composition, as well as *generalization* (white arrow).

Figure 2 shows how multiple *bdd*-diagrams can be used to granularly define different aspects of the system. Meanwhile, the `bridge`-block in (a) shares the same object with the `bridge`-block in (b) (as in: a change in that particular block will propagate to both diagrams). Separating aspects into different diagram views is a suitable way to illustrate the system while still maintaining necessary associations by storing them in the underlying model.

### 3.2 Requirements

The requirements of the bridge can either be defined at the beginning of the project lifetime and extended later on or derived from the modeled behavior. SysML also allows for the deriving and refining of requirements, as well as their satisfaction through other components. Many other system model components can satisfy a particular requirement, such as a block, an activity, or others. These requirements, defined by plain text and an id, are also part of the resulting model. Further detailing of the requirements can be achieved through *refining*, *tracing*, and *verification*, all of which are part of the SysML specification.

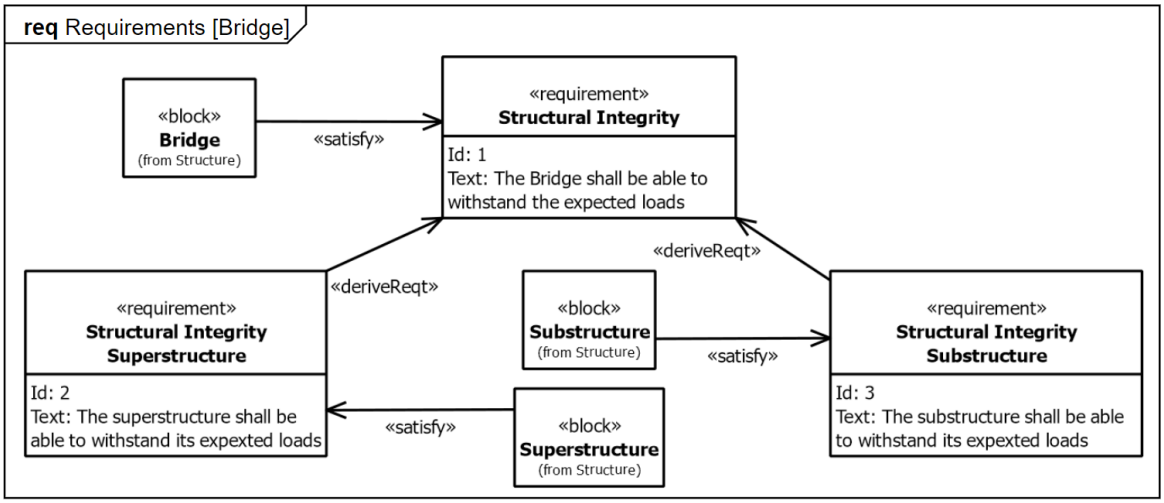


Figure 3: Example requirements of the bridge. Each requirement is currently satisfied by a respective block from the systems *structure*.

## 4 Model Testing

As several diagrams have now been created, the underlying model is also defined. Most SysML software provides the user with the tools to create the diagrams from which the modeling software derives the model. This is the case with the modeling software *Gaphor*, an open-source UML and SysML modeling tool. The graphical application used to model the diagrams also includes a Python library with which the objects within the model can be accessed [8]. *Gaphor* saves its models using an XML file, which can then be parsed by using the Python library. This allows the creation of a testing framework with which certain conditions can immediately be assessed. A prototypical implementation was developed to prove the concept of a simple system-level analysis of the model, ensuring model consistency and compliance across its development. Two examples of this would be (1) checking for requirement satisfaction and (2) testing the semantic embedding of new components. The first example is simple to implement and checks if all requirements inside the model are satisfied, i.e., have a 'satisfies' relationship with another component. In the following *req* diagram example in Figure 4, the test script will throw an error since not all requirements are satisfied.

Furthermore, a check for correct semantics can be implemented by automatically testing if new blocks that inherit from the block ConcreteModule are part of the bridge assembly - by traversing the composition associations until we arrive at the `bridge` block. This way, modeling consistency can be

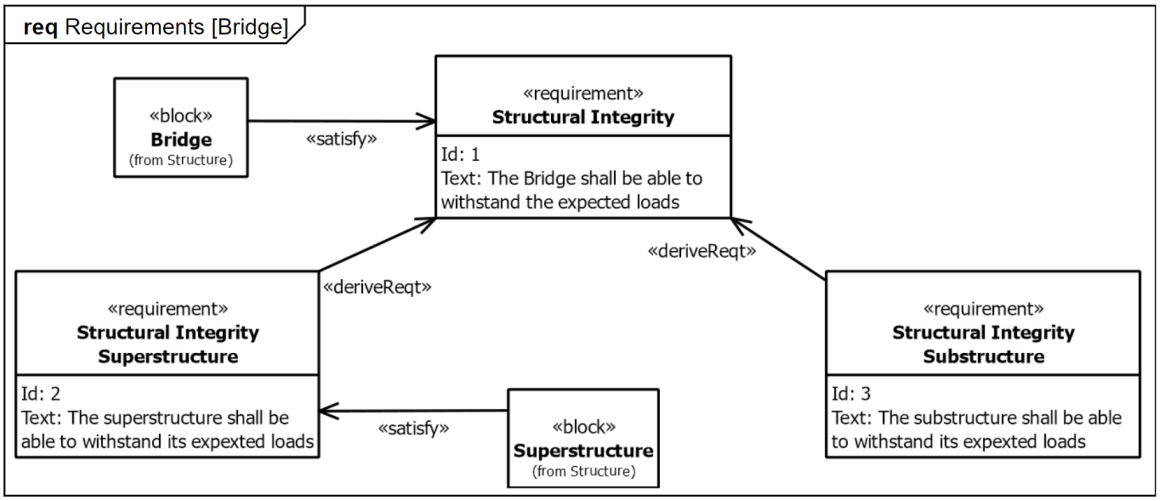


Figure 4: Example *req* diagram with one missing satisfaction relationship. In this case, the test would warn the user that not all requirements are satisfied. This can ensure model compliance

assured as components of a certain type must belong to a certain assembly. An example of this can be seen in Figure 2 in the (b) subfigure: If either `WallModule`, `GirderModule`, or `PierModule` were not part of the `bridges` composition, the text would warn the user.

The testing was scripted and executed using the *pytest* framework while using the *Gaphor* python library to extract and represent the model. One interesting point to make about this setup concerns the Object Modeling Group's (OMG) Meta Object Facility (MOF): Languages such as UML and SysML are defined on the M2 level and used on the M1 level. Concrete instances, on the other hand, are situated within the M0 level [9]:

Table 1: The Object Modeling Group's (OMG) Meta Object Facility (MOF) Hierarchy. [9]

| | |
|---|---|
| M3 (MOF) | Defines a language for specifying a metamodel. |
| M2 (SysML) | Defines a language for specifying models. |
| M1 (User Models) | Defines a language That describes semantic domains. |
| M0 (Instance Models) | Contains run-time instances of the model. |

The *pytest* framework exclusively tests on the M0 level, as it can only assert values or states during the runtime of the script or program. However, a workaround is necessary since we want to check for compliance on the M1 level (Where the SysML diagram exists). The *Gaphor* python library's solution is to map SysML objects to instantiated python objects when the model is loaded. An example of this would the SysML's *block*, which would be the equivalent to a UML *class*. When a model containing a *block* is loaded using the library, an object of type `SysML.Block` is instantiated. This kind of abstraction is a solution to make model testing with pre-existing frameworks simple and convenient.

## 5 Conclusion and Final Remarks

Adapting tools for systems engineering into the AEC domain is a challenging task, and this paper has only scratched the surface as to what is possible. SysML includes 9 different diagram types to model various aspects of a system [3], of which only 2 have been discussed here. Analyzing and dissecting these diagrams to find out which are necessary and which are not already a challenge in 'classical' systems engineering proves even greater of a challenge when adopting this method to a somewhat foreign domain. Yet, the use case of cyber-physical systems looks to be a promising starting point for the adoption of the method. Furthermore, existing software, including powerful libraries or APIs such as *Gaphor*, can prove to be useful for further automation of not only the design of the system itself but also for executing and simulating said system. One such example could be the previously mentioned feedback loops that can automatically propagate changes in one component to others, expressed through the system's behavior. Specifically, more research needs to be conducted on this kind of use case.

## Acknowledgements

We gratefully acknowledge the financial support of the Deutsche Forschungsgemeinschaft (DFG) as part of the program SPP 2187 "Adaptive modularized constructions made in flux" (Project 423969184).

## References

[1] A. Borrmann, M. König, C. Koch, and J. Beetz, *Building Information Modeling - Technologische Grundlagen und industrielle Praxis*, 2nd ed. Springer Vieweg, 2021.

[2] L. Delligatti, *SysML distilled: A brief guide to the systems modeling language*. Addison-Wesley, 2013.

[3] *Sysml faq: What is sysml?* [Online]. Available: https://sysml.org/sysml-faq/what-is-sysml.html.

[4] M. Broy, *Cyber-physical systems: Innovation durch softwareintensive eingebettete Systeme*. Springer, 2011.

[5] H. Nassereddine, M. E. Jazzar, and M. Piskernik, "Transforming the aec industry: A model-centric approach", Eigenverlag, 2020, pp. 13–18. DOI: 10.3311/CCC2020-076. [Online]. Available: https://repositum.tuwien.at/handle/20.500.12708/62873.

[6] P. Geyer, "Systems modelling for sustainable building design", *Advanced Engineering Informatics*, vol. 26, pp. 656–668, 4 Oct. 2012. DOI: 10.1016/J.AEI.2012.04.005.

[7] O. Badreddin, V. Abdelzad, T. Lethbridge, and M. Elaasar, "Fsysml: Foundational executable sysml for cyber-physical system modeling", 2016.

[8] *Gaphor: About*. [Online]. Available: https://gaphor.org/#about.

[9] O. 2. E. Team, "Meta-modeling and the omg meta object facility (mof)", 2017. [Online]. Available: https://www.omg.org/ocup-2/documents/Meta-ModelingAndtheMOF.pdf.

# Implementing information container to link multi-models for Semantic Digital Twins

Yingying Zhang[1]
[1]RWTH Aachen University, Schinkelstraße1, 52062, Aachen, Germany
E-mail(s): yzhang@dc.rwth-aachen.de

**Abstract:** Infrastructure Digital Twins (DTs) are commonly understood as up-to-date virtual representations of the physical infrastructure assets. The Digital Twins data pattern contains not only geometric and spatial aspects of the physical entities but also incorporates heterogeneous information including specifications, sensor data, performance metrics, maintenance records, and operational reports. At the same time, the continued expansion of the Digital Twin system without proper modeling, decoupling, and optimization of control workflows will further reduce its manageability and reliability. This paper presents a data archiving method using an Information Container for linked Document Delivery (ICDD), which is primarily based on ISO 21597, to containerize heterogeneous Digital Twins payload in arbitrary formats and provide validation services. The proposed container uses a standardized structure to implement services such as data linking, version control, and access control, thus making the Digital Twin data archiving more efficient and reliable.
*Keywords:* Digital Twin (DT), Information Container for linked Document Delivery (ICDD), Linked Data, Semantic Web

Erschienen in Tagungsband 35. Forum Bauinformatik 2024, Hamburg, Deutschland, DOI: 10.15480/882.13551
© 2024 Das Copyright für diesen Beitrag liegt bei den Autoren. Verwendung erlaubt unter Creative Commons Lizenz Namensnennung 4.0 International.

## 1 Introduction

The emergence of digital twins has led to the enrichment of static BIM systems in the temporal dimension, which has improved AEC productivity to some extent, but at the same time, more complex data management challenges need to be faced [1]. The initial challenge is how the digital twin infrastructure in the AEC domain can manage data from heterogeneous sources efficiently. Heterogeneous data formats and communication protocols require standardized processes. Linked data provides a way to facilitate the integration of heterogeneous datasets that might otherwise be incompatible, and can address interoperability issues to some extent to provide a more comprehensive DT model [2].

Secondly, the analysis of digital twin systems is highly reliant on large datasets, usually consisting of a collection of dynamic data of the temporal evolution of physical entities. This type of dynamic data is usually stored for access in time series databases, whereas contextual information about the DT system such as geometric data, and sensor contextual information is often stored separately in a static format. The underlying raw data does not need to be exposed to the top users, either for security or

administrative reasons, who only need access to the high-level knowledge or optimization conclusions generated by synthesizing the raw data. Therefore, the integration and unified access to dynamic data and static contextual information is far from easy and is still an active research area.

The emergence of the ICDD (Information Container for Linked Document Delivery) standard provides a container that can be used to standardize the management and delivery of data and documents in AEC engineering projects. It can provide a common platform to support multiple data formats and standards to ensure interoperability between different systems and tools, and at the same time can create links for heterogeneous resources. Currently, ICDD has been applied to solve some complex heterogeneous project unified information management, such as the infrastructure documentation management [3], or the automatic linkage of BIM model and external systems [4].

DT systems that collaborate across multiple domains rely on high-quality native data, and the use of information containers allows for effective management of DT projects to ensure that digital twins are always synchronized with physical entities. However, ICDD is an information container designed for static data, and the representation of DT, a system based on time-series iterations, becomes more complex. In this paper, we propose a research method that aims to link heterogeneous dynamic DT data in ICDD container and realize fully automatic updating of the linked information in the information container. This approach achieves effective linking of DT heterogeneous data while ensuring data storage efficiency, and saves the effort required to repeatedly create information in the container.

# 2 Background

## 2.1 DT data archival

Interoperability has always been one of the issues facing in the AECO as it is an industry that requires multi-disciplinary collaboration resulting in heterogeneous and highly fragmented data. While DT compared to static BIM systems the temporal evolution characteristic is added, which requires well-defined data structures to maintain the accurate operation of this system for decision support and prediction.

Currently the BIM domain is starting to evolve to address interoperability issues by using Linked Data approaches to ensure the exchange of heterogeneous data, such as the evolution of the IFC format to ifcOWL, and the emergence of open data paradigms such as the building topology ontology (BOT), where closed BIM systems are starting to move towards the stage of open BIM based on semantic modeling. The Semantic Web has proven its feasibility in addressing the interoperability of static BIM systems, e.g., using Linked Data to link BIM with IoT systems. Still, most of these studies have converted the data uniformly into RDF or OWL formats for storage and querying.

Apart from this, some research has started to focus on the effectiveness of the Semantic Web in representing dynamic data [5] [6]. Hybrid storage approaches have been proposed for the data characteristics of DTs, either in the form of data lakes or decentralized data modeling, which are able to combine data from multiple sources to provide a unified view and enable more efficient native data storage for data-intensive analytics (e.g., machine learning). Nevertheless this hybrid storage

approach has increased difficulty in unified access to data, and a number of data federated querying approaches have been proposed [7]. Overall, hybrid data storage approaches can effectively utilize the potential of linked data in solving interoperability problems as well as enabling flexible and efficient storage of massive amounts of data.

### 2.2 ICDD as the information container for AECO sectors

Document-based collaboration has been used in the AECO field until now, but traditional document management methods can lead to information fragmentation and confusion. Originally an information container for multi-domain data exchange was developed in the Dutch COINS project, and this approach to information containers was eventually standardized as ICDD. The ICDD, i.e. Information Container for Linked Document Delivery, defines a standardized method for managing and delivering linked documents in projects in the AEC field. In ISO 21597 [8], the structure of ICDD container is defined in detail and two ontology resources, Container ontology and Linkset ontology, are proposed to be used for interlinking documents inside the container.

The effectiveness of ICDD in managing static AEC documents has been demonstrated many times and continues to evolve, whether it is for the effective management of BIM models and drawings [4], to facilitating the integrated delivery of BIM models and other heterogeneous information. Ye [9] in this study explores the use of information containers and blockchain to ensure automated payment for construction, through the use of ICDD, where the BIM model, BoQs (Bill of Quantities) and QTO (Quantity Take-Off) are effectively interconnected in the information container. A micro-service based approach for BIM project document delivery has also been proposed, applying ICDD in open CDE can provide web-based online services [10]. However, projects in the AEC domain are based on the process of continuous time synchronization, so the dynamic functionality extension for information containers is concerned, and a dynamic information container feature is proposed to enable automatic update of version control [11]. The question of how to handle high volume time series data, which is the essential part of Digital Twin, can be efficiently represented in information containers will be explored in this paper.

## 3 Prototype design: ISO 21597-ICDD

Linked Data has been applied to address the interoperability of DT heterogeneous data sources, meanwhile it has become common sense in recent years Linked Data is not optimally efficient in representing high throughput data like sensor data, so this study envisions an ICDD-based Digital Twin data modeling approach that manages dynamic data in chunks in information containers and abstracts them into knowledge represented on Linked Data, thus facilitating interlinking of contextualized DT data and faster query paths.

Research Questions (RQs) outline the scope of how the data modeling method can effectively archival heterogeneous DT data, below lists the research questions:

- ***RQ1***: How can heterogeneous DT data be more efficiently archived?
- ***RQ2***: How to facilitate real-time collaboration and communication of DT's dynamic data?

- ***Hypothesis 1***: Hybrid storage scheme: the time series raw data is decomposed into different json files according to the chunking principle, and descriptive labels are generated and stored in the knowledge graph for querying.

- ***Hypothesis 2***: Use ICDD to facilitate standardized DT data exchange: ICDD is appropriate for federating heterogeneous project data while adhering to industry standards and regulatory document management and delivery processes, which helps to ensure that projects efficiently facilitate standardized DT data exchange in a compliant manner.

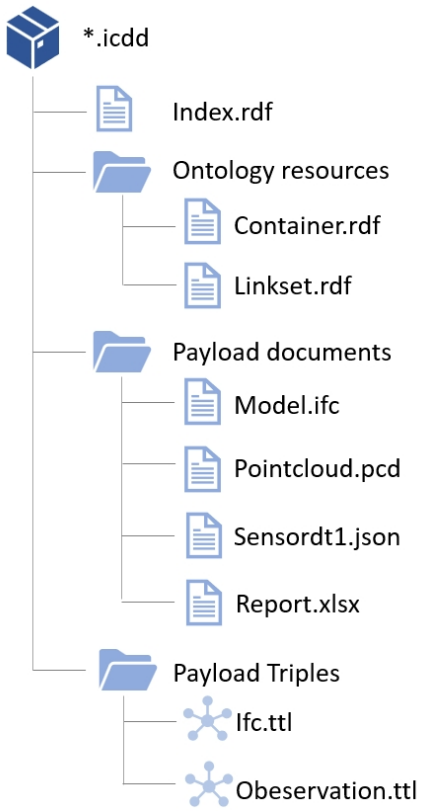


Figure 1: The file structure of the proposed scheme

### 3.1 Automated Dynamic data linking in ICDD

The growing volume and complexity of data generated by DT compared to static BIM systems require more effective data archiving strategies for efficient data storage, retrieval, and analysis. The DT model in the AEC domain, mainly consists of several data models, which also can be seen in Figure 2:

- ***Time series model***: it mainly consists of real-time monitoring information generated from actuators and sensors, and is mainly stored in databases that are optimized for time-stamped or time series data, such as InfluxDB.

- ***Geometric model***: the virtual representation of physical entities, used to represent relationships and interactions within a DT system and to facilitate pattern recognition.

- ***Relational model***: mainly includes structured data, including system log records, texts, spreadsheets, etc.
- ***NoSQL model***: includes both semi-structured and structured data, such as document-based storage, key-value storage, and wide-column storage, etc.

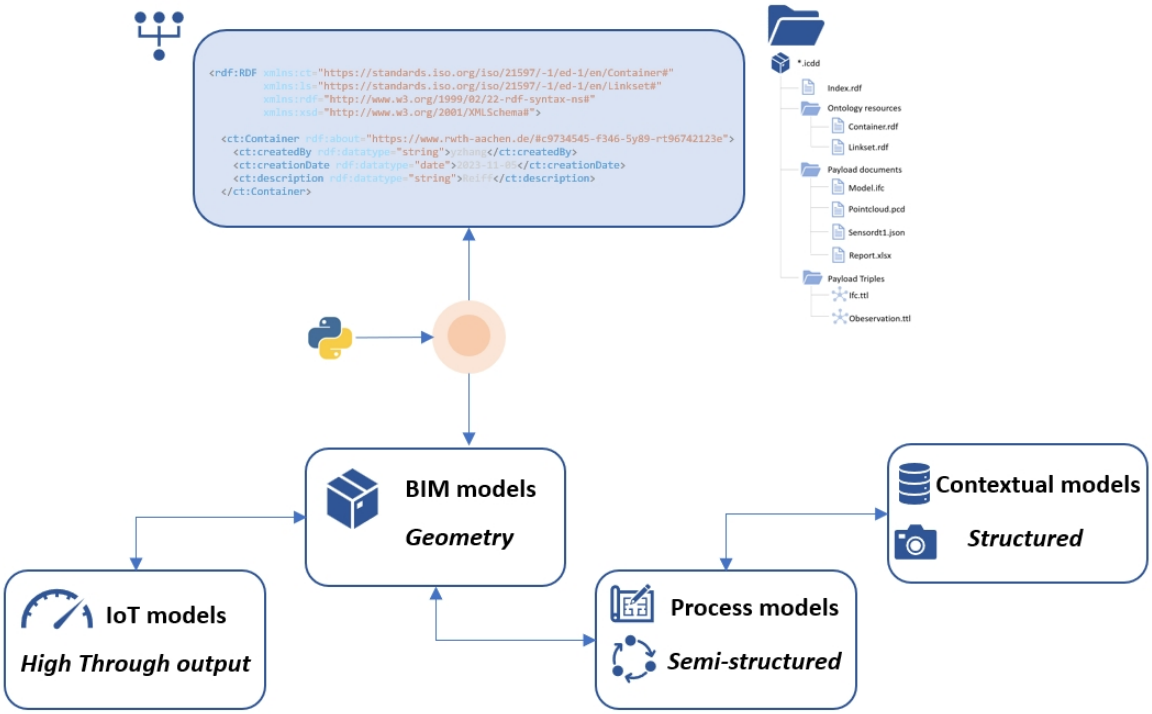


Figure 2: Information container work as the media for Multi-model digital twin data

So in this paper we designed a multi-data model for DT data from physical entity to virtual migration, and manage the DT data dynamically in the information container, using the function of ICDD to create links between different data elements in the container and also between multiple containers. The specific steps are as follows:

1 Physical entity information is transmitted via MQTT to the time series database for storage

2 Automatically create links to ICDD containers from InfluxDB datastore buckets chunked according to the chunking principle

3 The time series data is divided into different payload documents to store and automatically generate Identifier and RDF document reference, which is stored in index.rdf

To validate the proposed method of multi-modeling application, a case study was executed using sensor monitoring data in a university building, which is more complex compared to a static BIM model, where firstly, spatial information is modeled as an IFC model, while three air quality sensors are placed in different rooms to monitor the air quality in real-time. The specific data schema is shown in Figure

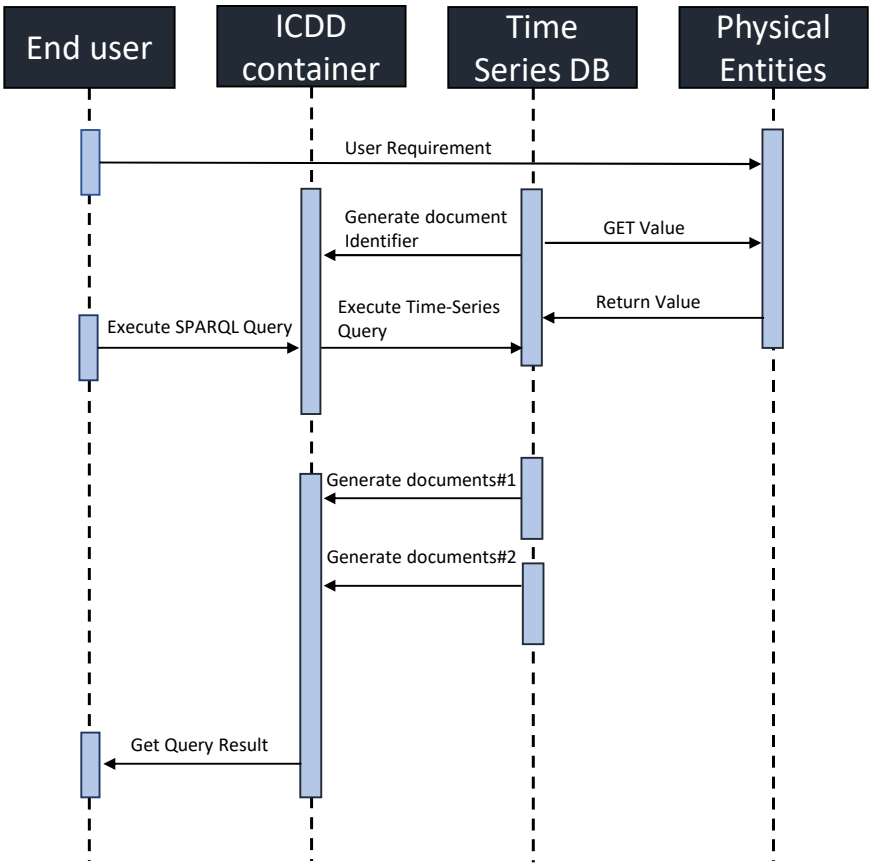


Figure 3: Overview sequence diagram of the proposed solution

4 Information from the environment is collected and converted into digital signals by micro-sensors and Raspberry Pi, subscribed and stored in buckets in the time series database through the MQTT protocol, and converted by the Python middleware, which allows linking the time series database directly to information containers and dividing them into different json files according to the chunking principle.

In this case study it is possible to provide the client with: links between the representation of the physical entity through the IFC space and the values of the aggregation operations on the observation values, links between physical entity model elements and inspection reports and photos.

## 4 Disscussion and Conclusion

This paper highlighted how dynamic data and heterogeneous data models can be efficiently stored and interlinked with each other in the information container. It explored how dynamic and contextualized data interoperability can be achieved while ensuring storage and querying efficiency. Hence, an approach based on linking data in information containers is used, which by dynamically linking time-series databases and automatically generating summarized information in information containers, is able to create formal links between dynamic data and contextualized information is necessary for the

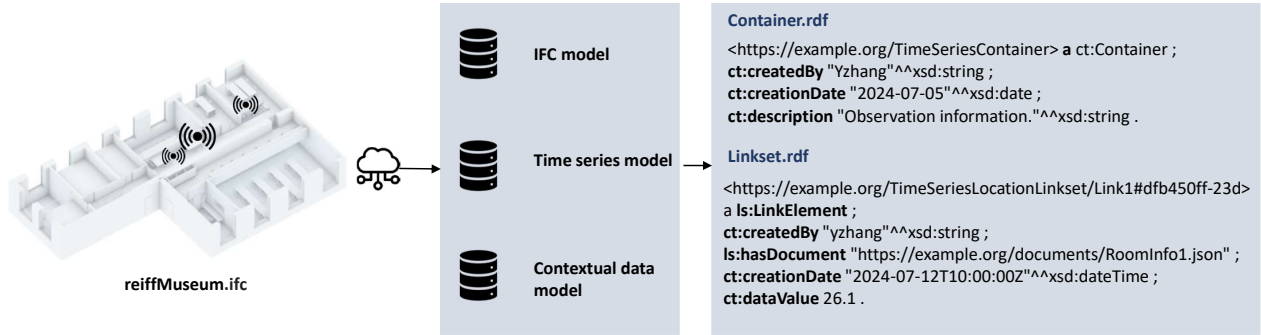


Figure 4: Using multiple containers to link multiple models in the use case Digital Twin scenario

Digital Twin system for data archiving, pattern validation and support for retrieval of context-supported observation information.

The AEC domain has brought great progress to the industry with the collaboration of multiple stakeholders, from drawing design to virtual modeling of physical entities, the intercommunication between multiple specialized models and systems plays an increasingly important role. From BIM to dynamic DT systems, the constantly proposed models put high demands on the matching of legacy data, so the significance of this research is to explore the usage of information containers as a medium to link BIM and complex DT systems by trying to use ICDD as the top-level data model architecture, heterogeneous geometric models, time series models, process models, and structured context models can be effectively integrated and linked in the information container.

Meanwhile, using ICDD containers can facilitate standardized data exchange workflows, thus resulting in increased reliability and consistency throughout the project lifecycle. However, ICDD currently stays at the standard level, and the compatibility with existing tools and legacy data is yet to be developed. In addition, whether the use of information containers to federate digital twin data is an optimal solution needs to be explored and verified, and the ability of Linked Data to effectively federate heterogeneous data has been demonstrated, but its current ability and efficiency to handle dynamic data still needs to be explored.

## References

[1] A. Borrmann, J. Schlenger, N. Bus, and R. Sacks, “Aec digital twin data-why structure matters”, in *International Conference on Computing in Civil and Building Engineering*, Springer, 2022, pp. 651–669.

[2] C. Boje, A. Guerriero, S. Kubicki, and Y. Rezgui, “Towards a semantic construction digital twin: Directions for future research”, *Automation in construction*, vol. 114, p. 103 179, 2020.

[3] A. Göbels and J. Beetz, “Using icdd containers for documentation data archives: Semi-automated creation of linked documentation data archives using an information container for linked document delivery”, in *Proceedings of the 27th International Conference on Cultural Heritage and New Technologies*, 2022.

[4] A. Borrmann, J. Abualdenien, and T. Krijnen, “Information containers providing deep linkage of drawings and bim models”, in *Proc. of the CIB W78 Conference 2021*, 2021.

[5] S. Hu, E. Corry, E. Curry, W. J. Turner, and J. O’Donnell, “Building performance optimisation: A hybrid architecture for the integration of contextual information and time-series data”, *Automation in Construction*, vol. 70, pp. 51–61, 2016.

[6] Y. Zhang and J. Beetz, “Semantic sensor data federation in dynamic knowledge graphs using rdf-star”, in *Proceedings of 30th EG-ICE: International Conference on Intelligent Computing in Engineering*, European Group for Intelligent Computing in Engineering, vol. 30, 2023.

[7] M. Bakken and A. Soylu, “Chrontext: Portable sparql queries over contextualised time series data in industrial settings”, *Expert Systems With Applications*, vol. 226, p. 120 149, 2023.

[8] ISO, “Information container for linked document delivery—exchange specification—part 1: Container”, *ISO 21597-1*, 2020.

[9] X. Ye, K. Sigalov, and M. König, “Integrating bim-and cost-included information container with blockchain for construction automated payment using billing model and smart contracts”, in *ISARC. Proceedings of the International Symposium on Automation and Robotics in Construction*, IAARC Publications, vol. 37, 2020, pp. 1388–1395.

[10] M. Senthilvel, J. Oraskari, and J. Beetz, “Implementing information container for linked document delivery (icdd) as a micro-service”, in *EG-ICE 2021 Workshop on Intelligent Computing in Engineering*, Universitätsverlag der TU Berlin, 2021, pp. 66–73.

[11] N. N. Al-Sadoon, R. Scherer, and K. Menzal, “From static to dynamic information containers”, in *EC3 Conference 2023*, European Council on Computing in Construction, vol. 4, 2023, pp. 0–0.

# Teil VIII

# Simulation & Optimization

# Building Resilience to Heatwaves: Parametric Simulation Approach Aiding Passive Design Strategies for Thermal Comfort in Future Climate

Agata Dalach[1]
[1]Technical University of Munich, Arcisstraße 21, 80333 Munich, Germany
E-mail(s): agata.dalach@tum.de

**Abstract:** Future weather predictions indicate more frequent and intense heatwaves, demanding that buildings ensure adequate comfort during those events. Current research focuses on climate adaptation and estimating thermal comfort with rising temperatures. This study investigates heatwave-resilient architecture, particularly where air conditioning is unavailable and cooling relies on passive strategies. Numerous simulations were conducted on a simplified building model using future-updated weather data and a parametric approach. This method enabled a detailed exploration of the effects of specific parameters (One-at-a-time Sensitivity Analysis) on thermal comfort during early design stages. The results suggest that buildings without mechanical air conditioning will struggle to maintain thermal comfort. The most influential parameters were window shading style, solar heat gain coefficient, and window-to-wall ratio. The main contribution of this study is developing a highly applicable model for a medium-sized residential building and a sensitivity analysis of thermal comfort during heatwaves, considering key geometric and physical parameters.
*Keywords:* heatwave resilience, thermal comfort, design in early stages, sensitivity analysis

Erschienen in Tagungsband 35. Forum Bauinformatik 2024, Hamburg, Deutschland, DOI: 10.15480/882.13501
© 2024 Das Copyright für diesen Beitrag liegt bei den Autoren. Verwendung erlaubt unter Creative Commons Lizenz Namensnennung 4.0 International.

## 1 Introduction

Extreme weather events are expected to increase in frequency and intensity in the future [1]. Among those events are heatwaves, which are natural hazards that may potentially harm human health [2]. Buildings should serve as shelters, isolating their users from such harmful external conditions, and achieving this goal requires both adaptation and resilience.

Climate adaptation involves strategies to reduce risks and vulnerability, ensuring buildings maintain comfortable conditions despite the rising temperatures [3]. Resilience, similarly, refers to the building's ability of systems to withstand, adapt to, and recover from temporary disruptions like extreme weather events [4]. The key attributes of resilience include robustness, redundancy, resourcefulness, and rapidity, ensuring that systems can adapt, learn, and transform in the face of challenges [5]. This

implies that resilient buildings could potentially be unsustainable, as their resilience features might contradict the sustainability aspect of resource sufficiency.

The response of a building to a heatwave depends both on the character of the heatwave and the properties of the building. For instance, building materials can mitigate shorter heatwaves, whereas longer and more intense heatwaves would likely require air conditioning systems. This study evaluates building heatwave resilience and user thermal comfort during extreme heat events, focusing on sustainability and sufficiency by relying on passive design strategies instead of air conditioning. A parametric approach was used to generate numerous design variants and perform one-at-a-time (OAT) sensitivity analyses, assessing thermal comfort using a broadly applicable shoebox-like building model. The research questions addressed are: What insights can parametric simulations provide on building heatwave resilience? What parameters are the most critical for buildings without air conditioning?

## 1.1 Thermal comfort

Elevated temperatures impact the thermoregulation processes of the human body, making prolonged exposure especially dangerous [2]. Thermal comfort models can be used to assess whether a building can protect its users against such events. Thermal comfort assessment is a topic that has been largely studied and utilized in the building industry and research. Developed in the 1970s by Ole Fanger, the PMV (Predicted Mean Vote) model assesses thermal comfort on a scale from +3 (hot) to -3 (cold), and then calculates the PPD (Predicted Percent of Dissatisfied) [6]. While widely adopted, some researchers argue its accuracy is limited, particularly for naturally ventilated spaces, leading to the development of adaptive comfort models, whose also include the influence of user behavioural adaptation and other factors [7]. The DIN EN 15251 norm defines a comfortable interior temperature in relation to outdoor temperature, as 22 °C for outdoor temperatures below 16 °C, 26 °C for outdoor temperatures above 32 °C and linearly interpolated values for outdoor temperatures between 16 °C and 32 °C [8]. However, predicting thermal comfort in the event of a heatwave could require a different approach. Related research on this topic includes a predictive model for overheating, considering that the human body can somehow tolerate hot temperatures if they are followed by the lower ones [9], and metrics to estimate the building heatwave resilience to extreme temperatures [10]. However, no established methodology exists to evaluate building design decisions in the early design stage.

## 1.2 Parametric modelling and building performance simulation

Building simulation allows for accurate reality emulation using complex equations and virtual experiments to evaluate building performance. Thermal comfort simulation in the context of climate change and heatwave resilience has already attracted researchers' attention, leading to the use of estimated future weather data for simulations. Approaches to estimating the influence of climate change on the built environment include evaluating thermal comfort in multi-family houses in Spain [11], assessing overheating risks in multi-family houses in Sweden [12], and examining impacts on buildings with various functions across U.S. climate zones [13]. The analysis of resilient strategies to mitigate these effects includes studies on the influence of the selection of insulation material in single-family homes in Brazil [14] and Central Europe [15], classroom retrofitting methods in Malaysia [16], and the effects of green facades on reducing operative temperatures inside buildings [17]. Despite the significant

contributions of previous works, there is still a need for a general approach that considers basic geometry and highly applicable scenarios, which could be especially beneficial in the early stages of building design when limited information is available, but the potential for design changes is greatest.

# 2 Methodology

The methodology employed in this study involves generating a large number of variants of the building model and conducting a performance simulation for each of them. The models were created using the parametric modeling Grasshopper plug-in for Rhino 3D modeling software. Thermal comfort simulations were conducted with components from the Ladybug Tools' Honeybee and Honeybee-Energy sets, which through OpenStudio SDK, utilize EnergyPlus simulation engine, allowing for complex thermodynamic modeling. The iterative process and result aggregation utilized Colibri components from the TTToolbox. Custom Python scripts facilitated data visualization and analysis.

## 2.1 Parametric building model

The basic model for the experiment consisted of a residential building, whose footprint was 10x45 m with 3 floors, each 4 meters high. Each variant of the model, representing an early-stage building, was defined by a combination of selected geometric and physical parameters, including, among others, window properties of the U-Factor (non-solar thermal transmittance) and the solar heat gain coefficient (SHGC) - ratio of the transmitted solar radiation to the total radiation hitting the element. As detailed in Table 1, 1,440 distinct model variants were formed, to facilitate a OAT sensitivity analysis. The influence of green building elements (roofs, façade greening) was deliberately omitted. Despite its decisive influence on climate adaptation [18], this topic requires a different kind of experiment.

Table 1: Set of the selected and tested simulation parameters

| # | Parameter name | No. val. | Values |
|---|---|---|---|
| P1 | Construction Set | 4 | sand-lime brick, clay brick, wood massive, wood light |
| P2 | Building Orientation | 5 | 0°, 30°, 60°, 120°, 150° |
| P3 | Window Shading Style | 4 | nothing, louvers, overhang, external roll |
| P4 | Window U-Factor $[W/m^2K]$ | 2 | 0.6, 1.2 |
| P5 | Window SHGC | 3 | 0.4, 0.6, 0.8 |
| P6 | Window-To-Wall-Ratio | 3 | 0.2, 0.3, 0.4 |
| | Total no. Variants | 1,440 | |

## 2.2 Weather data and analysis period

Ladybug Tools uses the EnergyPlus EPW weather format, which typically contains Representative Meteorological Years for various locations. However, this study focuses on heatwaves and extreme temperature events, which require the analysis of extreme rather than typical temperatures. To achieve this, the EPW files were updated using Meteonorm, which incorporates satellite data and future climate models from the IPCC CMIP5 framework. The pessimistic RCP8.5 scenario for the year 2100 was selected, representing a predicted future with high greenhouse gas concentrations. This scenario was chosen to simulate an extremely hot year. In order to focus on a heatwave event, the period between

June and August was chosen as the analysis period. Including the preceding month of June in the simulation allowed for accounting for the energy stored in the building's thermal mass, enhancing the accuracy of the simulation results. Figure 1 presents hourly charts for the outdoor dry bulb temperature in the selected location (Bamberg, Bavaria) for the years 2020 and 2100.

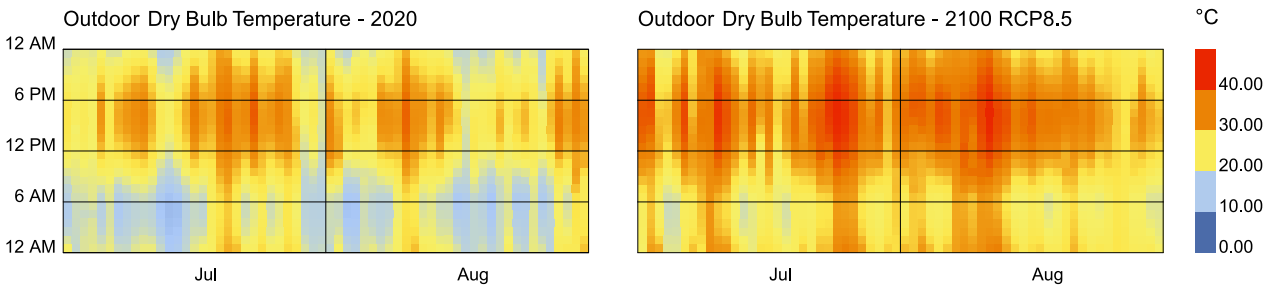


Figure 1: Temperature outside in 2020 and 2100 according to the RCP8.5 scenario

### 2.3 Thermal comfort indicators

Although there are many thermal comfort metrics, as described in Section 1.1, it was decided to compare the simulation's most general and universal information. These indicators allow for the calculation of other values, especially when considering additional details such as user characteristics. The sensor grid for the analysis was placed on the top floor, typically the most prone to overheating. The selected indicators are summarized in Table 2:

Table 2: Selected thermal comfort indicators

| # | Indicator Name | Unit | Description |
|---|---|---|---|
| IC1 | Number of Hot Hours | Hours | Total hours classified as "hot," determined by the HB-Energy component "Adaptive Comfort Map." This includes hours when at least 20% of building sensors exceed the defined comfortable temperature, based on the norm described in 2.1. |
| IC2 | Average Temp. Difference Outdoor-Indoor | ℃ | Measures the building's ability to mitigate high outdoor temperatures. |
| IC3 | Maximum Average Operative Temperature | ℃ | Operative Temperature, a measure of perceived temperature, considers factors such as air temperature, velocity, and mean radiant temperature, with guidelines set by DIN EN 15251 for various outdoor temperatures. |

## 3 Results

The results from 1440 simulations on thermal comfort in naturally ventilated buildings during extreme heatwaves showed diverse results. However, none of the designs fully achieved heatwave resilience. Notably, the IC2 and IC3 indicators demonstrated an almost linear relationship (Figure 2), while IC1 and IC3 plots demonstrate first stable and then value growth, clustered by the highest IC1 values (Figure 3). Some designs facilitated effective nighttime cooling and heat storage within the thermal mass, maintaining indoor temperatures between 28 and 36 ℃ without exceeding 40 ℃. However, a significant proportion of models experienced indoor conditions hotter than comfortable for 90% of the time, with extreme cases exceeding 50 ℃, making it uninhabitable. Only eight (out of 1440) parameter

configurations provided comfortable temperatures for at least 10% of the time. The extreme values and the average indicator values are detailed in Table 3.

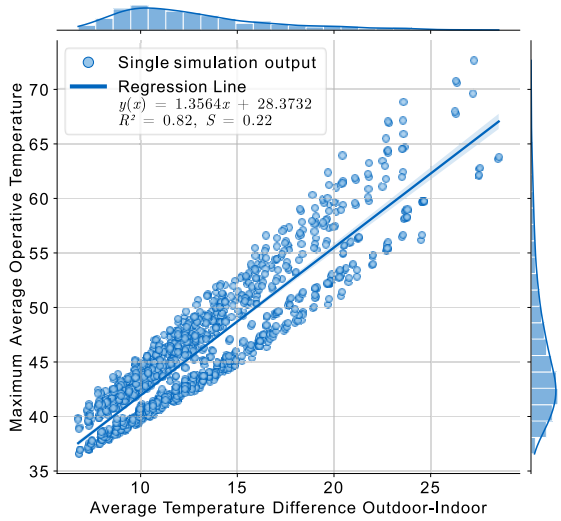


Figure 2: Comparison of Average Temperature Difference Outdoor-Indoor and Maximum Average Operative Temperature

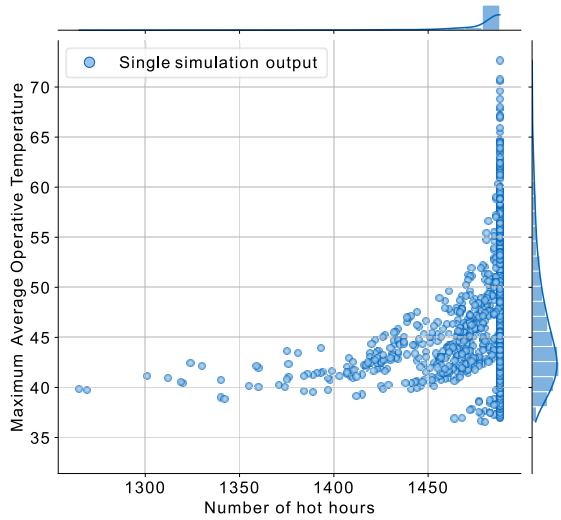


Figure 3: Comparison of Number of hot hours and Maximum Average Operative Temperature

## 3.1 Parameter sensitivity

The indicator values were averaged for all unique parameter values. The results for the IC3 indicator, presented in Figure 4, demonstrate that variants without shading devices performed the worst, with an average temperature of 50.29 °C. Louver shades (42.44 °C) and external roll screens (42.55 °C) were more effective than overhangs (47.97 °C). The window solar heat gain coefficient (SHGC) and the window-to-wall ratio significantly impacted the results, while the Construction Set had a lesser but still notable impact, with P1=[1] and [2] performing the best and [4] worst. The building rotation and the U factor of the window were the least significant. The sensitivity analysis (Figure 5) showed consistent relative importance of parameters across indicators, with Construction Set more influential for the Number of Hot Hours due to thermal mass and insulation effects. Ultimately, none of the variants is resilient in the given scenario, and mechanical conditioning will be essential to ensure adequate protection against heatwaves.

Table 3: Mean and extreme values for the thermal comfort indicators and corresponding parameters (P1-P6, see Table 1)

| Indicator | Mean | Lowest | Parameters | Highest | Parameters |
|---|---|---|---|---|---|
| IC1: Number of hot hours [no. hours, max: 1488] | 1477 | 1265 | 4, 60, 1, 1.2, 0.4, 0.2 | 1488 | Many |
| IC2: Average Temperature Difference Outdoor-Indoor [°C] | 12.86 | 6.77 | 4, 120, 1, 1.2, 0.4, 0.2 | 28.52 | 2, 0, 0, 0.6, 0.8, 0.4 |
| IC3: Maximum Average Operative Temperature [°C] | 45.81 | 36.57 | 1, 120, 1, 1.2, 0.4, 0.2 | 72.66 | 4, 0, 0, 0.6, 0.8, 0.4 |

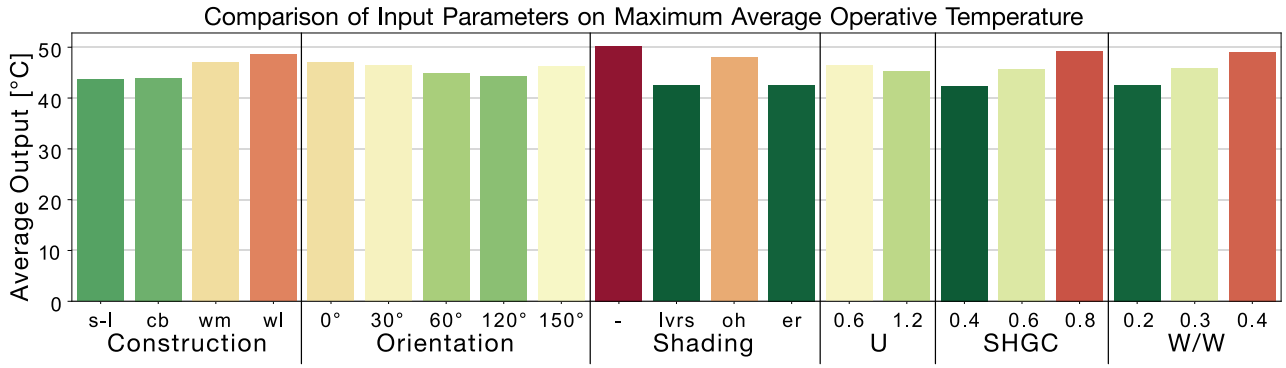


Figure 4: Average parameter values

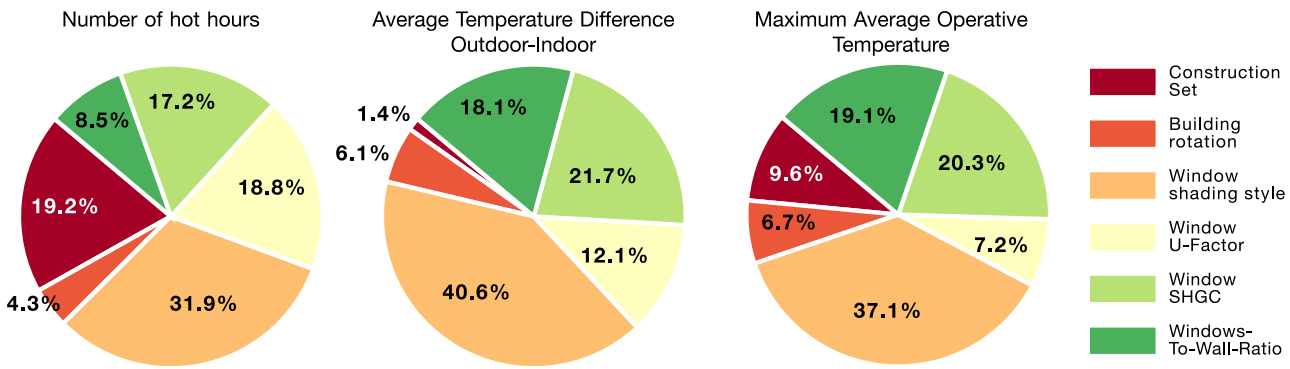


Figure 5: Parameter sensitivity of the three indicators

### 3.2 Comparison with a milder summer

After concluding that no building variants could provide comfort under the worst-case scenario (RCP 8.5) for 2100, the focus shifted to a more optimistic 'sustainability' scenario (RCP 2.6). This scenario features lower outdoor temperatures and fewer extremely hot days, allowing building elements more time to cool down. The same parameter combinations were simulated with the weather file exchanged. Analysis showed that in the RCP 2.6 scenario, some building variants could prevent overheating, with maximum interior temperatures on average over 5℃ lower than in the RCP 8.5 scenario. The number of uncomfortable hot hours decreased on average by 150, and while 572 variants still couldn't provide any comfortable hours, 496 offered more than 10% comfortable hours, and 80 provided comfortable conditions for half the time. The best-performing variant maintained indoor temperatures between 24 and 32℃, providing comfortable conditions for 62.5 % of July and August.

## 4 Discussion and conclusion

The described experiment provides valuable insights into the topics of thermal comfort and heatwave resilience. A OAT sensitivity analysis evaluated various parameters' influence on internal temperatures under extreme outdoor conditions, highlighting the critical importance of selecting appropriate shading devices, high-quality glass, and lower fenestration ratios to mitigate the effects of severe heatwaves. In contrast, building orientation and material selection played a minor role in the simulated setup, giving architects more flexibility when maintaining optimal values for the critical parameters described.

However, the methodology had some limitations, primarily due to the reduced scope of the model. The number of parameters and their selected values were significantly reduced to manage long computation times and the chosen evaluation method. Although this setting clarified which parameters are decisive and which are less influential, a more developed model could yield different results. Future studies should explore this further, possibly by employing a methodology that allows faster computation of numerous variants.

Despite these limitations, this research addresses critical issues of building resilience and thermal comfort in the context of climate change. As climate change continues to impact indoor thermal comfort, these findings underscore the necessity of integrating heatwave resilience into architectural design. Buildings constructed today will face future weather conditions; therefore, designs should not only adhere to current norms and requirements but also anticipate predicted future challenges. Making informed design choices now can minimize the need for future modifications or, in extreme cases, the demolition of structures that do not adapt to new conditions.

## References

[1] S. Seneviratne, X. Zhang, M. Adnan, *et al.*, “Weather and climate extreme events in a changing climate”, in *Climate Change 2021: The Physical Science Basis. Contribution of Working Group I to the Sixth Assessment Report of the Intergovernmental Panel on Climate Change*, V. Masson-Delmotte, P. Zhai, A. Pirani, *et al.*, editors, Cambridge, United Kingdom and New York, NY, USA: Cambridge University Press, 2021, pp. 1513–1766. DOI: 10.1017/9781009157896.013.

[2] S. N. Gosling, J. A. Lowe, G. R. McGregor, M. Pelling, and B. D. Malamud, “Associations between elevated atmospheric temperature and human mortality: A critical review of the literature”, *Climatic Change*, vol. 92, no. 3-4, pp. 299–341, Feb. 2009. DOI: 10.1007/s10584-008-9441-x.

[3] A. E. Stagrum, E. Andenæs, T. Kvande, and J. Lohne, “Climate Change Adaptation Measures for Buildings—A Scoping Review”, *Sustainability*, vol. 12, no. 5, p. 1721, Feb. 25, 2020. DOI: 10.3390/su12051721.

[4] S. Attia, R. Levinson, E. Ndongo, *et al.*, “Resilient cooling of buildings to protect against heat waves and power outages: Key concepts and definition”, *Energy and Buildings*, vol. 239, p. 110 869, May 2021. DOI: 10.1016/j.enbuild.2021.110869.

[5] M. Moench, “Experiences applying the climate resilience framework: Linking theory with practice”, *Development in Practice*, vol. 24, no. 4, pp. 447–464, May 19, 2014. DOI: 10.1080/09614524.2014.909385.

[6] P. O. Fanger, “Thermal comfort. Analysis and applications in environmental engineering.”, *Thermal comfort. Analysis and applications in environmental engineering.*, 1970.

[7] N. Djongyang, R. Tchinda, and D. Njomo, “Thermal comfort: A review paper”, *Renewable and Sustainable Energy Reviews*, vol. 14, no. 9, pp. 2626–2640, Dec. 2010. DOI: 10.1016/j.rser.2010.07.040.

[8] "DIN EN 15251:2012-12, Eingangsparameter für das Raumklima zur Auslegung und Bewertung der Energieeffizienz von Gebäude - Raumluftqualität, Temperatur, Licht und Akustik; Deutsche Fassung EN_15251:2007", Beuth Verlag GmbH, 2012. DOI: 10.31030/1912934.

[9] D. Robinson and F. Haldi, "An integrated adaptive model for overheating risk prediction", *Journal of Building Performance Simulation*, vol. 1, no. 1, pp. 43–55, Mar. 2008. DOI: 10.1080/19401490801906460.

[10] S. Flores-Larsen, C. Filippín, and F. Bre, "New metrics for thermal resilience of passive buildings during heat events", *Building and Environment*, vol. 230, p. 109 990, Feb. 2023. DOI: 10.1016/j.buildenv.2023.109990.

[11] R. Escandón, R. Suárez, J. J. Sendra, F. Ascione, N. Bianco, and G. M. Mauro, "Predicting the Impact of Climate Change on Thermal Comfort in A Building Category: The Case of Linear-type Social Housing Stock in Southern Spain", *Energies*, vol. 12, no. 12, p. 2238, Jun. 12, 2019. DOI: 10.3390/en12122238.

[12] A. Dodoo and L. Gustavsson, "Energy use and overheating risk of Swedish multi-storey residential buildings under different climate scenarios", *Energy*, vol. 97, pp. 534–548, Feb. 2016. DOI: 10.1016/j.energy.2015.12.086.

[13] H. Wang and Q. Chen, "Impact of climate change heating and cooling energy use in buildings in the United States", *Energy and Buildings*, vol. 82, pp. 428–436, Oct. 2014. DOI: 10.1016/j.enbuild.2014.07.034.

[14] E. L. A. da Guarda, E. Gabriel, R. Mansuelo Alves Domingos, *et al.*, "Adaptive comfort assessment for different thermal insulations for building envelope against the effects of global warming in the mid-western Brazil", *IOP Conference Series: Earth and Environmental Science*, vol. 329, no. 1, p. 012 057, Sep. 1, 2019. DOI: 10.1088/1755-1315/329/1/012057.

[15] J. Hollý and A. Palková, "Climate change impact – residential unit", *MATEC Web of Conferences*, vol. 279, K. Prušková, M. Vochozka, I. Juhásová Šenitková, *et al.*, editors, p. 03 007, 2019. DOI: 10.1051/matecconf/201927903007.

[16] N. M. Alwi, J.-F. Flor, N. H. Anuar, *et al.*, "Retrofitting measures for climate resilience: Enhancing the solar performance of Malaysian school buildings with passive design concepts", *IOP Conference Series: Earth and Environmental Science*, vol. 1102, no. 1, p. 012 014, Nov. 1, 2022. DOI: 10.1088/1755-1315/1102/1/012014.

[17] D. Marx, R. Reitberger, M. Kleeberger, and W. Lang, "Automated workflow for simulating the effect of green façades on indoor thermal comfort", *Journal of Physics: Conference Series*, vol. 2600, no. 9, p. 092 007, Nov. 1, 2023. DOI: 10.1088/1742-6596/2600/9/092007.

[18] D. Dodman, B. Hayward, M. Pelling, *et al.*, "Cities, Settlements and Key Infrastructure", in *Climate Change 2022: Impacts, Adaptation and Vulnerability. Contribution of Working Group II to the Sixth Assessment Report of the Intergovernmental Panel on Climate Change*, H. O. Pörtner, D. C. Roberts, M. Tignor, *et al.*, editors, Cambridge, UK and New York, NY, USA: Cambridge University Press, 2022. DOI: 10.1017/9781009325844.008.

# A Comparative Study of Deep Learning and Evac4BIM in Building Evacuation Design

Patrick Berggold[1], Ann-Kristin Dugstad[1,2] and Mohab Hassaan[1]
[1]Chair of Computational Modeling and Simulation, Technical University of Munich, Arcisstraße 21, 80333 Munich, Germany
[2]Division of Fire Safety Engineering, Lund University, John Ericssons väg 1, 22363 Lund, Sweden
E-mail(s): patrick.berggold@tum.de, ann-kristin.dugstad@brand.lth.se, mohab.hassaan@tum.de

**Abstract:** The integration of pedestrian simulations into the design process of a building is an inevitable step to improve its evacuation performance. This becomes particularly important during the initial design stages, when countless building configurations are explored and evaluated through interdisciplinary discussions. However, conventional simulators typically operate as stand-alone tools, necessitating several manual export and conversion steps and time-consuming runtimes. To address these challenges, recent developments have led to the integration of Building Information Modeling (BIM) with the widely-used pedestrian simulator Pathfinder in an open source tool called Evac4BIM. In this study, we explore the potential for further accelerating the generation and integration of evacuation simulation results through neural networks, trained on a comprehensive, synthetic dataset to enable real-time predictions. Subsequently, we analyze and compare the applicability of Evac4BIM and our deep learning approach in terms of practicality and accuracy.

*Keywords:* Pedestrian simulation, Building information modeling, Deep learning, Evacuation performance

Erschienen in Tagungsband 35. Forum Bauinformatik 2024, Hamburg, Deutschland, DOI: 10.15480/882.13518
© 2024 Das Copyright für diesen Beitrag liegt bei den Autoren. Verwendung erlaubt unter Creative Commons Lizenz Namensnennung 4.0 International.

## 1 Introduction

The simulation of building evacuations is vital for enhancing building design and preparing for disaster scenarios. However, these simulations are oftentimes computationally intensive, especially when using microscopic, agent-based models that make it unfeasible to investigate the evacuation performance of every single building variant that emerges throughout the planning and design stages of a building [1], [2]. To mitigate this computational burden, researchers have recently explored neural networks trained on simulation results to produce fast predictions that enable real-time evacuation assessment, thus aiding the decision-making during building design.

Moreover, Building Information Modeling (BIM) has gained widespread popularity due to its ability to provide a comprehensive digital representation of a building. Such a digital model facilitates the sharing of information among various stakeholders, making it easier to explore different design

options from a multidisciplinary perspective. As a result, BIM enables more efficient collaboration and decision-making during the design and planning stages [3]. BIM Models can be exported in standard file formats such as the Industry Foundation Classes (IFC). This capability is particularly advantageous for investigating evacuation performance, as IFC files can be imported into evacuation simulators. Recently, there have been significant advancements in integrating IFC with evacuation tools and employing deep learning approaches using floorplan or layout inputs.

In this study, we aim to investigate and compare the efficacy of a traditional simulation-based tool and a deep learning approach for predicting evacuation performance. Specifically, we develop a parametric model using a BIM-authoring tool to generate a comprehensive synthetic dataset for training our neural network. Distinct from previous studies, our approach relies solely on image-related inputs, encoding occupant information in input tensors without additional use case-specific inputs. In addition, we examine a novel IFC-based evacuation tool, namely Evac4BIM [4], which employs Pathfinder [5] to produce evacuation simulation results. We conduct a comparative analysis of these two methodologies, assessing their practicality and effectiveness in predicting evacuation performance. Through this investigation, we aim to provide insights into the potential advantages and limitations of each approach, contributing to the optimization of building design and safety planning.

# 2 State of the art

## 2.1 Evacuation modeling

Three primary methodologies are utilized to model evacuation behavior: macroscopic, microscopic, and mesoscopic modeling [6]. A macroscopic modeling approach simulates the movement of the whole crowd as a continuous flow, often by subdividing the area into cells and defining the in- and output flow of pedestrians per cell, similar to how eularian transport is modeled in particle flow models. A microscopic modeling approach focuses on the individual itself, by simulating the movement of individual agents with specific characteristics and behaviours. This approach is comparable to Lagrangian transport in transport models [2]. While the microscopic approach - the models employing this approach are often so called agent-based models - is more suitable for detailed studies, it also is more computationally intensive. Alternatively, a solution inbetween the macroscopic and microscopic model can be employed, the so called mesoscopic modeling approach, which represent groups of people with similar characteristics as single entities.

## 2.2 BIM-based evacuation tools

BIM is a methodology widely utilized in the architecture and construction industry to create and manage building models enriched with comprehensive information throughout the entire lifecycle of a structure [3]. A common format to store those three dimensional information rich models is IFC. BIM-models in IFC format can then be used in evacuation dynamics research to analyse evacuation dynamics in buildings. Pathfinder is one evacuation dynamics simulator which can import geometrical features such as walls, floors and stairs from IFC files [7]. However, those IFC files must be enriched manually by the user. [4] aimed to fill this interface gap between Revit and Pathfinder by developing the add-in Evac4BIM, which allows to export simulation-relevant BIM data such as alarm times and

pre-evacuation times from Revit and import of Pathfinder's simulation results such as evacuation times and occupancy flow rates into Revit. All parameters which are included in this Add-in are displayed in Table 1.

Table 1: Evac4BIM's analysis on the Simulation Input and Output Parameters from Pathfinder [8].

| **Simulation input** | **Simulation output** |
|---|---|
| Alarm time | Simulation Brief |
| Pre evacuation time | Initial Occupant Number |
| Number of occupants | Evacuation Time |
| Occupant load | Overall Evacuation Time |
| Peak number of occupants | Occupant History |
| Building occupancy day/night | Travel distances |
| Component status | First occupant in |
| Required door flow rate | Last occupant out |
| Occupant profiles | Total use |
| Admitted profiles | Door Flow rate History |
| | Average occ. flow rate |

### 2.3 Machine learning in evacuation planning

Machine learning, and particularly deep learning, are increasingly used to enhance building evacuation predictions – for instance by estimating total evacuation time (TET). Recent studies have demonstrated the ability to predict TET from vector inputs that encompass environment or crowd configuration parameters, using different regression methods [9] or an artificial neural network (ANN) [10]. Similarly, Testa et al. [11] estimate per-room evacuation time from vector input with an ANN, and aggregate these results for the overall TET prediction. Other research has focused on converting floorplans into images to capture the full complexity of building geometries. For instance, [1] predict TET from train station platforms by combining a convolutional neural network (CNN) with supplementary vector inputs describing the layout geometry. Extending this methodology, further studies simultaneously predict TET and other evacuation-related metrics to aid in building design. For example, Berggold et al. [12] utilize a single neural network to predict TET and density over time from image and vector inputs. Similarly, Nourkojouri et al. [13] separate density and TET predictions through a neural network and Extreme Gradient Boosting, respectively. Further works integrate trajectory prediction into the design process, from which TET can be derived [14].

In contrast to these approaches, we propose a general, streamlined neural network model that predicts TET exclusively from image-based inputs. This model eliminates the need for supplementary vector inputs, which are often specific to particular use cases and architectural descriptions, thus simplifying the prediction process and enhancing its applicability across diverse building designs.

## 3 Methodology

We aim at predicting evacuation time via a deep neural network directly from the BIM model, provided initialization information. Thus, in the following, we outline our proposed methodology in Figure 1, incorporating the dataset generation from a parametric BIM model, its associated export as semantic

map, and the neural network training. As a result, once the network is trained, it can be called directly called from the Dynamo script for an instant evacuation time prediction.

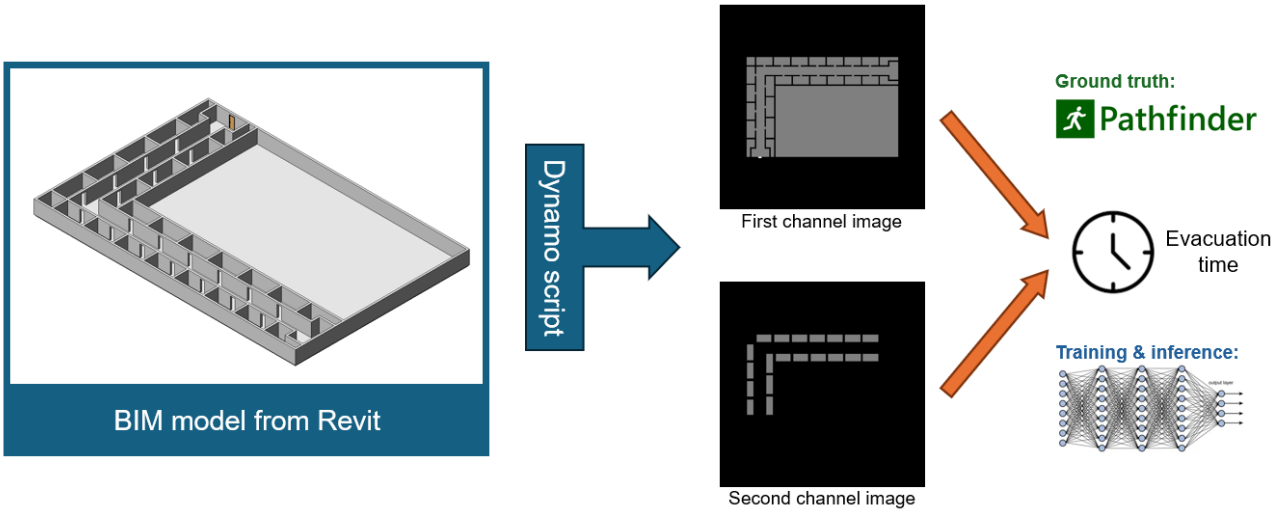


Figure 1: Our methodology, including the BIM model generation based on the parameters in Table 2, its image export via Dynamo, and the resulting tensor map with two channels. The first image channel encompasses walkable areas visualized in gray, the non-walkable areas in black, and the destination in white. The second channel resembles per-room densities at initialization.

### 3.1 Dataset generation

To train our neural network, we utilize a BIM model that is based on the input parameters in Table 2. Specifically, we present 256 samples, where each represents a unique combination of those input parameters. We use two options for the hallway width, four options for the room length, and four options both for site width and length. Additionally, we incorporate eight options for the initial number of occupants per room, ranging from single agents to dense crowds. Consequently, we investigate high-risk evacuation scenarios, where bottlenecks may form during an emergency situation with only one exit.

Table 2: The input parameters of the BIM model, resulting in 256 unique combinations.

| | **Number of Configurations** | **Values** |
|---|---|---|
| **Hallway Width (m)** | 2 | [2, 3] |
| **Room Length (m)** | 4 | [5, 6, 7, 8] |
| **Site dimensions [width × length] (m×m)** | 4 | $[32\times32, 64\times64, 48\times64, 32\times48]$ |
| **Number of Occupants per room** | 8 | [1, 4, 7, 10, 13, 16, 19, 22] |

The models were generated using Dynamo, which is Revit's integrated parametric modeling system. The Dynamo script creates a single-story, parametric model given the parameters detailed in Table 2, as depicted in Figure 1. Additionally, the script includes the number of occupants as an IFC parameter and generates an exit door. Notably, the number of occupants per room is constant across each dataset sample.

After model generation inside Revit, we export the model as an IFC file and run evacuation simulations using Pathfinder, as presented in Figure 2. As a result, we obtain the evacuation time for each dataset configuration. Intuitively, rising occupant numbers correspond to significantly higher evacuation times due to congestion effects both at the door of each room and at the final exit of the building.

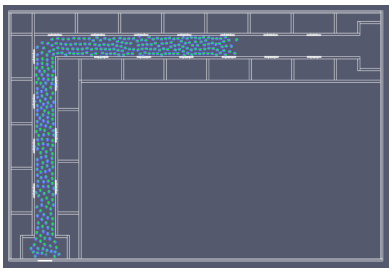

Figure 2: An evacuation simulation with only one exit inside Pathfinder.

### 3.2 Deep neural network

Different from previous works, we propose an image-only approach, without adding any supplementary parameters to the network. The neural network architecture is visualized in Figure 3. Initially, we process both channels individually through convolutional blocks, extracting geometry and density information, respectively. One convolutional block (*C-Block*) is made up of a batch norm and ReLU activation, with a preceding two-dimensional convolution that includes different input and output channels, as well as kernel size and stride. Subsequently, the extracted features are flattened and concatenated, and a two-layer MLP merges the vectors for the final prediction. The hidden layers in the MLP have the input dimensions 128 and 64, respectively, with a one-dimensional output that is the evacuation time prediction.

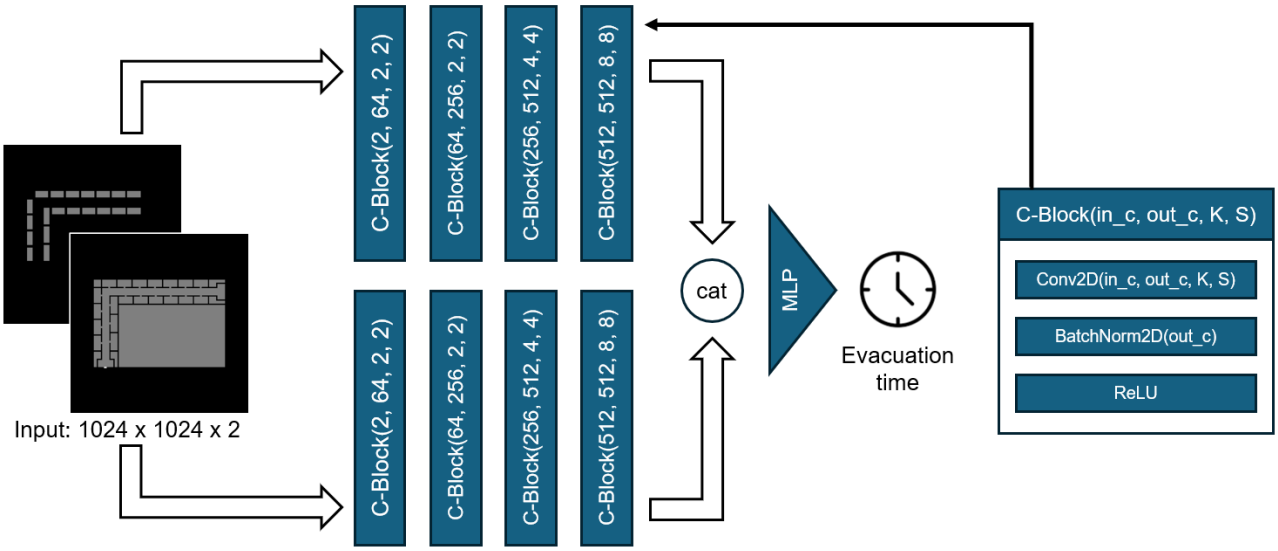


Figure 3: The neural network architecture.

### 3.3 Training results

We train the neural network by splitting our dataset into 70% training samples, while 15% are used both for validation and for testing. The resulting plots of training and validation are displayed in Figure 4, utilizing the Mean-Squared-Error (MSE) as loss function to effectively reduce the number of outlier predictions. Furthermore, in the following, we present the mean absolute and the relative errors on the test set, which are more intuitive than MSE.

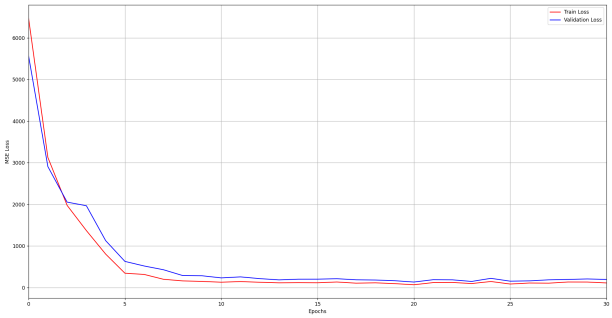


Figure 4: The result of our training process, including training (red line) and validation (blue line) results.

The evaluation of the neural network follows on the test set. We assess the results in terms of the absolute error ($\text{AE}_i$) between true evacuation time $T_{evac,i}$ from the simulation, and neural network prediction $\hat{T}_{evac,i}$ . Specifically, we provide the mean (MAE), the relative error (RE) and the standard deviation (SD) of the absolute error:

$$\text{MAE} = \frac{1}{N_{test}} \sum_{i=1}^{N_{test}} \left| T_{evac,i} - \hat{T}_{evac,i} \right| = \frac{1}{N_{test}} \sum_{i=1}^{N_{test}} \text{AE}_i = 8.31\,\text{sec}$$

$$\text{RE} = \frac{1}{N_{test}} \sum_{i=1}^{N_{test}} \frac{\text{AE}_i}{T_{evac,i}} = 7.38\% \;\text{ and }\; \text{SD} = \sqrt{\frac{1}{N_{test}} \sum_{i=1}^{N_{test}} (\text{AE}_i - \text{MAE})^2} = 9.93\,\text{sec}$$

Based on these results, it is evident that our deep learning approach serves as an effective approximation, aligning with its intended role as a supportive tool in the design process. Nonetheless, in edge cases where higher precision is required, a real simulation remains necessary. In addition, the current dataset size is constrained due to the time-intensive nature of its creation. To enhance the applicability of this approach in real-world scenarios, expanding the dataset is essential.

## 4 Comparison between deep learning and Evac4BIM

In the following section, we compare the practicality of using our straightforward Dynamo script and the neural network, to Evac4BIM for generating simulation results.

With respect to the deep learning approach, as detailed in Section 3, each dataset sample requires an IFC export from the Dynamo script, including the building's geometry and its simulation parameters, namely the number of occupants per room. Subsequently, the IFC files can be imported into Pathfinder to execute the evacuation simulations – the results of which constitute our synthetic dataset, utilized for training the neural network depicted in Figure 3. The major advantage of this method is the neural network's inference time, which is less than one second, thereby enabling real-time evacuation assessments. The critical limitation is the reliability of the network's performance, which is intrinsically linked to the quality and comprehensiveness of the dataset. To ensure the practical applicability

across diverse scenarios and building layouts, the dataset must be substantially expanded to facilitate interpolation on previously unseen samples.

In comparison, the usage of Evac4BIM involves some additional, manual steps, such as initializing the geometry elements, adding occupant profiles, assigning room categories, or pairing doors to their adjacent rooms, among others. Subsequently, the IFC file can be exported to be used as input to Pathfinder. While Evac4BIM's approach is thorough, for the purpose of generating this dataset, it is quite excessive; many of the steps are not required to generate our dataset. As an alternative, we used the Dynamo script method described in Section 3. The script is used to assign all the required parameters, resulting in lower effort. Comparing the average time taken by both approaches to generate one IFC file, we report that the Dynamo script method is significantly faster than the usage of Evac4BIM, taking us 17 seconds and 109 seconds, respectively.

## 5 Conclusion

In this study, we compared a traditional simulation-based method for predicting evacuation performance in buildings using Revit, Pathfinder, and the Revit Add-in Evac4BIM with our deep learning approach. By employing both the traditional method and a custom Dynamo script, we generated a synthetic dataset to train a neural network that predicts TET based solely on image-related inputs. This neural network offers rapid inference, making it suitable for real-time evacuation assessments during the building design process.

Our comparative analysis revealed that, while the neural network's performance is highly dependent on the dataset's quality and comprehensiveness, it significantly reduces prediction time. Conversely, the IFC-based tool Evac4BIM, despite requiring extensive manual input, provides detailed and accurate simulation results. Additionally, generating IFC files using a Dynamo script proved to be significantly faster than using Evac4BIM, highlighting its practicality for large dataset creation.

In conclusion, the neural network approach offers quick and efficient evacuation predictions, whereas traditional tools like Evac4BIM deliver detailed and reliable results. Future research should focus on expanding and enhancing the training dataset for neural networks and exploring the integration of both approaches to improve building design and safety planning.

## Acknowledgements

This research was supported by the project FORWARD, funded by the TUM Georg Nemetschek Institute. We would like to thank Enrico Ronchi for his guidance in leveraging this project.

## References

[1] J. Clever, J. Abualdenien, R. K. Dubey, and A. Borrmann, "Predicting occupant evacuation times to improve building design", in *Proc. of European Conference on Product and Process Modeling 2022*, Sep. 2022.

[2] E. J. Charlesworth, A.-K. Dugstad, F. Fritsch, P. Jöckel, and F. Plöger, "Impact of lagrangian transport on lower-stratospheric transport timescales in a climate model", *Atmospheric Chemistry*

*and Physics*, vol. 20, no. 23, pp. 15 227–15 245, 2020. DOI: 10.5194/acp-20-15227-2020. [Online]. Available: https://acp.copernicus.org/articles/20/15227/2020/.

[3] A. Borrmann, M. König, C. Koch, and J. Beetz, *Building Information Modeling: Technologische Grundlagen und industrielle Praxis*. Springer-Verlag, 2015.

[4] N. Yakhou, P. Thompson, A. Siddiqui, J. Abualdenien, and E. Ronchi, "The integration of building information modelling and fire evacuation models", *Journal of Building Engineering*, vol. 63, p. 105 557, 2023. DOI: https://doi.org/10.1016/j.jobe.2022.105557. [Online]. Available: https://www.sciencedirect.com/science/article/pii/S2352710222015637.

[5] T. Engineering, *Pathfinder*, 2024. [Online]. Available: https://www.thunderheadeng.com/pathfinder/.

[6] A. Rohaert, N. Janfeshanaraghi, E. Kuligowski, and E. Ronchi, "The analysis of traffic data of wildfire evacuation: The case study of the 2020 glass fire", *Fire Safety Journal*, vol. 141, p. 103 909, 2023. DOI: https://doi.org/10.1016/j.firesaf.2023.103909. [Online]. Available: https://www.sciencedirect.com/science/article/pii/S0379711223001777.

[7] T. Engineering, *Ifc import to pathfinder (and pyrosim)*, 2024. [Online]. Available: https://support.thunderheadeng.com/tutorials/pathfinder/ifc-import/.

[8] N. Yakhou, P. Thompson, and E. Ronchi, "Development of the 'evac4bim' add-in for revit", in *Proceedings of the Fire and Evacuation Modeling Technical Conference (FEMTC)*, Brno, Czech Republic, 2022. [Online]. Available: https://www.femtc.com/events/2022/d1-08-yakhou/.

[9] M. Abadeer, F. Ebeid, and S. Gorlatch, "Integration of machine learning methods into agent-based simulations for predicting evacuation time in disaster scenarios", in *2022 3rd Asia Symposium on Signal Processing (ASSP)*, IEEE, 2022, pp. 71–81.

[10] K. Hu, S. Yoon, V. Pavlovic, P. Faloutsos, and M. Kapadia, "Predicting crowd egress and environment relationships to support building design optimization", *Computers & Graphics*, vol. 88, pp. 83–96, 2020.

[11] E. Testa, R. C. Barros, and S. R. Musse, "Crowdest: A method for estimating (and not simulating) crowd evacuation parameters in generic environments", *The Visual Computer*, vol. 35, pp. 1119–1130, 2019.

[12] P. Berggold, S. Nousias, R. K. Dubey, and A. Borrmann, "Towards predicting pedestrian evacuation time and density from floorplans using a vision transformer", *Proc. of the 30th Int. Conference on Intelligent Computing in Engineering (EG-ICE)*, 2023.

[13] H. Nourkojouri, A. Nikkhah Dehnavi, S. Bahadori, and M. Tahsildoost, "Early design stage evaluation of architectural factors in fire emergency evacuation of the buildings using pix2pix and explainable xgboost model", *Journal of Building Performance Simulation*, vol. 16, no. 4, pp. 415–433, 2023.

[14] P. Berggold, S. Nousias, and A. Borrmann, "Integrating pedestrian simulation into early building design: A deep learning approach for trajectory prediction", in *i3CE 2024: 2024 ASCE International Conference on Computing in Civil Engineering*, Jul. 2024.

# Anwendung des Simulationsmodells *Transreac* bei zweidimensionalem, korrosivem Angriff auf zementgebundene Baustoffe

Heike Heizmann[1]

[1]Institut für Baustoffe, Bauphysik und Bauchemie, Technische Universität Hamburg, Eißendorfer Straße 42, 21073 Hamburg, Deutschland

E-mail(s): heike.heizmann@tuhh.de

**Abstract:** Zur Prognose der langfristigen Dauerhaftigkeit zementgebundener Baustoffe in chemisch angreifender Umgebung werden neben zeit- und kostenintensiven Laborversuchen zunehmend rechnerische Simulationen eingesetzt. Das Simulationsmodell *Transreac* berechnet für korrosiven chemischen Angriff die ablaufenden Transport- und Reaktionsprozesse zeit- und ortsabhängig und kann für eindimensionale Systeme bereits zuverlässige Vorhersagen treffen. In dieser Arbeit wird untersucht wie zuverlässig und unter welchen Bedingungen auch eine Prognose hinsichtlich des zweidimensionalen korrosiven Angriffs, beispielsweise entlang eines Risses, getroffen werden kann. Dazu wurden Probekörper aus Zementmörtel mit künstlich eingebrachten Fehlstellen für definierte Zeiträume in Lithiumbromid- bzw. Ammoniumnitrat-Lösung eingelagert, um die ablaufenden Transport- (Lithiumbromid) bzw. Reaktionsprozesse (Ammoniumnitrat) im Versuchsmaßstab darzustellen. In den anschließenden Simulationsberechnungen wurde geprüft, ob die Versuchsergebnisse korrekt abgebildet werden können. Die Berechnung symmetrischer, zweidimensionaler Systeme kann zum Teil asymmetrische Ergebnisse aufweisen. Als Grund werden geringe Unterschiede bei der Rundung iterativer Berechnungsschritte in verschiedenen, symmetrisch gleichwertigen Ortselementen angenommen. Es wird für unterschiedliche Randbedingungen geprüft, ob der Fehler innerhalb systemspezifischer Toleranzgrenzen liegt. Diese Grenzen ergeben sich aus den Abweichungen bei der experimentellen Ermittlung von für die Simulation relevanten Baustoffkennwerten (z.B. Porositätskennwerte und Transportparameter). Liegt die Abweichung von der Symmetrie innerhalb dieser Grenzen wird sie als vernachlässigbar angesehen.

*Keywords:* Simulation, zementgebundene Baustoffe, chemischer Angriff, Dauerhaftigkeit

Erschienen in Tagungsband 35. Forum Bauinformatik 2024, Hamburg, Deutschland, DOI: 10.15480/882.13492
© 2024 Das Copyright für diesen Beitrag liegt bei den Autoren. Verwendung erlaubt unter Creative Commons Lizenz Namensnennung 4.0 International.

# 1 Einleitung

Das komplexe Porensystem zementgebundener Baustoffe ermöglicht Gasen, Wasser sowie gelösten Ionen und Neutralteilchen den Transport ins Baustoffinnere. Das eingedrungene Medium kann den Zementstein angreifen und zu einer Veränderung der chemischen Zusammensetzung sowie der Transportparameter führen. In flächigen, intakten Baustoffbereichen erfolgt dieser Transport eindimensional und senkrecht zur Oberfläche (Abbildung 1(a)). Im Bereich von Bauteilanschlüssen, Rissen oder Fehlstellen kann der Transport der eindringenden Gase oder Flüssigkeiten beschleunigt stattfinden. Dies kann zu einem Transport bzw. einem chemischen Angriff entlang einer zweiten Achse führen (Abbildung 1(b)).

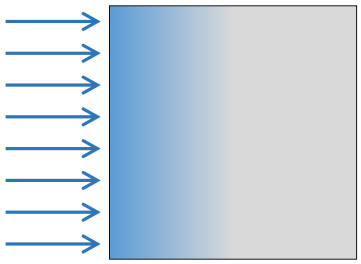

(a) Eindimensionaler Transport an intakter Baustoffoberfläche

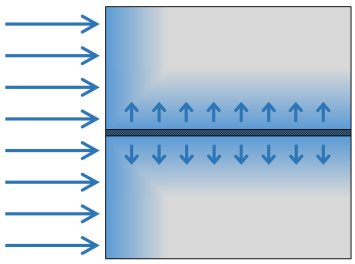

(b) Zweidimensionaler Transport an Baustoffobrefläche mit Riss

Abbildung 1: Darstellung des ein- bzw. zweidimensionalen Transportverhaltens im Porenraum zementgebundener Baustoffe

Gelöste Ionen oder Neutralteilchen können per Ionendiffusion, per Permeation oder per Huckepacktransport bei kapillarem Saugen in das Porensystem des zementgebundenen Baustoffes eindringen. Die vorgestellten Versuche fanden unter Atmosphärendruck an Probekörpern statt, deren Porensystem komplett wassergesättigt war. Dies reduziert die möglichen Tranpsortprozesse auf die Diffusion gelöster Teilchen. Abweichend vom Diffusionskoeffizienten in freier Lösung $D_0$ gilt im Porenraum des Zementsteins ein abgeminderter, effektiver Ionendiffusionskoeffizient $D_c$, der experimentell ermittelt werden kann (vgl. Abschnitt 3.1) [1].

Zhang et al. [2] entwickelten auf Basis verschiedener vorhandener Überlegungen ein Modell zur Berechnung eines Rissdiffusionskoeffizienten $D_{cr}$ in Abhängigkeit der Rissbreite $w_{cr}$:

$$
\begin{aligned}
D_{cr} &= D_c, && w_{cr} \leq 30\mu m \\
D_{cr} &= \frac{D_c + D_0}{2} + \frac{D_0 - D_c}{2} \sin\left[\frac{\pi}{120-30}\left(w_{cr} - \frac{120+30}{2}\right)\right] && 30\mu m < w_{cr} < 120\mu m \\
D_{cr} &= D_0 && w_{cr} \geq 120\mu m
\end{aligned}
$$

Durch die erhöhten Transportparameter, die laut Zhang et al. [2] bereits in Rissen ab 0,03 mm Rissbreite vorliegen, kann die Lösung in diesen Bereichen schneller und weiter ins Baustoffinnere vordringen. Hier kann es dann auf Grund der Konzentrationsunterschiede zwischen Riss und umliegendem Bauteil über die Rissflanken zu Transport und chemischem Angriff senkrecht zum Riss kommen.

Je nach Art der in den Porenraum eindringenden Gase oder Lösungen kann es zu einem chemischen Angriff auf die Zementsteinmatrix kommen. Bei einem treibenden Angriff ist die ablaufende chemische Reaktion mit einer Volumenzunahme verbunden. Überschreitet diese den zur Verfügung stehenden Porenraum können durch den entstehenden Druck Risse entstehen, die zu einem Festigkeitsverlust

des Baustoffs führen. Bei einem lösenden Angriff sind die Reaktionsprodukte leichter löslich als die Ausgangsprodukte und können so über den sich dadurch vergrößernden Porenraum abtransportiert werden. [3, S. 402 ff.]
Bei einem lösenden Angriff durch Ammoniumnitrat, welcher im Folgenden genauer betrachtet wird, beruht die Schädigung auf zwei Mechanismen: Zum Einen reagiert das Ammonium-Ion unter Verbrauch von Hydroxid-Ionen zu gasförmigem Ammoniak. Dies resultiert in einer Neutralisierung der Porenlösung was eine Destabilisierung von Calciumhydroxid und C-S-H-Phasen zur Folge hat. Zusätzlich ist die Löslichkeit von Calciumhydroxid im Vergleich zu der in reinem Wasser erhöht. [4]
Zum Anderen führen die Nitrat-Ionen durch Ionenaustausch zu einer Umwandlung des Calciumhydroxides in leichtlösliches Calciumnitrat [5].

## 2 Das Simulationsmodell *Transreac*

Die Entwicklung des Simulationsmodells *Transreac* (transport and reaction) begann durch Schmidt-Döhl [6] in den 1990er-Jahren. Rigo [7] erweitertete *Transreac* zu einem probabilistischen Modell, während Bruder [8] die Möglichkeit der adaptiven Berechnung ergänzte. Aktuelle Neuerungen verbessern das Programmsystem insbesondere für zweidimensionale Berechnungen. Durch eine Erweiterung der maximalen Ortselementanzahl können größere Systeme abgebildet werden. Die Ausnutzung paralleler Programmstrukturen und moderner Rechnerarchitekturen kann die Berechnungsdauer umfangreicher Simulationen stark reduzieren. Die Implementierung der thermodynamischen Daten aus der Thereda-Datenbank ([9], [10]) stellt für die Berechnungen den modernsten, intern konsistenten Datensatz für zementgebundene Baustoffe zur Verfügung.
*Transreac* ermöglicht die gekoppelte Berechnung von Transport- und Reaktionsprozessen zeit- und ortsaufgelöst. Die Wärme- und Feuchtetransportprozesse (Wärmetransport, kapillares Saugen inklusive Huckepacktransport, Ionendiffusion, Wasserdampfdiffusion, Permeation) werden auf Basis des Modells von Künzel [11] berechnet. Zur Berechnung der ablaufenden chemischen Reaktionen wird ein modifizierter Ansatz zur Minimierung der Gibbs-Energie (GEM-Algorithmus) von Storey und van Zeggeren [12] verwendet. Dieser Optimierungsalgorithmus nähert sich iterativ dem thermodynamisch stabilen Phasenbestand an. Er hat den Vorteil, dass die ablaufenden chemischen Reaktionen nicht genau bekannt sein müssen.
Insbesondere bei großen, mehrdimensionalen Simulationssystemen kommt ein Problem iterativer Berechnungsalgorithmen zum Tragen. Die Ergebnisse der einzelnen Iterationsschritte werden während der Berechnung gerundet. Dies geschieht unabhängig für jedes Ortselement eines Berechnungssystems mehrere tausend Male. So kann es im Laufe der Berechnung bei einem symmetrischen System zu asymmetrischen Ergebnissen kommen. Um die Größenordnung dieser Abweichungen zu erfassen, wurden umfangreiche Testberechnungen an zweidimensionalen, quadratischen und symmetrischen Simulationssystemen mit unterschiedlichen lösenden Angriffsszenarien und unterschiedlicher Diskretisierung durchgeführt. Als Beispiel sei das in Abbildung 2(a) dargestellte zweidimensionale System mit vierseitigem, lösendem chemischem Angriff genannt, welches bei den bisherigen Betrachtungen die stärksten Abweichungen von der Symmetrie aufwies. Abbildung 2(b) zeigt farblich hervorgehoben die jeweiligen symmetrisch gleichwertigen Ortselemente. Bei einer symmetrischen Berechnung wären in allen Elementen einer Farbgruppe die Ergebnisse gleich. Die von der Symmetrie abweichenden

Simulationsergebnisse werden in Abbildung 2(c) veranschaulicht. Dazu wird das Simulationsergebnis, in diesem Fall der Calciumhydroxidgehalt, über alle Ortselemente einer Gruppe symmetrisch gleichwertiger Elemente gemittelt. Anschließend wird die prozentuale Abweichung der Einzelwerte vom Mittelwert berechnet. Die Färbung dient zur Veranschaulichung der höchsten positiven (grün) und negativen (rot) Abweichungen. In den ausgekreuzten Ortselementen ist das Calciumhydroxid vollständig gelöst.

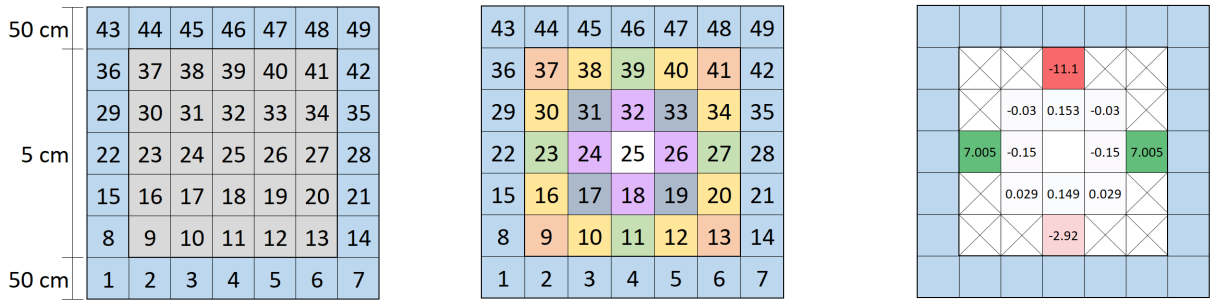


(a) Darstellung des Simulationssystems aus angreifender Lösung (blau) und Zementmörtel (grau)

(b) Farbliche Veranschaulichung der Gruppen symmetrisch gleichwertiger Elemente

(c) Proz. Abweichung des $Ca(OH)_2$ vom Mittelwert symmetrisch gleichwertiger Elemente nach 365 Tagen

Abbildung 2: Simulationsberechnungen zur Untersuchung der Asymmetrieproblematik

Neben den Abweichungen in den Simulationsberechnungen treten Abweichungen auch bei der Ermittlung von Baustoffkennwerten auf. Es erfolgt in der Regel eine Mehrfachbestimmung mit anschließender Mittelwertbildung. Liegen die Abweichungen auf Grund der Asymmetrieproblematik unter denen der Kennwertermittlung wird davon ausgegangen, dass der Einfluss der Asymmetrie vernachlässigt werden kann. Tabelle 1 zeigt eine Auswahl relevanter Materialkennwerte für einen am Institut für Baustoffe, Bauphysik und Bauchemie der TUHH häufig verwendeten Referenzmörtel und enthält zusätzlich die größten prozentualen Abweichungen der Einzelwerte vom Mittelwert. Der jeweils zugehörige Einzelwert ist hervorgehoben.

Tabelle 1: Materialkennwerte des Referenzmörtels REF-0

| Kennwert | Goedeke [1] | | Schulenberg [13] | eigene Werte | | Mittelwert | maximale Abweichung |
|---|---|---|---|---|---|---|---|
| Trockenrohdichte [g/cm$^3$] | 2,12 | 2,08 | **2,28** | 2,08 | 2,09 | 2,13 | 7,04 % |
| MIP-Porosität [Vol.-%] | **14,9** | 13,61 | 13,44 | 13,24 | 12,97 | 13,632 | 9,30 % |
| freie Wasseraufnahme [Vol.-%] | **18,5** | 15,15 | 13,96 | 14,72 | 16,85 | 15,836 | 16,82 % |
| offene Porosität [Vol.-%] | **20,0** | 17,42 | 16,43 | 16,20 | - | 17,513 | 14,20 % |

Die maximale Abweichung bei der Kennwertermittlung von 16,82 % liegt deutlich über der maximalen Abweichung der Simulationsergebnisse von 11,10 %. Die bisherigen Untersuchungen stützen die Vermutung, dass die Abweichungen auf Grund der Ungenauigkeiten in den Simulationsberechnungen nicht stärker ins Gewicht fallen als experimentelle Unsicherheiten bei der Kennwertermittlung der betrachteten Materialien.

# 3 Experimentelle Untersuchungen zum zweidimensionalen Transport- und Reaktionsverhalten zementgebundener Baustoffe

Zur Untersuchung des zweidimensionalen Transport- und Reaktionsverhaltens zementgebundener Baustoffe fanden Untersuchungen an Mörtelprüfkörpern mit künstlich eingebrachten Fehlstellen statt. Eine Einlagerung vollständig gesättigter Probekörper in Lithiumbromid ermöglicht eine Datenerhebung zum Transportverhalten im Mörtelsystem, während die Einlagerung in Ammoniumnitrat zusätzlich den Einfluss eines lösenden chemischen Angriffes abbildet. Der verwendete Mörtel ist der in Abschnitt 2 erwähnte Referenzmörtel (REF). Seine Zusammensetzung kann Tabelle 2 entnommen werden. Zum Einbringen künstlicher Fehlstellen wurden die hergestellten Mörtelprismen in 2 cm dicke Scheiben zersägt. Jeweils zwei der Scheiben wurden mit Epoxidharz und der Hilfe von Abstandshaltern zu Probekörperwürfeln mit einer Kantenlänge von ca. 4 cm zusammengesetzt. Die Probekörper wurden anschließend an vier Seiten mit Epoxidharz abgedichtet, sodass ein Eindringen der Lösungen nur über zwei gegenüberliegende Flächen erfolgen konnte. Im Anschluss an die Versuche wurden die tatsächlichen Rissbreiten per Messung am Mikroskop ermittelt. Eine Auswahl der tatsächlichen Rissbreiten $w_{cr,ist}$ kann Tabelle 3 entnommen werden.

Tabelle 2: Zusammensetzung REF in $\mathrm{kg/m^3}$

| | | |
|---|---|---|
| **Zement** | CEM I 42,5 R-SR 0/NA | 501,7 |
| **Gesteinskörnung** | CEN Normsand (≤ 2 mm) | 1505,2 |
| **Wasser** | | 225,8 |
| **w/z-Wert** | | 0,45 |

Tabelle 3: Rissbreiten der Probekörper in $\mu\mathrm{m}$

| **Probenbezeichnung** | $w_{cr,ist}$ **[$\mu m$]** |
|---|---|
| Sa | 110,23 |
| Sc | 165,20 |
| Se | 187,06 |

## 3.1 Diffusionsversuche

Zur Untersuchung des Diffusionsverhaltens in Probekörpern mit künstlich eingebrachten Fehlstellen wurden die eingangs beschriebenen Probekörper für 14 Tage in eine Lithiumbromid-Lösung mit einer Konzentration von 50 g/l eingelagert. Anschließend wurden die Probekörper entlang der Eindringrichtung und senkrecht zur Fehlstelle aufgesägt und die Bromid-Verteilung im Probekörper mittels Mikroröntgenfluoreszenzanalyse (µRFA) ortsaufgelöst gemessen. Für vergleichende Simulationsberechnungen mit *Transreac* wird der Riss über rechteckige Festkörper-Ortselemente mit angepassten Transportparametern idealisiert. Mit Hilfe von Simulationsberechnungen erfolgt eine rekursive Bestimmung des Ionendiffusionskoeffizienten durch eine bestmögliche Anpassung an das mittels µRFA gemessene Intenstitätsprofil. Der Bromid-Diffusionskoeffizient im Mörtel $D_{c,Br^-}$ wurde nach der gleichen Vorgehensweise an ungeschädigten Probekörpern ermittelt. Für den Referenzmörtel gilt $D_{c,Br^-}$ = 1,04·10$^{-11}$ m/s. Abbildung 3 stellt die Ergebnisse der Diffusionsversuche den Simulationsberechnungen für einen Probekörper mit $w_{cr,ist}$ = 187,06 µm gegenüber. Nach dem Modell von Zhang et al. gilt für $w_{cr}$ > 120 µm $D_{cr,Br^-}$ = $D_{0,Br^-}$ = 2,08·10$^{-9}$ m$^2$/s.

Die Versuchsergebnisse sind über vier Einzelproben gemittelt. Die Schwankungen der Kurven resultieren aus der starken Inhomogenität der Probe. Die Bromid-Ionen dringen nur in den Zementstein ein, während die Gesteinskörnung nach Versuchsende unverändert vorliegt. Abbildung 3 zeigt eine gute Übereinstimmung zwischen Versuchsergebnis und Simulationsberechnung. Während an der gesamten Probekörperoberfläche ein Eindringen der Bromid-Ionen erkennbar ist, ist in größeren Tiefen eine erhöhte Konzentration im Bereich der Fehlstelle zu verzeichnen. Es ist anzumerken, dass lediglich qualitative Verläufe und keine tatsächlichen Konzentrationen verglichen werden.

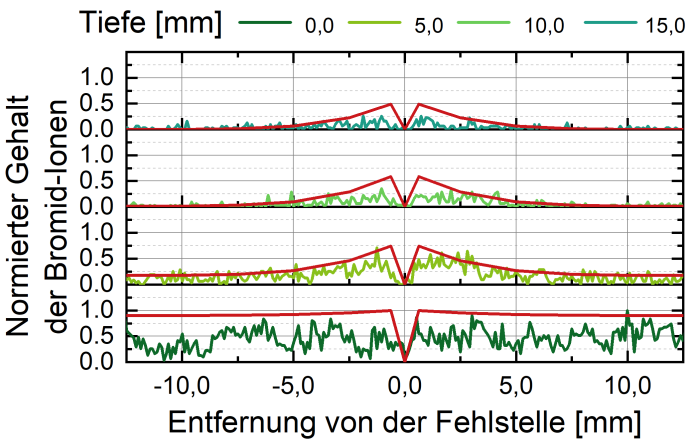


Abbildung 3: Vergleich von Diffusionsversuchen (grün) und Simulationsberechnungen (rot) über die Tiefe der Probekörper mit $w_{ist}$ = 187,058 µm

## 3.2 Korrosionsversuche

Zur Untersuchung des Korrosionsverhaltens in Probekörpern mit künstlich eingebrachten Fehlstellen wurden die eingangs beschriebenen Probekörper für 42 und 63 Tage in eine Ammoniumnitrat-Lösung mit einer Konzentration von 50 g/l eingelagert. Die Konzentration der Lösung wurde durch Austausch und Durchmischen konstant gehalten. Nach der Auslagerung wurden die Probekörper entlang der Eindringrichtung und senkrecht zur Fehlstelle aufgesägt. Mittels µRFA wurde die Elementverteilung in den Probekörpern ortsaufgelöst gemessen. Am deutlichsten lässt sich die Veränderung der Zusammensetzung durch den chemischen Angriff an der Abnahme der Calcium-Konzentration erkennen. In Abbildung 4 zeigt die Calcium-Konzentrationsprofile nach 63 Tagen Einlagerungsdauer. In allen Aufnahmen ist der verringerte Calciumgehalt an der am linken Bildrand liegenden Probekörperoberfläche gut zu erkennen. Die Tiefe dieser Abnahme ist in den weiter vom Riss entfernten, ungeschädigten Probenbereichen erwartungsgemäß für alle Rissbreiten ähnlich. Zusätzlich ist eine schwache Abnahme des Calciumgehaltes entlang der mittig liegenden Fehlstelle zu erkennen. Mit Hilfe eines zweidimensionalen Simulationssystems, welches den Riss als rechteckige Flüssigkeits-Ortselemente mit angepassten Transportparametern idealisiert, wird der

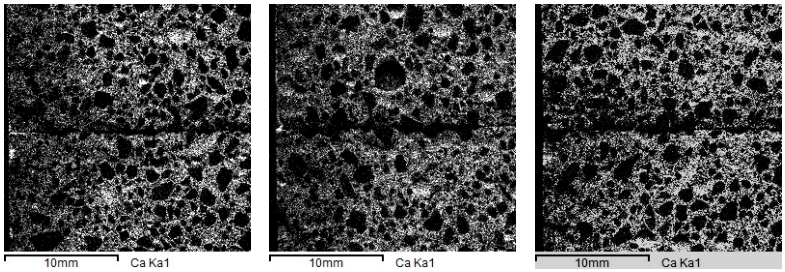


(a) $w_{cr,ist}$ = 110,23 µm (b) $w_{cr,ist}$ = 165,20 µm (c) $w_{cr,ist}$ = 187,06 µm

Abbildung 4: Elementverteilungsbilder der Calcium-Konzentration in Probekörpern mit verschiedenen Rissbreiten nach 63 Tagen Einlagerung in Ammoniumnitrat-Lösung (50 g/l)

lösende korrosive Angriff durch eine Ammoniumnitrat-Lösung rechnerisch nachgebildet. Die Diffusionskoeffizienten werden entsprechend der Rissbreite nach Zhang et al. [2] angepasst. Für die weiteren in der Porenlösung des Zementsteins vorhandenen Ionen erfolgt die Anpassung über gleichbleibende Verhältniswerte der Ionendiffusionskoeffizienten in freier Lösung bezogen auf den experimentell ermittelten Kennwert $D_{c,Br^-}$. Abbildung 5 zeigt den Vergleich zwischen Experiment und Simulation an Beispiel des Calciumgehaltes, normiert auf den Wert im unkorrodierten Material. Die Schwankungen in den Versuchsergebnissen sind auf die Inhomogenität des Probenmaterials zurückzuführen. Es zeigt sich sowohl für die Ergebnisse der experimentellen Korrosionsversuche als auch für die Simulationsberechnungen ein geringerer Calcium-Gehalt an der Probekörperoberfläche sowie, in geringem Maße, im Bereich der Fehlstelle. Die Abweichungen zwischen Experiment und Simulation sind größer als bei der Betrachtung von Diffusionsprozessen. Es ist anzumerken, dass lediglich qualitative Verläufe und keine tatsächlichen Konzentrationen verglichen werden.

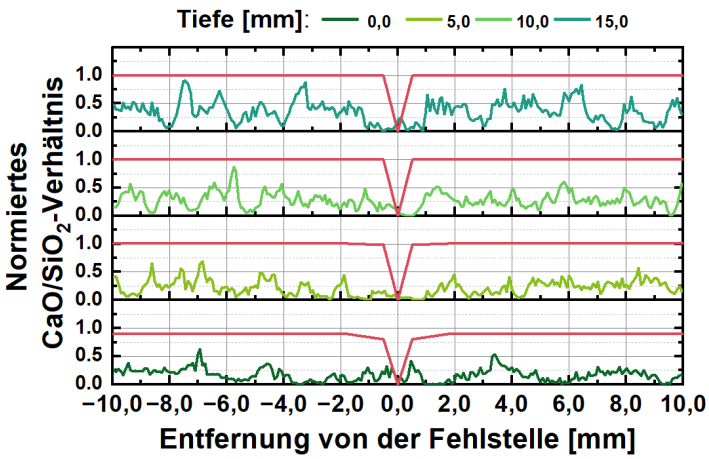


Abbildung 5: Vergleich von Korrosionsversuchen (grün) und Simulationsberechnungen (rot) über die Tiefe der Probekörper mit $w_{ist}$ = 187,058 µm

## 4 Zusammenfassung und Ausblick

Die bisherigen Simulationsberechnungen an zweidimensionalen Simulationssystemen mit *Transreac* zeigen eine gute Übereinstimmung mit den Ergebnissen experimenteller Untersuchungen. Unter Verwendung aktueller Modelle zur Ermittlung des Ionendiffusionskoeffizienten im Riss $D_{cr}$ ist eine sehr gute Abbildung des Stofftransportes in gesättigten Probekörpern möglich (vgl. 3.1). Bei der Simulationsberechnung eines zweidimensionalen, lösenden Angriffs ist die Übereinstimmung zwischen bisherigen experimentellen Versuchsergebnissen und Simulationsberechnungen weniger eindeutig (vgl. 3.2). Die Abnahme des Calciumgehaltes ist gering und daher sowohl mittels µRFA-Mapping als auch mittels Simulationsberechnung schwer abbildbar. Anpassungen der Auswertungsmethoden sowie Betrachtungen an weiteren Angriffsszenarien sind notwendig um eine eindeutige Aussage über die Eignung von *Transreac* für die Berechnung eines zweidimensionalen korrosiven Angriffs auf zementgebundene Baustoffe zu treffen.

Die Betrachtung des Asymmetrieproblems zeigt für die bisherigen Testberechnungen keine Abweichungen, die die typischen Abweichungen der experimentellen Kennwertermittlung überschreiten. Dies soll durch weitere Simulationsberechnungen, insbesondere auch an Systemen mit treibendem chemischem Angriff, gestützt werden.

## Literatur

[1] H. Goedeke, »Lösender Angriff auf zementgebundene Baustoffe - Veränderungen der Porenstruktur und Folgen für Transport- und Korrosionsprozesse«, Diss., Technische Universität Hamburg, Hamburg, 2018. DOI: 10.15480/882.1634.

[2] R. Zhang, L. Jin, M. Liu, X.-l. Du und Y. Li, »Numerical investigation of chloride diffusivity in cracked concrete«, *Magazine of Concrete Research*, Jg. 69, Nr. 16, S. 850–864, 2017. DOI: 10.1680/jmacr.16.00511.

[3] R. Benedix, *Bauchemie: Einführung in die Chemie für Bauingenieure und Architekten*, 7. Auflage. Wiesbaden und Heidelberg: Springer Vieweg, 2020.

[4] E. Nägele, B. Hillemeier und H. K. Hilsdorf, »Der Angriff von Ammoniumsalzlösungen auf Beton«, *Betonwerk + Fertigteil-Technik*, Nr. 11, S. 877–883, 1984.

[5] B. Siebert und J. Gerlach, »Chemischer Angriff auf Beton«, in *Beton Kalender 2019*, K. Bergmeister, F. Fingerloos und J.-D. Wörner, Hrsg., Wiley, 2018, S. 905–939. DOI: 10.1002/9783433609330.ch17.

[6] F. Schmidt-Döhl, »Ein Modell zur Berechnung von kombinierten chemischen Reaktions- und Transportprozessen und seine Anwendung auf die Korrosion mineralischer Baustoffe«, Diss., Technische Universität Braunschweig, Braunschweig, 1996. DOI: 10.24355/dbbs.084-201409231252-0.

[7] E. M. Rigo, »Ein probabilistisches Konzept zur Beurteilung der Korrosion zementgebundener Baustoffe durch lösenden und treibenden Angriff«, Diss., Technische Universität Braunschweig, 2005. DOI: 10.24355/dbbs.084-201409121437-0.

[8] S. Bruder, »Adaptive Modellierung der Dauerhaftigkeit im Zuge der Überwachung von Betonbauwerken«, Diss., Technische Universität Braunschweig, 2007. DOI: 10.24355/dbbs.084-201407171458-0.

[9] M. Altmaier, V. Brendler, S. Hagemann u. a., »THEREDA - Ein Beitrag zur Langzeitsicherheit von Endlagern nuklearer und nichtnuklearer Abfälle«, *ATW - International Journal for Nuclear Power*, Jg. 2008, Nr. 53, S. 249, 2008. Adresse: https://www.thereda.de/de/.

[10] H. C. Moog, F. Bok, C. M. Marquardt und V. Brendler, »Disposal of nuclear waste in host rock formations featuring high-saline solutions – Implementation of a thermodynamic reference database (THEREDA)«, *Applied Geochemistry*, Jg. 55, S. 72–84, 2015. DOI: 10.1016/j.apgeochem.2014.12.016.

[11] H. M. Künzel, »Verfahren zur ein- und zweidimensionalen Berechnung des gekoppelten Wärme- und Feuchtetransports in Bauteilen mit einfachen Kennwerten«, Diss., Universität Stuttgart, Stuttgart, 1994.

[12] F. van Zeggeren und S. H. Storey, *The computation of chemical equilibria*. London: Cambridge University Press, 1970.

[13] D. Schulenberg, »Osmotische Prozesse in mineralischen Baustoffen«, Diss., Technische Universität Hamburg, Hamburg, 2024. DOI: 10.15480/882.9144.

# Entwicklung eines Optimierungsverfahrens zur Strukturidentifikation von Brückenbauwerken

Lukas Guntermann[1] und Bjarne Sprenger[1]
[1]Institut für Massivbau, Universität Duisburg-Essen, Universitätsstraße 15, 45141 Essen, Deutschland
E-Mails: lukas.guntermann@stud.uni-due.de, bjarne.sprenger@uni-due.de

**Abstract:** Die Anpassung eines Finite-Elemente (FE)-Modells an die Tragwerksreaktionen eines realen Bauwerks im Rahmen eines Structural Health Monitorings (SHM) wird als Modelladaption bezeichnet. Die Adaption erfolgt durch die iterative Modifikation von unbekannten Modellparametern, bis die Reaktionen des numerischen Modells möglichst genau mit den gemessenen Größen am Bauwerk übereinstimmen. Um dieses hochdimensionale Optimierungsproblem zu lösen, werden Evolutionäre Algorithmen (EA) eingesetzt.
In diesem Beitrag wird ein Monitoringkonzept auf Basis einer FE-Modelladaption für vorgespannte Stahlbetonbrücken vorgestellt und das prototypische Optimierungsverfahren am Beispiel eines parametrisierten FE-Modells eines vorgespannten Fertigteildachbinders in Bezug auf die Identifizierbarkeit der Modellparameter validiert. Die Strukturidentifikation des Konzepts erfolgt über die Adaption der Modellparameter an zuvor numerisch generierten Messdaten des Tragwerks mithilfe von Genetischen Algorithmen (GA). Diese basieren auf der MATLAB Optimization Toolbox und verwenden automatisiert das FE-Programm DIANA FEA zur Berechnung der Modelle. Die Effizienz des Optimierungsalgorithmus wurde anhand einer Parameterstudie, die den Einfluss der Strategieparameter auf die Konvergenzgeschwindigkeit untersucht, optimiert und die Anbindung an das Monitoringkonzept einer realen Spannbetonbrücke diskutiert.
*Keywords:* Structural Health Monitoring (SHM), FE-Modelladaption, Evolutionäre Algorithmen (EA), Genetische Algorithmen (GA), MATLAB Optimization Toolbox

Erschienen in Tagungsband 35. Forum Bauinformatik 2024, Hamburg, Deutschland, DOI: 10.15480/882.13510
© 2024 Das Copyright für diesen Beitrag liegt bei den Autoren. Verwendung erlaubt unter Creative Commons Lizenz Namensnennung 4.0 International.

## 1 Einleitung und Motivation

Im Infrastrukturbau findet seit einigen Jahren der Wandel von einem reaktiven Handeln bei Schäden zu einer vorausschauenden prädiktiven Instandhaltung statt, die in Form des **Structural Health Monitoring (SHM)** angewendet wird [1]. Durch die Implementierung numerischer Rechenmodelle sowie Fortschritte im Gebiet der Messtechnik (bspw. faseroptische Sensoren oder 3D-Punktwolken), kann im Rahmen der Zustandsüberwachung das Tragverhalten eines Bauwerks untersucht werden.

Zur Strukturidentifikation von Tragwerken werden Finite-Elemente-Modelle (FE-Modelle) im Rahmen einer **FE-Modelladaption**, die auch als FE-Model-Updating-Verfahren bezeichnet wird, eingesetzt. In diesem Adaptionsprozess werden die Parameter des FE-Modells iterativ angepasst bis die gemessenen Tragwerksreaktionen des realen Bauwerks und die numerische Antwort des FE-Modells möglichst genau übereinstimmen [2]. Die iterative Adaption der Modellparameter stellt bei einer FE-Modelladaption das Optimierungsproblem dar.

## 2 Parameteridentifikation auf Grundlage Evolutionärer Algorithmen

**Evolutionäre Algorithmen (EA)** zählen zu den bionischen Optimierungsverfahren [3] sowie dem Machine Learning und bündeln als Oberbegriff eine Reihe von Optimierungsverfahren, wie **Genetische Algorithmen (GA)**, Evolutionäre Programmierung und Evolutionsstrategien, die auf der Evolutionstheorie basieren. Der Einsatz von EA ist bei Problemen möglich, bei denen Standardverfahren keinen Lösungsansatz bieten [3]. Sie sind insbesondere bei hochkomplexen Problemen mit unbekannten Optima und mehreren Optimierungsvariablen sinnvoll, sodass auch Probleme mit unendlich vielen möglichen Zuständen und nicht differenzierbaren Fitnessfunktionen gelöst werden können [4] und dabei ein globales Optimum identifiziert wird.

Dabei stellt der Genotyp das Gen-Set eines Zustands dar, das z. B. als Array definiert ist (z. B. Parameter des FE-Modells) und der Phänotyp das äußere Erscheinungsbild und somit die Bedeutung der im Array gespeicherten Informationen (z. B. die Tragwerksreaktion). Aus den so repräsentierten Individuen einer Population werden durch fitnessbasierte Selektion (survival of the fittest) Elternindividuen zur Bildung der Folgegeneration gewählt. Dazu werden genetische Operationen (auch Variationsoperatoren) angewendet [5]: Rekombination bezeichnet dabei die Vermischung der genetischen Informationen von $\rho$ Elternindividuen. Es existieren verschiedene Möglichkeiten der Rekombination, wie z. B. Crossover (CO) [6]. Mutationen stellen die zweite genetische Operation dar: Sie rufen eine zufällige Änderung des Genoms eines Individuums hervor [3] und sorgen dafür, dass eine hohe Diversität innerhalb der Population bestehen bleibt, wodurch der Optimierungsalgorithmus das globale Optimum der Fitnessfunktion, die verschiedene Extrema aufweist und auf der verschiedenen Individuen eine Fitness zugeordnet wird, identifizieren kann. Ein zusätzlicher Vorgang zur Sicherung fitter Genotypen ist der Elitismus, durch den Individuen für die Folgegeneration beibehalten werden, ohne einem Variationsoperator unterzogen zu werden. Durch die iterative Aneinanderreihung der beschriebenen Vorgänge ergibt sich der EA, der eine zufällige Grundpopulation erzeugt, diese durch die Variationsoperatoren optimiert und kontinuierlich prüft, ob das Optimierungsziel erreicht wurde.

# 3 FE-Modelladaption von Massivbrücken

## 3.1 Konzept zur Schadensdetektion

Das entwickelte Überwachungskonzept umfasst eine Schadensdetektion auf Basis einer nichtlinearen Modelladaption und soll innerhalb des Schwerpunktprogramms 2388 der DFG „SPP Hundert Plus“ anhand einer Spannbetonbrücke – der Nibelungenbrücke in Worms – validiert werden. Die Adaption der Modell- und Belastungsparameter erfolgt über die statische Antwort des Bauwerks.

Die Strukturidentifikation erfolgt über die iterative Modifikation der Parameter eines FE-Modells auf Basis eines GA. Dieser Optimierungsprozess wird bis zum Erreichen eines Abbruchkriteriums wiederholt. Die aus dem Optimierungsprozess adaptierten Modelle werden anschließend im Hinblick auf Parameterstreuung und Ungenauigkeiten untersucht. Zur Visualisierung der Modelle wird der hochkomplexe Parameterraum mithilfe eines autoassoziativen künstlichen neuronalen Netzwerkencoders (KNN-Autoencoder) in eine niedrigdimensionale Darstellung überführt. Mittels Clusteranalyse kann anschließend ein Modell zur Adaption des realen Tragwerks identifiziert werden. Die Schadensdiagnose erfolgt dann durch den Vergleich der Systemparameter des aus der Strukturidentifikation identifizierten Modells zu zuvor identifizierten Modellen. Allmähliche Änderungen über einen ausgedehnten Zeitraum weisen auf Alterung bzw. Abnutzung hin, plötzliche Änderungen stellen Indikatoren für auftretende Schädigungen dar.

## 3.2 FE-Modellierung eines Dachbinders als Validierungsbauwerk

Die prototypische Implementierung des Konzepts – die Anbindung des FE-Programms an den Optimierungsalgorithmus zur Strukturidentifikation mittels GA – erfolgt zunächst am Beispiel eines vorgespannten Fertigteildachbinders (Abbildung 1). Für die Reduzierung der Berechnungsdauer wurde zunächst ein linear-elastisches Materialverhalten des Betons angenommen. Die Berechnung erfolgt mit dem FE-Programm DIANA FEA [7].

Zur Validierung des Optimierungsalgorithmus wurde ein parametrisiertes FE-Modell des Dachbinders mit implementierten Schadens- und Belastungsfunktionen in Form von Wertetabellen erstellt. Die in zuvor durchgeführten Untersuchungen [8–10] ermittelten aussagekräftigen Modellparameter (der E-Modul, die äußere Belastung, die Vorspannkraft und die Bewehrungsfläche) werden mit sieben zu identifizierenden Modellparametern beschrieben. Eine Schädigung infolge von Betonabplatzungen oder Rissen wird durch die Reduzierung des E-Moduls mit den Parametern $e_{\mathrm{E}}$ (Ort) und $a_{\mathrm{E}}$ (Intensität) beschrieben. Eine Abnahme der Bewehrungsfläche (infolge von Korrosion) wird mit den Parametern $e_{\mathrm{R}}$ (Ort) und $a_{\mathrm{R}}$ (Intensität) beschrieben. Für eine realitätsnahe Approximation der Schädigungen infolge von Betonabplatzungen, Rissen oder Korrosion der Bewehrung, wird der Schaden mit einer gaußschen Glockenkurven dargestellt [8, 9]. Eine Schädigung am Vorspannsystem wird über den Parameter $m_{\mathrm{P}}$ (Intensität der Vorspannkraft) simuliert. Die äußere Belastung wird mit den Parametern $m_{\mathrm{S}}$ (Intensität einer gleichförmigen Streckenlast) und $e_{\mathrm{Q}}$ (Ort einer Wanderlast) beschrieben. Die Antwort der Modelle infolge der

Belastungs- und Materialparameter wird durch 28 virtuelle Sensoren gemessen (Abbildung 1). Die vertikale Verschiebung wird in einem Abstand von 2,0 Metern an der Unterseite erfasst. Die horizontale Verschiebung wird am rechten Auflager gemessen. Dehnungen werden in einem Abstand von 2,0 Metern an der Ober- und Unterseite des vorgespannten Dachbinders erfasst.

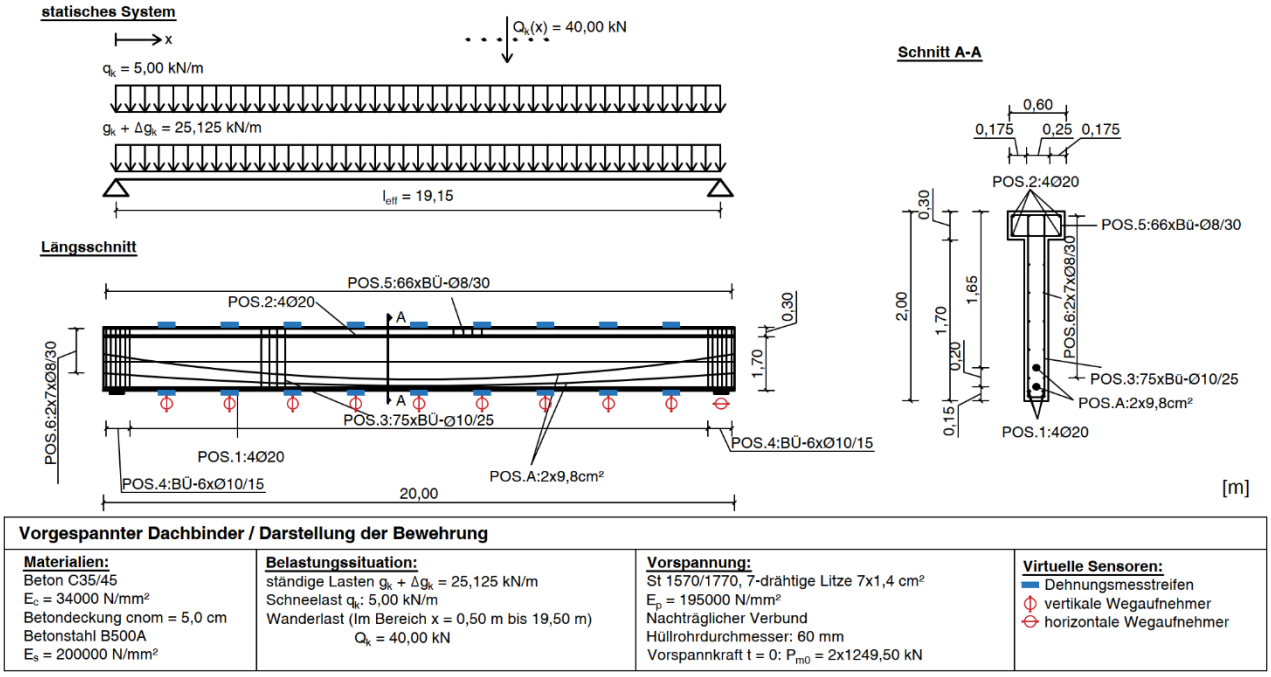


Abbildung 1: Anwendungsbeispiel – vorgespannter Dachbinder.

## 3.3 Konzept und Implementierung des Optimierungsverfahrens

Um das FE-Modell an das reale Tragwerk zu adaptieren, muss der GA verschiedene Parametersets (als Genotypen) mit dem FE-Programm DIANA FEA berechnen, um anschließend die Fitness der Tragwerksreaktion des FE-Modells (als Phänotyp) durch einen Abgleich mit der realen Tragwerksreaktion festzustellen. Als Programmierumgebung wird dazu MATLAB [11] und insbesondere die **Optimization Toolbox** gewählt, die über vielfältige Funktionen für die Implementierung von GA verfügt. Die Optimierung läuft dabei in MATLAB ab, während die einzelnen Individuen in DIANA FEA berechnet werden. Das entwickelte Konzept ist in Abbildung 2 dargestellt.

Als Schnittstelle dienen *.dat-, *.dcf- und *.tb-Dateien, die das Modell, die Berechnungseinstellungen und die Ergebnisse im Textformat enthalten. Die Anbindung von DIANA FEA erfolgt über einen CMD-Befehl in MATLAB, der die diana.exe-Anwendung aufruft und die *.dat- und *.dcf-Datei als Argumente übergibt. Die Berechnungseinstellungen (lineare oder nichtlineare Berechnung und Definition des Ergebnisformats) sind für alle FE-Modelle (Individuen) identisch. Die Modelldatei jedes Individuums wird in Abhängigkeit der sieben Modellparameter angepasst. Dies erfolgt über eine MATLAB-Routine, die in den *.dat-Dateien die Schlüsselwörter („FACTOR“) sucht, nach denen die Werte der Schäden bzw. Belastungen deklariert werden, und dort für alle betrachteten Stellen

mittels der mathematischen Schadens- bzw. Belastungsfunktionen die Funktionswerte berechnet. DIANA FEA startet als Konsolenanwendung die Berechnung und speichert, wie in der Berechnungseinstellungsdatei definiert, die Ergebnisse der betrachteten Knoten oder Elemente als einzelne *.tb-Dateien. Diese werden anschließend durch MATLAB ausgelesen und mit den Tragwerksreaktionen in der Fitnessfunktion verglichen. Für die Bestimmung des Fitnessscores wurde eine modifizierte Hyperbelfunktion angesetzt (Abbildung 2).

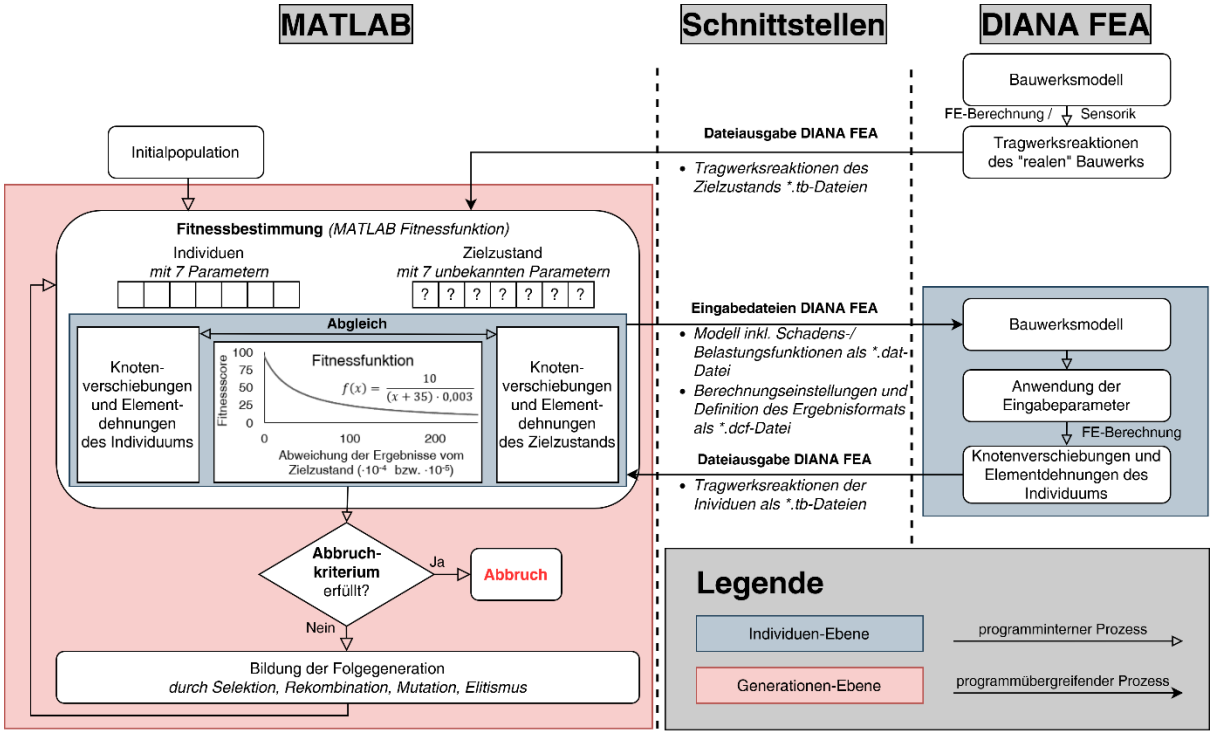


Abbildung 2: Konzept der Programmierung des GA aus [12].

## 3.4 Identifikation optimaler Strategieparameter und Algorithmen

Bei der Entwicklung des Optimierungsverfahrens wurde eine Parameterstudie durchgeführt [12], mit der geeignete Strategieparameter des GA (u. a. Populationsgröße, Rekombinations-, Mutations- und Elitismusrate) [5] und die Abbruchkriterien ermittelt wurden, um den Programmcode möglichst effizient aufzusetzen. Dazu wurde ein genotypischer anstelle eines phänotypischen Ansatzes verfolgt und somit innerhalb der Fitnessbestimmung durch MATLAB (Abbildung 2) lediglich eine Approximation von vorher gewählten Zielparametern durchgeführt. Die FE-Berechnung konnte im Testaufbau so vermieden werden, wodurch der Algorithmus die Optimierung stark beschleunigt durchführen konnte. Außerdem wurden geeignete Unter-Algorithmen für die Erstellung der Initialpopulation, die Selektion sowie die Variationsoperatoren identifiziert.

Für die Populationsgröße wurden N = 50 Individuen gewählt. Durch diese vergleichsweise geringe Populationsgröße [4] kann trotz der verringerten Konvergenzgeschwindigkeit und der daraus resultierenden erhöhten Generationenanzahl deutlich Berechnungszeit der FE-Modelle pro

Optimierung reduziert werden. Die Rekombinationsrate bzw. die Crossoverrate wurde als p(C) = 0,8 und der Elitimus bzw. die Reproduktionsrate als p(R) = 0,05 festgelegt. Die Mutationsrate liegt bei p(M) = 0,15 und ergibt sich nach [4] aus p(C) + p(R) + p(M) = 1, womit die verwendeten Variationsraten den bekannten Standardraten [4, 6, 13] entsprechen. Für die Initialpopulation wurde eine uniforme Verteilung („gacreationuniform“) und als Selektionsalgorithmus die Turnierselektion („selectiontournament“) verwendet, die die schnellste Konvergenz gemessen an den benötigten Generationen erzielt und in vergleichbaren Anwendungsfällen genutzt wird [13]. Als Rekombinationsalgorithmus wurde das Laplace-CO („crossoverlaplace“) und als Mutationsalgorithmus die Power-Mutation („mutationpower“) gewählt.

## 3.5 Validierung des entwickelten Konzepts

Die Konvergenz des GA wurde in sechs unabhängigen Versuchen mit N = 50 Individuen geprüft, in denen eine Konvergenz oberhalb eines festgelegten minimalen Fitnessscores innerhalb von durchschnittlich 85 Generationen erreicht wurde (Tabelle 1). Dargestellt ist die prozentuale Abweichung der approximierten Parameter.

Tabelle 1: Konvergenzergebnisse des in [12] entwickelten GA für das Validierungsbauwerk.

| | $e_{\mathrm{E}}$ E-Modul Ort | $a_{\mathrm{E}}$ E-Modul Intensität | $e_{\mathrm{R}}$ Bewehrung Ort | $a_{\mathrm{R}}$ Bewehrung Intensität | $m_{\mathrm{P}}$ Vorspannung Intensität | $m_{\mathrm{S}}$ Streckenlast Intensität | $e_{\mathrm{Q}}$ Wanderlast Ort |
|---|---|---|---|---|---|---|---|
| Durchschnitt | 0,2 % | 3,8 % | 9,5 % | 33,9 % | 1,7 % | 16,7 % | 8,3 % |
| Min. Fehler | 0,0 % | 1,3 % | 2,0 % | 16,9 % | 1,2 % | 4,6 % | 0,0 % |
| Max. Fehler | 0,3 % | 6,0 % | 21,2 % | 63,0 % | 2,6 % | 26,5 % | 22,2 % |

Schädigungen approximiert durch eine Reduzierung des E-Moduls (Parameter $e_{\mathrm{E}}$ und $a_{\mathrm{E}}$) lassen sich mit durchschnittlich ca. 0,2 % bis 3,8 % Abweichung detektieren. Ebenfalls kann der Ort (durchschnittliche Abweichung von 4 cm) genauer detektiert werden als die Intensität des Schadens. Eine Simulation eines Schadens des Vorspannsystems durch Reduzierung der Vorspannkraft (Parameter $m_{\mathrm{P}}$) kann durch den GA präzise detektiert werden. Die Intensität der Streckenlast (Parameter $m_{\mathrm{S}}$) kann mit durchschnittlichen Abweichungen von 16,7 % erfasst werden. Die vergleichsweise höheren Fehler der Adaption der Parameter zur Identifikation der Bewehrungskorrosionsschäden (Parameter $e_{\mathrm{R}}$ und $a_{\mathrm{R}}$; Fehler durchschnittlich bis zu 33,9 %) resultieren aus der linearen-elastischen Berechnungsanalyse, da infolge des linear-elastischen Verhaltens des Betons der Einfluss der Bewehrung auf die Biegesteifigkeit des Tragwerks gering ist. Durch die Implementierung eines nichtlinearen Materialverhaltens des Betons wird der Einfluss der Steifigkeit der Bewehrungselemente ab der Erstrissbildung des Betons auf die Biegesteifigkeit des Tragwerks erhöht [8–10]. Der Ort der Wanderlast (Parameter $e_{\mathrm{Q}}$) weist bei der Bestimmung eine hohe Streuung auf und erreicht teilweise Abweichungen bis zu 22,2 %. Dies resultiert aus dem teils geringen Einfluss der Last auf die Tragwerksreaktionen. Eine Positionierung der Last im Auflagerbereich führt zu geringeren Änderungen der Dehnungen und Verschiebungen als eine Positionierung der Last in der Mitte des Tragwerks. Zur Reduzierung der Fehler bzw. für eine Erhöhung der Zuverlässigkeit kann durch eine modellspezifische Sensitivitätsstudie, welche den

Einfluss der einzelnen Parameter auf die in der Fitnessfunktion ausgewerteten Tragwerksreaktionen untersucht, wodurch eine entsprechende Sensorkonfiguration zur Detektion der Last gewählt werden kann (vgl. [9, 10]), erhöht werden.

## 4 Zusammenfassung und Ausblick

Durch die Anbindung des FE-Programms DIANA FEA an die MATLAB Optimization Toolbox konnten Parameter eines FE-Modells an numerisch generierten Messdaten adaptiert und somit in erster Validierung des Verfahrens Schädigungen des Betons sowie des Vorspannsystems präzise identifiziert werden. Für eine realitätsnahe Modellierung von Schädigungen des Bewehrungsquerschnitts ist der Einbezug des nichtlinearen Materialverhaltens von Beton notwendig und wird bereits durch die Programmierung ermöglicht. Die daraus resultierende Erhöhung der Berechnungsdauer pro Individuum kann durch die Verteilung der ressourcenintensiven FE-Berechnungen auf ein Rechencluster mittels der MATLAB Parallel Computing Toolbox kompensiert werden. Eingebettet in einen digitalen Zwilling unter Einbezug weiterer Datenerfassungsstrategien zeigt eine mit GA implementierte Strukturidentifikation ihr möglicherweise größtes Potenzial, da das Verfahren durch nichtnumerische Ermittlung einzelner Parameter (bspw. Verkehrsbeanspruchung) beschleunigt werden kann. Im Rahmen eines Live-Monitorings einer realen Spannbetonbrücke ist die Reduzierung der Rechendauer des entwickelten Optimierungsverfahrens notwendig. Hierfür kann ein umfangreiches KI-basiertes Ersatzmodell, das auf Grundlage einer Datenbasis von zuvor durchgeführten Sensitivitätsstudien [9] trainiert wurde und die zeitaufwändigen nichtlinearen FE-Berechnungen ersetzen kann [14], zur Berechnung der Reaktionsgrößen der einzelnen Modelle an den entwickelten Optimierungsalgorithmus angebunden werden.

## Danksagung

Die Veröffentlichung innerhalb des Projekts (Projektnummer: 501496870) ist Teil des Schwerpunktprogramms 2388 „SPP Hundert Plus – Verlängerung der Lebensdauer komplexer Baustrukturen durch intelligente Digitalisierung“, das von der Deutschen Forschungsgemeinschaft (DFG) finanziert wird. Die Autoren bedanken sich bei der DFG für ihre Unterstützung.

## Literatur

[1] P. Rizzo und A. Enshaeian, "Challenges in Bridge Health Monitoring: A Review," *Sensors (Basel, Switzerland)*, Jg. 21, Nr. 13, 2021, doi: 10.3390/s21134336.

[2] M. Friswell, M. I. Friswell und J. E. Mottershead, *Finite element model updating in structural dynamics* (Solid mechanics and its applications 38). Dordrecht: Kluwer Academic Publishers, 1995.

[3] *Bionische Optimierung: Evolutionäre Algorithmen in der Anwendung*, VDI 6224 Blatt 1, Verein Deutscher Ingenieure e.V., Berlin, Jun. 2012.

[4] W. Kinnebrock, *Optimierung mit genetischen und selektiven Algorithmen,* 2018. Aufl. Berlin, Boston: Oldenbourg Wissenschaftsverlag, 1994.

[5] *Computational Intelligence: Evolutionäre Algorithmen: Begriffe und Definitionen*, VDI/VDE 3550 Blatt 3, Verein Deutscher Ingenieure e.V. und Verband der Elektrotechnik Elektronik Informationstechnik, Berlin, Feb. 2003.

[6] V. P. Patil und Pawar D.D., "The optimal crossover or mutation rates in genetic algorithm: a review," *International Journal of Applied Engineering and Technology ISSN: 2277-212X (Online), 2015 Vol. 5 (3)*, S. 38–41, 2015.

[7] *DIANA Finite Element Analysis (Release 10.7)* (2023). DIANA FEA BV.

[8] B. Sprenger und M. Schnellenbach-Held, "Schadensmodellierung mittels nichtlinearer FE-Simulationen zur Bauwerksüberwachung im Rahmen eines Digitalen Zwillings," *Baustatik – Baupraxis 15, Technische Universität Hamburg*, 2024.

[9] B. Sprenger und M. Schnellenbach-Held, "Sensitivity Analysis of Model Parameters in a Nonlinear Model-Updating Approach for Prestressed Concrete Bridges," *EWSHM 2024 - 11th European Workshop on Structural Health Monitoring*, 2024.

[10] M. Schnellenbach-Held und B. Karczewski, "Nonlinear Model-Updating in Long-Term Structural Health Monitoring: Sensitivity Analyses," *Proceedings of the EG-ICE Workshop, Twente University, Enschede, The Netherlands*, 2011.

[11] *MATLAB (R2024a)* (2024). The MathWorks Inc.

[12] L. Guntermann, "Entwicklung eines Optimierungsverfahrens zur Strukturidentifikation von Brückenbauwerken," Masterthesis (unveröffentlicht), Institut für Massivbau, Universität Duisburg-Essen, Essen, 2024.

[13] D. Y. Harvey und M. D. Todd, "Structural health monitoring feature design by genetic programming," *Smart Mater. Struct.*, Jg. 23, Nr. 9, S. 95002, 2014, doi: 10.1088/0964-1726/23/9/095002.

[14] S. Qin, Y.-L. Zhou, H. Cao und M. A. Wahab, "Model Updating in Complex Bridge Structures using Kriging Model Ensemble with Genetic Algorithm," *KSCE J Civ Eng*, Jg. 22, Nr. 9, S. 3567–3578, 2018, doi: 10.1007/s12205-017-1107-7.

# Neuartige selektive Massenskalierungsmethoden für transiente Analysen dünnwandiger Strukturen mit Volumenelementen und expliziter Zeitintegration

Moritz Hoffmann[1]
[1]Technische Universität Hamburg, Institut für Baustatik, Denickestraße 17, 21073 Hamburg, Germany
E-mail(s): m.hoffmann@tuhh.de

**Abstract:** Die Effizienz transienter Analysen unter Verwendung expliziter Zeitintegrationsverfahren ist durch die kritische Zeitschrittweite bestimmt. Die höchsten Eigenfrequenzen des diskreten Systems begrenzen die erlaubte kritische Zeitschrittweite, während sie meist nur einen geringen Einfluss auf das tatsächliche Strukturverhalten haben. Methoden der selektiven Massenskalierung (SMS) zielen darauf ab, die höchsten Eigenfrequenzen zu reduzieren, während die relevanten niedrigen Eigenfrequenzen idealerweise unverändert bleiben. Die meisten der bestehenden SMS-Methoden wurden für Volumen- oder Volumenschalenelemente entwickelt und darauf ausgelegt, dass die translatorische Trägheit und damit der Impuls erhalten bleibt. In diesem Beitrag werden neuartige SMS-Methoden vorgestellt, die intrinsisch impuls- *und* drehimpulserhaltend sind und sich durch eine hohe Genauigkeit auszeichnen. Die neuen SMS-Methoden werden hinsichtlich Genauigkeit und Effizienz untersucht und mit dem Stand der Technik verglichen.
*Keywords:* selektive Massenskalierung, explizite Dynamik, Finite-Elemente-Technologie, dünnwandige Strukturen, Volumenelemente

Erschienen in Tagungsband 35. Forum Bauinformatik 2024, Hamburg, Deutschland, DOI: 10.15480/882.13545
© 2024 Das Copyright für diesen Beitrag liegt bei den Autoren. Verwendung erlaubt unter Creative Commons Lizenz Namensnennung 4.0 International.

## 1 Einleitung

Im Bereich der Strukturdynamik wird bei transienten Analyseverfahren zwischen expliziten und impliziten Verfahren unterschieden. Explizite Algorithmen zur direkten Zeitintegration sind besonders gut für stark nichtlineare und nichtglatte Problemstellungen geeignet, da sie keine iterative Lösung der globalen dynamischen Bewegungsgleichungen erfordern. In bestimmten Ingenieuranwendungen sind sie robuster als implizite Algorithmen. Jedoch begrenzt die lediglich bedingte Stabilität expliziter Algorithmen die erlaubte kritische Zeitschrittweite $\Delta t_{\mathrm{crit}}$. Diese hängt direkt von der höchsten Eigenkreisfrequenz $\omega_{\max}$ des diskreten Systems ab,

$$\Delta t_{\text{crit}} = \frac{2}{\omega_{\max}}. \tag{1}$$

Die höchsten Eigenfrequenzen begrenzen die kritische Zeitschrittweite $\Delta t_{\text{crit}}$, haben aber meist nur einen geringen Einfluss auf das tatsächliche Strukturverhalten. Bei transienten Analysen dünnwandiger Strukturen ist dieser Aspekt besonders dominant, da die geringe Dicke in der Regel zu hohen Eigenfrequenzen, inakzeptabel kleinen Zeitschritten und hohen Rechenkosten führt. Werden dünnwandige Strukturen mit Volumen- oder Volumenschalenelementen diskretisiert, sind die höchsten Eigenfrequenzen zu Dickenänderungsmoden assoziiert, siehe [1].
Massenskalierungsmethoden zielen auf eine Vergrößerung der kritischen Zeitschrittweite $\Delta t_{\text{crit}}$ ab, um damit die Anzahl der benötigten Zeitschritte und somit die numerischen Kosten zu senken. Bei Massenskalierungsmethoden wird zwischen konventioneller Massenskalierung (*conventional mass scaling*, CMS) und selektiver Massenskalierung (*selective mass scaling*, SMS) unterschieden. Bei allen Massenskalierungsmethoden wird künstlich Trägheit addiert. Werden im Kontext von diagonalen, konzentrierten Massenmatrizen (*lumped mass matrix*, LMM) nur die Diagonaleinträge künstlich erhöht, spricht man von CMS. Die wünschenswerte Diagonalstruktur bleibt dabei erhalten, jedoch führt die Nutzung der CMS zur Erhöhung der translatorischen Trägheit, wodurch das gesamte Eigenfrequenzspektrum modifiziert wird. Somit wird die Anwendung von CMS in der Regel auf wenige kleine, steife Elemente in einem FE-Netz begrenzt [2].
SMS-Methoden zielen darauf ab, die höchsten Eigenfrequenzen zu reduzieren, ohne die relevanten niedrigen Eigenfrequenzen zu stark zu verändern. Die meisten der bestehenden SMS-Methoden wurden für Volumen- oder Volumenschalenelemente entwickelt (siehe beispielsweise [1], [3]–[5]) und darauf ausgelegt, dass die translatorische Trägheit und damit der Impuls erhalten bleibt. Die Erhaltung der rotatorischen Trägheit bzw. des Drehimpulses geht mit erhöhter Genauigkeit einher, bringt bei gängigen SMS-Methoden, wie beispielsweise [4], jedoch zusätzliche Rechenkosten mit sich. Die SMS kann in allgemeiner Form dargestellt werden als

$$\mathbf{M}^\circ = \mathbf{M} + \lambda^\circ, \tag{2}$$

wobei $\mathbf{M}^\circ$ die skalierte Massenmatrix, $\mathbf{M}$ die Ausgangsmassenmatrix und $\lambda^\circ$ die künstliche Massenmatrix beschreibt.
Verschiedene SMS-Methoden unterscheiden sich maßgeblich in Konstruktion und Struktur der künstlichen Massenmatrix $\lambda^\circ$. Es existieren beispielsweise zahlreiche SMS-Methoden, die auf algebraischen Konstruktionen basieren, unter ihnen die steifigkeitsproportionale SMS, d. h. $\lambda^\circ = \alpha\mathbf{K}$, welche unter anderem in [4], [6], [7] beschrieben wird und sich durch eine hohe Genauigkeit auszeichnet. Die praktische Anwendung ist allerdings auf lineare dynamische Problemstellungen beschränkt, da sich die Steifigkeitsmatrix für nichtlineare Problemen fortlaufend verändert und $\lambda^\circ$ stets neu assembliert werden muss. Die dadurch verursachten numerischen Mehrkosten sind der Hauptgrund dafür, dass steifigkeitsproportionale SMS-Methoden bezüglich der Effizienz nicht konkurrenzfähig sind.
In diesem Beitrag werden neuartige SMS-Methoden vorgestellt, die intrinsisch impuls- *und* drehimpulserhaltend sind und sich durch eine hohe Genauigkeit auszeichnen. Die neuen, erstmals in [8], [9] vorgestellten SMS-Methoden basieren auf der Discrete-Strain-Gap(DSG)-Methode [10], eines aus der

Finite-Elemente-Technologie bekanntes Verfahren zur Vermeidung geometrischer Locking-Effekte. Die resultierenden DSGSMS-Methoden haben in den Vorarbeiten [8], [9] bereits ihr großes Potenzial aufgezeigt. Im Wesentlichen wird hierbei eine steifigkeitsproportionale SMS mit hoher Genauigkeit approximiert, ohne die effizienzmindernde Reassemblierung zu erfordern.
In Kapitel 2 wird die DSGSMS-Methode für schlanke Volumenelemente eingeführt und mit der SMS-Methode nach Olovsson U.A. [4] verglichen, da diese zum Stand der Technik in kommerziellen expliziten FE-Solvern wie LS-DYNA zählt. In Kapitel 3 werden die Eigenschaften der vorgestellten DSGSMS-Methoden im Rahmen numerischer Experimente untersucht und mit existierenden SMS-Methoden verglichen. Kapitel 4 fasst die gewonnenen Erkenntnisse zusammen und gibt Anreize für zukünftige Entwicklungen.

## 2 Das DSGSMS-Konzept für schlanke Volumenelemente

Wie in [8] beschrieben, stammt die Inspiration für das DSGSMS-Konzept von dem kürzlich in [11] vorgestellten Konzept der intrinsisch selektiven Massenskalierung (ISMS). Das DSGSMS-Konzept basiert auf der theoretischen Verbindung von intrinsisch lockingfreien, hierarchischen Strukturelementformulierungen [12], [13] und DSG-Formulierungen zur Vermeidung von Querschublocking. Für Details zur DSG-Methode und Locking-Effekten in finiten Elementen wird an dieser Stelle auf [10] verwiesen. Die DSG-Methode ist eine universell einsetzbare Methode zur Beseitigung aller Arten von geometrischen Locking-Effekten in Balken-, Platten-, Schalen-, Volumen- oder Volumenschalenelementen. Das neu entwickelte DSGSMS-Konzept nutzt die im Rahmen der DSG-Methode konstruierte Strain-Gap-Funktion, eine modifizierte Verschiebungsfunktion, zur Konstruktion einer künstlichen Massenmatrix.
Bei einer dreidimensionalen Diskretisierung dünnwandiger Strukturen sind die höchsten Eigenfrequenzen in der Regel mit Dickenänderungsmoden assoziiert, siehe [1]. Um die höchsten Eigenfrequenzen mithilfe der DSGSMS-Methode zu skalieren, werden *discrete strain gaps* der Normalverzerrungen $\varepsilon_{33}$ in Dickenrichtung integriert, kollokiert und interpoliert. Aus der interpolierten Strain-Gap-Funktion $u_3^{\mathrm{mod}}$ wird ein zusätzlicher Beitrag zur virtuellen kinetischen Energie konstruiert

$$\delta W^{\mathrm{kin}}_{\mathrm{DSGSMS-33}} = \alpha_{\text{DSGSMS-33}} \int_{\Omega} \left( \delta u_3^{\mathrm{mod}} \rho \ddot{u}_3^{\mathrm{mod}} \right) \, \mathrm{d}\Omega, \tag{3}$$

wobei $\rho$ die Dichte und $\alpha_{\text{DSGSMS-33}}$ einen künstlichen, skalaren Massenskalierungsparameter der DSGSMS-33-Methode bezeichnet. Die aus der interpolierten Strain-Gap-Funktion $u_3^{\mathrm{mod}}$ berechnete künstliche Massenmatrix $\lambda^{\circ}_{\mathrm{DSGSMS-33}}$ ist entsprechend an der $33$- bzw. Dickenrichtung ausgerichtet und somit *anisotrop*, d. h. es wird lediglich künstliche Trägheit in Dickenrichtung addiert. Für nachfolgende Darstellungen wird von achtknotigen finiten Hexaeder-Elementen ausgegangen. Im Sinne einer kompakten Darstellung werden die Verschiebungsfreiheitsgrade auf Elementniveau blockweise nach $x-$, $y-$ und $z-$Komponenten sortiert, d. h.

$$\mathbf{d} = \left[ d_x^1 \, d_x^2 \, \ldots \, d_x^8 \, d_y^1 \, d_y^2 \, \ldots \, d_y^8 \, d_z^1 \, d_z^2 \, \ldots \, d_z^8 \right]^{\mathrm{T}}. \tag{4}$$

Damit ergibt sich für die aus Gleichung (3) hergeleitete künstliche Massenmatrix $\lambda^{\circ}_{\mathrm{DSGSMS-33}}$ der DSGSMS-33-Methode eine algebraische Struktur der Form

$$\lambda^{\circ}_{\mathrm{DSGSMS-33}} = \begin{bmatrix} \mathbf{0} & \mathbf{0} & \mathbf{0} \\ \mathbf{0} & \mathbf{0} & \mathbf{0} \\ \mathbf{0} & \mathbf{0} & \lambda^{\circ,8\times 8}_{\mathrm{DSGSMS-33}} \end{bmatrix}, \tag{5}$$

wobei

$$\lambda^{\circ,8\times 8}_{\mathrm{DSGSMS-33}} = \alpha_{\mathrm{DSGSMS-33}} \cdot f \begin{bmatrix} 1 & 1/2 & 1/4 & 1/2 & -1 & -1/2 & -1/4 & -1/2 \\ 1/2 & 1 & 1/2 & 1/4 & -1/2 & -1 & -1/2 & -1/4 \\ 1/4 & 1/2 & 1 & 1/2 & -1/4 & -1/2 & -1 & -1/2 \\ 1/2 & 1/4 & 1/2 & 1 & -1/2 & -1/4 & -1/2 & -1 \\ -1 & -1/2 & -1/4 & -1/2 & 1 & 1/2 & 1/4 & 1/2 \\ -1/2 & -1 & -1/2 & -1/4 & 1/2 & 1 & 1/2 & 1/4 \\ -1/4 & -1/2 & -1 & -1/2 & 1/4 & 1/2 & 1 & 1/2 \\ -1/2 & -1/4 & -1/2 & -1 & 1/2 & 1/4 & 1/2 & 1 \end{bmatrix} \tag{6}$$

gilt. Ein zusätzlicher Parameter, der von der Elementgeometrie und den Materialkennwerten abhängt, ist durch $f$ gekennzeichnet.
Die Methode nach Olovsson U.A. [4] ist als Vergleichspartner von besonderem Interesse, da diese den Stand der Technik in kommerziellen FE-Codes wie LS-DYNA repräsentiert. Sie führt auf

$$\lambda^{\circ}_{\mathrm{Olov}} = \begin{bmatrix} \lambda^{\circ,8\times 8}_{\mathrm{Olov}} & \mathbf{0} & \mathbf{0} \\ \mathbf{0} & \lambda^{\circ,8\times 8}_{\mathrm{Olov}} & \mathbf{0} \\ \mathbf{0} & \mathbf{0} & \lambda^{\circ,8\times 8}_{\mathrm{Olov}} \end{bmatrix}, \qquad \text{mit} \qquad \lambda^{\circ,8\times 8}_{\mathrm{Olov}} = \frac{\beta m^{\mathrm{e}}}{56} \begin{bmatrix} 7 & -1 & \dots & -1 \\ -1 & 7 & & \\ \vdots & & \ddots & \\ -1 & & & 7 \end{bmatrix}, \tag{7}$$

wobei $\beta$ einen skalaren Massenskalierungsfaktor und $m^{\mathfrak{R}}$ die gesamte Elementmasse beschreibt.
Aus den algebraischen Strukturen von $\lambda^{\circ}_{\mathrm{DSGSMS-33}}$ und $\lambda^{\circ}_{\mathrm{Olov}}$ aus den Gleichungen (5) und (7) ist zu erkennen, dass $\lambda^{\circ}_{\mathrm{Olov}}$ *isotrop* ist. Die künstliche Massenmatrix $\lambda^{\circ}_{\mathrm{DSGSMS-33}}$ ist hingegen *anisotrop*, d. h. künstliche Trägheit wird nur in Dickenrichtung addiert, was wiederum bei nichtlinearen Problemstellungen mit großen Rotationen zu numerischen Mehrkosten führt, da sich die Dickenrichtung permanent verändert. Die Konstruktion einer isotropen Variante der DSGSMS-33 ist in Hinblick auf anvisierte nichtlineare Probleme von großer Bedeutung. Eine DSGSMS-33-iso kann konstruiert werden, indem die künstlichen Trägheiten in $z$-Richtung in analoger Weise auf die $x$- und $y$-Richtung übertragen werden. Dies resultiert in einer künstlichen Massenmatrix

$$\lambda^{\circ}_{\mathrm{DSGSMS-33-iso}} = \begin{bmatrix} \lambda^{\circ,8\times 8}_{\mathrm{DSGSMS-33}} & \mathbf{0} & \mathbf{0} \\ \mathbf{0} & \lambda^{\circ,8\times 8}_{\mathrm{DSGSMS-33}} & \mathbf{0} \\ \mathbf{0} & \mathbf{0} & \lambda^{\circ,8\times 8}_{\mathrm{DSGSMS-33}} \end{bmatrix}, \tag{8}$$

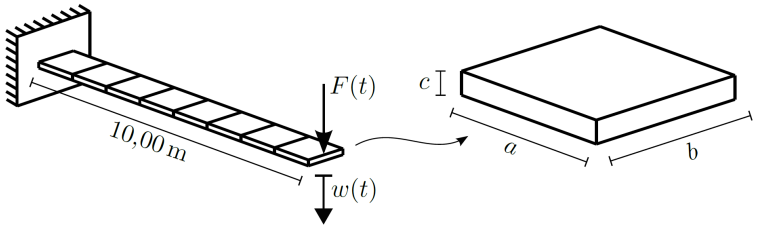


$a = b = 1,25\,\mathrm{m}$
$E = 200\,\mathrm{GPa}$
$\nu = 0,3$
$\rho = 8.000\,\mathrm{kg/m^3}$

Abbildung 1: Kragarm mit Einzellast, Problembeschreibung.

die unter Rotation konstant bleibt. Die Auswirkungen dieser Modifikation auf die Ergebnisqualität wird nachfolgend im Rahmen numerischer Experimente untersucht.

# 3 Numerische Experimente

## 3.1 Eigenfrequenzspektren

Die Effektivität der anisotropen DSGSMS-33 und der isotropen DSGSMS-33-iso werden zunächst anhand von Frequenzspektren untersucht. Analysiert wird ein mit acht achtknotigen Enhanced-Assumed-Strain(EAS)-Volumenelementen diskretisierter Kragarm, siehe Abbildung 1. Es wird das generalisierte Eigenwertproblem der Form

$$(\mathbf{K} - \omega^2\mathbf{M})\boldsymbol{\phi} = \mathbf{0} \tag{9}$$

gelöst. Die zugehörigen Ergebnisse sind in Abbildung 2 dargestellt. Die Massenskalierungsparameter sind dabei so gewählt, dass die maximale Eigenfrequenz um $90\,\%$ der ursprünglichen Eigenfrequenz (LMM) abgesenkt wird. Die CMS skaliert das gesamte Spektrum auf $\frac{\omega^\circ}{\omega_{\mathrm{LMM}}} = 0,1$ und ist damit für viele Anwendungen unbrauchbar. Wird die SMS nach Olovsson U.A. [4] gewählt, so weist schon die erste Eigenfrequenz einen Fehler von ca. $40\,\%$ auf. Alle weiteren Eigenfrequenzen zeigen noch stärkere Abweichungen.
Die höchste Genauigkeit im vorderen Teil des Frequenzspektrums, d. h. in den niedrigen Frequenzen, wird mit der anisotropen DSGSMS-33 erreicht. Die Methode ist derart selektiv, dass lediglich der Zweig mit den höchsten Eigenfrequenzen, welche zu Dickenänderungsmoden assoziiert sind, skaliert wird. Diese eigentlich positive Eigenschaft führt allerdings auch dazu, dass die maximale Skalierbarkeit limitiert ist. Zudem ist die bereits erwähnte Anisotropie der DSGSMS-33 für zukünftig anvisierte nichtlineare Analysen unter großen Rotationen mit numerischen Mehrkosten verbunden.
Die isotrope DSGSMS-33-iso scheint einen guten Kompromiss zwischen Effizienz und Genauigkeit bereitzustellen. In den niedrigsten zehn Eigenfrequenzen ergibt sich ein maximaler Fehler von $7,4\,\%$, während die SMS-Methode nach Olovsson U.A. [4] einen maximalen Fehler von $87,1\,\%$ aufweist.

## 3.2 Transiente Analyse

Die Genauigkeit der isotropen Massenskalierungsmethoden wird nun im Rahmen einer transienten Problemstellung mit expliziter Zeitintegration nach dem Zentrale-Differenzen-Verfahren, siehe beispielsweise [14], verglichen. Der in Abbildung 1 dargestellte Kragarm wird durch eine Stoßbelastung $F(0 \leq t \leq 0,005\,\mathrm{s})$ an der Kragarmspitze, verteilt auf die vier Eckknoten, belastet. Die Last ist so

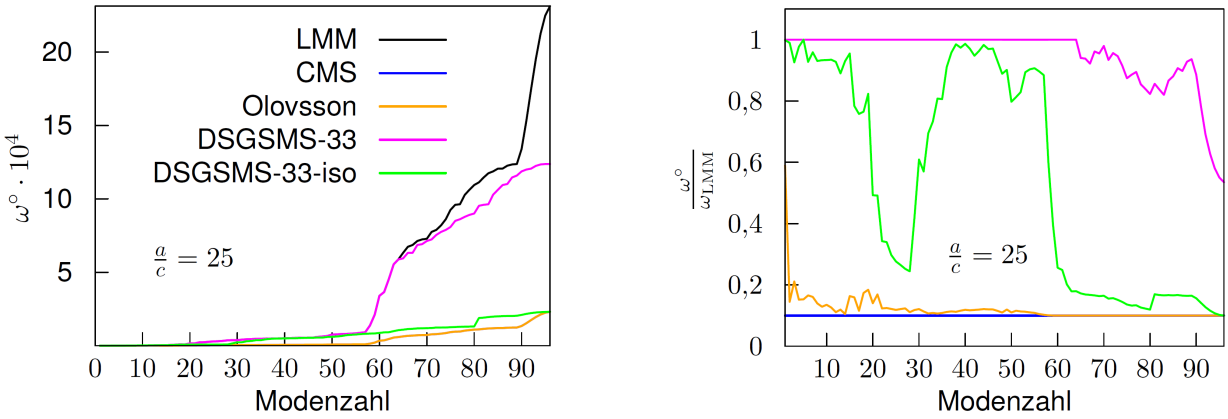


Abbildung 2: Frequenzspektren des Kragarms für $c = 0,05\,\mathrm{m}$, links: Eigenfrequenzspektren verschiedener Massenskalierungsmethoden im Vergleich, rechts: Verhältnis von skalierten zu unskalierten Eigenfrequenzen.

gewählt, dass die Verschiebungen klein bleiben und geometrisch lineares Verhalten angenommen werden kann. Des Weiteren wird ein linear-elastisches Materialmodell verwendet. Zur Auswertung dient die maximale Vertikalverschiebung $w(t)$ der Kragarmspitze. Die Berechnungszeit ist so gewählt, dass der Referenzverlauf ohne Massenskalierung, d. h. LMM, drei Schwingungsperioden abdeckt. Die kritische Zeitschrittweite $\Delta t_{\mathrm{crit}}$ nach Gleichung (1) wurde in allen Fällen durch die Lösung des generalisierten Eigenwertproblems nach Gleichung (9) exakt ermittelt.
Die Referenzlösung (LMM, ohne Massenskalierung) aus Abbildung 3 (links) benötigt für eine Berechnungszeit von $t_{\mathrm{end}} = 7,455\,\mathrm{s}$ insgesamt $862.935$ Zeitschritte. Für alle Massenskalierungsmethoden ist der entsprechende Skalierungsfaktor so gewählt, dass die benötigte Anzahl an Zeitschritten um $90\%$ auf $86.293$ reduziert wird. Sowohl die CMS als auch die SMS nach Olovsson U.A. [4] zeigen eine deutlich zu träge Strukturantwort. Die DSGSMS-33-iso bildet die Periodendauern und die maximalen Amplituden im Vergleich zur Referenzlösung (LMM) gut ab. In Abbildung 3 (rechts) sind lediglich geringe Abweichungen bei genauerer Betrachtung eines kleinen Ausschnitts der ersten maximalen Amplitude zu erkennen.

## 4 Zusammenfassung und Ausblick

Es wurde eine neuartige Klasse selektiver Massenskalierungsmethoden für transiente Analysen dünnwandiger Strukturen unter Verwendung von Volumenelementen und expliziter Zeitintegration vorgestellt. Diese DSGSMS-Methoden basieren auf der DSG-Methode, sind intrinsisch impuls- und drehimpulserhaltend und zeichnen sich durch eine hohe Genauigkeit aus.
Es wurden Eigenschaften der anisotropen und isotropen DSGSMS-Methode aufgezeigt und diskutiert. Speziell die isotrope Variante, d. h. die DSGSMS-33-iso, ist eine vielversprechende SMS-Methode, welche einen guten Kompromiss zwischen Effizienz und Genauigkeit bietet. Die zugehörige künstliche Massenmatrix $\lambda^\circ_{\mathrm{DSGSMS-33-iso}}$ weist im Vergleich zur Matrix $\lambda^\circ_{\mathrm{Olov}}$ nach [4] einen identischen Fill-In auf. Die Genauigkeit der DSGSMS-33-iso ist allerdings deutlich höher. Für die dargestellten numerischen Experimente konnten gute spektrale Eigenschaften der DSGSMS-33-iso sowie deutliche Effizienzsteigerung bei gleichzeitig hoher Genauigkeit demonstriert werden.

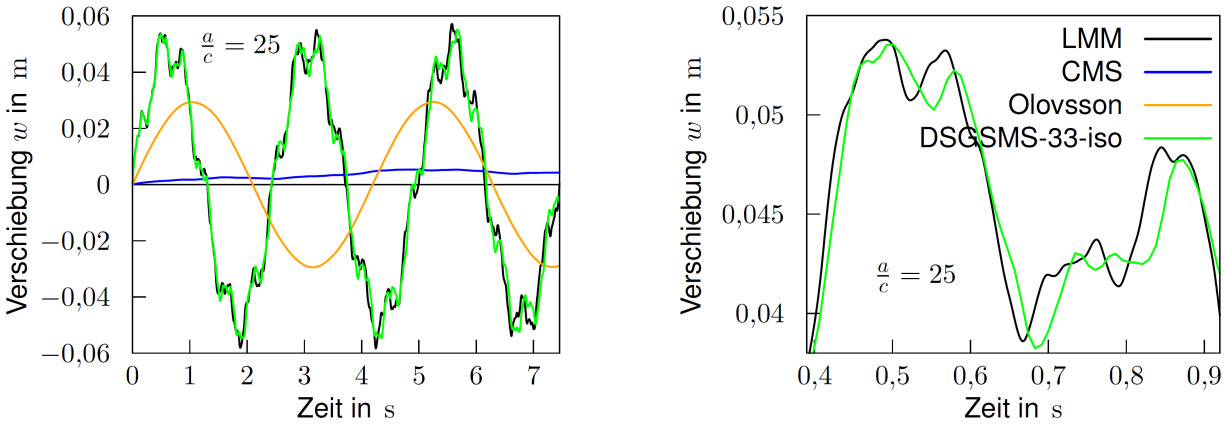


Abbildung 3: Transiente Analyse des Kragarms für $c = 0,05\,\mathrm{m}$, $F(0 \leq t \leq 0,005\,\mathrm{s}) = 31,25\,\mathrm{kN}$ und eine Reduktion der max. Eigenfrequenz um $90\,\%$ im Vergleich zu LMM (Zeitschrittfaktor von $10$), links: volle Berechnungszeit, rechts: Detail der ersten maximalen Amplitude.

Die DSGSMS-33-iso ist eine vielversprechende SMS-Methode für nichtlineare transiente Analysen mit großen Rotationen und verzerrten Netzen. Dieses Potenzial soll in zukünftigen Arbeiten detailliert untersucht werden. Des Weiteren stehen die Erweiterung der DSGSMS-33-iso auf Volumenschalenelemente sowie eine detaillierte Untersuchung der tatsächlichen Reduktion numerischer Kosten für größere und komplexere nichtlineare Problemstellungen im Fokus. In diesem Kontext bedarf es auch der Entwicklung effizienter und genauer Zeitschrittschätzer.

## Danksagung

Der Autor bedankt sich für die Förderung durch die Deutsche Forschungsgemeinschaft (DFG) im Rahmen des Projekts OE 728/3-1 – Projektnummer 512271632.

## Literatur

[1] G. Cocchetti, M. Pagani und U. Perego, »Selective mass scaling and critical time-step estimate for explicit dynamics analyses with solid-shell elements«, *Computers & Structures*, Jg. 127, S. 39–52, 2013. DOI: 10.1016/j.compstruc.2012.10.021.

[2] A. Tkachuk und M. Bischoff, »Variational methods for selective mass scaling«, *Computational Mechanics*, Jg. 52, Nr. 3, S. 563–570, 2013. DOI: 10.1007/s00466-013-0832-0.

[3] L. Olovsson, M. Unosson und K. Simonsson, »Selective mass scaling for thin walled structures modeled with tri-linear solid elements«, *Computational Mechanics*, Jg. 34, Nr. 2, S. 134–136, 2004. DOI: 10.1007/s00466-004-0560-6.

[4] L. Olovsson, K. Simonsson und M. Unosson, »Selective mass scaling for explicit finite element analyses«, *International Journal for Numerical Methods in Engineering*, Jg. 63, Nr. 10, S. 1436–1445, 2005. DOI: 10.1002/nme.1293.

[5] S. Mattern, C. Schmied und K. Schweizerhof, »Highly efficient solid and solid-shell finite elements with mixed strain–displacement assumptions specifically set up for explicit dynamic simulations

using symbolic programming«, *Computers & Structures*, Jg. 154, S. 210–225, 2015. DOI: 10.1016/j.compstruc.2015.03.009.

[6] R. W. Macek und B. H. Aubert, »A mass penalty technique to control the critical time increment in explicit dynamic finite element analyses«, *Earthquake Engineering & Structural Dynamics*, Jg. 24, Nr. 10, S. 1315–1331, 1995. DOI: 10.1002/eqe.4290241003.

[7] H. Askes, D. C. D. Nguyen und A. Tyas, »Increasing the critical time step: micro-inertia, inertia penalties and mass scaling«, *Computational Mechanics*, Jg. 47, Nr. 6, S. 657–667, 2011. DOI: 10.1007/s00466-010-0568-z.

[8] B. Oesterle, A. Tkachuk und M. Bischoff, »Finite element technology-based selective mass scaling for shear deformable structural element formulations«, in *COMPDYN 2023, 9th ECCOMAS Thematic Conference on Computational Methods in Structural Dynamics and Earthquake Engineering, M. Papadrakakis, M. Fragiadakis (eds.), Athens, Greece, 12-14 June 2023*, 2023, S. 1965–1973. DOI: 10.7712/120123.10534.20662.

[9] M. Hoffmann, A. Tkachuk, M. Bischoff und B. Oesterle, »Finite element technology-based selective mass scaling for explicit dynamic analyses of thin-walled structures using solid elements«, in *COMPDYN 2023, 9th ECCOMAS Thematic Conference on Computational Methods in Structural Dynamics and Earthquake Engineering, M. Papadrakakis, M. Fragiadakis (eds.), Athens, Greece, 12-14 June 2023*, 2023, S. 1974–1982. DOI: 10.7712/120123.10535.20771.

[10] K.-U. Bletzinger, M. Bischoff und E. Ramm, »A unified approach for shear-locking-free triangular and rectangular shell finite elements«, *Computers & Structures*, Jg. 75, Nr. 3, S. 321–334, 2000. DOI: 10.1016/S0045-7949(99)00140-6.

[11] B. Oesterle, J. Trippmacher, A. Tkachuk und M. Bischoff, »Intrinsically Selective Mass Scaling With Hierarchic Structural Element Formulations«, in *Book of Extended Abstracts of the 6th ECCOMAS Young Investigators Conference 7th-9th July 2021, Valencia, Spain, accepted for publication.*, 2021, S. 383–405. DOI: 10.4995/YIC2021.2021.12418.

[12] R. Echter, B. Oesterle und M. Bischoff, »A hierarchic family of isogeometric shell finite elements«, *Computer Methods in Applied Mechanics and Engineering*, Jg. 254, S. 170–180, 2013. DOI: 10.1016/j.cma.2012.10.018.

[13] B. Oesterle, S. Bieber, R. Sachse, E. Ramm und M. Bischoff, »Intrinsically locking–free formulations for isogeometric beam, plate and shell analysis«, *Proc. Appl. Math. Mech.*, Jg. 18, Nr. 1, 2018. DOI: 10.1002/pamm.201800399.

[14] T. Belytschko, W. K. Liu, B. Moran und K. I. Elkhodary, *Nonlinear finite elements for continua and structures*, en, 2. Aufl. Nashville, TN: John Wiley & Sons, 2014.

# LLM Assistant for heterogeneous multi-robot system dynamic task planning

Miguel Guzmán-Merino[1] and Nils Sören Krause[1]
[1]AI for Sustainable Construction, University of Rostock,
Justus-von-Liebig-Weg 2, 18059 Rostock, Germany
E-mail(s): miguel.merino@uni-rostock.de, nils.krause@uni-rostock.de

**Abstract:** Multi-robot systems find good implantation in construction applications. The combination of the skills of the robots creates systems with high flexibility. However the combination of these skills is not enough to ensure complex task completion. Task planning needs to face the dynamic behaviors of construction environments. In this paper, a heterogeneous multi-robot system for construction tasks is presented. The system is composed by three robots that present complementary skills and is commanded through natural language requirements, imposing low training requirements for the user. Task planning is managed by a large language model assistant, which receives information about the environment and the state of the system along with the user request. With this information, the assistant provides the execution plan for the robots in a dynamic environment. The system is tested through different situations with real-world tasks, involving extensive interaction with the environment and dynamic planning. Environment recognition, tool manipulation, or obstacle removal are some of the tasks presented in the system.

*Keywords:* Construction robotics, Human-robot interaction, Large language model, Multi-robot systems, Task planning

Erschienen in Tagungsband 35. Forum Bauinformatik 2024, Hamburg, Deutschland, DOI: 10.15480/882.13508
© 2024 Das Copyright für diesen Beitrag liegt bei den Autoren. Verwendung erlaubt unter Creative Commons Lizenz Namensnennung 4.0 International.

## 1 Introduction

Construction environments are complex dynamic scenarios. Constant changes, limited information and unclear references complicate the implantation of robotic systems in construction sites. These problems often required close human assistance during the robotic system performance. Multi-robot systems (MRS) are an alternative to this human interaction. Combining robots it is possible to face situations where single robot systems do not satisfy the requirements. This combination can be between robots with the same features (homogeneous MRS) or different types of robots (heterogeneous MRS). The combination of the robot's skills increases the flexibility of the systems. This flexibility allows MRS to execute complex tasks in dynamic construction environments. Along with the combination of the skills, task planning is an essential part of MRS to address complex tasks. In the task planning process, a complex task is divided into sub-tasks for the robots to perform. Robots

coalitions are build if necessary and sub-tasks are allocated to the robots. Environment information and the state of the system are taken into account during the processes. Only through proper task planning it is possible to ensure task completeness. Another important aspect in robotic systems is the human-system interaction. One of the issues included in the human-system interaction is users training requirements. Natural language user-system communication is an interesting solution to this issue. Large Language Models (LLM) can be used to assist in the natural language analysis and understanding. These models also present good performance in information abstraction. Therefore they have been used to face task planning problems. In this paper, a heterogeneous MRS composed by three robots and a LLM Assistant is presented. The LLM Assistant is used to compute the natural language requests from the user and generate the execution plan for the robots to perform. It also takes into account environment information, the state of the system and the robots features. This proposal is detailed in the paper as follows: the related work is presented in Section 2 followed by the description of the robots in the system in Section 3. The system architecture and the integration of the large language model assistant are presented in Section 4. The response of the system in different scenarios is discussed in Section 5. In Section 6, a discussion about the system is presented along with further developments proposals.

## 2 Related work

MRS present higher flexibility than single robot systems. That makes them more suitable for construction applications. Collaboration between robots allows for instance the exploration of tasks in large working areas [1], [2]. In [3] it is possible to remove the scaffolding process thanks to the collaboration between robots. This task could not be performed by a single robot system. Task planning is an important part of MRS. In [4] they present the main parts that integrate the task planning process as (i) task decomposition, the division of a complex task into sub-tasks for the robots to perform, (ii) coalition formation, to build teams dedicated to the same sub-task, (iii) task allocation, where sub-tasks are assigned to the appropriate robots or team of robots, and (iv) task execution, where the robots in the system execute the sub-task to complete the task. As it will be explained in Section 3, the actions proposed in this paper are single robot actions, therefore coalition formation is not considered. Several solutions for the task planning problem can be found in the literature. Solutions for optimal automatic task decomposition [5], [6] or task allocation [7], [8] focus on one of the parts of the task planning process. However, due to the high interconnection of the parts into the task planning process, studies like [9] target task allocation and planning problems simultaneously. Natural language processing approaches were proposed in [4] to solve the task planning problem. This approach has been successfully implemented in [10], [11]. Common house activities are studied in simulation environments in these papers. In [10] a LLM is trained to solve the task planning problem. They use a heterogeneous robot team to test the generated plans. Compound tasks are presented as the execution of the same task using different agents. In [11] they do not train the LLM previously and only a single agent perform the actions. It is stressed that the untrained LLM can develop accurate plans. In both studies a deterministic environment is presented, where the location of the objects is known and there are no obstacles during the plan execution. The requests are expressed as natural language high-level tasks, implying low or no user training. User training has been identified as one of the challenges for the

implantation of technology in construction [12], [13]. The benefit of natural language interaction is demonstrated in [14]. The system identifies the best tools for specific tasks using a probabilistic graph reasoning approach based on the weights derived from the language and computer vision model. The user can interact with the system using natural language prompts, implying no previous user training. In this paper a LLM Assistant is used to solve the task planning problem in non-deterministic scenarios. With this approach it is intended to study whether LLM can be used for dynamic task planning.

## 3 Robot system

The proposed system is intended to perform in dynamic environments with no or little previous information. The selection of the robots for the system is based on the combination of their features and the tasks they are likely to perform. A **legged robot** is proposed for environment recognition, remove obstacles and interact with the environment. These robots are appropriate for navigation through irregular terrains like the ones in a construction site. Sensors like RGB camera and LiDAR as well as a manipulator need to be mounted on the robot. A **mobile manipulator** is proposed to perform power-demanding tasks. Tasks like drilling or painting are not suitable for the legged robot manipulator. A mobile manipulator can reach the target location or relocate the robot arm during task execution. To ensure safe navigation, the mobile manipulator platform needs to integrate sensors like LiDAR or depth cameras. Finally a **mobile platform** is proposed for supplies transportation. An extra mobile platform adds flexibility to the system. By using and extra mobile platform it would be possible to perform parallel actions. For example, while the mobile manipulator performs an action in a working area, the mobile platform could travel back and forth to collect supplies. Navigation sensors would also be included in the mobile platform. Table 1 shows the robots' sub-tasks included in the current research. Each sub-task is composed by a robot and information about locations and/or objects. These sub-tasks are used by the LLM Assistant to generate the execution plan. The sub-task implementation is not discussed in this paper.

Table 1: Robots' sub-tasks integrated in the system. Each sub-task specifies the robot that performs it and information about locations or objects

| **Robot** | **Sub-tasks** |
|---|---|
| Legged robot | Move (LeggedRobot, location1, location2), Find (LeggedRobot, location), Remove (LeggedRobot, object) |
| Mobile manipulator | Move (MobileManipulator, location1, location2), Paint (MobileManipulator, location), Drill (MobileManipulator, location) |
| Mobile platform | Move (MobilePlatform, location1, location2), Carry (MobilePlatform, object) |

## 4 System architecture

There are different sources of information in the system. Figure 1 shows how these sources are integrated in the LLM Assistant to generate a feasible execution plan. Assuming resting state, a execution starts with a user request like: "Paint the left wall in the room number 3", "Drill a hole in the right wall of the office, 1 metre from the floor and 2 meters from the window" or "Sand the floor of the room number 2 and bring paint from the storage room". The request is provided to the LLM

Assistant along with the Environment Information, the Robots' sub-tasks from Table 1 and the System State. The Robots' sub-tasks do not change during the execution. However, the System State and the Environment Information can be updated. The System State includes the information about the location of the robots, or whether they are available. Another kind of information, not included in the current discussion, could be the battery level of the robots. This information is not considered in the current discussion. It is possible to have full, partial or no environment information. This information can proceed from Building Information Models (BIM) or from previous executions. GPT4o is used to implement the LLM Assistant without previous training. The performance of untrained LLM for task planning in deterministic scenarios was tested in [11]. Here the LLM Assistant would be used to solve the task planning problem in non-deterministic scenarios. The Environment Information, the Systems State and the Robots' sub-tasks are provided to the LLM Assistant as context information. No examples of task decomposition or allocation are provided to the LLM Assistant. Some guidance about how to handle the information and how to generate the plans are also part of the context of the LLM Assistant. Once the LLM Assistant has all the context information, the user request is provided. The Assistant's response is an ordered list of sub-tasks. The sub-tasks include information about the robots that perform them. This ensures proper task allocation. The robots updated their state in the system and the environment information during the plan execution. For example, the environment information could be updated with semantic information captured with the Legged Robot camera. It is also possible to update information like the location of an obstacle. The updated information is then communicated to the LLM Assistant. The Assistant generates a new plan if the new information demonstrates that the original plan is no longer feasible. This is how the system captures dynamic changes and how these changes modify the performance of the robots. The scenarios presented in the next section would help to clarify how the system architecture works.

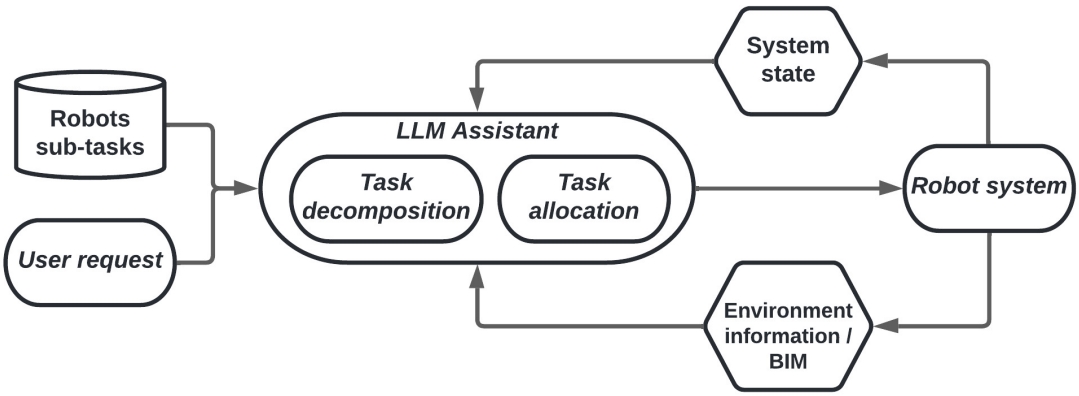


Figure 1: System architecture. The LLM Assistant generates the execution plan for the robots to perform. To do it the Environment information, the System state and the Robots' sub-tasks are provided to the LLM Assistant along with the User request.

## 5 System analysis

Three different scenarios are proposed to test the system performance. Sub-tasks from Table 1 are common to all the scenarios and do not change. The environment information is treated here as locations information and no time variable is assumed. Each step in the execution plan starts and

ends with the corresponding sub-task execution. It is intended to analyse the system performance with the following scenarios: (i) There is partial knowledge of the environment and the state of the system is updated. (ii) An obstacle does not allow the task completeness. (iii) A situation with a parallel sub-tasks execution is proposed.

## 5.1 Partial known environment

In the scenario proposed in Table 2 there is no information about the "left wall in the room 3" in the Environment information. A Find() sub-tasks is proposed in the point 2 of the Plan 1 to find the missing location before the Paint() sub-task. The context provided to the LLM Assistant is good enough to generate a logic sub-tasks sequence. Following Plan 1 it is possible to complete the User request. The update of the System State interrupts the execution of the plan. The LLM Assistant generates the Plan 2 in response. It is proposed to find the Paint location in the Store location in steps 1-3. Steps 4-6 describe how the Legged Robot takes the paint can from the Paint location and how the Mobile platform carries it. Steps 7-11 describe the replacement of the paint in the Mobile manipulator. The second plan shows the main flow needed to complete the task, but it is possible to detect some missing information or wrong steps. In Step 4 the Legged robot removes the paint can for the paint can location, but there is no step to put the can in the Mobile platform. In the step 11, the structure of the sub-task does not correspond with the right sub-task structure. Although Plan 2 is not fully correct, some interesting facts should be taken into account.

Table 2: Partial known environment scenario. The Room 3 left wall location is missing and an update of the system state forces the generation of a new plan.

| | |
|---|---|
| **Environment information** | Room 1 location, Room 3 location, Room 3 right wall location, LeggedRobot location, Mobile-Manipulator location, MobilePlatform location, Store location |
| **System State** | LeggedRobot(operative), MobileManipulator(operative), MobilePlatform(operative) |
| **User request** | Paint the left wall in the room 3 |
| **Plan 1** | **1**. Move (LeggedRobot, LeggedRobot location, Room 3) **2**. Find (LeggedRobot, left wall) **3**. Move (MobileManipulator, MobileManipulator location, Room 3) **4**. Paint (MobileManipulator, left wall) |
| **System State** | Low paint level |
| **Plan 2** | TASK: Refill paint for MobileManipulator<br>Subtask List:<br>**1**. Move (LeggedRobot, LeggedRobot location, Store location) **2**. Find (LeggedRobot, Paint location) **3**. Move (LeggedRobot, Store location, Paint location) **4**. Remove (LeggedRobot, Paint can) **5**. Move (MobilePlatform, MobilePlatform location, Paint location) **6**. Carry (MobilePlatform, Paint can) **7**. Move (MobilePlatform, Paint location, Room 3 left wall location) **8**. Move (LeggedRobot, Paint location, Room 3 left wall location) **9**. Remove ( LeggedRobot, Empty paint can from MobileManipulator) **10**. Move ( LeggedRobot, Room 3 left wall location, Store location) **11**. Carry (MobilePlatform, Full paint can to MobileManipulator) |

(i) The LLM Assistant keeps track of the previous events. For instance, the Legged robot and the Mobile platform are moved to the "Room 3 left wall location" where the Mobile manipulator was painting. (ii) There is a coherent sequence of actions. The dependency between sub-tasks is taken into account during the plan. For instance, it is planned to remove the empty can before placing the

full one. (iii) Sub-tasks are correctly assigned to robots. The legged robot is used to remove the paint can and the mobile platform is used to carry it.

## 5.2 Unknown obstacle

Table 3 presents a scenario where the request contains the same information as in Table 2, but presented in a different way, "Paint room 3 left wall". The Room 3 left wall location is included in the environment information in this case. The first plan generated by the LLM Assistant does not take into account whether there is a door in the way or not. Just when the Mobile Manipulator finds an obstacle and updates the environment information, Plan 2 is generated in response. Find() and Remove() sub-tasks refer to the Room 3 door in this plan. It is interesting to stress that the updated information does not specify location about the door. In spite of Plan 2 execution completes the user request, an error is presented. In the parallel sub-task proposed in step 4, there is no need of moving the Legged Robot to the room 3 left wall location after the obstacle was removed.

Table 3: Unknown obstacle scenario. All the information about environment is known. The environment information is updated when an obstacle is found and a new plan is generated in response.

| | |
|---|---|
| **Environment information** | Room 1 location, Room 3 location, Room 3 right wall location, Room 3 left wall location, LeggedRobot location, MobileManipulator location, MobilePlatform location, Store location |
| **System State** | LeggedRobot(operative), MobileManipulator(operative), MobilePlatform(operative) |
| **User request** | Paint room 3 left wall. |
| **Plan 1** | **1**. Move (MobileManipulator, MobileManipulator location, Room 3 location) **2**. Move (MobileManipulator, Room 3 location, Room 3 left wall location) **3**. Paint (MobileManipulator, Room 3 left wall). |
| **Environment information** | Door closed. |
| **Plan 2** | **1**. Move (LeggedRobot, LeggedRobot location, Room 3 location) **2**. Find (LeggedRobot, Door location) **3**. Remove (LeggedRobot, Room 3 door) **4**. Move (MobileManipulator, MobileManipulator location, Room 3 location) // Move (LeggedRobot, Room 3 location, Room 3 left wall location) **5**. Move (MobileManipulator, Room 3 location, Room 3 left wall location) **6**. Paint (MobileManipulator, Room 3 left wall). |

## 5.3 Parallel sub-task execution

The requested task in Table 4 includes two sub-tasks that can be executed at the same time. All the locations are known in this scenario and the Legged robot is involved in a Find() sub-task. In Table 4 Plan 1, the Carry() and the Move() sub-tasks are executed at the same time. The Mobile platform carries paint when moving to the room 1. Nevertheless the main parallels sub-tasks are not properly planned. The main idea of parallel sub-task is to execute actions without dependencies at the same time. In this scenario the robots could move simultaneously to the desired locations and perform the Drill() and Carry() sub-tasks in parallel. An example of the expected plan is proposed at the end of Table 4.

Table 4: Parallel sub-task execution scenario. The user request includes two tasks that can be executed in parallel.

| | |
|---|---|
| **Environment information** | Room 1 location, Room 3 location, Room 3 right wall location, LeggedRobot location, MobileManipulator location, MobilePlatform location, Store location |
| **System State** | LeggedRobot(finding), MobileManipulator(operative), MobilePlatform(operative) |
| **User request** | Drill a hole room 3 right wall and bring paint to room 1. |
| **Plan 1** | **1**. Move (MobileManipulator, MobileManipulator location, Room 3 right wall location) **2**. Drill (MobileManipulator, Room 3 right wall location) **3**. Move (MobilePlatform, MobilePlatform location, Store location) **4**. Carry (MobilePlatform, paint) // Move (MobilePlatform, Store location, Room 1 location) |
| **Alternative plan (not generated by Assistant)** | **1**. Move (MobileManipulator, MobileManipulator location, Room 3 right wall location) // Move (MobilePlatform, MobilePlatform location, Store location) **2**. Drill (MobileManipulator, Room 3 right wall location) // Carry (MobilePlatform, paint) **3**. Move (MobilePlatform, Store location, Room 1 location) |

## 6 Conclusion

In this paper a heterogeneous MRS assisted by a LLM for task planning has been presented. The proposed robots for the system and their features have been discussed. It has also been shown how the proposed system architecture can handle multiple information sources. The analysis of the scenarios demonstrates that LLM Assistants are good candidates to solve dynamic task allocation and planning problems. Although the proposed plans are not accurate enough, interesting features has been exposed. The LLM Assistant can dynamically elaborate plans while keeping previous relevant information into account. The generated plans also present a logic sequence of action. Further development like include new sub-tasks into the robots would help to generate more accurate plans. It is also proposed the implementation of reinforcement learning methods in combination with the LLM Assistant. The system would also be recreated in simulation. A more precise analysis of the system will be possible including time variable and the implementation of sub-tasks.

## References

[1] X. Zhang, M. Li, J. H. Lim, *et al.*, “Large-scale 3d printing by a team of mobile robots”, *Automation in Construction*, vol. 95, pp. 98–106, Nov. 2018. DOI: https://doi.org/10.1016/j.autcon.2018.08.004.

[2] A. Adel, “Co-robotic assembly of nonstandard timber structures”, *42nd Annual Conference of the Association for Computer Aided Design in Architecture, ACADIA 2022*, pp. 604–613, Oct. 2023.

[3] S. Parascho, I. Han, S. Walker, A. Beghini, E. Bruun, and S. Adriaenssens, “Robotic vault: A cooperative robotic assembly method for brick vault construction”, *Construction Robotics*, vol. 4, pp. 117–126, Dec. 2020. DOI: 10.1007/s41693-020-00041-w.

[4] Y. Rizk, M. Awad, and E. W. Tunstel, “Cooperative heterogeneous multi-robot systems: A survey”, *ACM Computing Surveys (CSUR)*, vol. 52, no. 2, pp. 1–31, Apr. 2019. DOI: 10.1145/3303848.

[5] B. Fu, W. Smith, D. Rizzo, M. Castanier, M. Ghaffari, and K. Barton, "Robust task scheduling for heterogeneous robot teams under capability uncertainty", *IEEE Transactions on Robotics*, vol. 39, no. 2, pp. 1087–1105, Apr. 2023. DOI: 10.1109/TRO.2022.3216068.

[6] A. Messing, G. Neville, S. Chernova, S. Hutchinson, and H. Ravichandar, "Grstaps: Graphically recursive simultaneous task allocation, planning, and scheduling", *The International Journal of Robotics Research*, vol. 41, no. 2, pp. 232–256, Nov. 2021. DOI: 10.1177/02783649211052066.

[7] F. Quinton, C. Grand, and C. Lesire, "Market approaches to the multi-robot task allocation problem: A survey", *Journal of Intelligent and Robotic Systems*, vol. 107, no. 2, pp. 1–29, Feb. 2023. DOI: 10.1007/s10846-022-01803-0.

[8] Y. Emam, S. Mayya, G. Notomista, A. Bohannon, and M. Egerstedt, "Adaptive task allocation for heterogeneous multi-robot teams with evolving and unknown robot capabilities", *2020 IEEE International Conference on Robotics and Automation (ICRA)*, pp. 7719–7725, Sep. 2020. DOI: 10.1109/ICRA40945.2020.9197283.

[9] F. Faruq, D. Parker, B. Laccrda, and N. Hawes, "Simultaneous task allocation and planning under uncertainty", Jan. 2019, pp. 3559–3564. DOI: 10.1109/IROS.2018.8594404.

[10] S. S. Kannan, V. L. N. Venkatesh, and B.-C. Min, "Smart-llm: Smart multi-agent robot task planning using large language models", *ArXiv*, 2024.

[11] W. Huang, P. Abbeel, D. Pathak, and I. Mordatch, "Language models as zero-shot planners: Extracting actionable knowledge for embodied agents", *International Conference on Machine Learning*, pp. 9118–9147, Mar. 2022.

[12] M. Yahya, Y. Hui, A. Md. Yassin, R. Omar, R. Robin, and N. Kasim, "The challenges of the implementation of construction robotics technologies in the construction", *MATEC Web of Conferences*, vol. 266, p. 05 012, Jan. 2019. DOI: 10.1051/matecconf/201926605012.

[13] M. S. R. Espinoza, M. A. C. Contreras, K. M. A. Estela, C. J. N. Varillas, and G. F. R. Torpoco, "Robotics in building construction: Advantages and barriers", in *2023 Congreso Internacional de Innovación y Tendencias en Ingeniería (CONIITI)*, Oct. 2023. DOI: 10.1109/CONIITI61170.2023.10324131.

[14] L. Fischer, S. Hasler, J. Deigmoeller, *et al.*, "Which tool to use? grounded reasoning in everyday environments with assistant robots", *CogRob@ KR*, pp. 3–10, 2018.

FORUMBAUINFORMATIK